

INDIAN JOURNAL OF PHYSICS

VOL. XXIV

AND

PROCEEDINGS

OF THE

Indian Association for the Cultivation of Science, Vol. XXXIII

(Published in Collaboration with the Indian Physical Society)

(With Thirtyseven Plates)

PRINTED BY SIBENDRANATH KANJILAL, SUPERINTENDENT (OFF-G.), CALCUTTA
UNIVERSITY PRESS, 48, HAZRA ROAD, BALLYGUNGE, CALCUTTA, AND
PUBLISHED BY THE REGISTRAR, INDIAN ASSOCIATION FOR
THE CULTIVATION OF SCIENCE
210, Bowbazar Street, Calcutta

1950

Price Rs. 20 or £2

BOARD OF EDITORS

K. BANERJEE	S. K. MITRA
D. M. BOSE	P. RAY
S. N. BOSE	M. N. SAHA
D. S. KOTIARI	S. C. SIKKAR.

Secretary

EDITORIAL COLLABORATORS

DR. R. K. ASUNDI, M.A., PH.D.
PROF. H. J. BHABHA, PH.D., F.R.S.
DR. P. K. KICHLU, D.Sc.
PROF. K. S. KRISHNAN, D.Sc., F.R.S.
PROF. G. P. DUBEY, M.Sc.
DR. K. RANGADHAMA RAO, M.A., D.Sc.
DR. N. D. SARWATTEY, D.Sc.
DR. N. N. DASGUPTA, M.Sc., PH.D.
PROF. N. R. SEN, D.Sc., F.N.I.
PROF. P. C. MAHANTI, D.Sc., F.N.I.
PROF. S. R. PALIT, D.Sc.,
DR. H. RAKSHIT, D.Sc.,
PROF. K. R. DIXIT, PH.D.
DR. VIKRAM A. SARABHAI, M.A., PH.D.

ASSISTANT EDITOR

MR. A. N. BANERJEE, M.Sc.

NOTICE TO INTENDING AUTHORS

Manuscripts for publication should be sent to Mr. A. N. Banerjee, Assistant Editor, 2 & 3, Lady Willingdon Road, Jadavpur, Calcutta-32.

The manuscript of each paper should contain in the beginning a short abstract of the paper.

All references to published papers should be given in the text by quoting the surname of the authors followed by the year of publication within braces, *e.g.*, Sen (1942). The actual references should be given in a list at the end of the paper according to the following specimen :

Sen, B. K., 1942, *Ind. J. Phys.*, **16**, 329.

The references should be arranged alphabetically in the list.

All diagrams should be drawn on thick white paper in Indian ink, and letters and numbers in the diagrams should be written in pencil.

Annual Subscription—

Inland Rs. 20

Foreign £ ?

INDIAN JOURNAL OF PHYSICS.

VOL. 24, 1950

CONTENTS

Subject	Page
1. On the Dispersion and Absorption of Supersonic Waves in Water —By B. B. Ghosh	1
2. Studies of the Joshi-effect in Chlorine under Ozonizer Excitation —Influence of Temperature—By K. S. Visvanathan and K. Kuppuswamy	13
3. Relativistic Thomas-Fermi Atom—By R. P. Singh	19
4. Dielectric Constants of Commercial Cashew Shell Oils—By S. Krishnamurthy and B. R. Y. Iyengar	23
5. The Complex Band Spectrum of Columbium Oxide (The Diatomic Molecule CbO)—By V. Ramakrishna Rao	35

No. 2

6. Term Values of f^4 -Electron Configuration—By K. Suryanarayana Rao	51
7. A Note on the Thermal Inertia of Cloud Particles—By B. K. Agarwala and N. K. Saha	57
8. On the Distribution of Ions in Solutions of Strong Electrolytes— By M. Dutta and S. N. Bagchi	61
9. The Spectro-Chemical Analysis of Molybdenum in Green Peas— By M. K. Ghosh and K. C. Mazumder	67
10. On the Variation of Current with Distance between the Electrodes of a Glow Discharge in Gases at Low Pressure—By M. Khurshed Husain	73
11. Microseisms—By A. N. Tandon	80
12. A Study on the Polarisation of X-Rays—By H. K. Pal	91

No. 3

13. Circular and Elliptical Quantum Orbits—By M. F. Soonawala	95
14. Spectrum of the Flame above a Copper Arc in Air—By S. P. Sinha and Shyam Chandra Prasad	103
15. A New Laboratory Hydrogen Continuum—By S. K. Bhattacharya	109
16. Raman Spectra of Organic Crystals at Different Low Temperatures. I. Chlorobenzene and Toluene—By A. K. Ray
17. Studies of Schrage Three-Phase Shunt Commutator Motor. III. Circle Diagram—By H. P. Bhattacharyya	119

Subject	Page
18. Effect of Temperature on Ultrasonic Absorption in Acetic Acid— By R. N. Ghosh and Gurudeva Sharan Varma	125
19. Determination of Moisture in Lac by Infra-red heating—By G. N. Bhattacharyya and S. C. Mukherjee	131

No. 4

20. Application of Stokes' Law to estimate the Solvation of Ions in a Solution—By H. Mukherjee	137
21. Electrical Constants of Sand at Ultra High Frequencies—By S. K. Chatterjee	143
22. The Raman Spectra of Trichloro-ethylene and Tetrachloro-ethylene in the Solid state—By S. B. Sanjal	151
23. Thermodynamics of an Oscillator Assembly—By R. P. Singh	155
24. Absorption of U.H.F. Radiowaves in some Substituted Benzene compounds—By S. N. Sen	163
25. A Comparative Study of the Different Methods of Heat-run Tests on Electrical Machines. I. Single Phase Transformers—By H. K. Basu	171

No. 5

26. A Note on Weyl's Inequality—By V. S. Nanda	181
27. Multiplet Separation Factors and Γ -sum Rule—By S. Sengupta	185
28. On the Raman Spectra and Heat Capacity of Benzene at Low Temperatures—By S. C. Sirkar and A. K. Kay	189
29. Fading of Short Wireless waves due to the Interference between Magneto-ionic Components—By S. N. Mitra	197
30. A Simple method of producing Wide-band Frequency Modulation —By H. Rakshit and N. L. Sarkar	207
31. Generalized Impedance Circle-diagrams in the Analysis of Coupled Net-works—By Chandrasekhar Ghosh	223

No 6

32. B.E.C. and Crystalline structure of Silicate Minerals related to Soils and Clays—By S. K. Mukherjee and A. K. Ganguli	233
33. Some New Relations in the Interval Factors and the General case of I' -Electron Configuration—By V. Ramakrishna Rao	257
34. Effect of 'Time-lag in the Measurement of Delayed Coincidence with G. M. Counters—By B. D. Nag, S. Sen and S. Chatterjee	261
35. On the X-Ray Luminescence Spectra of Alkali Halides—By Aparesh Chatterjee	265
36. A Note on the Critical Area of Surface-films and Evaporation through them—D. S. Subrahmanyam	271

Contents

Subject	No. 7	Page
37. Some Random Fading Records with Short-Wave Signals—By P. M. Das and S. R. Khastgir	...	277
38. Linear Analysis of Electronic Switching—By Rais Ahmed	...	281
39. An Explanation of the Influence of the Frequency of the Exciting Potential on Joshi-effect—By G. V. Bakore	...	291
40. Multiplet Separations in the f^4 -electron Configuration—By K. Suryanarayana Rao	...	296
41. An Experimental Study of the Illuminating system of the Electron Microscope—By M. L. De	...	303
42. Crystal Structure of Phenanthrene—By B. S. Basak	...	309
43. Some Nuclear Levels—By M. F. Soonawala	...	315
No. 8		
44. A Spectroscopic Study of a Condensed Spark between Copper Electrodes in Illumination gas, Air and Carbondioxide at various pressures—By Jagdeo Singh	...	321
45. On the X-Ray Luminescence Spectra of Thallium-activated Alkali Halide Crystals—By Aparesh Chatterjee	...	331
46. The Relativistic Theory of Scattering in Coulomb Field by Atom—By K. C. Kar, S. Sengupta and P. P. Chatterjee	...	339
47. Scintillation type Alpha-Counter and its Application in U and Th Estimation of Minerals—By Santinoy Chatterjee and Sobhana Dhar	...	346
48. A Study of the Switching Action in a Multivibration Circuit—By B. M. Banerjee	...	361
Reviews	...	371
No. 9		
49. A Spectroscopic Study of an Uncondensed Spark between Copper Electrodes in three different Gases at Various Pressures—Part III—By Jagdeo Singh	...	373
50. On the Raman Spectra of three Mono-substituted <i>n</i> -Butane Compounds in the Solid state—By S. B. Sanyal	...	378
51. Tides in the Ionosphere—By A. P. Mitra	...	387
52. On the Structure of Soda Cellulose from Raw Jute Fibre—By N. N. Saha and Mrs. Usha Saha	...	405
53. A Speed Limit for Rockets?—By William Squire	...	410
54. A Time Base Circuit for a High Precision Ionospheric Sounding Apparatus—By B. M. Banerjee and R. Roy	...	411
Review	...	420
No. 10		
55. Absorption Spectrum of Anisole—By K. Sreerainamurty	...	421

Subject	Page
56. Absorption Spectrum of Thallium Halides—By P. Tiruvenganna Rao	434
57. On the Origin of Fluorescence in Diamond—By B. M. Bishui ...	441
58. Ultrasonic Velocities in Organic Solution, I—By K. C. Lal ...	461
59. An Automatic Pressure Stabilizing Device for a Diaphragm-type Wilson Cloud Chamber—By Ranjit Kumar Das ...	466

No. 11

60. The Electrical Constants of Soil at Ultra High Frequencies—By P. N. Sundaram	469
61. On the Disintegration of Scandium(46) and the Method of Delayed Coincidence for the Study of Short-lived Meta-stable States in Isomeric Nuclei—By B. D. Nag, S. Sen and S. Chatterjee ...	479
62. A Triggering Device for Arc-discharge Lamps in Cloud Chamber Photography—By Ranjit Kumar Das	497
63. Photographic Emulsion Studies of the Latitude Effect—By K. R. Dixit	501
64. On the Absorption of U.H.F. Radio Waves by Opalescent Binary Liquid Mixtures—By (Miss) Anjali Choudhury	507
65. Fine Structure in the East-West Cosmic Ray Intensity at Lahore ($\lambda = 22^\circ\text{N}$), India—By Om Parkash	513

No. 12

66. On Alpha Disintegration, Part I. Some Useful Theoretical Tabulations and Graphical Plots—By Ranjit Kumar Das ...	523
67. On the Raman Spectra of Naphthalene at Low Temperatures—By A. K. Ray	539
68. The Wave Statistical Theory of Alpha Disintegration—By K. C. Kar and M. L. Chaudhury	545
69. The 43-Day Isomer of Cadmium (115)—By P. S. Gill, C. E. Mandeville and E. Shapiro	566
Review	571

AUTHOR INDEX

Author	Subject	Page
Agarwala, B. K. and Saha, N. K.	A Note on the Thermal Inertia of Cloud Particles.	57
Ahmed, Rais ..	Linear Analysis of Electronic Switching.	281
Bakore, G. V. ...	An Explanation of the Influence of the Frequency of the Exciting Potential on Joshi-effect.	291
Banerjee, B. M. ...	A Study of the Switching Action in a Multivibrator Circuit.	361
Banerjee, B. M. and Roy, R.	A Time Base Circuit for a High Precision Ionospheric Sounding Apparatus.	411
Basak, B. S.	Crystal Structure of Phenanthrene	309
Basu, H. K. ..	A Comparative Study of the Different Methods of Heat-run Tests on Electrical Machines. I. Single Phase Transformers.	171
Bhattacharya, G. N. and Mukherjee, S. C.	Determination of Moisture in Lac By Infra-red Heating	131
Bhattacharyya, H. P.	Studies of Schrage Three Phase Shunt Commutator Motor III. Circle Diagrams.	119
Bhattacharya, S. K.	A New Laboratory Hydrogen Continuum.	109
Bishui, B. M. ...	On the Origin of Fluorescence in Diamond.	441
Chatterjee, Aparesb	On the X-Ray Luminescence Spectra of Alkali Halides.	265
" "	On the X Ray Luminescence Spectra of Thallium-activated Alkali Halide Crystals.	331
Chatterjee, S. K. ...	Electrical Constants of Sand at Ultra High Frequencies.	143
Chatterjee, Santimoy and Dhar, Sobhana	Scintillation type Alpha Counter and its Application in U and Th Estimation of Minerals.	346

Author		Subject	Page
Choudhury, (Miss) Anjali	...	On the Absorption of U.H.F. Radio Waves by Opalescent Binary Liquid Mixtures.	507
Das, P. M. and Khastgir S. R.	...	Some Random Fading Records with Short Wave Signals.	277
Das, Ranjit Kumar	...	An Automatic Pressure Stabilizing Device for a Diaphragm-type Wilson Cloud Chamber.	466
	..	A Triggering Device for Arc-discharge Lamps in Cloud Chamber Photography.	497
	...	On Alpha Disintegration. Part I. Some Useful Theoretical Tabulations and Graphical Plots.	523
De, M. L.	...	An Experimental Study of the Illuminating System of the Electron Microscope.	303
Dixit, K. R.	...	Photographic Emulsion Studies of the Latitude Effect.	501
Dutta, M. and Bagchi, S. N.	..	On the Distribution of Ions in Solutions of Strong Electrolytes.	61
Ghosh, B. B.	...	On the Dispersion and Absorption of Supersonic Waves in Water.	
Ghosh, Chandrasekhar	..	Generalized Impedance Circle-diagrams in the Analysis of Coupled Net-works.	223
Ghosh, M. K. and Mazumder, K. C.	..	The Spectro-Chemical Analysis of Molybdenum in Green Peas.	67
Ghosh, R. N. and Varma, Gurdeva Sharan	..	Effect of Temperature on Ultrasonic Absorption in Acetic Acid.	125
Gill, P. S., Mandeville, C. E. and Shapiro, E.	..	The 43-day Isomer of Cadmium (115).	566
Husain, M. Khurshed	..	On the Variation of Current with Distance between the Electrodes of a Glow Discharge in Gases at Low Pressure.	73

Author Index

Author	Subject	ix Page
Kar, K. C. and Chaudhury, M. L.	... The Wave-statistical Theory of Alpha Disintegration.	545
Kar, K. C., Sengupta, S. and Chatterji, P. P.	... The Relativistic Theory of Scattering in Coulomb Field by Atom.	339
Krishnamurthy, S. and Iyengar, B. R. Y.	... Dielectric Constants of Commercial Cashew Shell Oils.	23
Lal, K. C.	... Ultrasonic Velocities in Organic Solutions. I.	461
Mitra, A. P.	... Tides in the Ionosphere.	387
Mitra, S. N.	... Fading of Short Wireless Waves due to the Interference between Magneto-ionic Components.	197
Mukherjee, H.	... Application of Stokes' Law to estimate the Solvation of Ions in a Solution.	137
Mukherjee, S. K. and Ganguli, A. K.	... B. E. C. and Crystalline Structure of Silicate Minerals related to Soils and Clays.	233
Nag, B. D., Sen, S. and Chatterjee, S.	... Effect of Time-lag in the Measurement of delayed Coincidence with G. M. Counters	261
	... On the Disintegration of Scandium (46) and the method of Delayed Coincidence for the Study of short-lived Metastable States in Isomeric Nuclei.	479
Nanda, V. S.	... A Note on Weyl's Inequality	181
Pal, H. K.	... A Study on the Polarisation of X-Rays.	91
Parkash, Om	... Fine Structure in the East-West Cosmic Ray Intensity at Lahore ($\lambda = 22^\circ N$), India.	513
Rakshit, H. and Sarkar, N. L.	... A Simple Method of Producing Wide-band Frequency modulation.	207
Rao, P. Tiruvenganna	... Absorption Spectrum of Thallium Halides.	434
Rao, K. Suryanarayan	... Term Values of f^4 -Electron Configuration.	51
" "	... Multiplet Separations in the f^4 -Electron Configuration.	296

Author	Subject	Page
Rao, V. Ramakrishna	... The Complex Band Spectrum of Columbium Oxide (The Diatomic Molecule CbO).	... 35
" "	... Some New Relations in the Interval Factors and the General case of l' -Electron Configuration.	... 257
Ray, A. K.	... Raman Spectra of Organic Crystals at Different Low Temperatures. I. Chlorobenzene and Toluene.	... 111
" "	... On the Raman Spectra of Naphthalene at Low Temperatures.	... 539
Saha N. N. and Saha, Mrs. Usha	... On the Structure of Soda Cellulose from Raw Jute Fibre	... 405
Sanyal, S. B.	... The Raman Spectra of Trichloroethylene and Tetrachloroethylene in the Solid State.	... 151
" "	... On the Raman Spectra of three Mono-substituted <i>n</i> -Butane Compound in the Solid State.	... 378
Sen, S. N.	... Absorption of U. H. F. Radio Waves in some Substituted Benzene Compounds.	... 163
Sengupta, S.	... Multiplet Separation Factors and Γ -sum rule.	... 185
Singh, Jagdeo	... A Spectroscopic Study of a Condensed Spark between Copper Electrodes in Illuminating Gas, Air and Carbon dioxide at various Pressures.	... 321
	A Spectroscopic Study of an Uncondensed Spark between Copper Electrodes in three different Gases at various Pressures. Part III.	... 373
Singh, R. P.	... Relativistic Thomas Fermi Atom	... 19
" "	... Thermodynamics of an Oscillator Assembly.	... 155
Sinha, S. P. and Prasad, Shyam Chandra	Spectrum of the Flame above a Copper Arc in Air.	... 103

Author Index

xi

Author	Subject	Page
Sirkar, S. C. and Ray, A. K.	On the Raman Spectra and Heat Capacity of Benzene at Low Temperatures.	... 189
Soonawala, M. F. ...	Circular and Elliptical Quantum Orbits.	... 95
	Some Nuclear Levels. 315
Squire, William ...	A Speed Limit for Rockets ?	... 410
Sreeramamurty, K.	Absorption Spectrum of Anisole.	... 421
Subrahmanyam, D. S.	A Note on the Critical Area of Surface-films and Evaporation through them.	... 271
Sundaram, P. N. ...	Electrical Constants of Soil at Ultra High Frequencies.	... 460
Tandon, A. N. ...	Microseisms. 80
Visvanathan, K. S. and Kuppuswamy, K.	Studies of the Joshi-effect in Chlorine under Ozonizer Excitation. Influence of Temperature.	... 13

SUBJECT INDEX

Subject	Author	Page
Absorption Spectrum of Anisole	K. Sreeramamurty ...	421
Absorption Spectrum of Thallium Halides	P. Tiruvenganna Rao ...	434
Alpha-disintegration. Part I. Some Useful Theoretical Tabulations and Graphical Plots. On	Ranjit Kumar Das ..	523
Alpha-disintegration The Wave Statistical Theory of	K. C. Kar and M. L. Chaudhury .	545
B. E. C. and Crystalline Structure of Silicate Minerals related to Soils and Clays	S. K. Mukherjee and A. K. Ganguli ..	233
Cadmium (115). The 43-day Isomer of	P. S. Gill, C. E. Mandeville and E. Shapiro ..	566
Complex Band Spectrum of Columbium Oxide (The Diatomic Molecule CbO). The	V. Ramakrishna Rao ...	35
Critical Area of Surface Films and Evaporation through Them. A note on the	D. S. Subrahmanyam ..	271
Crystal Structure of Phenanthrene	B. S. Basak ...	309
Delayed Coincidences with G. M. Counters. Effect of time-lag in the Measurement of	B. D. Nag, S. Sen and S. Chatterjee ...	261
Dielectric Constants of Commercial Cashew Shell Oils	S. Krishnamurthy and B. R. V. Iyengar ...	23
Electrical Constants of Sand at Ultra High Frequencies	S. K. Chatterjee ...	143
Electrical Constants of Soil at Ultra High Frequencies. The	P. N. Sundaram ...	469
Electron Microscope. An Experimental Study of the Illuminating System of the	M. L. De ...	303
Electronic Switching. Linear Analysis of	Rais Ahmed ...	281
Fading of Short Wireless Waves due to the Interference between Megneto-Ionic Components	S. N. Mitra ...	197
Fading Records with Short Wave Signals. Some Random	P. M. Das and S. R. Khastgir ...	277

Subject Index

xiii

Subject	Author	Page
Fine Structure in the East-West Cosmic Ray Intensity at Lahore ($\lambda = 22^\circ\text{N}$), India.	Om Parkash	513
Fluorescence in Diamond. On the Origin of	B. M. Bishui	441
Generalized Impedence Circle-diagrams in the Analysis of Coupled Networks.	Chaudrasekhar Ghosh	223
Glow Discharge in Gases at Low Pressure. On the Variation of Current with Distance between the Electrodes of a	M. Khurshed Husain	73
Heat-run Tests on Electrical Machines. I. Single Phase Transformers. A Comparative Study of the Different Methods of	H. K. Basu	171
Hydrogen Continuum. A new Laboratory	S. K. Bhattacharya	109
Interval Factors and the General Case of f^4 -Electron Configuration. Some New Relations in the	V. Ramakrishna Rao	257
Ions in Solutions of Strong Electrolytes. On the Distribution of	M. Datta and S. N. Bagchi	61
Ionospheric Sounding Apparatus. A Time Base Circuit for a High Precision	Banerjee, B. M. and Roy, R.	411
Joshi Effect in Chlorine under Ozonizer Excitation. Studies of the—Influence of Temperature	K. S. Visvanathan and K. Kuppuswami	13
Joshi Effect. An Explanation of the Influence of the Frequency of the Exciting Potential on	G. V. Bakore	291
Latitude Effect. Photographic Emulsion Studies of the	K. R. Dixit	501
Microseisms	A. N. Tandon	80
Moisture in Lac by Infra-red Heating. Determination of	G. N. Bhattacharya and S. C. Mukherjee	131
Multiplet Separation Factors and T-sum rule	S. Sengupta	185
Multiplet Separations in the f^4 -Electron Configuration	K. Suryanarayana Rao	296
Multivibrator Circuit. A Study of the Switching Action in a	B. M. Banerjee	361
Nuclear Levels. Some	M. F. Soonawala	315

Subject	Author	Page
Oscillator Assembly. Thermodynamics of an	R. P. Singh	155
Quantum Orbits. Circular and Elliptical	M. F. Soonawala	95
Raman Spectra of Organic Crystals at Different Low Temperatures.	A. K. Ray ...	
1. Chlorobenzene and Toluene		
Raman Spectra of Trichloro ethylene and Tetrachloro-ethylene in the Solid State. The	S. B. Sanyal	151
Raman Spectra and Heat capacity of Benzene at Low Temperatures. On the	S. C. Sirkar and Ray, A. K.	189
Raman Spectra of three Mono-substituted <i>n</i> -Butane Compounds in the Solid State. On the	S. B. Sanyal	378
Raman Spectra of Naphthalene at Low Temperatures. On the	A. K. Ray	539
Relativistic Theory of Scattering in Coulomb Field by Atom. The	K. C. Kar, S. Sen-upta and P. P. Chatterjee	339
Scandium (46) and the method of Delayed Coincidence for the study of Short-lived Metastable States in Isomeric Nuclei. On the Disintegration of	B. D. Nag, S. Sen and S. Chatterjee	479
Schrage Three Phase Shunt Commutator Motor. Studies of-III. Circle Diagrams.	H. P. Bhattacharyya	119
Scintillation type Alpha Counter and its Application in U and Th estimation of Minerals	Santimoy Chatterjee ... and Sobhana Dhar	346
Soda Cellulose from Raw Jute Fibre. On the Structure of	N. N. Saha and Mrs. Usha Saha	405
Solvation of Ions in a solution. Application of Stokes' Law to Estimate the	H. Mukherjee	137
Spectrochemical Analysis of Molybdenum in Green Peas. The	M. K. Ghosh and K. C. Mazumder	67
Spectroscopic Study of a Condensed Spark between Copper Electrodes in Illuminating Gas, Air and Carbon-dioxide at various Pressures. A	Jagdeo Singh	321

Subject Index

xv

Subject	Author	Page
Spectroscopic Study of an Uncondensed Spark between Copper Electrodes in three Different Gases at various Pressures. Part III.	Jagdeo Singh	373
Spectrum of the Flame above a Copper arc in Air	S.P. Sinha and Shyam Chandra Prasad	103
Speed Limit for Rockets ? A,	William Squire	410
Supersonic Waves in Water. On the Dispersion and Absorption of	B. B. Ghosh	1
Term Values of f^4 -Electron Configuration	K. Suryanarayana Rao	51
Thermal Inertia of Cloud Particles A note on the	B. K. Agarwala and N. K. Saha	57
Thomas-Fermi Atom. Relativistic	R. P. Singh	19
Tides in the Ionosphere.	A. P. Mitra	387
Triggering Device for Arc-discharge Lamps in Cloud Chamber Photography. A	Ranjit Kumar Das	497
U. H. F. Radio Waves in some Substituted Benzene Compound. Absorption of	S. N. Sen	163
U. H. F. Radio Waves by Opalescent Binary Liquid mixtures. On the absorption of	(Miss) Anjali Choudhury	507
Ultrasonic Absorption in Acetic acid. Effect of Temperature on	R. N. Ghosh and Gurdeva Sharau Varma	125
Ultrasonic Velocities in Organic Solutions. I.	By K. C. Lal	461
Weyl's Inequality. A note on	V. S. Nanda	181
Wide-band Frequency Modulation. A simple method of producing,	H. Rakshit and N. L. Sarkar	207
Wilson Cloud Chamber. An automatic Pressure stabilizing device for Diaphragm-type	Ranjit Kumar Das	466
X-Rays. A Study on the Polarisation of	H. K. Pal	91
X-Ray Luminescence Spectra of Alkali Halides. On the	Aparesh Chatterjee	265
X-Ray Luminescence Spectra of Thallium-activated Alkali halide Crystals. On the	Aparesh Chatterjee	331

	Author	Subject	Page
<i>Reviews :</i>			
(i)	A General Kinetic theory of liquids—M Born and H. S. Green. K. C. K		371
(ii)	History of Physics—Max Von Laue S. C. S.		371
(iii)	Principles of a new Energy Mechanics—J. Mandelker D. B.		420
(iv)	Physical aspects of Colour—P. J. Bouma S. C. S.		571

Vol. 23

INDIAN JOURNAL OF PHYSICS

No. 1

(Published in collaboration with the Indian Physical Society)

AND

Vol. 33

PROCEEDINGS

No. 1

OF THE

INDIAN ASSOCIATION FOR THE
CULTIVATION OF SCIENCE

JANUARY, 1950

PUBLISHED BY THE
INDIAN ASSOCIATION FOR THE CULTIVATION OF SCIENCE
210, Bowbazar Street, Calcutta

BOARD OF EDITORS

K. BANERJEE	S. K. MITRA
D. M. BOSE	P. RAY
S. N. BOSE	M. N. SAHA
D. S. KOTHARI	S. C. SIKKAR

Secretary

EDITORIAL COLLABORATORS

DR. R. K. ASUNDI, M.A., PH.D.
PROF. H. J. BHABHA, PH.D., F.R.S.
PROF. D. M. BOSE, M.A., PH.D.
DR. P. K. KICHLU, D.Sc.
PROF. K. S. KRISHNAN, D.Sc., F.R.S.
PROF. G. P. DUBEY, M.Sc.
DR. K. RANGASWAMI RAO, M.A., D.Sc.
DR. N. D. SARWATY, D.Sc.
DR. N. M. DASGUPTA, M.Sc., PH.D.
PROF. N. R. SEN, D.Sc., F.N.I.
PROF. P. C. MAHANTY, D.Sc., F.N.I.
PROF. S. R. PALIT, D.Sc.
DR. H. RAKSHIT, D.Sc.
PROF. K. R. DIXIT, PH.D.
DR. VIKRAM A. SARABHAI, M.A., PH.D.

ASSISTANT EDITOR

MR. A. N. BANERJEE, M.Sc.

NOTICE TO INTENDING AUTHORS

Manuscripts for publication should be sent to Mr. A. N. Banerjee, Assistant Editor, 97a Bowbazar Street, Calcutta.

The manuscript of each paper should contain in the beginning a short abstract of the paper.

All references to published papers should be given in the text by quoting the surname of the authors followed by the year of publication within braces, e.g., Sen (1942). The actual references should be given in a list at the end of the paper according to the following specimen:

Sen, B. K., 1942, *Ind. J. Phys.*, **16**, 329.

The references should be arranged alphabetically in the list.

All diagrams should be drawn on thick white paper in Indian ink, and letters and numbers in the diagrams should be written in pencil.

Annual Subscription

Volume No. 16
Price Rs. 10

ON THE DISPERSION AND ABSORPTION OF SUPERSONIC WAVES IN WATER

By B. B. GHOSH

(Received for publication, Sept. 13, 1949)

ABSTRACT A theoretical expression for the dispersion of supersonic waves in water has been deduced on the basis of water structure and structural compressibility. The experimental results as reported in previous papers, have been compared with the results calculated from this expression and are found to be in good agreement. Further, theoretically deduced formula for absorption, similar to one published in an earlier paper, has been used to calculate the frequency for maximum absorption for water due to structural vibrations at different temperatures. The calculated values indicate that the mean frequency region for dispersion for associated liquids such as water, lies in the neighbourhood of 10^8 to 10^{10} c p s.

INTRODUCTION

The gas dispersion formula, as derived by Kueser and others on the basis of relaxational principle, was further modified by Dutt (1938) with the help of thermodynamical relations to fit in the case of liquids in general. Subsequently some theoretical expressions for absorption of supersonic waves in liquids in general were reported by Dutt and Ghosh (1939).

The expressions given there are

$$\alpha/v^2 = \frac{2\mu_m}{v \cdot v_m} \cdot \frac{1}{1 + \left(\frac{v}{v_m}\right)^2} \quad \dots (1)$$

where α/v^2 = the expression for the measure of absorption of supersonic waves in liquids.

μ_m = the co-efficient of maximum absorption per unit wave length.

v = the supersonic velocity at frequency v .

v_m = the frequency for maximum absorption and corresponds to v_w , the mean dispersive frequency

μ_m is given by :

$$\mu_m = \pi^2 \frac{\alpha^2 - v_w^2}{v_w^2} = \pi \left[\frac{C_0 - C_1 + \frac{aV_m T}{\beta_0}}{C_0 - C_1} \cdot \frac{C_0}{C_0 + \frac{aV_m T}{\beta_0}} - 1 \right] \quad \dots (2)$$

where α = the coefficient of expansion

β_v = the compressibility

V_m = the molar volume

T = the absolute temperature

v_∞, v_0 = velocities at very high and very low frequencies.

$C_v = C_p$ = the sp. heat at constant volume.

and C_i = the amount of energy assimilated in the vibrational degrees of freedom of the molecules and is considered to be a function of frequency of the impressed sound energy.

It is here that the relaxation principle, based on the incomplete excitation of these energy levels by the sound waves, is introduced such that the difference

$$C_p = C_v + C_i$$

becomes dependent on the relaxation time factor.

In equation (2) all constants are known except " C_i " which was further calculated from the relation given by Einstein function as

$$C_i = \frac{\theta^2 e^{\theta}}{(e^{\theta} - 1)^2} \quad \dots \quad (R\text{-units})$$

$$= \frac{(\hbar\nu/kT)^2 \cdot e^{\hbar\nu/kT}}{(e^{\hbar\nu/kT} - 1)^2} \quad \dots \quad (3)$$

and also from the data given by Raman effect and the infra-red spectra. Thus the value of

$$\frac{v_\infty^2 - v_0^2}{v_0^2}$$

in equation (2) becomes known and so the value of μ_m . For most liquids the supersonic velocities are known from direct experiments and the frequency ν at which they are measured. Also, employing the experimentally measured values for α/ν^2 for different liquids, the values for v_m for different liquids were calculated and were generally found to be of the order of 10^9 c/s (Dutt and Ghosh, 1939). It was also considered that since the dispersive region of supersonic waves for gases generally lies in the region of 10^6 c/s and since the packing of molecules for liquids, is about 10^3 times the packing in the gaseous state, therefore, (since the effective collision number for the excitation of an oscillatory quantum state is constant), the dispersive region for liquids can be expected to lie in the neighbourhood of 10^8 to 10^9 c/sec. The value of v_m , which corresponds to the frequency of inflexion ν_m —the centre of the dispersive region of supersonic waves in liquid (Fig. 1), as found from equation (1) with the help of the

experimental values, agrees well with this prediction and thus afforded an indirect test for the validity of the relaxational theory as applied above using the thermodynamical relations for liquids. The behaviour of water and other associated type of liquids and also that of polyatomic unassociated liquid CS_2 , among the number of liquids considered, however, could not be accounted for by these theoretical expressions. According to this theory, we could not indicate definitely whether water would show any dispersion or absorption as the theoretical values became rather ambiguous (Table III). Experimentally, however, rather high amount of absorption (Pukerton, 1947; Sorensen, 1936; Fock and Hartmann, 1940) and quite an appreciable amount of dispersion (Dutt, 1938; Dutt and Ghosh, 1941) were reported by a number of workers in the line. In regard to dispersion in water, it was also found experimentally that the amount of dispersion decreases slightly with rise in temperature, as also with increasing concentration of electrolytic solution of water (Dutt and Ghosh, 1941). From all these informations, it was also concluded that although the relaxational heat capacity lag, as applied in the case of liquids by us, generally indicates the behaviour of non-associated type of liquids such as, toluol, xylol, benzene, etc. in respect of dispersion and absorption, we require a separate treatment for all associated type of liquids like alcohols, specially for water. A theory was outlined on the basis of inter-molecular interaction occurring in the regions of compressions under supersonic pressures and the consequent changes in or breaking of water structure resulting into decrease in compressibilities. The observed dispersion in water and in water solution of electrolytes was qualitatively explained on the basis of this theory (Ghosh, 1949).^{*} An attempt is made here to give a mathematical representation of the theory as reported there.

STRUCTURE OF WATER, STRUCTURAL ACTIVATION
ENERGY DUE TO HYDROGEN BONDS AND
STRUCTURAL COMPRESSIBILITY

X-ray studies of liquid water and water in ice state by a number of workers (Bernal and Fowler, 1933; Morgan and Warren, 1938; Stewart, 1939) indicate that each water molecule has four nearest neighbours arranged tetrahedrally and has thus an open structure. The tetrahedral structure is mainly maintained by the intermolecular hydrogen bonds. Introduction of ions, like an increase in temperature has, in general, the effect of breaking down this open water structure and has thus the effect of closer packing. This was shown to be actually the case by Morgan and Warren from the changes in height of the second maxima curve of the X-ray diffraction pattern of water.

^{*} Reported in the thesis for P.R.S. of the University of Calcutta, 30th November, 1945 and later published in part in Indian Journal of Physics, Vol. 23, No. 2, p. 79, 1949

Ewell and Eyring (1937), from a theory on viscosity of liquids, have shown that those associated type of liquids containing OH or NH groups have usually higher viscosities due to their hydrogen-bonded structures. The rapid decrease in η the viscosity co-efficient and ΔE_{vis} , the activation energy of viscous flow, with rising temperature, is due to the decrease in the number of hydrogen bonds that have to be broken for the flow to take place. This activation energy due to hydrogen bonds was termed the Structure Activation Energy.

STRUCTURAL COMPRESSIBILITY AND DISPERSION IN WATER

The possibility of the existence of some sort of a structural compressibility undergoing changes due to the breaking of water structure by the introduction of ions or increase in temperature and affecting the supersonic velocities in water solution of electrolytes at different concentrations and temperatures was suggested previously by Dutt and Ghosh (1941, 1943) and on the basis of the changes in structural compressibilities the physical principle of the observed dispersion of supersonic waves in water and electrolytic solutions was explained (Ghosh, 1945, 1949).

Randall (1932) has shown, as a result of accurate compressibility measurements that the adiabatic compressibility decreases with increasing temperature to a minimum at about 44°C. Further Tamman, (1893) had shown theoretically that when the "internal pressure" of water is increased, as by the introduction of ions in electrolytic solutions, the compressibility decreases.

From the foregoing observations, we may now assume, that the total or effective compressibility is the result of two effects under acoustical pressures of supersonic waves. Firstly, we may think of some free water molecules at any instant. Under a compression these molecules will be brought uniformly closer together and due to increased packing and increased molecular energy, the liquid will behave as if it has some sort of a molecular compressibility, say, β_n . Secondly, under a compression, the open tetrahedral structures will undergo a contraction in volume. When the compression is withdrawn, the structures will normally come back to their normal positions. But if before this another compression is impressed on them, the expanding structures will oppose the compression and it may appear as if the whole system has been subjected to an "internal pressure." The effective compressibility will be lowered: and this behaviour can be looked upon as having another form of compressibility, say, β_i , which may be called Structural Compressibility. Evidently, the structures will require a time to relax and hence when the time period of the sound frequency is comparable to this time, β_i will become relaxational, in the same way as the relaxational heat capacity. This will give rise to dispersion. For

absorption, the structures, due to these increased vibrations as a whole or due to increased molecular energy, will break up. As the energy (about 3000 cal. per each OH bond per mol) for breaking up of these structures (Cross, Burnham and Leighton, 1937) will have to be derived from the impressed sound energy; there will be an excess absorption than what is expected from a non-associated liquid.

We can therefore have

$$\beta_0 = \beta_a + \beta_i \quad (4)$$

where β_0 is the static or ordinary compressibility.

β_0 at any temperature can be obtained from various sources. The compressibility β_a , as stated above, may be considered to have its origin on what may be termed as the "Molecular Compression" and may, therefore, be considered common to all liquids, associated or non-associated. This is evidently dependent on the changes in molecular energy, as by transfer of translational energy into molecular energy by the propagating supersonic beam. The effect of it on the supersonic velocity in liquids is, therefore, expected to be the same as caused by the relaxational specific heat which, as we have shown already, indicates the relaxational time for most liquids to be near 10^{-11} sec. For water, theoretically, the dispersion from this source was shown to be nil even at frequencies of 10^6 or 10^8 c.p.s. (Dutt and Ghosh, 1939). But according to our experiments, there is dispersion, although small, even at this region of frequencies (Dutt and Ghosh, 1941). As stated before, this dispersion may have its origin on the changes in water structure brought about by supersonic pressures and therefore on structural compressibility " β_i " which, we have assumed to be associated with the relaxational time period of the water structure. Under harmonic sound pressure, the effective compressibility can, therefore, be expressed in the form,

$$\text{Effective compressibility} = \beta_a + \frac{\beta_i}{1 + i\omega t_0} \quad (5)$$

much in the same form that we had used in the case of relaxational heat capacity, viz.

$$\text{Effective sp. heat} = C_a + \frac{C_i}{1 + i\omega t_0}$$

Now, the velocity of sound can be written as,

$$\begin{aligned} v^2_{(\text{complex})} &= \frac{1}{\rho (\text{effective compressibility})} \\ &= \frac{1}{\rho \left(\beta_a + \frac{\beta_i}{1 + i\omega t_0} \right)} \end{aligned} \quad (6)$$

where, ρ is the density of water and t_0 is the relaxational time of the water structures. The real part of this complex velocity is given by,

$$v^2 = \left\{ \frac{\beta_0 + \omega^2 t_0^2 \beta_a}{\beta_0^2 + \omega^2 t_0^2 \beta_a^2} \right\} \cdot \frac{1}{\rho} \quad \dots (7)$$

and the dispersion is given by,

$$v_\infty^2 / v_0^2 = \frac{\beta_0 + \omega_\infty^2 t_0^2 \beta_a}{\beta_0^2 + \omega_\infty^2 t_0^2 \beta_a^2} \bigg/ \frac{\beta_0 + \omega_0^2 t_0^2 \beta_a}{\beta_0^2 + \omega_0^2 t_0^2 \beta_a^2} \quad \dots (8)$$

where, v_∞ and v_0 are the supersonic velocities at two frequencies ν_∞ and ν_0 and ν_∞ is much higher than ν_0 , the time period corresponding to ν_∞ being of the order of t_0 .

In the above expression, it is difficult to obtain a correct estimate of the value of β_a and its dependence on the change in temperature in water. With increasing temperature, there will be increasingly greater number of molecules, freed from associations due to the breaking of structures, and therefore it is expected that β_a will be slightly increasing and β_0 will be slightly decreasing till all the structures are broken. Probably, this explains why the value of the effective compressibility has a minimum at a particular temperature after which it rises. A rough estimate, however, can be made of the value of β_a from intermolecular potential functions for water molecules. The molecules under the acoustical pressure will approach each other till the force acting on them due to the potential energy existing between members of nearest neighbours, is just sufficient to balance the effect of the acoustic pressure. Now X-ray analysis shows that the distance between nearest neighbour molecules in ice is 2.76 Å and that in water at 1.5°C is 2.90 Å. We may therefore suppose, that 2.76 Å being the average distance of nearest approach, which occurs in ice, the value of β_a should be comparable in magnitude with the adiabatic compressibility in ice. According to Dorsey (1940) this can be taken as $12 \cdot 10^{-12}$ cm²/dyne. As the force acting on the molecules is also a controlling factor in the vibrational or oscillatory motion of the molecules, a rough estimate of this force can be made from the force constants and potential functions as obtained from Raman scattering spectra for water. The value of t_0 is also expected to be dependent on the temperature and should be decreasing with temperature. An estimate of the value of t_0 and its variation with temperature, can be therefore, made by employing the theoretical expressions for dispersion and absorption (Equations 8, 12 and 14) and using the experimental values for the same.

Dispersion and Absorption of Supersonic Waves in Water 7

DISPERSION AND ABSORPTION

For a plane propagating wave, following the usual procedure, we may put,

$$I_x = I_0 \cdot e^{3i\omega} \cdot \{t - \lambda / v(\text{complex})\} \quad \dots (9)$$

and putting $v(\text{complex}) = v' \cdot e^{i\phi}$

$$\text{we get, } I_x = I_0 \cdot e^{2i\omega \left(t - \frac{\lambda}{v'} \cdot \cos \frac{\phi}{2} \right)} \cdot e^{-2\omega \cdot \frac{\lambda}{v'} \cdot \sin \frac{\phi}{2}} \quad (10)$$

where the second factor determines the damping of the wave or the absorption. When ϕ is small, as is actually the case here, the co-efficient of absorption per unit wavelength is given by

$$\mu = 2\pi \tan \phi$$

where $\tan \phi$ is the quotient of the imaginary to the real parts of the velocity expressed in equation (6). Further, putting the condition, $d\mu/d\omega = 0$ in equation (11), we get the expressions,

$$\mu_m \pm \pi \frac{v_x' - v_0'}{v_0' v_s'} = \pi \frac{v_x'' - v_0''}{v_0'^2} \quad (\text{compare eqn 2})$$

since $v_x \neq v_0$ near the point "E" in Fig

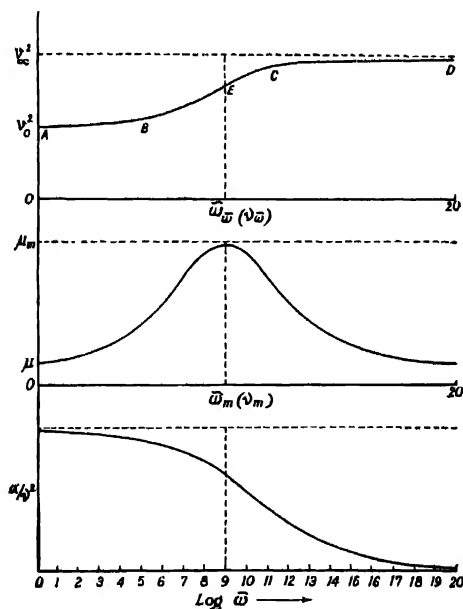


FIG. 1

and
$$\alpha/v^2 = \frac{2\mu_m}{v v_m} \cdot \frac{1}{1 + \left(\frac{v}{v_m}\right)^2} \quad (\text{compare eqn. 1}) \quad \dots (13)$$

$$= \frac{2\mu_m}{v v_m} \quad (\text{approximately}) \quad \dots (14)$$

In equation (8) t_0 and ω_0 correspond to some point near C in Fig. 1. The equation may still hold when it is referred to a point near E representing the mean frequency region for dispersion for which the relaxation time and frequency are, say, t_m and v_m . Hence the equation can be rewritten, as,

$$v_m^2/v_0^2 = \frac{\beta_0 + \omega_0^2 t_m^2 \beta_a}{\beta_0^2 + \omega_0^2 t_m^2 \beta_a^2} \bigg/ \frac{\beta_0 + \omega_0^2 t_m^2 \beta_a}{\beta_0^2 + \omega_0^2 t_m^2 \beta_a^2} \quad \dots (15)$$

The two frequencies, used by us in our experiments for dispersion in water, are $3 \cdot 10^7$ c.p.s. and $3 \cdot 10^6$ c.p.s. We may then assume that v_m and t_m correspond to some point very near to $\omega_0 = 3 \cdot 10^7$ c.p.s., time period of which is just comparable to t_m ; v_0 and ' ω_0 ' may then correspond to $v_0 = 3 \cdot 10^6$ c.p.s.

DISCUSSION OF THE THEORETICAL AND EXPERIMENTAL RESULTS

In Table I, the values of v_m and t_m have been calculated by employing the experimental value of $v_m^2/v_0^2 = 1.004$ at about 30°C . This dispersion as reported earlier, decreases slightly with temperature. Hence, the value of $v_m^2/v_0^2 = 1.004$ and μ_m calculated from Eqn. (12) cannot be taken as constant as has been done here. But from the nature of variation in v_m and t_m , it can be observed that the values for t_m will only be just slightly less than the values shown here. In any case the mid frequency region for dispersion due to structural relaxation, calculated by using the excess absorption lies in the neighbourhood of 10^9 c.p.s. and hence it is quite reasonable to expect dispersion at these frequencies. The excess absorption, denoted by the difference between experimental values and theoretical values calculated from classical formula of Stokes for viscosity absorption, according to our assumption, is the absorption due to both structural vibrations or breaking off of structures. Hence, in calculating v_m or t_m these values of excess absorption have been used.

Again applying these values of t_m in equation (15), values of v_m^2/v_0^2 for different temperatures have been calculated. These calculated values are in good agreement with the experimental results and also indicate a decrease with rising temperature.

After the preparation of this paper on the basis of the physical interpretations of the experimental observation reported in previous papers, the author came across two other papers, one by Hall (1948) and another

TABLE I

Temperature in °C	Dispersion $\frac{v_2^2 - v_1^2}{v_1^2 v_2^2}$ Experimental	$\mu_w = \pi \frac{v_2^2 - v_1^2}{v_1^2 v_2^2}$ Eqn 12 Calculated	a_1^2 in sec ² /cm ² /10 ¹⁰		α_1 in meters per sec Exptl	ν_w in 10 ⁹ c p s. calculated Eqn. 14	λ_w in 10 ⁹ sec calculated
		Stokes Theor	Pinkerton Exptl	Difference = 2-1			
0° C		17.09	26.9	30.81	14.9	0.4391	2.277
5° C		13.26	44.14	37.70	14.22	0.5593	1.785
10° C		11.34	26.10	24.76	12.53	0.6531	1.464
20° C		8.16	25.30	17.14	12.82	0.9676	1.033
30° C	0.004	6.15	10.10	12.95	12.11	1.253	0.7982
40° C	average	4.82	12.60	9.72	15.53	1.614	0.6082
50° C		3.90	12.00	8.10	15.42	1.986	0.5032

TABLE II

Temperature in °C	" β_n " in $\text{cm}^2/\text{dyne} \cdot 10^{-12}$ (Experimental)	" β_s " in $\text{cm}^2/\text{dyne} \cdot 10^{-12}$	ν_ω in c.p.s. Experimental	ν_0 in c.p.s. Experimental	l_ω in second calculated	Calculated Eqn. 15	τ_ω^2/τ_0^2
0° C	50.78				$2.77 \cdot 10^{-8}$	1.033	
5° C	49.92				1.788 "	1.021	
10° C	47.83				1.464 "	1.112	1.004 at 27°C
20° C	45.78	12.00	$3 \cdot 10^7$	$3 \cdot 10^6$	1.033 "	1.007	1.0036 at 33°C
30° C	44.74				$6.7982 \cdot 10^{-8}$	1.030	
40° C	44.23				0.6082 "	1.006	
50° C	44.08				0.5032 "	1.002	

Dispersion and Absorption of Supersonic Waves in Water 11

by Bauer (1949). Hall had used similar ideas and with a value of 18.10^{-12} cm²/dyne for β_∞ (i.e., β_a) has explained the excess absorption in water. The value of t_w as calculated by him, was of the order of 10^{-12} sec. He also had admitted the variation of β_a with temperature but the effect of this variation was considered to have been counterbalanced by the variation of another term $(1 + e^{4F/RT})$ which he used in the expression for absorption. Hence as regards the value of the relaxational time $t_w = 10^{-9}$ sec. as found by us the assumption that this may correspond to the mean dispersive frequency, ranging over 10^6 c.p.s. and 10^{12} c.p.s. corresponding to the point L in the portion BC in Fig. 1, appears to be in order. The working frequency range used by us lie between B and L and therefore dispersion, although small, should be experimentally observed. Our theoretical and experimental observations are, therefore, completely in order.

Bauer in his paper has reported similar theoretically derived expressions for absorption and dispersion for unassociated liquids, as was reported by us in early papers (Dutt and Ghosh, 1939). These were derived by Bauer from similar considerations as of ours, and based on relaxational heat capacity due to incomplete assimilation of sound energy by molecules and similar thermodynamical relations for liquids were employed.

TABLE III

Liquids	Characteristic frequencies of the molecules in cm ⁻¹	$\nu_0^2 t_w^2$ (theor.) from relaxational heat capacity Eqn. (2)	μ_0 (theor.) $\times 10^3$ Eqn. (12)	$\alpha \times 10^{17}$ Exptl. from Kneser	c velocity in metres per sec. Exptl.	ν_m in c.p.s. calculated from :—	
						Dutt and Ghosh (1939) $\alpha, \nu^2 = \frac{2\mu_0}{1\nu_m}$ Eqn. (14)	Bauer (1949) $\nu_m = \frac{2\mu_0}{c} \cdot \frac{1}{\alpha/\nu^2}$ $c = \text{velocity}$
Toluol	217	1.022	69.11			0.69 10^9	7.5 10^9
	730	1.010	31.42	130	1310	0.31 10^9	
Xylol	733	1.008	25.4	123	1330	0.30 10^9	—
Chloroform	261	1.033	103.7			0.22 10^9	2.2 10^9
	667	1.015	47.1	940	1001	0.10 10^9	
CCl ₄	218	1.027	85.0			0.18 10^9	
	459	1.020	62.8	1000	928	0.13 10^9	3.4 10^9
	759	1.11	34.5			0.08 10^9	
Benzene	401	1.053	166.5	1600	1310	0.15 10^9	1.2 10^9
	802	1.009	28.28			0.03 10^9	
CS ₂	395	1.057	179.1			0.14 10^9	
	676	1.032	100.6	21500	1140	0.08 10^9	0.5 10^9
	796	1.022	69.11			0.05 10^9	
Water	1652	1.000	0	60	1494		
	3420	1.000					
	3580	1.000					

The mean dispersive frequency for these liquids calculated from an expression similar to equation (14) was shown to be of the order of 10^9 c.p.s. almost exactly the same as calculated by us, (*vide* Table III). As pointed out by us, the case of CS_2 , being of special interest, was treated separately and numerical estimates of the individual dispersion frequencies for different vibrational levels which relax at different frequencies have been made for this particular liquid.

The foregoing observations suggest that if the passage of supersonic waves through water produces the same effect in causing change in the structures as is done by introducing ions or increasing the temperature, an experimental study of the X-ray diffraction curve of water with supersonic waves propagating through it may reveal the same results as reported by Morgan and Warren (1938). A direct experimental observation on the actual diminution in volume due to the breaking of water structure under supersonic pressure causing decrease in effective compressibility may also be carried out. Attempts are being made in this direction.

ACKNOWLEDGMENTS

The author's thanks are due to Dr. A. K. Dutt for many valuable discussions on this subject. He also expresses his gratitude to Prof. D. M. Bose, Director, Bose Research Institute, for help received from him in carrying out this work.

BOSE INSTITUTE,
Calcutta

REFERENCES

- Bauer, F., 1949, *Proc. Phys. Soc. A*, **62**, 3.
 Bernal, J. D. and Fowler, R. H., 1934, *J. Chem. Phys.*, **1**, 515.
 Cross, P. C., Burnham, J. and Leighton, P. A., 1937, *J. Amer. Chem. Soc.*, **59**, 1134.
 Dancy, 1940, The properties of water substance,
 Dutt, A. K., 1938, *Trans. Bose Res. Inst.*, **12**, 115.
 Dutt, A. K., 1938, *Phys. Zeits.*, **39**, 186.
 Dutt, A. K., and Ghosh, B. B., 1938, *Trans. Bose Research Inst.*, **13**, 115.
 Dutt, A. K., and Ghosh, B. B., 1941, *Trans. Bose Research Inst.*, **14**, 127.
 Dutt, A. K., and Ghosh, B. B., 1943, *Ind. Jour. Phys.*, **17**, 19.
 Ewell, R. H., and Eyring, H., 1937, *J. Chem. Phys.*, **5**, 726.
 Focke, A. B., and Hartmann, G. K., 1940, *Phys. Rev.*, **57**, 221.
 Ghosh, B. B., 1949, *Ind. Jour. Phys.*, **23**, 77.
 Hall, L., 1948, *Phys. Rev.*, **73**, 775.
 Morgan, J., and Warren, B. F., 1938, *J. Chem. Phys.*, **6**, 666.
 Pinkerton, J. M., 1947, *Nature*, **160**, 128.
 Randall, C. R., 1932, *Burr. Stand. J. Research*, **8**, 79.
 Sorensen, C., 1936, *Ann. d. Phys. Lpz.*, **26**, 121.
 Tammann, G., 1893, *Zeits. Physik. Chemie.*, **11**, 670.

STUDIES OF THE JOSHI-EFFECT IN CHLORINE UNDER OZONIZER EXCITATION—INFLUENCE OF TEMPERATURE

By K. S. VISVANATHAN AND K. KUPPUSWAMY

(Received for publication, May 26, 1959)

ABSTRACT The influence of temperature, varied in the range 8° – 67°C . on the magnitude of the Joshi Effect in Cl_2 taken in the pressure range 55.5–39.1 mm. and excited in a Siemens ozonizer due to potentials of 50 cycles frequency has been studied. The magnitude of both the net as well as the relative effect decreases with increase of temperature, the influence of applied potential is to increase the net effect and decrease the relative effect. This inhibitive influence of temperature is more in evidence at lower than at higher applied potentials. The intercorrespondence between light absorption by Cl_2 which increases, and the Joshi Effect, which decreases with increase of temperature, is in accord with Joshi's view that ΔI is not entirely a consequence of selective light absorption by the excited gas but rather a quantum or frequency effect.

The Joshi Effect having been originally discovered in chlorine (Joshi, 1913, 1915), most of the workers in this field have naturally devoted their attention to a detailed investigation of the production of the effect in this gas and the influence of the various factors which affect the nature and magnitude of the effect. It was only subsequently that other gases, e.g., H_2 , O_2 , Br_2 , etc., and metallic vapours, e.g., Hg , K , Na , etc., were taken up for similar exhaustive study. But a survey of the now considerable literature on the effect in chlorine revealed the absence of any information regarding the influence of temperature on the Joshi-Effect in chlorine, except for the preliminary note of a general nature by Joshi and Deshmukh (1941) and by Deo and Padmanabhaiah (1944). The present investigation was hence undertaken in order to find the dependence of the Joshi-Effect in Cl_2 on temperature.

EXPERIMENTAL

The general nature of the apparatus was the same as used in some of the previous investigations. The discharge vessel was a Siemens ozonizer which was excited by single phase alternating potentials of 50 cycles frequency, obtained from a rotary converter worked off the 220 volt D.C. mains and stepped up by means of a transformer of ratio 227:1. The source of illumination was a 200-volt 200-watt incandescent bulb enclosed within a box provided with a movable shutter.

Chlorine was prepared electrolytically from strong HCl , using graphite electrodes. A current of 0.25 ampere was employed for electrolysis. The current was first passed in one direction and then in the other alternately for some time in order that the acid might be saturated with chlorine and any organic impurities in the acid destroyed. After this precaution was

taken, it was found that hydrogen and chlorine were evolved in equivalent quantities. The gas, Cl_2 was then passed through a water trap in order to remove vapours of HCl and allowed to stand over fused CaCl_2 and P_2O_5 for the removal of moisture. The gas was finally purified by freezing it out in a liquid air trap and pumping off any uncondensed impurities by means of a Topley pump. It was then stored in a reservoir kept in communication with the drying tubes in order that the gas might be thoroughly dried.

Since chlorine attacks mercury easily, the use of a mercury manometer was precluded. Hence a Bourdon gauge of glass-spoon type, used by one of the authors (K.S.V.) in connection with his work on NO_2 and described earlier (Visvanathan, 1948), was employed.

The influence of temperature on the magnitude of the Joshi-effect in chlorine was studied by taking the gas in the pressure range 55.5–390 mm and observing the variation in the effect at three different temperatures, viz., 8° , 30° and 67°C , and for some pressures, also at 25° , 50° and 60°C the applied potential being kept constant. The temperature variation of the Joshi-effect was determined at different applied potentials, viz., 6.68, 8.01, 9.35, 9.88, 10.68, 12.02 and 13.35 kV (i.m.s.), the frequency of the A.C. supply being the same in all cases, viz., 50 cycles per second.

The discharge currents, i_0 and i_1 (i.e., when the ozonizer was in dark and under irradiation respectively), were measured by means of an oxide rectifier type micro-ammeter. The net Joshi-effect, Δi (i.e., $i_1 - i_0$) as well as the relative effect, $\% \Delta i$ (i.e., $100 \times \Delta i / i_0$) has been calculated. Results indicated in Tables I–VI are selected as being typical of a large mass of data obtained for a number of initial pressures of the gas and applied potentials and temperatures. The initial pressures of chlorine thus selected are 55.55, 137, 224, 238, 381 and 390 mm.

INFLUENCE OF TEMPERATURE ON THE JOSHI-EFFECT IN Cl_2 UNDER OZONIZER EXCITATION

TABLE I

Pressure of Cl_2 : 55.5 mm

Applied Potential →	6.68 kV				8.01 kV				9.35 kV			
Temperature	i_0	i_1	$-\Delta i$	$-\% \Delta i$	i_0	i_1	$-\Delta i$	$-\% \Delta i$	i_0	i_1	$-\Delta i$	$-\% \Delta i$
8°	34.3	37.0	2.7	50.4	41.8	21.8	20.0	47.8	50.0	28.0	22.0	44.0
30°	35.8	24.0	11.8	33.0	44.0	31.8	12.2	27.7	55.0	37.0	18.0	32.7
67°	40.0	5.0	35.0	17.5	50.5	41.8	8.7	17.2	63.0	51.5	11.5	18.3

TABLE II

Pressure of Cl_2 : 137 mm

8°	34.8	21.8	13.0	37.3	49.0	34.0	15.0	30.0	62.8	43.8	19.0	30.3
30°	28.0	22.0	6.0	21.4	45.8	35.0	10.8	23.6	59.0	45.0	14.0	23.7
67°	42.8	32.0	10.8	25.2	50.0	13.0	13.0	23.2	69.0	55.0	14.0	20.3

TABLE III

Pressure of Cl_2 : 224 mm.

8°	21.5	3.3	18.2	84.7	32.3	6.8	25.5	78.9	43.4	10.3	34.5	75.1
35°	23.8	7.8	16.0	67.2	36.0	13.3	22.7	63.1	48.3	18.8	29.5	61.1
60°	24.0	8.8	15.2	53.3	35.3	14.0	21.0	61.0	50.0	22.0	28.0	50.0
75°	25.8	10.8	15.0	58	38.0	18.0	20.0	54.6	54.0	26.3	17.7	51.3

TABLE IV

Pressure of Cl_2 : 238 mm

	9.88 kV				10.68 kV				12.02 kV			
8°	45.5	30.3	15.2	33.1	54.8	36.0	18.8	34.3	69.0	48.0	21.0	30.4
30°	30.0	29.3	10.7	20.8	59.0	39.5	19.5	33.1	68.0	48.8	19.2	28.2
67°	53.8	37.5	16.3	30.3	58.0	13.8	14.2	21.5	73.1	54.8	18.5	25.2

TABLE V

Pressure of Cl_2 : 381 mm.

	9.88 kV				11.04 kV				13.35 kV			
8°	10.0	0	10.0	100	26.0	6.3	19.7	75.8	38.3	11.3	27.0	70.5
30°	11.8	1	10.8	91.5	31.0	9.3	20.7	69.9	43.0	15.8	26.2	60.9
67°	15.1	4.3	11.0	71.9	33.8	13.8	20.4	59.2	48.8	27.8	26.0	53.3

TABLE VI

Pressure of Cl_2 : 390 mm.

8°	16.0	0	16.0	100	34.0	2.3	31.7	93.2	51.3	8.5	42.8	83.4
30°	15	0	15.3	100	35.0	3.3	31.7	90.6	48.0	7.8	40.2	83.7
50°	20.8	3.3	17.5	81.1	42.8	18.0	24.8	57.9	58.3	19.3	39.0	60.9
67°	20.3	3.3	17.0	83.7	43.8	10.0	27.8	63.5	60.3	15.0	35.3	58.5

DISCUSSION

The results for the net and relative Joshi-effect in Cl_2 show the characteristic and distinctive behaviour of the gas in regard to the facility with which Joshi-effect of large magnitude is produced. Thus the occurrence of 100% Joshi-effect at the pressures 381 and 390 mm of Cl_2 bears out the above observation. The range of pressure, viz., 55.5–390 mm over which chlorine continues to give the Joshi-effect of such large magnitude is remarkable, when it is seen that most of the other systems studied, e.g., H_2 , N_2 , air, etc., show the Joshi-effect only for a limited range of pressure, which abruptly falls off to almost zero on crossing either of the limiting pressures. For example, in H_2 subjected to ozonizer excitation at 50 cycles frequency, the Joshi-effect which is maximum at 70 mm, falls off sharply in value and vanishes outside the range 30–200 mm. In conformity with earlier findings for Cl_2 and other gases, the net effect $-\Delta I$ increases (numerically) while the relative effect, $-\% \Delta I$ decreases (numerically) with increase of applied potential. Thus, e.g., at 55.5 mm (cf. Table I), the net Joshi-effect at 6.68, 8.01 and 9.35 kV at 8°C is 17.3, 20.0 and 22.0 respectively, while the relative effect is 50.4, 47.8 and 44.0 respectively. Similar results are obtained at the other temperatures as well. But a close examination of the results shows that, in general, the inhibitive influence of the applied potential on the production of the Joshi-effect is greater at lower than at higher temperatures.

It is also seen from the results that temperature exerts an appreciable inhibitive influence on the system in respect of its ability to show the effect. It is significant that though v_p increases with temperature, v_i increases much faster than v_p with the result that both $-\Delta I$ and $-\% \Delta I$ show a (numerical) diminution as the temperature is increased. Thus, e.g., at 6.68 kV, the values of $-\Delta I$ at 8° , 30° and 67° are 17.3, 11.8 and 7.0 respectively, and those of $-\% \Delta I$, 50.4, 33.0 and 17.5 respectively. It may also be generalised from the data that the influence of temperature in lowering the magnitude of the Joshi-effect is less at higher than at lower potentials.

The above observations would appear to emerge from a consideration of the general theory proposed by Joshi for the effect (Joshi, 1946, 1947; Visvanathan, 1949).

Joshi assumes that an absorption-like boundary layer s' (Joshi, 1945 b), ionic plus molecular, is formed on the excited walls of the ozonizer, that this layer is characterised by a low work function so as to allow of photo-electric emission even under extreme red which is insufficient to cause a direct photo-ionisation of the excited gas; that these photo-electrons are captured by the atoms and molecules of the gas, on account of their electron affinity enhanced by electrical excitation, to form negative ions which, on account of their low mobility, bring about a diminution of the discharge current as a space charge effect.

It is well known that the adsorption process is exothermic and hence, according to the Le Chatelier-Braun principle of mobile equilibrium, the amount adsorbed at equilibrium should decrease with increase in temperature. This has actually been found to be the case for numerous adsorption reactions. Now, since Joshi's theory also contemplates an 'adsorption-like boundary layer (s)' (Joshi, 1945 *b*) formed by the ions and neutral molecules and atoms of the gas on the walls of the ozonizer as the chief seat of the phenomenon of the Joshi-Effect, it is to be anticipated that the adsorbed layer would be deformed or destroyed by rise of temperature, resulting in a decrease in the number of photoelectrons with the consequent reduced fall in the discharge current.

Evidence has been adduced by one of the authors (K. S. V.) in his work on the Joshi-Effect in H_2 that selective absorption, by the gas, of the incident light cannot be the cause of the Joshi-Effect. Earlier, Joshi (1945 *a*) had shown that the Joshi-Effect in Cl_2 cannot be the consequence of selective absorption of light by chlorine. He observed that while chlorine absorbs selectively chiefly in the region 6400 \AA to 2500 \AA with a pronounced maximum at 3340 \AA , the production of the effect of as much as 15% occurred in the yellow region of the spectrum (*e.g.*, radiation from a sodium vapour lamp) where absorption by chlorine is minimum and only 3.5% in the relatively more absorbed and intense red band, *viz.*, 6100 to 7100 \AA . Now the following considerations would appear to furnish additional evidence to establish the absence of any relation between selective absorption of the incident light by a medium and the production of the Joshi-Effect in it.

That photochemical reactions, in general, possess temperature coefficients of small magnitude, ranging between 1.04 to 1.4 is well known. It was thought that this temperature coefficient might be due to the increased light absorption by the reacting system at the higher temperature. This led to the investigation of the influence of temperature on the absorption of light by various systems. Thus Ribaud (1919) studied the absorption of light by bromine at various temperatures. Dobbie and Fox (1921) observed in the case of chlorine an extension of absorption towards longer wavelengths at higher temperatures. Later Kuhn (1926) studied the influence of temperature on absorption in the region of the band absorption spectrum around 5000 \AA . It is seen from his data that the temperature coefficient of light absorption in this spectral region is 1.12 at room temperature.

Thus if selective absorption of the incident light were to play any significant part in the production of the Joshi-Effect, an enhancement of the effect should be expected at higher temperatures on account of increased light absorption. The observed decrease in the magnitude of the effect with increase of temperature, therefore, points to the conclusion that the effect is independent of any selective absorption.

There are strong reasons for not identifying the 'photoelectric layer' responsible for the Joshi-Effect with that due to mere physical or chemical

adsorption. The fact that gases like NH_3 and SO_2 which show large physical adsorption do not show the Joshi-Effect as readily and as markedly as other gases, e.g., H_2 , air etc. which show poor physical adsorption, discounts the possibility of any physically adsorbed layer as the seat of the phenomenon. Similarly the anti correspondence between temperature and Joshi-Effect rules out chemisorption as the sole cause of the phenomenon, since chemisorption is favoured by rise of temperature. The fact that electrical excitation for various periods, i.e., ageing, is necessary before the system develops the Joshi-Effect and that the magnitude and even the nature, i.e., sign of the Effect depends upon any pre-treatment given to the walls of the discharge tube, such as coating the walls with various substances, points to a "variable adsorption-like layer" (Joshi, 1945). Further electrical excitation will give rise to particles of various life periods and activity and in the absence of light, these particles deposited on the walls of the containing vessel, due to their surface activity may give rise to an "excited layer" (Joshi, 1946a).

ACKNOWLEDGMENTS

In conclusion, the authors express their grateful thanks to Prof. S S Joshi for the suggestion of the problem and his kind interest and helpful discussions during this work.

PHYSICAL CHEMICAL LABORATORIES,
BENARAS HINDU UNIVERSITY.

REFERENCES

- Deo and Padmanabhan, 1944, *Proc. Ind. Sci. Cong. Chem. Sec.*, Abst. 30
 Dobbie and Fox, 1921, *Proc. Roy. Soc.*, A 99, 450
 Joshi and Deshmukh, 1941, *Nature*, 147, 800
 Joshi, 1943, *B. H. U. Journal*, 3, 99
 --, 1945, *Proc. Ind. Acad. Sci.*, 22, 389
 --, 1945a, *Curr. Sci.*, 14, 317.
 --, 1945b, *ibid.*, 14, 175
 --, 1946, *Proc. Ind. Sci. Cong. Chem. Sec.*, Abstract 20
 --, 1946a, *Curr. Sci.*, 15, 28.
 --, 1947, *Curr. Sci.*, 16, 19.
 Kuhn, 1926, *Z. Physik*, 39, 77.
 Ribaud, 1919, *Ann. Physique*, 12, 107.
 Visvanathan, 1948, *Proc. Ind. Acad. Sci.*, 27, 300.
 --, 1949, *J. I. C. S.*, 26, 205.

RELATIVISTIC THOMAS-FERMI ATOM

By R. P. SINGH

(Received for publication, Aug 18, 1949)

ABSTRACT A relativistic generalization of the well known Thomas-Fermi equation for the density of electronic charge in an atom, as a function of distance, is worked out and its importance in the study of the internal conditions prevailing in a white-dwarf star has been pointed out

INTRODUCTION

The well-known statistical method of Thomas (1927) and Fermi (1928) for the determination of the density of electronic charge in an atom as a function of distance is based on the assumption that the electrons in an atom constitute a non-relativistic degenerate gas in the Fermi-Dirac sense. The assumption of a non-relativistic degenerate gas is quite justified when one is dealing with an atom in free state or in combined state as in metals, but it would fail when one considers highly compressed atoms as they are in white dwarfs. On account of the astrophysical importance we consider in this note a relativistic formulation of the well-known Thomas-Fermi equation

The electron density of a relativistic Fermi-Dirac gas in absence of any field in completely degenerate case is given by

$$n = \frac{8\pi}{3(ch)^3} \left(\xi_0^2 + mc^2 \xi_0 \right)^{\frac{3}{2}}, \quad \dots (1)$$

where m is the rest mass of the electron and ξ_0 is the energy corresponding to the top of the Fermi level. Now if we consider the same gas present in a field of potential $V(x, y, z)$ the equation (1) will be modified to the form

$$n(x, y, z) = \frac{8\pi}{3(ch)^3} \left[c^2 \left(\frac{\xi_0 + V}{c} \right)^2 + 2mc^2 c \left(\frac{\xi_0 + V}{c} \right) \right]^{\frac{3}{2}} \quad \dots (2)$$

Putting

$$\frac{\xi_0 + V}{c} = U$$

we get the electron density as

$$\begin{aligned} n(x, y, z) &= \frac{8\pi}{3(ch)^3} \left[c^2 U^2 + 2mc^2 c U \right]^{\frac{3}{2}} \\ &= \frac{8\pi c^3 U^3}{3(ch)^3} \left[1 + \frac{2mc^2}{cU} \right]^{\frac{3}{2}} \quad \dots (3) \end{aligned}$$

and the corresponding charge density $\rho = -ne$ is

$$\rho = -\frac{8\pi e^4 U^3}{3(ch)^3} \left[1 + \frac{2mc^2}{cU} \right]^{\frac{3}{2}} \quad \dots (4)$$

If we assume a static distribution of charge the Poisson equation can be written in the form

$$\begin{aligned}\nabla^2 U &= -4\pi\rho \\ &= \frac{32\pi^2 e^4 U^3}{3(ch)^3} \left[1 + \frac{2mc^2}{eU} \right]^{\frac{3}{2}} \quad \dots (5)\end{aligned}$$

Further if we take the potential function U as spherically symmetrical so that it is a function of r only, we have,

$$\begin{aligned}\nabla^2 U &= \frac{d^2 U}{dr^2} + \frac{2}{r} \frac{dU}{dr} \\ &= \frac{32\pi^2 e^4 U^3}{3(ch)^3} \left[1 + \frac{2mc^2}{eU} \right]^{\frac{3}{2}} \quad \dots (6)\end{aligned}$$

The solution of the above equation must satisfy the following boundary conditions.

$$\lim_{r \rightarrow 0} U \rightarrow Zc \text{ and } \int ndr = \infty,$$

Z being the atomic number and the integration is to be extended over all space.

Equation (6) can be further simplified by putting,

$$U = \frac{Zc}{r} \phi \quad \dots (7)$$

where ϕ satisfies the boundary conditions,

$$\phi \rightarrow r \text{ as } r \rightarrow 0 \text{ and } \phi \rightarrow 0 \text{ as } r \rightarrow \infty.$$

Using relation (7) we get

$$\frac{d^2 U}{dr^2} + \frac{2}{r} \frac{dU}{dr} = \frac{Zc}{r} \frac{d^2 \phi}{dr^2}.$$

and so, (6) becomes

$$\frac{Zc}{r} \frac{d^2 \phi}{dr^2} = \frac{32\pi^2 e^4 \phi^3}{3(ch)^3} \times \left(\frac{Zc}{r} \right)^{\frac{3}{2}} \left[1 + \frac{2mc^2}{Zc^2 \phi} \right]^{\frac{3}{2}}$$

$$\text{or} \quad \frac{d^2 \phi}{dr^2} = \frac{32\pi^2 e^6 Z^2 \phi^3}{3(ch)^3 r^2} \left[1 + \frac{2mc^2}{Zc^2 \phi} \right]^{\frac{3}{2}}.$$

We now change the variable from r to x using the relation $r = ax$, where a is the radius of the first Bohr orbit $\left(a = \frac{h^2}{4\pi^2 m e^2} \right)$, and get (8) in the form

$$\begin{aligned}\frac{d^2 \phi}{dx^2} &= \frac{32\pi^2 e^6 Z^2 \phi^3}{3(ch)^3 a^2} \left[1 + \frac{2mc^2}{Zc^2 \phi} \right]^{\frac{3}{2}} \\ &= \alpha \frac{\phi^3}{a^2} \left[1 + \beta \frac{x}{\phi} \right]^{\frac{3}{2}} \quad \dots (9)\end{aligned}$$

where

$$\alpha = \frac{32\pi^2 e^6 Z^2}{3(ch)^3} \text{ and } \beta = \frac{2mc^2 a}{Zc^2}$$

We have so far considered a completely degenerate case. In what follows we take the effect of temperature into account.*

In this case the electron density in absence of the field is

$$n = \frac{8\pi m^3 c^3}{3h^3} \gamma^3 \left[1 + \left(\frac{\pi k T}{mc^2} \right)^2 \frac{\gamma^2}{2\gamma^4} + 1 \right],$$

where

$$\gamma = \frac{(\xi_0^2 + 2mc^2\xi_0)^{1/2}}{mc^2},$$

i.e.,

$$n = \frac{8\pi}{3(ch)^3} \times (\xi_0^2 + 2mc^2\xi_0)^{3/2} \times \left[1 + \frac{(\pi k T)^2}{2} \times \frac{\{2(\xi_0^2 + 2mc^2\xi_0) + (mc^2)^2\}}{(\xi_0^2 + 2mc^2\xi_0)^2} \right] \quad (10)$$

And in the presence of field we have

$$\begin{aligned} n(r, \gamma, z) &= \frac{8\pi}{3(ch)^3} \times \left[r^2 \left(\frac{\xi_0}{r} + 1 \right)^2 + 2mc^2 e \left(\frac{\xi_0}{e} + 1 \right) \right]^{3/2} \\ &\times \left[1 + \frac{(\pi k T)^2}{2} \times \frac{\left\{ 2 \left\{ e^2 \left(\frac{\xi_0}{e} + 1 \right)^2 + 2mc^2 e \left(\frac{\xi_0}{e} + 1 \right) \right\} + (mc^2)^2 \right\}}{\left\{ e^2 \left(\frac{\xi_0}{e} + 1 \right)^2 + 2mc^2 e \left(\frac{\xi_0}{e} + 1 \right) \right\}^2} \right] \\ &= \frac{8\pi}{3(ch)^3} \times (e^2 l^2 + 2mc^2 e l)^{3/2} \\ &\times \left[1 + \frac{(\pi k T)^2}{2} \times \frac{2\{e^2 l^2 + 2mc^2 e l\} + (mc^2)^2 l}{(e^2 l^2 + 2mc^2 e l)^2} \right] \quad (11) \end{aligned}$$

The equation is as before,

$$\begin{aligned} \frac{d^2 l}{dr^2} + \frac{2}{r} \frac{dl}{dr} &= \frac{32\pi^2 e^4 l^3}{3(ch)^3} \times \left[1 + \frac{2mc^2}{e l} \right]^{3/2} \\ &\times \left[1 + \frac{(\pi k T)^2}{2} \times \frac{(e^2 l^2 + 2mc^2 e l) + \frac{(mc^2)^2}{2}}{(e^2 l^2 + 2mc^2 e l)^2} \right] \quad (12) \end{aligned}$$

Changing (12) from l to ϕ as before we get,

$$\begin{aligned} \frac{d^2 \phi}{dr^2} &= \frac{32\pi^2 e^6 Z^2 \phi^3}{3(ch)^3 r^2} \left[1 + \frac{2mc^2 r}{Ze^2 \phi} \right]^{3/2} \\ &\times \left[1 + (\pi k T)^2 \times \frac{\frac{e^4 Z^2 \phi^2}{r^2} \left(1 + \frac{2mc^2 r}{Ze^2 \phi} \right) + \frac{(mc^2)^2}{2}}{\frac{e^6 Z^4 \phi^4}{r^4} \left(1 + \frac{2mc^2 r}{Ze^2 \phi} \right)^2} \right] \quad (13) \end{aligned}$$

* In the non-relativistic case the temperature effect has been considered by Bethe and Marshak, (1940).

and if we put $r = ax$ we have,

$$\begin{aligned} \frac{d^2\phi}{dx^2} &= \frac{32\pi^2 e^6 Z^2 \phi^3}{3(\epsilon h)^6 x^2} \times \left[1 + \frac{2mc^2 ax}{Z\epsilon^2 \phi} \right]^{\frac{3}{2}} \\ &\times \left[1 + (\pi k T)^2 \times \frac{\frac{e^4 Z^2}{a^2} \cdot \frac{\phi^2}{x^2} \left(1 + \frac{2mc^2 ax}{Z\epsilon^2 \phi} \right) + \frac{(mc^2)^2}{2}}{\frac{e^8 Z^4}{a^4} \cdot \frac{\phi^5}{x^4} \left(1 + \frac{2mc^2 ax}{Z\epsilon^2 \phi} \right)^2} \right] \\ &= \alpha \frac{\phi^3}{x^2} \left(1 + \beta \frac{x}{\phi} \right)^{\frac{3}{2}} \\ &\times \left[1 + (\pi k T)^2 \times \frac{\frac{(2mc^2)^2}{\beta^2} \cdot \frac{\phi^2}{x^2} \left(1 + \beta \frac{x}{\phi} \right) + \frac{(mc^2)^2}{2}}{\frac{(2mc^2)^4}{\beta^4} \cdot \frac{\phi^4}{x^4} \left(1 + \beta \frac{x}{\phi} \right)^2} \right] \end{aligned}$$

or

$$\begin{aligned} \frac{d^2\phi}{dx^2} &= \alpha \frac{\phi^3}{x^2} \left(1 + \beta \frac{x}{\phi} \right)^{\frac{3}{2}} \\ &\times \left[1 + (\pi k T)^2 \times \frac{\frac{\phi^2}{x^2} \left(1 + \beta \frac{x}{\phi} \right) + \frac{\beta^2}{8}}{\frac{(2mc^2)^2}{\beta^2} \left(1 + \beta \frac{x}{\phi} \right)^2} \right] \quad (14) \end{aligned}$$

where α and β have their usual meaning as mentioned before

A numerical integration of the above equation is very desirable since it will enable one to deduce accurately expressions for such astrophysically significant quantities as free electron density and gas pressure, the knowledge of which will help one in exact investigations of the internal constitution of white dwarfs.*

ACKNOWLEDGMENT

My thanks are due to Dr. K. S. Singwī for his kind interest in the progress of this work.

DEPARTMENT OF PHYSICS,
ALLAHABAD UNIVERSITY.

* A very accurate knowledge of density and temperature prevailing at the centre of white dwarf is essential before any light can be thrown on the nature of energy production process in such stars.

REFERENCES

- Bethe and Marshak, 1940, *Ast. Phys. Jour.* **91**, 239.
Thomas, 1927, *Proc. Camb. Phil. Soc.*, **23** 542.
Fermi, 1928, *Z. Physik*, **49**, 650.

DIELECTRIC CONSTANTS OF COMMERCIAL CASHEW SHELL OILS

BY S. KRISHNAMURTHY AND B. R. V. IVENGAR

(Received for publication, Nov. 12, 1949)

ABSTRACT For the first time the dielectric constants of commercial cashew shell oil and its constituents have been studied. The investigations carried out on seven commercial samples reveal that the behaviour with temperature of the dielectric constants of the three main constituents of the oil, the sodium bicarbonate insolubles, the sodium bicarbonate solubles and the neutrals is widely different from one another and typical of each.

The differences in the dielectric constant-temperature curves of the oils and the bicarbonate insolubles are attributed to the viscosity effects due to the presence of self-polymerised products depending on the pre-treatment given to the oil during extraction, and to the considerable variation in the proportion of anacardol (decarboxylated anacardic acid) in the oils and their bicarbonate insolubles.

INTRODUCTION

It is an established fact that the dielectric constant of a substance is not a mere insignificant physical property but has a very great bearing on molecular structure. A study of the dielectric properties of the oils is interesting and informative from more than one aspect. There are a number of naturally occurring oils (triglycerides) whose chemical structures are sufficiently well established. In such cases a study of dielectric constant and dipole moments would enable one in probing into the molecular structure of the constituents of the oil. On the other hand the data on dielectric constants might be used in identifying the oil or establishing its purity. It is also interesting to follow up by means of dielectric constant studies some important physical and chemical changes which occur, for example, when the oil is gradually oxidised, heat bodied, or reacted to form polymers of various degrees etc. An exhaustive study of the dielectric constants as a function of temperature and frequency enables one to assess the insulating and dielectric properties of the varnishes or enamels of which the oil might form an important constituent.

All the oils that have been studied so far belong to the general category of triglycerides. A feature of the present paper is that for the first time the dielectric constant of an oil which is not a triglyceride, but essentially a mixture of phenolic bodies, have been determined. Another special feature about the present investigation is that a careful study has been made to find

out as to how the dielectric properties of an oil vary with the source, method of extraction and the extent of the initial processing. In the present work, the constituents of the oil have been separated and their dielectric properties have been studied.

Stoops (1931) made the first significant contribution to the study of dielectric constants of oils. He determined the dielectric constants and densities of tung, linseed and castor oils over a wide range of temperature, (-70 to 100°C) and in dilute solutions of benzene and concluded that "probably all the animal and vegetable oils and fats of this class have moments between 2.7 to 3.7."

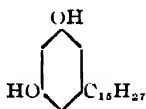
Paranjpe and Deshpande (1935) and Bhattacharya (1936) have measured the dielectric constants of various vegetable oils. Electric moments in dilute benzene solutions have been evaluated and interpreted on the basis of molecular structure.

Caldwell and Payne (1941) undertook the investigation of the dielectric properties of a number of vegetable oils with the purpose of (a) determining as to what extent the dielectric constant, molar polarisation or effective dipole moment could be employed as means of identifying various drying oils and mixtures thereof and (b) investigating the effect of degree of heat bodying on the dielectric constant, molar polarisation and effective dipole moments of these oils.

Hazlehurst (1943) described the measurement of dielectric constant of raw, polymerised and oxydised linseed oils and showed how the absorption of oxygen and subsequent oxidation of the oil could be followed by the measurement of dielectric constants at different frequencies. It has been claimed that as a result of this study of linseed oil, products which compare more than favourably with dehydrated castor oil have been prepared.

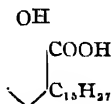
EXPERIMENTAL

The review of the literature has revealed that most of the work on the dielectric constants of oils has been made only on the triglycerides like castor oil, linseed oil, oiticica oil, perilla oil, tung oil, etc. Unlike other oils which are glycerides, cashew shell oil is completely phenolic in nature. It has been shown that the liquid contains two phenols. Approximately 10 per cent of the oil is present as cardol which is a substituted resorcinol of the following formula.

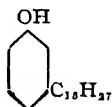


The substituent group is a linear chain, containing two double bonds, the position of which has not yet been determined.

The major constituent of the cashew shell oil is a salicylic acid dervative to which has been given the name anacardic acid. It has the following constitution:



The same substituent group which has been found in cardol is present in anacardic acid. Anacardic acid decarboxylates smoothly on thermal treatment to give a monohydric phenol known as anacardol of the formula :



The dielectric study of such a phenolic oil has not been undertaken so far. Cashew shell oil is very much used in insulating varnish and it makes an interesting study to find out the dielectric properties of the oil as well as its chief constituents. Commercial oils from various sources extracted under varying conditions (heat treatment, solvent extraction, etc.) have been chosen for the study to find out whether all the oils are similar in behaviour so far as the dielectric properties are concerned. Such a study becomes interesting in view of the fact that cashew shell oil is known to vary in composition depending on the source and method of extraction (*c f.* Table I).

Materials.—The following seven typical samples with the respective compositions mentioned have been studied. Of these, two samples were solvent extracted from commercial shells, while the rest were typical commercial oils.

A novel and thorough method of investigating the types of constituents present in the various commercial specimens has been adopted in this paper. The method consists in extracting each of the commercial oils with dilute alkali so as to dissolve the phenolic and acidic portion and enabling the neutral body to be extracted with a suitable solvent. The alkali solution is next saturated with carbon dioxide to liberate the purely phenolic part of the oil from carboxylic portion, extracting the former again with a suitable solvent. Each commercial oil is separated into a neutral, acidic (sodium bicarbonate soluble), and phenolic (sodium bicarbonate insoluble) portion; and their dielectric properties have been studied. Table I gives an analysis

of the various commercial samples of cashew shell oil obtained from different producing centres.

TABLE I

Analysis of various samples of commercial oil.

Sample	Neutrals %	Bicarb. soluble, %	Bicarb insolubles. %
Benzene extracted roasted shell (<i>Mangalore</i>)	2.0	5.0	93.0
Cardol corporation (<i>Mangalore</i>)	15.0	5.0	80.0
Pierce Leslie & Co. (<i>Calicut</i>)	1.0	3.0	96.0
Stanes & Co. (<i>Coimbatore</i>)	1.5	3.4	95.0
Fernandes Bros. (<i>Mangalore</i>)	2.0	6.0	92.0
Alcohol extracted roasted shell (<i>Mangalore</i>)	2.0	6.0	92.0
Naik & Co. (<i>Kasseigand</i>)	3.0	2.5	94.5

All the commercial samples of the oil have been obtained by drastic thermal treatment resulting in some polymerisation. The materials used represent the standard grade of industry available in India. No additional purification, except filtration and drying under vacuum for the removal of moisture, was made because it was desired to relate the results to actual industrial practice.

Apparatus.—The mostly widely used method of measuring the capacity of a condenser, first empty and then filled with the material, was employed to obtain the dielectric constants.

A very simple circuit similar to the one used by Nagmani and Jatkar (1942) was used for the measurement of capacities.

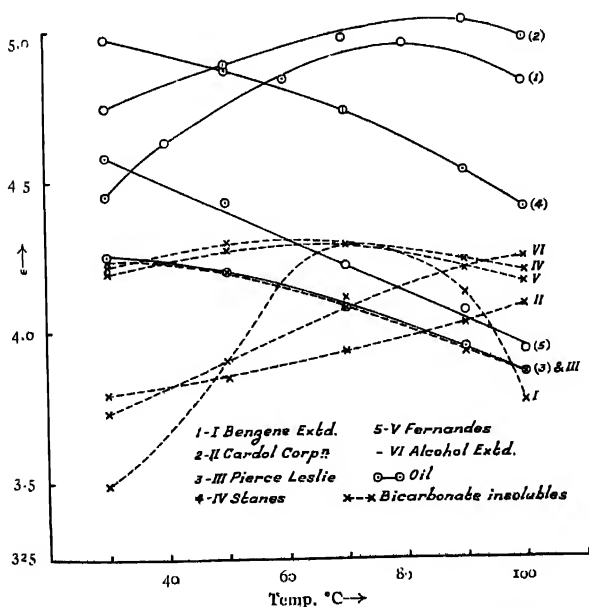
RESULTS

Table II gives the dielectric constants of various samples of cashew shell oil.

TABLE II

No.	Sample of cashew shell oil	ϵ	
		30°C	100°C
1.	Pierce Leslie & Co (Calicut)	4.26	3.87
2.	Benzene extracted (Laboratory)	4.45	4.84
3.	Fernandes Bros (Mangalore)	4.58	3.95
4.	Cardol Corpn. (Mangalore)	4.73	4.99
5.	Naik & Co (Kassergaud)	4.77	—
6.	Stanec & Co. (Coimbatore)	4.97	4.12
7.	Alcohol Extracted (Laboratory)	6.00	—

The dielectric constants of the oils have been arranged in order of decreasing viscosity.



Dielectric constants of cashew shell oils and their bicarbonate insolubles

FIG. 1

In Table III comparative dielectric constants of vegetable oils obtained by various experimenters are enlisted.

TABLE III

No.	Name of the oil	Temp in °C	ϵ	Frequencies
1	Cashew shell oil (author)	30	4.60 'average)	800 k c
2.	Castor oil (2)	34	4.55	1 k c.
	Castor oil (1)	30	4.54	300-1000 k c
	Castor oil (5)	26	4.45	10,000 k.c.
	Castor oil (3)	25	3.96	45-60 M.c.
3	Cocoanut oil (2)	34	3.41	1 k c.
	Cocoanut oil (5)	26	3.25	10,000 k.c.
4.	Dehydrated Castor oil (3)	25	3.03	45-60 M.c.
5.	Linseed oil (3)	25	3.20	60 c.
	Linseed oil (2)	34	3.30	1 k c.
	Linseed oil (4)	30	3.23	200 k.c
	Linseed oil (1)	30	3.35	300-1000 k c.
	Linseed oil (3)	25	3.17	45-60 M.c
6	Olive oil (2)	34	3.15	1 k.c.
	Olive oil (5)	26	3.25	10 000 k c.
7.	Oiticica oil (3)	25	6.14	60 c.
	Oiticica oil (3)	25	4.22	45-60 M.c
8.	Poppy seed oil (2)	34	3.55	1 k c.
9.	Perilla oil (3)	25	3.54	60 c.
	Perilla oil (3)	25	3.23	45-60 M.c.
10	Rapeseed oil (2)	34	3.08	1 k.c.
11.	Sesame oil (2)	34	3.16	1 k.c.
	Sesame oil (5)	26	3.37	20,000 k.c.
12.	Tung oil (1)	30	3.33	300-1000 k.c
	Tung oil (3)	25	3.34	60 c.
	Tung oil (3)	25	3.13	45-60 M.c.

(1) Stoops (1931) (2) Bhattacharyya (1936) (3) Caldwell and Payne (1941)
 (4) Hazlehurst (1943) (5) Paranjpe and Deshpande (1935)

DISCUSSION

Table II shows that the dielectric constants of different commercial samples of cashew shell oil vary from one another (4.25 to 6 at 30°C and 3.87 to 4.99 at 100°C). The value for the alcohol extracted oil is unusually high. This may be due to (a) some resinous constituent dissolved in the oil (b) due to traces of some alcohol retained in the oil in spite of vacuum distillation after dissolving the extracted oil in benzene. In view of its high dielectric constant the presence of even a small quantity of ethyl alcohol ($\epsilon = 25$ at 25°C) could easily be responsible for the observed high value of the dielectric constant of the alcohol extracted oil. In many cases the dielectric constants are still in the increasing trend at 30°C. Hence the dielectric constants at 100°C have been tabulated in order to eliminate the dispersion effect. It is seen from Fig. 1 that at 100°C the dielectric constants are in the falling region. The dielectric constant at room temperature is found to increase with decrease in the viscosity of the sample.

The available data on the dielectric constants of all the vegetable oils studied so far have been tabulated in Table III. It is interesting to see that all the other oils, except castor and oiticica oils, have a decidedly lower dielectric constant than cashew shell oil at room temperature and near about the frequencies used in the present investigation. Castor oil and oiticica oil show anomalous dispersion. The dispersion of cashew shell oil has been studied by varying the temperature but maintaining a fixed frequency for measurement (c.f. Fig. 1). It may be mentioned here that the dielectric dispersion can be studied by two alternative methods: (1) By varying the frequency but maintaining a constant temperature, (2) By varying the temperature at a fixed frequency. The latter method has been employed in the present study. It is well known from the behaviour of the molecule in an electrical field that the dielectric constant-temperature curve should attain a maximum after an initial increase with temperature and finally should follow a gradual and continuous fall.

At very low temperatures there is very little orientation of the molecules due to increased viscosity which results in a low dielectric constant. With increase in temperature, polarisation increases owing to enhanced orientation of molecules. This is responsible for the gradual initial rise of dielectric constant with temperature. With further rise in temperature forces due to thermal agitation become predominant and consequently the number of oriented molecules diminish resulting in a lower dielectric constant. The results of our studies on the temperature coefficient of the dielectric constants of the various commercial cashew shell oils and their constituents fully conform with the above picture. These curves (Fig. 1) are similar in nature to those obtained by Bhattacharya (1944) for lac and Mead and Fuoss (1941) and Dakin (1943) for vinyl chloride and vinyl acetate and are typical of the behaviour of viscous liquids in an electrical field. The maximum

dispersion is shown by the alcohol extracted sample whose dielectric constant varies from 6.00 at 30°C to 7.1 at 80°C.

Cardol and benzene extracted samples also show dispersion but on a smaller magnitude. From the curves (1,2) of the above oils it is obvious that the dielectric constant is very near the static value at 100°C at which point the dielectric constant—temperature curve has already started falling with increase in temperature. The other samples (3, 4 and 5) do not show any dispersion in the temperature region studied.

The dielectric properties of the constituents of cashew shell oil separated according to the new scheme have been studied and the results are plotted in Fig. 2. In the first instance the individual constituents obtained from different samples have been mixed together and their dielectric properties investigated.

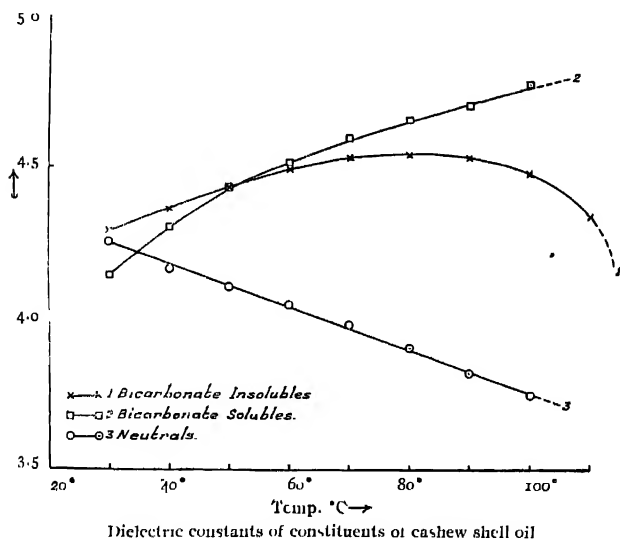


FIG. 2

The behaviour of the dielectric constants of the three constituents with temperature is widely different from one another and typical of each. The curve for bicarbonate solubles shows a continuous increase with temperature even up to 100°C. This behaviour is typical of a carboxylic acid like benzoic acid.

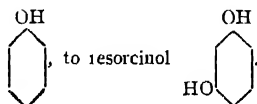
This abnormal increase with temperature may be either due to dispersion effects or the molecular association. In view of the fact that bicarbonate solubles are less viscous than the oils, such a large dispersion effect is not probable. It has been shown that benzoic and other carboxylic acid molecules

associate to form dimers. The observed gradual increase in dielectric constant may be due to gradual dissociation of dimers of anacardic acid with increase in temperature.

Bicarbonate insolubles, the major constituent of the oils behave much like the oil as regards the variation of dielectric constant with temperature. The neutrals which form a negligible portion of the oil have a lower dielectric constant with a negative temperature coefficient

A comparative study of the dielectric constant—temperature curves of the oils and their bicarbonate insolubles shows (Fig. 1) that in the case of Cardol Corporation oil, benzene extracted oil and Stanes oil, the curves for the bicarbonate insolubles fall much below those of the respective oils. This is due to the higher viscosity of the bicarbonate insolubles as compared with these oils. In the case of Fernandes oil, the curves cross near 60°C. At lower temperature (30–60°C) the Fernandes oil has a higher dielectric constant than the bicarbonate insolubles while after 60°C the situation is just the reverse. This means that though initially the viscosity forces are stronger in the case of the bicarbonate insolubles, the decrease in viscosity of the bicarbonate insolubles with temperature is so high that at higher temperatures the viscosity forces of the bicarbonate insolubles exert a lesser influence than that of the oils. For the Pierce Leslie oil both the curves go hand in hand. In the case of Pierce Leslie sample, evidently the viscosity of both are of the same magnitude. In the case of the alcohol extracted sample the difference in behaviour between the bicarbonate insolubles and the oil is enormous. Though in both cases the dielectric constant is still in the increasing trend in the range of temperature studied, yet the values for the oil are progressively very much higher than that of bicarbonate insolubles. All the anomaly between the dielectric behaviour of the oils and their bicarbonate insolubles are, as has been explained above, due to the viscosity effects. It will be, however, interesting to find out as to what exactly is responsible for these differences in viscosity between the oils and the bicarbonate insolubles. It is a well-known fact that cashew shell oil polymerises with heat and in this process the viscosity of the oil is increased. It is not yet established as to how the heat polymerisation of the oil occurs, and the mechanism of polymerisation is still to be understood. It is this polymer that is responsible for the high viscosity of the oil and its constituents. Comparatively, however, the oil is less viscous in that it is diluted by the relatively mobile solubles, (anacardic acid) and the neutrals. Again due to the differences in the extent of initial heat treatment and the method of extraction of samples the degree of polymerisation varies from sample to sample. This explains the difference in the magnitude of the anomalies that exist between the viscosity and the nature of the dielectric constant—temperature curve for the oils and the bicarbonate insolubles.

There is one more point which requires careful study and consideration. The bicarbonate insoluble portion of the oil is known to consist essentially of two main constituents: (1) anacardol derived from anacardic acid by decarboxylation and (2) cardol which is existing in the original oil. A comparative study of the dielectric constants of cardol and anacardol has not so far been undertaken for the very simple reason that it has not been possible to separate them from a mixture. Structural considerations would, however, indicate that their dielectric constants would be related to each other, at least qualitatively, in the same manner as that of the structurally analogous phenol



The essential difference between the two sets of compounds is the fact that 'H' of the latter is replaced by the nonpolar $C_{15}H_{27}$ in anacardol and cardol. Phenol has a dielectric constant of 8.02 at 113°C and resorcinol 14.5 at 110°C . (Kulkarni 1948). It is evident from this that the introduction in the phenol molecule of a 'OH' group in the meta position results in a marked increase in the dielectric constant. On the same analogy one could expect that the 'm' dihydroxy phenol, cardol should have a decidedly higher dielectric constant than that of the monohydroxy phenolanacardol. Hence the dielectric constant of the binary system, cardol—anacardol, would depend on the proportion of the individual constituents present. Consequently the magnitude of the dielectric constant of the oil or the bicarbonate insolubles would be, to a great extent, a function of the relative proportions of cardol and anacardol present in the sample under consideration. A study of the literature reveals the diversity of the composition of the raw cashew shell oil.

TABLE IV

Author	Percentage of anacardic acid
Joseph et al (1922)	90
Patel and Patel (1935)	40
Pillay (1935)	90
Backer and Haack (1941)	67

It is seen from Table IV that the percentage of anacardic acid of raw oil varies right from 40 to 90. The lowest value of 40 percent is not very reliable in that Patel and Patel have arbitrarily assumed the yield of oil as 33½ percent. Still Backer and Haack have given a value of 67 percent which is far less than the often quoted literature value of 'about 90%.' The consequence of such a wide variation in the percentage of anacardic acid in the raw oil is that the percentage of anacardol (which is anacardic acid decarboxylated) in the commercial oil is subject to correspondingly large variations depending on the source. Thus the dielectric constant of the oil or the bicarbonate insolubles is a function of its anacardol content which again depends on the source of the oil.

Hence in addition to the viscosity effects caused by the heat polymerised products the variation of the percentage of anacardol in the oil or in the bicarbonate insolubles could also be responsible for the differences in the dielectric behaviour of the different oils and their constituents. In other words each of the sample of the oil and its constituent is characterised by its dielectric behaviour depending upon (1) viscosity which is a function of the amount of polymerised product present and (2) its anacardol content, which varies from source to source.

In view of the above observations it is obvious as to how futile it is to speculate on a stray reading of dielectric constant of a sample of a particular oil. The influences governing the dielectric behaviour are many and varied and the exhaustive studies made in this present work on cashew shell oil clearly illustrate the valuable features of this point. It would be very interesting to study the dielectric properties of other oils with a view to finding out as to how factors like the source methods of extraction and pre-treatment influence the dielectric properties.

ACKNOWLEDGMENT

Thanks of the authors are due to Prof. P. Ramaswami Ayyar, M.A. for his helpful suggestions during this work.

The authors are indebted to Dr. S. K. K. Jatkan, D Sc for having provided facilities for conducting this research

GENERAL CHEMISTRY SECTION,
INDIAN INSTITUTE OF SCIENCE,
BANGALORE 5.

REFERENCES

- Backer and Haack, 1941, *Rec Trav Chim*, **60**, 661-67.
Bhattacharya, 1937, *Ind. J. Phy*, **10**, 290.

B. R. Y. Iyengar and S. Krishnamurthy

- Bhattacharya, 1941, *Ind. Jour Phys.*, **18**, 1
Caldwell and Payne, 1941, *Ind Eng. Chem.*, **33**, 954.
Dakin, 1943, *Trans. Elect Chem. Soc.*, **83**, 175.
Hazlehurst, 1943, *Paint Manuf.*, **13**, 275.
Joseph et al, 1922, *J. Ind. Inst. Sci* , **V**, 155.
Kulkarni, 1948, *Proc. Ind. Sci. Cong.*, Part III, **38**, 26.
Nagmani and Jatkari, 1942, *Q J Ind. Inst. Sci.*, **V-3**, 81
Mead and Fuoss, 1941, *J. Am. Chem. Soc.*, **63**, 2832.
Paranjpe and Deshpande, 1935, *Proc Ind. Acad. Sci.*, **A-1** , 880.
Patel and Patel, 1935, *J. Bomb Univ* , **4-6**, 111.
Pillay, 1935, *J. Ind Chem. Soc* , **12**, 226-231.
Stoops, 1931, *J. Phys. Chem* , **35-II**, 1704

THE COMPLEX BAND SPECTRUM OF COLUMBIUM OXIDE (THE DIATOMIC MOLECULE Cbo)

By V. RAMAKRISHNA RAO

Plates IA, B, C

(Received for Publication, Aug. 6, 1949).

ABSTRACT. An extensive band system attributable to the diatomic molecule Cbo is obtained in the region from λ 4200 to the limit of sensitivity of the panchromatic plates. The bands are divided into three systems, A, B, C, analogous to the α , β , γ -systems in TiO and ZrO , found by Lowater. The following vibrational constants are determined for the three systems:—

	ν_e	ω_e'	$\tau_e'\omega_e'$	ω_e''	$\tau_e''\omega_e''$
System A	21400	855.2	3.9	1002.9	6.5
System B	(18280)	998	16	1000	6.5
System C	(16260)	992	7.5	1000	6.5

Evidence of multiplet structure is found and electronic transitions between quartet terms are suggested as probable.

INTRODUCTION

The spectra of the diatomic molecules of the transition group of elements are of particular interest both theoretically and experimentally. The interest lies in the fact that the elements contain an incomplete 'd' electron shell and form molecules which give rise to bands of a very complex structure,—in appearance line-like, with a considerable overlap of multiplet and partially resolved rotational structure. These complex features are explained by the identification of high multiplicity terms among the electronic states for these molecules such as those established in the case of MnH (Nevin 1942, 1945), Mn halides (Muller, 1943; Bacher, 1948, and Rao, 1948) and CrCl (Rao and Rao, 1949). Another set of examples of bands of this type are those of TiO and ZrO (Lowater 1929, 1932). The multiplicity of terms involved in the emission of this later type of bands may not be "high" but the mechanism of electron configuration and transitions is analogous to the first type of bands. There is further an astrophysical interest associated with these oxide bands, since some of them are conspicuously present in the stellar spectra. The band spectra of the oxides known till now are those of Sc , Ti , V , Cr , Mn , Fe , Co and Ni in the first transition group and Yt and Zr in the second transition group, but there is no mention or reference till now in the literature to the band

spectrum of the oxide of columbium. While engaged on a study of the lines of Cb the author first observed bands in an arc excited between Cb electrodes, which are of a high degree of spectroscopic purity and are specimens of the H. S. brand supplied by Adam Hilger. Subsequently, in an attempt to obtain the bands of CbCl molecule (a small quantity of the pentachloride was supplied by Johnson and Mathey) in a heavy current discharge, the same bands were observed. These are not coincident with any known bands and are assigned to the oxide molecule of columbium. An investigation on these bands is described in the following pages:—

EXPERIMENTAL

The bands are obtained in three different sources:

1. In the flame of direct arc between columbium electrodes run at 22½ volts and 3 amperes
2. In the flame of D.C. arc between graphite electrodes fed by columbium pentachloride.
3. In a heavy current discharge from a D.C. two kilo-watt generator with columbium pentachloride in the quartz discharge tube. The excitation in this case may be due to the formation of the oxide as a result of the easy decomposition of the pentachloride.

Photographs are taken on S.R. Panchromatic plates with a Hilger two prism Littrow spectrograph of very high resolving and light gathering power. Measurements of the plates are made as usual and the columbium lines are eliminated by both observation and comparison with the list due to Humphreys and Meggers (1945).

DESCRIPTION OF THE BANDS

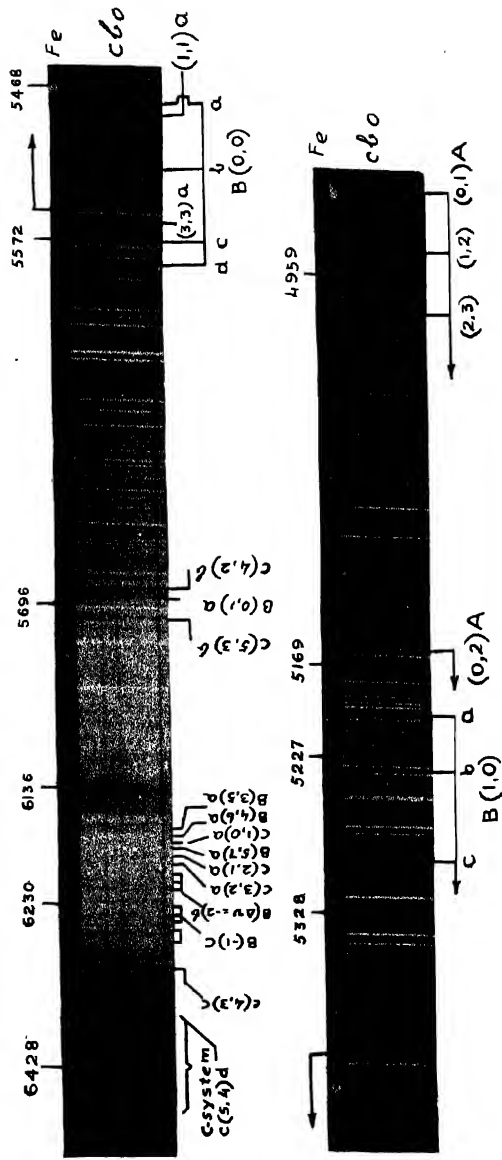
Extensive band systems from λ 4200 to the limit of sensitivity of the Ilford Panchromatic plate are obtained. The bands may be divided into three groups: (Plates IA, B and C).

1. From λ 4200—5100:—Definite well-marked and red-degraded sequences of which five are conspicuous: we shall designate these as system *A* (after Lowater's system α in ZrO).

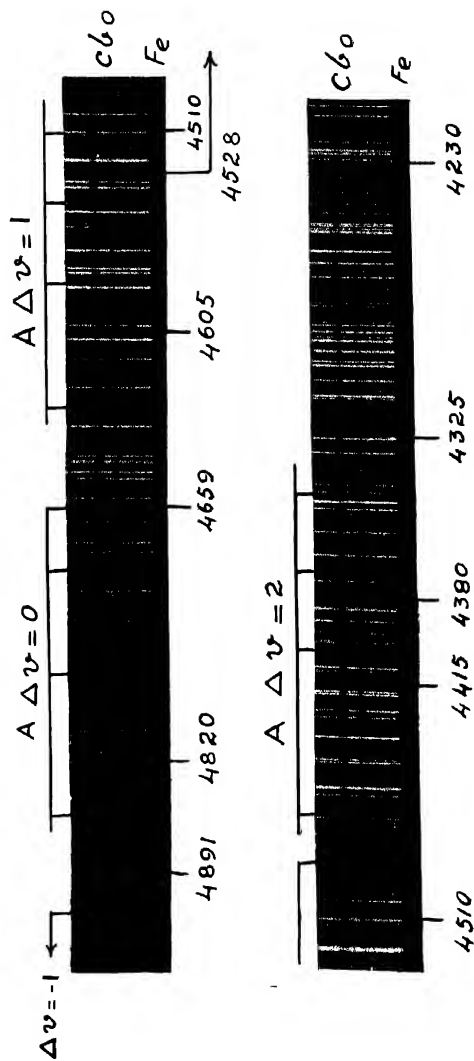
2. From λ 5100—6100:—Another group of red-degraded bands which does not present any apparent sequence structure. This may be designated as system *B* (corresponding to the β system of ZrO).

3. A third group from λ 6100 to a long wave-length limit which could not be ascertained as the system appears to extend into and beyond the panchromatic region; as can be seen from the photograph. These are closely packed red-degraded bands and shall be considered as a part of system *C* (analogous to $\text{ZrO-}\gamma$ system).

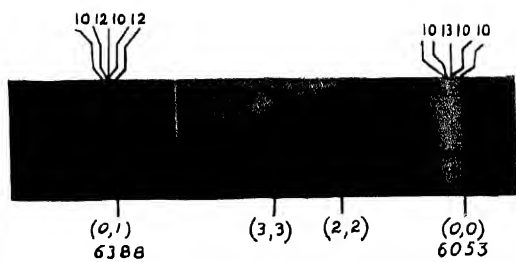
The possibility of the bands forming into three systems is suggested from an examination of the Plates.



Band spectrum of columbium oxide molecule



Columbium oxide bands (contd.).



Chromium oxide bands.

(Glass Littrow)

1. The intensity distribution in each differs from that in any other. There is a comparatively regular distribution of intensity in the sequence-starts of system *A* while the sequences in system *B* are not so conspicuous. As we follow the sequences in system *A* there is an abrupt rise in intensity at one stage of the spectrum which suggested the need for considering it as part of another system *B*. An analogous change in intensity characteristics and an apparent discontinuity in the band formation at λ 6100 is very conspicuous on plates with long exposures. It is quite likely that there is an overlap of continuum in this region extending to longer wave-lengths.

2. The structure of the bands also conspicuously differs from group to group and leads to the division into three different systems. There is an apparent partially open rotational structure in system *A*, the structure is much less open in system *B*, and, in system *C* there is no rotational structure at all.

3. Comparison with the other known oxide bands also supports this division into three systems. TiO and ZrO have three systems of analogous bands in the corresponding regions with similar characteristics. In the spectrum of vanadium oxide (Mahanti, 1935) though only one system corresponding to system *A* was analysed, mention was made of other bands lying on the long wave-length side of these. The VO system has an open rotational structure like that of ChO . Comparison with CrO bands also suggests that the system analysed by Ghosh (1932) probably corresponds to the system *A* in ChO and the α systems in TiO and ZrO . The measurements of Furguson (1932) suggest the possibility of extensive band systems lying in the infra-red region for CrO and VO molecules.

ANALYSIS

The three systems described above are not isolated ones with wide separations between them: there is a considerable amount of overlap which makes the process of picking out the sequence members a matter of difficulty especially in system *B*. There is, however, a large portion of system *A* in the region of shorter wave-lengths which is comparatively free from overlap. This helped in the easy identification of the structure of the sequences in the system *A*, and hence this is taken up as a starting point of the analysis. The most intense sequence appears at ν 21320 and is likely to be the $\Delta\tau=0$ sequence. When successive differences between the sequence starts are taken we get, beginning from the violet end the values are 830, 840, 981, 971, 960, etc. It is presumed that 981, 971, 960, are the $\Delta G(\nu)$ values of one electronic state and 840, 830, etc., of another state. As the bands are conspicuously red-degraded we may expect ω_e' less than ω_e'' , and assume that the higher intervals, 981 etc., correspond to the ground state differences. Thus the band heads at ν 21320 and ν 20340 are considered as (0,0) and (0,1) respectively, while that at ν 22163 is taken as the (1,0) head. After fixing up these three bands the (1,1) band is located in the calculated position and is identified as such. With these four bands the analysis of the other bands is developed, as shown in Table I.

TABLE I
Deslanders' Scheme Cbo System A.

$\frac{v''}{v'}$	0	1	2	3	4	5	(518)	6 901
0	21320 5(10) (842.7)	20330 9(16) (840.1)	19367 6(4) (813.2)					
1	22163 3(8) (837.1)	21180 0(3) (838.6)	20210 9(4) (809.1)					
2	23000 4(3)	22018 6(5) (831.8)	21879 5(2) (818.7)	20887 2(5) (827.8)	19967 4(1) (807.5)			18119 3(3)
3		22850.4(2)		(91.5)				
4			22098 4(4) (814.7)					
5			23313 1(5)					
6					21603 7(4) (802.1)	193.9	20670 8(1)	19752
7					23352 3(3)			20554 6(1)
8					19416 21		22269 8(3) 1792.7 23062 3(3)	

TABLE II

Vibrational constants of systems corresponding to system C in CbO.

Molecule	ω_0'	ω_0''	$x_0'\omega_0'$	$x_0''\omega_0''$
TiO	833.1	1003.5	4.5	5.1
VO	864.8	1012.3	5.7	5.3
CrO	750.7	893.8	8.9	6.5
MnO	792.0	840.7	18.3	4.9
ZrO	820.6	937.2	3.3	3.5
CbO	855.2	1002.9	3.9	6.5

The ground state differences, etc., agree well with the corresponding values of ZrO (Zr being the element preceding Cb in the periodic table). A comprehensive table of the ground and upper state frequencies of the oxide molecules of some of the elements of the transition groups is given above (Table II.) The order of magnitude and the general variation show a regularity and support the correctness of the identification in CbO.

INTENSITY DISTRIBUTION IN SYSTEM A

The most intense heads of the group are the sequence-starts: they fall on a typically wide Condon parabola. Considering any single sequence, the intensity falls rapidly. The fall is very conspicuous in $\Delta v=0$ sequence. But, one peculiarity is the abrupt change in intensity in the $\Delta v=0$ sequence; the (2,2) band is not observed at all although higher members of the sequence are developed. In the other sequences as well, some of the earlier members of the sequence are absent while the higher members are sufficiently intense, as is evident from the Table I. Such a general feature is not uncommon in the complex oxide bands; notably in the CrO the (1,1) band is very weak while the (2,2) (3,3) etc., are much stronger.

Another characteristic feature of the intensity distribution deserving particular mention is the relative intensity of the (0,1) and the (1,0) bands. The latter is much more intense than the former, and even comparable with the (0,0) band. This feature also seems to be present in other complex bands as well the oxide bands of Ti, V and Cr and also the halide bands of Mn and Cr.

STRUCTURE OF THE BAND SYSTEM

On account of the above peculiarities in the intensity distribution, considerable difficulty is experienced in arriving at the vibrational structure of the system. Another factor also has contributed to this difficulty. Although each sequence could be generally followed upto the start of

the next sequence, still the following up of each of the sequences after the first two members presented considerable difficulty. It can be seen from the plates and the wave-length list (Table V) that between the (0,0) and (1,1) bands there are at least half a dozen heads with fairly considerable intensity. Whether these bands are rotational heads or multiplet heads could not be decided. Multiplets were detected in the bands of ZnO by Lowater. An attempt to find out similar multiplet structure in the present CuO system *A* is not fruitful. The question of structure (rotational or multiplet) can be considered only after a detailed rotational analysis is obtained. The interpretation of many of the heads which are still unclassified, particularly those at the end of each sequence, might then be clear. The intensity characteristics of the bands alone do not give us any clue to their interpretation. Unless the rotational analysis is completed even the question of the existence or otherwise of multiplet structure cannot be decided. Even if the multiplet structure exists, the separations that are involved may be very small, as will be seen from a discussion given subsequently.

SYSTEM B

With the vibrational differences obtained from the structure of system *A* an analysis of system *B* is attempted. The identification of the $\Delta v=0$ sequence has not been as easy as in system *A*. From analogy with the ZnO molecule we may expect this system to have a common state with system *A* probably the lower state. Attempts are therefore made to see if the ground state differences of system *A* occur in any of the pairs formed from what might be the sequence starts in appropriate regions of system *B*. This resulted in the identification of a number of pairs with the same ground state intervals over short regions of the spectrum. This is in definite contrast to system *A* where no existence of such pairs could be found. A close scrutiny of these pairs and a consideration of the relations between the wave-numbers of this and of the remaining heads, resulted in the vibrational scheme shown in Table III. Under each v', v'' combination four members are given. These are designated as *a*, *b*, *c*, *d* in increasing order of wave-lengths. These members might arise from the multiplicity of the term.

A discussion of the interpretation of these components is given later. It should be noted that all the (v', v'') bands do not develop these four components still their existence and the regularities among them appear quite definite.

The following approximate vibrational constants are derived. The constants in the upper state of system *B* are less than those for the lower state consistent with the red-degraded bands. But the difference between the values is very small.

$$\omega_e' \sim 998 \text{ cm}^{-1}$$

$$x_e' \omega_e' \sim 16 \text{ cm}^{-1}$$

$$\omega_e'' \sim 1000 \text{ ,,}$$

$$x_e'' \omega_e'' \sim 6.5 \text{ ,,}$$

Complex Band Spectrum of Columbium Oxide

41

TABLE III
System I_b

	0	979.3	1	968.9	2	964.9	3	940.8	4	5	6	7	8
a	18275.4 (4) 198 01	17205.4 (4)	(970.4) 16325.0 (3)										
	(138.3)	(137.2)	(136.4)										
b	18137.1 (2) 197.8 91	17138.2 (4)	(969.6) 16182.6 (2)										
	(166.5)	(197.3)	(196.8)										
c	17940.6 (3) 197.9 71	16927.1 (4)	(969.1) 15991.8 (4)										
	(166.5)	(162.6)	(162.0)										
d	17886.1 (4) 198.1 8	16898.3 (2)	(966.5) 15931.8 (3) ?										
948	19222.0 (8) 197.6 31	18245.7 (3)					16313.6 (1)						
	(133.7)						(137.7)						
1	19083.3 (4) 1						16175.9 (3)						
	(202.0)						(196.4)						
18886.3 (2)							15976.5 (2)						
							(58.5)						
928			17822.4 (4)	(968.8) 16883.6 (3)			15918.0 (1)						
2				18569.2					16163.9 (5)				
									(196.4)				
									15997.5				
									(63.2)				
915	19753.1 (3)								15904.3				
									17078.2 (3)				
3			19550.2 (2)							16143.7 (3)			
			(197.6)							(195.1)			
			19753.1 (3)							15948.6 (6)			
										157.4			
913										15891.2 (0)			
										17201.9 (4)			
										(931.7)	16270.2 (4)		
											16130.6 (2)		
4												16256.7 (6)	
										16501.5 (2)	(932.3)	16069.0 (2)	
5													15994.6 (0)
6													15731.3 (1)

Intensity Distribution:—The intensity distribution in system *B* is highly complex. There is no systematic variation of the intensity of the different sequences or their individual members. This might be attributed to the partially open rotational structure, multiplicity of the band heads, and overlap of systems *B* and *C*.

SYSTEM C

Only one group is detected definitely in this system (Table IV). It presents a kind of fluted structure. A definite vibrational assignment of a single group like this is not possible. The first attempt was to see if this can be the (0,0) group, in view of its intensity but the intervals between the component heads are not of the expected order of magnitude to justify such an assignment. Intensities, and interval characteristics have suggested on the other hand that it might be the (1,0) sequence. The relatively large intensity of this group does not preclude the assignment as the (1,0) group instead of as the (0,0) group for, in this type of spectra the (1,0) sequence is nearly as intense as the (0,0) group. On the assumption that it might be the (1,0) sequence, evidence is found on the plate of a possible existence of the (2,0) sequence in the appropriate region but it is partially developed and overlapped considerably by bands belonging to system *B*.

Multiple heads are identified in some of the members of the sequence and are designated as *a*, *b*, *c*, *d* similar to those found in system *B*. But it should be noted that the component separations in the two systems are different.

If the above tentative assignment of the observed group as the (1,0) sequence prove to be correct the (0,0) sequence should lie further to the red. An investigation into this region was not possible for want of suitable photographic plates.

TABLE V

List of unclassified bands in CbO

Wave number	Int	Wave number	Int	Wave number	Int
23673.6	3	23528.7	2	23270.5	3
661.7	1	483.6	3	263.7	2
651.3	2	475.8	3	249.5	3
629.3	5	460.1	3	229.1	8
616.7	4	452.5	2	224.7	3
613.7	3	445.4	3	210.3	2
606.3	2	439.4	2	180.2	1
599.8	3	426.7	3	172.8	1
586.2	3	414.7	3	161.8	2
578.1	4	391.4	2	146.4	3
566.4	3	342.6	4	121.6	3
556.7	4	332.6	3		
548.7	5	325.1	4	23075.7	4
540.8	1	303.4	2		

TABLE V (contd)

Wave number	Int.	Wave number	Int.	Wave number	Int.
22968.7	2	20948.8	4	18350.5	3
955.1	3	910.7	5	332.9	2
936.6	3	876.1	6	282.4	5
905.7	2	832.9		269.0	3
878.2	2	803.3	3	255.3	2
837.0	2	740.9	4	230.7	5
821.1	2	731.4	3	196.1	3
805.0	2	587.9	4	168.4	4
791.6	3	565.2	2	153.1	2
772.0	3	527.0	2	119.3	3
750.8	2	504.3	1	069.2	3
746.7	2	471.3	2	055.8	3
741.0	2	408.9	3	025.8	2
730.1	3	327.5	2		
678.4	3			17987.3	2
648.2	2	20316.5	5	852.4	4
627.9	3	291.1	1	833.7	4
609.9	3	270.4	2	795.4	3
596.7	3	249.3	1	667.0	3
591.4	2	197.0	3	587.6	3
566.8	3	167.3	2	509.3	2
497.0	5	113.4	1	423.2	2
447.6	3	053.9	4	307.3	1
373.5	4	021.7	4	263.6	3
346.9	2			145.1	3
294.1	4	10975.9	2	011.1	2
268.6	2	914.3	3		
191.9	2	803.4	1	16741.5	1
182.3	1	823.2	2	733.4	2
104.0	4	723.9	2	676.5	1
081.8	5	714.5	3	646.7	2
069.6	2	671.6	2	622.1	2
032.6	4	574.5	1		
		552.6	2	16612.1	2
21949.4	2	428.5	4	601.0	1
926.9	4	384.2	6	564.4	1
911.8	3	351.1	4	526.7	2
893.7	4	346.8	1	493.6	3
870.5	2	323.5	8	475.2	2
		287.5	6	458.0	2
21831.1	3	236.4	2	442.8	1
811.5	6	120.8	5	427.9	1
799.6	3	126.3	5	390.2	2
781.6	3	027.6	3	369.5	1
777.1	2	075.2	2	362.2	1
755.0	4	067.1	2	352.5	1
676.3	6			336.0	2
626.3	6	18985.3	2	232.8	2
583.9	5	970.8	4	207.1	0
574.4	6	943.7	1	069.0	2
546.4	6	907.6	2	053.3	4
528.9	5	874.8	2		
490.5	6	838.7	3	15846.8	4
447.0	6	695.0	0	834.2	1
411.3	3	651.9	1	820.0	1
306.2	2			784.0	0
261.5	4	18571.9	3	764.0	1
252.9	4	568.1	3	731.3	1
225.0	3	561.4	2	706.3	1
217.1	2	511.8	3	671.2	2
163.2	4	480.0	2	651.3	1
080.4	4	473.8	3	628.4	0
024.1	4	433.1	1	587.7	2
011.2	2	366.7	3		

The author, however, desires to suggest that it is a very important investigation as it would lead firstly, to the analysis of system C. There is in addition a possibility of deciding the question of the multiplicity of the electronic states involved. The system C is specially suited for the purpose as it is obviously not complicated by the existence of the rotational structure.

The intensity distribution in this system cannot be discussed in the absence of a complete analysis.

VIBRATIONAL DATA

All the vibrational constants determined for the three systems are collected in Table VI. At least for systems B and C the order of magnitude alone should be taken as having been determined in the present work. Accurate formulae are not possible to derive without measurements on higher dispersion. In Table VII the values of the energies of dissociation etc., are given for a few allied molecules of the type CbO. The data for the oxides of Ti, V, Cr, Mn are taken from Mahanti (1935). For ZrO the values are calculated from Lowater's vibrational constants for system α . The values for CbO are derived from system A.

TABLE VI
Vibrational constants in CbO.

System A	21400	855.2	3.9	1002.9	6.5
System B	(18240)	998	16.0	1020	6.5
System C	1,6260	992	7.5	1000	6.5

TABLE VII
Heat of dissociation, etc. (from systems corresponding to system A in CbO)

	E_{mol}	D'	D''	E_{atom}
ScO	2.5	4.6	7.5	-0.4
TiO	2.4	4.8	6.9	+0.3
VO	2.2	4.2	6.4	0.0
CrO	2.0	1.9	3.3	+0.1
MnO	2.2	1.7	4.4	-0.5
ZrO	2.67	6.2	6.4	+2.47
CbO	2.6	5.7	4.7	+3.6

A few points of interest are :

1. In the horizontal row of molecule ScO , etc., E_{atom} is negligibly small, suggesting the probable dissociation of molecules into two neutral atoms in both the states.

2. In the second transition group (Zr, Nb oxides) E_{atom} is large with the result that the molecules may be expected to dissociate probably into an excited metal atom and neutral oxygen in one of the states (perhaps the upper).

There is thus a similarity in members of the same horizontal row but molecules belonging to different rows exhibit largely differing characteristics, as may be reasonably expected.

ELECTRONIC TRANSITIONS

No definite conclusions about the electronic states of the molecule can be reached without a further investigation of the rotational structure of system A , or without a complete development and analysis of system C . Still the following observations from the allied molecules may help in forming a general and tentative idea of the transitions involved in the emission of the NbO bands.

In TiO and ZrO the multiplicity of the terms involved is three. The three systems detected in each of these are supposed to arise out of the following transitions.

System α	$^1\Pi - ^1\Pi$
β^*	$^3\Sigma - ^3\Pi$
γ	$^3\Sigma - ^1\Pi$

In dealing with these molecules Lowater suggested the above transitions considering the following points.

1. The total number of electrons in the molecule being even the multiplicity is odd.

2. Christy (1927) in the rotational analysis of TiO (α system) suggested that the multiplicity of the terms is three. The occurrence of multiplets (each member consisting of three components) supports this view of multiplicity.

3. Lowater also referred to a suggestion made by Pearse that there should be a resemblance between the electronic configuration of the molecule of TiO and of the atom of Ca . "Each constituent of the molecule not only retains its own two K- electrons but also has a complete ring of eight L- electrons. If so, for the molecule of TiO , oxygen, gaining two electrons from Ti atom, resembles as a constituent of the molecule inactive neon, while Ti having lost two electrons resembles Ca ." Thus,

* In TiO this is due to a singlet transition. But, refer also, Gaydon and Pearse: "Identification of molecular spectra," page 192.

Ti has the outer configurations $3d^2 4s^2$ and oxygen $2s^2 2p^4$.

(perhaps it is the $4s^2$ electrons of Ti that go out to oxygen)

The above view is borne out, as Lowater has shown, from a correspondence between the region of occurrence of the bands of TiO, and the region of the atomic transitions in Ca. In general we get bands in regions corresponding to the atomic transitions in the element iso-electronic with the metallic constituent.

These general considerations may profitably be applied to interpret the electronic transitions in the CbO molecule thus.

Cb atom has the outer most electrons $4d^3 5s^2$ and oxygen has $2s^2 2p^4$.

(a) The total number of electrons is 11: the multiplicity must be even and may be two or four. (Higher multiplicities cannot be possibly expected).

There is experimental evidence, as shown above, of the existence of four components in each (v' , v'') member definitely in system B and probably also in system C. There is therefore a greater probability of the multiplicity being four.

(b) Applying Parse's suggestion, if there is a transfer or promotion of two electrons from the Cb atom to oxygen, there remains three electrons in the constituent of the molecule effective in giving rise to molecular terms in CbO. The CbO molecule may be considered as resembling in its electronic configuration the atom of yttrium which has $4d^3$ outermost electrons giving rise to quartet terms. Similar quartets may be expected in the CbO bands. Comparing also the corresponding regions of transitions in CbO and Yt we obtain a satisfactory ratio as in the case of TiO and Ca obtained by Lowater.

ν_e for system A is 21420 cm^{-1} .

In Yt I- $3d^2 4s$ $^1P = 15477 \text{ cm}^{-1}$.

$3d^2 4p$ $^1P^o = 37476 \text{ ,,}$

Difference = 21990 ,,

Ratio is $\frac{21999}{21420} = 1.03$

The following transitions might be tentatively considered for the different band systems observed in CbO.

System A: $^1\Pi - ^4\Pi$

System B: $(^4\Sigma) - ^4\Pi$

System C: $^4\Sigma - ^4\Pi$

Consistent with this scheme of electronic transitions we observed four components in each member in system C. In system B as well similar multiplets are observed, but the separations between them are smaller—a feature which may be expected if the $^4\Sigma$ involved in the emission of

system *B* has a small splitting. In system *A* however, the question of multiplet structure as shown in an earlier section is complicated by the existence of rotational structure. The multiplicity corresponding to the ground ${}^1\Pi$ state has not been detected in system *A*. There is no evidence of recurring frequency intervals that are found in systems *B* and *C*. Perhaps the effective separations are reduced to zero by the very near equality of the intervals in the upper and lower Π states. It is necessary to investigate the rotational structure of system *A* in detail before the above view can be established.

COMPARISON WITH SIMILAR MOLECULES

O_2^+ and VO are like CbO , eleven electron systems and may be expected to give similar electronic states. In O_2^+ the transition was established by Nevin (1938) from a study of the rotational analysis as ${}^4\Sigma - {}^1\Pi$ and there was good correlation between Budo's calculations (1937) of the rotational characteristics expected for such a transition. In VO , however, Mahanti (1935) analysing the rotational structure in one system suggested a transition ${}^2\Delta - {}^2\Delta$. The absence of Ω -type of doubling even at high rotational quantum numbers seem to have led Mahanti to exclude the possibility of a ground Π state and the presence of a short and strong Q branch ruled out a Σ ground state. Still, as Mahanti himself has stated, the criteria of missing lines and intensity relations between the branches for low rotational quantum numbers could not be used to settle the question definitely. If a similarity of electronic transitions can be predicted from the resemblance between the electronic configurations of O_2^+ and VO , it would be more probable to assume a ${}^1\Pi$ as the ground state. The transition of the system may be a ${}^4\Pi - {}^4\Pi$. A more complete evidence for determining these electronic transitions would be available only if the VO bands are photographed further in the red than Mahanti has done. Mahanti has also indicated the probable existence of such bands in the infrared region.

Chromium Oxide Bands.—The chromium oxide molecule gives band systems having a similar complex structure. From a partial vibrational analysis Ghosh (1932) suggested the probability of transitions between singlet or triplet terms. Observations of his pictures and also those obtained by the author and reproduced in the Plate I C, reveal four component heads following each band at the sequence start *i.e.* five component heads in all are observed, associated with each of the sequences starts. Arguing from the analogy and studying the variation of the multiplicities in a row of molecules such as TiO , VO and CrO it would appear that quintet terms are involved in the transition giving rise to CrO bands. Probably a ${}^7\Pi - {}^5\Pi$ transition may be occurring. A study of the detailed rotational structure of this and the other molecules in the transition groups is very desirable and would lead to an understanding of this subject of electronic states in such molecules.

ACKNOWLEDGMENT

The author wishes to thank Dr. K. R. Rao, for his guidance.

REFERENCES

- Bacher, 1948, *Helv. Phys. Acta.*, **21**, 379.
Budo, 1937, *Zs. f. Phys.*, **73**, 105.
Ferguson, 1932, *Brav. Stand. J.*, **78**, 382.
Ghosh, 1932, *Ibid*, **78**, 521.
Lowater, 1929, *Proc. Phys. Soc*, **41**, 557.
Lowater, 1932, *Ibid* **44**, 51.
Mahant, 1935, *Ibid*, **47**, 433.
Mcggers and Humphreys, 1945, *B. S. J.*, **34**, 477.
Muller, 1943, *Helv. Phys. Acta* **16**, 1.
Nevin, 1945, *Proc. Roy. Irish. Acad. A*, **48**, 1.
1942, *Ibid*, **60**, 123.
1938, *Phyl Trans. Roy. Soc A*, **237**, 471.
Rao, P. T., 1948, *Ind. J. Phy* (in press).
Rao, V. and Rao, K. R., 1949, *Ibid* (in press).

TOMORROW'S INSTRUMENTS TODAY

RAJ-DER-KAR & CO.

COMMISSARIAT BUILDING

HORNBY ROAD

FORT

BOMBAY

OFFERS

FROM STOCK

GLASS METAL DIFFUSION PUMPS, METAL BOOSTER
PUMPS, OILS AMOILS OCTOILS OCTOIL,
BUTYL SABACATE

MANUFACTURED

By

DISTILLATION PRODUCTS
(U. S. A.)

SPENCER MICROSCOPE

CENCO HIGHVACS

BESLER EPIDIASCOPE

COMPLETE WITH FILM STRIP ARRANGEMENTS

Telephone 27304
2 Lines

Telegrams
TECHLAB

GOVERNMENT OF INDIA

Ministry of Education.

Applications are invited for the following posts in the Faculty of Science, Kabul University, Afghanistan :

- (a) Professor of Physics
- (b) Professor of Plant Physiology

The terms and conditions of appointment are as follows :—

Pay : About Rs. 1,000/- (Indian) per month. A higher salary may be given to exceptionally well qualified candidates.

House rent allowance : 700 Afghanis per month

Travelling Expenses : First class railway fare plus other travelling expenses while joining and on the expiry of the contract.

Duration of contract : Three years

Candidates must possess a *first class* post-graduate degree, preferably Doctorate degree in the subject, together with *at least* 12 years' research experience in a well-established research laboratory in India or abroad. They must also be able to organise and develop departments for post-graduate teaching and research in the subject. Previous experience in an University Institution will be considered as an additional qualifications. For Physics Professorship preference will be given to those possessing working knowledge of French or Persian.

Applications together with copies of necessary testimonials, reprints of published research papers and any other relevant documents in support of the applicant's attainments should be addressed to Secretary, Ministry of Education (Technical Division) Government of India, New Delhi, so as to reach him not later than the 10th March, 1950.

The following is a list of the books and pamphlets for sale at the University of California Press, 2215 Center Street, Berkeley, California 94720. The prices are in dollars and cents.

Book	Author	Price
Methods in the History of Science	Ed. by J. H. E. D. Russell	\$12.50
The Origin of the Species	Charles Darwin	\$1.50
Separation of Variables	Prof. P. M. A. A. A.	\$1.50
Garnets and their Role in the Earth's Crust	Dr. David L. Farnham	\$1.50
(a) The Role of Garnets in the Earth's Crust	Dr. Arthur H. H.	\$1.50
(b) Studies in the Crust of the Earth		
Interatomic Forces	Prof. L. E. Landau-Rumer	\$1.50
The Educational Aims and Practices of the California Institute of Technology	Dr. A. A. A.	\$1.50
Active Nitrogen	Prof. S. K. Mitra	\$1.50
A New Theory		
Theory of Valency and the Structure of Chemical Compounds	Prof. P. Ray	\$1.50
Petroleum Resources of India	Dr. V. Wadia	\$1.50
The Role of the Electrical Double Layer in the Electro-Catalysis of Cellulose	J. N. Mather	\$1.50

A discount of 25% is allowed to Bookshelves and Agents.

RATES OF ADVERTISEMENTS

Third page of book	First page of book
10	10
20	20
30	30
40	40
50	50
60	60
70	70
80	80
90	90
100	100

CONTENTS

1. On the Dielectric and Absorption of Certain Organic Compounds in Glass	1
2. Studies of the Jahn Effect in Chlorine under Complex Excitation—Influence of Temperature—By K. S. Varshni and K. Raghunath	13
3. Relativistic Thomas-Fermion—By R. P. Singh	19
4. Dielectric Constants of Commercial Cashew Seed Oil—By S. K. Samanta and B. R. V. Iyengar	23
5. The Complex Band Spectrum of <i>Glyptotendipes</i> Ovipositor Diatom—Molecular CH_3 —By V. Ramakrishna Rao	35

Printed by Sankardevi Press, Bangalore

Price, 15 Paise

Copyright, 1954, by Sankardevi Press, Bangalore

24

INDIAN JOURNAL OF PHYSICS

No. 2

(Published in collaboration with the Indian Physical Society)

AND

33

PROCEEDINGS

No. 2

OF THE

**INDIAN ASSOCIATION FOR THE
CULTIVATION OF SCIENCE**

FEBRUARY, 1950

PUBLISHED BY THE
INDIAN ASSOCIATION FOR THE CULTIVATION OF SCIENCE
210, Bowbazar Street, Calcutta

BOARD OF EDITORS

K. BANERJEE	S. K. MITRA
D. M. BOSE	P. RAY
S. N. BOSE	M. N. SAHA
D. S. KOTHARI	S. C. SIKHAR.

Secretary

EDITORIAL COLLABORATORS

DR. R. K. ASUNDI, M.A., PH.D.
PROF. H. J. BHABHA, PH.D., F.R.S.
DR. P. K. KICHLU, D.Sc.
PROF. K. S. KRISHNAN, D.Sc., F.R.S.
PROF. G. P. DUBEY, M.Sc.
DR. K. RANGADHAMA RAO, M.A., D.Sc.
DR. N. D. SARWATHEY, D.Sc.
DR. N. N. DASGUPTA, M.Sc., PH D.
PROF. N. R. SEN, D.Sc., F.N.I.
PROF. P. C. MAHANTI, D.Sc., F.N.I.
PROF. S. R. PALIT, D.Sc.,
DR. H. RAKSHIT, D.Sc.,
PROF. K. R. DIXIT, PH.D.
DR. VIKRAM A. SARABHAI, M.A., PH.D.

ASSISTANT EDITOR

MR. A. N. BANERJEE, M.Sc.

NOTICE

AL

Manuscripts for publication should be sent to Mr. A. N. Banerjee, Assistant Editor, 210, Bowbazar Street, Calcutta.

The manuscript of each paper should contain in the beginning a short abstract of the paper.

All references to published papers should be given in the text by quoting the name of the authors followed by the year of publication within braces, e.g., (1942). The actual references should be given in a list at the end of the paper according to the following specimen :

Sen, B. K., 1942, *Ind. J. Phys.*, 18, 3

The references should be arranged alphabetically in the list.

All diagrams should be drawn on the white paper in Indian ink, and letters and numbers in the diagrams should be in pencil.

Annual Subscription—

Inland Rs. 20

Foreign 25

TERM VALUES OF f^4 ELECTRON CONFIGURATION

By K. SURYANARAYANA RAO

(Received for publication, Nov. 15, 1949)

ABSTRACT. Using Slater's wave-mechanical method term values have been calculated for the complex f^4 electron configuration in terms of the well-known F 's and G 's of Slater with the help of Condon's tables for a 's and b 's. A table of these values for the different terms of this configuration is given.

INTRODUCTION

In a recent paper term values have been calculated by Rao (1949) for an f^4 electron configuration using Slater's method (Slater, 1929) and compared with those obtained by Racah (1943) who adopted the tensor method. The present paper deals with the calculation of term values for the more complex f^4 configuration of electrons which so far has not been carried out by either the Slater or the tensor method. A derivation of these term values may be of interest in the analysis of the spectra of the rare earth elements, the structure of which is still unknown.

Slater's method is employed for the purpose of this calculation. Briefly, the method may be stated thus: the solution for the Schrodinger's equation for an atom consisting of N electrons, will be the product of the wave functions of the individual electrons if the wave function for the i th electron is denoted by $u(n_i, x_i)$, where n_i stands for the four quantum numbers n, l, m_l and m_s , and x_i for the four co-ordinates (x, y, z, m_s) . To get the required antisymmetry so as to obey Pauli's exclusion principle, any two x 's can be interchanged, thereby obtaining an approximate solution with the same energy. Any linear combination of such solution which will also be an approximate solution can be written down as a determinant (Slater, 1929) which has got two important properties: (1) It is intrinsically anti-symmetric and (2) it treats all electrons alike so that no two states obtained by the mere interchange of quantum numbers of two electrons can be treated as different. Using the method of perturbations to introduce the interaction between the various angular momenta, Slater has shown that the energy matrix computed with respect to the approximate but incorrect wave functions gives in its diagonal terms good approximations to the actual energy values, the non-diagonal terms being negligible when the magnetic interaction is neglected. The method of separating terms occurring more than once is omitted here.

CALCULATION

The total number of zero-order wave functions for any general configuration of the form l^N is $(4l+2) C_N$ and so in the case of the f^4 configura-

tion the number is equal to ${}^{14}C_4=1001$. Out of these only those with positive values of Σm_l and Σm_s need be taken. The number of valid functions have been actually put down, taking care to see that no function repeats itself and also that, in the same function the m_l, m_s values of no two electrons should coincide. They have been found to be 400 in number which has been checked up by a less tedious method, starting from the allowed states of the f^4 configuration. It is as follows:

The allowed states for this configuration, are

$${}^5(SDFGI), {}^3(P D F G H I K L M), {}^1(S D F G H I K L N)$$

$$3 \quad 2 \quad 4 \quad 3 \quad 4 \quad 2 \quad 2 \qquad 2 \quad 4 \quad 4 \quad 2 \quad 3 \quad 2$$

where the small number placed directly below the term symbol indicates the number of such identical terms. Taking the quintets, the value of $\Sigma m_s=2$ and the corresponding highest Σm_l value from the allowed quintets of f^4 configuration is 6, giving the 5I state. This function, $(3^+, 2^+, 1^+, 0^+)$ occurs uniquely and all the other quintet functions are

TABLE I

Σm_s	Σm_l	N	L_1	K	I_2	H_2	G_4	F	D_4	S_1	Total
0	10	1									1
0	9	1									1
0	8	1	2								3
0	7	1	2	1							4
0	6	1	2	1	3						7
0	5	1	2	1	3	2					9
0	4	1	2	1	3	2	4				13
0	3	1	2	1	3	2	4	1			14
0	2	1	2	1	3	2	4	1	4		18
0	1	1	2	1	3	2	4	1	4	2	18
0	0	1	2	1	3	2	4	1	4	2	20

degenerate in this. Now the positive values of Σm_l are combined with the other two positive values of Σm_s , namely, 1 and 0 and the degenerate functions corresponding to the quintets are thus obtained. The same procedure has been adopted with respect to the triplets and singlets, the unique functions in these cases being $(3^+, 2^+, 1^+, 3^-)$ and $(3^+, 2^+, 2^-, 3^-)$ which correspond to 3M and 1N respectively. It must be noted here that ${}^5I, {}^3M$ and 1N occur uniquely and all the other states are degenerate in one or the other or all these, the degree of degeneracy of such states being equal to the number of times the possible wave-functions with the charac-

teristic $\Sigma m_s, \Sigma m_l$ values occur. For example, the function $\Sigma m_s = 0, \Sigma m_l = 0$ corresponding to the 1S state, is degenerate in all the higher- l singlet, triplet and quintet states. Thus the number of (0,0) functions can be seen to be 47 from Table II. Similarly, the number of functions with a given set of $\Sigma m_s, \Sigma m_l$ values and hence the total number of valid functions can be determined. A representative table (Table I) is given above for singlets, showing how the number of functions with a given set of $\Sigma m_s, \Sigma m_l$ values is determined. Table II is given showing the number of functions of each kind arising from various states and also the total number of valid functions.

The effect of degeneracy is that we cannot independently calculate the term values of the degenerate state and we have to resort to the diagonal sum rule of Slater (1929). For example, 6G which is degenerate in 3I is characterised by these two wave-functions ($3^+, 2^+, 1^+, 2^-$) and ($3^+, 2^+, 0^+, 1^-$). The energy is computed with respect to these two, giving $^3I + ^6G$. From this subtracting the known value of 3I , the value of 6G is obtained. Similarly all the other degenerate states can be

TABLE II

$\Sigma m_s, \Sigma m_l$	Quintets	Triplets	Singlet	Total
2 6	1	1
2 5	1	1
2 4	2	2
2 3	3	3
2 2	4	4
2 1	4	4
2 0	5	5
1 9	...	1	...	1
1 8	...	2	...	2
1 7	...	4	...	4
1 6	1	6	...	7
1 5	1	10	...	11
1 4	2	13	...	15
1 3	3	17	...	20
1 2	4	19	...	23
1 1	4	22	...	26
1 0	5	22	...	27
0 10	1	1
0 9	...	1	1	2
0 8	...	2	3	5
0 7	...	4	4	8
0 6	1	6	7	14
0 5	1	10	9	20
0 4	2	13	13	28
0 3	3	17	14	34
0 2	4	19	18	41
0 1	4	22	18	44
0 0	5	22	20	47

Total

400

treated in the same way. The energies are computed in terms of the well-known F 's and G 's of Slater with the help of the tables for a^k 's and b^k 's, given by Condon (1930). In the case of equivalent electrons, the G 's will be equal to the F 's. For terms occurring more than once only the average values are given and are indicated by bracketing the term. The calculations for 3I term whose function, $(3^+, 2^+, 1^+, 0^+)$, occurs uniquely are given below to illustrate the procedure

$$(\frac{1}{2}^3, \frac{1}{2}^2) = F_0 + 0F_2 - 21F_4 - 6F_6 - 25G_2 - 30G_4 - 7G_6$$

$$(\frac{1}{2}^3, \frac{1}{2}^1) = F_0 - 15F_2 + 3F_4 + 15F_6 - 10G_2 - 54G_4 - 28G_6$$

$$(\frac{1}{2}^3, \frac{1}{2}^0) = F_0 - 20F_2 + 18F_4 - 30F_6 - 0 - 63G_4 - 84G_6$$

$$(\frac{1}{2}^2, \frac{1}{2}^1) = F_0 + 0 - 7F_4 - 90F_6 - 15G_2 - 32G_4 - 105G_6$$

$$(\frac{1}{2}^2, \frac{1}{2}^0) = F_0 + 0 - 42F_4 + 120F_6 - 20G_2 - 3G_4 - 224G_6$$

$$(\frac{1}{2}^1, \frac{1}{2}^0) = F_0 + 12F_2 + 6F_4 - 860F_6 - 2G_2 - 15G_4 - 350G_6$$

$$^3I = 6F_0 - 95F_2 - 240F_4 - 1079F_6$$

since G 's = F 's for equivalent electrons.

The term values are collected in Table III. It can be seen that the values of 3F and 3S have come out to be the same.

TABLE III

Term	Term value
3I	$6F_0 - 95F_2 - 240F_4 - 1079F_6$
3G	$6F_0 - 40F_2 - 174F_4 - 2080F_6$
3F	$6F_0 - \left(85 - \frac{25}{225}\right)F_2 - \left(207 - \frac{9}{1089}\right)F_4 - \left(1717 - \frac{1}{7361.64}\right)F_6$
3D	$6F_0 - 5F_2 - 132F_4 - 2717F_6$
3S	$6F_0 - \left(85 - \frac{25}{225}\right)F_2 - \left(207 - \frac{9}{1089}\right)F_4 - \left(1717 - \frac{1}{7361.64}\right)F_6$
3M	$6F_0 - \left(80 - \frac{25}{225}\right)F_2 - \left(159 - \frac{9}{1089}\right)F_4 - \left(212 - \frac{1}{7361.64}\right)F_6$
3L	$6F_0 - 70F_2 - 105F_4 - 316F_6$
(^3K)	$6F_0 - \left(55.5 - \frac{25}{2 \times 225}\right)F_2 - \left(124 - \frac{9}{2 \times 1089}\right)F_4 - \left(526.5 - \frac{1}{2 \times 7361.64}\right)F_6$
(^3I)	$6F_0 - 15F_2 - 81F_4 - 1065F_6$
(^3H)	$6F_0 - \left(29.75 - \frac{3 \times 25}{4 \times 225}\right)F_2 - \left(57.75 - \frac{3 \times 9}{4 \times 1089}\right)F_4 - \left(712.25 - \frac{3}{4 \times 7361.64}\right)F_6$

TABLE III (contd.)

$$(^3G) \quad 6F_0 - 22F_2 - 69.33F_4 - 1058F_6$$

$$(^3F) \quad 6F_0 - \left(23.5 - \frac{25}{2 \times 225}\right)F_2 - \left(74.75 - \frac{9}{2 \times 1089}\right)F_4 - \left(596.5 - \frac{1}{2 \times 7361.64}\right)F_6$$

$$6F_0 - 3F_2 - 85.5F_4 - 1170F_6$$

$$(^3D) \quad 6F_0 - \left(18.67 - \frac{25}{225}\right)F_2 - \left(18.67 - \frac{9}{1089}\right)F_4 - \left(958.67 - \frac{1}{7361.64}\right)F_6$$

$$(^3P) \quad 6F_0 - \left(50 - \frac{25}{225}\right)F_2 - \left(95 - \frac{9}{1089}\right)F_4 - \left(2 - \frac{1}{7361.64}\right)F_6$$

$$^1N \quad 6F_0 - \left(55.5 - \frac{25}{2 \times 225}\right)F_2 - \left(75 - \frac{9}{2 \times 1089}\right)F_4 + \left(103.5 + \frac{1}{2 \times 7361.64}\right)F_6$$

$$(^1L) \quad 6F_0 - 46F_2 - 23F_4 - 148F_6$$

$$^1K \quad 6F_0 - \left(8.67 - \frac{25}{3 \times 225}\right)F_2 + \left(26 + \frac{9}{3 \times 1089}\right)F_4$$

$$(^1I) \quad - \left(192.67 - \frac{1}{3 \times 7361.64}\right)F_6$$

$$6F_0 - \left(3 - \frac{25}{225}\right)F_2 - \left(92.5 - \frac{9}{1089}\right)F_4 - \left(72 - \frac{1}{7361.64}\right)F_6$$

$$(\quad 6F_0 - \left(1.25 - \frac{25}{4 \times 225}\right)F_2 - \left(22.5 - \frac{9}{4 \times 1089}\right)F_4$$

$$(^1G) \quad - \left(379.25 - \frac{1}{4 \times 7361.64}\right)F_6$$

$$6F_0 + 8F_2 + 74F_4 - 1324F_6$$

$$(^1F) \quad 6F_0 + \left(10.75 + \frac{85}{4 \times 225}\right)F_2 + \left(20.25 + \frac{9}{4 \times 1089}\right)F_4$$

$$(^1D) \quad - \left(536.75 - \frac{1}{4 \times 7361.64}\right)F_6$$

$$6F_0 + \left(97.5 + \frac{25}{2 \times 225}\right)F_2 + \left(106.5 + \frac{9}{2 \times 1089}\right)F_4$$

$$(^1S) \quad + \left(103.5 + \frac{1}{2 \times 7361.64}\right)F_6$$

ACKNOWLEDGMENTS

The author is deeply indebted to Prof. K. R. Rao for his valuable guidance during the course of this work. The author is also thankful to Mr. V. Ramakrishna Rao for many helpful suggestions.

REFERENCES

- Condon, 1930, *Phys. Rev.*, **36**, 1121.
Condon and Shortley, 1931, *Phys. Rev.*, **37**, 1025.
Racah, 1943, *Phys. Rev.*, **62**, 438.
Ramakrishna Rao, 1949, *Current Science*, (in course of publication).
Slater, 1929, *Phys. Rev.*, **34**, 1293.

A NOTE ON THE THERMAL INERTIA OF CLOUD PARTICLES

By B. K. AGARWALA AND N. K. SAHA

(Received for publication, Nov. 21, 1949)

ABSTRACT. In the present note the thermal lag of small liquid droplets losing heat to the surroundings by the processes of convection and radiation is calculated, the thermal lag being defined as the time required by the initial (small) temperature difference between the drop and the surroundings to be reduced to $\frac{1}{e}$ th of its value. The results seem to be of some application to meteorology in explaining the formation of an average rain drop from droplets. The thermal lag being a function of the radius of the drop, a temperature difference will exist between larger and smaller droplets in any cloud layer. On account of this temperature difference the cooler drops will grow at the expense of the warmer ones.

The present note is concerned with the determination of the thermal lag of small droplets (liquid or solid) losing heat to the surroundings by the processes of conduction, convection and radiation, the thermal lag being defined as the time required for the initial (small) temperature difference between the drop and the surroundings to be reduced to $1/eth$ of its value. The results seem to have some application to meteorology but before these could be profitably discussed, the calculations will have to be extended to take account of the heat interchange through condensation and evaporation of the liquid, in this case water. This is proposed to be done in the next communication.

As we can verify by an order of magnitude argument,* conduction does not play any important part in the cooling of small water drops. The cooling takes place mostly by the processes of convection and radiation

* If K be the thermal conductivity of the liquid we have

$$\frac{KA\theta}{R} = -VSd \frac{d\theta}{dt}$$

Integrating and simplifying we have

$$\theta = \theta_0 \exp. \left\{ -\frac{3h}{D^2} t \right\}$$

where $h = \frac{K}{Sd}$ is the thermal diffusivity. Thermal lag is thus given by

$$T \sim \frac{R^2}{h}$$

In case of water $h = 1.3 \times 10^{-3}$ so that a drop of $R \sim 10^{-3}$ cm., $T \sim 1$ second.

from the drop surfaces, and the whole drop takes the temperature of the surface by conduction practically in no time. The effect of conduction is, however, being examined more closely and will be reported later.

If the drop is stationary and loses heat only by radiation, the application of Stefan's law gives

$$4A\sigma T_0^4\theta = -VSdJ\frac{d\theta}{dt} \quad \dots (1)$$

where σ is the Stefan's constant and $J = 4.2 \times 10^7$ ergs/calorie. A , V , S , and d represent respectively the surface area, volume, specific heat and density of the water drop, T_0 is the temperature of the surrounding and $-\frac{d\theta}{dt}$ denotes the rate of cooling of the water drop. The temperature difference θ between the drop and the surroundings is assumed to be small.

Integrating (1) and simplifying we have

$$\theta = \theta_0 \exp. \left\{ -\frac{12\sigma T_0^4 t}{RJ} \right\}$$

R being the radius of the drop and S and d being unity in case of water.

The mean life T of the drop will thus be given by

$$T = \frac{RJ}{12\sigma T_0^4} \quad \dots (2)$$

In the case of freely falling drops the loss of heat will be mainly by convection. If α be the heat transfer coefficient we have

$$A\alpha\theta = -VSd\frac{d\theta}{dt} \quad \dots (3)$$

The coefficient α is connected with the Nusselt's number Nu by the relation

$$Nu = \frac{2R\alpha}{\lambda} \quad \dots (4)$$

where λ is the thermal conductivity of the flowing medium.

Recently Kramers (1946) has measured the heat transfer coefficient of small spherical particles of water in a forced flow of these in a viscous medium and has given the following empirical relation between the Nusselt's number Nu and two other dimensionless quantities, the Reynolds number Re and the Prandtl number Pr

$$Nu = 2.0 + 1.3 (Pr)^{0.15} + 0.66 (Pr)^{0.21} (Re)^{0.50} \quad \dots (5)$$

The Reynolds number Re is determined by the relation

$$Re = \frac{2Rv\rho}{\mu} \quad \dots (6)$$

where ρ and μ are respectively the density and viscosity of the medium; v denotes the velocity of free fall of the spherical drop and is determined by Stokes' law

$$6\pi\mu Rv = \frac{4\pi}{3} dR^4 g \quad \dots (7)$$

The Prandtl number Pr is determined by

$$Pr = \frac{\mu C_p}{\lambda} \quad (8)$$

where C_p denotes the specific heat of air at constant pressure. The heat transfer coefficient α may thus be determined in terms of R by using the relations (4) to (8). The various constants involved may be taken to be those for air at 0°C . From (3) we thus have

$$T = \frac{R}{3\alpha} \quad \dots (9)$$

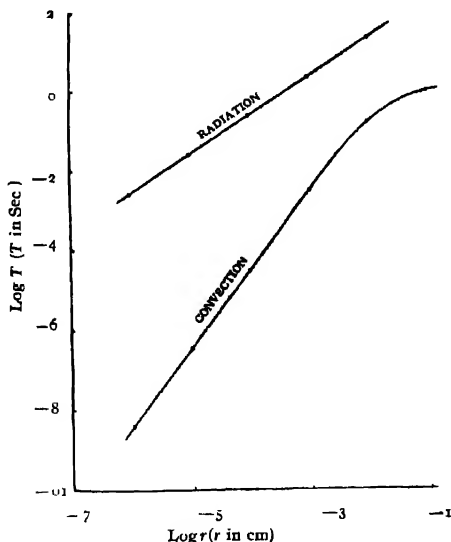


FIG. 1

In Fig. 1 $\log T$ has been plotted against $\log R$. The curve marked 'radiation' represents equation (2) and the convection curve represents equation (9). Comparing the two we find that the radiation curve gives the upper limit for the values of T and the 'convection' curve gives the lower limit. It must, however, be noted that on account of the electric field existing in a cloud the assumption of a drop falling freely seems difficult

to maintain. The actual value of T would thus depend on the effect of this electric field in controlling the velocity of the drop relative to that of air. All the same the two curves in the diagram provide the upper and lower limits for the possible values of T .

The considerations outlined above may have a possible bearing on the mechanism of formation and growth of cloud drops in the atmosphere. Thus it seems clear that water droplets of widely different sizes which may start originally at the same temperature will at a certain height show considerable temperature differences among themselves the smaller droplets taking readily the lower temperature of the layer while the larger drops lagging behind and conserving to some extent the higher temperatures of the lower layers. At a height where the smaller droplets are substantially cooler than the larger ones, it is possible that the cooler droplets will begin to grow at the expense of the warmer ones and a kind of colloidal instability helping the growth of the droplets by coalescence will set in. A similar process has been visualized by Petterssen (1911) in his theory of growth of cloud droplets in tropical countries.

ACKNOWLEDGMENT

Our thanks are due to Prof. D. S. Kothari for his kind interest in this work.

UNIVERSITY OF DELHI,
DELHI

REFERENCES

- Krammers, H., 1946, *Physica*, **12**, 61.
Petterssen, S., 1941, *Introduction to Meteorology*, p. 46.

ON THE DISTRIBUTION OF IONS IN SOLUTIONS OF STRONG ELECTROLYTES

By M. DUTTA AND S. N. BAGCHI

(Received for publication, Nov. 4, 1949)

ABSTRACT In a recent paper (Bagchi, 1949), it has been shown that a better and closer agreement between the theoretical and the experimental values of activity coefficients are obtained, if instead of Boltzmann's distribution functions a new distribution function, similar in form to that of Fermi-Dirac, be used in Debye-Huckel theory of strong electrolytes. No deduction has been given yet for the function used by Bagchi. In this paper, the distribution function has been deduced from simple physical properties of ions by a method developed by Dutta (1947, 1948, 1949).

In a recent paper one of the authors (Bagchi, 1949) has shown that a better and closer fit between the theoretical and experimental values of the activity coefficients are obtained, if instead of Boltzmann's distribution function, a new form of distribution, analogous to that of Fermi-Dirac, be used in Debye-Huckel's theory of strong electrolytes. For the distribution of ions in the field of any ion, the law was assumed to be of the form

$$\left. \begin{aligned} n_+ &= \frac{A}{B_+ \exp\left(\frac{e_+ \psi}{kT}\right) + 1} \\ n_- &= \frac{A}{B_- \exp\left(\frac{e_- \psi}{kT}\right) + 1} \end{aligned} \right\} \quad \dots \quad (1)$$

where n_+ and n_- are concentrations of positive and negative ions of charges e_+ and e_- respectively, ψ is the electric potential at the place, k is the Boltzmann's constant, T the absolute temperature and A , B_+ , B_- are some suitable constants. In the paper referred to above, this distribution was supposed to be a special type of Fermi-Dirac distribution, in the potential field, exactly analogous to that of Boltzmann's distribution under similar conditions, so no justification for the assumption of this particular form was given. Moreover, it was implied that the non-ideality of the solution was due to the effect of this contribution of the potential field, the contribution in the distribution due to the kinetic energy would give the ideal part. Hence only the distribution due to the field was considered. But a careful analysis would show that such a separation of the effect of the total energy into the kinetic and the potential parts could not be conveniently carried out with the usual distribution formula of Fermi-Dirac statistics. Fermi-Dirac statistics gives the distribution with respect to total energy. In order to determine the distribution in the potential field, the distribution function is to be integrated with respect to the kinetic energy, but integration with respect to the kinetic energy will change the form of the function, and so a distribution

function for the field alone cannot be obtained in the same form as in equation (1).

In the present paper, a complete derivation of the above distribution (Eqn. 1) has been given following a method developed by one of the authors in connection with the statistical investigations of real gases (Dutta, 1947, 1948, 1949 a). In this method the distributions with respect to configurational and momenta coordinates are treated separately and independently. It is assumed here that due to electrical repulsions and due to the finite size of ions, they cannot come infinitely close to each other so there occurs some rigid volumes of exclusion viz., b_+ , b_- and b_{+-} , which means that no more than one positive ion can be located inside the volume of extension b_+ , not more than one negative ion in the volume b_- and not more than one either a positive or negative ion in the volume of extension b_{+-} . The available configuration space is then divided into elementary cells of extension b_+ during distribution of positive ions and into elementary cells of extension b_- during the distribution of negative ions. For statistical considerations the ions are considered as points and are distributed into the respective cells according to the principle of exclusion, similar to that of Pauli-Fermi, namely that not more than one particle can come in a single cell. A cell may be either vacant or be occupied by a single ion. The distribution in the configurational space has been calculated after Fermi.

The distribution with respect to momenta (i.e. kinetic energy) has been considered separately in the usual way after Planck and Lorentz.

Description of the assembly

The assembly under consideration consists of N^+ , N^- ions enclosed in a volume V . It is assumed that there is no recombination of ions and that they are completely ionised.

For considering the distribution of ions in the configurational space, the total volume in the configurational space has been divided into potential layers of volumes $V_1, V_2, \dots, V_m, \dots$ corresponding to the potentials $\psi_1, \psi_2, \dots, \psi_m, \dots$ respectively (Dutta, 1949). Let, at any instant, $N_1^+, N_2^+, \dots, N_m^+, \dots$ and $N_1^-, N_2^-, \dots, N_m^-, \dots$ be the numbers of positive and negative ions in layers of volumes $V_1, V_2, \dots, V_m, \dots$ respectively.

Now for investigating the distribution, every volume is at first divided into cells of volume b_+ , the number of such cells in every layer being V_m/b_+ . The positive ions are then distributed in these cells. After the distribution of the positive ions, the volume of every layer available for the negative ions would be $(V_m - N_m^+ b_{+-})$ and this available space is again divided into cells of volume b_- . The number of such cells is $(V_m - N_m^+ b_{+-})/b_-$. Into these cells the negative ions are then distributed.

Let a_i^+ be the number of positive ions with kinetic energy E_i^+ and a_i^- be the number of negative ions with kinetic energy E_i^- .

Calculations

Calculating the thermodynamic probability (cf. Dutta 1947, 1949) we have

$$W_{+-} = \Pi_m \frac{\left(\frac{V_m}{b_+}\right)!}{N_m^+ \left(\frac{V_m}{b_+} - N_m^+\right)!} \cdot \frac{\left(\frac{V_m - N_m^+ b_{+-}}{b_-}\right)!}{N_m^- \left(\frac{V_m - N_m^+ b_{+-}}{b_-} - N_m^-\right)!} \cdot \frac{N^+!}{\Pi a_i^+!} \cdot \frac{N^-!}{\Pi a_n^-!}$$

Now, as usual, using Stirling's formula for approximation and taking logarithm, we have

$$\begin{aligned} \log W_{+-} = & \left[\sum_m \left\{ \left(\frac{V_m}{b_+}\right) \log \left(\frac{V_m}{b_+}\right) - N_m^+ \log N_m^+ - \left(\frac{V_m}{b_+} - N_m^+\right) \log \left(\frac{V_m}{b_+} - N_m^+\right) \right. \right. \\ & + \left(\frac{V_m - N_m^+ b_{+-}}{b_-}\right) \log \left(\frac{V_m - N_m^+ b_{+-}}{b_-}\right) - N_m^- \log N_m^- \\ & \left. \left. - \left(\frac{V_m - N_m^+ b_{+-}}{b_-} - N_m^-\right) \log \left(\frac{V_m - N_m^+ b_{+-}}{b_-} - N_m^-\right) \right\} \right. \\ & \left. + N^+ \log N^+ - \sum_i a_i^+ \log a_i^+ + N^- \log N^- - \sum_n a_n^- \log a_n^- \right] \end{aligned}$$

In the above expression for W_{+-} , N_m^+ 's and N_m^- 's involve differently. This is due to the fact that for convenience of our calculation, we have supposed that the positive ions are distributed first and then the negative ions. We could have also considered the distribution of negative ions first and then the positive ions. But the thermodynamic probability, which is connected with the entropy, should evidently be symmetrical with respect to N_m^+ , N_m^- , b_+ and b_- . Now this is achieved by symmetrisation (cf. Dutta IV, 1949),

$$\log W = \frac{1}{2} (\log W_{+-} + \log W_{-+})$$

Thus we get

$$\begin{aligned} \log W = & \left[\frac{1}{2} \sum_m \left\{ \left(\frac{V_m}{b_+}\right) \log \left(\frac{V_m}{b_+}\right) - N_m^+ \log N_m^+ - \left(\frac{V_m}{b_+} - N_m^+\right) \log \left(\frac{V_m}{b_+} - N_m^+\right) \right. \right. \\ & + \left(\frac{V_m - N_m^+ b_{+-}}{b_-}\right) \log \left(\frac{V_m - N_m^+ b_{+-}}{b_-}\right) - N_m^- \log N_m^- \\ & - \left(\frac{V_m - N_m^+ b_{+-}}{b_-} - N_m^-\right) \log \left(\frac{V_m - N_m^+ b_{+-}}{b_-} - N_m^-\right) \\ & + \left(\frac{V_m}{b_-}\right) \log \left(\frac{V_m}{b_-}\right) - N_m^- \log N_m^- - \left(\frac{V_m}{b_-} - N_m^-\right) \log \left(\frac{V_m}{b_-} - N_m^-\right) \\ & + \left(\frac{V_m - N_m^- b_{+-}}{b_+}\right) \log \left(\frac{V_m - N_m^- b_{+-}}{b_+}\right) - N_m^+ \log N_m^+ \\ & \left. \left. + \left(\frac{V_m - N_m^- b_{+-}}{b_+} - N_m^+\right) \log \left(\frac{V_m - N_m^- b_{+-}}{b_+} - N_m^+\right) \right\} \right. \\ & \left. + N^+ \log N^+ - \sum_i a_i^+ \log a_i^+ - N^- \log N^- - \sum_n a_n^- \log a_n^- \right] \end{aligned}$$

Now this is to be maximised subject to the following conditions

$$\left. \begin{aligned} \sum_i a_i^+ &= N^+, \\ \sum_n a_n^- &= N^-, \\ \sum_m N_m^+ &= N^+, \\ \sum_m N_m^- &= N^-, \\ \sum_i a_i^+ E_i^+ + \sum_n a_n^- E_n^- + \sum_m N_m^+ e_+ \psi + \sum_m N_m^- e_- \psi &= E \end{aligned} \right\} \quad \dots (3)$$

where N^+ , N^- and E remain constant in this variation.

Hence variation subject to the above conditions gives

$$\begin{aligned} \sum_i a_i^+ &= e^{-\lambda_+ - \mu E^+} \quad (\text{for all } i's) \\ \sum_n a_n^- &= e^{-\lambda_- - \mu E^-} \quad (\text{for all } n's) \\ \left(\frac{V_m}{N_m^+ b_+} - 1 \right)^{\frac{1}{2}} \left(\frac{V_m - N_m^- b_{+-}}{N_m b_+} - 1 \right)^{\frac{1}{2}} \left(1 - \frac{N_m^- b_{+-}}{V_m - N_m^+ b_{+-}} \right)^{\frac{b_{+-}}{2b_+}} &= e^{\nu_+ + \mu e_+ \psi} \\ \left(\frac{V_m}{N_m^- b_-} - 1 \right)^{\frac{1}{2}} \left(\frac{V_m - N_m^+ b_{+-}}{N_m b_-} - 1 \right)^{\frac{1}{2}} \left(1 - \frac{N_m^+ b_{+-}}{V_m - N_m^- b_{+-}} \right)^{\frac{b_{+-}}{2b_-}} &= e^{\nu_- + \mu e_- \psi} \end{aligned}$$

(for all m 's)

where λ_+ , λ_- , ν_+ , ν_- and μ are Lagrange's undetermined multipliers.

It will now be assumed that

$$N_m^+ b_+, N_m^+ b_{+-}, N_m^- b_-, N_m^- b_{+-} \ll V_m$$

Neglecting higher order terms, we get

$$\begin{aligned} \frac{V_m}{N_m^+ b_+} \left(1 - \frac{N_m^+ b_{+-}}{V_m} - \frac{N_m^- b_{+-}}{V_m} \right) &= e^{\nu_+ + \mu e_+ \psi} \\ \frac{V_m}{N_m^- b_-} \left(1 + \frac{N_m^- b_{+-}}{V_m} - \frac{N_m^+ b_{+-}}{V_m} \right) &= e^{\nu_- + \mu e_- \psi} \end{aligned}$$

Writing $n_m^+ = \frac{N_m^+}{V_m}$, $n_m^- = \frac{N_m^-}{V_m}$ and omitting suffices, we have, for any layer

where the potential is ψ ,

$$\frac{1}{n^+ b_+} \left(1 - n^+ b_{+-} - n^- b_{+-} \right) = e^{\nu_+ + \mu e_+ \psi}$$

and

$$\frac{1}{n^- b_-} \left(1 - n^- b_{+-} - n^+ b_{+-} \right) = e^{\nu_- + \mu e_- \psi}$$

or,

$$n_+ b_+ (1 + n^- b_{+-}) = \frac{1}{e^{\nu_+ + \mu e_+ \psi} + 1},$$

and

$$n_{-}b_{-}(1+n_{+}^{*}b_{+-}) = \frac{1}{e^{\nu_{-}+\mu\epsilon_{+}\psi} + 1}$$

Approximating we have

$$n_{+}^{*} = \frac{\frac{1}{b_{+}}}{e^{\nu_{+}+\mu\epsilon_{+}\psi} + 1} = \frac{A_{+}}{B_{+}e^{\mu\epsilon_{+}\psi} + 1}$$

$$n_{-}^{*} = \frac{\frac{1}{b_{-}}}{e^{\nu_{-}+\mu\epsilon_{-}\psi} + 1} = \frac{A_{-}}{B_{-}e^{\mu\epsilon_{-}\psi} + 1}$$

where A_{+} , A_{-} , B_{+} and B_{-} are constants.

Now we shall have to find out the value of μ . From Boltzmann's hypothesis and correcting upto first approximation, we have from (2)

$$S = k \left[\sum_m \left\{ N_m^{+} \log \left(\frac{V_m}{N_m^{+} b_{+}} - 1 \right) + N_m^{-} \log \left(\frac{V_m}{N_m^{-} b_{-}} - 1 \right) \right. \right. \\ \left. \left. - \left(\frac{V_m}{b_{+}} \right) \log \left(1 - \frac{N_m^{+} b_{+}}{V_m} \right) - \left(\frac{V_m}{b_{-}} \right) \log \left(1 - \frac{N_m^{-} b_{-}}{V_m} \right) \right. \right. \\ \left. \left. + \frac{1}{2} \frac{N_m^{+} b_{+-}}{b_{-}} \log \left(1 - \frac{N_m^{-} b_{-}}{V_m} \right) + \frac{1}{2} \frac{N_m^{-} b_{+-}}{b_{+}} \log \left(1 - \frac{N_m^{+} b_{+}}{V_m} \right) \right. \right. \\ \left. \left. + \frac{1}{2} N_m^{+} \log \left(1 - \frac{N_m^{-} b_{+-}}{V_m} \right) + \frac{1}{2} N_m^{-} \log \left(1 - \frac{N_m^{+} b_{+-}}{V_m} \right) \right\} \right. \\ \left. + N^{+} \log N^{+} - \sum_i a_i \log a_i + N^{-} \log N^{-} - \sum_n a_n \log a_n \right]$$

Substituting the values

$$\frac{N_m^{+} b_{+}}{V_m} = \frac{1}{e^{\nu_{+}+\mu\epsilon_{+}\psi} + 1}$$

and

$$\frac{N_m^{-} b_{-}}{V_m} = \frac{1}{e^{\nu_{-}+\mu\epsilon_{-}\psi} + 1}$$

obtained from equation (4), we have

$$S = k \left[\sum_m \left(\frac{V_m}{b_{+}} \right) \log \left(1 + e^{-\nu_{+}-\mu\epsilon_{+}\psi} \right) + \left(\frac{V_m}{b_{-}} \right) \log \left(1 + e^{-\nu_{-}-\mu\epsilon_{-}\psi} \right) \right. \\ \left. - \frac{1}{2} \frac{b_{+-}}{b_{-}} \left[\frac{V_m}{b_{+}} \right] \frac{\log \left(1 + e^{-\nu_{-}-\mu\epsilon_{-}\psi} \right)}{1 + e^{\nu_{+}+\mu\epsilon_{+}\psi}} + \frac{1}{2} \frac{b_{+-}}{b_{+}} \left(\frac{V_m}{b_{-}} \right) \frac{\log \left(1 + e^{-\nu_{+}-\mu\epsilon_{+}\psi} \right)}{1 + e^{\nu_{-}+\mu\epsilon_{-}\psi}} \right. \\ \left. + \frac{1}{2} \left[\frac{V_m}{b_{+}} \right] \frac{\log \left(1 - \frac{b_{+-}}{b_{-}} \frac{1}{1 + e^{\nu_{-}+\mu\epsilon_{-}\psi}} \right)}{1 + e^{\nu_{+}+\mu\epsilon_{+}\psi}} + \frac{1}{2} \left[\frac{V_m}{b_{-}} \right] \frac{\log \left(1 - \frac{b_{+-}}{b_{+}} \frac{1}{1 + e^{\nu_{+}+\mu\epsilon_{+}\psi}} \right)}{1 + e^{\nu_{-}+\mu\epsilon_{-}\psi}} \right] \\ \left. + N^{+} \log N^{+} + N^{-} \log N^{-} + N^{+} (\lambda_{+} + \nu_{+}) + N^{-} (\lambda_{-} + \nu_{-}) + \mu E \right]$$

Then by well-known thermodynamic relation

$$\frac{1}{T} = \left\{ \frac{\delta S}{\delta E} \right\}_v$$

we have

$$\frac{1}{T} = k\mu \quad \text{or} \quad \mu = \frac{1}{kT}.$$

The other Lagrangian constants λ_+ , λ_- , ν_+ , ν_- are to be determined from the equation (3) as shown already (Dutta, 1947, 1949).

Thus finally we have

$$n_+ = \frac{A_+}{B_+ e^{\epsilon_+ \psi / kT} + 1},$$

$$n_- = \frac{A_-}{B_- e^{\epsilon_- \psi / kT} + 1},$$

In Bagchi's paper referred to above, the constants A_+ and A_- were both taken to be equal to N , the concentration of the total number of ions. Now when the charges on the ions are of equal magnitude, the average distance of closest approach between two positive charges should be equal to that between two negative charges. The crystal structure of alkali halides also point to the same conclusion. Hence in these cases b_+ should be equal to b_- so, A_+ to A_- . Moreover, it is found to be of the same order of magnitude as N .

DEPARTMENTS OF PURE PHYSICS
AND PHYSICAL CHEMISTRY,
UNIVERSITY COLLEGE OF SCIENCE,
CALCUTTA.

REFERENCES

- Bagchi, S. N., 1949, *J. Ind. Chem. Soc.* (in press).
Dutta, M., 1947, *Proc. Nat. Inst. Sc. India*, **13**, 247
" , 1948, *ibid*, " , **14**, 163.
Dutta, M , 1949, *Proc Nat Inst. Sc India* (in press)
" , 1949a " "

THE SPECTRO-CHEMICAL ANALYSIS OF MOLYBDENUM IN THE GREEN PEAS

By M. K. GHOSH AND K. C. MAZUMDER

(Received for publication, Nov. 28, 1949)

(Plate II)

ABSTRACT The spectrum of the green pea ash consists mostly of the lines of P, Mg, Ca, K and Al and these can be taken as the major elements present in the ash. The lines of Zn, Mn, Mo, Cu, Na, Ba, Fe and Si are also found, from the intensities of the lines these latter elements can be considered to be the trace elements in peas. The quantitative estimation of the Mo-contents has been carried out. For the Indian peas it is found to be 0.015% and for the American tinned peas, 0.007%.

INTRODUCTION

Spectroscopes are being used in the western countries not only for estimating the ferrous and non-ferrous alloys but also for that of the trace elements in soils and agricultural and garden products. The spectroscopes have been found quite helpful in controlling both quality and quantity of these products. The technique of spectro-chemical analysis of the ferrous and some of the non-ferrous alloys having been developed at Tata. We have tried to employ spectroscopes for the study of the trace elements in the plants and vegetables grown in the neighbourhood of Jamshedpur. The soil of the locality is known not to have pronounced productivity for vegetables and it is of interest to know if this is due to the absence, shortage or superfluity of these trace elements generally found in particular vegetables. We have decided to start our investigation into this field with green peas grown in our garden at Jamshedpur. A preliminary survey of the spectrum of the ash of the peas showed that it consisted mostly of the lines of the elements P, Mg, Ca, K and Al. The lines are very bright and numerous indicating that the elements exist in the ash as more than mere traces. Lines belonging to the elements Zn, Mn, Mo, Cu, Na, Ba, Fe and Si are also found in the spectrum; but from their intensities it can be concluded that their percentages cannot be very large and some of them are mere traces. The spectrum of the carbon rods used for holding the ash contains faintly visible primary lines of Ca, Mg and Cu. A few iron lines and two Si-lines are barely visible. Two primary Na-lines are occasionally visible. The carbon rods (graphite rods when used) are kept in dilute acid for a fairly long time, then washed and heated to whiteness. Just before putting the sample they

are sparked for some time. After these treatments mere traces of the lines of Mg, Ca, and Cu only are visible showing indisputably that the elements listed above are really present in the ash. The ash of the plant as well as that of the covers have also been sparked and the spectrum photographed in the same way as that of the seeds. The spectrum of the salt recovered from the garden soil has also been taken. All the elements found in pea ash exist also in these substances. The barium lines for the soil are very bright; those corresponding to the plant are next in brightness: those corresponding to the pea and its cover are rather faint. The Mo-lines for the soil are very faint. The supply of the garden peas being insufficient we decided to carry on the preliminary work with the dried peas, obtained from the local market. These, it seems, are imported from different parts of Bihar Province. The relative intensities of the lines belonging to the different elements are almost the same for both varieties of the peas. After these qualitative work we started quantitative test for a few selected elements like, Mo, Zn, and Ba but have succeeded in finishing the work on Mo only.

For photographing the spectra the medium quartz spectroscop has generally been used. But for identifying lines in doubtful cases the large quartz spectroscop has occasionally been used.

EXPERIMENTAL

For the quantitative work Hilger medium quartz spectroscop only has been used. The following are the conditions for the excitation of the spectra.

Voltage	... 15,000
Capacity	... 0.005 μ F
Inductance	... 0.06 MH
Sp. gap	... 2.0 mm
Upper electrodes	Pointed C-rods
Lower	... C-rods with a cup formed at the tip

As mentioned previously, for the initial work the peas (also plants and soil) were obtained from the garden attached to our house at Jamshedpur. For the quantitative test by the spectroscop a thorough chemical analysis for the major elements occurring in the ash being necessary and the supply of the garden peas being quite insufficient the necessary stock of dried peas has been purchased in the local market. Peas are first washed thoroughly in tap water and then in distilled water. After drying in the sun the weight is taken. They are then burnt for about three hours in an oven, the temperature of which is about 750°C. All these are done in a platinum

crucible. The ash is then cooled in a desiccator and weighed. For a particular lot the percentage of the ash has been found to be 2.70. The creepers and the covers are also similarly treated. For recovering salts of the soil 250 gms. of it have been kept in dilute HCl for twelve days. The solution is then filtered and dried. The spectrum of the salt has been taken in the same way as those of the ashes of peas, plants and covers.

The quantitative work has been confined to the ash of the seeds for the present and the test has been completed only for the Mo-contents. The standard samples of ash necessary for the spectro-chemical work have to be prepared synthetically. To do so, one has to know the percentages of the major elements present in a typical ash by the chemical method. The results of such a chemical analysis are as follows :—

SiO ₂	...	0.20%
Fe ₂ O ₃	...	0.04%
Al ₂ O ₃	...	1.51%
MnO	...	0.19%
CaO	...	4.6
MgO	...	8.45%
K ₂ O	...	50.06%
Na ₂ O	...	trace
P ₂ O ₅	...	30.65%

These add up to 95.79%. The preparation of the synthetic ash has been carried out by adding together the above items (excluding Fe₂O₃ and Na₂O) in the following way :

SiO ₂	0.29 gm. fused and ppt. sample
Al ₂ O ₃	1.51 ,, made by burning alum
MnO	0.20 ,, Merk
CaCO ₃	8.20 ,, ,,
K ₂ CO ₃	64.80 ,, ,,
MgO	8.40 ,, U.S.A.
H ₃ PO ₄	42.00 ,,

equivalent of 47.20 gr. of Merk 86% acid.

H_3PO_4 is first added to K_2CO_3 and mixed well. MgO is next added. All other items are then added and mixed well. The mixture is ignited at 950°C . The ash thus prepared is found in the form of lump. It is broken into small pieces which are weighed in different weighing bottles. The ash thus prepared is hygroscopic and should be kept in a desiccator. The requisite amounts of Am. molybdate solution (Merk) is then added to the ash transferred to an agate mortar. They are then thoroughly mixed. The mortar containing the mixture is next placed in an air-bath at a temperature of about 140°C . The mixture is then finally powdered while the mortar is still hot and transferred to the weighing bottles. The bottles are kept in the desiccator. In this way the ashes containing 0.01, 0.02, 0.05, 0.10, 0.20 and 0.3% molybdenum have been prepared.

Each of these samples is placed in the cup of the lower electrode (using a fresh pair of electrodes for each sample), sparked and the spectrum photographed. A smooth calibration curve for Mo has been obtained with these synthetic ashes showing that the procedure adopted is correct. The Mo-content of the real ash can now be determined by photographing the spectrum of it on the same plate as those of the synthetic ashes. The quantitative estimation of Mo by photometric measurement of the intensities of the spectral lines has been carried out in the usual way. It has been described previously Ghosh and Mazumder (1948).

RESULTS

The spectrum reproduced in Plate II shows that the lines of K, P, Mg, Ca, and Al are very bright; these are then the major elements contained in the ash. This conclusion is supported by the result of the chemical analysis. The lines of Zn, Mn, Mo, Cu, Na, Ba, Fe and Si are also seen in the figure; some of them are barely visible. These elements exist in the ash as mere traces. They can, therefore, be spectroscopically estimated and we have undertaken the work of such quantitative estimation for some of these elements, namely, Mo, Zn, and Ba. But the time at our disposal has permitted us to complete the work on Mo only. The different estimations of the molybdenum contents in the ash of the dried peas, obtained from the local market and those of our garden have yielded the values 0.015, 0.014 and 0.015%. Two of the calibration curves, from which these values have been obtained, are given in Figs. 1 and 2. The curves are regular and smooth. The values read from them are therefore accurate. The estimation of the Mo-contents in the tinned peas of the American origin has also been attempted. Two estimations from a particular sample have yielded the values 0.008 and 0.006%. These are much lower than those of the Indian dried peas. It cannot, however, be inferred from this result that the American peas contain smaller amount of Mo than those grown in India.

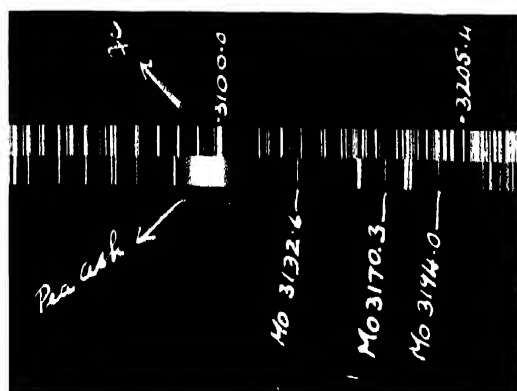


Fig. 1.

The treatment given to the peas for tinning may be responsible for such lower values.

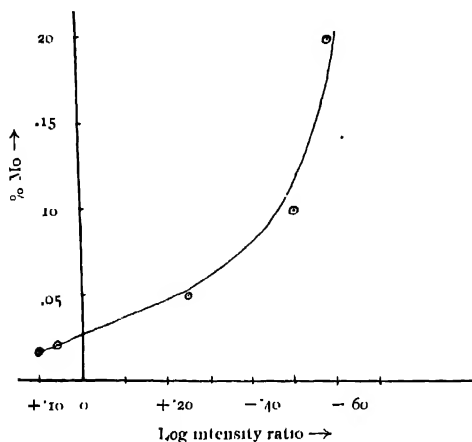


FIG. 1

Mo in pea ash Local pea "Crossed circle" - 0.015%

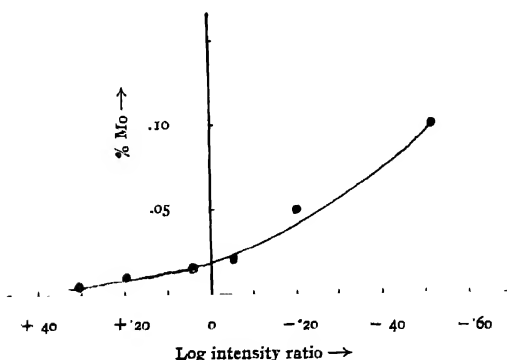


FIG. 2

Mo in pea ash Local pea - "Dot" - 0.014% American pea - "Dot" - 0.06%

We have not had the privilege of seeing the report of such work done in India or abroad. We even do not know if spectro-chemical (quantitative) analysis of this nature has ever been attempted in India. Our interest, however, is in the development of the technique primarily for the study of the local vegetables.

ACKNOWLEDGMENTS

In conclusion the authors record their gratefulness to the Tata Authorities and Dr. J. C. Ghosh, the Chief Chemist, for permission and facilities given for this investigation. They also appreciate very much the help rendered by Mr. R. C. Dutta, the Chemist, by carrying out the chemical analysis of the ash.

THE NEW CONTROL AND RESEARCH
LABORATORY, TISCO, JAMSHEDPUR.

REFERENCE

Ghosh, M. K. and Mazumder, K. C., 1948, *Ind. Jour. Phys.*, **22**, 409.

ON THE VARIATION OF CURRENT WITH DISTANCE BETWEEN THE ELECTRODES OF A GLOW DISCHARGE IN GASES AT LOW PRESSURE

By M. KHURSHED HUSAIN

(Received for publication, June 24, 1949)

ABSTRACT. Measurement of current strength with variation of distance between the electrodes of a glow discharge reveal that with the anode in the negative glow the current shows a maxima before falling to zero when the anode reaches the boundary of the cathode dark space. In the present paper it is suggested that when the anode is in the negative glow a stream of positive ions flows from the negative glow to the cathode dark space, which is not inconsistent with the assumptions of Sir J. J. Thomson.

INTRODUCTION

According to Sir J. J. Thomson's theory (1905) the glow discharge, in a gas at low pressure, is maintained by the continuous liberation of the secondary electrons from the cathode surface by the bombardment of the positive ions, that are produced wholly in the cathode dark space by the electrons. Aston (1911), Geddes (1925), and Guntherschulze (1923-24) also working on electric discharge through gases under similar conditions found the dark space to be the most active region of the glow. Observations by Schuster (1890) and Wehnelt (1890) on the formation of shadows on the cathode by placing solid obstacles in the dark space and the diminution of the thickness of the cathode dark space by the application of a magnetic field at right angles to the discharge studied first by Guntherschulze (1924) support very much the theory put forward by Thomson.

Different explanations have, however, been given by various experimenters with respect to the supply of the positive ions which bombard the cathode surface and thus maintain the discharge. Ryde (1923) holds that the supply of positive ions to the cathode dark space is mainly from the negative glow which acts as an emitter and the cathode as a collector. Loeb (1939) believes that there is always a rush of the positive ions from the negative glow to the cathode dark space. Compton and Moise (1927) assume that the flow of the positive ions from the negative glow will take place particularly when the discharge is abnormal. Compton's view is probably based on the fact that in an abnormal discharge the ionisation in the dark space is much less intense than in the normal case and it is, therefore, likely that a part of the supply of the positive ions may be from the negative glow. No sufficient experimental evidence is, however, available to substantiate these views.

A detailed study of the variation of current with the distance between the electrodes of a glow discharge under different conditions of pressure and voltage can only throw light on this problem. Thomson (1931) observed that if the distance between the electrodes is much greater than the thickness of the cathode dark space and the anode is gradually moved towards the cathode without disturbing the pressure in the tube, no change in the current is observed till the anode reaches very near to the boundary of the cathode dark space when the current begins to fall very rapidly as the distance between the electrodes is decreased and it requires a very small further diminution in the distance to stop the discharge altogether. These observations which were probably carried out at lower voltages, as is evidenced by our observations, substantiated his theory.

No systematic work appears to have been done which may throw sufficient light on this problem. The author has, therefore, carried out experiments under various pressures and voltages to study in greater details the variation of the current with the anode at different distances from the cathode in order to throw further light on the mechanism of the maintenance of the glow discharge.

APPARATUS

The main apparatus consisted of a discharge tube of pyrex glass 5 cm. s. in diameter sealed at its two ends by means of sealing wax to two hollow brass cases fitted with a fixed and a movable electrode—both being brass discs of 4 cms. diameter and 3 mm. thickness. The upper movable electrode was made to move up and down by the rotation of a brass rod r sealed firmly

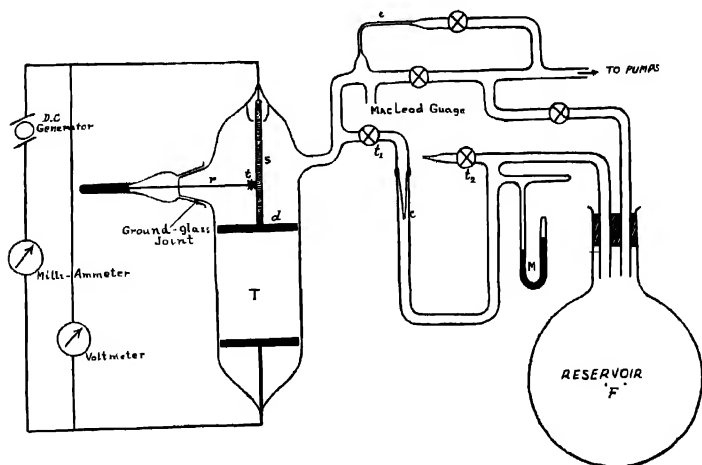


FIG. 1

in a ground glass joint by means of sealing wax. The rod r has a toothed wheel t at its other end, the teeth of which were fixed in the groves of the stem s fitted with the disc d . The arrangement was such that a motion of even a fraction of a millimetre was practicable without disturbing the pressure in the discharge tube.

In order to maintain a desired pressure in the discharge tube the apparatus was fitted with a 'leak system'. A flask F of a considerable capacity was connected to the main apparatus through a leak of a very finely drawn capillary c . The reservoir F was also connected to the pumps and could be exhausted to any desired pressure.

The apparatus was exhausted by Gaede's all-steel mercury diffusion pump backed by a Cenco Hyvac pump, and then the leak, c , was connected to the main apparatus by opening the stop cock l , and at the same time the discharge tube was also connected to the pumps through another capillary e . After a short time the gas entering and leaving the tube regulates its flow resulting in the maintenance of a constant pressure in the discharge tube. As the pressure in the discharge tube depends on the pressure in the reservoir, it can be varied by altering the pressure in the reservoir. The pressure adjusted by this method remains constant for several hours.

The pressure of the discharge tube was measured by a McLeod gauge connected to the main apparatus. The distance between the electrodes was measured by means of a cathetometer.

EXPERIMENTAL PROCEDURE AND RESULTS

Having obtained the steady pressure in the discharge tube, the electrodes were connected to a D C motor-generator and were kept at a fairly good distance. The readings of current and voltage were taken when they attained a constant value. The upper electrode was then gradually moved towards the cathode and its positions with the current and voltage were recorded at different distances. The movement was made slower when the variation in the current took place till the discharge went off. At a constant pressure a number of sets of observations with different voltages were taken.

At lower voltages the current remains practically constant by the gradual decrease in the distance between the electrodes till the anode reaches very near the boundary of the cathode dark space when it begins to fall rapidly and goes off abruptly for further diminution in the distance between the electrodes. At higher voltages, however, the current does not remain constant, but increases when the anode enters the negative glow till a certain stage comes when it attains a maximum value and then on further decreasing the distance, the current begins to fall and the discharge goes off. The maximum is always very near to the boundary of the cathode dark space. The increase in the current is followed by a decrease in the voltage and vice-versa. The increment of current was found proportional to the voltage.

The graphs between current and distance between the electrodes show that the current after reaching the maximum value decreases approximately to the same value, which it had when the distance between the electrodes was fairly large. Observations are given graphically in Figs. 2, 3, 4 and 5.

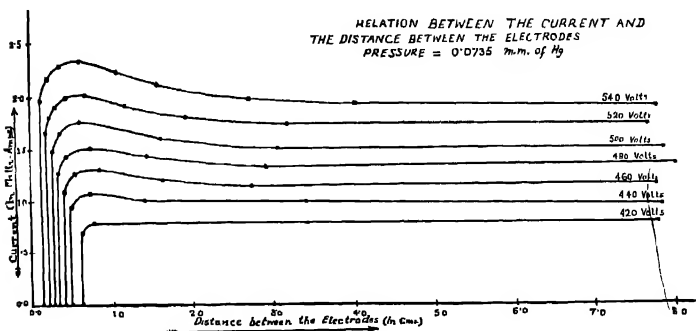


FIG. 2

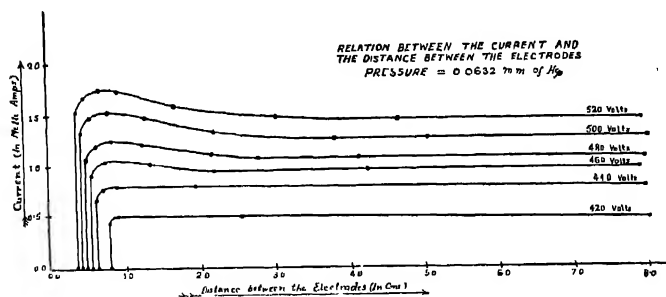


FIG. 3

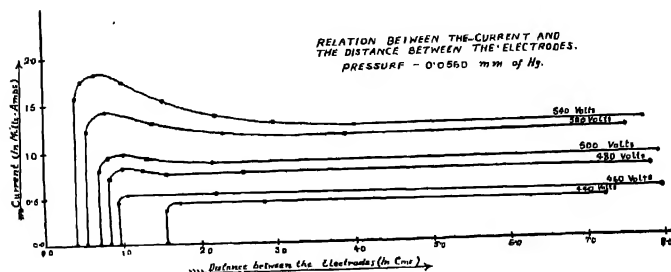


FIG. 4

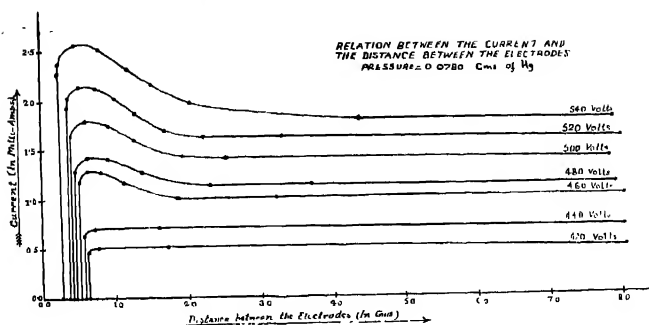


FIG. 5

DISCUSSION OF RESULTS

Thomson believes that positive ions flowing to the cathode come wholly from the cathode dark space. On this assumption there should be no change in the discharge current when the distance between the electrodes is gradually decreased till the anode reaches the boundary of the cathode dark space. At the slightest decrease in this distance the current should at once drop to zero.

Observations by the author confirm this fact to a great extent at only lower voltages when the current strength is very low. At higher voltages the current begins to increase when the anode reaches the negative glow. In every curve there is a maximum which is always very near the boundary of the cathode dark space. The current then begins to decrease rather rapidly and falls to zero for the slightest decrease in the distance when the anode is on the boundary of the dark space. As the curves show that the rate of rise of the current is proportional to the voltage applied at a constant pressure; it can perhaps be assumed that the same phenomenon occurs even at lower voltages but cannot be detected on account of the insensitiveness of the detecting instrument for variation of current of this order.

"The electric force in the negative glow is exceedingly small, so small that it is doubtful if we have at present the means of determining it with any approach to accuracy." (Thomson, 1933). Hence the density of the positive ions is approximately equal to that of electrons in this region. As there is no force sufficient to drag the positive ions and the electrons away, there will be a great loss of ions due to their recombination. This should hold only so long as the anode is at a sufficiently large distance from the cathode, i.e., away from the region of the negative glow. When the anode enters the negative glow, the electrons present in this region are attracted by it. On account of its potential according to Langmuir and Mott-Smith (1924), these electrons do not act as a sheath in front of the anode but pass

into it. Thus a number of electrons, that would have been lost due to recombination in the negative glow in the absence of the anode in that region, will now pass on to it, giving an increase in the current. Also the positive ions present in the negative glow will be repelled when the anode reaches there and will tend to move towards the cathode dark space. This will result in sending a stream of positive ions from the negative glow into the cathode dark space. Thus the ions reaching the cathode will increase giving a rise in the current. As the anode will move towards the dark space the number of ions entering the cathode dark space will also go on increasing till a stage will come when most of the negative glow will be cut off and the ions present in the remaining portion of the dark space will themselves decrease, causing a diminution in the number of ions entering from the negative glow to the cathode dark space. There will be practically no ions in the negative glow that can be sent to the dark space when the anode reaches very near to its boundary and hence the current should be the same as it was when the anode was at a fairly large distance from the cathode. Thus a kink should be observed in current-distance graph. The increment of the current should be proportional to the voltage as the force required to send the ions to the cathode dark space from the negative glow increases with the increase of the voltage.

This shows that for fairly large distances between the electrodes the positive ions striking the cathode come wholly from the dark space and a very few may enter from the negative glow; but when the distance is such that the anode is in the region of the negative glow the positive ions continuously flow from it to the cathode dark space. Thomson's assumption, is, therefore, true for only large distance between the electrodes. For such small distances there must also be a potential gradient in the negative glow and there must be a deviation from Aston's law for the electric force in the cathode dark space.

Experiments with different electrodes in different gases are still in progress.

ACKNOWLEDGMENT

The author is under deep sense of gratitude to Dr. Sh. Nawazish Ali, Chairman, Department of Physics Muslim University, Aligarh, for his continuous assistance and valuable suggestions without which this work could not be completed.

DEPARTMENT OF PHYSICS, MUSLIM UNIVERSITY,
ALIGARH.

REFERENCES

- Aston, P. W., 1911, *Proc. Roy. Soc. A*, **84**, 526.
Compton and Morse, 1927, *Phys. Rev.*, **30**, 305.
Geddes, A. D. M., 1925, *Roy. Soc. Edin. Proc.*, **46**, 2.
Gunther Schulze, 1923, *Zeits. f. Phys.*, **20**, 1
Gunther Schulze, 1924, *Zeits. f. Phys.*, **23**, 334
Gunther Schulze, 1924, *Zeits. f. Phys.*, **24**, 140
Langmuir, I. and Mott Smith, 1924, *Gen. Elect. Rev.*, **27**, 538.
Loeb, L. B., 1939, *Fundamental Processes of Electrical Discharge in Gases*
Ryde, J. W., 1923, *Phil. Mag.*, **11**, 1149
Schuster, 1890, *Proc. Roy. Soc.*, **44**, 557.
Thomson, J. J., 1905, *Camb. Phil. Soc. Proc.*, **13**, 212
Thomson, J. J., 1931, *Phil. Mag.*, **11**, 677.
Thomson, J. J. and Thomson, G. P., 1933, *Conduction of Electricity Through Gases*,
3rd Edition, 2 pp. 350
Wehnelt, 1890, *Wied. Ann.*, **47**, 557

MICROSEISMS

BY A. N. TANDON

(Received for publication, Dec. 6, 1949)

ABSTRACT. The type, nature and origin of different microseismic phenomenon have been summarised. The relation existing between microseisms and disturbed weather has been discussed and the latest work in America on the tracking of storms when they are far out at sea, with the help of microseisms, has been described.

Sensitive type of seismographs which are used for recording distant earthquakes also record in addition certain earth tremors of very small amplitudes, the origin of which cannot be attributed to any tectonic phenomenon. These minute vibrations have periods which cover a wide range, and the amplitudes vary from day to day. Vibrations of this nature have been given the name "microseisms". In most of the studies of this subject the term "microseisms" has been restricted to mean those vibrations which have a period ranging from about 2 to 10 seconds.

CLASSIFICATION OF MICROSEISMS

Microseisms have mainly been classified according to their periods and forms, which largely depend on the source of origin of the microseisms. Benerji (1930) found the existence of at least three distinct types of microseisms as recorded on a Milne-Shaw seismograph installed in an underground room at a depth of 15 feet at the Colaba observatory, Bombay. The results of his investigations are tabulated below (Table I).

TABLE I

Type of Microseisms	Range of periods	Form	Period of the year when most prominent	Probable cause
Long period	10 - 30 s	Irregular	Winter months	Gusty winds producing waves in shallow water.
2 Monsoon type		Regular & continuous wave trains.	May-Sep	Generation of waves by monsoon winds in deep sea.
3 Storm type	4-6 secs	Characteristic irregular variation of amplitude	During pre & post monsoon period whenever there is storm in Indian sea.	Large waves generated in storm causing pressure fluctuation on sea bed

In addition to the above there are other types of short period microseisms caused by road and rail traffic, blasting operations, vibrations of buildings, etc. These will be described in the next section. As has already been mentioned earlier most workers have confined their attention to the study of microseisms with periods ranging between 2 and 10 seconds, and which are associated with some kind of disturbed weather. Gilmore (1946) has published a classification of microseisms associated with weather disturbances. His classification is based on a study of seismographic records during periods of storms in the Caribbean Sea by the method of tripartite station. The details of this method are described later. According to him different kinds of atmospheric phenomena give rise to microseisms which can be classified according to their periods, amplitude, form and duration. Any change in weather phenomenon over the sea within a distance of nearly 300 miles of a microseismograph station, can usually be recorded as distinct type of microseisms. Well developed hurricanes can be followed up to a distance of 2000 miles. Gilmore's classification is given in Table II

TABLE II

Kind of weather.	Type	Period secs	Amplitude	Form	Average duration.
Hurricanes	Well formed peak good build ups.	2-7 Slow change.	3 to 30	Very regular	3 to 10 days
Cold Fronts	Fair peaks & build ups.	1-4 rapid change	3 to 12	Regular to irregular.	1 to 3 days
Thunder storms	Good peaks & fair build ups	1-3 nearly constant	3 to 5	Do	3 to 7 hours
High Winds	No definite peaks, irregular.	1-10 rapid change	3 to 10	Very irregular.	1 to 10 days
Fair	No definite peaks, irregular	Irregular	Normal 1.5 to 2.5	Very irregular.	1 to 15 days

PERIODS OF MICROSEISMS

As has already been mentioned above microseisms have been found to cover a very large range of periods. The prominence of microseisms of particular range of frequency depend upon the free period of the instrument used. While long-period seismographs record microseisms of longer period prominently, the record of the short-period instruments have shown

microseisms of shorter periods. The most prominent group of periods which arrest our attention was that in the 4-8 secs range. As early as 1908 Milne, and Galitzin in 1910 recognized, on the records of long period instruments, microseisms having periods ranging from 20-40 secs. Banerji (1930) pointed out the existence of microseisms having periods ranging from 10 to 30 seconds caused by high winds blowing over shallow sea. These microseisms are more prominent in winter than during the rest of the year.

Microseisms having periods ranging from 1 to 3 seconds are always found on the records of short-period instruments like Sprengnether, Macelwane, Wood-Anderson and Benioff seismographs. These microseisms correspond to one of the types described by Gilmore.

About 1930 Macelwane had noticed regular microseisms of periods between .2 to .5 secs appearing daily on the records of short-period Wood-Anderson seismographs. These microseisms have been characterised by their true wave form, long series of waves and exceedingly low amplitudes. Carder and Gilmore (1945) have also mentioned about these short-period microseisms. The range of periods found by them lies between .15 and 0.5 seconds. Besides the above, microseisms of shorter periods (.01 to .05 secs) have been found in the records sensitive geophones and also on the records of seismographs installed on a foundation consisting of fine sand.

A detailed study of the microseisms of the period range .2 to .5 is being conducted in America by Ramirez (1948) who is using the method of tripartite stations. The units of the station are situated at a distance of 600 to 800 ft. Each station has been equipped with 3 components of sensitive capacity seismographs made by Sprengnether and Co., a short period Benioff microbarograph and a long-period Macelwane microbardiograph. A magnification of about half a million is achieved for these seismographs by means of high-gain capacity pick-up device. Recording is done centrally on single tape recorder. A galvanometer bank consisting of 12 d'Arsonval galvanometers has been specially designed. Results of the investigations have not yet been published.

AMPLITUDE OF MICROSEISMS

The amplitude of microseisms on a seismogram depends mainly on the sensitivity of the seismograph, the distance of the source of microseisms, the type of lithologic foundation of the seismograph station and the intensity of the disturbance at the source. Therefore, in order to compare the relative amplitudes at different stations it is necessary to reduce the amplitudes to standard conditions of rock. The standard generally chosen is that of Rayleigh waves in the underlying 'granitic layer'. The standard amplitude is determined by measuring the observed amplitude and dividing it by a factor which represents the magnification due to the sedimentary layers. This factor depends upon the ratio of the horizontal amplitude A_H to the vertical amplitude A_z .

In the case of rock, the value of A_H/A_Z has been found to be 0.7. A_H/A_Z for consolidated rocks is nearly unity and the horizontal amplitudes are 20 to 100% larger. For weak formations the horizontal amplitudes are found to be 4 to 5 times larger.

For a single station using a seismograph with the same constants the day-to-day amplitudes can be compared by directly measuring the amplitudes on the seismogram. In order to compare the amplitudes recorded by various types of instruments having different periods and damping constants it is necessary to express the microseismic amplitudes in terms of earth motion. This is generally expressed in Microns (1 Micron = 0.001 mm). It has been found that the amplitudes of microseisms is much larger at stations situated at or near the sea coast than those at inland stations. Systematic observations of microseismic amplitudes at both coastal and inland stations have been taken and it has been shown that the amplitudes show a simultaneous increase on all the seismographic stations over a whole continent and also decrease simultaneously. The change is more noticeable at the coastal stations. Various studies relating to the amplitudes of microseisms have been undertaken by different workers in nearly all the parts of the world. The general approach has been to calculate from seismograms the average amplitude at fixed hours, and then make a statistical study. Microseismic amplitudes for many seismological stations are available in printed tabulations. Lee (1934) has made a study of the geographical distribution of microseismic amplitudes, over the European continent. In India systematic study of microseisms was first undertaken by Banerji at the Colaba Observatory, Bombay. Average values of periods and amplitudes of microseisms have been published by him for the years 1924 to 1926 in the Colaba Observatory's annual publication. Banerji (1930) has also shown that the microseismic amplitudes of Colaba or Calcutta show an increase whenever there is a storm in the Arabian Sea or Bay of Bengal. The amplitudes increase as the storm approaches the recording station and show a marked decrease when the storm enters inland. During the period of approach of the S.W. monsoon, the amplitudes show a steady increase until the monsoon has set in when the amplitude changes according to the strength of the south-west winds.

NATURE OF MICROSEISMS

The works of Gutenberg, Lee and others have shown that microseismic waves are surface waves in which nearly all the energy is confined to a depth equal to the wave length of the waves. Lee has further shown that in these waves the more prevalent types are the Rayleigh types of waves in which the earth particles move in ellipses with the longer axis along the direction of propagation. Longitudinal surface waves of the Love type in which the vibrations take place along the direction of propagation are nearly absent.

He has also studied the effect of geological structure of a station on the recorded amplitudes of microseisms and has been able, on the assumption that microseismic waves are surface waves of Rayleigh type, to explain the anomalies in the recorded amplitudes of different stations as well as the variation in the observed ratios of the horizontal to vertical amplitudes at different stations.

The horizontal amplitudes are generally greater for stations situated on recent formations than those situated on rock. The ratio of the horizontal to vertical amplitudes depends upon the thickness of the surface layer over the underlying granitic layer. This effect is more pronounced on horizontal amplitudes than on vertical amplitudes upto a thickness of 1 Km. of the superficial layer. For stations situated on Archaen rocks the ratio of horizontal to vertical amplitudes has been found to be 0.7 which is in agreement with theory. For stations with consolidated foundations the ratio has been found to be nearly unity, as would be anticipated from the theory of Rayleigh waves in stratified media. For weak formations like alluvium, the amplitude of the horizontal component is 2 to 3 times larger than that of vertical. According to the theory, no variation of ratio of amplitudes with the periods is to be expected on rock, but on other formations the effect would be larger for shorter period microseisms than for the larger period ones.

MICROSEISMS AND WEATHER

A great deal of work has been done in many countries of the world correlating the occurrence of microseisms with different adverse weather phenomena. With the exception of earth tremors caused by road or rail traffic or other artificial means, it is now well established that microseisms are closely associated with weather phenomena and particularly with the occurrence of rough weather over the seas. Linke (1909) found that microseisms in Apia Samoa showed a considerable increase in amplitude when a storm approached the station. In the same way Ghezi (1930) found that a close relationship existed between the microseisms recorded at Zi-Ka-Wei (near Shanghai) and approaching typhoons in the China Sea.

In India the work on microseisms was started at the Colaba Observatory by Banerji (1930). He classified the microseisms recorded by Milne-Shaw seismograph according to their periods and showed that microseisms of 4 to 7 seconds periods, which have a characteristic variation of amplitude and are mostly recorded during the pre-monsoon and post-monsoon periods, are caused by storms in the Arabian Sea or the Bay of Bengal. He made a special study of a few storm in the Arabian Sea and the Bay of Bengal and was able to correlate the variation in microseismic amplitudes at Colaba with the distance and intensity of the storm. It was shown by him how the microseisms can be of practical help to the weather forecaster. Banerji also showed that the high winds at sea during the monsoon period cause microseisms whose

amplitudes may be considerable, depending upon the strength of monsoon winds. The types of microseism caused by the monsoon winds can be easily identified from those caused by storm. These vibrations are characterised by their regular and continuous wave form. They are first visible on records when the monsoon advances in the month of May. The periods range from 4 to 10 seconds.

A detailed study of microseisms associated with disturbed weather in the Bay of Bengal has been undertaken by Pramanik, Sengupta and Chakraverti (1946) from a study of the records of the Alipore Observatory, Calcutta.

The other types of microseism associated with weather and their classification has already been mentioned earlier

STORM TRACKING BY MICROSEISMS

As storms over the seas are now known to give rise to microseismic movements, attempts have been made to find out the exact location of a storm over the sea with the help of microseisms. Lee (1935) made an attempt to find out the direction of approach of microseisms by observing the amplitude ratio of two horizontal component seismographs. His attempts, however, were not very successful. A partial success was made by Krug in Germany in 1937 in finding the direction of approach of microseismic waves. He used four portable seismographs round about Gottingen and showed that microseisms approached from a N-E direction and their speed was slightly more than 1 Km. per sec. Better results were obtained by Trommsdorff in 1939 who used 3 of 4 sets of instruments with 2 or 3 components each.

Ramirez (1940) in America during 1940 made a thorough study of the direction of approach of the microseism at St Louis, Missouri, by using a tripartite station. In this method three sensitive seismographs were placed at the vertices of a triangle having sides of a few kilometres, and records of all the three instruments were taken on the same drum. He was able by this method to track a few storms successfully. The method of tripartite station is described later. During the period of war when observations from the sea areas were meagre, it became necessary for the American navy to find out some method of detecting hurricanes when they are far out at sea. The tripartite station method was found to have potentialities which could be utilised for locating a hurricane successfully. During the year 1944 Gilmore was entrusted with the project in the Caribbean Sea and the first tripartite station was started at the Naval operating base, Guantanamo Bay, Cuba in September, 1944. The technique was improved later and more stations started at Porto Rico and Florida in 1946. The instruments used were specially designed by Macelwane and Sprengnether (1946). They utilised the electromagnetic method with galvanometric recording. The static magnification of instruments could be increased up to 20,000. A special recorder was designed which could record the traces from all the three

galvanometers on single drum. Special provision was made in the recorder for changing the speed of rotation of the drum as well as the spacing between the different traces. This method therefore could be used even when the recorded amplitude of microseisms were very large.

The method of tripartite station recording is briefly described below.

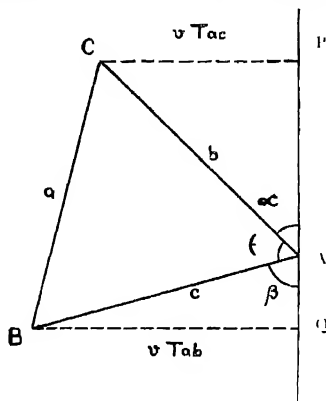


FIG. 1

A, B & C are electromagnetic seismographs situated on the vertices of a triangle ABC. They are all connected by means of underground cable to three galvanometers placed side by side whose coil movements can be recorded photographically on the same drum. Let PQ be a microseismic wave front. The wave first arrives at A, then at C and finally at B. Let the time interval between the arrival time of the same phase at A & B be given by T_{ab} and that between A & C by T_{ac} . Knowing the sides a, b, c , the angle ϵ , T_{ab} & T_{ac} the angle, ϵ , the inclination of the wave front to the side AC can be easily calculated from the following relations

$$\sin \alpha = \frac{v T_{ac}}{b}, \quad \sin \beta = \frac{v T_{ab}}{c}$$

$$\tan \alpha = \frac{\sin \epsilon}{k - \cos \epsilon}$$

$$k = \frac{b T_{ab}}{c T_{ac}}$$

For simplification of calculation it is better to use an equilateral triangle. The velocity v can be eliminated.

With this method Gilmore (1946, 1948) was able to track nearly all the storms which occurred in the Caribbean Sea from 1945 on-ward. He has published his results in a number of publications. This technique has now been extended to the Pacific and one tripartite station opened at Guam.

ORIGIN OF MICROSEISMS

It is now well known that microseisms are related to some type of adverse weather phenomenon. High winds and storms over deep sea cause microseisms which have periods ranging from 2 to 10 seconds. The manner in which the storms or high winds over the sea give rise to these earth motions which are recorded thousands of miles away is not very clearly understood, and several theories have been suggested to explain the observed results. Gherzi in 1924, proposed that the air pumping in regions of lows caused by typhoons is the cause of storm type microseisms. In 1930 Banerji has theoretical explanation of the origin of both storm and monsoon type microseisms. He derived a mathematical expression to explain the periods and amplitudes of the microseisms and showed how a steady monsoon current would be able to give rise to and maintain minute earth vibrations at the bottom of the sea which travel forward as surface seismic waves of the Rayleigh type. In 1935 he further explained how the changes of pressure caused by the sea waves are communicated to the bottom of the sea. Normally the effect of changes in pressure at the surface should die off exponentially with depth, and in deep sea no small pressure fluctuations should be noticeable but Banerji showed that if the compressibility of water is taken into account the pressure disturbance can be communicated to the sea bottom. He also performed experiments in small water tanks and showed that small pressure fluctuations caused by generating small waves by a vibrator on the water surface are communicated to the bottom. According to Banerji's theory the period and wave lengths of microseismic waves should be the same as those of the sea waves which produce the disturbance. Gutenberg (1936, 1946) following an idea of Wiechert, postulated that microseisms are caused by the beating of large ocean waves against a steep coast. According to this view the beating of waves against the steep coast of Norway was responsible for the generation of microseisms in north and eastern Europe. He was able to explain with the help of this theory that the energy associated with microseisms could be explained if it was assumed that only 1/1000 part of the total energy of the beating waves was communicated for producing the vibrations of the coast. It has however been found that large microseisms are recorded at stations which have no steep coast near them. Moreover, as pointed out by Banerji, the monsoon microseisms make their appearance several days before the actual arrival of the monsoon air near the coast. Tropical cyclones and hurricanes give rise to large microseisms when they are far away at sea without any noticeable surf near the coast. These observations clearly indicate that the "Surf theory" cannot account for the microseisms of 3 to 10 secs. period associated with high winds and storms over open sea. It is, however, not unlikely that surf is also a contributory cause to the microseismic movements. The periods associated with surf microseisms are expected to be of smaller values.

Observations of microseisms during periods of storms made by Gilmore (1948) with the help of tripartite stations have led him to the following conclusions.

(1) Typhoons and hurricanes always cause an increase in microseisms at a station near enough to the storm centre. Microseisms are also caused by frontal systems, and extratropical lows accompanied by sufficient wind.

(2) Recorded amplitudes are directly proportional to the intensity of the storm and inversely to the distance of storm from the recording station. This effect is demonstrated by the presence of geological discontinuities in the path of the microseismic waves.

(3) Different types of weather phenomenon give rise to distinct type of microseisms which can be identified by an experienced observer.

(4) Severe storms on the open sea can generally be detected when they are as far as 1600 miles, if geological discontinuities or large islands do not intervene in the path of microseismic waves.

(5) It is possible to calculate the bearings of the centre of the hurricane with the help of tripartite stations, the accuracy in the determination being directly proportional to the skill of the observer.



FIG. 2

Microseisms recorded at Poona on a locally made Torsion seismograph between 08.00 hours I. S. T. and 10.00 I. S. T. on 22nd November 1948, due to a cyclone in the Arabian Sea near Bombay.

Experiments performed by the Admiralty in England and by workers in America to measure the changes in pressure at sea bottom caused by gravity waves have shown that the pressure due of the waves is communicated to the bottom. Deacon (1947) has pointed out that the existing explanations about the origin of microseisms in deep water are not satisfactory as the amplitudes of waves in deep waters should diminish exponentially with depth. He has also objected to Bauerji, Whipple and Lee and the surf theory on the ground that the sea waves are short in comparison to the wave length of microseisms and hence the pressure variations due to them would tend to cancel out and the net effect would be very small. This objection has been answered by Bernard (1937, 1941) by stating that microseisms are produced at places where wave trains coming in opposite direction produce stationary waves. Such condition exists in the

centre of a cyclone. In order to explain microseisms caused by high winds at-sea, Bernard postulates the formation of stationary waves to be formed by interference between the waves travelling towards and the waves reflected by a neighbouring steep coast.

An analysis of wave records obtained by Deacon, shows that the wave periods are double of the periods of microseisms. He has also quoted an observation of Bernard on the coast of Morocco where the observed wave periods are nearly double the microseismic periods. As has been mentioned earlier, the period of microseismic waves and sea waves according to Banerji's theory should be equal.

It would appear, however, that the observations of wave periods by Bernard or Deacon have all been taken in shallow water. As shown by Banerji the wave periods in deep sea and shallow water by the same wind force are likely to be different. He showed that due to the slope of bottom near the coast the waves caused by wind will have a higher period. An increase of wind from 20 miles per hour to 27 miles per hour will increase the period from 7 seconds to 30 seconds. It is therefore to be expected that, in wave records near the coast, with wind speed fluctuating between 20 and 30 miles per hour, all periods ranging from 6 to 30 seconds should be obtained. The larger period waves will be superposed on the shorter period waves. Presumably the records of Deacon bring out their presence. According to Banerji's theory waves with periods between 10 and 30 secs., should give rise to microseisms of periods ranging between 10 and 30 secs. These movements were actually observed by him at Colaba during periods of pronounced land and sea breeze. The microseisms of long period (10-30 seconds) which have small amplitudes are not likely to be observed in the presence of strong shorter period microseisms. A harmonic analysis of the microseismic records may, however, bring out the presence of the longer period microseisms in the presence of shorter period microseisms.

Deacon has also referred to an unpublished work of Longuet Hyggins and Ursell in which they have developed a theory according to which the average pressure on the sea bottom below a standing wave varies sinusoidally with twice the frequency of the waves and does not decrease to zero with depth. This theory may be able to explain the storm type of microseisms but will not be able to give any convincing answer to the monsoon type of microseisms which are detected several days before the arrival of any appreciable surf or swell near the coast.

CONCLUSION

It has now been established that cyclones over the sea give rise to microseismic movements which can be detected at a far off station. The exact location of storm can be found by using the tripartite station and central recording technique. This method can be of great use to weather forecaster

who has to issue storm warnings. During the period of war or adverse weather, meteorological observations from sea areas are lacking. Under such circumstances this may perhaps prove to be the only way of locating storms. The presence of storms by this method, can be detected a day or two earlier than by means of methods using meteorological observations.

From the theoretical point of view it appears that of all the theories proposed, the one proposed by Banerji in 1930 still holds ground, and is able to explain most of the observed features of microseisms.

METEOROLOGICAL OFFICE
POONA

REFERENCES

- Banerji S. K., 1930, *Phil. Trans. Roy. Soc. Lond.*, **230**, 287.
 Banerji S. K., 1935, *Proc. Ind. Acad. Sci. B*, **727**, 753.
 Bernard, P., 1937, *C. R.*, **208**, 163.
 Carder, D. S. and Gilmore, M. H., 1945, *Bull. Seis. Soc. Am.*, **35**, 13.
 Deacon, G. E. R., 1947, *Nature*, **160**, 419.
 Gherzi, E., 1930, *Gerlands, Beil. Geophysik.*, **28**, 145.
 Gilmore, M. H., 1946, *Bull. Seis. Soc. Am.*, **36**, 89.
 Gilmore, M. H., 1946, *Trans. Am. Geophysical Union*, **27**, 466.
 Gilmore, M. H., 1948, *Bull. Seis. Soc. Am.*, **38**, 195.
 Gutenberg, B., 1936, *Bull. Seis. Soc. Am.*, **26**, 111.
 Gutenberg, B., 1936, *Jour. of Meteorology*, **4**, 21.
 Lee, A. S., 1932, *Mon. Not. R. Astro. Soc. Geophys. Suppl.*, **3**, 83.
 Lee, A. S., 1935, *Proc. Roy. Soc. Lond. A*, **1497**, 183.
 Pramanik, S. K., Sengupta, P. K., and Chakraborty, K. C., 1946, *J. Met. D. Scientific Notes*, Vol. X No. 120.

A STUDY ON THE POLARISATION OF X-RAYS*

By HIRENDRA KUMAR PAL

(Received for publication, Aug. 15, 1949)

ABSTRACT In this paper the variations of the polarisation of a heterogeneous primary beam of X-rays with the variation in the (i) magnitude of the generating H.T. and (ii) thickness of an aluminium filter through which the rays were transmitted, have been studied. It is observed that a lowering of the voltage applied or an increase in the thickness of the filter has the effect of producing an increased p.c. polarisation of the beam.

INTRODUCTION

In connection with the work on the energy distribution of scattered X-radiation by the author (Pal, 1948) it was found necessary to determine the ratio P/U for the various beams experimented upon, where P and U respectively denote the intensities of the polarised and unpolarised components of the incident beam. If i_s and i_u represent the intensities of the scattered rays in a direction perpendicular to the primary, when the cathode stream is (A) perpendicular and (B) parallel respectively to the above scattered rays, then,

$$P/U = (i_s - i_u) / 2i_s,$$

$$\text{and p.c. polarisation} = \frac{100P}{P+U} = \frac{100(i_s - i_u)}{i_s + i_u} = Q \text{ (say).}$$

i_s and i_u were measured and hence the values of P/U and the p.c. polarisation were computed for the different incident radiations which were either excited at different voltages or filtered to different extents through aluminium, at the same voltage. For a description of the apparatus employed reference should be made to the aforesaid paper.

The difference shown by the two scatterers (70 sheets of filter paper and a 1.8 c.m. thick paraffin slab) in the value of P/U is insignificant. In Figs. 1 and 3 the mean values of the p.c. polarisation have been plotted against the generating voltage and the thickness of the filter respectively.

Fig. 1 shows that an increase in the excitation voltage diminishes the p.c. polarisation of the unfiltered radiation. Thus, in the present case, the effect of stepping up the voltage from 30 K. V. (peak) to 100 K. V. (peak) was to bring down the mean p.c. polarisation from 8.8 to 1.3 in successive stages. This is in qualitative agreement with the results obtained originally

* A part of the thesis approved for the Ph.D. Degree of the University of Edinburgh.

by Barkla as early as 1908, which indicated that the polarisation varied from about 9 to 2.5% on hardening the rays by increasing the P. D. applied—

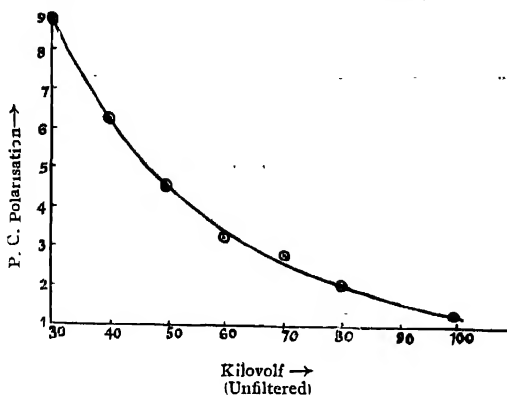


FIG. 1

and subsequently by Khubchandani who raised the voltage from 30 K. V (peak) to 80 K. V. (peak) in a single step with a consequent degradation in the p.c. polarisation from 8.5 to 2.0 Bassler (1909) also noticed a progressive fall from 16 to 2% as the spark-length (Funkenstoecke) of the generating induction coil was extended gradually from a minimum of 4 c.m. to a maximum of 20 c.m. But in these early works of Barkla and of Bassler information is lacking with respect to the actual values of the H. T. applied to the X-ray tube. The diminution in the polarisation with increasing voltage may partly be ascribed to the fact that at higher voltages, a greater amount of secondary radiation, which is unpolarised, is emitted from the anticathode, thus cutting down the proportion of the polarised part.

It is also interesting to note that if $\log_{10} Q$ is plotted against the corresponding voltage V , a graph is obtained which is fairly a straight line as may be seen from Fig. 2. Hence the relation between Q and V may

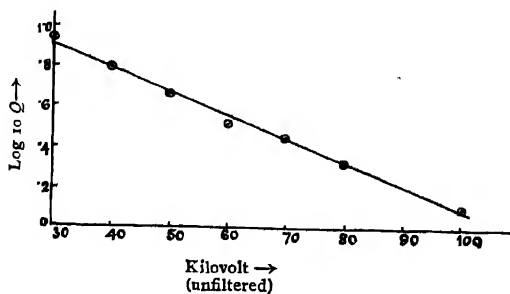


FIG. 2

be expressed to a considerable degree of accuracy by an empirical equation of the form $Q = A \exp. (-BV)$; at least within the range of voltage used in these investigations,—where A and B are constants presumably depending upon the tube emitting the radiation.

Fig. 3 shows that when the incident radiation at a constant H. T. is hardened more and more by filtering through increasing thicknesses of alumi-

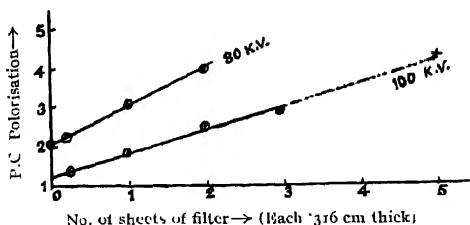


FIG. 3

nium, the p.c. polarisation steadily rises up. This also is in accord with the results of Barkla (*loc. cit.*) and Ham (1910) and of Klubchandani, the last of whom found that at 80 K. V. (peak) the proportion of polarisation suffered an increase from 2 to 3.03% when the unfiltered radiation was passed through 5 m.m. thickness of aluminium. A similar increase produced by the process of transmission of the rays through absorbers such as platinum, water, etc., was also reported by Bassler (1909). This increase in the polarised component is usually explained on the supposition that the filter absorbs more of the softer secondary radiation leaving behind a greater percentage of the polarised primary radiation.

The relation between the p.c. polarisation of the filtered radiation (at a constant voltage) and the thickness of the aluminium filter appears to be a fairly linear one as in Fig. 3, at any rate up to the maximum absorption occurring in these experiments.

ACKNOWLEDGMENT

The author acknowledges his indebtedness to late Prof. C. G. Barkla, F.R.S., N.L. of the University of Edinburgh for his interest and kind supervision and to Prof. K. Banerjee of the Indian Association for the Cultivation of Science for helpful discussions.

A. M. COLLEGE,
MYMENSINGH.

REFERENCES

- Barkla, C. G., 1908, *Jahrbuch der Radio-aktivität und Electronik* V. Band Heft 3.
 Bassler, E., 1909. *Ann. der Physik*. 28, 808
 Ham, 1910. *Phys. Rev.* 30, 96.
 Pal, H. K. 1948. *Ind. Jour. Phys.*, 22, 291.

ANNOUNCEMENT

We intend to purchase the following Old Volumes of *Indian Journal of Physics* at Rs. 6/- per complete volume :
Volumes 1, 2, 3, 4, 5, 6
and 7.

TOMORROW'S INSTRUMENTS TODAY

RAJ-DER-KAR & CO.

COMMISSARIAT BUILDING

HORNBY ROAD

FORT

BOMBAY

OFFERS

FROM STOCK

GLASS METAL DIFFUSION PUMPS, METAL BOOSTE
PUMPS, OILS AMOILS OCTOILS OCTOIL,
BUTYL SABACATE

MANUFACTURED

By

DISTILLATION PRODUCTS
(U. S. A.)

SPENCER MICROSCOPE

CENCO HIGHVACS

BESLER EPIDIASCOPE

COMPLETE WITH FILM STRIP ARRANGEMENTS

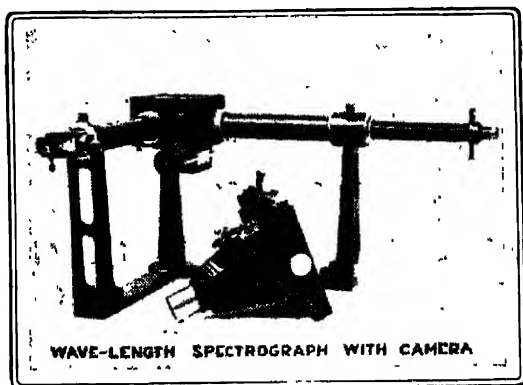
Telephone 27804
2 Lines

Telegrams
TECHLAB

THE ANDHRA SCIENTIFIC CO., LTD.

Head Office & Works: MASULIPATAM.

Registered Office: 4, BLACKERS ROAD, MOUNT ROAD, MADRAS.



MANUFACTURERS OF ALL VARIETIES OF:-

*Spectrographs And Accessories, Goniometers,
Precision Measuring Instruments like Micro-
meter Microscopes, Cathetometers, Spectrometers
And All Other Scientific Instruments For
Research, Industry And Instruction.*

BOMBAY - -

Asian Building,

Nicol Road,

Ballard Estate.

ALLAHABAD

CUTTACK

VIZAGAPATAM

GUNTUR

The following special publications of the Indian Association for the Cultivation of Science, 210, Bowbazar Street, Calcutta, are available at the prices shown against each of them :—

Subject	Author	Price Rs. A. P.
Methods in Scientific Research	Sir E. J. Russell	0 6 0
The Origin of the Planets	Sir James H. Jeans	0 6 0
Separation of Isotopes	Prof. F. W. Aston	0 6 0
Garnets and their Role in Nature	Sir Lewis L. Fermor	2 8 0
(1) The Royal Botanic Gardens, Kew.	Sir Arthur Hill	1 8 0
(2) Studies in the Germination of Seeds.		
Interatomic Forces	Prof. J. E. Lennard-Jones	1 8 0
The Educational Aims and Practices of the California Institute of Technology.	R. A. Millikan	0 6 0
Active Nitrogen A New Theory.	Prof. S. K. Mitra	2 8 0
Theory of Valency and the Struc- ture of Chemical Compounds.	Prof. P. Ray	3 0 0
Petroleum Resources of India	D. N. Wadia	2 8 0
The Role of the Electrical Double layer in the Electro Chemistry of Colloids.	J. N. Mukherjee	5 12 0

A discount of 25% is allowed to Booksellers and Agents.

RATES OF ADVERTISEMENTS

Third page of cover	Rs. 32, full page
do. do.	„ 20, half page
do. do.	„ 12, quarter page
Other pages	„ 25, full page
do.	„ 16, half page
do.	„ 10, quarter page

15% Commissions are allowed to *bonafide* publicity agents securing orders for advertisements.

CONTENTS

PAGE

✓ 6.	Term Values of f^4 Electron Configuration—By K. Suryanarayana Rao	... 51 ✓
✓ 7.	A note on the Thermal Inertia of Cloud Particles—By B. K. Agarwala and N. K. Saha	... 57 ✓
✓ 8.	On the Distribution of Ions in Solutions of Strong Electrolytes—By M. Dutta and S. N. Bagchi	... 61 ✓
✓ 9.	The Spectro-Chemical Analysis of Molybdenum in Green Peas—By M. K. Ghosh and K. C. Mazumder	... 67 ✓
✓ 10.	On the Variation of Current with Distance between the Electrodes of a Glow Discharge in Gases at Low Pressure—By M. Khurshed Husain	... 73 ✓
✓ 11.	Microseisms—By A. N. Tandon	... 80 ✓
✓ 12.	A study on the Polarisation of X-Rays—By H. K. Pal	... 97 ✓

PRINTED BY SIBENDRANATH KANJILAL, SUPERINTENDENT (OFFG.), CALCUTTA UNIVERSITY
 PRESS, 48, HAZRA ROAD, BALLYGUNGE, CALCUTTA AND PUBLISHED BY THE
 REGISTRAR, INDIAN ASSOCIATION FOR THE CULTIVATION OF SCIENCE,
 210, Bowbazar Street, Calcutta.

Vol. 24

INDIAN JOURNAL OF PHYSICS

No. 3

(Published in collaboration with the Indian Physical Society)

AND

Vol. 33

PROCEEDINGS

No. 3

OF THE

INDIAN ASSOCIATION FOR THE
CULTIVATION OF SCIENCE

MARCH, 1950

PUBLISHED BY THE
INDIAN ASSOCIATION FOR THE CULTIVATION OF SCIENCE
210, Bowbazar Street, Calcutta

BOARD OF EDITORS

K. BANERJEE	S. K. MITRA
D. M. BOSE	P. RAY
S. N. BOSE	M. N. SAHA
D. S. KOTHARI	S. C. SIKKAR.

Secretary

EDITORIAL COLLABORATORS

DR. R. K. ASUNDI, M.A., PH.D.
PROF. H. J. BHABHA, PH.D., F.R.S.
DR. P. K. KICHLU, D.Sc.
PROF. K. S. KRISHNAN, D.Sc., F.R.S.
PROF. G. P. DUBEY, M.Sc.
DR. K. RANGADHAMA RAO, M.A., D.Sc.
DR. N. D. SARWATTEY, D.Sc.
DR. N. N. DASGUPTA, M.Sc., PH.D.
PROF. N. R. SEN, D.Sc., F.N.I.
PROF. P. C. MAHANTI, D.Sc., F.N.I.
PROF. S. R. PALIT, D.Sc.,
DR. H. RAKSHIT, D.Sc.,
PROF. K. R. DIXIT, PH.D.
DR. VIKRAM A. SARABHAI, M.A., PH.D.

ASSISTANT EDITOR

MR. A. N. BANERJEE, M.Sc.

NOTICE TO INTENDING AUTHORS

Manuscripts for publication should be sent to Mr. A. N. Banerjee, Assistant Editor, 210, Bowbazar Street, Calcutta.

The manuscript of each paper should contain in the beginning a short abstract of the paper.

All references to published papers should be given in the text by quoting the surname of the authors followed by the year of publication within braces, e.g., Sen (1942). The actual references should be given in a list at the end of the paper according to the following specimen :

Sen, B. K., 1942, *Ind. J. Phys.*, 16, 329.

The references should be arranged alphabetically in the list.

All diagrams should be drawn on thick white paper in Indian ink, and letters and numbers in the diagrams should be written in pencil.

Annual Subscription—

Inland Rs. 20

Foreign £ 2

CIRCULAR AND ELLIPTICAL QUANTUM ORBITS

By M. F. SOONAWALA

(Received for publication, Sept. 25, 1948)

ABSTRACT. Some further implications of the gravitational inverse cube law of attraction between two particles deduced in a previous paper from a generalization of the quantum laws are discussed here. The treatment is extended to elliptical orbits and expressions derived for the force of attraction between the particles, the energy of one of the particles, and the conditions for the change in the quantum numbers.

In a previous paper (Soonawala, 1947), the fundamental laws, as given by Bohr for circular electronic orbits, were slightly modified to be applicable to the nucleus also. Generalising this for a system of two particles of any mass and charge an alternative expression was derived for the force of attraction between the two particles in terms of their masses and the distance between them. Logically, this expression assumes the same role as the one for the electric force of attraction, $E_1 E_2 / r^2$, as either of these has been derived from the centrifugal force. We are hence led to the equivalence of the two kinds of forces expressed by

$$\frac{E_1 E_2}{r^2} = \frac{h^2 s^2 (m_1 + m_2)^3}{4\pi^2 M m_1 m_2 r^3} \quad (1)$$

giving

$$r = \frac{h^2 (m_1 + m_2)^3 s^2}{4\pi^2 M m_1 m_2 E_1 E_2} \quad (2)$$

and the energy

$$W = \frac{2\pi^2 M m_1 m_2 E_1^2 E_2^2}{h^2 (m_1 + m_2)^3 s^2} \quad \dots \quad (3)$$

The gravitational force can also be expressed as

$$F = G \frac{s^2 M^3 (m_1 + m_2)^3}{m_1 m_2 r^3} \quad \dots \quad (4)$$

where $G = \frac{h^2}{4\pi^2 M^4} = 1.40 \times 10^{11} . M$ and $(m_1 + m_2)$ is the sum of the masses of the particles. An alternative expression is

$$F = \frac{h^2 s^2 m_1^2 m_2^2 M^2}{4\pi^2 \mu^3 r^3} = 3.03 \times 10^{-101} \times \frac{s^2 m_1^2 m_2^2}{\mu^3 r^3} \quad \dots \quad (5)$$

where μ is the reduced mass given by

$$\frac{1}{\mu} = \frac{1}{M} \left(\frac{1}{m_1} + \frac{1}{m_2} \right) \quad \dots \quad (6)$$

Eqn (2) gives the equilibrium values of r , and for these the orbits are quantized. The gravitational force preponderates at shorter distances and the electric one at greater distances. By the ordinary dynamical theory, the inverse cube law leads to spiral orbits of the type

$$a = A \cos n(\theta - \alpha) \quad (7)$$

according as $\frac{n^2 h^2}{4\pi^2 M^2 m_1 m_2}$ is less than or greater than $\frac{h^4 s^2 (m_1 + m_2)^4}{4\pi^2 M m_1 m_2}$. It is the latter condition that is satisfied in our case. This would give orbits of the type (7) with only the gravitational force acting as when both or either of the two particles are uncharged.

ELLIPTICAL ORBITS

The treatment can now be extended to elliptical orbits for two oppositely charged particles. Let m_1 and m_2 be the mass-numbers of the particles, M the mass of the proton so that the masses of the particles are Mm_1 and Mm_2 , and E_1 and E_2 the charges upon them one being positive and the other negative. Let the co-ordinates of the two particles referred to the centre of mass be x_1, y_1, z_1 , and x_2, y_2, z_2 . The equations of motion will be

$$\left. \begin{aligned} Mm_1 \frac{d^2 x_1}{dt^2} &= -E_1 E_2 \frac{(x_1 - x_2)}{r^3} \\ Mm_1 \frac{d^2 y_1}{dt^2} &= -E_1 E_2 \frac{(y_1 - y_2)}{r^3} \\ Mm_1 \frac{d^2 z_1}{dt^2} &= -E_1 E_2 \frac{(z_1 - z_2)}{r^3} \\ Mm_2 \frac{d^2 x_2}{dt^2} &= -E_1 E_2 \frac{(x_2 - x_1)}{r^3} \\ Mm_2 \frac{d^2 y_2}{dt^2} &= -E_1 E_2 \frac{(y_2 - y_1)}{r^3} \\ Mm_2 \frac{d^2 z_2}{dt^2} &= -E_1 E_2 \frac{(z_2 - z_1)}{r^3} \end{aligned} \right\} \quad \dots (8)$$

Also,

$$\left. \begin{aligned} m_1 x_1 + m_2 x_2 &= 0 \\ m_1 y_1 + m_2 y_2 &= 0 \\ m_1 z_1 + m_2 z_2 &= 0 \end{aligned} \right\} \quad \dots (9)$$

Or,

$$m_1 r_1 = m_2 r_2 \quad \dots (10)$$

and

$$\frac{m_1}{r_2} = \frac{m_2}{r_1} = \frac{m_1 + m_2}{r_1 + r_2} \quad \dots (11)$$

where r_1 and r_2 are the distances of the particles from the centre of mass and $r = r_1 + r_2$. Combining (8) with (9) we get

$$M m_1 \frac{d^2 x_1}{dt^2} = - \frac{E_1 E_2}{r^3} \left(x_1 + \frac{m_1 x_1}{m_2} \right) = - \frac{E_1 E_2}{r^3} x_1 \left(\frac{m_1 + m_2}{m_2} \right) \quad \dots (12)$$

$$\text{or} \quad \frac{d^2 x_1}{dt^2} = - \frac{E_1 E_2}{M r^3 \mu} x_1; \quad \dots (13)$$

and two similar equations.

μ is the reduced mass number given by

$$\frac{1}{\mu} = \frac{1}{m_1} + \frac{1}{m_2}$$

We may take the plane of the orbit to be the xy -plane. Then the orbit will be an elliptical one given by

$$\frac{d^2 x}{dt^2} = - \frac{E_1 E_2}{r^3} x, \quad \text{and} \quad \frac{d^2 y}{dt^2} = - \frac{E_1 E_2}{r^3} y \quad \dots (14)$$

for one particle referred to the other.

Here

$$\begin{cases} x = x_2 - x_1 \\ y = y_2 - y_1 \end{cases} \quad \dots (15)$$

The orbit for the second particle is also a similar ellipse with the centre of mass as one focus. As the relations (11)

$$\frac{m_1}{r_2} = \frac{m_2}{r_1} = \frac{m_1 + m_2}{r}$$

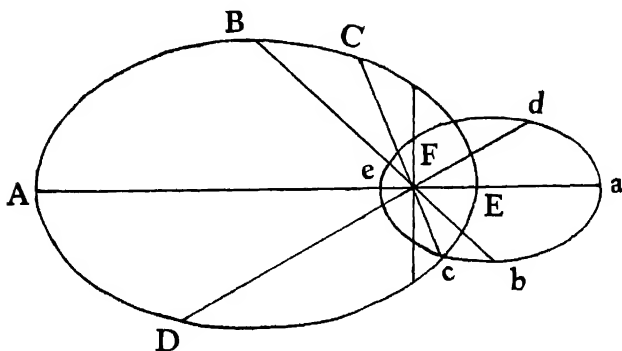


FIG. 1

are to hold simultaneously, the paths of the two orbits will be as shown (Fig. 1). aA , bB , cC , dD , eE , are corresponding positions of the particles in

their orbits. If a_1 and a_2 are the semi-major axes and l_1 and l_2 the latus recta, then, also,

$$\left. \begin{aligned} m_1 a_1 &= m_2 a_2 \\ m_1 l_1 &= m_2 l_2 \end{aligned} \right\} \quad \dots \quad (16)$$

The quantum conditions for the two orbits will be, as usual,

$$M m_1 r_1^2 \left(\frac{d\theta}{dt} \right)_1 = \frac{n_1 h}{2\pi} \quad \dots \quad (17)$$

$$M m_2 r_2^2 \left(\frac{d\theta}{dt} \right)_2 = \frac{n_2 h}{2\pi} \quad \dots \quad (18)$$

$$\int_0^{2\pi} p_1 r_1 d\tau = n_1' h \quad \dots \quad (19)$$

$$\int_0^{2\pi} p_2 r_2 d\tau = n_2' h \quad \dots \quad (20)$$

n_1, n_2, n_1' , and n_2' are the four quantum numbers. We can see from Fig. 1. that the angular velocity, $d\theta/dt$, must be the same at any instant for both the particles. Hence, since $m_1 r_1 = m_2 r_2$,

$$\frac{n_1}{n_2} = \frac{m_1 r_1^2}{m_2 r_2^2} = \frac{r_1}{r_2} = \frac{m_2}{m_1} \quad (21)$$

$$\text{Let } n_1 = s m_2 \text{ and } n_2 = s m_1 \quad (22)$$

Also, for an elliptical orbit derived from the inverse square law,

$$r^2 \frac{d\theta}{dt} = \sqrt{\frac{E_1 E_2 b^2}{M \mu a}} = \sqrt{\frac{E_1 E_2 a}{M \mu}} \cdot \frac{b}{a} = \sqrt{\frac{E_1 E_2 a}{M \mu}} \cdot \frac{n}{n+n'} = \frac{n h}{2\pi m M} \quad (23)$$

where a and b are the semi-axes of the ellipse

$$\text{Then,} \quad \frac{a_1}{a_2} = \frac{m_2^2}{m_1^2} \frac{(n_1 + n_1')^2}{(n_2 + n_2')^2} = \frac{m_2}{m_1} \quad (24)$$

$$\text{giving} \quad \left(\frac{n_1 + n_1'}{n_2 + n_2'} \right)^2 = \frac{m_1}{m_2} = \frac{n}{n_1} \quad (25)$$

$$\text{Let} \quad n_1 = s m_2, \quad n_2 = s m_1, \quad (n_1 + n_1')^2 = s' m_1, \quad \text{and} \quad (n_2 + n_2')^2 = s' m_2 \quad (26)$$

$$\text{then,} \quad n_1' = \sqrt{s' m_1 - s m_2}, \quad \text{and} \quad n_2' = \sqrt{s' m_2 - s m_1} \quad (27)$$

THE FORCE OF ATTRACTION

The central force of attraction between the particles is given by

$$F = M m_1 \left(\frac{d\theta}{dt} \right)^2 - M m_1 \frac{d^2 r}{dt^2} \quad (28)$$

$$\begin{aligned}
\text{Also, } \frac{dp_i}{dt} &= Mm \frac{d^2 r}{dt^2} = \frac{d}{dt} \left(Mm \frac{dr}{dt} \right) = \frac{d}{dt} \left(Mm \frac{dr}{d\theta} \frac{d\theta}{dt} \right) \\
&= \frac{d}{dt} \left(Mm \frac{dr}{d\theta} \frac{d\theta}{dt} \right) = \frac{d}{dt} \left(\frac{h}{r^2} \frac{dr}{d\theta} \right) = \frac{h}{r^2} \frac{dr^2}{dt d\theta} + \frac{h}{r^2} \frac{d^2 r}{d\theta^2} \frac{d\theta}{dt} \\
&= -\frac{h}{r^3} \left(\frac{dr}{d\theta} \right)^2 \frac{d\theta}{dt} + \frac{h}{r^2} \frac{d^2 r}{d\theta^2} \frac{d\theta}{dt} = \frac{h}{r} \frac{d\theta}{dt} \left\{ \frac{1}{r} \frac{d^2 r}{d\theta^2} - \frac{1}{r^2} \left(\frac{dr}{d\theta} \right)^2 \right\} = \frac{h}{r} \frac{d\theta}{dt} \frac{d}{d\theta} \left(\frac{1}{r} \frac{dr}{d\theta} \right) \\
&= \frac{h}{r} \frac{nr}{2\pi Mmr^2} \left\{ \frac{1}{l^2} (e^2 - 1) + \frac{1}{l} \right\} = \frac{h}{r} \frac{n}{2\pi Mmr^2} \left\{ \frac{1}{l} - \frac{1}{l^2} \left(\frac{n}{n+u} \right)^2 \right\} \\
&= \frac{n^3 h^2}{4\pi^2 m M l} \left\{ \frac{1}{r^2} - \frac{1}{rl} \left(\frac{n}{n+u} \right)^2 \right\} \quad \dots (29)
\end{aligned}$$

Here,

$$p = Mmr^2 \frac{d\theta}{dt} = \frac{nh}{2\pi} \quad \dots (30)$$

and the equation of the ellipse is

$$1/r = 1 + e \cos \theta \quad \dots (31)$$

The force of attraction is, then, given by

$$\begin{aligned}
F &= -\frac{h^2}{8\pi^2 M} \left\{ \frac{n_1^2}{m_1 l_1 r_1^2} + \frac{n_2^2}{m_2 l_2 r_2^2} - \left(n_1 + \frac{n_1^2}{n_1 l_1} \right) \frac{1}{m_1 r_1 l_1^2} - \left(n_2 + \frac{n_2^2}{n_2 l_2} \right) \frac{1}{m_2 r_2 l_2^2} \right\} \\
&\quad + \frac{M}{2} \left\{ m_1 r_1 \left(\frac{d\theta}{dt} \right)^2 + m_2 r_2 \left(\frac{d\theta}{dt} \right)^2 \right\} \\
&= -\frac{h^2}{8\pi^2 M} \left\{ \frac{s^2 m_2^2 r_2^2 m_2 l_2 + s^2 m_1^2 r_1^2 m_1 l_1}{m_1 m_2 l_1 l_2 r_1^2 r_2^2} - \frac{s^4}{s'} \frac{m_2^2 r_2^2 l_2^2 + m_1^2 r_1^2 l_1^2}{m_1^2 m_2^2 l_1^2 l_2^2 r_1 r_2} \right\} \\
&\quad + \frac{M}{2} \{ m_1 r_1 + m_2 r_2 \} \left(\frac{d\theta}{dt} \right)^2 \\
&= \frac{h^2}{8\pi^2 M} \left\{ \frac{s^4}{s'} (m_1^2 m_2 + m_2^2 m_1) \left(\frac{m_1 + m_2}{m_1 m_2} \right)^3 \frac{1}{(l_1 + l_2)^2 (r_1 + r_2)} \right. \\
&\quad \left. - 2s^2 m_1^2 m_2^2 \left(\frac{m_1 + m_2}{m_1 m_2} \right)^3 \frac{1}{(l_1 + l_2) (r_1 r_2)^2} \right\} \\
&\quad + \frac{h^2 M}{8\pi^2} (n_1^2 m_1^2 + n_2^2 m_2^2) \left(\frac{m_1 + m_2}{m_1 m_2} \right)^3 \frac{1}{(r_1 + r_2)}, \quad \dots (32)
\end{aligned}$$

CHANGE OF QUANTUM NUMBERS

Let the quantum number n_1 change to $n_1 + \Delta n_1$, so that (22) becomes

$$n_1 + \Delta n_1 = (s + \Delta s) m_1 \quad \dots (33)$$

and, correspondingly,

$$n_2 + \Delta n_2 = (s + \Delta s) m_2$$

If, simultaneously, n_1' changes to $n_1' + \Delta n_1'$, then,

$$n_1' + \Delta n_1' = \sqrt{m_1} (\sqrt{s'} + \Delta \sqrt{s'}) - s m_2 - (s + \Delta s) m_2$$

or

$$\Delta n_1 = \sqrt{m_1} \Delta \sqrt{s'} - \Delta s m_2$$

and,

$$\Delta n_2 = \sqrt{m_2} \Delta \sqrt{s'} - \Delta s m_1 \quad \dots (34)$$

The simultaneous fulfilment of the conditions that $n_1, n_2, \Delta n_1', \Delta n_2', m_1$ and m_2 are to be integers and that s and s' are restricted to the group defined by m_1 and m_2 imposes severe restrictions upon the selection of $\Delta n_1, \Delta n_2, \Delta n_1'$ and $\Delta n_2'$.

ENERGY OF A PARTICLE

The energy will be given by

$$W = \frac{E_1 E_2}{2a_1} = \frac{2E_1^2 E_2^2 \pi^2 M^2 m_1^2}{h^2 \mu (n_1 + n_1')^2} \quad \dots (35)$$

NON-ELLIPTICAL ORBITS

The condition

$$M m r^2 \frac{d\theta}{dt} = \frac{n h}{2\pi} \quad \dots (36)$$

holds good for all central orbits. If, further, the orbits are similar and described about the common centre of mass, then,

$$m_1 r_1 = m_2 r_2$$

or,

$$\frac{r_1}{r_2} = \frac{m_2}{m_1} = \frac{n_1}{n_2}$$

The relation,

$$\int p_r dr = n' h$$

would lead to expressions for n' as a function of mass-numbers and distance depending upon the shape of the orbit and its constants. The orbit will be given by the equations

$$\frac{d^2 u}{d\theta^2} + u = \frac{f(r)}{m A^2} \cdot \frac{1}{u^2} \quad \dots (37)$$

or,

$$\frac{f(r)}{m} = \frac{A^2}{p^3} \cdot \frac{dp}{dr} \quad \dots (38)$$

where

$$A = r^2 \frac{d\theta}{dt} \quad \dots (39)$$

$f(r)$ is the force of attraction between the particles, and p is the perpendicular from the origin to the tangent at any point.

We can here examine a little more closely the non-elliptical orbit given by the inverse cube law mentioned in (7). The equation of the orbit is

$$\frac{d^2 u}{d\theta^2} = -n^2 u \quad \dots (40)$$

$$\text{where} \quad -n^2 = \left(\frac{h^2 s^2 (m_1 + m_2)^3}{4\pi^2 M m_1 m_2} \times \frac{4\pi^2 m^2 M^2}{h^2 s^2 m^3} \right) - 1 \quad \dots (41)$$

$$\text{with} \quad u = \frac{1}{r}$$

The first term,

$$\frac{M(m_1 + m_2)^3}{m_1 m_2} \quad \dots (42)$$

is of the order 10^{-22} or less for any plausible values of m_1 and m_2 , and, hence, $n = 1$. The orbit becomes

$$u = A \cos(\theta - \alpha) \quad \dots (43)$$

which, in rectangular co-ordinates is of the form

$$Ax + By + C = 0 \quad \dots (44)$$

This denotes a straight line. Further, if $\alpha = 0$, the equation of the line becomes

$$x = c \quad (45)$$

a straight line parallel to the y -axis. The two particles approaching each other from infinity would move along parallel straight lines, pass each other at the apsidal distance, and move on to infinity. The paths will be straight lines described with uniform velocities.

CIRCULAR ORBIT UNDER INVERSE CUBE ATTRACTION

If the central acceleration is a^2/r^3 , the condition for a circular orbit will be

$$r\omega^2 = \frac{a^2}{r^3} \quad \dots (46)$$

$$\text{or,} \quad \omega = \frac{a}{r^2} \quad \dots (47)$$

SUPERPOSED INVERSE SQUARE AND INVERSE CUBE CENTRAL FORCES

For a central orbit

$$r^3 \frac{d\theta}{dt} = A, \text{ a constant.}$$

The equation of motion for the inverse square law of the form $\frac{\mu}{r^2}$ is given by

$$\frac{d^2 u}{d\theta^2} + u = \frac{\mu}{A^2} \quad \dots (48)$$

and the solution is

$$u = C + B \cos(\theta - \alpha) \quad \dots (49)$$

with

$$B = \frac{c}{a(1 - e^2)} \quad \dots (50)$$

and

$$C = \frac{1}{a(1 - e^2)} = \frac{\mu}{A^2} \quad \dots (51)$$

Let an inverse cube force be superposed on this so that the total force is

$$F = \mu u^2 + \mu_1 u^3 \quad \dots (52)$$

The equation of the orbit now is

$$\frac{d^2 u}{d\theta^2} + u \left(1 - \frac{\mu_1}{A^2} \right) = \frac{\mu}{A^2}$$

As seen from (17), (4), (41), (42), μ_1/A^2 is of the order 10^{-22} or less; hence, the equation of motion reduces to the ellipse (48) again. The existence of the inverse cube force is thus seen not to affect the elliptical motion under the inverse square law. This is a particular case of Newton's Revolving Orbit Theorem according to which the orbit described under a central force of attraction remains unaffected when a central inverse cube force is superposed on the original one excepting that the orbit revolves in its own plane about the centre of attraction with a uniform angular velocity. In our case, the revolution also vanishes.

MAHARAJA'S COLLEGE, JAIPUR
(RAJPUTANA)

REFERENCES

Soonawala, M. F., 1947, *Ind. Jour. Phys.*, **21**, 137.

SPECTRUM OF THE FLAME ABOVE A COPPER ARC IN AIR

By S. P. SINHA AND SHYAM CHANDRA PRASAD

(Received for publication, March 25, 1949)

Plate III

ABSTRACT. The spectrum of the flame above a copper arc in air has been photographed on a glass prism spectrograph with a dispersion of about 12 Å per mm at $\lambda 5500\text{Å}$, and all the radiations between $\lambda 4800$ and $\lambda 5400\text{Å}$ have been measured. A large number of bands exist. The origin and structure of most of them do not seem to be very well understood. A tentative arrangement for three systems of bands is given.

INTRODUCTION

The spectrum of the flame above a copper arc in air does not seem to have received the attention it deserves, by virtue of being associated with such a common source of radiation in a spectroscopic laboratory. It is believed that the radiation of the flame is chiefly due to Cu(I) which has an intense system of band in the orange and red region and some weak bands in the green. Several measurements of the orange and red bands have been published (Mulhken, 1925; Mahanti, 1920; Loomis and Watson, 1935; Pearce and Gaydon, 1941; Rosen, 1945 and Guntzsch, 1946), and some of these workers have also attempted an analysis of them, each in his own way. As for the bands in the other regions there does not seem to exist even a complete measurement of them (Hertenstein, 1912, Pearce and Gaydon, 1941; Rosen 1945; Lejuene and Rosen, 1945 and Rao, 1946). It was, therefore, considered necessary to photograph the spectrum of this flame and to make a complete measurement of the wavelengths of all the radiations present in it. This has been done and as a result it has been found that the spectrum is quite complicated and the structures are not easily understood. Full details are given in the following sections:

EXPERIMENTAL

The copper arc used was run from 110 volts D. C. supply. The electrodes were horizontal and the image of the flame above the level of the electrodes was thrown by means of a lens over the slit of a glass Littrow spectrograph having a dispersion of about 12 Å per mm. at $\lambda 5500\text{Å}$. Exposures of about one and a half hours on Ilford Special Rapid Panchromatic plates were necessary to get the fainter bands with an intensity so that they could be read in the microscope. The iron arc was used for comparison. A copper arc was also exposed side by side in order to eliminate the copper lines from the spectrum of the flame.

DESCRIPTION OF THE SPECTRUM

The spectrum of the flame is given in Plate III. The prominent features of the spectrum are the very intense bands in the orange region, one or two intense bands in the green, a large number of comparatively faint bands in the orange, yellow and green and the strong green and yellow lines of copper, which could not be eliminated, although their relative intensities have been considerably reduced. The fainter bands can apparently be put into several groups described below.

Beginning from the short wavelength side, the first group starts at 44828\AA and extends up to 4916\AA . There are 9 prominent bands in this region with heads at 44828.5 , 4836.5 , 4845 , 4852.5 , 4862.5 , 4871.5 , 4882.5 , 4893.5 and 4916\AA . The last band is the most intense of the lot, although the others also are quite strong. The fainter bands of this group have heads at 44852.5 , 4876 , 4901 , 4904 and 4911\AA .

The second group lies between 44976 and 45040\AA . Two bands at 45030.3 and 5039.5\AA have distinct heads, both degraded to the red. The bands at 44976.1 , 4982.7 and 4989.6\AA are somewhat less intense. These are also degraded to the red. There is a strong band at 44996\AA . This is quite broad and does not show any head. The measurement corresponds to the centre of the band. It is possible that there may be a faint structure at 45002\AA which is masked by the above band. The other faint structures are at 45005.9 , 5008.7 and 5011.9\AA .

A single intense band lies at 45071.4\AA . It is degraded to the red but is quite blurred. Another intense band occurs with head at 45227.8\AA , degraded to the red.

A third group starts at 45274\AA , 4 distinct bands appear with heads at 45274.0 , 5278.9 , 5282.7 and 5285.6\AA . They all appear degraded to the red, but they are all so narrow that they look more or less like lines. There are faint band heads at 45302.6 and 5304.6\AA , followed by two stronger ones at 45307.4 and 5312.0\AA .

Again there are two bands, comparatively isolated, the intense one with head at 45345.1\AA and the faint one, at 45347.9\AA .

A fourth group of bands appears between 45150 and 45500\AA . Nine heads have been measured, which seem to be gradually converging towards the short wavelength side. They all appear degraded to the red. The more prominent amongst them have their heads at 45496.1 and 5488.2\AA . The others follow at shorter wavelengths with gradually decreasing separation and intensity.

A moderately intense band is observed at 45529.5\AA , degraded towards the red. Another one which is a little blurred appears at about 45557\AA .

A fifth group of bands is observed between 45827 and 45895\AA . Some of the bands of this group are blurred. The stronger and more distinct ones are at 45847.6 and 5856.0\AA .

TABLE I

Wavelengths of bands in the flame above a copper arc in air.

$\lambda_{\text{air}} (\text{\AA})$	$\nu_{\text{vac}} (\text{cm}^{-1})$	Int.	$\lambda_{\text{air}} (\text{\AA})$	$\nu_{\text{vac}} (\text{cm}^{-1})$	Int.
4628.4	20704.5	s	5833.3	17138.2	m
36.5	670.4	s	44.9	113.0	w
45.2	633.2	s	43.4	108.6	
52.6	601.8	s	47.6	96.3	m
54.9	592.0	m	50.4	98.1	?
62.4	560.7	s	56.0	97.8	m
65.7	546.3	w	55.0	93.0	w
71.4	522.3	s	66.0	94.7	m
75.8	503.7	m	73.7	920.3	w
82.6	475.2	s	80.3	901.2	w
89.1	448.0	w	89.1	16975.8	m
93.5	420.6	s	95.0	958.8	m
4901.0	398.3	w	5912.6	879.8	w
04.2	385.0	m	26.4	809.0	w
10.9	357.2	m	32.2	852.5	m
16.2	335.3	vs	36.0	841.7	w
76.1	290.5	w	40.5	828.9	m
82.7	263.9	m	43.6	820.2	vw
89.6	236.1	m	48.2	807.2	m
95.7	211.6	s	50.5	800.7	w
5002.6	19984.0	w	57.5	780.9	m
05.9	970.9	w	65.0	759.8	m
08.7	959.7	w	6030.1	578.1	?
11.0	917.0	m	45.1	537.8	vv
30.3	874.0	s	46.0	535.3	?
39.5	837.7	s	48.3	529.0	s
71.4	712.0	vs	52.7	517.0	s
5227.8	123.2	vs	59.1	499.5	vv
32.4	105.4	m	64.1	485.9	w
34.3	099.4	s	69.0	172.6	w
35.8	094.0	vs	78.2	147.7	w
46.5	091.4		6146.8	264.1	vv
41.8	072.1	vv	51.1	252.8	w
74.0	18055.7	s	57.3	236.4	m
78.0	938.1	s	61.5	225.3	vv
82.7	924.5	s	68.7	206.4	m
85.6	914.1	w	74.5	191.2	w
92.6	889.7	m	91.5	146.7	vw
5302.6	853.4	?	6005.3	110.8	w
04.6	846.3	w	11.6	094.5	w
07.4	836.4	m	20.1	072.5	m
12.0	820.1	vs	23.0	065.0	m
45.1	703.5	s	70.3	15943.8	w
47.9	693.7	?	80.1	918.9	w
5385.0	18505.0	?	89.1	890.1	w
5457.7	317.7	w	94.0	883.8	vv
66.1	289.5	w	97.6	874.7	s
68.7	280.8	w	6302.6	862.1	m
72.7	267.5	w	13.5	834.7	m
77.0	253.1	m	23.9	808.7	w
82.2	235.8	m	78.5	074.3	w
88.2	215.9	m	84.9	657.6	vw
96.1	189.7	m	92.5	630.0	vw
5529.5	079.8	s	6400.3	620.0	s
56.8	17991.0	m	03.5	612.2	vw
57.9	987.4	s	15.2	583.7	vw
5827.6	155.0		30.2	547.3	vw
29.0	150.9	m			

A sixth group of bands appears between $\lambda 5922.6$ and $\lambda 5965\text{\AA}$. This group of bands is followed by the very strong bands in the orange and red regions extending up to $\lambda 6550\text{\AA}$. Our measurements in this region are in general agreement with those due to Pearse and Gaydon (1941). The bands are degraded to the red. The structure is complex, consisting of several heads of varying intensity.

A complete list of all wavelengths measured is given in Table I, and can be generally taken to be correct to within $\pm 1\text{\AA}$.

The intensities given are visual estimates, and the notations in that column have the following significance: *s* means strong, *m* means medium, *w* means weak, *v* means very and ? means that the band measured was so faint that its existence is doubtful. Measurements included in braces mean that the corresponding bands did not clearly indicate which way they were degraded and in such cases either both the ends and the centre or at least both of them have been measured. All the other bands were degraded to the red.

DISCUSSION

We will consider the strong bands in the red and orange and the fainter ones dispersed over the entire yellow and green regions separately.

(a) *Bands in the orange and red regions.* An analysis of the bands in this region was proposed by Mahanti (1930), but this is doubted by Loomis and Watson (1935). Rosen (1945) carried out a vibrational analysis of these bands and found that they could be represented by the equation

$$\nu = 16222 - 625 \nu'' + 3 \nu''^2 + 274 \nu'$$

A different equation for the vibrational analysis of these bands has been proposed by Guntch (1946). According to him

$$\nu_0 = 16273.9 + 285.6 \nu' - 9.2 \nu'^2 - 318.6 \nu'' + 4.4 \nu''^2, \text{ where } u = \nu + \frac{1}{2}$$

Guntch gives evidences in support of his equation. He has also carried out the rotational analysis for 5 bands of this system and believes them to be due to $^2\Sigma - ^2\Sigma$ transition of CuO molecule. The *B* values are $B''_0 = 0.632$ and $B'_0 = 0.591 \text{ cm}^{-1}$. Our own arrangements, as given in Table II, is in agreement with Guntch's equation, but it suffers from certain defects, viz, (1) the agreement is not as good as could be expected, (2) the vibrational differences are not very satisfactory and (3) all the bands in the region are not accounted for by this arrangement.

(b) *Bands in the green and yellow regions.* Although some of the measurements given in Table I in the yellow region may be associated with the orange bands, it seems doubtful if all of them can be accounted for in this way. Nor does there appear any clue for classifying the yellow and the green bands from an inspection of the spectrum. At any rate, then

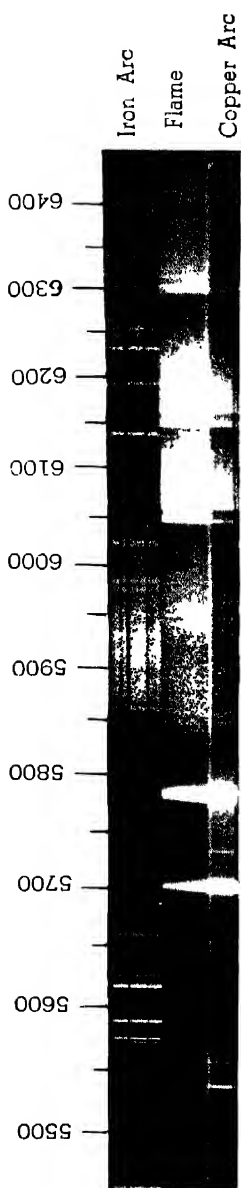
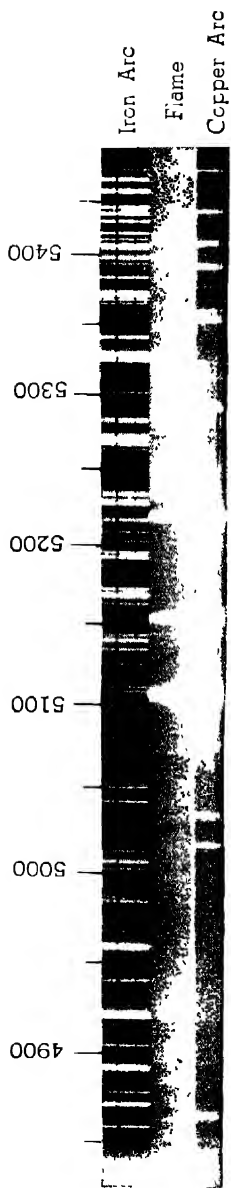


Fig 1.—Spectrum of the flame above a Copper arc in air

appearance is so different from that of the orange and red bands that it does not look probable that the entire stuff can be attributed to the same emitter. Yet certain bands, from their appearance, seem to suggest some sort of regularity. Thus the bands, referred to as belonging to the first group in the previous section, indicate, from their appearance, that it should be possible to arrange them in some sort of fragmentary system. This is easily done, as given in Table III.

TABLE II

$\nu' - \nu''$ scheme for orange-red bands

$\nu' \backslash \nu''$	0	1	2	3	4	5
0	16264					
1	16538	6225	- 15920	15670	15310*	
2		16499		15884		15270*
						15547

D₂ notes that the corresponding band has been taken from Pearse and Gaydon (1941).

TABLE III

$\nu' - \nu''$ scheme for the bands between $\lambda 4828$ and $\lambda 4916\text{\AA}$.

$\nu' \backslash \nu''$	0	1	2	3
0	20504	20385		
1	20592	20475	20357	
2	20670	20560	20448	20335
3		20633		20430

The ω 's are, however, so much different from those suggested for the orange-red system by Guntch that it is difficult to believe that those two systems are due to the same emitter.

The bands in the other groups mentioned in the previous section do not generally seem to suggest any order. Some bands, however, between $\lambda 5270$ and $\lambda 5530\text{\AA}$, can be picked up from the spectrogram and their separation indicated that they might belong to one system. Such bands are given in Table IV. This system may be attributed to the same emitter to which the orange system belongs, *i.e.*, to CuO. But here again none of the ω 's agree and if both the systems belong to CuO, the states involved are all different.

TABLE IV

 $\nu' - \nu''$ scheme for some bands in the green region.

$\nu' \backslash \nu''$	0	1	2	3	4
0	19093*	18827	18565	18318	18080
1		18956	18704		

* This band is strong, but its head is not distinct. The centre had to be measured. More work seems necessary to clarify all these points.

ACKNOWLEDGMENT

Finally, it is a great pleasure to record our thanks to Dr. M. M. Sengupta for giving us all the facilities for this work.

SCIENCE COLLEGE,
PATNA.

REFERENCES

- Guntzsch, A. 1946, *Ark. Mat. Astr. Fys.*, **33A**, 8.
 Hertenslein, H., 1912, *Wiss. Phot.*, **11**, 69, 119.
 Lejuene, J. M. and Rosen, B., 1945, *Bull. Soc. Sci. Liege*, **14**, 81.
 Loomis, F. W., and Watson, T. F. 1935, *Phys. Rev.*, **48**, 280.
 Mahanti, P. C., 1930, *Nature*, **125**, 819.
 Mulliken, R. S., 1925, *Phys. Rev.*, **26**, 1.
 Pearse, R. W. B., and Gaydon, A. G., 1941. *The Identification of Molecular Spectra*.
 Rao, V. R., 1946, *Curr. Sci.*, **15**, 69.
 Rosen, B., 1945, *Nature*, **156**, 570.

A NEW LABORATORY HYDROGEN CONTINUUM

By S. K. BHATTACHARYA

(Received for publication, Dec. 8, 1949)

ABSTRACT A simple high intensity hydrogen discharge tube as a source for ultra-violet light is described. This hydrogen continuum source is very simple and easy to set up in any laboratory.

INTRODUCTION

In this laboratory a special discharge tube was being made to study the emission spectra of the alkali hydrides. During this pursuit the present hydrogen discharge tube was made. Through this a continuous flow of pure hydrogen gas was maintained at a pressure less than 1 mm, a Cenco-Hyvac pump evacuating all the time and the discharge tube was then sparked. The spectrum photographed by an Adam Hilger E_2 spectrograph showed the performance of this hydrogen discharge tube as a hydrogen continuum very good. The present hydrogen discharge tube being extremely simple in comparison with those of the previous workers [Bay and Steiner (1927); Lawrence and Eldefassen (1930); Kistiakowsky (1931); Nanda (1945)] is described in detail here.

The Discharge Tube The discharge tube was entirely made of pyrex glass except the quartz windows W at the ends which were sealed in by shellac. The discharge tube is shown in Fig. 1. It consists of the long tube

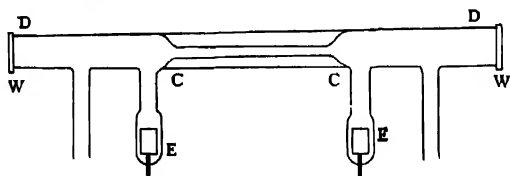


FIG. 1

DD (75 cm. long, 8 mm. bore) having a capillary tubing CC (22 cm long, 2 mm. bore). The electrodes EE used were hollow cylindrical tungsten electrodes sealed by tungsten pyrex seals. The electrodes were not touching glass walls.

EXPERIMENTAL PROCEDURE

Fig. 2 shows the experimental arrangement. Hydrogen gas, prepared from magnesium and hydrochloric acid, was collected in a gas holder. The

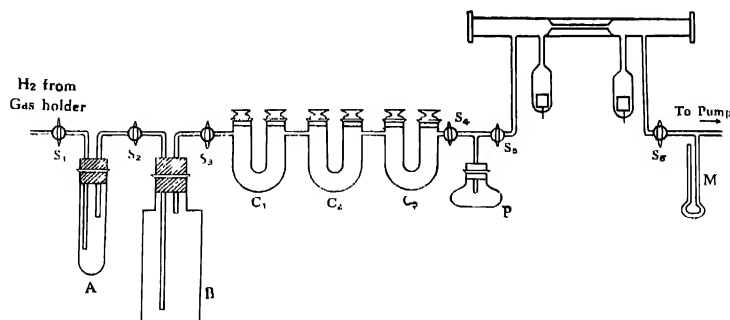


FIG. 2

hydrogen gas was passed through a water trap *A*, an empty flask *B*, a series of fused calcium chloride tubes *C*₁, *C*₂, *C*₃, and finally through phosphorous pentoxide tube *P* before it really entered the discharge tube. The discharge tube was connected to the Cenco-Hyvac pump through a manometer *M*. The water trap *A* was used for two reasons; firstly to absorb any traces of hydrochloric acid gas, if present, and secondly to indicate the rate of the flow of hydrogen gas passing through the discharge tube from the rates of bubbling within a period of time. An Adam Hilger H₂ spectrograph was used to record the spectrum. The sparking arrangement used to run the discharge tube was the sparking apparatus for spectroscopy (catalogue nos. F281, F282, F283) supplied by Adam Hilger, Ltd.

RESULTS

A number of plates were exposed at varying rates of flow of hydrogen gas through the discharge tube and also at different sparking voltages (8,000 V, 10,000 V; 12,500 V; and 15,000 V). The Ilford Special rapid panchromatic plates and metol-hydroquinone developer were used during the experiment. The most intense hydrogen continuum developed when the rate of hydrogen gas flow was 100 bubbles per 70 secs. and the sparking voltage was 10,000 volts. The duration of exposure in this case was 15 minutes.

ACKNOWLEDGMENT

The author wishes to express his gratitude to Prof. M. N. Saha, D.Sc. F.R.S., for his keen interest.

DEPARTMENT OF PHYSICS,
B. N. COLLEGE, PATNA.

REFERENCES

- Bay and Steiner, 1927, *Zeits. f. Phys.*, **45**, 337.
Kistiakowsky, 1931, *Rev. Sci. Inst.*, **2**, 549.
Lawrence and Bldefassen, 1930, *Rev. Sci. Inst.*, **1**, 45.
Nanda, 1945, *Ind. J. Phys.*, **19**, 8.

RAMAN SPECTRA OF ORGANIC CRYSTALS AT DIFFERENT LOW TEMPERATURES. I. CHLOROBENZENE AND TOLUENE*

By A. K. RAY

(Received for publication, Feb. 9, 1950)

Plate IV

ABSTRACT. The Raman spectra of solid chlorobenzene at two different temperatures -6°C and -28°C and of solid toluene at -105°C and -180°C have been investigated. In each case five new Raman lines have been observed. The frequency shifts of these lines lie between 45 cm^{-1} and 135 cm^{-1} . In the case of chlorobenzene all these lines are observed to shift away from the Rayleigh line, some by 3 cm^{-1} and others by about 6 cm^{-1} when the solid is cooled down from -6°C to -180°C , while in the case of solid toluene four of the five lines remain almost in their original positions and only one of them at 100 cm^{-1} shifts to 110 cm^{-1} when the crystal is cooled to -180°C . The intensities of these new lines do not diminish with the lowering of temperature. Some of the lines due to internal oscillations of the molecule are also observed to undergo changes with the change of temperature. It has been pointed out that the results cannot be explained satisfactorily by assuming the new lines to be due to angular oscillations of the molecules in the lattice as has been done by some previous workers.

INTRODUCTION

The Raman spectra of many organic compounds in the solid state at low temperatures were studied by previous workers in order to understand the cause of changes which take place in the Raman spectra when the substances are solidified at low temperatures. The most important change which takes place in the Raman spectrum of some organic compounds is the appearance of new lines in the neighbourhood of the Rayleigh line. This was first observed by Gross and Vuks (1935) who attributed the origin of these lines to lattice oscillations. Sirkar (1935, 1936) showed that some of the lines in the low frequency region observed in the case of solid diphenyl ether persist in the liquid state and even when the substance is dissolved in cyclohexane. It was also observed by him that the frequency-shifts of the new lines increase with the lowering of temperature of the crystal in the case of naphthalene. Later he pointed out (Sirkar, 1937) that the new lines were very intense in the case of naphthalene and similar other substances having centro-symmetrical molecules, although translational oscillations of the molecules in the lattice were forbidden in the Raman effect in these cases,

* Communicated by Prof S. C. Sirkar.

Bhagavantam (1941) investigated the problem with the help of group theory and came to the conclusions that although the lattice oscillations involving translational oscillations of the molecule are forbidden in the Raman effect in the case of centro-symmetrical molecules the three degrees of rotational freedom of the molecule can give rise to six Raman lines in the case of the naphthalene lattice the unit cell of which contains two molecules. He thus came to the conclusion that the new Raman lines yielded by the solid state were due to rotational oscillations of the molecules in the lattice and the hypothesis put forward by Sirkar (1937) that these lines might be due to formation of new intermolecular bonds in the solid state was unnecessary. Kastler and Rousset (1941) also independently pointed out that the new lines observed in the case of naphthalene and a few other aromatic compounds in the solid state were due to rotational oscillations of the molecules in the lattice about the three axes of the molecules. Nedungadi (1942) investigated the Raman spectra of single crystal of naphthalene using polarised incident light and different orientations of the crystal with respect to the incident light vector and came to the conclusion that the results were in agreement with the theory put forward by Bhagavantam (1941), because actually six new lines were observed in the neighbourhood of the Rayleigh line and also some of the lines were due to the internal oscillations of the molecule were found to be split up into doublets predicted by the theory. The theory was further tested by Rousset and Lochet (1942), Rousset (1944a, 1944b) and by Kastler and Fruhling (1944) and they came to the conclusion that the results obtained in the case of para dichloro-, dibromo- and diiodobenzene, benzene and naphthalene can be explained by the theory put forward by Bhagavantam (1941) and also independently by Kastler and Rousset (1941). A brief review of these works has also been published recently by Kastler and Rousset (1947).

Although the authors mentioned above have shown that group theoretical consideration predicts new lines in the neighbourhood of the Rayleigh line in the case of crystals they have not discussed in what way the position and the intensities of these new lines should depend on the temperature of the crystal. The theory can be tested only by studying such dependence in the case of a large number of different substances. A programme has, therefore, been undertaken to test this particular theory by observing the dependence of the intensities and position of the new lines on temperature. The present paper deals with results obtained in the case of two aromatic compounds having simple but similar molecules *e.g.*, chlorobenzene and toluene.

EXPERIMENTAL

Of the two liquids used toluene was obtained from U. S. A. and mono-chlorobenzene from May and Baker and both were of pure quality. They were distilled in vacuum before use and the purity was tested by comparing

the Raman spectra of the liquids with those published by previous workers. In order to investigate the Raman spectra of the solid at different low temperatures the liquid was put in a cylindrical Pyrex container about one inch in diameter provided with a long narrow neck, the mouth of which was sealed. The container was suspended in a transparent Dewar vessel of Pyrex glass closed by a cork and the height of the bottom of the container from level of the liquid oxygen in the Dewar vessel was adjusted to get the desired low temperature, which was measured with a pentane thermometer. Liquid oxygen was introduced in the Dewar vessel through a Pyrex glass tube passing through the cork and connected to another such tube immersed in liquid oxygen contained in a large metallic Dewar vessel. Whenever the pressure inside the Dewar vessel of Pyrex glass was reduced by a Cenco-hyvac pump, there was a flow of liquid oxygen into it from the larger vessel. The solidified organic substance in its container was illuminated by focussing light from two vertical mercury arcs placed on two sides with the help of condensers. A Fuess glass spectrograph having a dispersion of about 10.8 Å U. in the 4016 Å region was used to photograph the Raman spectra. Iron arc spectrum was used as comparison. The liquids were cooled very slowly to obtain homogeneous masses of solid and the spectrograms obtained were free from excessive extraneous light. In the case of chlorobenzene two spectrograms with the solid at about -60°C and -180°C were obtained and in the case of toluene the corresponding temperatures of the solid were about -105°C and -180°C respectively. The spectrograms obtained are reproduced in figures 1 and 2 in Plate IV.

RESULTS AND DISCUSSION

The frequency-shifts of the Raman lines observed in the two cases have been given in Tables I and II. The data for the liquids have also been included for comparison. Faint lines for the liquids have not been recorded because the continuous background in the spectrogram due to the solid state masked such lines.

The frequencies of Raman lines observed in the case of the two liquids agree closely with those given by previous authors (Magat, 1936). It can be seen from Tables I and II, however, that some changes occur in the Raman spectra when the liquids are solidified and also when the solid is further cooled down. In each case five new Raman lines appear in the low frequency region when the liquid is solidified and the lines shift a little when the temperature of the solid is further lowered to -180°C (figs. 4 and 5). The frequencies of the new lines in the case of chlorobenzene agree fairly well with those reported earlier by Sirkar and Gupta (1937) for the solid at -180°C . The faint line in 33 cm^{-1} was not observed by them. The lines nearer to the Rayleigh line at -60°C than at $+180^{\circ}\text{C}$ showing that

TABLE I
Chlorobenzene C_6H_5Cl

Liquid at about 30°C $\Delta\nu$ in cm^{-1}	Solid at about -60°C $\Delta\nu$ in cm^{-1}	Solid at about -180°C $\Delta\nu$ in cm^{-1}
	43 (2); e, h	46 (3); e, h
	60 (1); e, h	63 (2); e, h
	76 (2); e, h	83 (3); e, h
	96 (2); e, h	102 (3); e, h
	127 (0); e, h	135 (1); e, h
198 (3); e, h	215 (2b); e, h	217 (2b); e, h
295 (1); e, h	295 (0); e, h	298 (1); e, h
418 (3); e, h	412 (2); e, h	412 (2); e, h
615 (2); e, h	610 (1); e, h	608 (1); e, h
699 (3); e, h	701 (1); e, h	703 (3); e, h
1001 (5); e, i, h	1001 (5); e, i, h	1001 (5); e, i, h
1020 (2); e, h	1015 (1); e, h	1013 (1); e, h
1085 (2); e, h	1089 (2); e, h	1089 (2); e, h
1122 (ob); e, h	1122 (ob); e, h	1122 (ob); e, h
1155 (1); e, h	1158 (1); e, h	1158 (1); e, h
1355 (2); e, h		
1475 (0); e, h		
1565 (0); e, h	1565 (1); e, h	1565 (2); e, h
1580 (3); e, h	1580 (2); e, h	1580 (3); e, h
	3058 (1); e, h	3058 (3); e, h
3065 (8); e, i, h	3065 (3); e, h	3065 (5); e, h
	3090 (c); h	3090 (1); h
3151 (1b); e, h	3161 (7b); h	3161 (ob); h

whatever be the nature of oscillations which produce these lines, the restoring force increases at the lower temperature. This dependence on temperature observed in the case of toluene, however, seems to be different from that observed in the case of chlorobenzene. In the former case the four lines 48, 70, 88, and 128 cm^{-1} shift towards the Rayleigh line and the line 100 cm^{-1} shifts away from the Rayleigh line as the temperature of the solid is lowered to -180°C, while in the latter case all these new lines shift away from the Rayleigh line with the lowering of the temperature.

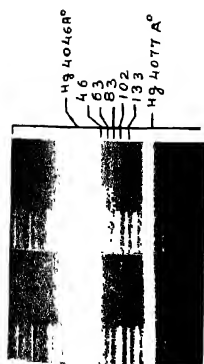
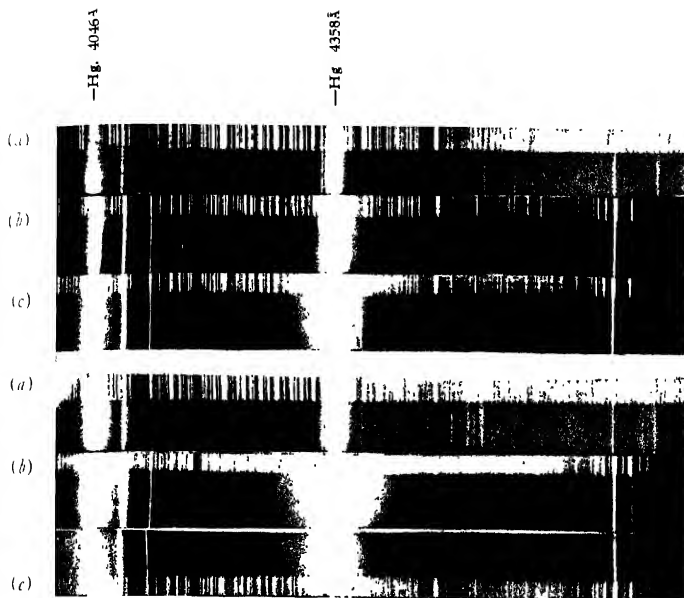


Fig 3

- (a) C_6H_5Cl —liquid at about $30^\circ C$
 (b) " solid at about $-60^\circ C$
 (c) " solid at about $-180^\circ C$
 (a) C_6H_5Cl —solid at about $-180^\circ C$
 (b) " solid at about $-60^\circ C$

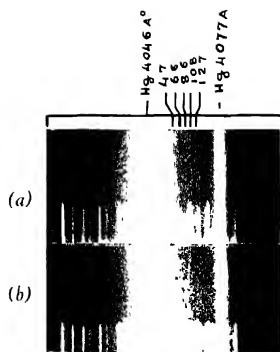


Fig 4

- Fig. 2 (a) $C_6H_5CH_3$ —liquid at about $30^\circ C$
 (b) " solid at about $-105^\circ C$
 (c) " solid at about $-180^\circ C$
 Fig 4 (a) $C_6H_5CH_3$ —solid at about $-180^\circ C$
 (b) " solid at about $-105^\circ C$

TABLE II
Toluene $C_6H_5CH_3$

Liquid at 30°C $\Delta\nu$ in cm^{-1}	Solid at -105°C $\Delta\nu$ in cm^{-1}	Solid at -185°C $\Delta\nu$ in cm^{-1}
	48 (1); <i>e, k</i>	47 (2), <i>e, k</i>
	70 (1), <i>e, k</i>	66 (2); <i>e, k</i>
	88 (0), <i>e, k</i>	86 (1); <i>e, k</i>
	100 (1); <i>e, k</i>	108 (2); <i>e, k</i>
	128 (0b); <i>e, k</i>	127 (0); <i>e, k</i>
215 (1); <i>e, l, k</i>	216 (2), <i>e, k</i>	220 (2); <i>e, k</i>
342 (1); <i>e, k</i>		
520 (3), <i>e, k</i>	520 (1), <i>e, k</i>	520 (2), <i>e, k</i>
620 (3), <i>e, k</i>	620 (1b); <i>e, k</i>	623 (2); <i>e, k</i>
734 (0); <i>e, k</i>		
786 (5), <i>e, k</i>	786 (3); <i>e, k</i>	788 (5), <i>e, k</i>
806 (0); <i>e, k</i>		
838 (0); <i>e, k</i>		
891 (0); <i>e, k</i>		
1003 (10); <i>e, l, k</i>	1003 (3); <i>e, l, k</i>	1005 (10); <i>e, l, k</i>
1029 (3); <i>e, k</i>	1032 (2); <i>e, k</i>	1033 (4); <i>e, k</i>
1057 (2); <i>e, k</i>		
1187 (0); <i>k</i>		
1213 (2); <i>e, k</i>	1217 (2); <i>e, k</i>	1217 (3); <i>e, k</i>
1380 (2); <i>e, k</i>	1380 (1); <i>e, k</i>	1380 (2); <i>e, k</i>
1590 (1); <i>e, k</i>	1596 (2); <i>e, k</i>	1592 (1); <i>e, k</i>
1604 (4); <i>e, k</i>	1610 (3), <i>e, k</i>	1608 (3), <i>e, k</i>
2865 (2b); <i>e, k</i>	2865 (0b); <i>k</i>	2865 (0b); <i>k</i>
2921 (10); <i>e, l, k</i>	2921 (3); <i>e, k</i>	2921 (5); <i>e, k</i>
2980 (1), <i>e, k</i>	2980 (0); <i>k</i>	2980 (0), <i>k</i>
3030 (4), <i>e, k</i>	3030 (2), <i>e, k</i>	3030 (3); <i>e, k</i>
3059 (10); <i>e, l, k</i>	3060 (5), <i>e, k</i>	3060 (8), <i>e, k</i>

As regards the other changes observed in the Raman spectrum of chlorobenzene the splitting up of the line 3065 cm^{-1} into three sharp lines at 3058, 3065 and 3090 cm^{-1} is striking. This line is due to symmetric C-H valence oscillation. The line 1001 cm^{-1} due to symmetric oscillation of

the carbon ring does not change its position when the liquid is solidified, but the frequency shift of its companion 1020 cm^{-1} diminishes a little. Also the line 198 cm^{-1} due to the liquid shifts to 215 cm^{-1} and the intensities of the lines 1565 and 1580 cm^{-1} tend to become equal in the case of the solid state. In the case of toluene on the other hand, no change takes place in the frequencies of the C-H valence oscillations when the liquid is solidified and also the line 215 cm^{-1} remains almost in its original position, but the lines 1029 , 1213 , 1590 and 1604 cm^{-1} shift respectively to 1032 , 1217 , 1596 and 1610 cm^{-1} when the liquid is solidified. The last two lines again shift respectively to 1592 and 1608 cm^{-1} when the solid is further cooled to -180°C , and also their intensities become equal to each other at -180°C .

If attempts are made to explain the changes which occur in the Raman spectra with the solidification of the liquids on the theory (Bhagavantham, 1941) that the molecules execute angular oscillations about their axes, the following difficulties arise. First, the amplitude of such oscillation should diminish with the lowering of temperature and therefore the intensity of the new lines should also diminish at the lower temperature. No such diminution is actually observed. Secondly, according to such a theory, six new Raman lines arise if there are two molecules in the unit cell having some particular symmetry elements, three of these being due to oscillations symmetric to the symmetry elements and the other three due to oscillations antisymmetric to these symmetry elements. In the present two cases if it is assumed that one of the five new lines is a doublet, the number will agree with those predicted by the theory mentioned above, but the difference of frequencies of the components of each pair is too much to account for the extreme sharpness of the lines due to inner oscillations of the single molecule. If the frequencies of lines due to angular oscillations of the molecules depend so much on the proximity of the neighbouring molecules, each inner oscillation can also be postulated to be of two types, one symmetric and the other antisymmetric to the symmetry elements of the unit cell, and the frequencies of these two types of oscillation should then have been appreciably different from each other. On the contrary, it can be seen from figures 1 and 2, Plate IV, that each of the prominent lines due to the inner vibrations of the single molecule becomes so sharp in the solid state that its width is not more than 2 to 3 cm^{-1} . Thirdly, it cannot be explained why the behaviour of the C-H valence oscillations in the two cases is different from each other, although the molecules are similar, and also, why the new lines behave differently in the two cases with the change of temperature of the solid. Finally, the moments of inertia of these two molecules being greater than that of the benzene molecule, the frequencies of angular oscillation cannot be larger than that observed in the case of benzene. Actually, however, these frequencies are larger than those observed in the case of benzene.

The change in the frequencies of the C-H valence oscillation in the case of solid chlorobenzene, on the other hand may be due to the presence of chlorine atoms in the lattice, there being strong tendency of this atom to form virtual HCl bond with the hydrogen atom of the surrounding molecule, and the shift of the other lines due to inner frequencies may also be indirect effect of the formation of such a virtual bond. In the case of toluene also as the molecules are polar they may be associated in the solid state. The origin of five new lines given by the solid state seems to be intimately connected with the presence of the benzene ring in both the molecules, but owing to the difficulties mentioned earlier they cannot be ascribed to oscillations of single molecules pivoted in the lattice as postulated by Kastler and Rousset (1941) and by Bhagavantam (1941). If it is assumed that the hindered rotations of the molecules in the liquid is transformed into angular oscillations in the solid state the magnitude of the intermolecular field is to be taken into consideration. It has been shown by Sirkar and Sen (1949) that the frequencies of hindered rotation of some polar molecules in the liquid deduced from the frequencies of radio waves observed by such liquids is so small that the corresponding frequency shift in the Raman effect would be of the order of a fraction of 1 cm^{-1} . There is also no reason to suppose that these forces of restitution increase enormously in the solid state because actually it is observed that with the lowering of temperature of the liquid the internal viscosity of the molecules increases and consequently the frequencies of the radio waves observed diminish considerably instead of increasing with the lowering of temperature in the case of all polar molecules studied so far. Hence it is evident that in order to explain the comparatively large frequencies of the new Raman lines observed in the present case, *e.g.*, those lying in the range from 46 cm^{-1} up to about 133 cm^{-1} , new type of force of restitution of larger order of magnitude than what is actually present in the liquid state has to be postulated. This force has been assumed to be that due to formation of virtual bond in the present paper. Probably this theory will also be able to explain the anomalies which may still exist in the explanation of the origin of new lines in the case of some non-polar aromatic compounds, *e.g.*, benzene, naphthalene, etc.

ACKNOWLEDGMENT

The author is indebted to Prof. S. C. Sirkar for his kind interest and guidance throughout the progress of the work.

INDIAN ASSOCIATION FOR THE CULTIVATION OF SCIENCE,
210, BOWBAZAR STREET, CALCUTTA.

REFERENCES

- Bhagavantam, S. 1941, *Proc. Ind. Acad. Sc.*, A, 13, 543.
Gross, E. and Vuks, M., *Nature*, 136, 100, 431 and 963 (1935).

- Kastler, A. and Fruhling, 1944, A. C. R. Acad. Sc , **213**, 998
- Kastler, A. and Rousset, A, 1941, C. R. Acad. Sc., **212**, 645; Jour de Physique, **2**, 49.
- Magat, M. 1935, Annual Tables, Paris, **26**. pp. 71 and 75
- Nedungadi, T. M. K., 1942, *Proc Ind. Acad. Sc A*, **18**, 376
- Rousset, A. 1944a, C R Acad Sc., **219**, 485.
- „ 1944b, „ , **219**, 546.
- Rousset, A, and Lochet, R. 1942, *Jour de. Physique*, **2**, 146
- Sirkar, S. C., 1935, *Science and Culture*, **1**, 361.
- „ „ 1936, *Ind. J. Phys.* **10**, 109
- „ „ 1937, *Ind. J Phys* **11**, 343.
- Sirkar, S. C. and Gupta, J , 1937. *Ind J Phys* , **11**, 55.
- Sirkar, S C. and Sen, S. N., 1949, *Nature*, **163**, 1048.

STUDIES OF SCHRAGE THREE PHASE SHUNT COMMUTATOR MOTOR, III. CIRCLE DIAGRAMS

By H. P. BHATTACHARYYA

(Received for publication, 8th Feb., 1950)

ABSTRACT. This paper reports the experimental verification of the theoretical locus diagrams as obtained from the author's equation in the brush position, where the machine runs super-synchronous at no-load and sub-synchronous on load, as well as in the brush position intermediate between short-circuit and synchronous.

INTRODUCTION

In a previous communication the author (Bhattacharyya, 1949) developed an equation for the circle diagrams of a Schrage three phase shunt commutator motor in the brush position where it runs super-synchronous at no-load and sub-synchronous on load. The present paper reports the experimental verification of this equation from data obtained on a B. T. H. machine. For this purpose the theoretical and experimental locus diagrams at different brush positions including the one which is intermediate between short-circuit and synchronous conditions have been drawn.

The specifications and design data of the B. T. H. machine under test are as follows :

Type :—CHT, No. 5622 G
 Cycles :— 50
 Primary Volts :— 220/400
 H. P. :— 6
 Speed :— 1800 r. p. m.
 Poles :— 6

	Stator	Rotor	
	Secondary	Primary	Commutator
Type of winding.	Double Layer Lap	Double Layer Lap	
Poles in parallel.	1, 2, 3, or 6	1	
Turns in series per phase.	90, 45, 30, or 15	180	1 per seg.
No. of slots.	54		36
Pitch of coils.	1-8	1-6	2 coils 1-6 2 coils 1-7

No. of commutator segments	= 144
Resistance of primary winding per phase at 60°C	= 0.738 ohm
Resistance of secondary winding per pole per phase at 60°C	= 0.044 „
Resistance of regulating winding referred to secondary with 6 poles in parallel at 60°C	= 0.0165 „
Reactance (at 50 cycles) of primary winding per phase	= 5.27 ohms
Reactance (at 50 cycles) of secondary winding per phase referred to primary	= 2.83 „

EXPERIMENTAL

The machine was run with its primary connected in star to a 400 V source and with the secondary having 6 poles in parallel. It was loaded by means of a Walker's Fan-Brake Dynamometer. An indexing device was made on the brush gear of the machine to indicate the position of the brush in order to be sure that the latter remained unchanged during a set of observations and was divided into 36 equal divisions. The brush position corresponding to the synchronous condition of the machine was marked zero on the indexing device. It was then found that at mark 2, the brushes were just short-circuited; at mark 1, they were crossed over and the speed of the machine was sub-synchronous, while at mark 34, the brushes were also crossed over but the no-load speed was super-synchronous, the brush and the stator secondary induced voltages being in opposition; on loading the machine the speed became, however, sub-synchronous and the above voltages became additive. Thus at mark 1, the brush and the stator induced voltages were additive both at no-load and on load while at mark 34, they were subtractive at no-load and additive on load. These two positions of the brush are, therefore, of interest in the present investigation. Data of primary voltage, current, wattage, power-factor and corresponding speed were noted by varying the load on the machine for each of these two positions of the brush. They are included in Tables I and II.

TABLE I
(Brush position at mark 34)

Volts (line)	Current (line amps.)	Watts	P. F.	Speed (r p m.)
400	5.05	1045.5	0.2988	1080
400	5.50	1931.8	0.5070	980
398	5.75	2204.5	0.5534	930
400	6.15	2636.4	0.6187	900
400	6.55	2954.5	0.6512	860

Studies of Schrage Three Phase Shunt Commutator Motor 121

TABLE II
(Brush position at mark 1)

Volts (line)	Current (line amps)	Watts	P. F.	Speed (r. p. m.)
400	4.60	818.2	0.2567	930
398	4.95	1409.0	0.4110	840
398	5.03	1568.2	0.4500	810
400	5.44	1818.2	0.5009	780
400	5.40	2000.0	0.5347	745

CIRCLE DIAGRAMS

In the previous communication (*loc. cit.*) the following equation was deduced for a symmetrical brush position of the motor having the same effective number of primary (rotor) and secondary (stator) turns,

$$\sin \psi (VR_2) + \cos \psi (VpX_2) = I_1 \left[R_1 p X_2 + X_1 R_2 - \frac{R_2 (X_2 + pX_1)}{1 + p} \right] \quad \dots (1)$$

where,

V = Primary volts applied per phase

R_1 = Primary resistance per phase

R_2 = Secondary resistance (lap-connected) per phase

X_1 = Primary leakage reactance at 50 cycles per phase

X_2 = Secondary leakage reactance at 50 cycles per phase and $p = \alpha n$, where $\alpha = \sin \beta/2$, β being the separation (in electrical degrees) between any pair of half brushes and n is the ratio of effective lap turns for 180 electrical degrees brush displacement to effective stator turns per phase. But in the machine under test this ratio of primary and secondary turns was found to be different from unity. It may be, however, shown that if a is the effective number of turns in the primary and b that in the secondary, the relation between I_1 and I_2 at any slip S is given by

$$I_1 = -I_2 b/a (S + p) \text{ while at standstill, by}$$

$$I_1 = -I_2 b/a (1 + p).$$

when both the brush and stator secondary induced voltages are additive. Moreover, since

$$S = \frac{R_2 \tan \theta - p^2 X_1 b/a}{X_2 + p X_1 b/a},$$

$$V \cos \psi = E_1 \cos \theta + I_1 R_1 \text{ and}$$

$$V \sin \psi = E_1 \sin \theta + I_1 X_1$$

the above equation (1) becomes

$$\sin \psi (VR_2) + \cos \psi (VpX_2) =$$

$$I_1 \left[R_1 p X_2 + X_1 R_2 - \frac{R_2 (X_2 + \frac{pX_1 b/a}{1+p})}{1+p} \right] \quad (2)$$

which is an equation of a circle whose centre is the point $\left(\frac{L}{2M'}, \frac{K}{2M'} \right)$ and

$$\text{whose radius is } \left[\left(\frac{L}{2M'} \right)^2 + \left(\frac{K}{2M'} \right)^2 \right]^{1/2},$$

where,

$$L = VR_2,$$

$$K = VpX_2 \text{ and}$$

$$M' = \left[X_1 R_2 + R_1 p X_2 - \frac{R_2 (X_2 + \frac{pX_1 b/a}{1+p})}{1+p} \right]$$

Equation (2) was actually utilised to obtain the theoretical circle diagrams for brush positions at marks 34 and 1, from the design data of the machine.

Excepting the no load speed and α (hence p) the value of the other constants remains unaltered for either brush position and these constants are given below as directly obtained or calculated from the design data of the machine.

$$V = 230 \text{ volts}$$

$$R_1 = 0.738 \text{ ohm}$$

$$R_2 = 0.327 \text{ ,,}$$

(It may be noted that in taking the lap winding resistance into account the fact that this resistance per phase does not increase after 120 electrical degrees of brush spread was marked)

$$X_1 = 5.270 \text{ ohms}$$

$$X_2 = 0.020 \text{ ohm}$$

$$\text{Primary winding factor} = 0.933$$

$$\therefore a = 180 \times 0.933$$

$$\text{Secondary winding factor} = 0.806$$

$$\therefore b = 15 \times 0.806$$

$$\text{Lap winding factor} = 0.966$$

and no. of lap turns for 180 electrical degrees brush displacement = 24

\therefore Effective lap turns for 180 electrical degrees brush displacement = 24×0.966
so that

$$n = \frac{24 \times 0.966}{15 \times 0.806}$$

The values of no-load speed, α , p , L , K , and M' for brush positions at marks 34 and 1 are given in Table III. It may be noted here that α was found from the relative displacement of the brushes over the commutator segments with respect to their short-circuit position.

TABLE III

	Brush position at mark 34	Brush position at mark 1
No-load speed.	1080 R.P. M.	930 R. P M
α	0.2807	0.1400
p'	0.5376	0.2688
I_{sc}	7.5190	7.5190
k_1	2.4730	1.2365
m'	0.1142	0.1326

From these data the co-ordinates of the centre point of the circle diagram were $\frac{L}{2M'} = 32.9$ amperes along X-axis and $\frac{K}{2M'} = 10.8$ amperes along Y-axis for brush position at mark 34, and 28.3 amperes along X-axis and 4.9 amperes along Y-axis for brush position at mark 1.

The theoretical circle diagram is represented by the full line curve in each of Figs 1 and 2. The point C represents the centre of the circle

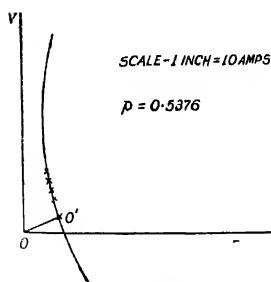


FIG. 1.

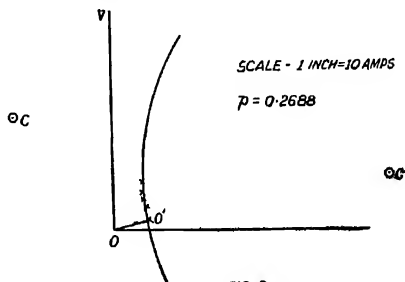


FIG. 2.

while OC its radius. O is the origin and OO' is the no-load current line. The points marked \times in each figure represent the actual load points, using the data of Tables I and II, and the curve obtained by joining these points gives the load or experimental curve. It will be seen that the experimental curve practically coincides with the theoretical curve in each case. The slight deviation may be attributed to the fact that in deducing the equation, the brush-contact resistance has not been taken into account.

ACKNOWLEDGMENTS

The author thanks Professor Dr. P. C. Mahanti, the Head of the Department, and Dr. A. K. Sengupta, Lecturer-in-charge, Electrical Machines Laboratory, for their helpful discussions and for giving all facilities to carry on the work.

ELECTRICAL MACHINES LABORATORY,
DEPARTMENT OF APPLIED PHYSICS,
UNIVERSITY COLLEGE OF SCIENCE & TECHNOLOGY,
CALCUTTA

REFERENCES

- Arnold, A. H. M., 1926. *J. I. E. E.*, **64**, 1139.
Bhattacharyya, H. P., 1949, *Ind. Jour. Phys.*, **23**, 459

EFFECT OF TEMPERATURE ON ULTRASONIC ABSORPTION IN ACETIC ACID

By R. N. GHOSH AND GURDEVA SHARAN VARMA

(Received for publication, Dec. 21, 1949)

ABSTRACT.—The theory of ultrasonic absorption based on the structural changes in the quasi-crystalline structure of the liquid state has been applied to acetic acid. Variation of maximum absorption frequency with the variation of temperature (20°C to 65°C), as observed by Lamb and Pinkerton, has been explained by this theory.

In the previous paper (Ghosh and Varma, 1949) we have calculated the values of absorption frequencies in the various unassociated liquids on the assumption of quasi-crystalline structure of the liquid state. The work function A was deduced on the basis of 'hole theory' of viscosity. All the values refer to 300°K. The value 4.87 Mcs. obtained in the case of acetic acid is high because here we had neglected the effect of temperature *viz.*, the value of $\left(\frac{\alpha}{N} \times 10^{17}\right) \text{sec}^2 \text{cm}^{-1} = 12,000$ which we have taken is a low value for 27°C and moreover dispersion in velocity with temperature was also neglected.

It may be pointed out that the work function A given as

$$A = R \frac{TT'}{T' - T} \log \frac{\eta T'}{\eta' T}$$

which depends upon the values of viscosity (η) of the liquid at two temperatures varies with temperature. As defined previously A is the work function required to remove N molecules from the interior of the body to infinite distance. Fig. 1 shows the plot of viscosity (η) against temperature and Table I gives the value of A at the various temperatures ranging from 25°C to 65°C. Fig. 2 shows the plot of work function A (cals/mole) against temperature.

It may be observed from the Fig. 2 that A at first decreases slowly with temperature and a minimum is obtained near about 55°C and it again rises sharply to high values. The variation of A with temperature is represented by $A = A_0 + \gamma (T - T')^2$ where A_0 is the minimum value of A at the corresponding temperature T' and on either side it increases. $A_0 = 3228$ cals/mole. The rate of increment with regard to the square of the temperature difference, *viz.* γ , is of the order 2 cals/mole per degree centigrade, for temperatures below T' °C and for temperatures above T' °C it

is of the order 2.6 cal/mole to 5 cal/mole per degree centigrade. Further dA/dT is of the order of 9 cal/mole per degree centigrade.

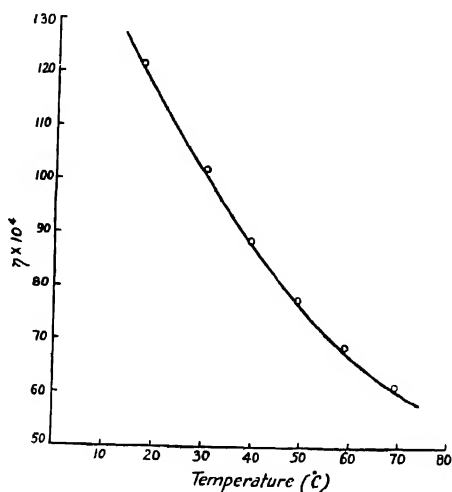


FIG. 1

$\eta \times 10^4$ (Viscosity) plotted against temperature for Acetic Acid, Range of Temp. 20°C – 70°C Values of viscosity have been taken from Physical Chemical Constants by Kaye and Laby

TABLE I

S NO	temperature	A cals/mole	$\frac{dA}{dT}$ cal deg $^{-1}$ mole $^{-1}$
1	25°C	3402	2034
2	30°C	3365	2359
3	35°C	3331	2531
4	40°C	3286	2831
5	45°C	3246	3095
6	50°C	3336	3234
7	55°C	3228	3414
8	60°C	3295	3550
9	65°C	3422	3459

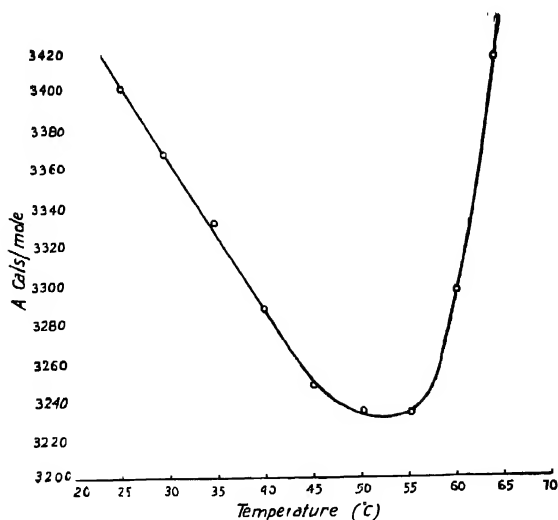


FIG. 2

Work function A cal/mole plotted against Temp for Acetic Acid (20°C–70°C)

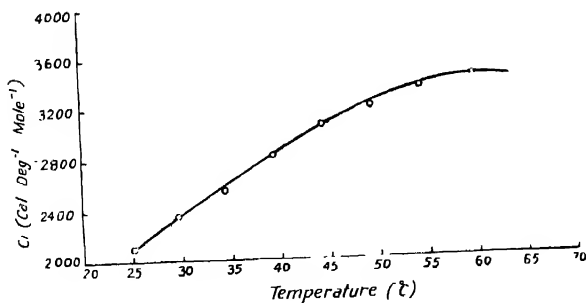


FIG. 3

The corresponding values of internal structural specific heat C_i calculated from the formula $C_i = R \left[\frac{A}{RT} \right]^2 - \frac{A}{RT}$ where R is the gas constant for the different temperatures are also given in Table I. Fig. 3 shows the plot of C_i against temperature.

The minima of A at 55°C indicates that most of the molecules at this particular temperature are in their equilibrium positions. This will at first sight appear to be wholly inappropriate in the case of a liquid with their characteristic fluidity. But it may be pointed out that the equilibrium positions of the molecule in the liquid body are not absolutely permanent, but have a temporary character for a given molecule. After performing more or less large no of oscillations about the same equilibrium position during a certain time T , each molecule can jump to a new equilibrium position. If the time T is large compared with the vibration period, this sporadic change of the equilibrium position cannot affect the magnitude of the specific heat, which is evident from Fig 3 where a plot of C_v against temperature is given in the neighbourhood of 55°C .

It may be observed from Fig. 3 that C_v at first increases linearly with temperature and then becomes flat, horizontal near about 60°C , the temperature where minima in A is observed. The values of the maximum absorption per wavelength (μ_m) at the absorption frequency (N_m) have been calculated as described in the previous paper. The values of $[\alpha/N^2]$ $N \ll N_m$ for the various temperatures ranging from 25°C to 60°C have been taken from Pinkerton's paper (1949). Here the dispersion of the velocity with temperature has also been taken into account.

TABLE II

S NO	Temperature	$(\alpha/N^2 \times 10^{17}) N \ll N_m$ sec ² cm ⁻¹	$C \times 10^5$ cm/sec	$2\mu_m$	$N_m(Mc)$
1	25°C	132,000	1.12	.061	13
2	30°C	107,000	1.10	.071	61
3	35°C	88,700	1.08	.076	.80
4	40°C	72,900	1.065	.086	1.10
5	45°C	58,800	1.05	.093	1.51
6	50°C	48,400	1.035	.098	1.94
7	55°C	41,100	1.02	.103	2.00
8	60°C	33,800	.99	.107	3.20
9	65°C	25,000	.97	.104	4.30

Column four in Table 2 gives the values of velocity at different temperatures. These have been taken from Lamb and Pinkerton's graph showing the plot of velocity against temperature. The values of the absorption frequencies at the various temperatures are given in the last column. The value for $(\alpha/N^2 \times 10^{17})$ for 65°C is the extrapolated one.

Fig. 4 shows the plot of $\log_{10} Nm$ against temperature reciprocal.

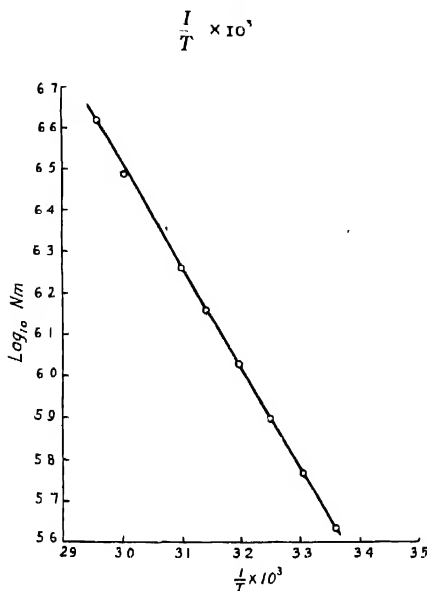


FIG 4

Dependence of $\log_{10} Nm$ against $1/T$, N_m being the absorption frequency

As it is evident from the graph that $\log_{10} N_m$ is a linear function of $1/T$, that is N_m (absorption frequency) is proportional to the factor $e^{-\Delta E/RT}$ where ΔE is the energy required for the creation of extra holes when ultrasonic waves pass through the medium. From the slope of graph of $\log_{10} N_m$ and $1/T$ we find that the value of ΔE comes out to be 8.69 kilocalories. This coincides with the activation energy obtained by Pinkerton.

Thus our theory of ultrasonic absorption in liquids "that the mechanism of absorption in the case of liquids is not entirely due to vibration of atoms, but that the structural changes in the quasi-crystalline state of the liquid molecules play an important part in the absorption of ultrasonic waves and that the phenomenon of absorption and viscosity are all related ones and both can be described in terms of 'hole theory' of liquid state" which has not only been able to explain the absorption and predict the absorption frequencies in most of the liquids successfully but also explains the temperature effect on the absorption frequency as well as on the maximum absorp-

tion per wavelength experimentally obtained by Lamb and Pinkerton in the case of acetic acid.

PHYSICS DEPARTMENT
ALLAHABAD UNIVERSITY
ALLAHABAD.

REFERENCES

- Ghosh, R.N. and Varma, G S., 1943, *I.S.I.R* , 8, 192
Lamb, J. and Pinkerton, J.M.M., 1949, *Proc. Roy Soc* **199**, 114

DETERMINATION OF MOISTURE IN LAC BY INFRA-RED HEATING

By G. N. BHATTACHARYA AND S. C. MUKHERJEE

(Received for publication, January 11, 1950)

ABSTRACT. A rapid method for the determination of moisture in lac has been found by using infra red heating and desiccation under vacuum. A simple apparatus has been devised to effect simultaneous heating and desiccation, so that moisture can be determined in about $1\frac{1}{2}$ hours' time only. The results obtained by this method are the same as those obtained by the time consuming methods at present in use for lac. The apparatus is simple and can be easily assembled in any laboratory with an ordinary vacuum desiccator.

INTRODUCTION

The moisture content of lac is usually small varying from about 1% to 3% depending mostly on the humidity of the surrounding atmosphere and to a lesser extent on some other factors, such as, exposed surface, organic impurities, etc. Although this figure appears to be small, the great influence of moisture on some important physical properties of lac, such as fluidity (Townend and Clayton, 1936) and solubility (Palit, 1940) as well as some chemical properties, such as polymerisability, makes its accurate determination often necessary. It is known, however, that the usual method of drying a substance to constant weight at 100°C or above is not applicable to lac, since it easily gives off its combined water at such high temperatures resulting in a partially polymerised product. Various methods (Rangaswami and Sen, 1942) are therefore in use employing lower temperatures and vacuum for the purpose of determining moisture in lac. These methods, however, are all time consuming and so a rapid method would be definitely helpful to the trade.

With this end in view the dielectric constant method of determining moisture was given a trial some time ago (Bhattacharya, 1947). But it was found that there is no direct correlation between the moisture content of lac and its dielectric constant; the increase in capacitance due to absorption of moisture being anomalous at a certain stage. It appeared, therefore, that the heating of the sample followed by desiccation was almost indispensable, since usual chemical methods, whereby moisture in solids can be determined, cannot be used for ordinary lac (Gidvani and Kamath, 1945). The various special features of infra-red heating and its successful application to many solids where quick and uniform heating is essential, at once suggested itself for a trial to minimise time in the determination of moisture in lac also.

PRELIMINARY EXPERIMENTS

A large number of experiments were first conducted with samples of lac containing various percentages of moisture to see if infra-red heating could be successfully used to reduce the drying time of lac. A Modinstal* dull emitting infra-red heater, fitted with a reflector was employed for this purpose and it was found that by this method the total time required for the determination of moisture in lac could be reduced from about 24 hours required by the British Standard (B. S. I., 1941) or the Indian Lac Research Institute method (Rangaswami and Sen, 1942) to less than 4 hours only. This period includes infra-red heating of the sample at about 45°C (i) either for only 30-45 minutes with regular raking to turn up fresh layers at intervals of 10 minutes, (ii) or for 75-90 minutes without any raking of the powdered sample whatsoever, followed by desiccation for 2-3 hours under vacuum at room temperature. The actual values obtained closely agree in all cases with those obtained by the present long-drawn Indian Lac Research Institute method. Further experiments to shorten the period of heating by raising the temperature appreciably above 45°C were unsuccessful since lac showed a tendency towards softening and consequent blocking. Experiments carried out to dispense with desiccation after heating were also not successful.

The arrangement was to heat a sample of lac contained in a flat-bottomed dish by means of infra-red rays inside an enclosure such as an ordinary laboratory oven fitted at the top with an infra red heater and a reflector. A vessel containing fused calcium chloride was kept inside the enclosure to obtain a somewhat uniform ambient atmosphere irrespective of the widely varying humidity conditions that might be present outside during the different seasons of the year. Without a dehydrant in the enclosure the time of heating required to obtain the same result varied from season to season. Immediately after heating, the sample was transferred to a vacuum desiccator and carefully weighed at the end of 2 to 3 hours' desiccation. The results were very satisfactory as may be seen from Table I :

TABLE I

Lac Sample	Wt of lac taken (gms.)	Heating time (mins.)	Desiccation time (hours)	Moisture %	Moisture by Inst. method %	Remarks
S I	2.0352	35	3	1.62	1.60	Raking of the sample at intervals of 10 mins to turn up fresh layers.
S II	2.0632	30	3	2.21	2.24	
S III	2.0859	35	3	1.90	1.90	
S V	2.0272	45	3	0.97	0.97	
S VI	2.0532	90	2½	2.10	2.05	No raking.

* Modinstal Electric Co., Ltd., England.

It may be noticed that the heating period was about 90 minutes when there was no raking of the sample. With regular raking, however, this heating time might be as short as 30 minutes only. The drying time curve of a sample of lac (S I) has been shown in Fig. 1, where it may be noticed that the determined moisture becomes more or less constant after a heating period of 30-35 minutes.

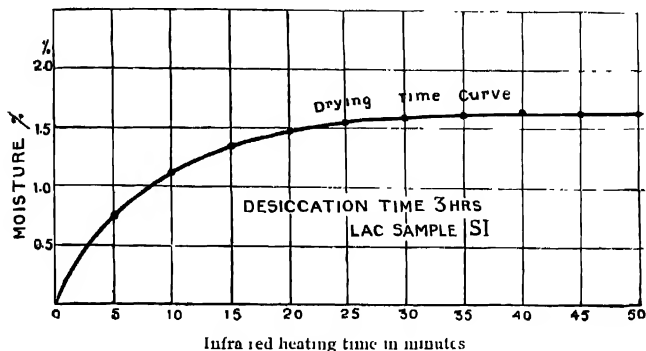


FIG. 1

FINAL EXPERIMENTS AND PROPOSED METHOD

Apparatus. It was subsequently thought if it was possible to combine both the heating and the desiccation processes together to save time still further. A special apparatus was, therefore, constructed with a vacuum desiccator as shown in Fig. 2.

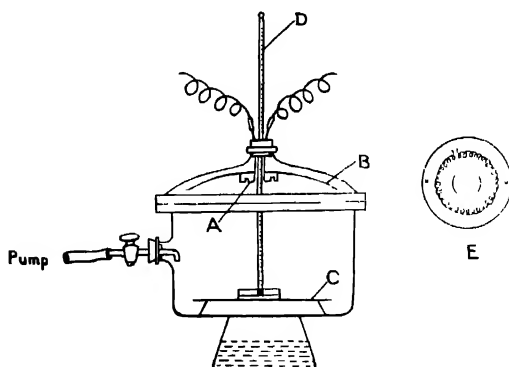


FIG. 2

A is a small ring type infra-red heater made on an asbestos-cement circular plate grooved to contain the heater element (shown separately at E).

A highly polished metal reflector *B* is fitted at the top to throw parallel heat rays down on the desiccator platform *C* below. A thermometer *D* passes through the rubber cork in such a way that its bulb is only a few mm. above the platform and the dish containing sample of lac can be just placed below without touching it. The pump may be connected with the side tube for evacuation. The desiccant is concentrated sulphuric acid. It has been found that an infra-red heating element of 15-25 watts capacity is quite satisfactory for a 6-7 inch desiccator assembly. Its design should be such that it should glow under the applied voltage without being white hot.

Procedure. The procedure for performing an experiment with this apparatus is to evacuate the desiccator to a few mm. of mercury and adjust current through the heater so that a constant temperature of $45 \pm 2^\circ\text{C}$ is indicated by the thermometer under equilibrium conditions. The carefully weighed dish containing a sample of lac should then be quickly placed on the platform of the desiccator by opening the cover through a temporary release of the vacuum. As quickly as possible the vacuum should be restored and the previous temperature obtained within a few minutes. The heating time should be noted from the time the thermometer shows 45°C again.

It has been observed that for most of the samples of lac, one hour's heating under these conditions is sufficient for the purpose of drying. But to be on the safe side $1\frac{1}{2}$ hours' heating will always be found more than enough for complete drying of all samples. This means that heating for some extra time when the sample is already dry does not interfere with the determination of moisture in any way. In other words, lac can be dried to constant weight under these conditions. In this connection, it must be clearly stated that dry lac is a hygroscopic substance and it readily absorbs moisture from the humid atmosphere when exposed to it. Too much stress cannot therefore be laid on using a dehydrating agent, inside the balance case as well as a weighing dish with a ground cover. In short, all precautions necessary for weighing a hygroscopic substance should be taken in the case of dry lac. This method is rapid and also independent of outside weather conditions. A few typical measurements have been shown in Table II. In these experiments petri dishes of 60-65 mm diameter with covers were used throughout and the weight of the sample of lac taken was nearly 2 gms., as advocated in the I. L. R. Institute method of moisture determination for lac.

Effect of particle size.

In all the above experiments samples of lac were powdered to pass a U. S. Standard sieve No. 60 (24 mesh per cm.). The effect of the size of lac particle on the drying time was also studied. It was found that practically no appreciable difference in drying time could be recorded when

TABLE II

Lac sample	Wt. of lac taken (gms.)	Heating time	Moisture %	Moisture by the last. method
S I	2.0272	60 mins.	1.62	1.60
"	"	90 "	1.62	1.60
S II	2.0354	60 "	2.22	2.24
"	"	90 "	2.24	"
"	"	120 "	2.22	"
S III	2.0042	60 "	1.85	1.90
"	"	90 "	1.92	"
"	"	120 "	1.92	"
S IV	2.0464	60 "	3.25	3.27
"	"	90 "	3.25	"
S V	2.0152	60 "	2.06	2.05
"	"	90 "	2.06	2.05

the powder was of the above size or finer, but when the size was between 10 to 60 mesh per inch (15-24 mesh per cm.) slightly more time (about 15 mins extra) was needed to obtain constant weight. Even then 90 minutes' heating time was found to be more than enough for these powders.

CONCLUSION

We find, therefore, that this method of determination of moisture in lac by infra-red heating is quite satisfactory and it gives results which are practically the same as obtained by the long drawn methods at present in use for lac. The determination of moisture can be done very rapidly in any laboratory where routine analysis of lac is carried out if only an apparatus is assembled as shown in the figure and set apart specially for this purpose. The apparatus is very simple and inexpensive and can be assembled in any laboratory without much difficulty.

ACKNOWLEDGMENT

The authors are grateful to Dr P. K. Bose, Director of this Institute, for his kind interest in this work.

PHYSICAL & H. V. ELECTRICAL LABORATORIES,
INDIAN LAC RESEARCH INSTITUTE, NAMKUM, RANCHI.

REFERENCES

- Bhattacharya, G. N., 1947, *Cur. Sci* 16, 117.
- B. S. Institution, 1941, B. S. S., No. 954, Appendix K, 24.
- Gidvani, B. S., and Kumath, N. R., 1945, Bull. No. 7, London. Shell. Res. Bur.
- Palit, S. R., 1940, *Ind. Chem. Soc.*, 17, 308.
- Rangaswami, M., and Sen, H. K., 1942, A Handbook of Shellac Analysis, 7, 8.
- Townend, R. V., and Clayton, W. R., 1936, *J. Ind. Eng. Chem., Anal. Edn.*, 8, 108

The following special publications of the Indian Association for the Cultivation of Science, 210, Bowbazar Street, Calcutta, are available at the prices shown against each of them :—

Subject	Author	Price	
		Rs.	A. P.
Methods in Scientific Research	... Sir E. J. Russell	0	6 0
The Origin of the Planets	... Sir James H. Jeans	0	6 0
Separation of Isotopes	... Prof. F. W. Aston	0	6 0
Garnets and their Role in Nature	... Sir Lewis L. Fermor	2	8 0
(1) The Royal Botanic Gardens, Kew.	... Sir Arthur Hill	1	8 0
(2) Studies in the Germination of Seeds.	...		
Interatomic Forces	... Prof. J. E. Lennard-Jones	1	8 0
The Educational Aims and Practices of the California Institute of Technology.	... R. A. Millikan	0	6 0
Active Nitrogen A New Theory.	... Prof. S. K. Mitra	2	8 0
Theory of Valency and the Struc- ture of Chemical Compounds.	... Prof. P. Ray	3	0 0
Petroleum Resources of India	... D. N. Wadia	2	8 0
The Role of the Electrical Double layer in the Electro. Chemistry of Colloids.	... J. N. Mukherjee	1	12 0

A discount of 25% is allowed to Booksellers and Agents.

RATES OF ADVERTISEMENTS

Third page of cover	Rs. 32, full page
do. do.	„ 20, half page
do. do.	„ 12, quarter page
Other pages	„ 25, full page
do.	„ 16, half page
do.	„ 10, quarter page

15% Commissions are allowed to *bonafide* publicity agents securing orders for advertisements.

CONTENTS

	PAGE
13. Circular and Elliptical Quantum Orbits—By M. F. Soonawala ...	98
14. Spectrum of the Flame above a Copper Arc in Air—By S. P. Sinha and Shyam Chandra Prasad ...	103
15. A new Laboratory Hydrogen Continuum—By S. K. Bhattacharya	109
16. Raman Spectra of Organic Crystals at Different Low Temperatures. I. Chlorobenzene and Toluene—By A. K. Ray ...	111
17. Studies of Schrage Three Phase Shunt Commutator Motor. III. Circle Diagrams—By H. P. Bhattacharyya ...	119
18. Effect of Temperature on Ultrasonic Absorption in Acetic Acid—By R. N. Ghosh and Gurdeva Sharan Varma	125
19. Determination of Moisture in Lac by Infra-red Heating—By G. N. Bhattacharya and S. C. Mukherjee ...	131

PRINTED BY SIBENDRANATH KANJILAL, SUPERINTENDENT (OFFG.), CALCUTTA UNIVERSITY
PRESS, 48, HAZRA ROAD, BALLYGUNGE, CALCUTTA AND PUBLISHED BY THE
REGISTRAR, INDIAN ASSOCIATION FOR THE CULTIVATION OF SCIENCE,
210, BOMBAY STREET, CALCUTTA.

VOL. 24

INDIAN JOURNAL OF PHYSICS

No. 4

(Published in collaboration with the Indian Physical Society)

AND

VOL. 33

PROCEEDINGS

No. 4

OF THE

**INDIAN ASSOCIATION FOR THE
CULTIVATION OF SCIENCE**

APRIL, 1950

**PUBLISHED BY THE
INDIAN ASSOCIATION FOR THE CULTIVATION OF SCIENCE
210, Bowbazar Street, Calcutta**

BOARD OF EDITORS

K. BANERJEE	S. K. MITRA
D. M. BOSE	P. RAY
S. N. BOSE	M. N. SAHA
D. S. KOTHARI	S. C. SIRKAR.

Secretary

EDITORIAL COLLABORATORS

DR. R. K. ASUNDI, M.A., PH.D.
PROF. H. J. BHABHA, PH.D., F.R.S.
DR. P. K. KICHLU, D.Sc.
PROF. K. S. KRISHNAN, D.Sc., F.R.S.
PROF. G. P. DUDEY, M.Sc.
DR. K. RANGADHAMA RAO, M.A., D.Sc.
DR. N. D. SARWATTEY, D.Sc.
DR. N. N. DASGUPTA, M.Sc., PH.D.
PROF. N. R. SEN, D.Sc., F.N.I.
PROF. P. C. MAHANTI, D.Sc., F.N.I.
PROF. S. R. PALIT, D.Sc.,
DR. H. RAKSHIT, D.Sc.,
PROF. K. R. DIXIT, PH.D.
DR. VIKRAM A. SARABHAI, M.A., PH.D.

ASSISTANT EDITOR

MR. A. N. BANERJEE, M.Sc.

NOTICE

TO INTENDING AUTHORS

Manuscripts for publication should be sent to Mr. A. N. Banerjee, Assistant Editor, 210, Bowbazar Street, Calcutta.

The manuscript of each paper should contain in the beginning a short abstract of the paper.

All references to published papers should be given in the text by quoting the surname of the authors followed by the year of publication within braces, e.g., Sen (1942). The actual references should be given in a list at the end of the paper according to the following specimen :

Sen, B. K., 1942, *Ind. J. Phys.*, 16, 324

The references should be arranged alphabetically in the list.

All diagrams should be drawn on thick white paper in Indian ink, and letters and numbers in the diagrams should be written in pencil.

Annual Subscription—

Inland Rs. 20
Foreign £ 2

APPLICATION OF STOKES' LAW TO ESTIMATE THE SOLVATION OF IONS IN A SOLUTION

By H. MUKHERJEE

(Received for publication, March, 15, 1950.)

ABSTRACT. Since the diameter of a solvated ion is fairly large in comparison with the distance between the molecules of the solvent, the motion of the ion under a constant force should conform to Stokes' law. The diameter, however, is not large enough to allow the solvent to be considered as a continuous medium with respect to the ion and so the law cannot be applied in its original form. By introducing in the expression of velocity, a correction term inversely proportional to the surface area of the ion, it has been shown that the calculated hydration values of ions relative to the hydration of H-ion are in close agreement with the experimental values of Washburn and Millard.

INTRODUCTION

In an earlier work the author (Mukherjee), 1949, published a method of approach to the problem of solvation of ions from the kinetic theory. The assumption made in the paper, viz., that a solvated ion could be represented by point-particles as regards charge, mass and velocity in an electric field, was rather bold, although, with its help, the values of hydrations of some ions obtained were in close agreement with Washburn and Millard's (1915) experimental values. Discrepancy, however, was found in the case of caesium and is likely to be found in the case of other heavy ions. The problem may, however, be attacked with the aid of Stokes' law regarding uniform motion of a particle in a viscous medium under a constant force, and this method appears to be more rational in as much as it takes into account the finite diameters of the solvated ions. The first attempt to obtain hydration values with the aid of Stokes' law seems to have been made by Riesenfeld and Reinhold (1932;1933); but they considered the medium (the solvent) as continuous with respect to the ions and applied the law as it is. Their results, therefore, were too high. The medium can, by no means, be considered as continuous with respect to the ions, for the intermolecular separation in the solvent is not negligibly small in comparison with the sizes of the ions. The present paper shows that the correction term required to be introduced in the expression for velocity in Stokes' equation should be inversely proportional to the surface area of the ion under consideration, and that the hydration values of ions at infinite dilution obtained with the help of the corrected equation are close to, and reasonably higher than, the experimental values of Washburn and Millard obtained with solutions of strength 1.25 N.

CORRECTION OF STOKES' EQUATION

When a particle moves under a constant force through viscous medium with constant velocity, the resistance offered by the medium is just equal to the force. This resistance is due to the impact of the molecules of the medium on the surface of the particle. The number of molecules impinging on the particle per second depends on (i) the surface area and the velocity of the particle and (ii) the intermolecular separation in the medium. When the surface area is large in comparison with the intermolecular space, the law of motion of the particle is, as deduced by Stokes,

$$6\pi\eta av = P \quad (1)$$

where η is the viscosity of the medium, a and v are, respectively, the radius and velocity of the particle and P , the constant force. The left hand member of the equation represents the resistance to the motion. In deducing the equation no account has been taken of the slipping of the molecules along the surface. But, as has been shown by Helmholtz, Piotrowsky, Kundt and Warburg, the molecules do slip along the surface of a foreign body. In consequence of this, the reduction in velocity caused by the impacts is somewhat less than what it would be otherwise. Cunningham has shown that, in view of the occurrence of slipping, the law should be corrected to,

$$6\pi\eta a \cdot \frac{v}{1 + \frac{A\lambda}{a} + \frac{A'\lambda^2}{a^2}} = P \quad \dots (2)$$

where λ is the mean intermolecular separation and A, A' , etc., are constants.

Furthermore, in the case of a large-sized particle, some part or other of the particle is struck by the molecules of the medium at every instant, so that the impacts on the particle as a whole may be regarded as continuous and sensibly the same at all instants. If, however, the size of the particle and the extent of the intermolecular space are mutually comparable, the number of impacts will be different at different instants and there may even be intervals between successive impacts. The result is that, area for area, the average number of impacts at any instant will be smaller for small particles than for large particles, and so the velocity of a small particle will be greater than that obtained by calculation from equation (2). The acting force P must now be

$$6\pi\eta a \cdot \frac{v}{1 + \frac{A\lambda}{a} + \frac{A'\lambda^2}{a^2} + \dots + k} = P$$

where k is a positive quantity, which is large or small according as the discontinuity in the impacts is large or small. The discontinuity is large if the surface area of the particle and the number of molecules per unit area

across its path are small. The latter is obviously inversely proportional to λ^2 . Therefore k may be written as $\frac{B\lambda^2}{a^2} + \frac{B'\lambda^4}{a^4} + \dots$. Since first approximations are sufficient in most cases, we may write Stokes' equation in the form.

$$6\pi\eta a \frac{v}{1 + \frac{A\lambda}{a} + \frac{B\lambda^2}{a^2}} = P \quad \dots (3)$$

It is this form which Millikan used in connection with his famous series of experiments for the determination of e .

In the case of a solvated ion, the slipping effect is nil, because the ion is surrounded by a sheath of the solvent and the free molecules of the latter come in contact *not* with the ion directly but *with* molecules of their own kind. The effect is as if a globule of the solvent were moving among the molecules of the solvent itself. The motion of the solvated ion, therefore, conforms to the equation

$$6\pi\eta a \frac{v}{1 + \frac{B\lambda^2}{a^2}} = P \quad \dots (4)$$

The force P acting on the ion is, when the solution is too dilute for appreciable interionic action, equal to eX , where e is the charge on the ion and X the intensity of the electric field in which the ion moves.

Therefore

$$6\pi\eta a \frac{v}{1 + \frac{B\lambda^2}{a^2}} = eX$$

$$\text{or } v = \frac{eX}{6\pi\eta a} \left(1 + \frac{B\lambda^2}{a^2} \right),$$

where all the quantities are expressed in C.G.S. F.M. units. If u denotes the velocity under a potential gradient of one volt per cm.,

$$u = \frac{v}{X} \cdot 10^8 = \frac{e \cdot 10^8}{6\pi\eta a} \left(1 + \frac{B\lambda^2}{a^2} \right) \quad \dots (5)$$

The ratio of the velocities of two ions having charges e, e' , and velocities v, v' , in the same solvent is,

$$\frac{u}{u'} = \frac{\Lambda}{\Lambda'} = \frac{e}{e'} \cdot \frac{a'}{a} \cdot \frac{1 + \frac{B\lambda^2}{a'^2}}{1 + \frac{B\lambda'^2}{a^2}} = \frac{1}{z} \cdot \frac{a'^2}{a^3} \cdot \frac{a^2 + B\lambda^2}{a'^2 + B\lambda'^2} \quad \dots (6)$$

where Λ, Λ' are the equivalent conductivities of the ions at infinite dilution and z is the ratio of the valency of the second ion to that of the first.

R E F E R E N C E S

- Davies, Hassid and Taylor, 1932, *J. C. S.*, 2497.
Mukherjee, 1949, *Ind. J Phys*, **23**, 503.
Riesenfeld and Reinhold, 1932, *Coll Czech Chem Comm* **4**, 200.
„ „ 1933 *Ibid*, **5**, 518,
Taylor and Sawyer, 1929, *J. C. S.*, 2095
Washburn and Millard, 1915, *J. C. S.*, **37**, 694

ELECTRICAL CONSTANTS OF SAND AT ULTRA HIGH FREQUENCIES

By S. K. CHATTERJEE

(Received for publication, Aug. 5, 1959)

ABSTRACT. Electrical constants of dry and moist sand (up to 5% moisture content) have been measured over a frequency range of 300 Mc/s to 500 Mc/s. Dielectric constant, conductivity and loss tangent increase with increasing moisture content. Dielectric constant and conductivity of dry sand vary between 2.6 to 2.7 and 0.25×10^{-8} e.s.u. to 1.04×10^{-8} e.s.u. respectively over the frequency range in question. Loss tangent for dry sand varies from 64×10^{-3} to 153×10^{-3} over the same frequency range. Reflection coefficient for dry sand remains practically constant at 0.24 over 300 Mc/s to 500 Mc/s. But phase change on reflection varies with frequency. Reflection coefficient increases from 0.24 to 0.35 at 500 Mc/s for dry sand to 5.6% moist sand. There occurs also, a variation of phase change on reflection with different moisture content.

THEORETICAL

Measurement of Dielectric Constant. If a pair of parallel wires excited at one end by an oscillator is first immersed wholly in air and then in a nonconducting dielectric material having dielectric constant ϵ , the ratio of the wavelengths in air λ and in dielectric λ_d gives the dielectric constant ϵ .

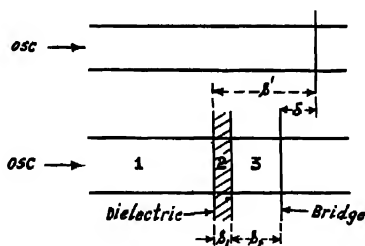


FIG. 1

If the dielectric is solid, it is difficult to measure λ_d directly. When the dielectric covers only a part of the parallel wires (Fig. 1.), the Lecher wire system is immersed in three media air-dielectric-air. In this case the principle of measurement is contained in the following derivation:

Maxwell's field equations are

$$\text{Curl } H = i_c + \frac{\partial D}{\partial t} \quad \text{and} \quad \text{Curl } E = -\frac{\partial B}{\partial t}$$

which when resolved into rectangular components given the following expressions;

$$\text{Curl}_x H = i_{c,x} + \frac{\partial D_x}{\partial t} \quad \text{Curl}_x E = -\frac{\partial B_x}{\partial t}$$

$$\text{Curl}_y H = i_{c,y} + \frac{\partial D_y}{\partial t} \quad \text{and} \quad \text{Curl}_y E = -\frac{\partial B_y}{\partial t}$$

$$\text{Curl}_z H = i_{c,z} + \frac{\partial D_z}{\partial t} \quad \text{Curl}_z E = -\frac{\partial B_z}{\partial t}$$

$$\text{where } i_c = \sigma E, \quad D = \epsilon E \quad \text{and} \quad B = \mu H$$

All the symbols have usual significance. These equations refer to the most general medium with the following restrictions:

1. It is homogeneous in that ϵ , μ and σ are constant over the regions in question.

2. It is isotropic in that these parameters ϵ , μ , σ have the same properties in all directions.

These requirements may be considered to be satisfied by media like air or free space rather exactly. But medium like soil is extremely inhomogeneous and anisotropic. Sand may be regarded to meet these requirements to an intermediate degree. The field equations then give approximately correct results depending on the degree of approximations.

Assuming $\mu = 1$ and considering the case of a plane wave of angular frequency ω , the electric and magnetic intensities in Gaussian units can be determined from the field equations as follows:

$$E = A e^{j(\omega t - \beta x)} + B e^{j(\omega t + \beta x)}$$

$$H = \frac{C\beta}{\omega} \left\{ A e^{j(\omega t - \beta x)} - B e^{j(\omega t + \beta x)} \right\}$$

where C is the velocity of light and $\beta = 2\pi/\lambda$, where λ is the wavelength in the medium and A and B involve wave amplitudes. The electric and magnetic intensities in the three media in which the Lecher wire is immersed are given by the following expressions:

$$E_1 = A_1 e^{j(\omega t - \beta_1 x)} + B_1 e^{j(\omega t + \beta_1 x)}$$

$$H_1 = \frac{C\beta_1}{\omega} \left\{ A_1 e^{j(\omega t - \beta_1 x)} - B_1 e^{j(\omega t + \beta_1 x)} \right\}$$

$$E_2 = A_2 e^{j(\omega t - \beta_2 x)} + B_2 e^{j(\omega t + \beta_2 x)}$$

$$H_2 = \frac{C\beta_2}{\omega} \left\{ A_2 e^{j(\omega t - \beta_2 x)} - B_2 e^{j(\omega t + \beta_2 x)} \right\}$$

$$E_3 = A_3 e^{j(\omega t - \beta_3 x)} + B_3 e^{j(\omega t + \beta_3 x)}$$

$$H_3 = \frac{C\beta_3}{\omega} \left\{ A_3 e^{j(\omega t - \beta_3 x)} - B_3 e^{j(\omega t + \beta_3 x)} \right\}$$

where $\beta_1 = 2\pi/\lambda_1$, λ_1 being the wavelength in the dielectric. The other components in this case can be ignored. By assuming perfect reflections at the bridge and applying boundary conditions, the above set of equations can be utilised (Lamont, 1940) to yield the following relation involving the thickness of the material s_1 and ϵ :

$$\sqrt{\epsilon} \cot \beta_1 s_1 (\cot \beta s' - \cot \beta s_2) + \cot \beta s' \cot \beta s_2 + \epsilon = 0$$

which gives

$$\tan \frac{1}{2} \beta (s_1 + \delta) = \sqrt{\epsilon} \tan \frac{1}{2} \beta_1 s_1 = \sqrt{\epsilon} \tan \frac{1}{2} \sqrt{\epsilon} \beta s_1 \quad \dots (1)$$

where $\delta = \text{bridge shift} = s' - (s_1 + s_2)$. Since $\sqrt{\epsilon} \gg 1$ it is evident that for $s_1/\lambda_1 = 0$, or even integer, that is s_1 equal to an even multiple of $\lambda_1/2$ equation (1) gives maximum bridge shift δ_{max} . If the position of the dielectric is adjusted such that the first boundary of the dielectric coincides with a node and then the thickness s_1 of the dielectric is adjusted (which in this case is easier, sand being the dielectric) so that it becomes an even multiple of $\lambda_1/2$ then the second boundary of the dielectric also coincides with a node. In this case the phase difference suffered by the wave in passing through the dielectric is dependent only on the optical path difference $(\beta_1 - \beta)s_1$ and so is independent of the position of the dielectric. But if the thickness of the dielectric is neither odd nor even multiple of $\lambda_1/2$ the total phase difference suffered by the wave will be given by

$$\beta\delta = \theta_1 + \theta_2 + (\beta_1 - \beta)s_1$$

where θ_1 and θ_2 are the phase differences suffered by the wave at the two boundaries of the dielectric. In this case, therefore, it is evident that the bridge shift will differ with different positions of the dielectric and consequently, the value of ϵ will be dependent on the position of the dielectric which is undesirable.

Measurement of Loss Angle. The loss tangent $\tan \delta$ can be determined from a knowledge of attenuation constant α and the line parameters R, L, G, C , per unit length of the lecher wire. The well known transmission line equation involving the sending end voltage V_1 , the receiving end voltage V_2 , receiving end current I_2 and the characteristic impedance of the line Z can be written as follows:

$$V_1 = V_2 \cosh \gamma l + I_2 Z \sinh \gamma l$$

where the propagation constant γ is given by $\alpha + j\beta$ involving the attenuation constant α and phase constant β . The attenuation constant α can be determined (Kusters, 1942) to be as follows:

$$\alpha = \frac{2\pi d\lambda}{\lambda^2} \cdot \frac{1}{\sqrt{m-1}}$$

where m is an integer. For $m=2$, $\alpha_m = \frac{2\pi d\lambda}{\lambda^2}$, where $2d\lambda$ represents the

value of the half power width of the resonance curve. So if the half power widths $2d\lambda_1$ and $2d\lambda_2$ of resonance curves for two different thicknesses s_1 and s_2 of the sample are determined, the attenuation constant can be derived to be

$$\alpha = \frac{\alpha_{m1}s_1 - \alpha_{m2}s_2}{s_1 - s_2} \quad \dots (2)$$

From transmission line equation α can be expressed in terms of line parameters as follows.

$$\alpha = \frac{R}{2} \sqrt{\frac{C}{L}} + \frac{G}{2} \sqrt{\frac{L}{C}}$$

which can be written as

$$G = 2\alpha \sqrt{\frac{C}{L}} - \frac{RC}{L}$$

The loss angle is given by $\tan \delta = \frac{G}{\omega C}$. So the value of $\tan \delta$ is given by

$$\tan \delta = \frac{2\alpha}{\omega \sqrt{LC}} - \frac{RC}{\omega CL} = \frac{\lambda}{\pi} \cdot \alpha - \frac{R}{\omega L} \quad \dots (3)$$

The values of R and L for the lecher wire can be calculated from the following relations (Hund, 1924):

$$\left. \begin{aligned} R &= \sqrt{\frac{\gamma_0 \omega}{1 - (d/a)^2}} \\ L &= 4 \ln \left\{ \frac{1 + \sqrt{1 - (d/a)^2}}{d/a} + \sqrt{\frac{\gamma_0}{\omega [1 - (d/a)^2]}} \right\} \end{aligned} \right\} \quad \dots (4)$$

where γ_0 represents the d.c. resistance per cm. length of the lecher wire, d represents the diameter in cm. of wire and a is the spacing in cm. between centre to centre of wires. So if α_{m1} and α_{m2} are measured, α can be calculated from equation (2). Then calculating R and L , the value of $\tan \delta$ can be determined from equation (3). The advantage of this form of equation is that $\tan \delta$ can be determined without a knowledge of the dielectric constant.

Measurement of Conductivity: The conductivity σ of the material can be determined from the following relation (Smith Rose and McPetrie, 1934):

$$\sigma = \frac{\alpha \omega \lambda^2}{4\pi^2 \lambda_s} = \frac{\alpha \omega \epsilon \lambda}{4\pi^2} \quad \dots (5)$$

EXPERIMENTAL

The experimental arrangement is similar to that reported earlier (Chatterjee, 1948). The detector used is of the resonant line type. Sand

placed in a wooden box of length 54 cm. and width 14 cm. The two boundary walls touching the lecher wires are made of thin mycalex sheets. One of the mycalex walls of the box is adjustable so that the thickness of the sand covering the lecher wire can be varied. The oscillator used is a R Type No 525-A. To keep the oscillator output constant, two regulator tubes have been used with the main supply and the supply to the oscillator is made through a Variac. The effect of moisture on ϵ , σ and $\tan \delta$ have been studied. Percentage of moisture content has been determined from the difference in weights of dry and moist sands. The variation of ϵ , σ and $\tan \delta$ at 500 Mc/s with different moisture content is shown in Fig. 2. The effect of

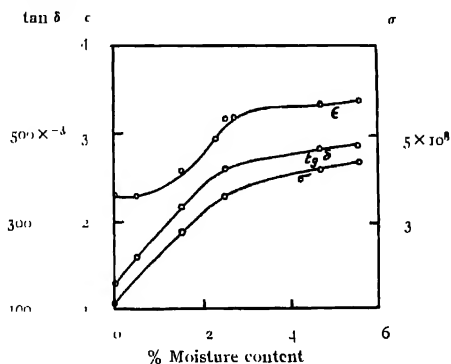


FIG. 2

Variation of ϵ , σ and $\tan \delta$ at 500 Mc/s with moisture content

more than 6% moisture content could not be studied as the resonance peak becomes flatter. The values of ϵ , σ and $\tan \delta$ at certain frequencies over a range of 300 Mc/s to 500 Mc/s for dry sand are given in Table I and for sand having moisture content nearly 2.5% are given in Table II.

TABLE I

Values of ϵ , σ , $\tan \delta$ over 300 Mc/s to 500 Mc/s for dry sand.

Frequency in Mc/s	ϵ	$\sigma \times 10^{-8}$ in esu	$\tan \delta \times 10^3$
300	2.7	0.26	64
350	2.7	0.35	82
400	2.6	0.5	95
450	2.6	0.84	127
500	2.6	1.04	153

TABLE II

Values of ϵ , σ , and $\tan \delta$ over 300 Mc/s to 500 Mc/s for sand having nearly 2.5% moisture content.

Frequency in Mc/s	% moisture content	ϵ	$\delta \times 10^{-8}$ e.s.u.	$\tan \delta \times 10^3$
300	2.8	3.6	2.5	477
350	2.9	3.7	3.0	464
400	2.4	3.3	3.1	476
450	2.3	3.3	3.2	424
500	2.5	3.4	3.6	420

Values of $R/\omega L$ for different frequencies have been calculated from the formula (4) and given in Table III. The constants of the Lecher wires are $a = 5$ cm., $d = 0.326$ cm., and $\gamma_0 = 4.27 \times 10^{-3} \frac{\Omega}{\text{cm.}}$

TABLE III

Frequency in mc/s.	300	350	400	450	500
$(R/\omega L) \times 10^3$	0.37	0.32	0.29	0.38	0.27

DISCUSSION

The values of $\tan \delta$ and σ increase with increasing moisture content whereas ϵ remains almost constant for low values of moisture and then increases. The values of $\tan \delta$ for sea sand measured by Løb (1943) at a wavelength 8.65 cms, vary from 100×10^{-4} to 500×10^{-4} over moisture content up to 0.5%, whereas for Rhine sand at the same wavelength $\tan \delta$ varies from 100×10^{-4} to 475×10^{-4} over the same percentage of moisture content. But ϵ maintains a constant value of 2.5 and 2.7 in case of sea sand and Rhine sand respectively over the same moisture content and the same wavelength. In the present investigation $\tan \delta$ at 60 cms. wavelength varies from 153×10^{-1} to 478×10^{-3} over a moisture content of 5.6%. The value of ϵ varies from 2.6 to 3.8 over the same percentage of moisture content at 60 cms. wavelength. The value of ϵ for very dry sandy loam measured by Ford and Oliver (1946) at 9 cms wavelength by using direct reflection method is $\epsilon = 2$.

The conductivity σ determined by Strutt (1930) is 4×10^{-14} e.m.u. at a wavelength of 1.42 metres. The value of σ measured by Løb (1943) is

4.3×10^{-11} e.s.u. at a wavelength of 8.6 cms. The conductivity value measured by Ford and Oliver (1946) for a very dry sandy loam is 3×10^{-8} e.s.u. The values of conductivity in the present case for dry sand varies from 0.26×10^{-8} e.s.u. to 1.04×10^{-8} e.s.u. over 100 cms. to 60 cms.

Reflection Coefficient. The solution of many of the problems relating to the propagation of radio waves necessitates a knowledge of the magnitude of the reflection occurring at the earth's surface. The reflection coefficient at the earth's surface is complex and may conveniently be represented by $K + jK'$. The magnitudes of the two rectangular components K and K' are functions of the dielectric constant ϵ , the ratio of the conductivity σ to the frequency f of radiation and also of the angles of incidence. Considering plane polarised radiation to be incident normally on the reflector, the values of K and K' are given by the following relation (McPetrie, 1934):

$$K = \frac{1 - \sqrt{\left(\epsilon^2 + \frac{4\sigma^2}{f^2}\right)}}{1 + \sqrt{(\epsilon^2 + 4\sigma^2/f^2)} + \sqrt{[2\{\epsilon + \sqrt{(\epsilon^2 + 4\sigma^2/f^2)}\}]}}$$

$$K' = \frac{\sqrt{[2\{-\epsilon + \sqrt{(\epsilon^2 + 4\sigma^2/f^2)}\}]}}{1 + \sqrt{(\epsilon^2 + 4\sigma^2/f^2)} + \sqrt{[2\{\epsilon + \sqrt{(\epsilon^2 + 4\sigma^2/f^2)}\}]}} \quad ;$$

where ϵ and σ are respectively dielectric constant and conductivity in e.s.u. A determination of the magnitudes of the modulus of the reflection coefficient and the ratio of its two rectangular components is sufficient to determine the electrical constants of the reflecting surface under consideration. It will be seen from the above relation that for infinitely high values of ϵ or σ , K' becomes zero and $K = -1$. This means for a perfect conductor the wave undergoes on reflection a phase change of 180° . For an imperfect conductor K and K' are negative and positive respectively. The values of K , K' , $\tan^{-1} K/K'$ and reflection coefficient R at a wavelength 60 cms. for different percentages of moisture content are given in Table V.

TABLE IV

Values of K , K' , $\tan^{-1} K'/K$ and R at $\lambda=60$ cms. for dry sand and sand having different moisture contents

% moisture contents	Dry	3.5	5.6
K	-0.237	-0.318	-0.31
K'	0.035	0.086	0.007
$\tan^{-1} \frac{K'}{K}$	$171^\circ.7$	$164^\circ.4$	$164^\circ.4$
R	0.24	0.33	0.35

The reflection coefficient of dry sand having $\epsilon=2$ and $\sigma=3 \times 10^8$ e.s.u. measured by Ford and Oliver (1946) at wavelength 9 cms varies from 0.2 to 0.09 for angles of incidence 68° to $43^\circ 5'$ for vertical polarisation and from 0.48 to 0.26 over the same angle of incidence for horizontal polarisation.

The value of $\tan^{-1} \frac{K'}{K}$ is $< 180^\circ$ which means that the advance of phase on reflection is $< 180^\circ$ and the amount of change is a measure of the ratio $\frac{K'}{K}$. The variation of reflection coefficient and $\tan^{-1} \frac{K'}{K}$ of dry sand over the frequency range 300-500 Mc/s. can be studied from Table V.

TABLE V

Values of reflection coefficient and $\tan^{-1} \frac{K'}{K}$ of dry sand over a frequency range of 300 Mc/s. to 500 Mc/s.

Frequency in Mc/s	300	350	400	450	500
$\tan^{-1} \frac{K'}{K}$	$175^\circ 1'$	$175^\circ 1'$	$171^\circ 0'$	173°	$171^\circ 7'$
R	0.24	0.243	0.237	0.238	0.24

It will be seen from Table V that the reflection coefficient remains practically constants at about 0.24 over the frequency range, whereas $\tan^{-1} \frac{K'}{K}$ decreases with frequency increasing from 300 Mc/s. to 500 Mc/s.

ACKNOWLEDGMENT

The author expresses his grateful thanks to Professor K. Sreenivasan, Head of the Department, for giving facilities to carry out the investigation.

DEPARTMENT OF ELECTRICAL COMMUNICATION ENGINEERING,
INDIAN INSTITUTE OF SCIENCE, BANGALORE.

REFERENCES

- Chatterjee, S.K., 1948, *Ind Jour Phys.*, **23**, 157.
 Ford, L.H. and Oliver, R., 1946, *Proc. Phy. Soc.*, **59**, 265
 Hund, A., 1924, *Bureau Standards Scientific papers*, **19**, 487
 Kusters, W., 1942, *Hochf. u. Elektroakustik*, **59**, 131
 Lamont, H.R.L., 1940, *Phil. Mag.*, **29**, 521
 Lob, E., 1943, *Hochf. u. Elektroakustik*, **61**, 35
 McPetrie, J.S., 1934, *Proc. Phy. Soc.*, **46**, 637
 Smith Rose, R.L., and McPetrie, J.S., 1934, *Proc. Phy. Soc.*, **46**, 649.
 Strutt, M.I.O., 1930, *E.N.T.*, **7**, 387.

THE RAMAN SPECTRA OF TRICHLORO-ETHYLENE AND TETRACHLORO-ETHYLENE IN THE SOLID STATE

By S. B. SANYAL *

(Received for publication, March 29, 1950)

Plate V

ABSTRACT - Raman spectra of trichloroethylene and tetrachloroethylene in the liquid state at about 26°C and in the solid state at about -150°C have been investigated. In the latter case the frequency-shifts of some of the Raman lines increase in the solid state, but no new line appears in the low frequency region. On the other hand, in the case of trichloroethylene only one new line at 60 cm^{-1} appears when the liquid is solidified and cooled to -150°C and the intensities and positions of some of the prominent lines change with the solidification of the substance. It is pointed out that these observations contradict the hypothesis put forward by previous authors that these lines may be due to rotatory oscillations of the molecules pivoted in the lattice. It is pointed out that these new lines are due to presence of a halogen atom and permanent electric moment in the molecule in this particular case.

INTRODUCTION

It was previously observed by the present author and Mazumdar (1949) that in the case of two compounds having similar molecules, e.g., chloroacetyl chloride and bromoacetyl chloride, the number of lines observed in the liquid state is not the same. It was further observed in the case of the latter compound, that the number of lines is actually more than that expected theoretically and this was explained by assuming that strongly associated molecules were present in liquid bromo-acetyl compound. Thus the behaviour of the two similar molecules, both polar in the liquid state, is different from each other. In both the cases when the liquids were solidified and cooled down to -150°C a feeble new line at 48 cm^{-1} was observed. It was pointed out that in the case of such a complicated molecule the appearance of only one line in the low frequency region in the solid state cannot be explained by assuming that the line is due to rotatory oscillations of the molecules pivoted in the lattice as suggested by Kastler and Roussel (1941). In order to find out whether the appearance of such a line is due to the presence of particular atom in the molecule or it is due to the presence of strong permanent electric moment, two similar compounds, e.g., tetrachloroethylene and trichloro-ethylene were selected and the Raman spectra of these two compounds in the liquid and solid states have been studied in the present investigation.

* Communicated by Prof. S. C. Sirkar.

EXPERIMENTAL

The liquids were obtained from an old stock of Kahlbaum's original packings. They were distilled in vacuum before use. Arrangement for recording the Raman spectra in the solid state at low temperature was the same as that used in this laboratory by previous workers, such as Bishui (1948) and Majumdar (1949). A Fuess spectrograph giving dispersion of about 13.5\AA per mm in the region of 4046\AA was used. In each case iron arc spectrum was used for comparison. The polarisation of the Raman lines was also studied in order to verify the data published in Annual Table of Constants (Magat, 1934).

RESULTS AND DISCUSSIONS

The spectrographs for liquid and solid states are reproduced in the Plate V. The results are given in Tables I and II in which the letters P and D mean that the value of the de-polarisation factor is less than $6/7$ and equal to $6/7$ respectively. The values of the frequency-shifts in the case of the liquid state as given in Annual Table of Constants by Magat (1934) are also included in these tables for comparison. It will be observed that in the case of tetrachloro-ethylene the lines 238 , 450 and 1572 cm^{-1} shift respectively to 242 , 454 , and 1576 cm^{-1} and thus the binding forces in the $\text{C}-\text{Cl}$ and $\text{C}=\text{C}$ increase with the solidification of the liquid. No new line in the low frequency region is observed, however, in this case. But there seems to be a faint line, 380 cm^{-1} in the spectrogram due to the solid and on closer examination the spectrogram due to the liquid also seems to show the existence of a faint band at this place. On the other hand, in the case of trichloro ethylene, it can be seen from Table II that much more prominent changes have occurred in the relative intensities and positions of the lines with the solidification of the substance. The line 1582 cm^{-1} due to $\text{C}-\text{C}$ valence oscillation does not shift in the solid state, and its intensity relative to that of the line 629 cm^{-1} remains also the same, but the intensity of the line 3081 cm^{-1} due to $\text{C}-\text{H}$ valence oscillation increases very much in the solid state and becomes larger than the intensity of the line 1582 cm^{-1} . The intensity of the line 1248 cm^{-1} at the same time, diminishes considerably in the solid state. As regards the lines due to $\text{C}-\text{Cl}$ valence oscillation the frequencies diminish in some cases and increase in others. Thus the lines 277 , 457 and 629 cm^{-1} shift to 270 , 450 and 623 cm^{-1} , while the lines 211 and 383 cm^{-1} shift respectively to 216 and 390 cm^{-1} . Thus it appears that the strength of the $\text{C}=\text{C}$ bond remains unaltered while the $\text{C}-\text{C}$ bond is affected by the intermolecular field in the solid state. Further a sharp line at 62 cm^{-1} appears in the solid state and since such a line is absent in the tetrachloroethylene, it is quite evident that it is not the presence of chlorine atoms in the molecules alone that is responsible for the appearance of such new lines, but the presence of permanent electric

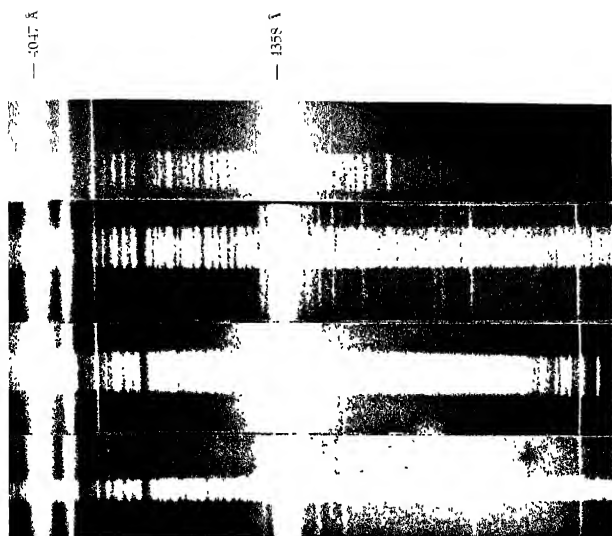


Fig. 1.

Raman Spectra

- | | | | |
|-----|---------------------|----|--------|
| (a) | Trichloroethylene | at | -150°C |
| (b) | " | at | 27°C |
| (c) | Tetrachloroethylene | at | 150°C |
| (d) | " | at | 27°C |

TABLE I

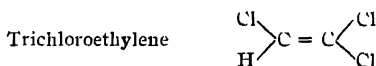


Liquid at 26°C

Solid at about -150°C

Magat (1934) $\Delta\nu$ in cm^{-1}	Present author $\Delta\nu$ in cm^{-1}	Present author $\Delta\nu$ in cm^{-1}
238(5)	238(7) , e, k, D	242(2) , e, k
344(3)	346(4) , e, k, D 382(6b) o, e, f	346(1) ; e 380(6) ; e
448(6)	450(9) ; e, i, k, P	454(1) , e, k
513(2)	516(3) ; e, k, D	-
1570(9)	1572(10) , e, k, D	1576 (55) , e, k

TABLE II



Liquid at 26°C		Solid at -150°C.
Simons (1932) $\Delta\nu$ in cm^{-1}	Present author $\Delta\nu$ in cm^{-1}	Present author $\Delta\nu$ in cm^{-1}
172(5)	174(4) , e, k, D	62(2) , e 174(1) ; e, k
211(4)	211(2b) , e, k, D	216(1) , e
274(5)	277(5) ; e, k, D	270(1) , e, k
380(5)	383(6) , e, k, D	390(4) , e, k
452(3)	457(3) , e, k, D	450(2) , e, k
628(5)	629(5) ; e, k, P	623(3) ; e, k
775(2)	765(2) , e, k, D	765(1) , e, k
933(1)	-	-
1248(2)	1248(2) ; e, k, P	1248(6b) , e, k
1585(6)	1582(7) , e, k, D	1582(6) ; e, k
3080(4)	3081(4) ; e, k, P	3076(6) , e, k

moment simultaneously with the presence of halogen atoms in the molecule seems to be the main cause for the appearance of this new line in the present case. The results obtained in the present investigation seem to contradict the hypothesis put forward by Bhagvantam (1943), and Kastler and Roussel (1941) that these new lines may be due to rotational oscillations of the molecules pivoted in the lattice. The molecules of trichloro-ethylene and tetrachloro-ethylene are similar to each other excepting the fact that one is polar and the other is non-polar, and if such rotational oscillations would give rise to new Raman lines in the solid state we would expect new Raman lines, at least three in number in each case, in the low frequency region when these substances are solidified. The change in the relative intensities of the lines due to the C-H oscillations and the shift in the lines due to C-Cl oscillations in the case of trichloro-ethylene suggest that something like a virtual bond is formed in the solid state between adjacent molecules, and this may also be responsible for the origin of the new line at 62 cm^{-1} in the case of trichloro-ethylene in the solid state.

ACKNOWLEDGMENT

The author is indebted to Prof. S. C. Sirkar for his guidance and kind interest in the work and to the authorities of the Indian Association for the Cultivation of Science for permission to work in the laboratory of the Optics Department.

INDIAN ASSOCIATION FOR THE
CULTIVATION OF SCIENCE,
210, BOU BAZAR STREET,
CALCUTTA.

REFERENCES

- Bhagavantam, S., 1943, *Proc. Ind. Acad. Sci. A*, **13**, 543.
Bishui, B.M., 1948, *Ind. J. Phys.*, **22**, 167.
Kastler, A. and Roussel, A., 1941, *Compt. Rendus*, **212**, 646, *Jour. de Physique*, **2**.
Magat, M., 1934, *Annual Table of Constants*, Paris, **23**, p. 59.
Majumdar, N. C., 1949, *Jour. Sci. and Indust. Research*, **8B**, 25.
Sanyal S. B. and Majumdar, M., 1949, *Ind. J. Phys.*, **23**, 1.

THERMODYNAMICS OF AN OSCILLATOR ASSEMBLY

By R. P. SINGH

(Received for publication, Nov. 12, 1949)

ABSTRACT. The thermodynamics of an assembly of linear harmonic oscillators is worked out. The expressions for specific heat obtained here for Bose and Fermi statistics are compared with those of Auluck and Kothari. Their results, obtained by use of partition theory of numbers, show that entropy and hence the specific heat is the same for both Bose and Fermi cases while here it is approximately the same, and not exactly. In the derivation here the sums have been replaced by integrals and it remains to investigate where the difference actually lies in the two cases. This will be done in the next communication.

The thermodynamical study of an assembly of linear oscillators is of considerable intrinsic interest, and also because of its close connection, as has been shown by Auluck and Kothari (1946), with the partition theory of numbers. In fact, one can profitably discuss processes of approximation, replacement of sums by integrals and so on for this assembly, and such a discussion is expected to furnish greater insight into these questions than one relating to a more complicated assembly. Further an examination of such questions is opportune as appears from Dingle's (1941) recent contribution.

We first take the case where the sums have been replaced by integrals in the usual manner. The distribution law of the assembly is

$$f(\epsilon) = \frac{1}{e^{\epsilon/kT} \frac{A}{\beta}} \quad \dots (1)$$

where $\beta = +1$ for Fermi-Dirac case and $\beta = -1$ for Bose-Einstein case, and

$$\begin{aligned} n(\epsilon) d\epsilon &= a(\epsilon) f(\epsilon) d\epsilon \\ &= \frac{a(\epsilon) d\epsilon}{e^{\epsilon/kT} \frac{A}{\beta} + \beta} \quad \dots (2) \end{aligned}$$

with

$$N = \int_0^\infty n(\epsilon) d\epsilon, \quad \dots (3)$$

and

$$E = \int_0^\infty \epsilon n(\epsilon) d\epsilon. \quad \dots (4)$$

For our case

$$a(\epsilon) = \frac{1}{\hbar\omega}$$

so for N and E we have

$$N = \frac{kT}{\hbar\omega} \int_0^{\infty} \frac{e^{-u}}{\frac{e^u}{A} + \beta} du \quad \dots (5)$$

and

$$E = \frac{(kT)^2}{\hbar\omega} \int_0^{\infty} \frac{u e^{-u}}{\frac{e^u}{A} + \beta} du \quad \dots (6)$$

where

$$u = \frac{\epsilon}{kT}.$$

1. For the case of non-degeneracy we have $A \ll 1$ and the distribution function is easily expanded as series. In this case the total number N of the oscillators in the assembly is given by

$$A_1 = \sum \frac{A^n}{n} (-\beta)^{n-1} \quad \dots (7)$$

where A_1 is defined by $A_1 = \frac{N\hbar\omega}{kT}$.

In above equation (7) a quantity A_1 has been defined and $\beta = -1$ for Bose-Einstein case and $\beta = +1$ for Fermi-Dirac case. The total energy of the assembly is given by

$$\begin{aligned} E &= \frac{(kT)^2}{\hbar\omega} \int_0^{\infty} \frac{u e^{-u}}{\frac{e^u}{A} + \beta} du \\ &= NkT \left\{ 1 + a\beta A_1 - b\beta^2 A_1^2 + c\beta^3 A_1^3 + \dots \right\} \quad \dots (8) \end{aligned}$$

where $a = \frac{1}{2}$, $b = \left(\frac{2}{3} - 1 \right)$

and $c = \frac{3}{4} + \frac{5}{2.8} - \frac{3}{6}$.

Substituting the value of A_1 we get for the energy of the assembly,

$$E = NkT + a\beta N^2 \hbar\omega - b\beta^2 \frac{N(N\hbar\omega)^2}{kT} + c\beta^3 N \frac{(N\hbar\omega)^3}{(kT)^2} + \dots (9)$$

and the specific heat of the assembly is given by

$$C_v = \frac{\delta E}{\delta T} = Nk \left[1 + b\beta^2 \left(\frac{N\hbar\omega}{kT} \right)^2 - 2c\beta^3 \left(\frac{N\hbar\omega}{kT} \right)^3 + \dots \right] \quad \dots (10)$$

The thermodynamical potential and the entropy of the assembly can also be obtained as follows for the non-degenerate case. They are

$$\frac{G}{NkT} = \log A = \log A_1 + a\beta A_1 - \frac{1}{2}b\beta^2 A_1^2 + \frac{1}{6}c\beta^3 A_1^3 + \dots \quad (11)$$

and

$$\frac{S}{Nk} = \frac{E-G}{NkT} = 1 - \log A_1 - a\beta A_1 + \frac{1}{2}b\beta^2 A_1^2 - \frac{1}{6}c\beta^3 A_1^3 + \dots \quad (12)$$

or

$$S = Nk \left[1 - \log A_1 + a\beta A_1 - \frac{1}{2}b\beta^2 A_1^2 + \frac{1}{6}c\beta^3 A_1^3 + \dots \right] \quad (13)$$

In the above G is the thermodynamic potential of the assembly and S is the entropy and again $\beta = +1$ corresponds to F. D. case and $\beta = -1$ to the B. E. case

The equation (10) demonstrates an interesting fact, that is, it shows that for non-degeneracy ($A \ll 1$) the specific heat C_v of the assembly is proportional to the number of oscillators in it and that it is the same for both Bose-Einstein and Fermi-Dirac cases to the approximation of the

order of $\left(\frac{N\hbar\omega}{KT} \right)^2$.

2. We shall now take up the degenerate case

In degeneracy the Fermi-Dirac and Bose-Einstein cases are considered separately. For Bose-Einstein degeneracy $A=1$ and $\beta=-1$ and so the energy of the assembly is,

$$E = \frac{(kT)^2}{\hbar\omega} \int_0^\infty \frac{u du}{e^u - 1} = \frac{\pi^2}{6} \cdot \frac{(kT)^2}{\hbar\omega}.$$

Hence

$$C_v = \frac{\delta E}{\delta T} = \frac{\pi^2}{3} k \left(\frac{kT}{\hbar\omega} \right). \quad (15)$$

Also

$$G = NkT \log A = 0, \quad (16)$$

and

$$S = \frac{E}{NkT} = \frac{\pi^2}{6} \cdot \frac{kT}{N\hbar\omega} = \frac{\pi^2}{6A_1}. \quad (17)$$

The degenerate case of Fermi-statistics is characterised by $A \gg 1$ and $\beta = +1$. In this case the integration is carried out by using Sommerfeld formula according to which for large A we have an asymptotic series expansion for the integral

$$\int_0^\infty \frac{d\phi(\epsilon)}{d\epsilon} \cdot \frac{1}{\frac{\epsilon - \xi}{e^{kT} - 1}} d\epsilon \quad (18)$$

$$= \{\phi(\epsilon) + 2C_2\phi^{II}(\epsilon)(kT)^2 + 2C_4(kT)^4\phi^{IV}(\epsilon) + \dots\}_{\epsilon=\xi} \quad \dots (18a)$$

$$\text{where} \quad C_{2n} = (1 - 2^{1-2n})\zeta(2n) \quad \dots (18b)$$

$\zeta(2n)$ being the well known Riemann-Zeta function. The numerical values of C_{2n} are (Mc-Dougall and Stoner, 1938)

$$C_2 = \frac{\pi^2}{12}, \quad C_4 = \frac{7\pi^4}{720}$$

$$\text{and} \quad C_6 = \frac{31\pi^6}{30240}.$$

The above expansion of (18) is subject to an error of the order of $e^{-\xi/kT}$ and holds good if $\xi/kT \gg 1$ and $\phi(\epsilon)$ is a regular function vanishing for $\epsilon=0$.

We have in this case for N the number of oscillators in the assembly

$$\begin{aligned} N &= \frac{1}{\hbar\omega} \int_0^\infty \frac{1}{\frac{\epsilon}{\hbar\omega} + 1} d\epsilon \\ &= \frac{1}{\hbar\omega} \int_0^\infty \frac{d(\epsilon)}{d\epsilon} \cdot \frac{1}{\frac{\epsilon}{\hbar\omega} + 1} d\epsilon \\ &= \frac{1}{\hbar\omega} \left[\epsilon \right]_{\epsilon=\xi}^\infty = \frac{\xi}{\hbar\omega} \\ &= \frac{kT}{\hbar\omega} \log A \quad \dots (19) \end{aligned}$$

or

$$\frac{N\hbar\omega}{kT} = A_1 = \log A. \quad \dots (20)$$

On the other hand the integral for N can be directly evaluated giving correct value of A_1 . We have

$$A_1 = \int_0^\infty \frac{du}{\frac{e^u}{A} + 1}.$$

putting $e^u = Z$ and changing the variable from U to Z we get

$$\begin{aligned} A_1 &= \int_1^\infty \frac{dZ}{Z \left(\frac{Z}{A} + 1 \right)} \\ &= \int_1^\infty \left[\frac{1}{Z} - \frac{1}{Z+A} \right] dZ \end{aligned}$$

$$\begin{aligned}
 &= \left[\log \frac{Z}{Z+A} \right]_1^{\infty} \\
 &= \left[-\log \frac{1}{1+A} \right] \\
 &= \log (1+A). \quad \dots (21)
 \end{aligned}$$

Thus we have $\log (1+A)$ for the accurate value of A_1 which can be put in the form of a series in powers of A

$$\begin{aligned}
 \log (1+A) &= \log A + \log \left(1 + \frac{1}{A} \right) \\
 &= \log A + \frac{1}{A} - \frac{1}{2A^2} + \dots (27)
 \end{aligned}$$

and because $A \gg 1$ we have $\log (1+A) \sim \log A$, i.e. $A_1 \sim \log A$ which is the same result as (20).

Now the energy in the Fermi-Dirac case is

$$\begin{aligned}
 E &= \frac{1}{\hbar\omega} \int_0^{\infty} \frac{\epsilon d\epsilon}{\frac{e^{-\xi}}{e^{kT} + 1}} \\
 &= \frac{1}{\hbar\omega} \int_0^{\infty} \frac{d(\frac{1}{2}\epsilon^2)}{d\epsilon} \cdot \frac{1}{\frac{e^{-\xi}}{e^{kT} + 1}} d\epsilon \\
 &= \frac{1}{\hbar\omega} \left[\frac{1}{2}\epsilon^2 + 2C_2 (kT)^2 \right]_{\epsilon=\xi}^{\infty} \\
 &= \frac{1}{\hbar\omega} \left[\frac{1}{2}\xi^2 + \frac{\pi^2}{6} (kT)^2 \right] \quad (23)
 \end{aligned}$$

We shall now find ξ using (21) and substitute in (23) for various orders of approximation.

To the zeroth order approximation $A_1 = \log A$

$$\text{or} \quad A = e^{\frac{\lambda \hbar\omega}{kT}}$$

$$\text{but} \quad A = e^{\xi/kT} \text{ and so } \xi/kT = \frac{N\hbar\omega}{kT}$$

$$\text{or} \quad \xi = N\hbar\omega. \quad \dots (24)$$

The energy E in this case is

$$E = \frac{1}{\hbar\omega} \left[\frac{1}{2} (N\hbar\omega)^2 + \frac{\pi^2}{6} (kT)^2 \right] \quad \dots (25)$$

$$= \frac{1}{2} N^2 \hbar \omega + \frac{\pi^2}{6} \cdot \frac{(kT)^2}{\hbar \omega}$$

and so

$$C_v = \frac{\delta E}{\delta T} = \frac{\pi^2}{3} k \left(\frac{kT}{\hbar \omega} \right) \quad \dots (26)$$

Here we see that we have got equation (26) identical with (15) for the Bose-Einstein case. Thus to a zeroth order approximation the specific heat is the same for both Bose-Einstein and Fermi-Dirac cases for degeneracy. The specific heat is seen to be independent of the number of oscillators in the assembly for the Fermi-Dirac case. That it is also the same for Bose-Einstein case is easily understandable.

$$C_v = \frac{\pi^2}{3} k \left(\frac{kT}{\hbar \omega} \right) \text{ exactly for Bose case}$$

and

$$C_v = \frac{\pi^2}{3} k \left(\frac{kT}{\hbar \omega} \right) \text{ approximately for F. D. case.}$$

We now proceed to obtain the value of C_v in the present case to a higher approximation using more accurate value of ξ .

From equation (21) we have again

$$\frac{N\hbar\omega}{kT} = \log (1 + A)$$

or

$$A = e^{\frac{N\hbar\omega}{2\pi kT}} - 1$$

and hence

$$e^{N\hbar\omega/kT} = e^{\frac{N\hbar\omega}{2\pi kT}} - 1$$

i.e.,

$$\begin{aligned} \xi/kT &= \log e^{\frac{N\hbar\omega}{2\pi kT}} + \log \left(1 - e^{-\frac{N\hbar\omega}{2\pi kT}} \right) \\ &= \frac{N\hbar\omega}{kT} + \log \left(1 - e^{-\frac{N\hbar\omega}{2\pi kT}} \right), \end{aligned}$$

which gives

$$\xi = N\hbar\omega + kT \log \left(1 - e^{-\frac{N\hbar\omega}{2\pi kT}} \right), \quad \dots (27)$$

and

$$\xi^2 = (N\hbar\omega)^2 + 2N\hbar\omega kT \log \left(1 - e^{-\frac{N\hbar\omega}{2\pi kT}} \right) + (kT)^2 \left\{ \log \left(1 - e^{-\frac{N\hbar\omega}{2\pi kT}} \right) \right\}^2.$$

Substituting this value of ξ^2 in (23), we get

$$\begin{aligned}
 E &= \frac{1}{\hbar\omega} \left[\frac{1}{2} \left\{ (N\hbar\omega)^2 + 2N\hbar\omega kT \log \left(1 - e^{-\frac{N\hbar\omega}{2\pi kT}} \right) \right. \right. \\
 &\quad \left. \left. + (kT)^2 \left(\log \left(1 - e^{-\frac{N\hbar\omega}{2\pi kT}} \right) \right)^2 \right\} + \frac{\pi^2}{6} (kT)^2 \right] \\
 &= \frac{N^2\hbar\omega}{2} + 2NkT \log \left(1 - e^{-\frac{N\hbar\omega}{2\pi kT}} \right) \\
 &\quad + \frac{(kT)^2}{\hbar\omega} \left[\frac{\pi^2}{6} + \left\{ \log \left(1 - e^{-\frac{N\hbar\omega}{2\pi kT}} \right) \right\}^2 \right]
 \end{aligned}$$

and hence the specific heat C_v is

$$\begin{aligned}
 C_v &= \frac{\delta E}{\delta T} = 2Nk \log \left(1 - e^{-\frac{N\hbar\omega}{2\pi kT}} \right) - \frac{2N^2\hbar\omega}{T} \frac{e^{-\frac{N\hbar\omega}{2\pi kT}}}{1 - e^{-\frac{N\hbar\omega}{2\pi kT}}} \\
 &\quad + \frac{2k(kT)}{\hbar\omega} \left[\frac{\pi^2}{6} + \left\{ \log \left(1 - e^{-\frac{N\hbar\omega}{2\pi kT}} \right) \right\}^2 \right] \\
 &\quad - \frac{(kT)^2}{\hbar\omega} \cdot \frac{2N\hbar\omega}{kT^2} \frac{e^{-\frac{N\hbar\omega}{2\pi kT}}}{1 - e^{-\frac{N\hbar\omega}{2\pi kT}}} \log \left(1 - e^{-\frac{N\hbar\omega}{2\pi kT}} \right) \quad \dots (29)
 \end{aligned}$$

$$\begin{aligned}
 C_v &= \frac{\pi^2}{3} k \left(\frac{kT}{\hbar\omega} \right) + 2Nk \left\{ 1 - \frac{1}{e^{\frac{N\hbar\omega}{2\pi kT}} - 1} \right\} \log \left(1 - e^{-\frac{N\hbar\omega}{2\pi kT}} \right) \\
 &\quad - \frac{2N^2\hbar\omega}{T} \cdot \frac{1}{e^{\frac{N\hbar\omega}{2\pi kT}} - 1} + \frac{2k(kT)}{\hbar\omega} \left\{ \log \left(1 - e^{-\frac{N\hbar\omega}{2\pi kT}} \right) \right\}^2 \quad \dots (30)
 \end{aligned}$$

Equation (30) shows that in the degenerate Fermi-Dirac case the specific heat has additional terms beyond $\frac{\pi^2}{3} k \left(\frac{kT}{\hbar\omega} \right)$. It can be seen that these terms have a very small contribution to specific heat. But on the other hand if we proceed by more exact method of sums (and not replace by integrals) as described by Auluck and Kothari (1946), we find that entropy and hence specific heat is exactly the same for Bose and Fermi statistics.

The above treatment shows that we get results by integral method which do not agree exactly with those obtained by sum method. It would be of interest to investigate where the difference actually lies and in this connection the work of Dingle and Liebfried and Kaempffer (1948) is relevant.

ACKNOWLEDGMENT

It is a great pleasure to acknowledge my indebtedness to Prof. D. S. Kothari for suggesting the problem and his kind help during the progress of the work

DEPARTMENT OF PHYSICS
UNIVERSITY OF ALLAHABAD.

REFERENCES

- Auluck P. C. and Kothari D. S., 1946, *Proc. Camb. Phil. Soc.* **42**, 272
 Dingle R. B., 1949, *Proc. Camb. Phil. Soc.* **45**, 275
 Liebfried G. and Kaempffer E., 1948, *Zettls für Phys.*, **12**, 441.
 Mc Dougall, J. and Stoner, E. C., 1938, *Phil. Trans.* **4**, **287**, 67

ABSORPTION OF U. H. F. RADIO WAVES IN SOME SUBSTITUTED BENZENE COMPOUNDS

By S. N. SEN *

(Received for publication March 31, 1950)

ABSTRACT In continuation of previous work, the absorption of ultra high frequency radio waves of frequencies ranging from 250–530 megacycles/sec in chlorobenzene, toluene, ethyl benzene and nitrobenzene at temperatures ranging from 27°C to –94°C in the first three cases and from 27°C to 5°C in the latter, has been investigated. It is observed that there is a broad peak in the absorption curve of chlorobenzene at 410 megacycles/sec when the liquid is cooled to –30°C. The absorption becomes negligible when the liquid is solidified and kept at a temperature of –45°C. In case of nitrobenzene at 26°.7C a similar peak is observed at a frequency of 505 megacycles/sec and in this case also, the absorption vanishes when the substance is solidified and kept at the melting point of the solid, *i.e.*, at 5°C. In the case of toluene and ethyl benzene there is no absorption in the frequencies mentioned above in the temperature range from –95°C to 27°C. Also, when solidified, these two substances did not show any absorption of the radio waves. These results have been discussed in the light of the theories put forward by previous authors to explain the origin of new lines in the Raman spectra of these compounds in the solid state. It is pointed out that the order of frequencies of rotational oscillations in the liquid state as indicated by absorption peaks mentioned above is different from that of the frequencies of the new Raman lines of these substances observed in the solid state. For this reason the explanation offered by previous workers that such rotational oscillations of molecules are the cause of the new lines observed in the Raman spectra of the compounds in the solid state is not correct.

INTRODUCTION

It was shown recently by the present author (Sen, 1949) that many liquids, in which anomalous absorption of U. H. F. radio waves could not be detected by previous authors, show absorption when the frequency of the radio-waves and temperatures of the liquid are adjusted. It was thus observed that acetone, ether and methyl ethyl ketone exhibit such anomalous absorption at different temperatures when the frequencies of the incident radio-waves range from 250 megacycles/sec to about 530 megacycles/sec. The significance of these results was mentioned in the paper mentioned above and it was pointed out that probably the intermolecular field produced by neighbouring molecules has an effect on the permanent electric moment of each molecule and due to thermal vibration there is a periodic fluctuation of permanent electric moment also. These results also indicated that natural frequency of angular oscillations could be obtained from the frequency

* Communicated by Prof. S. C. Sirkar,

of the radio-waves absorbed anomalously by these polar molecules. Recently, Ray (1950) has investigated the Raman spectra of chlorobenzene and toluene and has observed five new Raman lines in the low frequency region in each case. The oscillations producing these lines have frequencies varying from 45 cm^{-1} to about 130 cm^{-1} . Previous workers (Kastler and Roussel, 1941) have attributed the origin of such lines to angular oscillations of molecules pivoted at the crystal lattice about the three axes. Bhagavantam (1941) also independently put forward a similar hypothesis and indicated that when the substance passes from solid to liquid state, the oscillations giving rise to new lines in the solid state are transformed into hindered rotation and the wings accompanying the Rayleigh line in the Raman spectra may be due to these hindered rotations. In the case of chlorobenzene and toluene, the wing does not extend beyond 140 cm^{-1} from the centre of the Rayleigh line and if the interpretation given by Bhagavantam (1941) is correct, it appears that frequency of hindered rotation of the molecule in the liquid is of the same order of magnitude as that of the angular oscillation of the molecule pivoted in the crystal lattice. Hence, according to this theory, the frequencies of the radio waves which are absorbed by polar molecules in the liquid state should be of the same order of magnitude as that of the frequency-shifts at different points in the wing accompanying the Rayleigh line in these liquids. Since the frequencies at certain positions in the wing correspond to 10^{11} per sec in the two cases mentioned above, there should be no absorption of ordinary ultra high-frequency radio-waves by these liquids. In the present investigation, attempt has been made to test the correctness of the hypothesis put forward by Kastler and Roussel (1941) and independently by Bhagavantam (1941) by studying the absorption of ultra high-frequency radio waves of frequencies ranging from 250 Mc/sec. up to 530 Mc/sec. in chlorobenzene and toluene at different temperatures. The investigation has also been extended to nitrobenzene and ethyl benzene to find out how the frequency of absorption changes with change in the substitution group in the benzene ring. Attempts have also been made to detect the absorption of these ultra high-frequency waves by all the four substances in the solid state.

EXPERIMENTAL

The experimental arrangements are essentially the same as those described previously (Sen 1949) and these are shown diagrammatically in figure 1. It was observed that when cylindrical reflector *M* of parabolic cross section was used in the position shown, the waves were less divergent than without it so that the receiver could be placed at a distance of about 40 cms from the aerial. Without a reflector in this position there was much smaller current in the tuned detector due to incident radiation, at such a distance. The thickness of the glass cell in which the liquid was put was about 3.95 cms.,

and its width was about 14 cms., which was much larger than the diameter of the tuning condenser. The whole receiver was covered with an earth-connected metal sheet leaving only a window just in front of the tuning condenser, and as this window was completely covered by the cell containing the liquid it was not possible for any radiation from the oscillator to reach the tuning condenser without passing through the liquid in the cell. As it was intended to find only the frequencies of radiation in the region of anomalous absorption, no attempt was made to measure the attenuation co-efficient under ideal conditions. Allowance was, however, made for the absorption of waves in the empty glass cell itself as explained in the previous investigation (Sen, 1949).



FIG. 1

The current I_0 in the detecting circuit adjusted for resonance was first noted without placing the cell between the vertical aerial and tuning condenser of the detector. The cell was previously put inside a Dewar vessel above the surface of the liquid oxygen contained in the vessel and when a steady low temperature was indicated by the pentane thermometer inserted in the liquid through a cork fitted at the mouth of the cell, the cell was taken out quickly and inserted between the aerial and the tuning condenser. The condenser was immediately adjusted again for resonance and the current I_1 was noted. The liquid was then taken out and after the empty cell had been cooled to the same temperature as before it was placed between the aerial and the tuning condenser. The resonance was restored by adjusting the condenser and the new current I_2 was then noted. Since we have $I_1 = I_2 e^{-\mu x}$ where μ is the attenuation co-efficient and x denotes the thickness of the liquid in the cell, we get the attenuation co-efficient from the relation.

$$\mu = (1/x) \log_e (I_2/I_1).$$

This was repeated for different temperatures of the liquids and for different frequencies, the different temperatures being obtained by placing the cell at different heights above the surface of the liquid oxygen in the Dewar vessel. The value of I_2 was less than I_0 by about 5% to 8%. So the value of attenuation coefficient taken here is fairly accurate.

TABLE I
Chlorobenzene C_6H_5Cl

Temp. Frequency Mc/sec	$^{\circ}C$ μ	$-30^{\circ}C$ μ	$-45^{\circ}C$ (Melting point of solid). I_2/I_1	$26^{\circ}C$ I_2/I_1
520	.08818	.02446	1.004	1.002
500	.07750	.04002	1.001	1.001
480	.06882	.07285	1.000	1.000
460	.06153	.1050	1.000	1.004
440	.05050	.1325	1.001	1.001
420	.04531	.1365	1.000	1.001
400	.03384	.1275	1.001	1.001
380	.02975	.1027	1.001	1.000
360	.02678	.06750	1.000	1.000
340	.02514	.04512	1.002	1.001
320	.02414	.0350	1.002	1.000
300	.02014	.0225	1.002	1.001
280	—	.01560	1.000	1.001
260	—	.01450	1.001	1.001
250	—	.01232	1.001	1.000

TABLE II
Nitrobenzene $C_6H_5NO_2$

Temp Frequency Mc/sec	$26^{\circ}C$	$5^{\circ}C$ (Melting point of the solid) I_2/I_1
530	.2608	1.000
510	.2932	1.001
500	.2985	1.001
490	.2886	1.001
480	.2783	1.002
470	.2675	1.002
460	.2519	1.001
450	.2379	1.002
440	.2280	1.000
430	.2248	1.003
420	.2030	1.002
410	.1932	1.000
400	.1756	1.000
390	.1624	1.003
380	.1523	1.003
370	.1421	1.003
360	.1365	1.000
350	.1224	1.000
340	.1021	1.002
330	.1009	1.000
320	.0932	1.002
310	.0802	1.002
300	.0728	1.001
290	.0580	1.002
280	.0461	1.002
270	.0330	1.003
260	.0323	1.000
250	.0266	1.000

TABLE III.
Toluene $C_6H_5CH_3$

Temp.	27°C. I_2/I_1	0°C I_2/I_1	-30°C I_2/I_1	-65°C I_2/I_1	-95°C I_2/I_1
Frequency /sec.					
525	1.001	1.001	1.001	1.001	1.002
500	1.000	1.001	1.001	1.002	1.000
480	1.001	1.000	1.001	1.003	1.003
460	1.003	1.001	1.001	1.003	1.001
440	1.000	1.000	1.001	1.001	1.001
420	1.003	1.001	1.000	1.001	1.000
400	1.002	1.001	1.000	1.000	1.001
380	1.001	1.001	1.000	1.000	1.000
360	1.005	1.003	1.001	1.001	1.000
340	1.001	1.001	1.000	1.001	1.001
320	1.001	1.002	1.000	1.001	1.001
300	1.002	1.001	1.003	1.001	1.000
280	1.000	1.000	1.000	1.000	1.000
260	1.000	1.000	1.000	1.000	1.000
250	1.000	1.000	1.000	1.000	1.000

TABLE IV.
Ethyl Benzene $C_6H_4C_2H_5$

Temp.	27°C I_2/I_1	0°C I_2/I_1	-30°C I_2/I_1	-65°C I_2/I_1	-95°C. I_2/I_1
Frequency Mc/sec					
325	1.001	1.001	1.001	.000	.000
500	1.001	1.000	1.000	.000	.000
480	1.002	1.000	1.003	.004	.000
460	1.001	1.000	1.001	.000	.000
440	1.001	1.001	1.002	.001	.001
420	1.003	1.003	1.002	.002	.001
400	1.001	1.001	1.000	.001	.001
380	1.001	1.001	1.000	.001	.001
360	1.000	1.000	1.001	.001	.004
340	1.000	1.000	1.001	.001	.001
320	1.001	1.000	1.001	.001	.001
300	1.000	1.003	1.003	.001	.001
280	1.000	1.000	1.000	.000	.000
260	1.000	1.000	1.000	.000	.000
250	1.000	1.000	1.000	.000	.000

In this way the absorption in chlorobenzene was studied in the temperature-range from 26°C to -45°C, in toluene from 27°C to -92°C, in nitrobenzene from 27°C to 5°C and in ethyl benzene from 27°C to -94°C. The absorption of radio-waves in these substances in the solid state and kept at their freezing points was also studied in this way.

RESULTS AND DISCUSSION

The results are given in Tables I—IV. They are also shown diagrammatically in Figs. 2 to 5. It will be seen from the figures that in case of ethyl

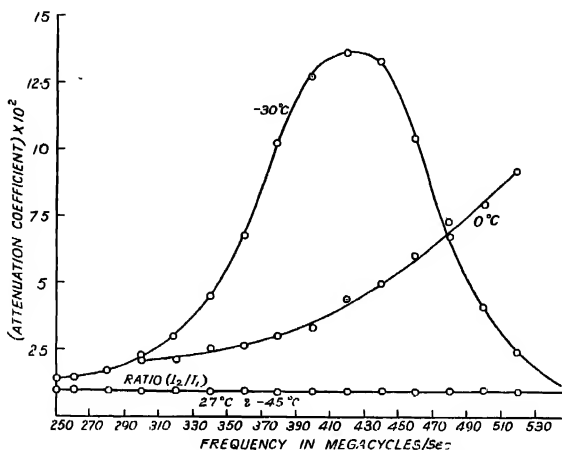


FIG. 2

(Chlorobenzene)

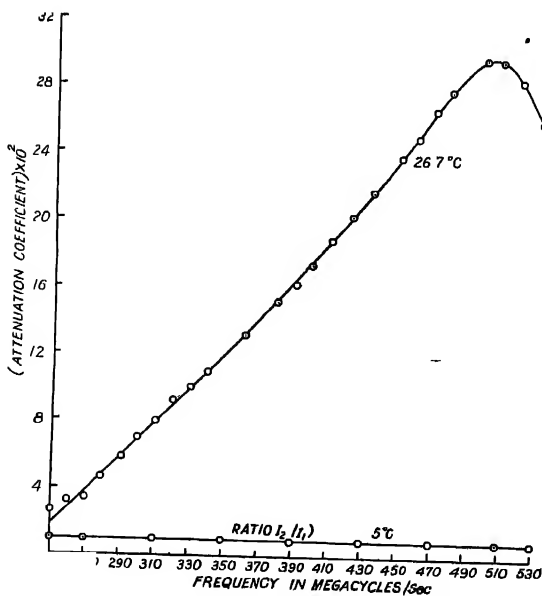


FIG. 3

(Nitrobenzene)

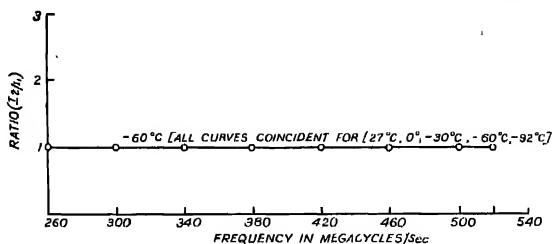
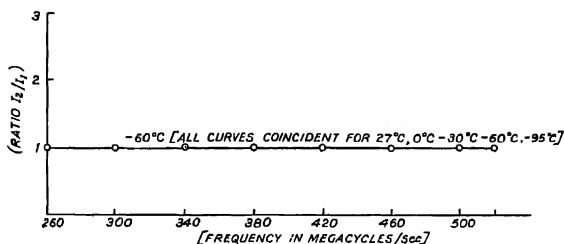


FIG. 4 (Toluene)



5FIG. (Ethyl benzene)

benzene and toluene in the liquid state there is no absorption of waves of frequencies ranging from .50 megacycles/sec up to 530 megacycles/sec. even when they are cooled down to temperatures just above their freezing points. In the case of chlorobenzene, at -30°C an absorption peak is observed at 420 megacycle/sec. and at 0°C the absorption increases with the increase of frequency up to 530 megacycles/sec. without showing any maximum. It is also seen from Table I that when chlorobenzene is solidified no absorption peak is observed in the region of frequencies mentioned above. Toluene and ethyl benzene also did not show any absorption when they were solidified.

In the case of nitrobenzene an absorption peak is observed at $26^{\circ}.7^{\circ}\text{C}$ at 505 megacycles/sec but when the liquid is solidified and kept at a temperature of 5°C the peak disappears and the absorption becomes negligible throughout the whole range of frequencies from 250--530 megacycles/sec.

The absorption of radio waves of wavelength 1.82 metres in nitrobenzene and chlorobenzene in the liquid state was studied previously by Szymanowski (1933) but he did not observe any anomalous dispersion in the temperature range from 10°C to 60°C in the former case and 0°C to 60°C in the latter case. The results obtained in the present investigation show that the absorption maximum is observed in both these cases when the frequencies of the radio waves are increased about three times and also the liquid is cooled to -30°C in the case of chlorobenzene.

The results mentioned above show that when the substances are solidified, either the radiations are not absorbed at all, or the region of absorption shifts towards higher frequencies because no absorption in the low frequency region is observed. It is, however, unlikely that shift towards higher frequency region may take place with the freezing of the substance, because with the lowering of temperatures of the liquid and consequent increase in viscosity of the liquid the frequency of the region of anomalous dispersion is observed to shift towards low frequency region and not towards high frequencies region. Hence with the freezing of the liquid and consequent increase in the viscosity of the liquid, the frequency of maximum absorption is expected to diminish. Since such a diminution in the frequency of maximum absorption is not observed, it is reasonable to assume that the anomalous absorption of radio waves disappears with the solidification of the substance. If this be true, then absorption of ultra high frequency radio waves seems to be intimately connected with the freedom of hindered rotational movement of the molecules and when such freedom is absent in the solid-state, the absorption ceases. The absence of absorption in case of toluene and ethyl benzene even in the liquid state at low temperatures down to their freezing point may be due to the fact that the value of dipole moment possessed by the molecules of these substances is very small.

The presence of an absorption peak at 420 megacycles/sec. in the case of chlorobenzene thus proves that the frequency of rotational oscillation of molecules in the liquid state at -30°C is of the order of 4.2×10^8 /sec. This order of magnitude is quite different from that of the frequencies of the new lines observed in the case of solid chlorobenzene and toluene by Ray (1950). Hence the lines observed by him cannot be due to such rotational oscillations and their origin is to be attributed to other causes.

ACKNOWLEDGMENT

The author is indebted to Prof. S. C. Sirkar for his interest and helpful discussions during the progress of the work and to Prof. S. K. Mitra, of Calcutta University for kindly lending the crystal detector used in the present investigation.

INDIAN ASSOCIATION FOR THE
CULTIVATION OF SCIENCE,
210, BOWBAZAR STREET,
CALCUTTA.

REFERENCES

- Bhagavantam, S. 1941, *Proc. Ind. Acad. Sc.* **13A**, 542.
Kastler, A., and Rousset, A., 1941, *Comptes Rendes* **212**, 645.
Ray, A. K. 1950, *Ind. J. Phys.* **24** (in press)
Sen, S. N. 1941, *Ind. Jour. Phys.* **23**, 495.
Szymanowski, W. T., 1933, *Jour. Chem. Phys.* **1**, 809.

A COMPARATIVE STUDY OF THE DIFFERENT METHODS OF HEAT-RUN TESTS ON ELECTRICAL MACHINES.

I. SINGLE-PHASE TRANSFORMERS.

By H. K. BASU

(Received for publication, March 14, 1950)

ABSTRACT. The paper makes a critical study of the different methods of making heat-run tests on a single-phase transformer and of estimating its final temperature rise when fully loaded. The results of test show definitely that the alternate open- and short-circuit run may be used where it is not possible to carry out the direct loading method

INTRODUCTION

It is well known that one of the main factors deciding the rating of an electrical machine is its temperature rise. A correct determination of the maximum temperature rise at its rated load is therefore one of the main problems confronting the designers, especially when a new design is undertaken. The temperature rise may, of course, be predetermined but the data necessary for the purpose are not always available. The normal practice is therefore to estimate the maximum temperature rise of a new design from the results of a heat-run test on it. There are many methods available for carrying out the test. Amongst them the direct loading method is known to yield the true result. In this method the machine under test is run at its rated load under rated conditions for about 5 to 18 hours, depending upon the size, till it attains a steady temperature, which is either read directly with the help of a thermometer suitably inserted into it or estimated from a measurement of the hot resistance of its winding or windings. Unfortunately the method is not always feasible in practice in a test room, especially in the case of large machines, since it involves a huge wastage of power. The other methods are, on the other hand, less expensive. It is therefore worthwhile investigating if these methods could be employed to determine the maximum temperature rise of an electrical machine under its rated load conditions. In the present paper the results obtained in the case of a single-phase transformer are reported.

METHODS OF HEAT-RUN TEST

In addition to the direct loading method noted above, the following alternative methods have been suggested by several workers (Madden, 1913; Stigant and Lacey, 1941) for carrying out a heat-run test on transformers without actually loading them:

- (a) Summer test, known also as Opposition test,
- (b) Equivalent Short-circuit run,
- (c) Equivalent Open-circuit run,
- (d) Alternate Open- and Short-circuit run

Since it is only the losses that are responsible for the temperature rise in an electrical machine, the basic idea underlying all the above alternative methods is to supply to the machine necessary electrical power to overcome its full load losses when operating otherwise normally so as to stimulate full load conditions as far as temperature rise is concerned.

METHODS OF ESTIMATING TEMPERATURE RISE

It is evident that the most direct and simple method of estimating the temperature rise in a heat-run test on a machine is to note the reading of a thermometer suitably inserted into it just before beginning the test and after it attains a steady hot state during the test. The difference in the readings of the thermometer gives the temperature rise. This method, however, takes several hours. It is hence necessary to keep a constant watch on the operating conditions during the test to ensure oneself that there has been no fluctuation or variation in any of these conditions as well as in the temperature of the surrounding atmosphere.

Another equally time-consuming method as above is to measure the resistance of the winding or windings of the machine undergoing a heat-run test at the temperature (θ_1) of the surrounding atmosphere, just before beginning the test and, also after the steady hot state is reached during the test. The rise in temperature of the machine is then calculated from the following relation,

$$\text{rise in temperature} = \left\{ (234.5 + \theta_1) \frac{R_2}{R_1} - 234.5 \right\} - \theta_1$$

where R_1 is the cold resistance of the winding at temperature θ_1 , and R_2 the hot resistance at the steady hot temperature. It may be noted that since for copper $\alpha_0 = 0.00426$, we have $\frac{1}{\alpha_0} = 234.5$. This method of calculating the temperature rise also necessitates the same care and precautions as the previous method, besides the choice of a suitable and accurate method for the measurement of resistance of the winding.

As both the above methods require a prolonged heat-run test on a machine, two other methods in which it is necessary to obtain data of temperature-rise over a comparatively very short period only for estimating the final temperature rise have been suggested. These methods are, therefore, called 'short heat-run tests'. They are essentially graphical methods.

In one of these the rate of temperature-rise, i.e., $\frac{d\theta}{dt}$ is plotted against the

temperature-rise ($\theta = \theta_2 - \theta_1$) at regular intervals during a given period of heat-run test and from the graph thus obtained, the maximum temperature rise is extrapolated since when $\frac{d\theta}{dt} = 0$, θ is maximum. In the other method, first suggested by Cotton (1932), only the initial portion of a time vs. temperature-rise curve is utilised. The initial slope of this curve is first noted and then a point over it is found at which the value of the slope is half that of the initial. The final temperature rise of the machine under test is therefore twice the temperature rise corresponding to this point as shown below.

Let θ be the temperature-rise at any instant, t , during a heat-run test.

Then we have $\theta = \theta_m \left(1 - e^{-\frac{t}{\tau}} \right)$

where θ_m is the maximum temperature rise and τ is the time constant. The slope of the curve for any value of θ is therefore given by

$$\begin{aligned} \left(\frac{d\theta}{dt} \right)_{\theta} &= \frac{1}{\tau} \theta_m \cdot e^{-\frac{t}{\tau}} \\ &= \frac{1}{\tau} (\theta_m - \theta) \end{aligned}$$

so that when $\theta = 0$,

$$\left(\frac{d\theta}{dt} \right)_0 = \frac{1}{\tau} \theta_m$$

Now if the initial slope is n times the slope at any point on the curve,

then at that point $\left(\frac{d\theta}{dt} \right)_{\theta} = \frac{1}{n} \left(\frac{d\theta}{dt} \right)_0 = \frac{1}{n} \cdot \frac{\theta_m}{\tau}$

$$\text{or } \frac{1}{\tau} (\theta_m - \theta) = \frac{1}{n} \cdot \frac{\theta_m}{\tau}$$

so that

$$\theta_m = \frac{n}{n-1} \cdot \theta$$

Hence when $n=2$, we have $\theta_m = 2\theta$. In other words, the final temperature rise θ_m is twice the temperature rise, θ , corresponding to the point at which the slope is half the initial slope of the time vs. temperature-rise curve.

Incidentally it may be noted here that the above two graphical methods have not yet been sufficiently tried in practice to ascertain the degree of accuracy with which the final temperature-rise of a machine in a heat-run test can be estimated by them.

EXPERIMENTAL

With a view to comparing the results obtained by the different methods of heat-run tests, including the direct loading method, a fairly small single-phase transformer manufactured by Messrs International G.E.C. and having the following specifications was chosen.

Type	AN
Output	2 KVA
Primary voltage	220 Volts
Secondary voltage	65 Volts
Frequency	50 c/s

The measuring instruments and the mercury-in-glass thermometers were all calibrated and checked from time to time during the investigation in comparison to the standards of the laboratory.

To carry out the heat-run test on the transformer by the direct loading method, the connections were made as shown in Fig. 1. The primary was connected across a 230 V. a.c. supply of 50 c/s in series with a suitable rheostat so that the primary voltage could be maintained constant at 220 V. when the transformer was loaded on the secondary to the rated value. Under the full load condition, the primary current was about 9.1 A and this value was maintained throughout the test.

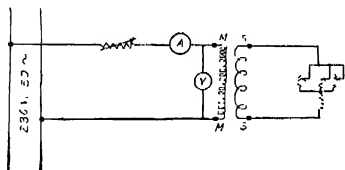


FIG. 1

Heat-run test by direct loading method.

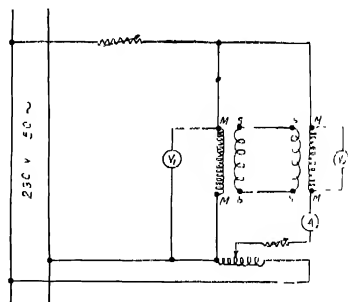


FIG. 2

Heat-run test by Sumpner test.

For the Sumpner test an identical auxiliary transformer was connected in opposition to the test transformer as shown in Fig 2. In actual practice the two primaries were first connected to the 230 V. a.c. mains of 50 c/s in series with a suitable rheostat so as to keep the applied voltage across their terminals constant at 220 volts. Thus the power was supplied to the primaries to overcome only the total core loss in the two transformers. Then one junction of the two primaries was opened and a suitable voltage injected between the two ends forming the junction in order to send the full load current (9.1 A) through them. The two secondaries carried also the full load current by transformer action and therefore gave rise to full load copper

loss in both the transformers. It is thus evident that the transformer under test would develop maximum heating because of the presence of its full load losses although it is not directly loaded.

Before carrying out the remaining heat-run tests the full load losses of the experimental transformer were determined in the usual way and it was found that the value of the copper loss was nearly double that of the core loss.

For the equivalent short-circuit run, a low voltage was applied to the primary of the test transformer with its secondary short-circuited and the applied voltage adjusted until the power input (in watts) into the transformer was equal to its total normal full load losses. The electrical connections are shown in Fig. 3.

The equivalent open-circuit run on the test transformer was carried out by applying a high voltage to the primary, keeping the secondary open as shown in Fig. 4, and adjusting the applied primary voltage until the input watts were equal to the total normal full load losses.

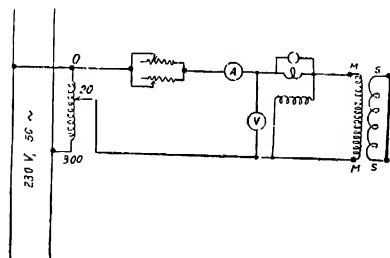


FIG. 3
Heat-run test by equivalent short-circuit run.

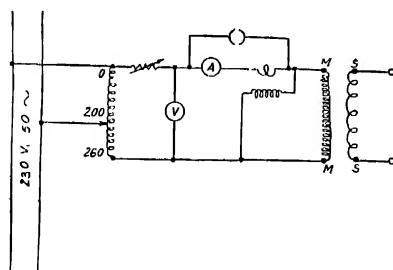


FIG. 4
Heat-run test by equivalent open circuit run.

For carrying out the alternate open-circuit and short-circuit heat-run, the transformer was connected as shown in Fig. 5. To begin with, a suitable voltage higher than the rated value was applied to the primary of the transformer with its secondary open, and this voltage was gradually increased

till the value of the core loss was equal to that of the total full load losses as previously determined. The transformer was run under this condition for 10 minutes. The primary was switched on to a low voltage source, with the secondary short-circuited, and this applied low voltage was adjusted till the copper loss was equal in value to that of the total full load losses. Under this condition the transformer was run for 20 minutes. This cycle was repeated till a steady hot temperature of the test transformer was reached. It may be noted that the period of each run was so chosen that the ratio of the two periods of the two heat-runs was equal to that of the core loss and

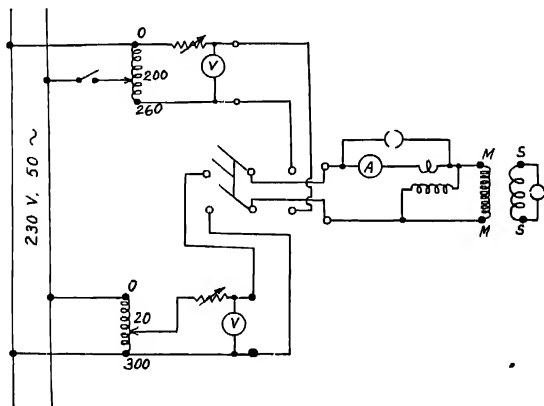


FIG. 5
Heat-run by alternate open-circuit
and short-circuit run

the copper loss of the test transformer. It has been shown by previous workers (McConahey and Fortescue, 1913, Madden, 1913) that if the length of the total period of the cycle is not too great, preferably not greater than 30 minutes, then this method gives results closely approximating those obtained by other methods.

It may be noted here that all the above tests were made under approximately still-air conditions. In each case the temperature of the transformer under test was measured with a mercury-in-glass thermometer (1 small div. = 0.1°C), suitably placed in contact with its upper primary winding. The reading of the thermometer was noted at an interval of 15 minutes for the first two hours and then at an interval of 1 hour till the hot temperature was found to be steady in all but the alternate open-circuit and short-circuit heat-run test. In the latter case the thermometer was, however, read at the middle of each short-circuit run. The temperature of the surrounding atmosphere during each test was also observed along with the hot temperature in order to note fluctuation or variation, if any, in the initial ambient

temperature of the test transformer. This was done by noting the reading of a similar thermometer inserted inside an identical transformer placed at the same level above ground but at a suitable distance from the test transformer (Johannasen and Wade, 1913). The resistance of the primary winding of the latter was measured before beginning each test and also at the hot temperature when it was steady. The readings obtained in all these tests are given in Tables I and II. Table III contains the data of temperature rise as estimated by each of the four methods described in a previous section for the different methods of heat-run test.

TABLE I

Test	Direct Loading.			Sumpner test.			Equivalent short-circuit run			Equivalent open-circuit run.		
	Temperature.		Resistance of primary winding.	Temperature.		Resistance of primary winding.	Temperature.		Resistance of primary winding.	Temperature.		Resistance of primary winding.
	Hot	Cold		Hot	Cold		Hot	Cold		Hot	Cold	
Time	in °C	in °C	in ohm.	in °C	in °C	in ohm	in °C	in °C	in ohm	in °C	in °C	in ohm
0.0	31.40	31.40	0.376	33.30	33.30	0.379	31.40	31.40	0.376	33.10	33.10	0.378
0.15	37.80	31.40		43.50	33.30		43.00	31.40		39.00	33.10	
0.30	44.70	31.40		51.60	33.30		53.50	31.40		43.40	33.10	
0.45	50.20	31.30		57.70	33.30		60.80	31.40		47.00	33.10	
1.0	54.40	31.00		62.60	33.30		66.40	31.40		50.30	33.10	
1.15	58.50	31.00		67.40	33.30		70.70	31.40		52.70	33.10	
1.30	61.90	31.00		71.00	33.40		71.00	31.50		55.20	33.20	
1.45	64.00	31.10		73.90	33.40		76.3	31.50		57.30	33.20	
2.0	67.50	31.20		76.20	33.40		78.10	31.55		59.10	33.25	
3.0	74.50	31.30		82.70	33.50		83.20	31.65		64.10	33.35	
4.0	78.00	31.40		86.40	33.50		85.50	31.70		66.80	33.40	
5.0	80.90	31.50		88.70	33.50		87.10	31.80		67.60	33.40	
6.0	81.90	31.60		89.70	33.50		88.25	31.90		67.90	33.40	
7.0	82.70	31.65		90.70	33.50		88.80	32.00		67.90	33.40	0.449
8.0	82.80	31.65		90.70	33.50	0.466	89.00	32.00	
9.0	82.80	31.65	0.451		89.00	32.00	0.473	

TABLE II

Test		Alternate open-circuit & short-circuit run		
Time		Temperature in °C		Resistance of Primary winding in ohm.
Hour.	Min	Hot	Cold.	
0	0	32.20	32.20	0.371
0	20	47.40	32.20	
0	50	59.10	32.25	
1	20	65.70	32.25	
1	50	70.70	32.45	
2	20	73.30	32.45	
2	50	74.50	32.50	
3	20	76.00	32.55	
3	50	77.40	32.60	
4	20	78.70	32.65	
4	50	79.60	32.75	
5	20	80.30	32.75	
5	50	80.50	32.75	
6	20	80.50	32.75	0.455

TABLE III

Methods of heat-run tests			Temperature rise in °C			
1			2	3	4	5
Direct loading	51.15	53.00	54.60	52.00
Sumpner test	57.50	61.60	52.70	060 C
Equivalent short-circuit run	...		57.00	68.80	52.60	58.00
Equivalent open-circuit run	...		34.50	45.30	34.90	38.00
Alternate open circuit & Short-circuit run			47.75	55.20	.	48.00

DISCUSSIONS

According to specifications of the standardising bodies of different countries, the temperature rise of an AN type of transformer with class A insulation and running continuously under full load conditions must not exceed 50°C when measured directly by a thermometer in contact with its windings or 55°C when estimated from a measurement of their hot resistances. It is evident from columns 2 and 3 of Table III that the direct loading method of heat-run test gives the best result as one would expect. Amongst the indirect methods, the Sumpner test as well as the equivalent short-circuit run give too high values while the equivalent open-circuit run gives too low values. But the temperature rise as estimated from the alternate open-circuit and short-circuit run is very close to that obtained by the direct loading method, the agreement specially between the results obtained by the measurement of the hot-resistance of the winding being remarkable. This leads one to suggest that the alternate open-circuit and short-circuit run may be employed for determining the temperature rise in a transformer where it is uneconomical or where facilities are wanting to carry out the direct loading method.

It is further interesting to note that the value of the temperature rise as estimated by either of the two graphical methods from data obtained by the direct load heat-run test is also in good agreement with that directly

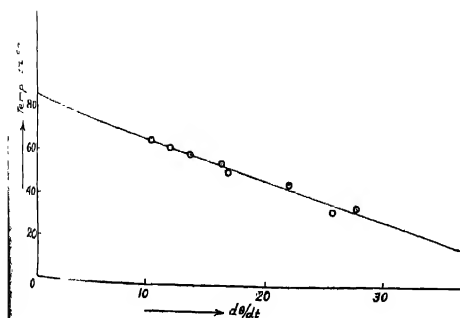


FIG. 6
First graphical method of determining
maximum temperature rise.

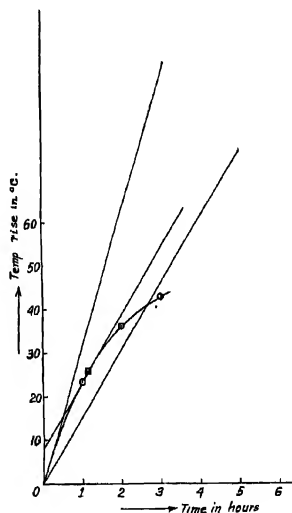


FIG. 7
Second graphical method of estimating
maximum temperature rise.

measured by the thermometer or calculated from the hot-resistance of the windings of the transformer. From this one may infer that any of the two graphical methods may be adopted to form a fair idea of the actual temperature rise of the transformer under test when it is not possible to carry through the heat-run test for several hours.

Incidentally it may be noted also from Table III that the temperature rise as estimated by the first graphical method (column 4) from the Sumpner test as well as from the equivalent short-circuit run agrees very closely with that obtained by direct load heat-run test. Another interesting point is the very close agreement between the values of temperature rise as measured directly by the thermometer and as estimated graphically by Cotton's method in the case of alternate open-circuit and short-circuit heat-run test. But these agreements may be quite accidental. It is therefore desirable to obtain more data on other machines for the confirmation of these observations. It may be noted that such observations are likely to help the designers of electrical machines in as much as a graphical method of estimating very closely the actual temperature rise from the data of an indirect heat-run test will avoid much wastage of energy otherwise involved in a direct load test.

ACKNOWLEDGMENTS

The author desires to express his heartfelt thanks to Prof. P. C. Mahanti, Head of the department and to Dr. A. K. Sengupta, Lecturer-in-charge of the Electrical Machine Laboratory for their helpful discussions and encouragements during the course of the investigation and to Sri P. Sen, Lecturer-in-charge of the Standardisation Laboratory for his valuable help in calibrating the measuring instruments.

ELECTRICAL MACHINE LABORATORY,
APPLIED PHYSICS DEPARTMENT,
UNIVERSITY COLLEGE OF SCIENCE & TECHNOLOGY,
CALCUTTA

REFERENCES

- Johannasen, S. E. and Wade, G. W., 1913, *Proc. A.I.E.E.*, **32**, 255
Madden, J. J. K., 1913, *Proc. A.I.E.E.*, **32**, 325
McConahey, W. M. and Fortescue, C., 1913, *Proc. A.I.E.E.*, **32**, 507.
Stigant, S. A. and Lacey, H. M., 1941 *The J. & P. Transformer Book.*

A n n o u n c e m e n t

INTERNATIONAL UNION OF CRYSTALLOGRAPHY

The Second General Assembly and International Congress of the International Union of Crystallography will be held in Stockholm from the 27th June to the 3rd July, 1951. Delegates to the General Assembly will be nominated by the National Committees. Crystallographers throughout the world are, however, cordially invited to attend the International Congress. Those who hope to attend are requested to complete Form A which is to be obtained from the Secretary to the Government of India, Department of Scientific Research, North Block, Central Secretariat, New Delhi, and to return it to the General Secretary of the Union, R. C. Evans, Crystallographic Laboratory, Cavendish Laboratory, Cambridge, England. (Telegraphic Address—Crystals, Cambridge, England).

TOMORROW'S INSTRUMENTS TODAY

RAJ-DER-KAR & CO.

COMMISSARIAT BUILDING

HORNBY ROAD

FORT

BOMBAY

OFFERS

FROM STOCK

GLASS METAL DIFFUSION PUMPS, METAL BOOSTER
PUMPS, OILS AMOILS OCTOILS OCTOIL,
BUTYL SABACATE

MANUFACTURED

By

DISTILLATION PRODUCTS
(U. S. A.)

SPENCER MICROSCOPE

CENCO HIGHVACS

BESLER EPIDIASCOPE

COMPLETE WITH FILM STRIP ARRANGEMENTS

Telephone 27304

2 Lines

TelegramS
TECHLAB

The following special publications of the Indian Association for the Cultivation of Science, 210, Bowbazar Street, Calcutta, are available at the prices shown against each of them :—

Subject	Author	Price Rs. A. P.
Methods in Scientific Research	Sir E. J. Russell	0 6 0
The Origin of the Planets	Sir James H. Jeans	0 6 0
Separation of Isotopes	Prof. F. W. Aston	0 6 0
Quanta and their Role in Nature	Sir Lewis L. Fermor	2 8 0
(1) The Royal Botanic Gardens, Kew.	Sir Arthur Hill	1 8 0
(2) Studies in the Germination of Seeds.		
Interatomic Forces	Prof. J. E. Lennard-Jones	1 8 0
The Educational Aims and Practices of the California Institute of Technology.	R. A. Millikan	0 6 0
Active Nitrogen A New Theory.	Prof. S. K. Mitra	2 8 0
Theory of Valency and the Struc- ture of Chemical Compounds.	Prof. P. Ray	3 0 0
Petroleum Resources of India	D. N. Wadia	2 8 0
The Role of the Electrical Double layer in the Electro Chemistry of Colloids.	J. N. Mukherjee	2 12 0

A discount of 25% is allowed to Booksellers and Agents.

RATES OF ADVERTISEMENTS

Third page of cover	Rs. 32, full page
do. do.	„ 20, half page
do. do.	„ 12, quarter page
Other pages	„ 25, full page
do.	„ 16, half page
do.	„ 10, quarter page

15% Commissions are allowed to *bonafide* publicity agents securing orders for advertisements.

CONTENTS

	PAGE
20. Application of Stokes' Law to Estimate the Solvation of Ions in a Solution By—H. Mukherjee 	137
21. Electrical Constants of Sand at Ultra High Frequencies—By S. K. Chatterjee	143
22. The Raman Spectra of Trichloro-ethylene and Tetrachloro-ethylene in the Solid State—By S. B. Sanyal 	151
23. Thermodynamics of an Oscillator Assembly—By R. P. Singh 	155
24. Absorption of U. H. F. Radio-waves in some Substituted Benzene compounds —By S. N. Sen 	163
25. A Comparative Study of the Different Methodes of Heat-run Tests on Electrical Machines. 1. Single Phase Transformers—By H. K. Basu 	171

PRINTED BY SIBENDRANATH KANJILAL, SUPERINTENDENT (OFFG.), CALCUTTA UNIVERSITY
 PRESS, 48, HAZRA ROAD, BALLYGUNGE, CALCUTTA AND PUBLISHED BY THE
 REGISTRAR, INDIAN ASSOCIATION FOR THE CULTIVATION OF SCIENCE,
 210, Bowbazar Street, Calcutta,

Vol. 24 INDIAN JOURNAL OF PHYSICS

No. 5

(Published in collaboration with the Indian Physical Society)

AND

Vol. 33

PROCEEDINGS

No. 5

OF THE

**INDIAN ASSOCIATION FOR THE
CULTIVATION OF SCIENCE**

MAY, 1950

PUBLISHED BY THE

INDIAN ASSOCIATION FOR THE CULTIVATION OF SCIENCE

210, Bowbazar Street, Calcutta

BOARD OF EDITORS

K. BANERJEE	S. K. MITRA
D. M. BOSE	P. RAY
S. N. BOSE	M. N. SAHA
D. S. KOTHARI	S. C. SIKHAR.

Secretary

EDITORIAL COLLABORATORS

DR. R. K. ASUNDI, M.A., PH.D.
PROF. H. J. BHABHA, PH.D., F.R.S.
DR. P. K. KICHLU, D.Sc.
PROF. K. S. KRISHNAN, D.Sc., F.R.S.
PROF. G. P. DUBEY, M.Sc.
DR. K. RANGADHAMA RAO, M.A., D.Sc.
DR. N. D. SARWATKEY, D.Sc.
DR. N. N. DASGUPTA, M.Sc., PH D.
PROF. N. R. SEN, D.Sc., F.N.I.
PROF. P. C. MAHANTI, D Sc., F.N.I.
PROF. S. R. PALIT, D Sc.,
DR. H. RAKSHIT, D.Sc.,
PROF. K. R. DIXIT, PH.D.
DR. VIKRAM A. SARABHAI, M.A., PH.D.

ASSISTANT EDITOR

MR. A. N. BANERJEE, M.Sc.

NOTICE

TO INTENDING AUTHORS

Manuscripts for publication should be sent to Mr. A. N. Banerjee, Asst Editor, 210, Bowbazar Street, Calcutta.

The manuscript of each paper should contain in the beginning a short abstract of the paper.

All references to published papers should be given in the text by quoting the surname of the authors followed by the year of publication within braces, e.g., Sen (1942). The actual references should be given in a list at the end of the according to the following specimen :

Sen, B. K., 1942, *Ind. J. Phys.*, 16, 339

The references should be arranged alphabetically in the list.

All diagrams should be drawn on thin white paper in Indian ink, and letters and numbers in the diagrams should be written in pencil.

Annual Subscription—

— Inland Rs. 20
Foreign £ 2

A NOTE ON WEYL'S INEQUALITY.*

By V. S. NANDA

(Received for publication, March 3, 1950)

ABSTRACT. In this paper Weyl's Inequality, is deduced from the commutation relation satisfied by the co-ordinates and their conjugate momenta

The present note gives an elementary proof of Weyl's Inequality which is used by Thomas (1942) in his theory of contact transformations. His object is to solve the problem of the anharmonic oscillator by the successive removal of terms from the Hamiltonian. In practice, it is very difficult to deal with polynomials of the fourth or higher degree in a co-ordinate and its conjugate momentum. This is however, facilitated by the use of Weyl's method (1927) which transforms the non-commutative algebra of operators to the ordinary one. In the actual application of the above procedure to the solution of quantum mechanical problems, Weyl's Inequality is a result of fundamental importance. It is shown here how this relation can be obtained from the commutation relation satisfied by a co-ordinate q and its conjugate momentum p instead of having recourse to group theory.

Weyl's Inequality is expressed by the relation,

$$e^{\alpha p + \beta q} \equiv e^{\alpha p} e^{\beta q} e^{i\hbar \alpha \beta / 2} \equiv e^{\beta q} e^{\alpha p} e^{-i\hbar \alpha \beta / 2} \quad (1)$$

or by its corollary,

$$\begin{aligned} e^{\alpha p + \beta q} e^{\gamma p + \delta q} &\equiv e^{(\alpha + \gamma)p} e^{(\beta + \delta)q} e^{i\hbar(\gamma\beta + \gamma\delta + 2\beta\gamma)} \\ &\equiv e^{(\alpha + \gamma)p + (\beta + \delta)q} e^{i\hbar(\beta\gamma - \alpha\delta)/2} \quad \dots \quad (2) \end{aligned}$$

where α, β, γ and δ are ordinary numbers while q, p satisfy the commutation relation,

$$qp - pq = i\hbar \quad \dots \quad (3)$$

Starting from this basic relation we shall first establish the second part of (2). The following relations can be easily deduced from (3) :

$$c\beta q p - p c\beta q = i\hbar \beta e^{\beta q} \quad \dots \quad (4a)$$

$$q e^{\alpha p} - e^{\alpha p} q = i\hbar \alpha e^{\alpha p} \quad \dots \quad (4b)$$

$$q e^{\alpha p + \beta q} - e^{\alpha p + \beta q} q = i\hbar \alpha e^{\alpha p + \beta q} \quad \dots \quad (4c)$$

$$e^{\alpha p + \beta q} p - e^{\alpha p + \beta q} p = i\hbar \beta e^{\alpha p + \beta q} \quad \dots \quad (4d)$$

It is easily noticed that the relations (4a) and (4b) are dissimilar in the respect that roles of p and q have been interchanged. This also holds for

* Communicated by Dr. F. C. Anluck.

(4c) and (4d). We shall prove the first and the third of these relations. An independent proof for the other two is unnecessary as these can be established in a similar manner.

We multiply both sides of the relation

$$\begin{aligned} p(\beta q) &= [(\beta p)p - i\hbar\beta], \text{ by } (\beta q/2) \text{ on the right. We get} \\ p(\beta q)^2/2! &= [(\beta q)p - i\hbar\beta](\beta q/2!) \\ &= \left[\frac{(\beta q)^2}{2!} p - i\hbar\beta(\beta q) \right] \end{aligned}$$

Similarly, multiplying now by $(\beta q/3)$ on the right,

$$p(\beta q)^3/3! = \left[\frac{(\beta q)^3}{3!} p - i\hbar\beta \frac{(\beta q)^2}{2!} \right]$$

We assume the result for the index m , that is, we take

$$p \frac{(\beta q)^m}{m!} = \frac{(\beta q)^m}{m!} p - i\hbar\beta \frac{(\beta q)^{m-1}}{(m-1)!} \quad (5)$$

Multiplying on the right with $(\beta q)/(m+1)$, we get

$$\begin{aligned} p \frac{(\beta q)^{m+1}}{(m+1)!} &= \frac{(\beta q)^m}{(m+1)!} (\beta q p - i\hbar\beta) - i\hbar\beta \frac{(\beta q)^m}{(m-1)!(m+1)!} \\ &= \frac{(\beta q)^{m+1}}{(m+1)!} p - i\hbar\beta \frac{(\beta q)^m}{m!}, \end{aligned}$$

which is the same as (5) if m is changed into $(m+1)$. Hence by induction it follows that equation (5) holds for all positive integral values of m . Taking the sum from zero to infinity for equation (6), we at once get,

$$p e^{\beta q} = e^{\beta q} p - i\hbar\beta e^{\beta q}$$

and

$$p e^{-\beta q} = e^{-\beta q} p + i\hbar\beta e^{-\beta q}.$$

Relation (4c) will now be proved on the same lines. Since

$$q(\alpha p + \beta q) = (\alpha p + \beta q)q + i\alpha\hbar$$

we have

$$\begin{aligned} q \frac{(\alpha p + \beta q)^2}{2!} &= \frac{(\alpha p + \beta q)}{2!} \left\{ q(\alpha p + \beta q) + i\alpha\hbar \right\} \\ &= \frac{(\alpha p + \beta q)^2}{2!} + i\alpha\hbar(\alpha p + \beta q). \end{aligned}$$

we assume the relation

$$q \frac{(\alpha p + \beta q)^m}{m!} = \frac{(\alpha p + \beta q)^m}{m!} q + i\alpha\hbar \frac{(\alpha p + \beta q)^{m-1}}{(m-1)!} \quad (6)$$

and multiply with $\left(\frac{\alpha p + \beta q}{m+1} \right)$ on the right. We obtain

$$\begin{aligned}\frac{q(\alpha p + \beta q)^{m+1}}{(m+1)!} &= \frac{(\alpha p + \beta q)^m}{(m+1)!} \left\{ (\alpha p + \beta q)q + i\hbar \right\} + \frac{i\hbar(\alpha p + \beta q)^m}{(m+1)(m-1)!} \\ &= \frac{(\alpha p + \beta q)^{m+1}}{(m+1)!} q + i\hbar \frac{(\alpha p + \beta q)^m}{m!}.\end{aligned}$$

This is of the same form as (6) except that $(m+1)$ now replaces m . Thus by induction (6) holds for all positive integral values of m including zero. Taking the sum for all these values, we get

$$qe^{\alpha p + \beta q} = e^{\alpha p + \beta q} q + i\hbar e^{\alpha p + \beta q},$$

which is (4c).

To prove Weyl's Inequality, we write (4a) in the form

$$e^{\beta q}(\alpha p) = (\alpha p + i\hbar\alpha\beta)e^{\beta q},$$

and therefore

$$\begin{aligned}e^{\beta q}(\alpha p)^2/2! &= \{(\alpha p + i\hbar\alpha\beta)e^{\beta q}\}(\alpha p)/2! \\ &= \{(\alpha p + i\hbar\alpha\beta)^2/2!\}e^{\beta q}.\end{aligned}$$

Assuming as before the relation

$$e^{\beta q}(\alpha p)^m/m! = (\alpha p + i\hbar\alpha\beta)^m e^{\beta q}/m!, \quad (7)$$

We multiply on the right by $\alpha p/(m+1)$, and get,

$$\begin{aligned}e^{\beta q} \frac{(\alpha p)^{m+1}}{(m+1)!} &= \frac{(\alpha p + i\hbar\alpha\beta)^m}{m!} e^{\beta q} \frac{(\alpha p)}{(m+1)} \\ &= \frac{(\alpha p + i\hbar\alpha\beta)^{m+1}}{(m+1)!} e^{\beta q}.\end{aligned}$$

Thus by induction (7) holds for all m . Summing up for all powers from 0 to ∞ we have,

$$e^{\beta q} e^{\alpha p} = e^{\alpha p + i\hbar\alpha\beta} e^{\beta q} \quad (8)$$

or

$$e^{\beta q} e^{\alpha p} e^{-i\hbar\alpha\beta/2} = e^{\alpha p} e^{\beta q} e^{i\hbar\alpha\beta/2},$$

which proves the second part of (1). Replacing α by $(-\alpha)$ and β by $(-\beta)$, we can write the above relation in the form

$$e^{-\beta q} e^{-\alpha p} = e^{-\alpha p + i\hbar\alpha\beta} e^{-\beta q} \quad (9)$$

Now if we start with (4c) we can derive the following relations by the same procedure as followed so far :

$$e^{\alpha p + \beta q} e^{-\alpha p} = e^{-(\alpha p + i\hbar\alpha\beta)} e^{\alpha p + \beta q} \quad \dots \quad (10)$$

$$e^{\alpha p + \beta q} e^{-\beta q} = e^{-(\beta q - i\hbar\alpha\beta)} e^{\alpha p + \beta q} \quad \dots \quad (11)$$

Multiplying on the left of (10) with $e^{-\beta q}$, we get,

$$\begin{aligned}e^{-\beta q} e^{\alpha p + \beta q} e^{-\alpha p} &= e^{-\beta q} e^{-\alpha p} e^{\alpha p + \beta q} e^{-(i\hbar\alpha\beta)} \\ &= e^{-\alpha p} e^{\alpha p + \beta q} e^{-\beta q} e^{-(i\hbar\alpha\beta)}\end{aligned}$$

and therefore

$$A \equiv e^{-\beta q} e^{\alpha p + \beta q} e^{-\alpha p} e^{i\hbar\alpha\beta/2} \quad B \equiv e^{-\alpha p} e^{\alpha p + \beta q} e^{-\beta q} e^{-i\hbar\alpha\beta/2},$$

where the nature of A is to be determined. If it can be shown that A is a pure number and equal to unity, Weyl's relation will be fully established. From the equation (12) we get

$$\begin{aligned} Ap &= \{ e^{-\beta q} e^{\alpha p + \beta q} e^{-\alpha p} \} e^{i\hbar\alpha\beta/2} \\ &= \{ e^{-\beta q} (p + i\hbar\beta) e^{\alpha p + \beta q} e^{-\alpha p} \} e^{i\hbar\alpha\beta/2} \\ &= \{ (p - i\hbar\beta) e^{-\beta q} e^{\alpha p + \beta q} e^{-\alpha q} \\ &\quad + i\hbar\beta e^{-\beta q} e^{\alpha p + \beta q} e^{-\alpha p} \} e^{i\hbar\alpha\beta/2} \\ &= p e^{-\beta q} e^{\alpha p + \beta q} e^{-\alpha p} \quad \text{from (5a)} \\ &= p.1. \end{aligned}$$

This shows that p commutes with A . Similarly it can be shown that q commutes with A . Therefore A must be a pure number, and evidently a real number because it is equal to its complex conjugate. Replacing $(-\alpha)$ by $(+\alpha)$ and $(-\beta)$ by (β) , equation (12) can be written as

$$e^{\beta q} e^{-(\alpha p + \beta q)} e^{\alpha p} e^{i\hbar\alpha\beta/2} = A$$

Multiplying this with the second part of (12), we get

$$A^2 = 1.$$

Therefore,

$$A = \pm 1.$$

The negative value of A is obviously untenable as it does not hold for the case $\alpha = \beta = 0$.

In order to verify the corollary we have merely to make use of (1) in

$$\begin{aligned} e^{\alpha p + \beta q} e^{\gamma p + \delta q} &= \{ e^{\alpha p} e^{\beta q} e^{i\hbar\alpha\beta/2} \} \{ e^{\delta q} e^{\gamma p} e^{-i\hbar\gamma\delta/2} \} \\ &= \{ e^{\alpha p} e^{(\beta + \delta)q} e^{\gamma p} \} e^{i\hbar(\alpha\beta + \gamma\delta)/2} \\ &= e^{(\alpha + \gamma)p} e^{(\beta + \delta)q} e^{i\hbar(\alpha\beta + \gamma\delta + 2\beta\gamma)/2} \end{aligned}$$

Combining the exponentials by the help of equation (1) we get

$$\begin{aligned} &e^{(\alpha + \gamma)p} e^{(\beta + \delta)q} e^{i\hbar(\alpha\beta + \gamma\delta + 2\beta\gamma)/2} \\ &= e^{(\alpha + \gamma)p + (\beta + \delta)q} e^{i\hbar(\beta\gamma - \alpha\delta)/2} \end{aligned}$$

which proves the corollary.

ACKNOWLEDGMENTS

It is a pleasure to thank Professor D. S. Kothari and Dr. F. C. Auluck for their kind interest in this work.

DELHI UNIVERSITY
DELHI

REFERENCES

- Thomas, L. H., 1942, *J. Chem. Phys.*, **10**, 539.
Weyl, H., 1927, *Zeits. f. Physik.*, **48**, 1.

MULTIPLY SEPARATION FACTORS AND Γ -SUM RULE

By S. SINGUPTA

(Received for publication, January, 5, 1950.)

ABSTRACT: Weak field Γ -sum rule has been used to give a general proof of the inversion of X-ray doublets and to calculate the multiplet separation factors in a simple way.

Goudsmit (1928) calculated the multiplet separation factors for equivalent electron configurations with the help of strong field Γ -sum rule and Γ -permanence rule. He applied the same method to prove the inversion of the X-ray doublets. Recently Rao (1948) has followed the same method to calculate the separation factors in f^2 configuration. In all these cases the calculations involve, preparation of big tables for the allowed values of m_l and m_s of the individual electrons, consistent with Pauli's exclusion principle, and then to calculate the individual γ -values of the electrons and their sums for the same value of M . The calculations are necessarily cumbersome.

Striking simplification can, however, be made if instead of using strong field Γ -sum rule and Γ -permanence rule, we use weak field Γ -sum rule and Lande interval rule. The weak field Γ -sum rule states that the sum of the Γ -values for terms of the same J -value, arising out of any configuration is independent of coupling. Since in jj -coupling the Γ -values of the terms depend on the γ -values of single electrons (which are of course well known), the Γ -sums in this case can be easily determined. From the weak field Γ -sum rule we know that these sums will be true even in the LS -coupling. Then the multiplet separation factors can be easily calculated since the term intervals satisfy Lande interval rule. In all these calculations it will be necessary to know the kind of terms arising out of any equivalent electron configuration in the jj -coupling. These have been calculated by Pauling and Goudsmit (1930). However, they give terms only for p and d electrons. In the following table we give the resultant J -values allowed by exclusion principle, for different numbers of electrons having identical quantum numbers n , l and j . From these the allowed terms for any equivalent electron configuration in the jj -coupling can be easily calculated.

If we want to calculate the allowed states for say d^3 configuration, then we proceed as follows. In this case individual j values of the electrons are $j_1 = 5/2$ and $j_2 = 3/2$. If all the three electrons have their $j = 5/2$, then from the table we get the resultant $J = 9/2, 5/2, 3/2$. This we represent by writing $(3)19/2, 5/2, 3/2$. If two electrons have $j = 5/2$ and one $j = 3/2$ then the resultant J 's are obtained by adding each of the angular momenta 4, 2, 0 (which are

the allowed resultant J for two $5/2$ electrons) with $3/2$ and taking all possible values resulting from the addition. This we represent by writing $(2j_1j_2)_{(4,2,0)(3/2)}$. Proceeding in this way we get all the states which are,

$$(3j_1)_{0/2, 5/2, 3/2}; (2j_1j_2)_{(4, 2, 0)(3/2)}; (j_12j_2)_{(5/2)(2, 0)}; (3j_2)_{3/2}$$

We shall illustrate the calculation of the separation factors by calculating the same for f^2 configuration. But before that we shall consider the inversion of the X-ray doublets.

TABLE I

j -value of the individual electrons.	Number of the electrons.	Allowed values of the resultant J .
$1/2$	1	$1/2$
$3/2$	2	0
	1 or 3	$3/2$
	2	2, 0
	4	0
$5/2$	1 or 5	$5/2$
	2 or 4	4, 2, 0
	3	$9/2, 5/2, 3/2$
	6	0
$7/2$	1 or 7	$7/2$
	2 or 6	6, 4, 2, 0
	3 or 5	$15/2, 11/2, 9/2, 7/2, 5/2, 3/2$
	4	8, 6, 5, 4, 4, 2, 2, 0
	8	0

Inversion of X-ray doublets.

Following Goudsmit's method, Compton and Allison (1935) showed the inversion of the X-ray doublets for the special case of p^2 configuration. In the following with the help of weak field Γ -sum rule, we give a very general proof which is applicable for any value of l .

For the nl shell the maximum number of electrons is $4l+2$ (from Pauli's principle). Let us consider the nl^{4l+1} configuration. The allowed terms in the LS-coupling are $^2l_{l+\frac{1}{2}}$ and $^2l_{l-\frac{1}{2}}$. The allowed terms in the jj -coupling are to be calculated. The j values of the individual electrons are $j_1=l+\frac{1}{2}$ and $j_2=l-\frac{1}{2}$. The maximum number of electrons that can have their $j=j_1$ is $2j_1+1=2l+2$. The maximum number of electrons with $j=j_2$ is $2j_2+1=2l$. Thus for nl^{4l+1} configuration, the allowed terms are

$$(2l+2)j_1(2l-1)j_2)_{l-\frac{1}{2}}; (2l+1)j_1(2l)j_2)_{l+\frac{1}{2}}$$

Now, for j_1 electrons the γ -value is $l\frac{b_1}{2}$ and for j_2 electrons it is $-(l+1)\frac{b_1}{2}$. If Γ_+ and Γ_- be the Γ -values of $^2l_{l+\frac{1}{2}}$ and $^2l_{l-\frac{1}{2}}$ terms in the nl^{4l+1} configuration then from the Γ -sum rule we get,

$$\Gamma_+ = (2l+1)l\frac{b_1}{2} - 2l(l+1)\frac{b_1}{2} = -l\frac{b_1}{2}$$

$$\Gamma_- = (2l+2)l\frac{b_1}{2} - (2l-1)(l+1)\frac{b_1}{2} = (l+1)\frac{b_1}{2}.$$

The corresponding Γ -values for doublets in the nl -configuration are

$$\Gamma_+ = l \frac{b_1}{2} \text{ and } \Gamma_- = -(l+1) \frac{b_1}{2}.$$

This shows that the X-ray doublets are inverted.

Separation factors for the multiplets in the f^2 -configuration.

In this case the terms in the LS -coupling are 1PFH 1SDGI . The corresponding terms in the jj -coupling can be easily determined with the help of the table given before. These are,

$$(2j_1)6, 4, 2, 0 \quad (j_1j_2)(7/2)(5/2) \quad (2j_2)4, 2, 0 \quad (1)$$

where $j_1 = 7/2$ and $j_2 = 5/2$. The corresponding γ -values are $3\frac{b}{2}$ and $-2b$ respectively. Let a_1 , a_2 and a_3 be the separation factors for the 3P , 3F and 3H multiplets. Then from Landé interval rule, the Γ -values of the terms are,

$$\begin{aligned} {}^1P_2 &= a_1 & {}^1P_1 &= -a_1 & {}^3P_0 &= -2a_1 \\ {}^3F_4 &= 3a_2 & {}^3F_3 &= -a_2 & {}^3F_2 &= -4a_2 \\ {}^3H_6 &= 5a_3 & {}^3H_5 &= -a_3 & {}^3H_4 &= -6a_3 \end{aligned} \quad (2)$$

For the singlets evidently the Γ 's are all zero. Comparing (2) with (1) and remembering Γ -sum rule, we get,

$$\begin{aligned} 5a_1 &= 2 \cdot \frac{3}{2}b + \frac{3}{2}b - 2b = \frac{5}{2}b \\ -6a_3 + 3a_2 &= 2 \cdot \frac{3}{2}b + \frac{3}{2}b - 2b - 4b = -\frac{3}{2}b \\ -4a_2 + a_1 &= 2 \cdot \frac{3}{2}b + \frac{3}{2}b - 2b - 4b = -\frac{3}{2}b \end{aligned} \quad (3)$$

Solving the above we get at once $a_1 = a_2 = a_3 = \frac{1}{2}b$. The same has recently been calculated by Rao (1948), by Goudsmit's method. Comparison will show the simplicity of the method we have used here.

It is evident from the above that the Γ -sum rule provides us with a number of equations (each for a particular value of J), connecting the separation factors of the multiplets. If the number of these equations is equal to or greater than the number of separation factors then only can the unknown factors be determined. The same limitation is also true for Goudsmit's method. It is for this reason that the above methods are not applicable in the case of f^3 or f^4 configurations. Rao, however, observes that Goudsmit's method can be extended to the above cases. But it may be easily shown that this is not possible.

ACKNOWLEDGMENTS

The author's thanks are due to Prof. K. C. Kar, D.Sc., of Presidency College, Calcutta for his kind encouragement during the progress of the work; and to the Government of West Bengal for awarding him a research scholarship which enabled him to carry on the work.

PHYSICAL LABORATORY
PRESIDENCY COLLEGE
CALCUTTA.

REFERENCES

- Compton and Allison, 1935, *X-rays in Theory and Experiment*.
Goudsmit, S. 1928, *Phys. Rev.* **31**, 946
Pauling and Goudsmit, 1930 *The Structure of Line Spectra*.
Rao, V. R., 1948 *Ind Jour Phys.* **22**, 423

ON THE RAMAN SPECTRA AND HEAT CAPACITY OF BENZENE AT LOW TEMPERATURES

By S. C. SIRKAR AND A. K. RAY

(Received for publication, March 31, 1930)

Plate VI

ABSTRACT The Raman spectra of solid benzene at -70°C , -100°C and -180°C have been investigated. At -180°C five new lines have been observed in the low frequency region at 47, 53, 78, 95 and 131 cm^{-1} respectively. It is observed that the lines 44, 60 and 100 cm^{-1} appearing at -70°C become more intense and shift to 53, 78 and 134 cm^{-1} respectively at -180°C and two more new lines appear at the latter temperature. The values of C_p calculated on the assumption that three frequencies, 58, 95 and 135 cm^{-1} contribute to the Einstein function at low temperatures between 4°K and 70°K are found to agree fairly well with the observed values. It is pointed out that if the line 35 cm^{-1} observed at about 0°C is taken to be that due to complete rotation of the molecule about an axis perpendicular to its plane, as has been done by Rousset (1944), the calculated values of C_p become many times higher than values observed for temperatures between 4°K and 25°K . It is concluded that at low temperatures virtual bonds are formed between adjacent molecules and oscillations in these groups produce the new Raman lines in the low frequency region.

INTRODUCTION

The Raman spectrum of benzene in the solid state was first studied by Gross and Vuks (1935) who discovered two new lines at 63 cm^{-1} and 108 cm^{-1} respectively. It was later reported by one of the authors (Sirkar, 1936) that at a temperature of -180°C benzene in the solid state yielded three new lines having frequency shifts 81 cm^{-1} , 98 cm^{-1} and 124 cm^{-1} respectively, instead of the two lines mentioned above. Sirkar and Gupta (1938) also calculated the specific heat of solid benzene at low temperatures along with that for a few other compounds and showed that the values of C_p calculated by taking into account Einstein functions corresponding to the new lines in the low-frequency region, besides the Debye function, agree with the observed values. Kastler and Fruhling (1944) recently studied the Raman spectrum of a single crystal of benzene at a temperature just below its freezing point and also studied the polarisation of the new lines in the low frequency region. They observed four new lines at 35 cm^{-1} , 55 cm^{-1} and 100 cm^{-1} and found that the line 35 cm^{-1} is totally polarised. They concluded from these results that the lines 55 cm^{-1} , 65 cm^{-1} were due to rotational oscillations of the benzene molecule, pivoted in the crystal lattice, about the b -axis and the line 100 cm^{-1} was probably due to similar oscillation of the molecule about an axis perpendicular to b -axis. Rousset

(1944) next calculated the specific heat of solid benzene at low temperatures taking into account the Einstein functions corresponding to these lines and taking the line 35 cm^{-1} to be due to complete rotation of the molecule about an axis perpendicular to its plane. He, however, overlooked the fact reported by Sirkar (1936) that the frequency-shifts of the new lines in the low frequency region observed in the case of solid benzene increase with the lowering of temperature.

As regards the hypothesis put forward to explain the origin of these lines by Kastler and Rousset (1941) and also independently by Bhagvantam (1941) it has been pointed out earlier by one of the authors (Ray, 1950) that it can be tested only by studying the changes which the new lines undergo in intensity and position with the lowering of temperature of the crystal. Further, in any attempt to calculate the specific heat of the crystal at very low temperatures the accurate values of the frequencies of the new lines at these temperatures should be used. It has already pointed out that in the line at 35 cm^{-1} was not observed by Sirkar (1936) in the case of benzene in the solid state at -180°C and this may be due to photographic spreading of the over-exposed Rayleigh line, as indicated by the microphotometric records reproduced by him. Thus accurate data regarding the frequency-shifts of all these new lines which may be observed in the case of solid benzene at very low temperatures were not known. It was, therefore, thought worthwhile to reinvestigate the Raman spectra of solid benzene at different temperatures going down up to about -180°C , using an improved technique, and to discuss the bearing of the results on the theories which have been put forward by previous workers to explain the origin of the new lines and also on the specific heat of solid benzene at low temperatures.

EXPERIMENTAL

Benzene used in the present investigation was obtained from U. S. A. and was of pure quality. It was distilled in vacuum before use. The arrangement used for studying the Raman spectra of solid benzene at different temperatures is the same as that described by Majumdar, (1949). Care was taken to solidify the liquid slowly in order to obtain a homogeneous mass so that the proportion of stray light due to diffuse reflection from the volume of the crystal was very small. The Fuess spectrograph used in the present investigation is more suitable than that used by one of the authors earlier (Sirkar, 1936), because it has a dispersion of about 10.8 \AA/mm and the line 4046 \AA is free from coma on the Stokes side, while in the case of the spectrograph used earlier the dispersion was slightly smaller. The Raman spectrum of solid benzene was photographed at three different temperatures, e. g., -10°C , -100°C and -180°C . These temperatures were produced in the region in which the sealed Pyrex tube containing the liquid was placed inside a transparent Dewar vessel by adjusting the level

of the liquid oxygen in this vessel. Iron arc spectrum was photographed in each spectrogram as comparison.

RESULTS AND DISCUSSION

The spectrograms are reproduced in Plate VI along with that for liquid benzene for comparison. As only the prominent lines appeared in the spectrograms due to solid benzene, no attempt was made to record the faint lines due to the liquid. The frequency-shifts of the prominent lines are given in Table I.

TABLE I
Benzene

Liquid at 30°C $\Delta\nu$ in cm^{-1}	Solid at -10°C $\Delta\nu$ in cm^{-1}	Solid at -100°C $\Delta\nu$ in cm^{-1}	Solid at -180°C $\Delta\nu$ in cm^{-1}
Continuous wing extending up to 110 cm^{-1}			47 (1) e, k , 53 (2) e, k 78 (5) e, k 95 (1b) e, k , 134 (3) e, k 603 (1) e, k 855 (2) e, k 989 (10) e, l, k , 1174 (4) e, k , 1581 (3) e, k , 1602 (2) e, k , 3042 (2) e, i, k 3046 (2) e, l, k 3063 (5) e, i, k
	44 (1) e, k 60 (1b) e, k 100 (1b) e, k 603 (1) e, k 850 (2) e, k 990 (10) e, l, k 1174 (3) e, k 1583 (3) e, k 1604 (2) e, k 3049 (3) e, l, k 3063 (5) e, i, k	48 (2) e, k 69 (6) e, k 116 (b) e, k 603 (1) e, k 852 (2) e, k 990 (5) e, l, k 1174 (4) e, k 1582 (2) e, k 1603 (1) e, k 3042 (2) e, l, k 3046 (2) e, l, k 3063 (5) e, i, k	

It can be seen from Table I that the remarkable change which takes place in the Raman spectrum of benzene with the solidification of the liquid is the appearance of the new lines in the low frequency region. At a temperature of about -10°C the crystal yields three new lines at 44, 60 and 100 cm^{-1} respectively. This fact seems to be in agreement with that observed by Kastler and Fruhling (1944); if it is assumed that the line at 60 cm^{-1} consists of a close doublet, and the line at 35 cm^{-1} observed by them, presumably at about 0°C , shifts to about 44 cm^{-1} at -10°C . When the crystal is cooled down to -100°C the three lines shift respectively to 48, 69 and 116 cm^{-1} . On further cooling the crystal up to -180°C , the lines

at 48, 68, and 116 cm^{-1} shift to 53, 73 and 134 cm^{-1} respectively and two more faint lines appear at 47 cm^{-1} and 95 cm^{-1} respectively. The intensity of the lines 48, 68 and 116 cm^{-1} relative to that of the line 990 cm^{-1} increases considerably and these lines become sharper, with the lowering of the temperature.

As regards the prominent Raman lines due to intramolecular oscillations of the benzene molecule, it is observed from Plate VI that all the lines become extremely sharp as the liquid is solidified and the line 3049 cm^{-1} due to C-H valence oscillation, which is broad at the room temperature, splits up into two sharp components separated by only about 4 cm^{-1} from each other in the solid state at -100°C . The line 992 cm^{-1} shifts to 989 cm^{-1} when the liquid is solidified and cooled to -180°C . Similarly the frequency shift of the line 607 cm^{-1} diminishes a little at the low temperature. On the other hand, the frequency shift of the line 849 cm^{-1} increases at low temperatures to 855 cm^{-1} .

The changes in position, number and intensity of the new lines in the low frequency region observed in the present investigation can hardly be explained by the theory put forward by Bhagavantam (1941) and Kastler and Rousset (1941). According to Bhagavantam the intramolecular vibration of the molecule as well as the angular oscillations of those molecules in the lattice may be of two types, symmetric and antisymmetric to the symmetry elements of the unit cell. The intensity of the Raman lines are assumed in this theory to be due to the change in the polarisability of the unit cell during the oscillation of the molecules in it. The benzene crystal belongs to an orthorhombic system in which the unit cell is pseudo-face-centred containing four molecules. The space group has been found by Cox (1932) to be V_h^{10} . If such a unit cell would execute a mode of oscillation in which the phases of all the four molecules were either the same or so adjusted as to make the oscillations antisymmetric to the symmetry elements of the unit cell, the frequencies of these two modes would be slightly different from each other. Thus each of the lines due to internal vibration of the benzene molecule would be split up into two components. No such splitting is actually observed, and on the contrary each of the lines becomes very sharp when this liquid is solidified. The line 3049 cm^{-1} is originally broad consisting probably of an unresolved doublet, and as each of the components becomes sharper in the solid state it is resolved from its companion. Thus this is not the splitting up of a single line into two components. Hence the sharpness of the lines due to benzene in the solid state clearly shows that the scattering does not take place according to the theory put forward by Bhagavantam (1941) and that it is due to individual molecules. Also there are certain fallacies in the arguments in this theory mentioned above. First, it is assumed that the unit cell acts as a large molecule and when one of the four benzene molecules executes any particular mode of internal oscillation, for instance, the breathing vibration, all the remaining three

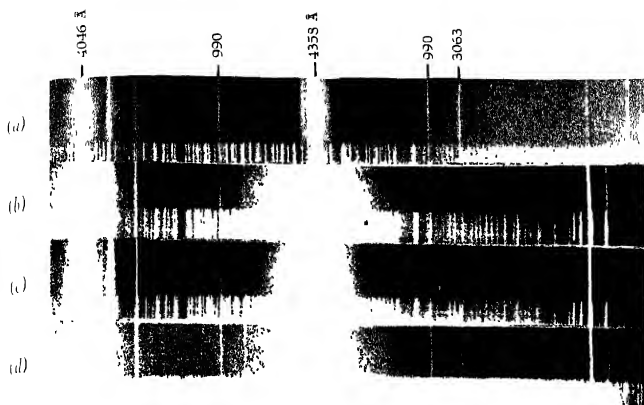


Fig. 1

- (a) Liquid at about 27°C
 (b) Solid " " -10°C
 (c) " " -100°C
 (d) " " -180°C

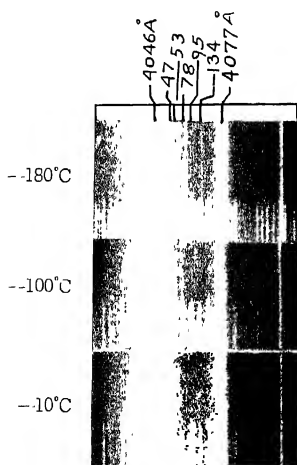


Fig. 2

Raman Spectra of benzene

molecules also execute the same mode of oscillation in only two distinct phases mentioned earlier. In fact, there is no reason to suppose that the remaining three molecules will execute the same mode of oscillation as the first one, and even if they do so, the relative phases may have any values. Hence the chance of having two distinct types of oscillation of the unit cell, in one of which the breathing vibrations of the molecules are all in phase and in the other the phases in the two molecules are opposite to those in the other two, is very small in comparison with that for the occurrence of this breathing vibration in any one of the four molecules independently. Thus the intensity of the scattering due to individual molecules is expected to be tremendously large in comparison with that due to the group of four molecules in this particular case. The extreme sharpness of all the prominent Raman lines of benzene in the solid state shows that the scattering is actually due to individual molecules. This question of probability of the occurrence of the definite phase relations in the oscillations of the different molecules in the unit cell has been overlooked by Bhagavantam (1941). Secondly, scattering takes place through a single electron belonging to a particular molecule in the group of the four molecules in the unit cell in this particular case. If the change in the polarisability of the single molecule during any mode of vibration of the molecule determines the intensity of the corresponding line, the relative intensities of the Raman lines observed in the liquid are expected to remain unaltered in the solid state. If on the other hand, the change in the polarisability of the unit cell would determine the intensity of the corresponding Raman line during a mode of vibration of the four molecules in the unit cell, this change in polarisability would depend on the relative phases of the vibration of the four molecules and in that case the relative intensities of the prominent Raman lines would alter with the solidification of the substance. It can be seen from Plate VI that actually the relative intensities of the prominent Raman lines in the solid state are the same as those in the liquid state. Hence this fact also leads to the conclusion that in the crystal only scattering due to individual molecule is more predominant than that due to the group of four molecules in the unit cell. The change in the intermolecular field which takes place with the solidification of the substance may, however, alter slightly the frequencies of the Raman lines due to internal vibrations of the molecule. The changes in the frequencies of the lines which are observed to take place when benzene is solidified, as shown in Table I, are probably due to this increased effect of the intermolecular field in the solid state.

As regards the origin of new lines in the low frequency region Bhagavantam (1941) and Kastler and Rousset (1941) suggest that these are due to angular oscillations of the molecules pivoted in the lattice. In the present case, Rousset (1944) has assumed the line 35 cm^{-1} observed by Kastler and Fröhling (1944) at about 0°C to be due to complete rotation of the benzene molecule about an axis perpendicular to its plane,

because the line is totally polarised. It has already been pointed out that this line shifts to 53 cm^{-1} when the crystal is cooled down to -180°C . This fact shows that the line cannot be due to complete rotation of the molecule, because according to the theory of rotational spectrum of polyatomic molecules by Placzek and Teller (1933), the position of maximum in the rotation spectrum would shift towards the centre of the Rayleigh line with the lowering of temperature. The distance of the maximum from the centre of the Rayleigh line is proportional to \sqrt{BkT} , where $B = h^2/8\pi^2 I$, I being the moment of inertia of the benzene molecule. The value of I cannot diminish at low temperatures so rapidly as to keep the value of BT constant. Hence the frequency-shift of the line would be much smaller than 35 cm^{-1} at -180°C , had it been due to rotation of the molecule. Further, it is difficult to understand how a sharp line can be produced by complete rotation of the molecule, because several quantised states of rotation are possible. Hence the origin of the line is to be attributed to some other cause. As regards the origin of the other lines in the low frequency region Rousset (1944) has assumed that they are due to angular oscillations of the molecules about the two axes of the Crystal. If this assumption were correct, the amplitude and the frequency of the angular oscillation would diminish at low temperatures, because in the case of polar molecules in the liquid state it has been observed by previous workers including Sen (1950a) that the frequency corresponding to hindered rotation of the molecules diminishes at low temperatures and Sen (1950b) has observed that the amplitude becomes almost zero when the liquid is frozen. Since actually both the intensity and the frequency-shift of the lines increase with the lowering of temperature, the lines cannot be due to angular oscillation as postulated by the authors mentioned above. As pointed out by Sirkar and Gupta (1938) the new lines may be due to formation of virtual bonds between adjacent molecules.

The above arguments will indicate that the values of specific heat calculated on the assumption that the line 35 cm^{-1} is due to complete rotational freedom of the benzene molecule about an axis perpendicular to its plane have very little significance. Rousset (1944) has actually made such an assumption in calculating the specific heat of benzene and has further included the contribution from Einstein functions due to two lines at 55 cm^{-1} and 100 cm^{-1} respectively even at such low temperatures as 24°K and 36°K . It will be seen from Table I, however, that the frequency-shifts of the lines increase considerably even when the temperature is lowered only to about 93°K and they are expected to become still larger at 24°K . Further, two more lines appear at 47 cm^{-1} and 95 cm^{-1} respectively when the crystal is cooled to 93°K . These two lines have not been taken into consideration by Rousset (1944). These facts explain why he had to assume a very high value of the Debye temperature, e.g., 1150°K .

for benzene which has a melting point of only $278^{\circ}.5$ K. On the other hand, Sirkar and Gupta (1938) assumed the Debye temperature of solid benzene to be as low as $121^{\circ}.5$ K and showed that if along with the Debye function Einstein functions due to the frequencies of the three lines 81 cm^{-1} , 98 cm^{-1} and 124 cm^{-1} are taken into consideration, the calculated values of C_v agree closely with those observed throughout the range from 4° K to 70° K. It was also shown that at higher temperatures similar agreement is obtained if the internal oscillations of the molecules are taken into consideration.

Since the number of lines is larger than three, the calculations made by Sirkar and Gupta (1938) are to be revised now. Actually if these lines are taken as those due to oscillations of a pair of molecules in which virtual bonds have been formed each line will contribute only half of the Einstein function to the value of C_v . If the line 95 cm^{-1} , which is broad, is taken as a doublet, there are altogether six lines and only three frequencies are to be taken for calculating the contributions of the Einstein functions. The mean values of the frequencies of these three lines are expected to be about 58 cm^{-1} , 90 cm^{-1} and 135 cm^{-1} respectively in the temperature range from 4° K to about 70° K. The corresponding values of θ_1 , θ_2 and θ_3 in the function $E(\theta_n/T)$ are $83^{\circ}.3$, $129^{\circ}.3$ and 194° respectively. The values of $R\Sigma_i^3 E(\theta_n/T)$ and $3 R.D(\theta'/T)$ with θ' equal to $121^{\circ}.5$ K are given in Table II. The values of C_p observed by Ahlberg, Blanchard and Landberg (1937) are given in the last column of the table. It will be observed that for temperatures 20° K, 30° K and 40° K the calculated values of C_v are slightly greater than those of C_p actually observed, but for the other temperatures the calculated values of C_v are slightly less than the observed values of C_p , as expected from theoretical point of view. Probably the frequency of the vibration corresponding to the line 53 cm^{-1} becomes a little larger than 58 cm^{-1} even at 40° K and if it is assumed that the frequency becomes about 64 cm^{-1} at 40° K the slight discrepancy observed at 20° K, 30° K and 40° K disappears. At temperatures lower than 10° K the contribution due to this line is so small in comparison with that due to the Debye function that the calculated values of C_v are not altered if the lowest frequency is increased to about 64 cm^{-1} . Similarly, at temperatures above 60° K the value of the frequency is probably slightly less than 58 cm^{-1} , because it diminishes to 53 cm^{-1} at 93° K.

Rousset (1944) has stated that the values of C_v of solid benzene calculated on the assumption that there is complete rotation of the molecule about an axis perpendicular to its plane even up to as low a temperature as 0.2° K agree with observed values. He has, however, overlooked the data published by Ahlberg, Blanchard and Landberg (1937) according to whom the values of C_p below 8° K are less than $0.14\text{ cal/mol./degree}$. This fact completely disproves the hypothesis put forward by Rousset that the line

TABLE II

T	$3RD(\theta'/T)$	$R \sum_{l=1}^{\infty} \frac{1}{l} \left(\frac{\theta_m}{T} \right)^l$	C_p Calc.	C_p (obs.)
4	0.17	0.0	.017	0.195
8	1.32	0.07	.140	0.147
10	0.26	0.33	.29	0.346
20	1.54	.635	2.18	1.84
30	2.96	1.72	4.68	4.24
40	3.91	2.64	6.58	6.47
50	4.51	3.40	7.91	8.14
60	4.90	3.95	8.85	9.32
70	5.14	1.36	9.50	10.16

34 cm^{-1} observed by Kastler and Fruhling (1944) is due to complete rotation of the molecule. If on the other hand it is assumed that the rotation stops suddenly at a temperature between 15°K and 20°K the contribution of the Debye function with such a high value of θ_m as 1150° assumed by him would be too small to account for the observed values of C_p .

The facts mentioned above thus confirm the view expressed by Sirkar and Gupta (1938) that Einstein functions corresponding to the new Raman lines in the low frequency region observed in the solid state can explain satisfactorily the observed specific heats of benzene at low temperatures, and therefore, the facts lead to the conclusion that these lines are due to vibrations in a pair of molecules connected together by virtual bonds

INDIAN ASSOCIATION FOR THE CULTIVATION OF SCIENCE,
210, BOWBAZAR STREET, CALCUTTA.

REFERENCES

- Ahlberg, J. E., Blanchard, R. R. and Landberg, W. O. 1937, *J. Chem. Phys.*, **5**, 539.
 Bhagavantam, S., 1941, *Proc. Ind. Acad. Sci.*, **13A**, 543.
 Cox, R. G., 1932, *Proc. Roy. Soc.*, **135A**, 491.
 Gross, R. and Vuks, M., 1935, *Nature*, **135**, 100, 998.
 Kastler, A. and Fruhling, A., 1944, *Comptes Rendus*, **219**, 998.
 Kastler, A. and Rousset, A., 1941, *Comptes Rendus*, **212**, 645.
 Placzek, G. and Teller, E., 1933, *Z. f. Phys.*, **81**, 209.
 Ray, A. K., 1950, *Ind. J. Phys.*, **28**, 111.
 Rousset, A. 1944, *Comptes Rendus*, **218**, 546.
 Sen, S. N., 1950a, *Ind. J. Phys.*, **23**, 495.
 Sen, S. N., 1950b, *Ind. J. Phys.*, **28**, in press.
 Sirkar, S. C., 1936, *Ind. J. Phys.*, **10**, 189.
 Sirkar, S. C. and Gupta, J., 1938, *Ind. J. Phys.*, **12**, 145.

FADING OF SHORT WIRELESS WAVES DUE TO THE INTERFERENCE BETWEEN THE MAGNETO-IONIC COMPONENTS

By S. N. MITRA

(Received for publication, February 16, 1950)

Plates VIIA and B

ABSTRACT. The various causes of fading of a downcoming wireless wave from the ionosphere are briefly discussed. It is pointed out that the periodic fading of a single downcoming wave as often observed may be due to the interference between the two overlapping magneto-ionic components when the difference between their equivalent heights of reflection is changing at a uniform rate. The design of a polarised aerial system accepting only one of the components is then described. By the use of such an aerial system and with pulsed transmission one can study the fading of a single magneto-ionic component. The effect on fading due to scattering from the ionospheric irregularities, having either a random motion or a steady drift with the existing wind velocity in the ionosphere, is also discussed. Previous experimental evidence shows that when random motion is predominant, the fading is peculiar and irregular and that due to a steady drift it is quasi-periodic in nature. In order to obtain unambiguous measurement of the motion of the ionospheric irregularities from the fading curves produced at a receiver, and specially at higher wave-frequencies where ionospheric absorption is low, a polarised aerial system is considered essential.

INTRODUCTION

That the intensity of downcoming wireless signals reflected from the ionosphere varies with time is known for a long time. This phenomenon is briefly known as "fading". A large amount of work has already been done on the subject but till now the cause of the fading has not been fully understood. The object of this paper is to describe one particular type of fading which may be assigned to a definite cause.

Ratcliffe and Pawsey (1933) and Pawsey (1935) have discussed the possible causes of the intensity variation of the downcoming waves. These have been broadly divided into absorption effects and interference effects. Although absorption is an important factor in explaining the difference between the over-all night-time and day-time intensities, its effect would certainly be small on short-period intensity fluctuations. Moreover, the fading curves (the curve of amplitude fluctuations of the wave with time) at two adjacent wave-frequencies as recorded simultaneously on two receivers at the same place were found to be independent of each other which showed that the absorption effect could be excluded from the possible causes of fading. It has, therefore, been suggested that the possible causes of fading may be due to the following interference effects :

(1) Interference between ground and skywaves when the receiver is close to the transmitter.

(2) Interference between multiple-reflected waves from one or more ionospheric layers.

(3) Interference between the wave reflected from different layers (the so-called M reflection)

(4) Interference between the ordinary and the extraordinary waves caused by the presence of the earth's magnetic field

(5) Interference between the waves scattered from the local irregularities in the ionosphere.

In all the cases, the time-variation of the intensity at the ground is assumed to be due to the characteristics of the downcoming waves (the phase, amplitude and path) varying with time

The resultant intensity of the downcoming wave may, therefore, depend upon many factors. It is, however, possible to eliminate some of the causes in the following way. The first three causes can be eliminated by using short duration pulses as a means of exploring the ionosphere. In that case, the ground wave, if any, and the different skywaves could be observed separately on the cathode ray time-base since all these are separated in time due to their different path-lengths. Now the effect of the interference between the magneto-ionic components may exist so long as the echo exhibits itself as a single one and not as a split pair. The effect of the last case, however, is often found in the experiment since the ionosphere presents considerable number of irregularities in a horizontal plane. In the present paper we shall describe the effects of the interference between the magneto-ionic components and in what way this fading curve differs from that due to the interference between the waves scattered from the local irregularities in the ionosphere.

Recently, Banerjee and Singh (1949) have observed periodic fading curves which they attribute to the interference between the magneto-ionic components. According to Khastgir (1949), however, the periodic fading curves observed by Banerjee and Singh during early morning or evening hours may be due to the beats produced between the Doppler frequency-shifts on the waves reflected simultaneously from the moving E and F layers, or, between the single and double reflections from the same moving layer.

THEORETICAL CONSIDERATIONS

It is known that a wave reflected from the ionosphere apparently as a single echo is often in fact composed of two overlapping magneto-ionic components with opposite senses of polarisation (Kruger and Plendl, 1930). These two magneto-ionic components combine at the ground to give in

general, a resultant wave of elliptic polarisation and if the two components are equal in amplitude, the wave degenerates into a straight line. If the phase difference between the two components now alters due to a change in the difference between their equivalent paths, the ellipse on the ground will rotate. If the resultant wave is now received on a loop or a horizontal wire aerial the recorded e.m.f. will be fluctuated periodically, being a maximum when the major axis of the ellipse lies in the reception place of the aerial. We shall consider here the simple case in which the two components are circularly polarised.

The two oppositely circularly polarised components can be expressed by the following simple equations :—

$$\begin{aligned} H_{xo} &= H_o \cos \omega t \\ H_{yo} &= H_o \sin \omega t \end{aligned} \quad \left| \begin{array}{l} \text{for the ordinary wave,} \end{array} \right.$$

$$\begin{aligned} \text{and, } H_{xe} &= H_o \cos (\omega t - \phi) \\ H_{ye} &= H_o \sin (\omega t + \phi) \end{aligned} \quad \left| \begin{array}{l} \text{for the extraordinary wave.} \end{array} \right.$$

where H_{xo} , H_{yo} are the magnetic fields of the ordinary wave along the x and y axes (z axis being along the vertical direction); H_{xe} , H_{ye} those for the extraordinary wave; ϕ is the phase difference introduced between the two waves because of their different velocities of travel; ϕ may be considered in terms of an equivalent path difference between the two waves. The interference between these two systems of waves will produce a wave in space whose components along the x and y -axes are given by the following expressions :

$$\text{along } x, \quad 2H_o \cos (\omega t + \phi/2) \cos \phi/2$$

$$\text{along } y, \quad 2H_o \cos (\omega t + \phi/2) \sin \phi/2.$$

Suppose a loop is placed with its horizontal side coinciding with the x -axis, then the e.m.f. induced in the loop will be proportional to $\cos \phi/2$. Now ϕ can be put equal to $\frac{2\pi}{\lambda} \cdot 2d$ where d is the difference between the effective heights of reflection for the ordinary and the extraordinary waves and λ is the wave-length of the radio wave. As the phase difference increases uniformly with time due to the levels of reflections for the two magneto-ionic components separating at a uniform rate, ϕ will change from 0 to $4n\pi$ for d changing from 0 to $n\lambda$. This would, therefore, produce a sinusoidal variation of the signal in the loop and the output from the receiver would also vary periodically representing the amplitude variation of the downcoming wave as time goes on.

Now, if another similar loop aerial is used at right angles to the above-mentioned one, its response would be proportional to $\sin \phi/2$. If, therefore,

during a magneto-ionic-interference fading, two identical receivers are used which are connected to the two loop aerials with their planes at right angles to each other, the fading curve at one receiver will be displaced by 90° with respect to the other. In other words, the maximum amplitude at one fading curve would correspond to the minimum of the other when the two fading curves are recorded simultaneously.

In general, when the vertical planes of the two loops are inclined at any angle, the fading pattern for one loop will be shifted by a certain amount (depending on this angle) with respect to that of the other and the two fading curves will be similar in nature.

EXPERIMENTAL DETAILS

(a) *Magneto-ionic interference.*

A simple experiment was carried out in order to test this hypothesis. Short duration pulses of 200 micro-seconds at a frequency of 4 mc/s were received at vertical incidence by a receiver and the amplitude fluctuation of the downcoming wave was recorded photographically in the following way. The echo was displayed on a monitor oscilloscope time-base in the usual way. Electronic height-marks were incorporated in the time-base to note the height from which the echo was being reflected. An electronic gate of variable width and variable delay was used to select the echo. A photograph of the echo-pattern with the height-marks and its selection by the gate is shown in Plate VIIA, (a). A photographic CR() tube was used, in the Y-plate of which was connected the receiver output and this CR() tube was brilliancy modulated by the electronic gate selecting the echo. There was no time-base for this CR() and when the echo was properly selected by the gate there appeared on the CR() screen a line of length proportional to the amplitude of the desired echo. A 35 mm camera was focused to the screen of the CR() and the fading pattern of the echo was photographed automatically by running the film at a predetermined rate (1 or 6 inches per minute).

Time-marks were produced on the film mechanically every 15 seconds by momentarily closing the camera lens so as to produce narrow gaps on the continuous fading curves. Provisions were made with three photographic oscilloscopes and a suitable optical arrangement so that three independent fading curves from three receivers could be simultaneously photographed on the same moving film.

It has been mentioned before that when the amplitude fluctuation of the downcoming wave is due to the interference between the magneto-ionic components, the fading curve would be a periodic one. A typical photograph of such a fading curve is shown in Plate VIIA, (b). It will be seen from this plate that the fading curve is very periodic in nature. In order to test whether

this fading is due to the interference between the magneto-ionic components, the following experiments were made :

Two identical receivers kept on the same table were tuned to the same wave-frequency. They were connected to two identical loop aerials with their planes making a certain angle between them. The receivers were placed parallel to each other to avoid any relative phase-shift. The same echo amplitude from the two receivers was displayed on the two photographic oscilloscopes and when the fading appeared to be periodic in nature the camera motor was switched on. Plate VIIA, (c) shows one such record. It will be noticed from the record that the fading curves at the two receivers were very similar in nature but displaced with respect to each other which showed that the fading was due to the interference between the magneto-ionic components, the displacement between the two fading curves being due to the angle between the loops. Plate VIIB, (d) shows what happens when the planes of the two loops are made parallel to each other in which case there is no displacement between the two periodic fading curves. The interval between any two consecutive small gaps in the fading curves represents a time-interval of 15 seconds.

(b) *Suppression of a magneto-ionic component*

In the previous section it has been observed that when the amplitude fluctuation of a downcoming wave is due to the interference between the

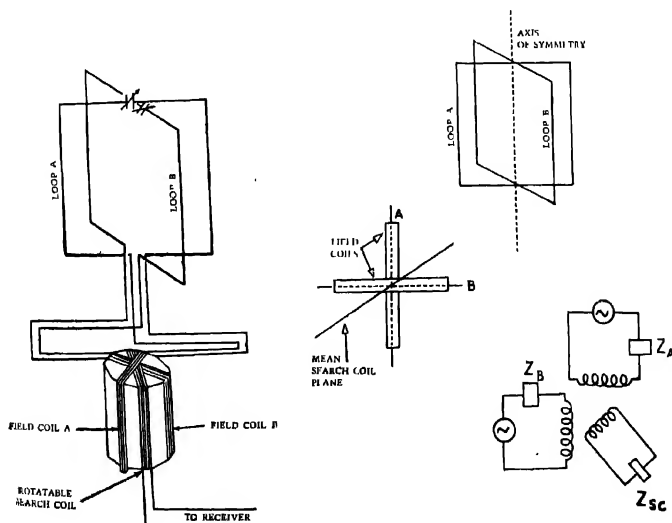


FIG. 1

FIG. 2

magneto-ionic components, periodic fading is observed. It is, however, possible to suppress one of the magneto-ionic components by means of a special receiving aerial. The fading of a single component may therefore be observed even when both the components are present in the downcoming wave. This was achieved in the following way :

First, a circularly polarised loop aerial was constructed. This aerial, when properly adjusted, should receive only one of the magneto-ionic components. This aerial is similar to that described by Lickersley (1932), Ratcliffe and White (1933), Ratcliffe and Pawsey (193b) and Lickersley and Millington (1939). It consisted of two vertical loops mounted at right angles to each other having a common axis of symmetry. The loops were tuned in the middle by series condensers and each was coupled to the field coils of a radio-goniometer as shown in Fig. 1. Fig. 2 shows the plan of the aerial system. The rotatable search coil was connected to the input circuit of the receiver in the usual way. The area of each loop was 1 sq.m. and consisted of four turns of wire. The tuning range with four turns of wire in the loop and the inductance of the field coil was from 2.8 mc/s to 4.5 mc/s. Both the loops were carefully screened to avoid any stray pick-ups and the whole goniometer was screened. The vertical planes of the two loops were made perpendicular to each other in order to avoid any mutual inductance between the two loops.

The working principle of such an aerial system can be seen from the following. The main object was to use this double frame as a polarimeter. The aerial was set so that the angle between the two frames was bisected by the incoming ground wave. The two loops were then separately tuned so that the currents in the two loops were in phase with the e. m. f's in the loops which were also in phase. The search coil of the goniometer can then be set at 45° so as to receive no signal. The loops were then mistuned, one being increased in natural period and the other reduced. The amount of mistuning should be 45° in each loop. This was achieved by first tuning the loop so as to receive some pulse-amplitude of the ground wave on the monitor time-base and then detuning continued on the same tuning condenser until the pulse amplitude was reduced to $1/\sqrt{2}$ times its tuned value. In this way a phase-lag (or phase-increase) of 90° was deliberately introduced between the currents in the two loops.

Let us now consider a downcoming wave from the ionosphere. If it were circularly polarised, then the e. m. f's in the two loops would be 90° out of phase. When the mistuning of the aerials had been properly carried out, the currents would be in phase or 180° out of phase according to the direction of the circular polarisation. For a circularly polarised wave, therefore, a balance was obtained with the pointer of the goniometer either at $+45^\circ$ or -45° according to the direction of circular polarisation. The presence of a split pair of echoes was also strikingly shown by the "see-saw effect" as one echo was suppressed and the other appeared when the search

coil was rapidly rotated from one 45° position to the other. Thus, when both the ordinary and the extraordinary components are present in the downcoming wave, it is possible to pick out either of them. The adjustment of the aerial was first done on the ground wave and then when the two components were properly split, as shown on the time base as a pair of adjacent echoes, the final adjustments were carried out. It was found that such a polarised aerial was quite efficient in suppressing one of the components and accepting the other in full strength.

In the experiment two identical receivers were placed on the same table; one was connected to a plane loop and the other to a circularly polarised loop-aerial of the type mentioned above. The polarised aerial was previously adjusted to ensure that only one component was being received. When the fading of the downcoming wave was observed to be periodic, the camera motor was switched on and the fading curves at the two receivers were simultaneously recorded. Plate VII B, (c) shows a typical example. In this plate the top pattern was taken by a loop aerial and the bottom by a circularly polarised aerial suppressing one of the components. It will be noticed that the amplitude of the single component was not varying but at the same time the interference between the two waves was producing a remarkable periodic fading.

An interesting result may, however, be obtained from a periodic fading pattern, namely, the rate at which the equivalent distance of separation between the two components is changing. It can be shown by simple calculation that d must change by a quarter wavelength in order to obtain one half cycle in the fading curve, i.e., from one minimum to the next. In the fading curve shown in Plate A (b), the rate of change of d is found to be about 2.5 meters per second, i.e., about 9 km. per hour. As time goes on, the effective distance of separation between the two components would go on increasing and the two waves will be shown as two split echoes on the time-base, provided no extra absorption takes place. On a 20 ms. time-base, using a radio-frequency pulse of width 200 μ s, the first sign of splitting would occur after about half an hour from the commencement of the periodic fading.

EFFECT OF IONOSPHERIC IRREGULARITIES ON MAGNETOIONIC FADING

So far we have considered the fading as only due to the interference between the magneto-ionic components. We have also seen that while a single component remains steady in amplitude the interference between the two components may produce at the same time a remarkable periodic fading. In this section we shall discuss what happens when the scattering from the irregularities in the ionosphere also contributes to the fading.

It is known that the ionosphere exhibits considerable irregularities which may be in the form of ion-clouds. If the dimension of these irregularities

becomes comparable with the wavelength of the incident radio wave, they will diffract the waves. This problem of diffraction has been described in detail by Ratcliffe and Pawsey (1935).

It has been shown (above) that the effect of the interference between the magneto-ionic components may be eliminated by using a circularly polarised aerial at the receiver. The ionospheric echo thus singled out may therefore be considered as a single downcoming wave. This single wave may now be considered as a resultant of a large number of wavelets diffractively scattered from the irregularities. If the ionosphere remained constant there would result an irregular 'diffraction pattern' of received signal changing in magnitude from point to point on the ground but the signal intensity would remain constant with time at one given point. A single magneto-ionic component received at one point will only exhibit fading if the ionosphere changes in some way and the resulting fading might be due to two different phenomena: (a) a steady motion of the ionosphere as a whole and (b) a random motion of the ionospheric irregularities; or it might be due to some combination of the two.

A uniform drift of the ionosphere corresponding to a steady wind would result in the sweeping of the diffraction pattern past the receiver with a velocity equal to twice the velocity of the wind. Two separated receivers would therefore record similar fading but with a time-displacement corresponding to the rate of drift of the diffraction pattern. In a previous paper (Mitra, 1949) the author has dealt with the wind-observations by three spaced receivers.

The other extreme would correspond to the random motion of the irregularities and would lead to random fading at the two receivers and if these were separated by a sufficient distance the two fading curves would cease to be similar (Ratcliffe, 1948). There would in particular be no regular time-shift between the two curves. Such irregular fading curves have been observed and the records statistically analysed in a previous paper by the author (Mitra, 1949). The results lead to a determination of the random motion of the ionospheric irregularities.

In practice, however, if one uses a loop or an ordinary aerial, the effects of wind and random motions will be present together with the effect of the interference between the magneto-ionic components. Then it becomes very difficult to decide which effect is predominant. It has, however, been observed that when the effect of wind predominates the fading curve of a single downcoming wave is quasi-periodic. On the other hand, when the random motion is the dominating factor, the curve appears peaky and very irregular. Thus, from an inspection of the fading curve an approximate idea may be formed regarding the cause of the fading. But the real difficulty comes when the curve appears to be quasi-periodic and the receiver is not

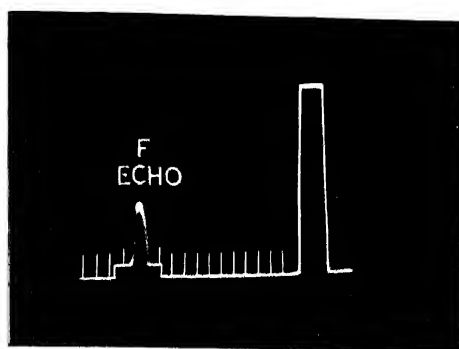


Fig. (a)—Gated echo, the ground pulse and the height-marks on the monitor time-base

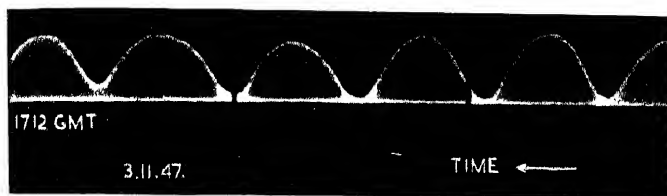


Fig. (b)—Fading curve due to the magneto-ionic interference. The receiver was connected to a plane loop aerial

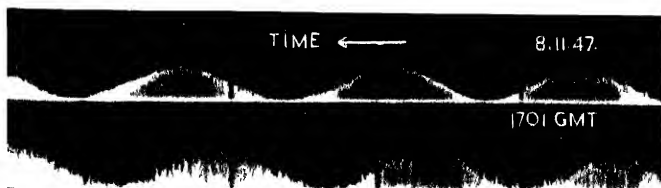


Fig. (c)—Displaced fading curves. Two receivers were placed on the same table, one was connected to a loop aerial the plane of which was making a certain angle to the other loop aerial connected to the other receiver.



Fig (d)—Similar periodic fading curves at the two receivers placed at the same place. Both the receivers were connected to plane loop aerials the reception planes of which were made parallel.

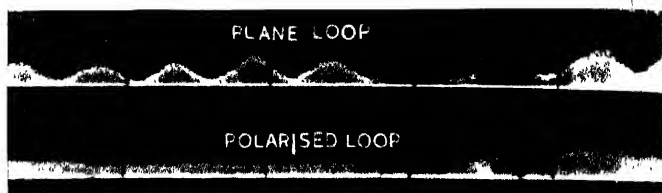


Fig (e)—Suppression of the interference due to the two overlapping magneto-ionic components by the use of a circularly polarised loop aerial. The receivers were placed on the same table (Wave-frequency = 4 Mc/s)

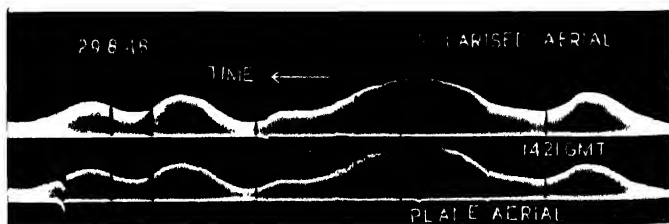


Fig. (f)—Quasi-periodic fading which is not due to the interference between the magneto-ionic components. (Wave-frequency = 4 Mc/s.).

connected to a circularly polarised aerial when the magneto-ionic interference may be suspected. In this case even, an approximate idea may be obtained regarding the cause of the fading from the following considerations :

It is known that in northern latitudes and specially in high altitudes, the extraordinary component at lower frequencies is heavily absorbed during day-time and only the ordinary component is present in the downcoming wave. However, during night, sunrise and sunset periods when absorption is low, the two components are found to be present in comparable amplitudes. The need of a polarised aerial is specially felt at these periods if one desires to investigate the fading of a single downcoming wave for the study of the wind or random motion of the irregularities. During day, when absorption is supposed to be high, quasi-periodic fading is also often observed. To ascertain whether the magneto-ionic interference is of any consequence in such fading the following experiment was conducted:

Two identical receivers were placed on the same table; one was connected to a circularly polarised loop aerial accepting only one component and the other connected to a horizontal dipole. Plate VII B, (f) shows a typical photograph of the two fading curves taken simultaneously. It will be seen that for the particular wave frequency used (4 mc/s) the fading curves were very similar and quasi-periodic in nature but not displaced. This shows that only one magneto-ionic component was present in the downcoming wave. The fading was primarily due to the motion of the scattering centres with a steady ionospheric wind. Thus, one may use ordinary aerial either loop or horizontal dipole for the study of the fading during daytime provided the wave frequency is kept low. At higher wave frequencies, however, the absorption will be low and a polarised aerial should be used for an unambiguous study of fading.

CONCLUSIONS

We conclude that a periodic fading of short wireless waves may be due to the interference between magneto-ionic components. It cannot, however, be generalised that all periodic fading patterns, as often observed, are due to this effect. Similar fading is also found which has been interpreted as due to an ionospheric wind. It is only by the use of a polarised aerial system that one is able to detect the effect of the interference between the magneto-ionic components in the fading.

ACKNOWLEDGMENTS

The present work was carried out in connection with the investigation of wind and turbulence in the ionosphere at the Cavendish Laboratory, University of Cambridge and it was supported by a grant from the Department of Scientific and Industrial Research. The author is grateful to (i) Mr. J. A. Ratcliffe, Reader in Physics, University of Cambridge under whose

guidance the experiment was conducted (ii) the Government of India for the award of a State Scholarship in England which enabled him to work in the Cavendish Laboratory (iii) Dr. H. Rakshit, Professor of Communication Engineering, Bengal Engineering College, Sibpore, for helpful discussion; and (iv) Mr. B. V. Baliga, the Chief Engineer, All India Radio for the permission to publish this paper.

RESEARCH DEPARTMENT
ALL INDIA RADIO
DELHI

REFERENCES

- Banerjee, S. S. and Singh, R. N., 1949, *Science and Culture*, **14**, 293.
 Eickersley, T. L., 1932, *Journal I. E. E.*, **71**, 439.
 „ 1932, *Nature*, **130**, 398
 „ 1937, *Nature*, **140**, 846.
 „ 1940, *Journal, I E E.*, **86**, 548.
 Eickersley, T. L. and Millington, G. 1939, *Proc. Phys. Soc.*, **51**, 110
 Khasigir, S. R., 1949, *Science and Culture*, **15**, 116.
 Kruger, V. K. and Plendl, M., 1930, *Zetts. f. Tech. Phys.*, **11**, 478
 Mitra, S. N. 1949, *Proc. I.E. E.*, pt. III, **96**, 441.
 „ 1949, *Proc. I. E. E.*, pt. III, **96**, 505
 Pawsey, J. L. 1935, *Proc. Camb. Phil. Soc.*, **31**, 125
 Ratcliffe, J. A. 1948, *Nature.*, **162** 9.
 Ratcliffe, J. A. and Pawsey, J. L. 1933, *Proc. Camb. Phil. Soc.*, **29**, 301
 Ratcliffe, J. A. and White, E. L. C., 1933, *Phil. Mag.*, **16**, 125

A SIMPLE METHOD OF PRODUCING WIDE-BAND FREQUENCY MODULATION

By H. RAKSHIT AND N. L. SARKAR

(Received for publication, March 28, 1950)

ABSTRACT The three-phase R-C tuned radio-frequency oscillator developed by Rakshit and Bhattacharyya (1946) can easily be made to generate frequency-modulated oscillations by varying the tuning resistance of one of the three stages in the oscillator. It has been found that if frequency modulation is produced by shunting any of the three oscillator valves by a triode with the modulating audio voltage on its grid, faithful wide-band modulation can be realised under proper adjustments. Frequency stability of the central unmodulated carrier has been attained by incorporating an automatic frequency-control system involving a phase discriminator. The experimental arrangement is fully described in the present paper and a typical set of results with a 1.44-megacycle carrier is presented. The preliminary observations have already given very good results and further studies are in progress.

INTRODUCTION

The R-C tuned oscillator is well known as a very good generator of audio frequency oscillations. Rakshit and Bhattacharyya (1946) have pointed out, however, that the conventional circuit of a three-phase system, with components selected for producing audio frequency oscillations, invariably generates radio frequencies by virtue of the unavoidable stray and inter-electrode capacities. In fact, with the simple three phase oscillator it is impossible to generate audio frequencies unless certain modifications are introduced in the circuit. It was further pointed out that the three-phase radio frequency oscillator can easily be made to generate frequency-modulated oscillations by varying the tuning resistance of one of the oscillator stages by the modulating voltage.

In a recent communication by the authors (Rakshit and Sarkar, 1949) it has been reported that if frequency-modulation is produced by shunting any of the three oscillator valves by a triode and applying the modulating audio voltage on the grid of this triode modulator, faithful wide-band modulation can be realised under proper adjustments. The present paper gives the details of the observations.

THEORETICAL CONSIDERATIONS

When the three stages are identical one of which being as shown in Fig. 1, and the anode load of each valve is composed of resistance r_1 shunted

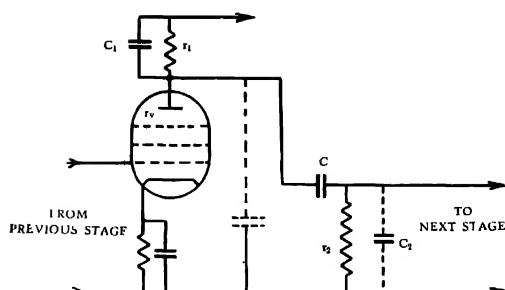


FIG. 1

One of the three stages in oscillator

by capacity C_1 it has been shown that the oscillations produced are of radio frequency given approximately by

$$f = \frac{\sqrt{3}}{2\pi r_1(C_1 + C_s)} \quad (1)$$

when r_2 as also the anode impedance r_a of valve $\gg r_1$ and $C_2 \ll C$. The quantity C_s in the above expression denotes the total stray capacity on both sides of the coupling condenser C . In regard to C_1 , it will be noted that the performance of the system remains unaltered if it is connected between anode and cathode. In practice the three condensers C_1 of the three stages are replaced by a three-gang condenser between the common H.T. negative line and the three anodes.

Let us consider the case in which the three stages which are otherwise identical in every respect have load resistances r_1 for the two and r for the third stage. If p be the angular frequency of the generated radio frequency oscillations, the phase shift in either of the first two stages having load resistances r_1 is given by

$$\phi_1 = \phi_2 = \tan^{-1} \frac{1 - p^2 r_1 r_2 C(C_1 + C_s)}{p C r_2}$$

when $C \gg C_2$ and $r_2 \gg r_1$. With further approximation

$$\phi_1 = \phi_2 = \tan^{-1} [-p r_1 (C_1 + C_s)] \quad (2)$$

The phase shift produced by the third stage is

$$\phi_3 = \tan^{-1} [-p r (C_1 + C_s)] \quad (3)$$

The total phase shift produced by the three stages is

$$\phi = 2 \tan^{-1} [-p r_1 (C_1 + C_s)] + \tan^{-1} [-p r (C_1 + C_s)] \quad (4)$$

The gain of a stage with load resistance r_1 is given by

$$\text{gain} = \frac{gr_1 r_2 pC}{\sqrt{[1 - p^2 r_1 r_2 C (C_1 + C_s)]^2 + (pCr_2)^2}}$$

In the symmetrical case it has been shown by Rakshit and Bhattacharyya (1946) that, as a first approximation, $pC_1 r_1 = \sqrt{3}$. Here also, as the variation in frequency is very small, $pC_1 r_1 \approx \sqrt{3}$ and hence

$$p^2 r_1 r_2 C (C_1 + C_s) = p r_1 (C_1 + C_s) p C r_2 > > 1$$

since

$$r_2 > > r_1.$$

Therefore,

$$\begin{aligned} \text{gain} &\approx \frac{gr_1 r_2 pC}{\sqrt{[p r_1 (C_1 + C_s) \times p C r_2]^2 + (p C r_2)^2}} \\ &= \frac{gr_1}{\sqrt{[1 + p^2 r_1^2 (C_1 + C_s)^2]}} \end{aligned}$$

The overall gain for the three stages

$$= \frac{g^3 r_1^2 r_2}{[1 + p^2 r_1^2 (C_1 + C_s)^2] [1 + p^2 r_2^2 (C_1 + C_s)^2]^{\frac{1}{2}}} \quad \dots (5)$$

For maintenance of oscillations we must have

$$(i) \quad \phi = 2\pi$$

and

$$(ii) \quad \text{overall gain} \ll 1.$$

Condition (i) is satisfied if

$$2 \tan^{-1} [-p r_1 (C_1 + C_s)] + \tan^{-1} [-p r_2 (C_1 + C_s)] = 2\pi$$

$$\text{or} \quad \tan^{-1} \left\{ \frac{\frac{-2p r_1 (C_1 + C_s)}{1 - p^2 r_1^2 (C_1 + C_s)^2} - p r_2 (C_1 + C_s)}{\frac{1 - 2p^2 r_1 r_2 (C_1 + C_s)^2}{1 - p^2 r_1^2 (C_1 + C_s)^2}} \right\} = 2\pi$$

$$\text{or} \quad \frac{2p r_1 (C_1 + C_s)}{1 - p^2 r_1^2 (C_1 + C_s)^2} + p r_2 (C_1 + C_s) = 0$$

$$\therefore \quad p = \frac{1}{r_1 (C_1 + C_s)} \left(1 + \frac{2r_1}{r} \right)^{\frac{1}{2}} \quad \dots (6)$$

If, as mentioned in the introduction, the anode load resistance of the third stage is composed of a resistance shunted by the modulator impedance then for a ganged condenser used for C_1 the effective value of C_s for the third stage would be slightly greater, C' , say, due to the extra capacitances involved. The frequency of the oscillations maintained is then given by

$$p = \frac{1}{r_1 (C_1 + C_s)} \left[1 + \frac{2r_1 (C_1 + C_s)}{r (C_1 + C'_s)} \right]^{\frac{1}{2}} \quad \dots (6a)$$

On substitution from (6) expression (5) for the overall gain becomes

$$\frac{g^3 r_1^2}{2 \left(1 + \frac{r_1}{r}\right) \left[1 + \frac{1}{r_1^2} \left(1 + \frac{2r_1}{r}\right)\right]^{\frac{1}{2}}} = \frac{g^3 r_1^2 r}{2 \left(1 + \frac{r_1}{r}\right) \left(1 + \frac{1}{r_1}\right)} = \frac{g^3 r_1^2 r}{2 \left(\sqrt{\frac{r}{r_1}} + \sqrt{\frac{r_1}{r}}\right)^2} \dots (5a)$$

Since $\left(X + \frac{1}{X}\right)$ is always greater than 2 for any positive value of X , it is evident that

$$\text{overall gain} < \frac{g^3 r_1^2 r}{8}$$

In practice r differs from r_1 by only a small percentage and hence overall gain $\approx \left[\frac{g r_1}{2}\right]^3$. Condition (ii) for maintenance of oscillations is thus satisfied if

$$g r_1 \ll 2 \quad \dots (7)$$

The expression (6) for frequency shows that if r is varied the generated frequency will also vary, producing frequency modulation.

CONDITIONS FOR FAITHFUL MODULATION

The schematic arrangement of the third stage of the three phase oscillator producing frequency modulation is shown in Fig. 2. The effective anode load of the third valve is r'_1 shunted by the anode impedance R_a of the

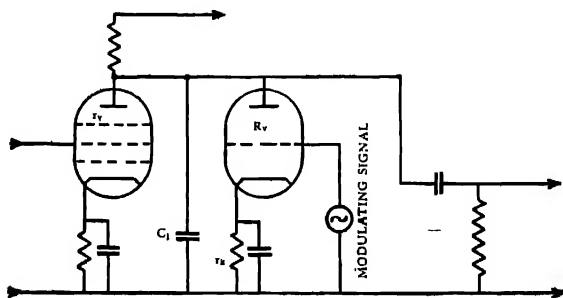


FIG. 2

Modulated stage of oscillator

modulating triode. Thus

$$\mu = \frac{r'_1 R_a}{r'_1 + R_a}$$

and according to (6) the frequency of the oscillations is

$$f = \frac{1}{2\pi r_1(C_1 + C_s)} \sqrt{\left(1 + \frac{2r_1}{r_1'} + \frac{2r_1}{R_v}\right)} \\ = \alpha \sqrt{\left(\beta + \frac{2r_1}{R_v}\right)} \quad \dots (8)$$

where

$$\left. \begin{aligned} \alpha &= \frac{1}{2\pi r_1(C_1 + C_s)} \\ \beta &= 1 + \frac{2r_1}{r_1'} \end{aligned} \right\} \quad \dots (9)$$

As shown in Fig. 2, frequency modulation is produced by changing the grid voltage of the modulator. Faithful modulation would, however, require linearity between change in oscillator frequency and amplitude of modulating voltage. Further, there should not be appreciable amplitude modulation introduced in the process.

Linearity of frequency modulation requires that, over a frequency range sufficient for wideband modulation

$$f = K(1 + mV_g) \quad \dots (10)$$

where K and m are constants of the system which do not change with V_g the modulator grid voltage. Comparing (8) and (10), we find

$$K(1 + mV_g) = \alpha \sqrt{\left(\beta + \frac{2r_1}{R_v}\right)},$$

giving

$$(K^2 - \alpha^2\beta) + 2K^2mV_g + K^2m^2V_g^2 = \frac{2\alpha^2r_1}{R_v}$$

or

$$R_v = \frac{2\alpha^2r_1}{(K^2 - \alpha^2\beta) + 2K^2mV_g + K^2m^2V_g^2} \\ = \frac{1}{A + BV_g + CV_g^2}, \text{ say} \quad \dots (11)$$

where

$$\left. \begin{aligned} A &= \frac{K^2 - \alpha^2\beta}{2\alpha^2r_1} \\ B &= \frac{K^2m}{\alpha^2r_1} \\ C &= \frac{K^2m^2}{2\alpha^2r_1} \end{aligned} \right\} \quad \dots (12)$$

$$\text{giving } B/C = 2/m \quad \dots (13)$$

It has been found possible to have, under proper working conditions, R_v varying very closely according to (11), at least over a range of V_g sufficient for wideband modulation,

OBSERVATIONS ON FREQUENCY STABILITY

To make a quantitative study of the variation of carrier frequency with change of voltage on modulator grid it is essential that the R-C oscillator has a good degree of inherent frequency stability. It is therefore desirable to discuss this question in detail and make an experimental study of the stability before we attempt to study the nature of frequency modulation capable of being produced by this system.

When all the three stages are identical, disregarding the presence of the modulator for the present, the radio frequency of the R-C oscillator is given by

$$f = \frac{\sqrt{3}}{2\pi\tau_1(C_1 + C_s)}$$

It has already been pointed out that in arriving at this approximate value, the impedance r_v of the oscillator valves has been neglected as being $\gg r_1$, since r_1 is actually in shunt across r_v .

(One of the causes of variation of oscillation frequency is the variation of r_v of the oscillator valves due to fluctuation of supply voltages. Taking

$$r_v \text{ into account we have } f = \frac{\sqrt{3}}{2\pi(C_1 + C_s)} \times \frac{1}{R_1}$$

$$\text{where } 1/R_1 = 1/r_1 + 1/r_v$$

The variation δf in frequency, due to variation δr_v in r_v ,

$$\text{is } \delta f = - \frac{\sqrt{3}\delta r_v}{2\pi(C_1 + C_s)r_v^2}$$

$$\text{or } \frac{\delta f}{f} = - \frac{R_1\delta r_v}{r_1^2} = - \frac{r_1}{r_1 + r_v} \cdot \frac{\delta r_v}{r_v}$$

So far as variation in r_v is concerned, it is obvious that for a high degree of frequency stability $\frac{\delta f}{f}$, r_v should be as large and r_1 as small as possible. A

large value of r_v necessitates the use of r. f. pentodes and a small value of r_1 necessitates the use of high- μ pentodes, since oscillations are maintained when $gr_1 \ll 2$. For a typical case in which $r_1 = 2 \times 10^3$ and $r_v = 10^6$ ohms,

$$\frac{\delta f}{f} = - 2 \times 10^{-3} \frac{\delta r_v}{r_v}$$

For one per cent variation in r_v , there would be 2×10^{-3} per cent variation of the frequency of the oscillations. For a one megacycle carrier the frequency variation due to one per cent increase in r_v will in this case be minus 20 cycles. Stabilisation of the voltages to the different electrodes is therefore essential to minimise this variation. In actual practice, the anode

and screen voltages were derived from a stabilised source as shown in Fig. 3 and the heaters of the valves were fed from a voltage regulation transformer.

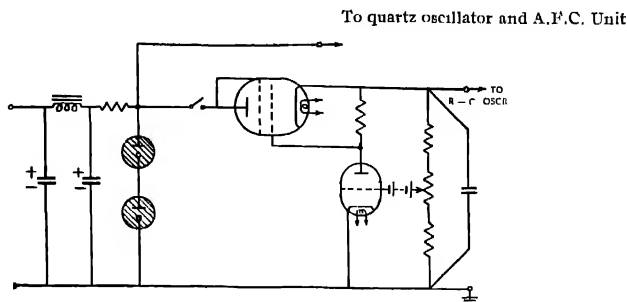


FIG. 3

Stabilized HT supply

Another important cause of frequency instability is the variation of the load resistance r_1 with change in temperature. To minimise the frequency variation due to change in r_1 caused by temperature change, the resistances r_1 must be wound with wires having low temperature coefficient. Proceeding as above, we get, for variation of r_1

$$\frac{\delta f}{f} = - \frac{R_1}{r_1^2} \delta r_1 = - \frac{r_p}{r_1 + r_p} \cdot \frac{\delta r_1}{r_1} \propto - \frac{\delta r_1}{r_1},$$

since $r_p \gg r_1$.

The resistances r_1 were actually wound on thin mica cards with manganin wires which have an average temperature coefficient of 10^{-5} per degree Centigrade. For a temperature rise of 1°C of the resistances r_1 , there will thus be a frequency change of minus 10 cycles on a one-megacycle carrier.

Frequency instability is also caused by changes in C_1 due to variations in temperature. Assuming an average temperature coefficient of capacity to be 2×10^{-5} , for small change in temperature, the change in frequency caused by change in capacity due to increase of temperature by 1°C is, for a one-megacycle carrier, minus 20 cycles.

From a consideration of the frequency change due to change in working temperature it is desirable to place both r_1 and C_1 in thermostatically controlled chambers.

The degree of stability attained in this way was checked by comparing with a quartz-controlled oscillator. In the absence of a direct frequency measuring equipment of high accuracy, the R-C oscillator was heterodyned with a quartz-controlled oscillator to produce a 1,000 cycle beat note. The R-C and quartz-controlled oscillators were both separated by buffer amplifiers before applying to the mixer, as shown in Fig. 4. The beat note produced

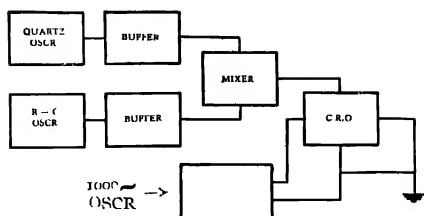


FIG. 4

Checking stability of R-C oscillator

was in turn compared with a valve-maintained tuning fork (1,000 cycle) oscillator. The observed stability was found to be sufficiently good for making quantitative studies in frequency modulation.

VARIATION OF OSCILLATOR FREQUENCY WITH MODULATOR GRID VOLTAGE

One of the oscillator valves was now shunted by a triode modulator as explained before and shown in Fig. 2. The load resistance of this valve was increased from r_1 to r'_1 so that under average grid bias on modulator the equivalent resistance formed by r'_1 and modulator anode impedance R_a in parallel is equal to r_1 . The beat frequency produced by heterodyning the R-C and quartz-controlled oscillators was then measured by comparison with a beat frequency audio oscillator of good frequency stability.

To start with, a preliminary investigation was made to find out the range of modulator grid bias, if any, over which the variation of frequency was approximately linear. This study revealed that for grid bias greater than 1 volts the variation was more or less linear. The cathode bias developed across r_k (figure 2) was accordingly set for 4 volts and the measurements of frequency for different values of grid voltage were made with all possible accuracy.

With 4.30 volts grids bias (negative) on the modulator the three ganged tuning condenser of the R-C oscillator was carefully adjusted to give a beat note of say 500 cycles/second with R-C oscillator-frequency below that of the quartz controlled one. From a knowledge of the quartz oscillator frequency, that of the R-C oscillator was thus ascertained. This setting of the tuning condenser was kept undisturbed. The modulator grid bias was then slightly increased with consequent decrease of the R-C oscillator frequency. The audio beat frequency accordingly increased and the grid bias carefully adjusted to make this exactly 1000 c/s. This grid bias was recorded and the process repeated for higher and higher beat frequencies. A typical set of results is shown in Table I and also plotted in Fig. 5.

TABLE I

Modulator grid voltage V_g (volts, negative)	Oscillator frequency f (kc/s)	Modulator grid voltage V_g (volts, negative)	Oscillator frequency f (kc/s)
4.30	999.5	5.35	995.5
4.47	999.0	5.45	995.0
4.60	998.5	5.60	994.5
4.75	998.0	5.70	994.0
4.87	997.5	5.82	993.5
5.00	997.0	5.95	993.0
5.10	996.5	6.05	992.5
5.20	996.0	6.15	992.0

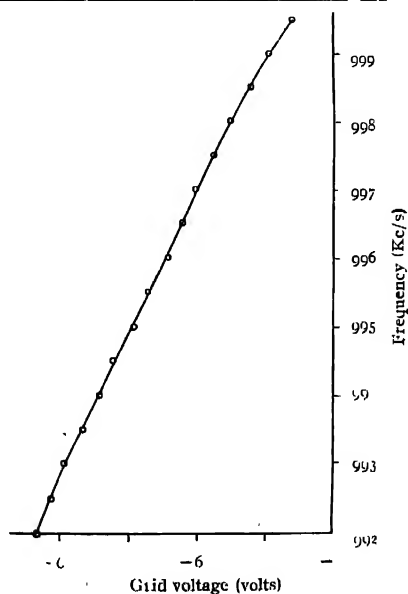


FIG. 5
Frequency—modulator grid voltage

From the plot in Fig. 5 it is obvious that R-C oscillator frequency is practically a linear function of modulator grid bias over the range $V_g = -4.75$ to $V_g = -6.0$ volts. Within this range the variation in frequency is 5.25 kc/s. It will be noted that the standard practice of wide-band frequency modulation is to have a frequency variation of ± 75 kc/s over an average carrier of, say, 50 Mc/s. This would require a frequency deviation of ± 1.5 kc/s over a one-megacycle carrier. In the plot of Fig. 5 there is a total deviation of 5.25 kc/s over the linear regime and hence if the modulator is worked with a static bias of -5.4 volts we can easily get faithful frequency modulation suitable for wide-band system. The modulating and frequency voltage is to be inserted in series with the D-C. grid bias and the resulting variation in R_g of modulator will produce a deviation of carrier frequency proportional to the amplitude of the modulating voltage.

Within the linear portion the variation of f with V_g may be represented by the equation

$$f = K(1 + mV_g) \quad (10)$$

In the particular plot under consideration,

$$\left. \begin{aligned} K &= 1.02 \times 10^6 \\ m &= 4.18 \times 10^{-1} \end{aligned} \right\} \quad \dots (11)$$

AMPLITUDE MODULATION ASSOCIATED WITH FREQUENCY MODULATION

Frequency modulation being produced by varying the effective anode load of one of the oscillator valves will automatically involve amplitude modulation. It must be remembered however, that the percentage change in frequency is very small. For example, wide-band frequency modulation requiring a deviation of ± 75 kc/s over an average carrier frequency of 50 Mc/s involves a frequency change of 0.0015%. This would require a very much smaller percentage change in r and hence the degree of amplitude modulation will also be negligibly small. A typical set of data is shown in Table II and plotted in Fig. 6.

TABLE II

f (kc/s)	992	993	994	995	996	997	μ_0
Output (volts)	1.400	1.390	1.383	1.380	1.370	1.365	1.360

VARIATION OF R_v WITH V_g OF MODULATOR

From the linearity of modulation it is obvious that over the range of grid voltage between -4.75 and -6.0 volts, the anode impedance of the modulator follows the relation (11). It was therefore considered desirable to make an experimental study of the variation of R_v with V_g . Table III gives the results of a typical set of observations and the plot is shown in Fig. 7.

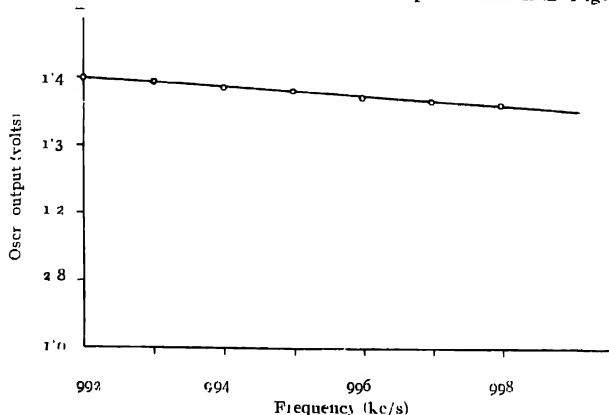


FIG. 6

Oscillator output—Frequency

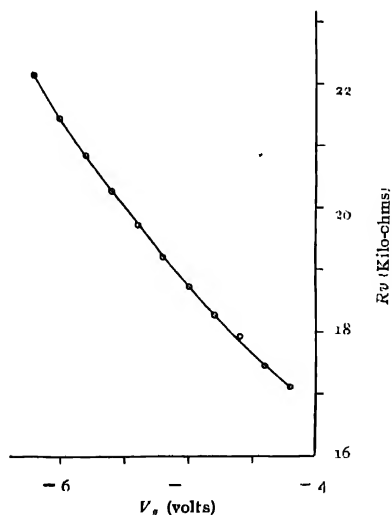


FIG. 7

Modulator impedance—Grid voltage

TABLE III

V_g (volts, -ve)	4.2	4.4	4.6	4.8	5.0	5.2	5.4	5.6	5.8	6.0	6.2
R_i (kilo-ohms)	17.10	17.45	17.85	18.25	18.69	19.18	19.69	20.23	20.80	21.40	22.11

Assuming R_i to vary according to (11), the constants A , B and C are found to be

$$\left. \begin{aligned} A &= 8.8 \times 10^{-2} \\ B &= 7.0 \times 10^{-5} \\ C &= 2.5 \times 10^{-5} \end{aligned} \right\} \dots (15)$$

within the grid voltage range from -5 to -6 volts. From the values in (15) it will be noted that

$$B/C = 280 \dots (16)$$

According to equation (13), $B/C = 2/m$. But this experimental value of B/C is not very close to the value of $2/m$ as obtained from (14). In this connection, it must be remembered that since the quantity C is very small, a slight error in measuring R_i may cause large changes in the value of C , making it even negative. The agreement between the observed values of B/C and $2/m$ is, therefore, sufficiently good for all practical purposes.

It may be noted that from the point of view of frequency stability it is better to work on that part of R_i vs. V_g characteristic (provided it satisfies the condition of fidelity), or with such valves, for which R_i changes slowly with V_g . In that case, slight changes in V_g will not appreciably alter the generated frequency.

STABILITY OF CENTRAL CARRIER FREQUENCY

It has been pointed out before that with proper regulation of the voltage to the different electrodes of the oscillator valves, the frequency stability obtained is sufficiently good for making quantitative observations on frequency modulation. If, however, we remember that to get the final radiation frequency of the order of 50 megacycles/sec, the R-C oscillator frequency is to be multiplied many times it is obvious that the stability of the R-C oscillator must be of a very high order.

In a previous communication by Rakshit and Bhattacharyya (1946) it was pointed out that the three-phase R-C oscillator can easily be controlled by a quartz crystal used as a connecting link between the anode of any one stage and the grid of the succeeding one. This method is quite simple but is applicable only when quartz-controlled oscillations at a fixed frequency are needed. It is not suitable for the present case where frequency modulation is wanted. A method very similar to the automatic frequency control system in superheterodyne reception has, however, been found to work satisfactorily.

EXPERIMENTAL ARRANGEMENT

The schematic arrangement of the control system is shown in Fig. 8. The R-C oscillator output, via buffer amplifier, is applied to the signal grid of the mixer valve and the crystal oscillator output similarly applied to the

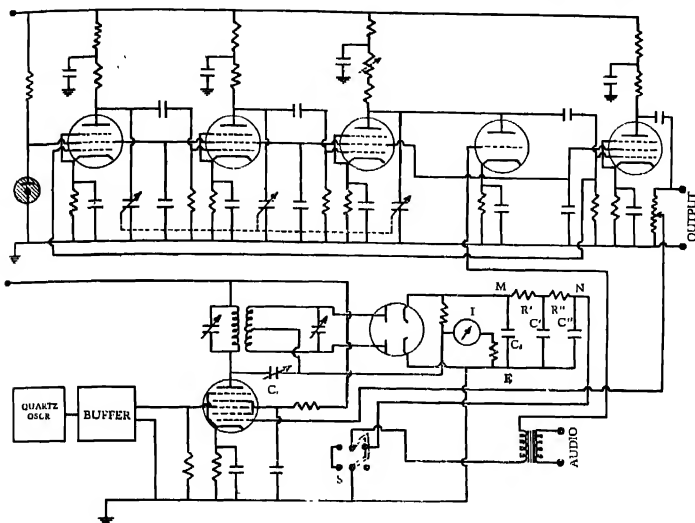


FIG. 8

Complete oscillator with stabilised central carrier

oscillator grid. The two tuned circuits on the anode of the mixer are separately tuned to a pre-determined frequency f_1 and are sufficiently loosely coupled so that the tuning of one does not appreciably affect the other. The crystal oscillator has a frequency of 1,000 kc/s and the R-C oscillator adjusted to 1,440 kc/s ($f_1 = 440$ kc/s) so that the difference frequency f_1 is applied to the phase discriminator as shown. The function of the discriminator is to distinguish between signals which are (i) above and (ii) below the proper frequency. When the R-C oscillator frequency is exactly 1,440 kc/s, i.e. the difference frequency is the same as the resonant frequency of the two tuned circuits, there is no D.C. voltage across the points marked *ME*. With zero voltage across *ME* the grid bias on modulator is such that R-C oscillator frequency is exactly 1,440 kc/s and under this condition the discriminator circuit has no effect upon the oscillator. If, however, the R-C oscillator frequency drifts from 1,440 kc/s the difference frequency accordingly changes and a D.C. voltage is developed across *ME* having its polarity dependent upon the nature of the drift. It is so arranged that with decrease of R-C oscillator frequency the voltage of *M* becomes positive with respect to *E* so that

R_o of modulator decreases and thereby tends to increase, and hence stabilise, the R-C oscillator frequency. Similarly, for increase of R-C oscillator frequency above the present value (1440 kc/s).

To start with, both the R-C and the quartz oscillators were disconnected and only a signal generator set for 440 kc/s applied to the signal grid of the mixer. The coupling condenser C_c was also disconnected and the two tuned circuits on the mixer anode were separately tuned to 440 kc/s, the resonance condition being indicated by the microammeter I . A sensitive D.C. valve voltmeter was connected across ME and suitable adjustments was made to see that under resonant condition no difference of potential existed between M and E . The coupling condenser C_c was then connected and the tuning of primary readjusted to restore resonance. On changing the signal generator frequency above and below 440 kc/s, the voltmeter across ME indicated voltages of opposite polarity and with proper adjustment these voltages were equal in magnitude for equal frequency deviations above and below 440 kc/s. As explained before, M has to be positive with respect to E for decrease of R-C frequency and vice versa. If instead of this it is found that for any particular set of connections M becomes negative with respect to E , E is to be connected to the modulator and M is to be earthed. With variation of C_c and the mutual inductance between the primary and the secondary the sensitivity of the arrangement could also be controlled.

The signal generator was now disconnected and the R-C and quartz oscillators connected as shown. The tuning condenser of the R-C oscillator was carefully adjusted, with modulator grid bias set for -5.4 volts as required for faithful modulation, so that the generated frequency was exactly 1440 kc/s as shown by zero reading of the D.C. voltmeter across ME . The R-C and quartz oscillator voltages as applied to the mixer were next adjusted to get the desired sensitivity in D.C. voltage output across ME for deviations of R-C oscillator frequency from 1440 kc/s.

To check the improvement in frequency stability attained with the incorporation of the discriminator, the points M and E were connected to the modulator through a double-throw switch S as shown in Fig. 8. When S was thrown to the left the discriminator output was not applied to the modulator and the D.C. voltmeter across ME occasionally showed perceptible fluctuations indicating variations of R-C oscillator frequency. When S was thrown to the right, there was absolutely no fluctuation in the reading of the voltmeter indicating greater frequency stability. The functions of the combinations $R'C'$ and $R''C''$ in the discriminator output circuit are to allow only the D.C. voltage output of discriminator to be applied to modulator.

From the nature of the arrangement shown in Fig. 8 it will be realised that the system maintains a stable central carrier and there is no change in voltage across NE even when modulating audiofrequency voltage is applied to the modulator. The discriminator is effective in eliminating frequency

Method of Producing Wide-band, Frequency Modulation 221

drifts or scintillations of long periods and the normal desirable modulations are not in any way affected. The stabilising system with discriminator cannot obviously be used for making observations on variation of oscillator frequency with modulator D.C. grid bias as depicted in Fig. 5.

DISTORTION PRODUCED IN THE SYSTEM

It has been pointed out in a previous communication by Rakshit and Bhattacharyya (1946) on the three-phase R-C oscillator that harmonic distortion of the unmodulated carrier can be kept low by maintaining three-phase symmetry. For introducing frequency modulation asymmetry has been deliberately adopted with resulting increase in harmonic distortion. But by adjusting the anode load resistance of the modulated stage in the three-phase system, the symmetry for the unmodulated condition can be maintained and hence harmonic distortion kept low. In any case, if the overall gain is the minimum required for maintenance of stable oscillations, the harmonic distortion is quite small although there might be slight asymmetry.

The presence of the modulator introduces other sources of distortion which are of interest. The modulator valve is essentially a non-linear element, its anode impedance varying with H.T. voltage used. Since the oscillator voltage is applied across the modulator, its impedance will vary over one period of the radio frequency oscillation and this is likely to produce some distortion. If the r.f. voltage on the modulator be not large, the distortion due to this cause will be very low.

It should also be noted that the modulating voltage on the grid of modulator will naturally be present on its anode and hence the frequency modulated output will have the modulating voltage superimposed upon it. This can easily be removed by using a high-pass filter of suitable design.

The frequency deviation required for wide-band modulation on a 1440 kc/s carrier being about ± 2.2 kc/s it is obvious that if the discriminator has a pull-in width of about 6 kc/s and the capacity C_d across the diode load (Fig. 8) has a value suitable for usual second detection, there will be audio output across C_d when the R-C oscillator will be frequency modulated by means of an audio signal. For sinusoidal modulating voltage, faithful modulation would give—assuming ideal discriminator characteristics—sinusoidal audio voltage across C_d . Preliminary observations have already been made with good results and further waveform studies are in progress.

Observations on frequency deviations resulting from modulation are also in progress.

CONCLUSION

The method of producing wide-band frequency modulation as described in this paper is very simple and the preliminary results, as reported, are

quite encouraging. The stability of the central carrier is no doubt dependent upon that of the phase discrimination assembly but is practically the same as the stability of the associated quartz-controlled oscillator. The overall stability attained is quite satisfactory for all practical purposes.

It must be pointed out that a large degree of frequency multiplication would be necessary to get the usual carrier of about 45 Mc/s starting from, say, a 1.5 Mc/s carrier. It was reported earlier (Rakshit and Bhattacharyya, 1946) that a carrier frequency as high as 9 Mc/s can be obtained by using 6SK7 valves as oscillators with 1,500 ohm load resistances and having no external C_1 's across them. The inter-electrode and stray capacitances alone then control the frequency and the stability is poor. To attain a high carrier frequency with good stability, it is desirable to have external tuning capacitances much greater than the inter-electrode and stray capacitances and to use high- μ pentodes requiring small anode load resistances for the maintenance of oscillations. Quantitative observations along this line and also on the different aspects of producing faithful frequency modulation are in progress.

ACKNOWLEDGMENT

The experimental observations reported in this paper were carried out in the Kanodia Electrical Communication Engineering Laboratory, Department of Applied Physics, University of Calcutta, when the senior author was a lecturer in the department.

Department of Physics and Communication
BENGAL ENGINEERING COLLEGE
SIBPORE, CALCUTTA

REFERENCES

- Rakshit, H., and Bhattacharyya, K K , 1946, *Ind. Jour. Phys* , 20, 171.
Rakshit, H , and Sarkar, N.L , 1949, *Nature* 163, 572.

GENERALIZED IMPEDANCE CIRCLE DIAGRAMS IN THE ANALYSIS OF COUPLED NETWORKS

By CHANDRASIKHAR GHOSH

(Received for publication, March 11, 1950)

ABSTRACT. The use of circle diagrams in the analysis of circuit behaviour in electrical engineering problems is well-known. When applied to the determination of circuit behaviour with reference to variation in the impedance of circuits, the impedance circle diagram is very useful in the solution of network problems where mutual impedances are involved. The analysis of circuit behaviour by considering the complete circuit as an equivalent T-section leads to a very useful way of visualizing the performance with the help of circle diagrams. In this paper the form of relation leading to circular loci for the impedance is developed and a practical method of developing the impedance circle diagrams for a representative T-section under different conditions of variation in the impedance is shown.

In electrical engineering, steady-state impedances, admittances, voltages and currents in simple series and parallel circuits are studied from the analytical point of view. Graphical representations, in the form of vector diagrams are of considerable help in the visualization of the analytical expressions.

In the simple plots of steady-state time vectors, the locus of the terminal of any individual rotating vector is a circle concentric with the origin and the angular displacement of the vector at any instant is proportional to the independent variable, time. The use of this vector diagram can be extended to include a range of steady-state conditions by letting a vector sweep out a locus in the complex plane as either a parameter or the frequency is varied. This application differs from the first concept in that the locus is not swept out by a *time* vector. By means of this extended vector diagram, the circuit behaviour can be visualized and quantitatively analyzed not only for a single steady-state condition but also for a range of conditions. This method is especially convenient and practically useful because these loci prove to be circles (or straight lines) in many useful cases. For these reasons such loci or *circle diagrams*, as they are commonly called, are widely used in both the power and the communication fields.

In problems on transmission of power, the entire transmission system, used to connect an electrical generating station with a distant load centre including a long transmission line and transformers at both ends, is usually analyzed as an *l*-loop network with the generating station as one source and the load as an equivalent of a negative source. Such an *l*-loop network with two pairs of terminals, one pair in each of two loops, to which sources

(or loads which, from the point of view of the l -loop network, are treated as sources) can be connected is often called a coupling network.

The coupling network is often rather complex and, in a broad use of the term, may, as mentioned above, contain long transmission lines or even energy-conversion devices, so that between the two pairs of terminals a mechanical, acoustical, or electric-wave link may exist. In the latter cases the equivalent electrical behaviour of the mechanical or other link must be known before the combination of such a link and electric circuits can be treated as a coupling or two-terminal pair network.

Thus considering a two-terminal-pair network, as shown in Fig. 1, the current and voltage relations at the terminals 1-1' and 2'-2 are given by

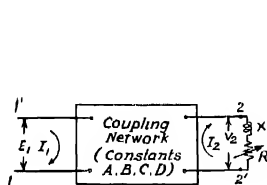


FIG. 1
Coupled net work

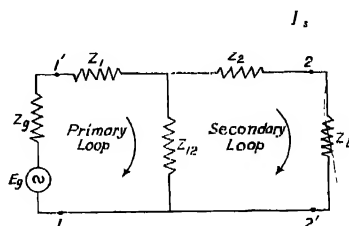


FIG. 2
T-section net work

$$E_1 = Z_{11} I_1 + Z_{12} I_2 \quad \dots (1)$$

$$E_2 = Z_{12} I_1 + Z_{22} I_2$$

where Z_{11} = impedance in loop 1

Z_{22} = impedance in loop 2

Z_{12} = mutual impedance between loops 1 and 2

For power engineering it is usually convenient to express the voltage and current at one end of a two-terminal-pair network in terms of the voltage and current at the other end. Such equations are much used by the power engineer in preference to the equations giving the two voltages in terms of the two currents and *vice versa*.

The equations of the coupling network as used in power circuits are customarily written

$$E_1 = AV_2 + BI_2 \quad \dots (2)$$

$$I_1 = CV_2 + DI_2$$

in which the parameters A , B , C and D are called *general circuit constants*, of which only three are independent. These constants are related to the Z 's in the former equations as follows

$$A = -\frac{Z_{11}}{Z_{12}}; B = -\frac{Z_{22}}{Z_{12}}; C = -\frac{1}{Z_{12}}; D = -\frac{Z_{22}}{Z_{12}}$$

where D_Z is the determinant of Z 's, i.e.

$$D_Z = \begin{vmatrix} Z_{11} & Z_{12} \\ Z_{12} & Z_{22} \end{vmatrix} = Z_{11} Z_{22} - Z_{12}^2$$

Considering now the branch containing the variable resistance R and constant reactance X as the load Z_L , if it is desired to determine the circle diagram of the current I_1 , as the resistance of any other branch is varied over a definite range, then the input impedance

$$Z_{1a} = \frac{E_1}{I_1} = \frac{AV_2 + BI_2}{CV_2 + DI_2}$$

$$= \frac{A\left(\frac{V_2}{I_2}\right) + B}{C\left(\frac{V_2}{I_2}\right) + D} = \frac{AZ_L + B}{CZ_L + D} \quad \dots (3)$$

Since $Z_L = R + jX$, in which R is variable

$$Z_{1a} = \frac{A(R + jX) + B}{C(R + jX) + D}$$

$$= \frac{AR + (jAX) + B}{CR + (jCX) + D} \quad \dots (3a)$$

Similarly, the input admittance

$$Y_{1a} = \frac{CZ_L + D}{AZ_L + B} = \frac{CR + (jCX) + D}{AR + (jAX) + B} \quad \dots (3b)$$

Both these expressions for Z_{1a} and Y_{1a} are in the general form of

$$F(\rho) = \frac{M(\rho) + N}{T(\rho) + U} \quad \dots (4)$$

in which M , N , T and U are complex constants. The locus of $F(\rho)$, as shown by Schumann (1922), is a circle. Hence the input impedance or admittance described by these expressions can be represented by a circular locus in the complex plane.

All such networks involving mutual impedance can be simplified into an equivalent T -section. The circle diagrams used for analytical work in such cases are usually referred to as *impedance circle diagrams*. Such diagrams are very helpful in various problems in connection with network solutions and also in relay work. The use of such diagrams show properties of the original circuit that might be overlooked without their use. As already noted, the impedance circle diagram is adaptable not only to problems in transmission and relaying, but also to problems relating to coupled circuits, electromechanical problems and even to any energy-conversion devices.

Thus taking the general case of a T-section network, shown in Fig. 2, the looking-in impedance, i.e., the impedance as on looking into end 1 is

$$Z_{LI} = Z_1 + \frac{(Z_2 + Z_L)Z_{12}}{Z_2 + Z_L + Z_{12}} \quad (5)$$

Put in a more convenient form

$$\begin{aligned} Z_{LI} &= \left\{ Z_1 + Z_{12} \right\} + \left\{ \frac{(Z_2 + Z_L)Z_{12}}{Z_2 + Z_{12} + Z_L} - Z_{12} \right\} \\ &= \left\{ Z_1 + Z_{12} \right\} - \frac{Z_{12}^2}{Z_2 + Z_{12} + Z_L} \end{aligned} \quad (6)$$

But as shown in Fig. 1, $Z_1 + Z_{12} = Z_{11}$ the total impedance of the primary loop of the T-section, and $Z_2 + Z_{12} + Z_L = Z_{22}$ the total impedance of the secondary loop. Hence we have

$$\begin{aligned} Z_{LI} &= Z_{11} - \frac{Z_{12}^2}{Z_{22}} \\ &= \frac{Z_{11}Z_{22} - Z_{12}^2}{Z_{22}} \end{aligned} \quad \dots \quad (6a)$$

This again is one of the particular forms of the general equation for a circle. The locus of Z_{LI} is therefore a circle under all conditions.

The construction and geometry of the impedance circle diagrams have been discussed by Stewart (1944). The construction of the impedance circle diagrams can, however, be modified to make it more convenient for use in problems concerned with coupled circuits and in relaying. In determining the limits of operation of relays one of the important requirements is to anticipate the possible variation in the looking-in impedance, as viewed by the relay, and thus to be able to provide the proper setting for the relay.

In relay operations the possible variations in the circuit constants to be anticipated are in the value of resistance, reactance and/or power-factor angle. The modified relations for the circles with reference to these conditions are now discussed.

Case I

Take $Z_{22} = \text{constant}$. Further let $\theta_{12} = \text{power factor angle of the mutual impedance}$, and $\theta_{22} = \text{power factor angle of the secondary loop impedance}$

$$\text{Then} \quad Z_{LI} = Z_{11} - \frac{|Z_{12}|^2}{|Z_{22}|} \frac{1}{180^\circ - \theta_{22}} \quad \dots \quad (7)$$

$$= Z_{11} + \frac{|Z_{12}|^2}{|Z_{22}|} \frac{1}{180^\circ + 2\theta_{12} - \theta_{22}} \quad \dots \quad (7a)$$

The locus of Z_{LI} is a circle with the centre at the end point of vector Z_{11} and radius equal to $\left| \frac{Z_{12}^2}{Z_{22}} \right|$, the angle parameter of the vector Z_{LI} starts from zero position at angle $180^\circ + 2\theta_{12}$ and rotates in a negative direction.

Case II

Take $R_{22} = \text{constant}$; θ_{22} varies

$$\begin{aligned} \text{Then } Z_{LI} &= Z_{11} - \left| \frac{Z_{12}^2}{Z_{22}} \right| / \underline{2\theta_{12} - \theta_{22}} \\ &= Z_{11} - \frac{|Z_{12}|^2}{R_{22}} \cdot \frac{R_{22}}{|Z_{22}|} / \underline{2\theta_{12} - \theta_{22}} \end{aligned} \quad \dots (8)$$

$$\text{But } \frac{R_{22}}{|Z_{22}|} = \cos \theta_{22}$$

$$\text{Hence } Z_{LI} = Z_{11} - \frac{|Z_{12}|^2}{R_{22}} \cos \theta_{22} / \underline{2\theta_{12} - \theta_{22}} \quad \dots (8a)$$

$$\begin{aligned} &= Z_{11} - \frac{|Z_{12}|^2}{R_{22}} \cos \theta_{22} [\cos (2\theta_{12} - \theta_{22}) + j \sin (2\theta_{12} - \theta_{22})] \\ &= Z_{11} - \frac{|Z_{12}|^2}{R_{22}} \left[\cos 2\theta_{12} + j \sin 2\theta_{12} \right] + \left[\cos (2\theta_{12} - 2\theta_{22}) + j \sin (2\theta_{12} - 2\theta_{22}) \right] \\ &= Z_{11} - \left[\frac{|Z_{12}|^2}{2R_{22}} / \underline{2\theta_{12}} + \frac{|Z_{12}|^2}{2R_{22}} / \underline{2\theta_{12} - 2\theta_{22}} \right] \\ &= Z_{11} + \frac{|Z_{12}|^2}{2R_{22}} / \underline{180^\circ + 2\theta_{12}} + \frac{|Z_{12}|^2}{2R_{22}} / \underline{180^\circ + 2\theta_{12} - 2\theta_{22}} \end{aligned} \quad \dots (8b)$$

This is again a circle with centre at $Z_{11} + \frac{|Z_{12}|^2}{2R_{22}} / \underline{180^\circ + 2\theta_{12}}$ and radius equal to $\frac{|Z_{12}|^2}{2R_{22}}$, the angle starts from $180^\circ + 2\theta_{12}$.

Case III.

Let $X_{22} = \text{constant}$

$$\begin{aligned} \text{Then } Z_{LI} &= Z_{11} - \frac{|Z_{12}|^2}{|Z_{22}|} / \underline{2\theta_{12} - \theta_{22}} \\ &= Z_{11} - \frac{|Z_{12}|^2}{|X_{22}|} \cdot \frac{|X_{22}|}{|Z_{12}|} / \underline{2\theta_{12} - \theta_{22}} \end{aligned} \quad \dots (9)$$

$$= Z_{11} - \frac{|Z_{12}|^2}{|X_{22}|} \sin \theta_{22} / \underline{2\theta_{12} - \theta_{22}} \quad \dots (9a)$$

$$\begin{aligned}
 &= Z_{11} - \frac{|Z_{12}^2|}{|X_{22}|} [\sin \theta_{22} \cos (2\theta_{12} - \theta_{22}) + j \sin \theta_{22} \sin (2\theta_{12} - \theta_{22})] \\
 &= Z_{11} - \frac{|Z_{12}^2|}{2|X_{22}|} \angle 2\theta_{12} - 90^\circ - \frac{|Z_{12}^2|}{2|X_{22}|} \angle 2\theta_{12} - 2\theta_{22} + 90^\circ \\
 &= Z_{11} + \frac{|Z_{12}^2|}{2|X_{22}|} \angle 2\theta_{12} + 90^\circ + \frac{|Z_{12}^2|}{2|X_{22}|} \angle 2\theta_{12} - 2\theta_{22} + 90^\circ \quad \dots (9b)
 \end{aligned}$$

The locus is a circle the centre of which is at $Z_{11} + \frac{|Z_{12}^2|}{2|X_{22}|} \angle 2\theta_{12} + 90^\circ$ and

radius $\frac{|Z_{12}^2|}{2|X_{22}|}$, the angle starts with zero at $2\theta_{12} + 90^\circ$

Case IV

Let $\theta_{22} = \text{constant}$

Then

$$\begin{aligned}
 Z_{LI} &= Z_{11} - \frac{|Z_{12}^2|}{|Z_{22}|} \angle 2\theta_{12} - \theta_{22} \\
 &= Z_{11} + \frac{|Z_{12}^2|}{|Z_{22}|} \angle 2\theta_{12} - \theta_{22} + 180^\circ \quad \dots (10)
 \end{aligned}$$

Thus the locus is a circle with centre at infinity and radius infinite, i.e., a straight line inclined to the R -axis at an angle $2\theta_{12} + 180^\circ$, and passing through Z_{11} when $Z_{22} = \theta$, i.e. open circuit.

Construction of Impedance Circle Diagrams for the above cases.

In all the above cases, the second term in the expression for Z_{LI} is of the form a^2/b , where a stands for Z_{12} in all the cases while b stands for Z_{22} in cases I and IV, for $2R_{22}$ in case II, and for $2X_{22}$ in case III. Hence, the

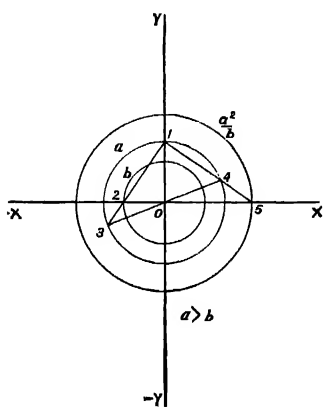


FIG. 3a

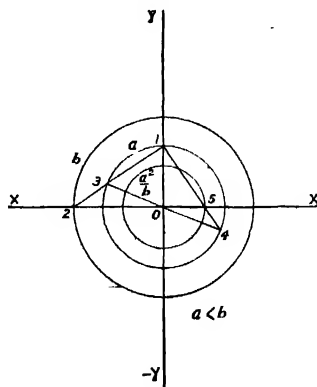


FIG. 3b

Determination of a^2/b

starting point in obtaining the impedance circle diagram is determining the magnitude of the expression for the radius. A very convenient graphical method of determining the magnitude of such an expression is indicated in Figs. 3a and 3b. Fig. 3a is for the case when $a > b$ and Fig. 3b is for the case when $a < b$. The successive steps are: join 1 on 'a' circle to get the point 3 on the 'a' circle; join 3 and the origin of co-ordinates and produce it to obtain point 4 on the 'a' circle. Join 1 and 4 and obtain the point 5 on the X-axis. Then 0-5 is the measure of a^2/b , the radius required.

On the normal rectangular co-ordinate paper first plot Z_{11} and draw a circle with the origin as centre and radius equal to a^2/b . Then in terms of the arc on the a^2/b circle, the angle $2\theta_{12} + 180^\circ$ in cases I and II, or the angle $2\theta_{12} + 90^\circ$ in case III is measured, the line through this angle gives the direction of the datum line. The datum line is next drawn parallel to this line through the end point of vector Z_{11} .

Case I.

The circle of radius a^2/b , i.e. $\frac{|Z_{12}|^2}{|Z_{22}|}$ drawn with the end point of vector

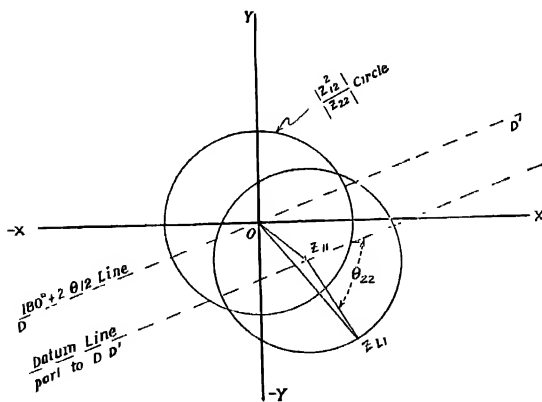


FIG. 4

Case I $Z_{22} = \text{constant}$

Z_{11} as centre, is the looking-in impedance circle for case I. θ_{22} is measured clockwise from the datum line, to obtain the value of Z_{11} . This is shown in Fig. 4.

Cases II and III

The point of intersection of the datum line through the end point of vector Z_{11} and the second a^2/b circle drawn with Z_{11} as centre, becomes

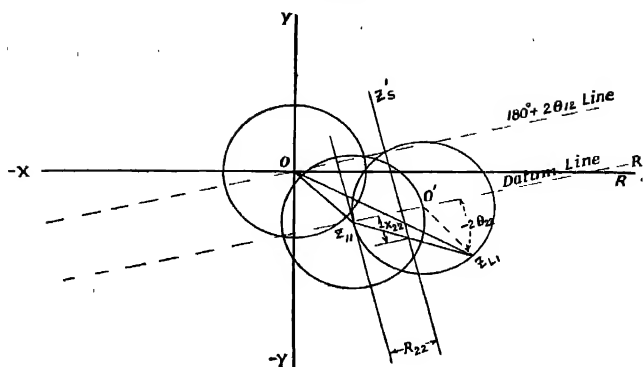


FIG. 5
Case II. $K_{22} = \text{constant}$

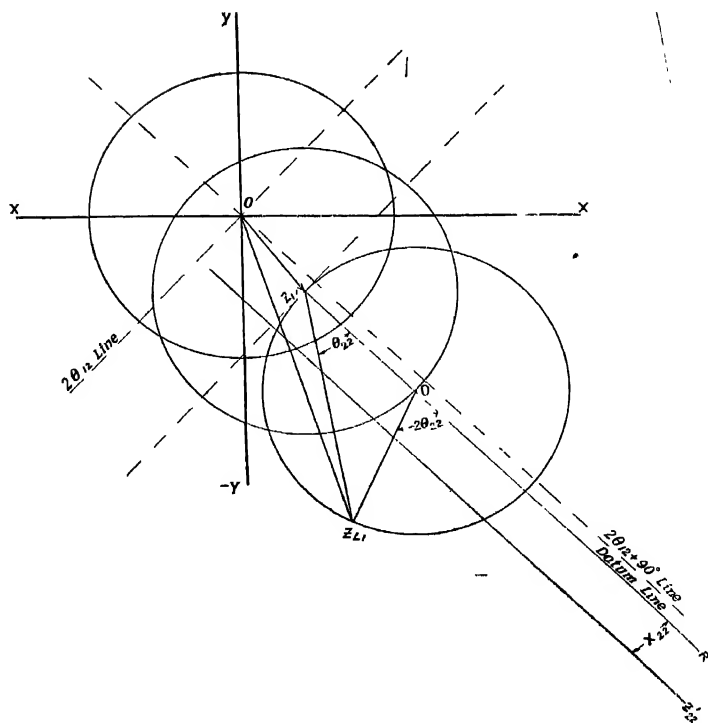


FIG. 6
Case III. $X_{22} = \text{constant}$

the centre of the required impedance circle Z_{LI} . With the same datum line as the zero angle line, the angle $2\theta_{22}$ is measured in the negative (*i.e.* clockwise) direction on the third circle. This point on the third circle, thus obtained, locates the end of the vector for the looking-in impedance Z_{LI} . These are shown in Figs. 5 and 6.

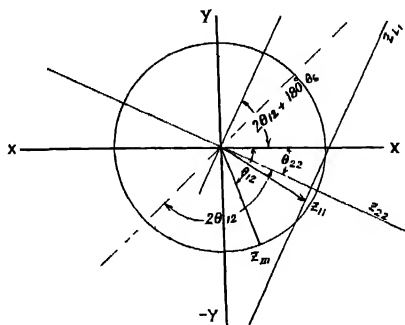


FIG. 7
Case IV. $\theta_{22} = \text{constant}$

The end point of the vector Z_{LI} can also be located by plotting the locus of Z_{22} in the new co-ordinates, joining Z_{11} with the proper point on the Z_{22} locus and producing this line to meet the third circle. This meeting point with the third circle locates the end point of the vector Z_{LI} . This is also shown in the figures.

Case II'

As already discussed above, the locus of Z_{LI} , in the event θ_{22} is a constant, is a straight line, that is, a circle with infinite radius. This is shown in Fig. 7.

Further analytic work on the above line is being carried on with different types of actual circuit conditions. These will be communicated later.

DEPARTMENT OF POWER ENGINEERING
INDIAN INSTITUTE OF SCIENCE
BANGALORE

REFERENCES

- Schumann, W. O., 1922, *Arch. f. Elek.*, 11, 140-46.
Stewart, H. L., 1944, *General Electric Review*, 47, 20-25.

TOMORROW'S INSTRUMENTS TODAY

RAJ-DERK-AR & CO.

COMMISSARIAT BUILDING

HORNBY ROAD

FORT

BOMBAY

OFFERS

FROM STOCK

GLASS METAL DIFFUSION PUMPS, METAL BOOSTER
PUMPS, OILS AMOILS OCTOILS OCTOIL,
BUTYL SABACATE

MANUFACTURED

By

DISTILLATION PRODUCTS
(U. S. A.)

SPENCER MICROSCOPE

CENCO HIGHVACS

BESLER EPIDIASCOPE

COMPLETE WITH FILM STRIP ARRANGEMENTS

Telephone 27304
2 Lines

Telegrams
TECHLAB

The following special publications of the Indian Association for the Cultivation of Science, 210, Bowbazar Street, Calcutta, are available at the prices shown against each of them :—

Subject	Author	Price Rs. A. P.
Methods in Scientific Research	Sir E. J. Russell	0 6 0
The Origin of the Planets	Sir James H. Jeans	0 6 0
Separation of Isotopes	Prof. F. W. Aston	0 6 0
Garnets and their Role in Nature	Sir Lewis L. Fermor	2 8 0
(1) The Royal Botanic Gardens, Kew.	Sir Arthur Hill	1 8 0
(2) Studies in the Germination of Seeds.		
Interatomic Forces	Prof. J. E. Lennard-Jones	1 8 0
The Educational Aims and Practices of the California Institute of Technology.	R. A. Millikan	0 6 0
Active Nitrogen A New Theory.	Prof. S. K. Mitra	2 8 0
Theory of Valency and the Struc- ture of Chemical Compounds.	Prof. P. Ray	3 0 0
Petroleum Resources of India	... D. N. Wadia	2 8 0
The Role of the Electrical [Double layer in the Electro Chemistry of Colloids.	... J. N. Mukherjee	Rs. 12 0

A discount of 25% is allowed to Booksellers and Agents.

RATES OF ADVERTISEMENTS

Third page of cover	Rs. 32, full page
do. do.	„ 20, half page
do. do.	„ 12, quarter page
Other pages	„ 25, full page
do.	„ 16, half page
do.	„ 10, quarter page

15% Commissions are allowed to *bonafide* publicity agents securing orders for advertisements.

CONTENTS

	PAGE
26. A note on Weyl's Inequality—By V. S. Nanda	181
27. Multiplet Separation Factors and Γ -sum Rule—By S. Sengupta	185
28. On the Raman Spectra and Heat Capacity of Benzene at Low Temperatures —By S. C. Sirkar and A. K. Ray	189
29. Fading of Short Wireless Waves due to the Interference between Magneto- Ionic Components—By S. N. Mitra	197
30. A Simple Method of Producing Wide-band Frequency Modulation—By H. Rakshit and N. L. Sarkar	207
31. Generalized Impedance Circle-diagrams in the Analysis of Coupled Net- works—By Chandrasekhar Ghosh	223

PRINTED BY SIBENDRANATH KANJILAL, SUPERINTENDENT (OFFG.), CALCUTTA UNIVERSITY
PRESS, 48, HAZRA ROAD, BALLYGUNGE, CALCUTTA AND PUBLISHED BY THE
REGISTRAR, INDIAN ASSOCIATION FOR THE CULTIVATION OF SCIENCE,
210, Bowbazar Street, Calcutta.

Vol. 24 **INDIAN JOURNAL OF PHYSICS** **No. 6**

(Published in collaboration with the Indian Physical Society)

AND

[Vol. 33 **PROCEEDINGS** **No. 6**

OF THE

**INDIAN ASSOCIATION FOR THE
CULTIVATION OF SCIENCE**

JUNE, 1950

**PUBLISHED BY THE
INDIAN ASSOCIATION FOR THE CULTIVATION OF SCIENCE
210, Bowbazar Street, Calcutta**

NOTICE

TO INTENDING AUTHORS

Manuscripts for publication should be sent to Mr. A. N. Banerjee, Editor, 210, Bowbazar Street, Calcutta.

The manuscript of each paper should contain in the beginning a short abstract of the paper.

All references to published papers should be given in the text by quoting the surname of the authors followed by the year of publication within braces, e.g., Sen (1942). The actual references should be given in a list at the end of the paper according to the following specimen :

Sen, B. K., 1942, *Ind. J. Phys.*, 18, 339.

The references should be arranged alphabetically in the list.

All diagrams should be drawn on thick white paper in Indian ink, and letters and numbers in the diagrams should be written in pencil.

BOARD OF EDITORS

K. BANERJEE	S. K. MITRA
D. M. BOSE	P. RAY
S. N. BOSE	M. N. SAHA
D. S. KOTHARI	S. C. SIKKAR.

Secretary

EDITORIAL COLLABORATORS

DR. R. K. ASUNDI, M.A., PH.D.
PROF. H. J. BHABHA, PH.D., F.R.S.
DR. P. K. KICHLU, D.Sc.
PROF. K. S. KRISHNAN, D.Sc., F.R.S.
PROF. G. P. DUBEY, M.Sc.
DR. K. RANGADHAMA RAO, M.A., D.Sc.
DR. N. D. SARWATTEY, D.Sc.
DR. N. N. DASGUPTA, M.Sc., PH.D.
PROF. N. R. SEN, D.Sc., F.N.I.
PROF. P. C. MAHANTI, D.Sc., F.N.I.
PROF. S. R. PALIT, D.Sc.,
DR. H. RAKSHIT, D.Sc.,
PROF. K. R. DIXIT, PH.D.
DR. VIKRAM A. SARABHAI, M.A., PH.D.

ASSISTANT EDITOR

MR. A. N. BANERJEE, M.Sc.

Annual Subscription—

Inland Rs. 20
Foreign £ 2

B. E. C. AND CRYSTALLINE STRUCTURE OF SILICATE MINERALS RELATED TO SOILS AND CLAYS*

BY S. K. MUKHERJEE AND A. K. GANGULY

(Received for publication, April, 3, 1950)

ABSTRACT. An approach to the problem of ion-exchange in silicate minerals related to soils and clays from the stand point of their crystalline character is presented.

Clay fractions of soils exhibit base exchange capacity in an enhanced degree (Atterberg, 1912). The clay fractions were often regarded as "absorption complexes" or mixed gels of silica, alumina, iron oxides, water, etc. (Van Bemmelen, 1888; Wiegner, 1924; Mattson, 1930). Mattson (1930-37) from a study of synthetic co-precipitates formed from solutions under varying conditions comparable with the expected conditions which give rise to the absorption complex of soils, tried to interpret the behaviour of soil colloids without reference to their possible crystalline character. The adaptability and handy nature of the "absorption complex" theory held in the back ground the crystalline character of soil colloid constituents. Detailed informations of the crystals structure of clay minerals are now available through X-ray (Hendricks and Fry, 1930), optical (Marshall, 1935), thermal (Grim & Rowland, 1942) and dehydration studies (Kalley *et al*, 1936; Hendricks *et al*, 1940). Four groups of clay minerals have been identified in soil colloids represented by kaolinite, montmorillonites, hydrous mica or illite and attapulgite. Of these again the first two are more abundant than the rest. Grim (1942) states—"at the present time there are a few students of clays who would dispute the premises that clays are composed of flake shaped particles." Still there does exist considerable amount of confusion in our understanding of the case exchange process because of our insufficient knowledge about the chemical, physical and as well the electrical nature of the surface of clay micro-particles. Wiegner's (1935) idea of meta-structure can still be invoked with advantage to explain some of the very important properties in base exchange systems.

The elucidation of the general scheme of structure of silicate is due to Bragg (1929) and Pauling (1930). Pauling (*loc. cit.*) laid the foundation of the crystal structure of clay minerals with three fundamental units of structure.

(1) The hydrargillite $\text{Al}(\text{OH})_3$ layer lattice structure constituted of octahedra each consisting of 6 OH^1 ions at the corners grouped about an

* Communicated by Prof. P. B. Sarkar.

Al^{+3} ion at the centre. Each octahedron in the layer shares three edges and the $(OH)^1$ ions are held by two bonds of half the strength. The $(OH)^1$ ions on the surface of such a layer are situated at the corners of an equilateral triangle of sides 2.9 \AA . In such a layer the 'electrostatic valence rule' of Pauling (1929) is satisfied. The H of OH ion of the hydrargillite is thus expected to possess a weak acid function. The pseudo-hexagonal hydrargillite layer has $a=8.7 \text{ \AA}$, $b=5.09 \text{ \AA}$. (Fig 1 (a)) and the thickness of such a layer calculates to 2.37 \AA .

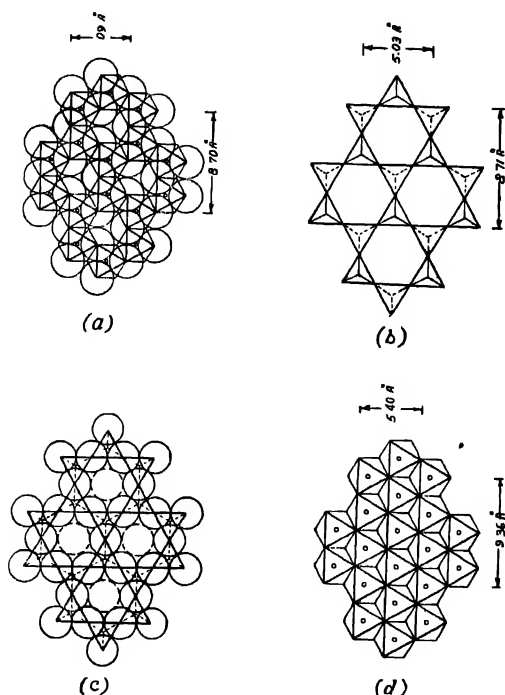


FIG. 1

(After Pauling)

(a) A hydrargillite layer of octahedra.

(b) A tetrahedral layer from β -cristoballite or β -tridymite. A silicon ion is located at centre of each tetrahedron and an oxygen atom at each corner,

(c) A tetrahedral layer in which all the tetrahedra point in the same direction

(d) A complete layer of octahedra (Brucite layer).

(2) The second fundamental unit is β -tridymite or β -cristoballite. X-ray diffraction patterns of different forms of quartz (Bragg, Gibbs, 1925) reveal that SiO_2 mineral lattice is best represented by four oxygen atoms

occupying the corners of a tetrahedra at the centre of which is an atom of Si. The corners of the tetrahedra are joined with the corners of four other similar tetrahedra. β -cristobalite or β -tridymite can be considered to have a layer-lattice type of structure (Pauling, 1930) in which the tetrahedra point in the opposite direction (Fig. 1b). On each side of such a layer is superimposed another similar layer as the mirror image. It is to be noted that in such a layer lattice (assuming perfect development of the lattice) the terminal tetrahedra on the surfaces have alternately one unshared corner. The hexagonal layer of silicon tetrahedra has the dimensions, $a = 8.71 \text{ \AA}$; $b = 5.03 \text{ \AA}$ which agree closely with those of the hydrargillite layer. These unshared corners are not electrically neutral. Each oxygen atom in SiO_4 lattice is common to two Si atoms only and held to each of them by one unit of the so called primary valency. Thus, there is left no valence force at these shared corners. The oxygens in the layers are situated at the corners of an equilateral triangle. The distance between oxygen atoms of a tetrahedron is between 2.5 and 2.6 \AA ; and it is found to be nearly the same for the oxygen around silicon in all silicates (Bragg, 1929).

Bragg (1929) suggests that in silicates and silica the Si-O linkage is only in the partly ionised state. Pauling (1929, 1945), assumes that Si-O, though not of the extreme ionic type, is largely so. The O-O distance in the oxygen plane of the layer lattice is 5.03 \AA at the corners of an equilateral triangle.

In a single layer of SiO_4 lattice the electrostatic valence rule can be satisfied if at the unshared corners H atoms are incorporated to give rise to (OH) ions. The composition of such a layer then turns out to be $\text{Si}_2\text{O}_3(\text{OH})_2$ (or if we have a single tetrahedra of Si, the composition becomes $\text{Si}(\text{OH})_4$ which is in accord with the valence rule) The compounds like $\text{H}_2\text{Si}_2\text{O}_5$, $\text{Si}(\text{OH})_4$ are expected to be weak acids (Pauling, 1945). Or, again, if we consider only the surface of a crystal of any size of β -tridymite or of β -cristobalite the unshared corners at the surface have each one unit of negative valency to be neutralised, which can be achieved by the incorporation of an atom of hydrogen or equivalent cation on each of the so called unshared tetrahedral corners occurring on the surface. In such a case also some sort of acidity at the surface can be visualised.

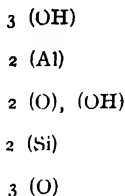
Another type of the hexagonal layer having the same dimensions can be obtained by pointing all the tetrahedra in the same direction. The basal oxygens of such a layer have their valencies satisfied, but the oxygen ions at the unshared corners have one of their valencies unsatisfied. The corners now give rise to a layer of O-ions arranged round the corners of a regular hexagon of sides 2.9 \AA (Fig. 1c) and the thickness of such a layer calculates to 2.05 \AA .

(3) The third fundamental unit is the brucite layer of $\text{Mg}(\text{OH})_2$, composed of octahedra, each consisting of 6 OH⁻ ions at the corners grouped

about a Mg^{+2} ion at the centre. Each octahedron in the layer shares six edges (Fig. 1d). The OH^1 ions are held by three bonds of one third strength. The OH^1 ions on the surface of such a layer are situated at the corners of an equilateral triangle of sides 3.12 \AA . In such a layer also the electrostatic valence rule is satisfied. The brucite layer has $a=9.36 \text{ \AA}$ and $b=5.4 \text{ \AA}$, and the thickness of such a layer calculates to 2.55 \AA .

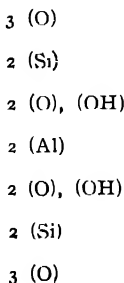
The structure of clay and other minerals have been built up by suitable and rational superposition of the above three fundamental units (viz., Figs. 1a, 1c, 1d)

It will be seen that a layer of unshared tetrahedral corners (cf. Fig. 1c) fits exactly with the pseudohexagonal layer of hydrargillite. On superimposing two such layers (OH^1 ions at the corners of the hexagon of the hydrargillite layer being eliminated we get an unsymmetrical layer lattice where the electrostatic valence rule holds. In the layer of fusion there occurs one OH^1 ion at the centre of each oxygen hexagon. The opposite faces of the newly formed layer are different. On the face there exists one of the OH surfaces of the original hydrargillite layer and on the other the basal oxygens of the tetrahedral layer. The stacking of the layer can be represented as :



i.e., $\text{Al}_2\text{Si}_2\text{O}_6(\text{OH})_4$. This is also the formula for the mineral kaolinite. The thickness of such a layer taking oxygen ion diameter to be 2.8 calculates to $(2.37 + 2.05 + 2.8) = 7.22 \text{ \AA}$.

If layers of silicon tetrahedra (Fig 1c) are condensed on both sides of a hydrargillite layer a symmetrical layer lattice packet is formed having the arrangement of the units as follows :



i.e., $\text{Al}_2\text{Si}_4\text{O}_{10}(\text{OH})_2$ which is the formula for pyrophyllite. The thickness becomes then to be equal to $(2.05 + 2.37 + 2.05 + 2.8) = 9.27 \text{ \AA}$

Now the opposite faces of the new layer are similar, on both sides of which there are the basal oxygens of the tetrahedral layers.

The H of OH^+ ions at the surface of the kaolinite are expected to have some acid function like the OH of the hydrargillite. In the second case, the layers have no ionising group at the boundary faces. The faces are neutral and therefore only stray weak electrical forces might be present there.

The brucite layer does not fit exactly with the unshared corners of the silicon tetrahedral (Figs. 1c and 1d) layer. By the fusion of two tetrahedral layers on both sides of the brucite layer a symmetrical layer lattice having the following arrangement results :

- 3 (O)
- 2 (Si)
- 2 (O), (OH)
- 3 (Mg)
- 2 (O), (OH)
- 2 (Si)
- 3 (O)

It has the composition of talc, i.e., $\text{Mg}_3\text{Si}_4\text{O}_{10}(\text{OH})_2$. But the fit in this case is somewhat strained and Pauling (1930) suggested that it would be too great for an unsymmetrical fusion as in the first case. The thickness of such a layer becomes then equal to $(2.05 + 2.55 + 2.05 + 2.8) = 9.45 \text{ \AA}$

In this symmetrical lattice also no ionising groups are present on the surface, making it neutral and hence only stray weak electrical forces are possible to exist.

KAOLINITE

The unsymmetrical layer lattice structure of kaolinite proposed by Pauling (1930) has been completely verified by Gruner (1932) $a = 5.138 \text{ \AA}$, $b = 8.9 \text{ \AA}$, $c = 14.506 \text{ \AA}$, $\beta = 100^\circ 12'$. Each layer is a neutral sheet stacked one above the other such that the base of the tetrahedral layer of one sheet faces OH layer of another sheet and is held to one another by some sort of OH..O binding. The neutral sheets are thus firmly held (i.e., not merely arranged by stacking of neutral sheets) because of attraction between the adjacent O and OH faces (Grim, 1942). The inter-sheet space becomes according to this representation very compact and entry of other ions to displace H of OH from these surfaces is restricted by their greater sizes. Mehmel (1935) identified also a lattice composed of the above unsymmetrical neutral sheets without any stacking as envisaged above (Mehmels metalhalloysite), $a = 5.15 \text{ \AA}$, $b = 8.9 \text{ \AA}$, $c = 7.57 \text{ \AA}$, $\beta = 100^\circ$. The value of the c -axis comes out to be equal to the calculated value of such a layer from the dimensions of

hydrargillite and SiO_4 layer (*viz.*, $7.22/\cos 10^\circ = 7.33 \text{ \AA}$) indicating absence of distortion of the fundamental units. The stacking of these layers gives rise also to a compact crystal the inter-sheet distance ($= 2.8 \text{ \AA}$) being equal to the diameter of an O (or OH) ion which is expected to be a close packed structure without distortion. And the lattice dimension of such a system becomes almost identical to that of kaolinite. (Experimental value is 14.51 and calculated value is 14.66) In fact, Hofmann, Endell and Wilm (1934) identified metahalloysite as kaolinite. When and if fusion does not take place between a tetrahedral layer and an octahedral layer, the composition of the two layers become $\text{H}_2\text{Si}_2\text{O}_5$ and $\text{Al}(\text{OH})_3$ respectively. According

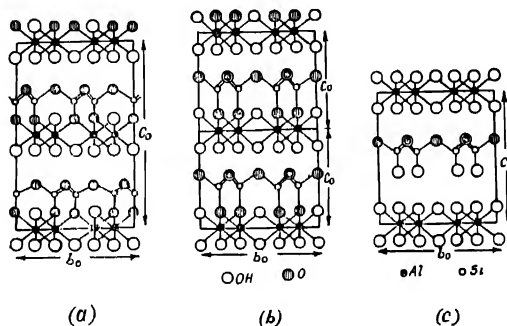


FIG. 2

(a—c After Mehmel)

- (a) Schematic diagram of the projection on the plane (100) of (a) kaolinite.
 (b) " " " " " " " in Halloysite.
 (c) Hydrated Halloysite.

to Mehmel, hydrated halloysite (Mehmel's halloysite) is built up in the direction of the c -axis from alternating layers of $\text{H}_2\text{Si}_2\text{O}_5$ and $\text{Al}(\text{OH})_3$. The value of the c -axis, calculated from the dimensions of the two layer, comes out to be $[(7.22 + 2.8)/\cos 10^\circ] = 10.17$ which agrees very closely to the experimental value. [*cf.* $a = 5.20 \text{ \AA}$, $b = 8.92 \text{ \AA}$, $c = 10.25 \text{ \AA}$, $\beta = 100^\circ$]

Almost complete absence of isomorphous replacement is a distinctive feature of kaolinite and kaolinitic minerals.

The exchange sites of kaolinite are on the exposed OH groups (Fig. 3) of the hydrargillite surface and the base exchange capacity is due to the dissociation of these surface OH groups. The small exchange capacity of kaolinite is in agreement with this picture. Potentiometric titrations of colloidal solutions of H-kaolinite show two inflexion points (Mitra, 1941-42) indicating a dibasic acid character. To explain this, the subsurface OH groups surrounded by O ions (*cf.* Fig. 3) are believed by some to be able

to exchange its H at higher pH for other cations but a consideration of the dimensions of the kaolinite lattice does not support such a possibility.

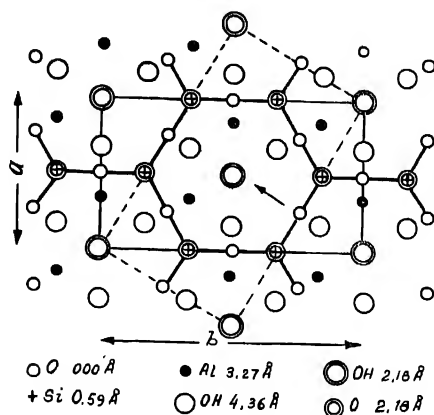


FIG. 3

(After Gruner)

Sheet of $2[(\text{OH})_4\text{Al}_2\text{Si}_2\text{O}_5]$ proposed by Pauling Height of atomic positions may vary slightly

Hendricks (1945) suggests that the exchange spots in kaolinite is distributed along the surfaces lateral to the cleavage planes. Evidence of these lateral exchange spots has been obtained by studying the effect of grinding on base exchange capacity. In all probability exchange seems to take place from both types of surfaces, *viz.*, cleavage and lateral. The difference in the binding energy of exchangeable hydrogen at the two surfaces might perhaps explain the dibasic acid character of H-kaolinite (cf. Ganguly 1949).

PYROPHYLLITE

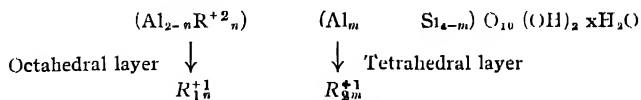
Pauling (1930) proposed the symmetrical layer lattice structure of pyrophyllite by the fusion of a hydrargillite layer with two tetrahedral layers of SiO_4 on the two faces of a hydrargillite layer. The sheets are stacked one above the other in the mineral. The calculated thickness of two such sheets stacked one above the other comes out to be $(2 \times 9.27) 18.54 \text{ \AA}$. Gruner (1934) found $c = 18.55 \text{ \AA}$ and $\beta = 99^\circ 55'$, *i. e.* the thickness equals 18.27 \AA . The layers are presumably held together by Van der Waal's forces. No acid function, unlike the OH surface of kaolinite, is expected to appear at the cleavage planes of such a layer lattice because of the absence of any ionisable group on the planes.

T A L C

Pauling (1930) proposed a similar structure for talc where the hydrargillite layer is replaced by a brucite layer having the same dimensions. Gruner (loc. cit.) has also confirmed this structure. The neutral sheets are compactly stacked as before. Gruner found $c = 18.81 \text{ \AA}$ and $\beta = 100^\circ$ (i. e., thickness equals 18.53) and the calculated thickness is 18.90. In this case the surface layers of the sheets are similar to that of pyrophyllite and possess similar properties.

MONTMORILLONITE

Hofmann, Endell and Wilm (1933) proposed the pyrophyllite structure of montmorillonite minerals, with considerable isomorphous replacement in the octahedral as well as in the tetrahedral layer. The negative charge developed in the silica layer as a result of replacement of Si by Al is balanced by the incorporation of mono- or bivalent cations as in micas (Marshall, 1935). Wherry, Ross and Kerr (1930) recognised Mg as an essential constituent of montmorillonite. From a large number of chemical analysis, Ross and Hendricks (1945) concluded: "The bases Al^{+3} , Fe^{+3} , Cr^{+3} , Fe^{+2} , Mn^{+3} , Mn^{+2} , Mg^{+2} , Ni^{+2} and Li^{+1} as naturally present in clays of the montmorillonite group, are essentially non-replaceable and clearly form part of the crystal lattice. Ca^{+2} and Na^{+1} , on the other hand, and perhaps minor amounts of other bases, are in general, replaceable. Wide variations in composition are encountered in which the octahedral Al is partly replaced by (1) Fe^{+3} , Cr^{+3} ions for which the neutrality of the layer is not disturbed. (2) Fe^{+2} , Mn^{+2} and most of all by Mg^{+2} giving rise to a negatively charged sheet whose charge is balanced by the incorporation of mono- or bivalent cations in the intersheet space. From analytical data and assuming presence of pyrophyllite skeleton in montmorillonite minerals, Ross and Hendricks (1941) (cf. Hendricks, 1942) gave the general formula:



for montmorillonite which the balancing cations are R_1^{+1} , R_2^{+1} are exchangeable.

The exchange spots and exchangeable cations of montmorillonite lie to a greater extent between the silicate layers and only to a smaller extent within them (Marshall, 1935). Nagelschmidt (1939) obtained a quantitative agreement between the observed *b. c. c.* and that calculated on the basis of isomorphous replacements. According to the estimate of Hendricks, Nelson and Alexander (1940), 80% of the exchange positions are situated in the basal planes, the remainder on the edges of the particle flakes. A distinction between the H-ions or other cations in between the cleavage planes and

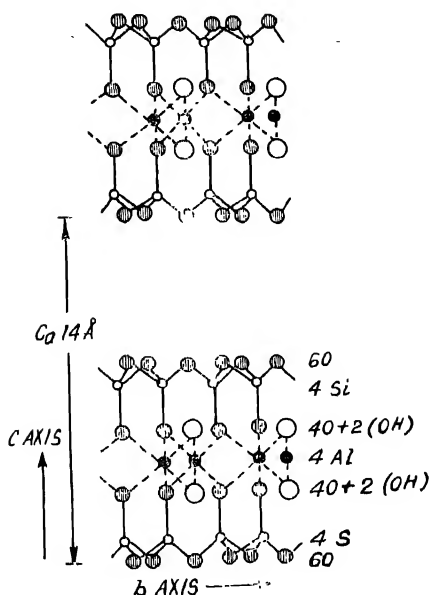


FIG. 4

(After Hofmann)

Schematic diagram of the crystal structure of pyrophyllite.

those on the external surfaces becomes possible on the basis of the intensity of the electrical field in these two locations; their behaviour in exchange reactions should therefore be different. Potentiometric titration of colloidal solutions of II-montmorillonite with alkalis, however, shows one inflexion point indicating a monobasic acid character. It is probable that the dissociation constants of the acids are too close to show more than one inflexion in the curve.

A characteristic feature of the montmorillonite lattice which distinguishes it from pyrophyllite is the reversible swelling of the former in water. Hofmann *et al* (1939) from X-ray diffraction studies observed that water taken up during swelling enters the space (where exist the replaceable cations of the mineral) between the silicate layers of the mineral (cf. Ross and Shannon, 1926) "The swelling is primarily due to the micaceous habit". Thus while the other lattice dimensions remain unaltered and are closely equal to those of pyrophyllite or kaolinite, (cf. below) the *c*-axis becomes variable; the distance depending on the water content. The adsorbed water molecules are readily

given off on heating. Hofmann observed reversible dehydration up to a temperature of 550°C . The lattice remains intact even up to a temperature of 800°C , above which it breaks down

Water absorption by montmorillonite is a complex phenomenon and they are very closely related to its crystalline structure. Bradley, Grim and Clark (1937) from X-ray diffraction studies of oriented samples of montmorillonite observed stepwise variation in swelling with humidity (cf. also Nagelschmidt, 1936). Bradley *et al* (loc. cit.) attributed the stepwise increase in swelling to the formation of definite hydrates containing 2, 8, 14, 20 and 26 molecules of water corresponding to (001) spacing respectively equal to 9.6\AA , 12.4\AA , 15.4\AA , 18.4\AA and 21.4\AA . The minimum value for (001) of montmorillonite agrees well with that for margarite (9.58\AA) and muscovite (9.96\AA) (cf. later), which suggests that isomorphous replacement in the lattice has not produced any change in lattice dimension and packing of the sheets takes place in a way similar to that in micas

Hofmann and Bilke (1937) showed that at a fixed humidity the swelling of montmorillonites depends on the nature of the exchangeable cations as well as on the pH. Hydration of the cations (Wiegner, 1931; Bar and Teudeloo, 1936) can explain neither the magnitude of the swelling nor the differences in the relative effects of the cations. From a study of low temperature endothermic effects shown by "Thermal curves", Hendricks *et al* (1940) concluded that a very small part of the water absorbed can be accounted for by the hydration of cations.

According to Hendricks and Jefferson (1938) water molecules in between the sheets form a hexagonal net by secondary bonds between O and H (also Hofmann, 1937) as in Fig 5. One-fourth of the hydrogen atoms in the net remains 'free' from bonding by secondary valence force. These hydrogens are anchored on the oxygen atoms of the adjacent layers like OH...O linking between two sheets in kaolinite. This OH...O bonding in the absorptions of water is not, however, as strong as a similar bonding in kaolinite

Russell (1934) attributed the swelling of montmorillonite to the polarising properties of the cations lying on the surface of the packets. In view of various isomorphous replacement in montmorillonite considerable strains are brought to bear on the lattice, which hamper the growth of the crystals to large dimensions and only minute crystallites are formed (cf. Hendricks, 1942). This gives rise to a large surface and a large number of exposed cations. The co-ordination valencies of these cations polarise the water

a	b
Pyro : 5.14	8.9
Kao : 5.14	8.9
Mont : 5.095	8.83

molecules and draw them to the surface where water molecule may be condensed into a pattern as suggested by Hendricks and Jefferson (*loc cit.*)

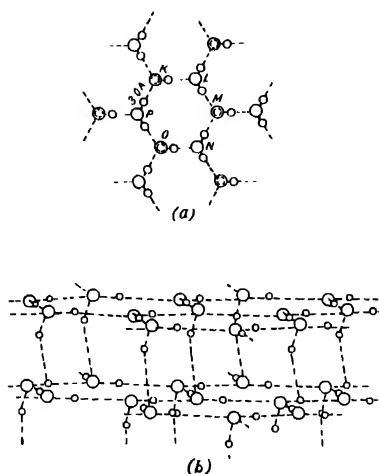


FIG 5

(After Hendricks and Jefferson)

- (a) Hexagonal net of water molecules. Large spheres represent oxygen atoms and small spheres hydrogen atoms, dotted lines indicate bonding through hydrogen
- (b) Probable structure of multiple water layers

Hendricks and Jefferson's mechanism of condensation of water molecules can also be visualised on the exposed surfaces of pyrophyllite, talc, kaolinite as well as on the surfaces of powdered micas. But because of the electrically neutral character of the compact packets expansion along the *c*-axis does not take place by the adsorption of water in between the sheets. The adsorbed water molecules in the above cases can be easily removed excepting some in the case of micas, depending on the nature of the cation exposed. In the case of montmorillonite too the observation is similar to that suggested for micas (Ganguly and Gupta, 1948). There is an essential difference between the adsorption of water on the surface of a particle composed of several packets (as in mica) and that in between the packets as in montmorillonite, whereas in the first case particles after maximum adsorption of water does not show any expansion along any axis while montmorillonite expands along the *c*-axis. Hendricks and Jefferson's mechanism, though offers an explanation for characteristic adsorption of water in the case of montmorillonites, does suggest why the same thing does not happen (i.e., adsorption of water in between the sheets of a mica particle) in the case of powdered micas (and pyrophyllite or talc).

Grim (1942) offered more convincing explanation for the non-expanding lattice of micas. In montmorillonite, isomorphous replacements by lower valent cation take place mainly in the octahedral layer, in micas it is almost entirely restricted to the silicate layer. The centre of the negative charges resides nearer to the surface in the latter case and thus the cations are strongly bound to the surface thereby strongly binding the sheets together. In the case of montmorillonite, the centre of negative charges reside predominantly deep within the body of the sheets, but the charge neutralisation is made by incorporating cations on the surface; the sheets are thus tied comparatively loosely. In the neighbourhood of the surface there exists a negative electric field to orient the water molecules with their hydrogen atoms directed towards the surface. The force of attachment between the sheets being loose the sheets can be comparatively easily lifted, so to say, allowing further water molecules to get in and attach themselves to the surface as well as to hydrate the cations in between the sheets.

ATTAPULGITE

De Lapparent (1935) gave the name attapulgite to a clay mineral in Fuller's earth from Attapulgus, Georgia and Mormoin, France. Bradley from X-ray studies proved it to be a fibrous mineral (1940). Bradley proposed the structure (Fig. 6) which consists of a brucite layer fused between two

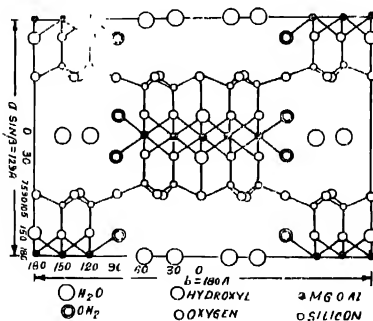


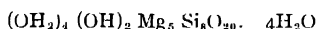
FIG. 6

(After Bradley)

Idealized proposed structure for attapulgite projected on to (001)

silica layers. The brucite structure, unlike that in talc, extends only in one direction instead of two. Consequently, instead of sheets, fibres or rods with the *c*-axis parallel to the length of the fibres are obtained. The Si-O chains running parallel to the *c*-axis are similar to amphibole chains (Warren, 1929) so that the silicate layer as viewed from above is continuous. Chains of water molecules also run parallel to the *c*-axis and fill the interstices

between the ions and this water is lost below 100°C without materially altering the diffraction patterns. An equal amount of water is co-ordinated about Mg. It is less easily removed. Finally, the water which is expelled above 500-600°C comes from the OH groups of the lattice, the unit cell containing four of them. The cell has the ideal composition.



In attapulgite, most of the charge on the silica chain frame-work is balanced by the structural brucite layers, leaving only a very small residue to be balanced by mobile cations (Marshall and Caldwell, 1947) and Marshall attributes the *b.e.c.* of the mineral to such cations.

MUSCOVITE, PHLOGOPITE, ETC.

By the replacement of one-fourth of the silicon ions in pyrophyllite and talc by Al ions, layers with a negative electric charge corresponding respectively to the composition, $\text{Al}_2\text{AlSi}_3\text{O}_{10}(\text{CH})_2$ and $\text{Mg}_3\text{AlSi}_3\text{O}_{10}(\text{OH})_2$ are obtained. The excess negative charge of such a sheet is neutralised by the incorporation of an equivalent quantity of K-ions in between the sheets as in muscovite (Fig. 7) or phlogopite. K-ions occupy the centre of two

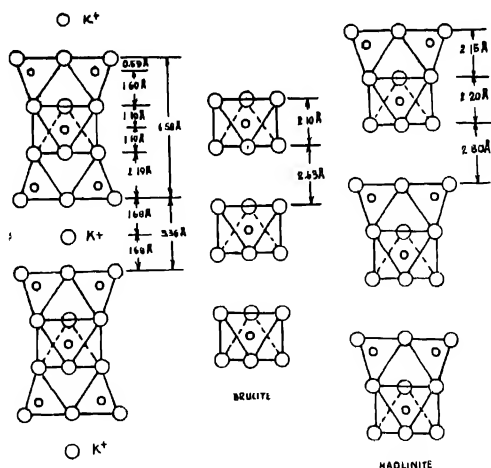


FIG. 7

(After Pauling)

The structure of mica, brucite, and kaolinite, showing the sequence of layers normal to the cleavage planes. Large circles represent O⁻ or OH⁻ (or K⁺ when so marked), small ones Si⁺⁺ or Al⁺⁺ at tetrahedron centres and Mg⁺⁺ or Al⁺⁺ at octahedron centres.

hexagonal oxygen rings on opposite sides as in Fig. 8. The intersheet distance can be calculated assuming a close-packing and the diameter of $K = 2.66 \text{ \AA}$ (Fig. 8).

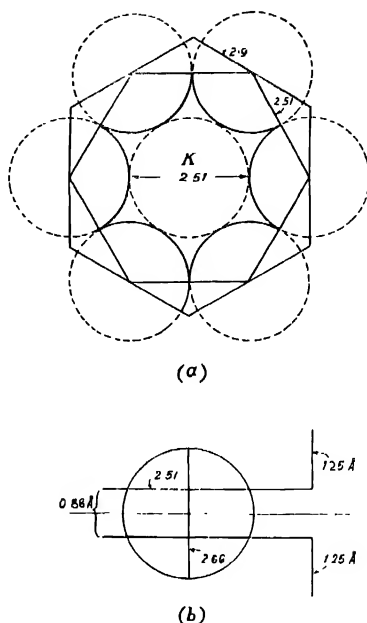


FIG. 8

The sides of the hexagonal ring equal those of a tetrahedron *i.e.*, $2.9 \sin 60 = 2.51 \text{ \AA}$. Picturing that in such a ring, the K can enter that section of its sphere whose diameter equals 2.51 \AA , the thickness equals to $2.51 + 0.88 = 3.39 \text{ \AA}$. This value of 2.51 is taken in this case, as well as in all cases of binding of adjacent layers by the incorporation of cations instead of 2.8 . Pauling (1945) has actually found such shortening of oxygen ion diameters in minerals such as rutile, anatase, corundum etc., and ascribes this shortening to the strongly ionic character of the minerals. A very strong electric field can easily be visualised to exist between the adjacent layers of muscovite and similar minerals.

The values calculated from Mauguin's data (1913) are, for intersheet distance, in muscovite $(10.06 \cos. 8^\circ 6' - 6.47) = 3.48 \text{ \AA}$, in phlogopite $(10.24 \cos. 10^\circ 2' - 6.65) = 3.43 \text{ \AA}$, and in biotite $(10.16 \cos. 9^\circ 3' - 6.65) = 3.38 \text{ \AA}$.

In margarite (Ca-mica) the sheets of interlinked tetrahedra have half of its silicon replaced by Al. The double negative charge thus developed is neutralised by the incorporation of Ca-ions just as by the K-ions in mus-

covite Pauling (1945) puts the radius of Ca equal to 0.99 Å. It therefore fits loosely in the hexagonal oxygen ring of two adjoining sheets. The intersheet distance then should equal to 2.51 Å, a value which is lower than Maugin's data (9.73 cos. $10^{\circ}8' - 6.47 = 3.11$ Å). Maugin's sample, however, does not correspond to the ideal formula, on the basis of which the theoretical value has been calculated. The results of calculation made with a number of minerals having the same basic structure as muscovite, but different isomorphous replacements are shown below. It is clear from these data that isomorphous replacements do not appreciably disturb the original compactness of the mica structure, and the agreement between the calculated values suggest the absence of distortion in the fundamental units

Because of the compact nature of these minerals, the cations trapped within the sheets do not become replaceable like the cations which occur on the surface. Except in the case of zinwaldite and lepidolite, the surface negative charges in the sheets developed as a result of isomorphous replacement almost entirely in the tetrahedral layer, are completely neutralised

Mineral	Formula	Calculated intersheet distance (Å)	(Observed distance Maugin's data) (Å)
Muscovite	$KAl_2(AlSi_3O_{10})(OH)_2$	3.39	3.48
Phlogopite	$KMg_3(AlSi_3O_{10}) \cdot (OH)_2$	3.39	3.43
Biotite	$K(Mg, Fe)_3(AlSi_3O_{10})(OH)_2$	3.39	3.38
Margarite	$CaAl_2(Al_2Si_2O_{10})(OH)_2$	2.51	3.11
Lepidolite	$KLi_2Al(Si_4O_{10})(OH, F)_2$	3.39	3.43
Zinwaldite	$KLiFeAl(AlSi_3O_{10})(OH, F)_2$	3.39	3.43

by the inclusion of cations. The sheets with equivalent cations in between them are as neutral in their behaviour towards a dipole like water as kaolinite, pyrophyllite, talc, etc. are. These minerals do not swell in water, they do not show the phenomenon of expanding lattice as do the montmorillonites. When these minerals are powdered, more and more of the intersheet cations are exposed to the surface, which then in water may absorb their water of hydration.

L I T E R

The micas exhibit a bewildering variety of composition in which isomorphous replacement may occur in the octahedral layer such as replacement of octahedral Al^{+3} by Mg^{+2} as in illite, as suggested by Hofmann and Maegdefiaw (1937), the excess negative charge in part may be balanced by the substitution of OH for O. Both Fe^{+2} and Fe^{+3} ions may also replace some octahedral Al^{+3} . The general formula of illite or the hydrous micas

is given by Grim (1937) as $2K_2O, 3R \cdot 0.8R_2O_3 \cdot 24SiO_2, 12H_2O$ and distinguished them from muscovite mica by their relatively small content of K and large percentage of water. Only 15% of the Si, and not 25% as in muscovite mica, is replaced by Al.

The K-ion of the micas becomes accessible for ionic exchange as soon as the cleavage surfaces become exposed. Besides these, some exchange positions will also be available at the lateral surfaces.

Effect of particle size on b.e.c

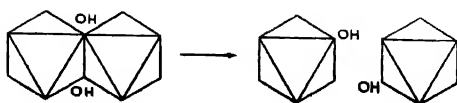
It has become clear from the above discussion that physical accessibility of the exchange spots is one of the limiting factors determining b.e.c. A decrease in particle size is therefore expected to increase the b.e.c. by way of exposing a large number of exchange spots. Without bringing in any further complications, it is possible to visualise a progressive breaking of the lattice to appropriate dimensions and thereby calculate the percentage exchange capacity.

On the basis of the crystal structure envisaged in the earlier section, a more detailed analysis is possible of the conditions arising out of breaking the lattice into smaller sizes. The particle size is usually reduced by a process of grinding. Naturally, the grinding results in the separation of the particles along the cleavage planes. But breaking along the lateral planes is not excluded and under certain conditions the latter type of breaking may be appreciably large.

Oxygen ions on the basal plane of the tetrahedral layer is arranged as in Fig. 1c.

Kaolinite—When kaolinite is powdered breaking is expected to take place (i) along the cleavage plane so as to give rise to thin plates, exposing more and more of OH planes of the hydrargillite and basal O plane of the silica; (ii) along the plane perpendicular to the basal plane, which may cut through the shared edges of the octahedral layer. If the tetrahedra and octahedra are looked upon as rigid configurations then breaking along this plane produces little complications. The breaking may also take place along any other plane perpendicular to cleavage plane in which case it will pass through the configurations of (a) Al octahedra, or (b) Si tetrahedra, in the latter case of course the plane must pass through the Al octahedra as well. However (a) involves the rupture of a smaller number of valence forces than (b).

A breaking of the Si-O-Si linkage in the presence of moisture may lead to hydrolysis, thus $Si-O-Si + H_2O = SiOH, OHSi$. The H ions of OH's on the site of cleavage become exchangeable. When the octahedron sharing the edges breaks along the edge, the two OH's at shared corners may distribute equally amongst the two units as follows



and also breaking of the Al-O-Si linkage in the presence of moisture may lead to hydrolysis, thus $\text{Al-O-Si} + \text{H. OH} = \text{Al-OH, Si-OH}$.

The H-ions of the OH's remain replaceable as in the unshated condition but Al atoms occurring on the broken surface may also be exchanged for other cations. The H of OH groups, thus developed on the Al-octahedron and Si-tetrahedron surfaces, will naturally be different in their reactivity (Ganguly, 1949). Phosphate fixation by kaolinite has been traced by Murphy (1939) to the —OH groups linked to Al.

Increase of *b. e. c.* of kaolinite on grinding has been observed by a number of workers (Shaw, 1942; Kelley and Jenny, 1936). It is obvious that the lateral breaking which takes place on grinding kaolinite will make more Al susceptible to attack by chemical reagents similar to that observed by Kelley and Jenny (1936) in the case of talc where Mg is exchanged for other cations. Marshall and Paver (1934) also observed that increasingly large quantities of Al could be extracted from soils and bentonites by treatment with dilute acids and salts. The large quantities of Al extracted by dilute acids and salts indicate that possibly Al-ions residing well within the lattice are attacked through the side of the lateral breaking. Therefore, no correlation between the amount of extractable Al and change in *b. e. c.* is to be expected.

It can be shown from consideration of the lattice dimensions that the position previously occupied by Al-except those on the surface, does, not become available for exchange by other cations except H^+ -ion*.

The displacement of Al through the lateral surface by H-ions causes a separation between the oxygen ion surface of the tetrahedral layer of the opposite sheet and the —OH ion surface of the sheet from which Al is displaced by a distance of 2.37\AA , assuming the crystal structure of kaolinite is not disturbed or distorted. Even the diameter of the non-hydrated cations K, Ba, NH_4 , etc. are greater than this distance of separation; the more so are all the hydrated ones. H-ion may be considered to behave as a single proton despite of its heavy hydration, which it perhaps does by slipping off from its hydration sheath, while entering a lattice. It thus appears that the OH's developed by the dissolution of Al from the body of the lattice are not physically accessible for ion exchange except those occurring near about the surface of the particles. The amount of Al_2O_3 extracted from the crystal and the change in *b. e. c.* are therefore not correlated. Mention may be made in this connection of the observation of Kelley and Jenny (1936), who observed that grinding renders the Mg of the octahedral layer of talc,

biotite, etc., exchangeable by NH_4 and eventually by hydrogen. They do not appear, however, to contribute to a corresponding increase in *b. e. c.* Although not exactly analogous, a similar process is also operative in kaolinite which makes octahedral Al susceptible to attack by dilute acids and salts

Mica—Grinding of micas will break the crystals mostly along the cleavage plane, exposing K-ions which become exchangeable. As the size of the crystallites is gradually reduced the total exchange spots increase in number and correspondingly more ions are displaced by exchange with other cations. Kelley and Jenny (1936) found that Mg, which occupies the octahedral position, is also extracted from biotite by means of an ammonium acetate solution. The relationship between the amounts of K and Al and the *b. e. c.* in mica has not, however, been clearly shown. The exchange spots of mica like the kaolinite, are by no means restricted to those occupied by K-ions at the cleavage surface. They may occur also at the lateral surfaces arising from the OH ions linked to Al and Si. Potentiometric titration curves of H-mica with alkalis obtained by Mitra (1934) demonstrate the existence of exchange spots having different bonding energies. Shaw (1942) and Grim (1942), in fact, believe that in illites the broken bonds developed on the lateral surface contribute to a large extent towards their *b. e. c.*'s.

Pyrophyllite.—When pyrophyllite is powdered, breaking takes place most easily along the cleavage plane, but thereby no surface with ionisable group appears. The stacking of sheets become thinner, so that only the area of exposed tetrahedral basal planes is increased. When breaking takes place along a plane perpendicular to the basal plane *i. e.*, along the one (as in kaolinite) that cuts through the shared edges of the octahedral layer and through the shared corners of the tetrahedral layer, then the OH spots developed along each face of the plane of powdering, are of two types (a) OH's linked to Si and (b) OH's linked to Al. By the above breaking and also breaking along any other plane not passing through the tetrahedral configuration, but passing through the octahedral configuration opens up Al for exchange by other cations.

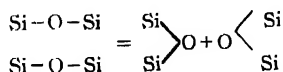
Talc.—In the case of talc, grinding along the cleavage plane does not produce any new surface condition different from that on a similar surface of the pyrophyllite sheets. But a plane perpendicular to the cleavage plane will pass through the configuration of Mg in the brucite layer and as such the Mg is rendered susceptible to attack by other cations. Moreover, the fit between the brucite layer and the tetrahedral Si layer is strained (on account of which, as Pauling (1930) stated, unsymmetrical lattice, analogous to kaolinite, cannot become stable). The Mg atoms or fit of their configurations on the surface of the broken faces are strained and as such they are more susceptible to attack by other cations *i. e.*, they are in a labile condition on the

surface like exchangeable ions and hence grinding renders a very large part (if not all) of Mg atoms on the surface sufficiently labile as to make it exchangeable.

Thus on the lateral surface of powdered talc develops two types of exchange spots, *viz.* (1) due to the development of Si-OH on the surface and (2) due to the development of -Mg-OH on the surface. Magnesium being a comparatively strongly electropositive metal, the H of OH linked to it, in all probability does not possess an acid function. Thus the development of these spots do not contribute to the base exchange capacity of powdered talc. Only the H of OH's linked to Si gives rise to the observed *b. e. c.* OH linked to Mg can be looked upon to give rise to the anion exchange properties such as phosphate fixation in powdered talc. Perkins (1944) made observation in which he attributes the phosphate fixation in kaolinite, talc and muscovite and phlogopite to the broken bonds of Al and Mg in these minerals. It has been observed by treatment of quartz and silica gel with N/20 H₃PO₄, that -OH linked to Si do not possess the anion exchange properties (Ganguly, 1949).

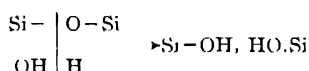
Montmorillonite.—The exchange capacity of montmorillonite, as stated earlier, is due almost entirely to isomorphous replacements. Hauser and Reed (1937) found that the *b. e. c.* of montmorillonite does not vary with particle size, since particle size in montmorillonite is merely a reflection of dispersion of the mineral particles. The suggestion of an ultimate dispersion of montmorillonite into unit plates was also made by Macgdefrau and Hofmann (1937). A definite increase in *b. e. c.* with diminishing *e. s. d.* (equivalent spherical diameter) has been observed by Marshall (1935) and also by Mitra *et al* (1942-43). A diminution of particle size is expected to increase the area of exchange along the lateral planes and hence there is a likely increase of the *b. e. c.* although small. However, the increase of cleavage surface area similar to the minerals described above will practically be meaningless in the case of montmorillonite. Kelley and Jenny (1936) and Jackson and Truog (1939) showed that the exchange capacity of montmorillonite could be greatly increased by fine grinding. Possibly the real difference between fractions of montmorillonite is only one of plate area. This increase could not, however, be accounted for by the isomorphous replacements. Most likely the increased value of *b. e. c.* is the contribution of the broken bonds on the lateral surfaces. Phosphate fixation by montmorillonite can also be traced to the presence of -OH groups linked to Al on the lateral surfaces.

Quartz.—Quartz as a whole has an electrically neutral lattice but it is not clear how this neutrality is maintained on the surface of quartz particles. On grinding quartz crystals the O-ions exposed on the surface may be shared as follows.



Accordingly, quartz powder will possess no base exchange property. Kelley suggested that as a result of the orientation of water molecule on the surface of quartz particles, they may show a low but appreciable *b.e.c.* Kelley and Jenny (1936), who attempted to estimate NH_4 adsorption by quartz powder could find almost none at all. Van der Meulen (1935) observed that Ca is adsorbed by powdered quartz but no NH_4 adsorption from NH_4NO_3 solution used to replace adsorbed Ca. It has been found earlier by one of the authors (Ganguly 1949) that the determination of exchange capacity of systems like silica by NH_4 adsorption is not correct.

If however, breaking is accompanied by the taking up of a molecule of water, the following hydrolytic cleavage may be pictured:



The H of the OH group may dissociate and thus gives rise to exchange spots on the surface. Naturally, the H ion will have only a weak acid function as in silicic acid (H_4SiO_4) to which grinding, according to this picture, ultimately leads to. Quartz will no doubt show increase in *b.e.c.* with decrease in particle size but Kelley and Jenny (1936) are of opinion that the increase will be much less than in the case of kaolinite and other minerals. It has been observed (Ganguly 1949) that quartz and silica gel possess base exchange capacities.

In a series of papers to be published shortly it is emphasised that the ion exchange behaviour of the exchange spots in ion exchange bodies is to a large extent determined by the chemical nature of the atoms or groups to which the exchangeable ions or groups are attached.

SUMMARY AND CONCLUSIONS

1. Previous investigations bring out markedly the ill-defined character of the *b.e.c.* of soils and clays. Concordant values are seldom obtained by the various methods in vogue. Though many treat colloidal clays as "adsorption complexes" or mixed gels, their crystalline nature is established now, still there does exist considerable amount of confusion in our understanding of the base exchange process because of our insufficient knowledge about the chemical, physical and as well the electrical nature of the surface of clay micro-particles.

2. In the proposed layer lattice structure of β -cristobalite and β -tridymite by Pauling the tetrahedra terminating on the surfaces of such minerals have alternately one unshared corner. At the unshared corners there is one unit of valency to be satisfied, which can be achieved by the incorporation of an atom of hydrogen or equivalent cation there. In such a case some sort of acidity at the surface can be visualised.

3. The H of OH⁺ ions on the cleavage surface of kaolinite are expected to have some weak acid function like the H of OH ion of a hydrargillite layer. Each of the layer lattice in kaolinite is a neutral sheet stacked one above the other, -OH face of one facing the basal oxygen face of another and are held to one another by hydrogen bonds. The stacking is a compact one and entry of cations to displace the H of OH ions from these trapped surfaces is restricted by their greater sizes. Fusion of the fundamental units by the stacking of layers does not produce any distortion in the fundamental units.

4. In kaolinite exchange reaction is likely to take place from the cleavage as well as from the lateral planes. The difference in the binding energy of exchangeable hydrogen at the two surfaces might give rise to dibasic acid character of H-kaolinite.

5. In hydrogen montmorillonites a distinction between the H-ions in between the cleavage planes and those on the external surfaces becomes possible on the basis of the intensity of the electrical field in these two locations. It is probable that the dissociation constants of the acids in two locations are too close to show more than one inflexion on potentiometric titration

6. The experimental value of *a* and *b*-axes for montmorillonite are closely equal to those of pyrophyllite and kaolinite. From water adsorption studies of montmorillonite it appears that isomorphous replacement in the tetrahedral or octahedral layers has not produced any change in the fundamental lattice dimensions and packing of the sheets takes place in a way similar to that in micas.

7. The calculated intersheet distances, assuming the proposed packing of K ion in micas agree well with the experimental value. The effective diameter of the basal oxygen ions being taken to be shortened to 2.51 Å from 2.8 Å which was taken in the cases of kaolinite, pyrophyllite and talc due to the very strong electric field existing between the adjacent layers of micas

8. In the case of micas too, isomorphous replacement does not appreciably disturb the original structure. Because of the compact nature of these minerals, the cations trapped within the sheets do not become replaceable like the cations which occur on the surface. In the case of hydrous micas the centre of negative charges in the packets lie removed from the surface (like that in montmorillonite) and as such the negative field appears somewhat diffused on the surface and hence, like montmorillonite, illite is expected to show some swelling in water.

9. Physical accessibility of the exchange spots is one of the limiting factors determining *b.e.c.* A decrease in particle size (*e.g.* by grinding) is therefore expected to increase the *b.e.c.* by way of exposing a large number

of exchange spots. Naturally, the grinding results in the separation of the particles, along the cleavage planes, but breaking along the lateral planes is not altogether excluded and under certain conditions the latter type of breaking may be appreciably large.

10. In kaolinite as well as in other minerals, breaking of the Si-O-Si linkage in the presence of moisture lead to SiOH, e.g., $\text{Si-O-Si} + \text{H}_2\text{O} = \text{Si-OH}$, OH-Si , when Al octahedron, sharing the edges, breaks along the edge, the two OH's at shared corners may distribute equally amongst the two units. The H of OH groups thus developed are expected to take part in cation exchange differing somewhat in their reactivity. It is obvious that lateral breaking which takes place on grinding kaolinite (or any other aluminosilicate) will make more Al susceptible to attack by chemical reagents. The large quantities of Al extracted from soils and bentonites by dilute acids and salts indicate that possibly Al-ions residing well within the lattice are attacked through the sides of lateral breaking. Therefore, no correlation between the amount of extractable Al and change in b.e.c. is to be expected.

11. The exchange spots on the surface of ground mica like the kaolinite, are not restricted to those occupied by K-ions on the cleavage surface. They may occur also at the lateral surfaces arising from the OH groups linked to Al and Si.

12. The b.e.c. of powdered pyrophyllite is traced to the OH groups linked to Si and Al, developed on the lateral broken surfaces.

13. The exchange capacity of montmorillonite is due almost entirely to isomorphous replacements and in all probability exchange predominantly takes place from the cleavage surfaces of unit plates or sheets of montmorillonite. Nevertheless, a diminution of particle size is expected to increase the area of exchange along the lateral surfaces and hence there is a likely increase of b.e.c. in montmorillonite with diminution in particle size.

14. It is proposed that quartz powder should have base exchange capacity, which they actually have.

ACKNOWLEDGMENT

Our best thanks are due to Prof. P.B. Sarkar, Dr. es. Sc., F.N.I., Ghosh Prof. of Chemistry, University College of Science and Techn., Calcutta, for his kind interest and constant encouragement during the progress of the work.

DEPARTMENT OF CHEMISTRY
UNIVERSITY COLLEGE OF SCIENCE AND TECHNOLOGY,
52, UPPER CIRCULAR ROAD, CALCUTTA

REFERENCES

- Atterberg, A., 1912, *Int. Mit. Fur Bodenk.*, **2**, 312.
- Bar and Tendeloo, 1936, *Koll. Beih.*, **47**, 97
- Bradley, W. F., 1940, *Am. Min.*, **25**, 405.
- Bradley, Grim, and Clark, 1937, *Zeit. Krist.*, **97**, 210
- Bragg, W. L., 1929, *Trans. Farad. Soc.*, **25**, 292.
- Bragg, and Gibbs, 1925, *Proc. Roy. Soc. A*, **109**, 409
- DeLapparent, 1935, *Compt. Rend.*, **201**, 401.
- Ganguly, A. K., 1949, *Sci. Cult.*, **15**, 337, 341
- Ganguly, and Gupta, 1948, *Sci. Cult.*, **14**, 81
- Gibbs, 1926, *Proc. Roy. Soc. A*, **110**, 443; **A 113**, 351
- Grim, R. E., 1937, *Am. Min.*, **22**, 855
- Grim, R. E., 1942, *Jour. Geol.*, **50**, 225
- Grim, and Rowland, 1942, *Am. Min.*, **27**, 746, 801.
- Gruner, J. W., 1932, *Zeit. Krist.*, **83**, 75, 394.
- Gruner, J. W., 1934, *Zeit. Krist.*, **88**, 412.
- Hausser, and Reed, 1937, *Jour. Phys. Chem.*, **41**, 911.
- Hendricks, S. B., 1942, *Jour. Geol.*, **50**, 270
- Hendricks, S. B., 1942, *Jour. Chem. Phys.*, **10**, 147
- Hendricks, S. B., 1945, *Ind. Eng. Chem.*, **37**, 625.
- Hendricks, and Fry, 1930, *Soil. Sci.*, **20**, 457.
- Hofmann, Rudell, and Wilm, 1934, *Zeit. Angew. Chem.*, **47**, 358.
- Hendricks, and Jefferson, 1938, *Am. Min.*, **23**, 851.
- Hendricks, Nelson, and Alexander, 1940, *Jour. Am. Chem. Soc.*, **62**, 1457.
- Hofmann, U., 1937, *Zeit. Krist.*, **98**, 31, 1937.
- Hofmann, and Bilke, 1937, *Koll. Zeit.*, **77**, 238.
- Hofmann, Rudell, and Bilke, 1939, *Zeit. Electrochem. Band.*, **41**, 469.
- Hofmann, Rudell, and Wilm, 1933, *Zeit. Krist.*, **86**, 340
- Hofmann, and Maegdefrau, 1937, *Zeit. Krist.*, **98**, 31.
- Jackson, and Troug, 1939, *Proc. Am. Soil. Sci. Soc.*, 136
- Kelley, Dore, and Brown, 1931, *Soil. Sci.*, **31**, 25.
- Kelley, Jenney, and Brown, 1936, *Soil. Sci.*, **41**, 259.
- Kelley, and Jenny, 1936, *Soil. Sci.*, **41**, 367.
- Le Chatelier, 1887, *Z. Physic. Chem.*, **1**, 396.
- Maegdefrau, and Hofmann, 1937, *Zeit. Krist.*, **98**, 290.
- Marshall, C. E., 1935, *Jour. Soc. Chem. Ind.*, **54**, 393 T
- Marshall, C. E., 1935, *Zeit. Krist.*, **90**, 8, 91 A, 433
- Marshall, and Caldwell, 1947, *Jour. Phys. Chem.*, **51**, 311.
- Marshall, and Paver, 1934, *Jour. Soc. Chem. Ind.*, **53**, 750
- Murphy, H. F., 1939, *Hilgardia*, **12**, 343

- Matlson, S. 1930-37, *Soil. Sci.*
- Maugin, C. 1913, *Compt. Rend.* **180**, 1246.
- Mehmel, M. 1935 *Zeit. Krist.* **90**, 35.
- Mitra, and Rajagopalan, 1948, *Proc. 35th Ind. Sci. Congr.* 15.
- Mitra, R. P. 1941-42, *Bull. Ind. Soil. Sci. Soc.* **4**, 41
- Mitra R. P. 1942, *Ind. Jour. Agric. Sci.* **12**, 6, 38.
- Mitra, R. P. 1943, *Ind. Jour. Agric. Sci.* **13**, 18
- Nagelschmidt, G. 1934, *Zeit. Krist.* **87**, 120.
- Nagelschmidt, G. 1936, *Zeit. Krist.* **93**, 481.
- Nagelschmidt, G. 1939, *Jour. Agric. Sci.* **29**, 477.
- Pauling, L. 1929, *Jour. Am. Chem. Soc.* **51**, 1010
- Pauling, I. 1930, *Proc. Nat. Acad. Sci. U. S. A.* **16**, 123, 578
- Pauling, L. 1945, *The Nature of Chemical Bond*
- Perkins, and King, 1944, *Proc. Soil. Sci. Soc. Am.* **8**, 154
- Ross, and Hendricks, 1941, *Proc. Soil. Sci. Soc. Am.* **6**, 58.
- Ross, and Hendricks, 1945, *Minerals of the Montmorillonite Group*, U. S. Dept. of Interior, Professional paper, 205 B
- Ross, and Shannon, 1926, *Jour. Am. Ceram. Soc.* **9**, 77
- Russell, E. S. 1934, *Phil. Trans. Roy. Soc. Lond.* **233A**, 361.
- Shaw, B. T. 1942, *Jour. Phys. Chem.* **46**, 1032
- Van Bemmelen, J. M. 1888, *Land vers. Stat.* **38**, 67
- Van der Meulen, 1935, *Rec. Trav. Chem.* **54**, 107
- Warren, B. E., 1929, *Zeit. Krist.* **72**, 42.
- Wherry, Ross, and Kerr, 1930, *Colloid Symp. Annual*, 191, 1930
- Wiegner, G., 1924, *Boden und Bodembau*, T. Steinkoff, Leipzig
- Wiegner, G., 1931, *Jour. Soc. Chem. Ind.* **50**, 65T 13T.
- Wiegner, G., 1935, *Trans. 3rd Int. Congr. Soil. Sci.* **3**, 109, 1935
- Wychoff, 1925, *Am. Jour. Sci.* **9**, 448

SOME NEW RELATIONS IN THE INTERVAL FACTORS AND THE GENERAL CASE OF THE l' ELECTRON CONFIGURATION

By V. RAMAKRISHNA RAO

(Received for publication, February 24, 1950)

ABSTRACT An investigation of the regularities in the multiplet separations in spectral terms due to p^n , d^n , and f^n electron configurations has led to the formulation of two new theorems. These enabled the calculation of multiplet separations for certain terms in any configuration of the type l' , thus avoiding the laborious work involved in Goudsmit's method. The theorems are stated and their *a priori* proofs are presented. Using these theorems, the separation factors are calculated for certain terms in f^4 , f^5 , f^6 configurations.

Following the method given by Goudsmit (1928), the author (Rao 1948, 1949) has calculated the multiplet separations in the spectral terms arising out of f^1 , f^2 and f^3 configurations. A comparative study of these results along with those already known (1928) for p^n and d^n electron configurations led to an observation of interesting regularities leading to certain general formulae for the calculation of the multiplet separations. It is the purpose of this paper to discuss these new regularities and present the formulae. *A priori* proofs of the formulae are also given. Applying these formulae, the separation factors are calculated for terms (to which they are applicable) in the configurations f^4 , f^5 , f^6 . A comprehensive table (Table II) of A factors for f configurations is given at the end, which is expected to be of use in working out the analysis of the highly complex spectra of rare earth elements, our knowledge of which is meagre.

Table I gives the known separation factors, for terms of different electron configurations calculated by the Goudsmit method. It is seen that the values of these factors for the higher multiplicity terms of a set of configurations are the same. For such terms, a simple generalisation seems to hold:—*the separation factors have the value a/r where r is the number of electrons.*

TABLE I

Configuration	Terms	A
p^2	3P	$1/2 a$
d^2	$^3F, ^3P$	$1/2 a$
f^2	$^3H, ^3F, ^3P$	$1/2 a$
d^3	$^4F, ^4P$	$1/3 a$
f^3	$^4I, ^4G, ^4F, ^4D$	$1/3 a$

The validity of this generalisation can be seen from the values for f^1 . We have here the unique wavefunction ($3^+ 2^+ 1^+ 0^+$) giving 5I_8 for which $\sum m_l m_s = 3/2 + 1 + 1/2 + 0 = 3$, which is $= 1/2 A$ (weak field). This gives the separation factor $A = 1/4 a$, and 4 is the number of electrons. This value is the same for all the quartets. The same verification can be made in other configurations as well. The results are given later. Hence the following generalisation.

That for all terms of the highest multiplicity occurring in any equivalent electron configuration of the type l^n the separation factor is given by $A = a/r$, where r (the number of electrons) is less than half the total capacity of the shell. The factor A is also independent of l .

An *a priori* proof of the generalisation is easy:

We have

$$r = 1/2 A [J(J+1) - L(L+1) - S(S+1)]$$

Since $J = L + S$, for the terms of the highest multiplicity with the highest L values,

$$\begin{aligned} r &= 1/2 A [(L+S)(L+S+1) - L(L+1) - S(S+1)] \\ &= A L S. \end{aligned}$$

This is equal to $\sum_r m_l m_s$, where \sum_r means summation over r electrons. For highest multiplicity terms, m_s is always $+1/2$ and $\sum_r m_l$ is $= L$. So the summation reduces to $(a/2)L$. So we have $A = (a/2)L/LS$, if L is not zero.

$$\text{So } A = a/2S \text{ and } S = r/2,$$

$$\therefore A = a/r. \quad \dots (1)$$

When $r = N/2$, where N is the total capacity of the shell, the maximum multiplicity term is an S term for which the factor is zero.

(2) A general formula for the separation factor for the next lower multiplicity term can also be derived particularly for those with highest L value.

We have

$$A = \frac{a \sum m_l m_s}{LS}$$

In the terms of multiplicity next to the highest we have $(r-1)$ electrons with parallel spins (m_s values $= +1/2$) and successively decreasing values of m_l i.e., $l, l-1, l-2$, etc., and one electron with antiparallel spin ($m_s = -1/2$) and $m_l = l$.

$$\therefore L = l + l + (l-1) + (l-2) \dots (l-r+2)$$

$$= \frac{2rl - (r-1)(r-2)}{2}$$

$$\text{and } S = (r-2)/2$$

$$\sum_r m_l m_s = \frac{1}{2} [(l-1) + (l-2) \dots (l-r+2)]$$

$$= \frac{2(r-2)l - (r-1)(r-2)}{4}$$

which gives for A

$$A = \left\{ \frac{2l+1+r}{2rl-(r-1)(l-2)} \right\}^a \quad \dots (2)$$

If $r=2$ singlet terms result for which the separation factor is zero.

EXAMPLES

Configuration	Term	Separation Factor
d^3	3H	$1/5 \ a$
d^4	3H	$1/10 \ a$
f^3	4L	$1/4 \ a$
f^4	3M	$1/6 \ a$
f^5	4M	$1/9 \ a$
f^6	5L	$1/16 \ a$

TABLE II

Multiplet Separations for Equivalent l^r electrons

Configuration	Multiplet	A	Total Separation	Configuration
f^1	2F	a	$7/2 \ a$	$-f^{13}$
f^2	3H	$1/2 \ a$	$11/4 \ a$	$-f^{12}$
	3F	$1/2 \ a$	$7/4 \ a$	
	3P	$1/2 \ a$	$3/4 \ a$	
f^3	4I	$1/3 \ a$	$13/2 \ a$	$-f^{11}$
	4G	$1/3 \ a$	$9/2 \ a$	
	4F	$1/3 \ a$	$7/2 \ a$	
	4D	$1/3 \ a$	$5/2 \ a$	
	2L	$1/4 \ a$	$17/8 \ a$	
	2K	$9/28 \ a$	$135/56 \ a$	
	2I	$2/21 \ a$	$13/21 \ a$	
	(^2H)	$3/10 \ a$	$33/20 \ a$	
	(^2G)	$1/30 \ a$	$3/20 \ a$	
	(^2F)	$1/6 \ a$	$7/12 \ a$	
	(^2D)	$1/2 \ a$	$5/4 \ a$	
	2P	0	0	$-f^0$
f^4	6I	$1/4 \ a$	$13/2 \ a$	
	6G	$1/4 \ a$	$9/2 \ a$	
	6F	$1/4 \ a$	$7/2 \ a$	
	6D	$1/4 \ a$	$5/2 \ a$	
	3M	$1/6 \ a$	$19/6 \ a$	
f^5	6H	$1/5 \ a$	$11/2 \ a$	$-f^9$
	6F	$1/5 \ a$	$7/2 \ a$	
	6P	$1/5 \ a$	$3/2 \ a$	
	4M	$1/9 \ a$	$19/6 \ a$	
f^6	7F	$1/6 \ a$	$7/2 \ a$	$-f^8$
	6L	$1/16 \ a$	$17/8 \ a$	
f^7	All terms	0	0	$-f^7$

The first three values agree with the values obtained by direct calculation. The values for the other three terms are our predictions from the formula (2) derived above.

The final results are collected in Table II. The values for the terms out of f' are zero as 7 is half the capacity of the f shell. Configurations containing more than 7 electrons give the same terms and so the same separation factors as those due to less than 7 electrons, i.e., f' gives the same terms as f^{n-r} where N is the total capacity. To indicate this, corresponding configurations are also given, with a negative sign to indicate inversion in the last column. Total separations are also calculated and given Column 4.

The Table II is given in two parts. The part relating to f^1, f^2, f' embodies the results obtained by the direct procedure of Goudsmit. In the other part are given the results in the other configurations for which the results are calculated from the two theorems given by the author.

ACKNOWLEDGMENT

It is a pleasure to thank Dr. K. R. Rao and Dr. S. Minakshisundaram for their interest in the work.

PHYSICS DEPARTMENT,
ANDHRA UNIVERSITY
WALTAIR

REFERENCES

- Goudsmit, 1928, *Phy Rev* **31**, 946
 Rao, V. Ramakrishna, 1948, *Ind J, Phy*, **22**, 189.
 „ „ 1949, *Comm Sci* (Communicated).

EFFECT OF TIME LAG IN THE MEASUREMENT OF DELAYED COINCIDENCES WITH G. M. COUNTERS

BY B. D. NAG, S. SEN AND S. CHATTERJI

(Received for publication, May, 1, 1950)

ABSTRACT. A mathematical expression for the delayed coincidences between two G M counters have been derived for both instantaneous and delayed radiations passing through the counters. In deriving the expressions, the time lag between the ionizing event and its recording by the G. M. counters has been assumed to have a Gaussian distribution as a first approximation. The distribution function for the time lag has been found to differ from the Gaussian error function. Experimental curves can be checked against deduced inequalities. These checks have been used to check published curves for the delayed coincidence method of determining short-lived meta-stable states in isomeric nuclei.

In measuring half lives of metastable nuclei, using the method of delayed coincidences between γ -rays as also between hard β -rays and γ -rays, calculations given in the literature (Rossi and Nercson, 1942; Benedetti and McGeowan, 1946; 1948; Bunyan and others, 1949) have to be modified to take into account the possibility of the β -or the γ -rays entering either counter. This is done assuming, with previous authors (Bunyan and others, 1949), that there is a Gaussian distribution of the pulses at the coincidence stage for a given time of the ionising event.

Let us consider the case of two exactly identical counters followed by two identical channels A and B and leading to the coincidence stage. If a variable time delay t_d can be introduced in channel A , then for an event in the counter connected to the channel B , the probability of recording the pulse at the input of the coincidence stage between time t and $t + dt$ is,

$$\frac{1}{t_0 \sqrt{\pi}} \exp. \left[- \left(\frac{t - \bar{t}_B}{t_0} \right)^2 \right] dt$$

Similarly for an event in the counter connected to the channel A , the probability of recording the pulse between time t' and $t' + dt'$ is,

$$\frac{1}{t_0 \sqrt{\pi}} \exp. \left[- \left(\frac{t' - \bar{t}_A - t_d}{t_0} \right)^2 \right] dt'$$

where \bar{t}_A and \bar{t}_B are assumed inherent mean time-lags in the two counters

and $\frac{t_0}{\sqrt{2}}$ is the standard deviation of the distribution function of each of the

counters. The probability of coincidence with a delay t_d in channel A , is

$$\psi(t_d) = \frac{1}{2} \left[\phi\left(\frac{t_d + \Delta + \tau}{t_0 \sqrt{2}}\right) - \phi\left(\frac{t_d + \Delta - \tau}{t_0 \sqrt{2}}\right) \right] \quad \dots (1)$$

where $\Delta = t_B - t_A$ and τ are the width in each of the pulse of the channels A and B and

$$\phi(x) = \frac{2}{\sqrt{\pi}} \int_0^x e^{-z^2} dz.$$

It will be no loss of generality to take $\Delta = 0$, (which is true when counters are identical), since this will only lead to a displacement of the curves in the figure along the t_d -axis by an amount Δ .

Considering the case of a radioactive source having a metastable state with a decay constant λ , the probability of delayed coincidence, when the first radiation enters channel A , in which a time delay t_d is introduced, and the following radiation enters channel B , is given by,

$$\begin{aligned} \psi_1(\lambda, t_d) &= \int_0^\infty \lambda e^{-\lambda t''} \psi(t_d - t'') dt'' \\ &= \frac{1}{2} \left[\phi\left(\frac{t_d + \tau}{t_0 \sqrt{2}}\right) - \phi\left(\frac{t_d - \tau}{t_0 \sqrt{2}}\right) \right] + \frac{1}{2} \left[\left\{ 1 + \phi\left(\frac{t_d - \tau}{t_0 \sqrt{2}} - \frac{\lambda t_0}{\sqrt{2}}\right) \right\} \exp(\lambda \tau) \right. \\ &\quad \left. - \left\{ 1 + \phi\left(\frac{t_d + \tau}{t_0 \sqrt{2}} - \frac{\lambda t_0}{\sqrt{2}}\right) \right\} \exp(-\lambda \tau) \right] \exp(-\lambda t_d + \frac{1}{2} \lambda^2 t_0^2) \quad \dots (2) \end{aligned}$$

Since it is equally probable, according to the usual geometry of the source and the counters, that the first radiation enters channel B and the following one channel A , then in that case the probability of delayed coincidence is

$$\psi_2(\lambda, t_d) = \int_0^\infty \lambda e^{-\lambda t''} \psi(t_d + t'') dt'' = \psi_1(\lambda, -t_d) \quad \dots (3)$$

and therefore the total probability for the delayed coincidence is,

$$\psi(\lambda, t_d) = \frac{1}{2} \psi_1(\lambda, t_d) + \frac{1}{2} \psi_1(\lambda, -t_d) \quad \dots (4)$$

The expressions (1) and (2) were given by Bunyan *et al.*

It can be shown analytically that at $t_d = 0$, $\frac{d\psi}{dt_d} = 0$, and $\frac{d^2\psi}{dt_d^2}$ is negative

for all values of the parameters t_0 , τ , and λ . This means that $\psi(\lambda, t_d)$ is maximum at $t_d = 0$ in all cases. This is entirely expected from a priori considerations and we have found that this expression gives a more accurate fit to the experimental curves. In the case where the geometry of the two counters is not symmetrical but each of the counters can receive both radiations in different proportions, the analytical expression is similar and similar results can be deduced.

In deriving the expressions (1) and (4) the integration over t has been taken from $-\infty$ to $+\infty$. But since there is no probability of coincidence during the time interval $-\infty$ to t_d , this integration introduces an error so

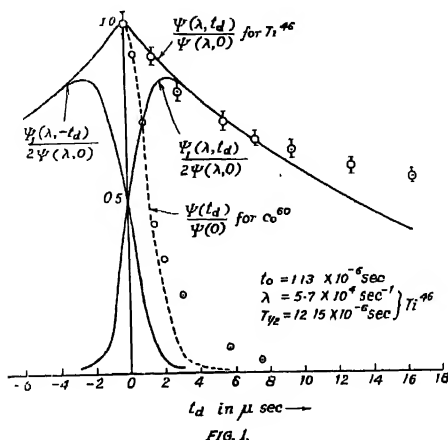


FIG. 1.

that the experimental curve appears to go to zero more slowly than the corresponding theoretical expressions as we have obtained in the case of Co^{60} (dotted curve). This raises the point as to whether it is justified in assuming a Gaussian distribution. The actual distribution in a counter can, in principle, be investigated and an analytical expression for the distribution function can be obtained.

The two function in the expressions (4) are plotted separately for Ti^{46} excited states (Nag, Sen and Chatterjee, 1949) and the resulting curve (in Fig. 1.) lies on the experimental points for the metastable state of Ti^{46} decayed from Sc^{46} . The delayed coincidence curve for Ti^{46} as well as that for Co^{60} shows that the maximum is at $t_d = 0$, as we should expect analytically. In the case where one of the counters cannot receive one of the radiations involved (as in α - β or α - γ coincidence experiments) only the first term in equation (4) will remain and $\frac{d\psi}{dt_d} \neq 0$ at $t_d = 0$. The maximum of the curve will then be at some positive value of t_d .

At $t_d = 0$, equation (4) becomes $\psi(\lambda, 0) = \psi_1(\lambda, 0)$ and for all values of t_d , $\psi(\lambda, t_d) \leq \psi(\lambda, 0)$ since $\psi(\lambda, t_d)$ is maximum at $t_d = 0$. From this it can

be shown that $\frac{\psi_1(\lambda, 0)}{\psi_1(\lambda, t_d)} \geq \frac{1}{2} + \frac{1}{2} \frac{\psi_1(\lambda, -t_d)}{\psi_1(\lambda, t_d)}$. Now because, $\frac{\psi_1(\lambda, -t_d)}{\psi_1(\lambda, t_d)}$ is a

positive quantity, the expression,

$$\frac{\psi_1(\lambda, 0)}{\psi_1(\lambda - t_d)} \geq \frac{1}{2}.$$

This is a good check for all experimental curves and deviations from this would imply that errors have been made in plotting the time co-ordinate.

A complete report on the experimental and theoretical portions of the work will be published in due course.

ACKNOWLEDGMENTS

Thanks are due to Prof. M. N. Saha, F R. S for his interest in the work and to Messers. U C. Guha, and S. Datta Majumder for discussions on the theoretical portions of the work.

INSTITUTE OF NUCLEAR PHYSICS
CALCUTTA UNIVERSITY.

REFERENCES

- Bunyan, D E., Laundby, A and Walker, D. · 1949, *Proc Phys Soc.*, **62**, 523
 De Benedetti, S and McGowan, I. K., 1946, *Phys Rev.*, **70**, 560.
 De Benedetti, S and McGowan, I. K., 1948, *Phys Rev.*, **74**, 728.
 Nag, B. D, Sen, S. and Chatterjee, S, 1949, *Nature*, **164**, 1001.
 Rossi, B and Nereson, N, 1942, *Phys Rev*, **62**, 417

ON THE X-RAY LUMINESCENCE SPECTRA OF ALKALI HALIDES

By APARESH CHATTERJEE

(Received for publication, April, 26, 1950)

PLATE VIII

ABSTRACT. The X-ray luminescence spectra of a few alkali halides have been reported in this paper. The pure crystals get coloured due to new absorption bands created on irradiation. The emission bands are not characteristic of any impurities present, and hence they represent lattice emission. The importance of lattice emission spectra in elucidating the electronic energy states of solids has been discussed.

INTRODUCTION

Physically, there are two methods of exciting a solid to give luminescence; (i) photoexcitation, i. e., excitation by ultraviolet light, and (ii) irradiation by corpuscular rays like cathode or β -rays, α -particles, etc. X-rays and γ -rays also behave like corpuscular rays, since the photoelectrons ejected from a solid are the real stimulating sources. The X-ray luminescence efficiency appears to be related simply to the ability of the material to absorb X-rays and its efficiency of light emission by the internal photoelectrons.

Unfortunately, the luminescence of solids excited by corpuscular rays has attracted very limited attention, though it has a few distinct advantages. Primary X-rays produce a large number of internal photoelectrons of various energy, so that all the energy levels which may not be indicated on ultraviolet excitation are made to play their part. With photoexcitation the question always remains whether the energy is absorbed at special points or by the parent substance, while with X-ray excitation it is always a case of transfer of energy. Direct activation will require an exciting source of white light extending far into ultraviolet; thus it is impossible to produce similar conditions by using ultraviolet radiations. X-ray excitation of luminescence is connected with the crystalline lattice through the mobility of the internal photoelectrons, the excitation energy being carried to the emitting centers by these electrons; the presence of the crystalline field facilitates such transfer. In the absence of the crystalline field, viz., in solutions, there is no perceptible luminescence under X-rays even in the case of uranyl salts.

X-ray luminescence of alkali halides has been observed by comparatively a few workers. Perrine (1923) reported some early measurements. Rose (1917) studied the X-ray luminescence spectra of these phosphors in the visible region with a glass spectrograph. In the present investigations, the measurements reported by Bose have been extended to the ultraviolet region with improved technique resulting in greater intensity and precision.

EXPERIMENTAL TECHNIQUE

An unrectified Hadding-Scherrer type of tube, run between 30 to 45 kv at 10 to 15 mA, was used as the exciting source. The phosphors were mostly of Merck or Kaulbalm varieties, though other sources were also tried for comparison. They were prepared for mounting in the form of thin sheets (in sizes 2 cm \times 2 cm \times 1 mm nearly) by pressing finely ground powders in a ball press, carefully avoiding contamination. A small Fuess spectrograph recorded the spectra which were standardized by a copper arc. The location and relative intensities of the bands were determined with the help of a Moll type microphotometer of magnification nearly 7. The measurements are uncertain by ± 25 AU in most cases.

RESULTS

The spectra are presented in Plate VIII, the microphotograms in figure 1, and the measurements in Table I. The following phosphors showed very weak glow—KF, KCl, LiCl, RbCl,—sometimes none, as in the case of LiBr. A few samples being highly hygroscopic (LiCl, RbCl, NaI), could not be photographed.

A characteristic colour change developed on irradiation; NaCl turned blue on light exposures, deep blue on moderate irradiation, blue plus yellow or brown on prolonged exposures, and finally brownish blue-black on very long irradiation. Obviously the blue colour is due to the \bar{A} -band at 4600 \bar{A} (Mollwo 1931), and the yellow and brown colours due to R_1 and R_2 bands at 5450 \bar{A} and 5960 \bar{A} (Molnar, 1941, 1944); the bluish black colour is

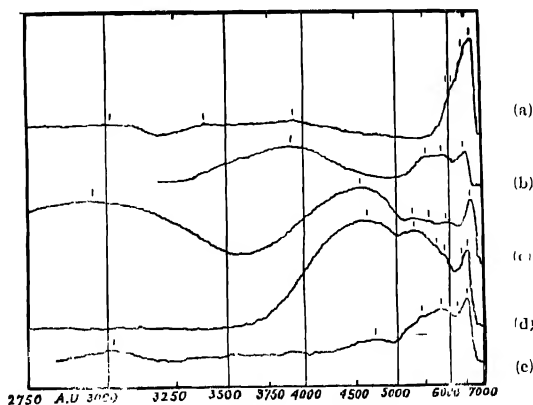


FIG 1

Microphotometer traces of the X-ray luminescence spectra of pure alkali halides, reduced, an wavelength scale is attached for comparison) (a) NaF. (b) NaCl; (c) NaBr; (d) KBr. (e) KI.

probably due to general widening of these absorption bands on heavy exposures. It has been noted that softer crystals, like KI, RbCl, are difficult to darken at ordinary temperatures, when colouration is produced, they are easily bleached when left undisturbed for a few hours, or on simple warming. On the other hand, harder crystals, like KCl, NaF, NaCl etc. darken well and retain their colour—an observation similar to that quoted by Seitz (1946).

TABLE I

Emission spectra of pure Alkali Halides

Wavelengths of the band maxima in Å U.

NaF	NaCl	NaBr	KBr	KI
6500*	6400	6700*	6600*	6650*
6285	5825	5940	6355*	6285
5990	5510	5600 ?	5970	5890
3900	3915	5295	5750 ?	5495
3380		4575	5310	4735
3010		2935	4630	3005 ?

DISCUSSIONS

It is apparent from the microphotograms that the extensions of many individual bands could not be estimated due to superposition of one into others. The modern theory of solids according to Bloch's scheme of crystal orbits demands that this is possible only when the optical levels responsible for these radiative transitions are wide.

It may seem probable that some of the emission bands are due to transitions associated with the formation of colour centres in alkali halides studied by Pohl, Hilsch, Ottmer, Mollwo (1931), Molnar (1941, 1944), Kalabuchov (1945), etc. These colour centres have been discussed in details by Seitz (1946) and presented as a tabular review by Ivey (1947). Hirschlaff 1938, is of opinion that the F-centre can occur in emission, but Mott and Gurney (1940,) report that no such emission is known. Though some of the bands of Table I can be found to agree with the locations of colour centre absorption peaks, a systematic sequence or correlation is not obtained; e.g., in NaF, the 3380Å and 3900Å bands correspond to F- and R₁-bands respectively, while no band in NaCl near to F-band is found in emission, but the 5510Å bands corresponds to R₁-band. Such accidental

* Denotes that the position of the band is uncertain by about ± 50 ÅU; ? denotes that the existence of the band is uncertain.

agreements cannot be regarded as tell-tale data, due to the following reasons:

(i) Even if some of the bands are assumed to be due to radiative colour centres, a suitable explanation as to the origin of the other emission bands has to be found out.

(ii) The levels arising out of colour centres are very much temperature-dependent, e.g., the F-band of KCl shifts from 7000\AA at 600°C to 6000\AA at -180°C . But these emission bands are relatively insensitive to temperature, as has been verified by photographing a few spectra at liquid oxygen temperature, where any such changes remain within the experimental error; the shape of the bands also does not change, as may be verified by comparing Fig. 1 with the cathodoluminescence spectra at -180°C studied by Bose and Sharma (1950).

(iii) It has been found that the glow of a fresh sample of any phosphor is greater than that of a coloured one. This shows that the available number of radiating electrons at the start is minimized on subsequent trapping on irradiation.

(iv) The colour centres are the centres created at vacant lattice sites where ions or electrons may be trapped, and remain trapped, unless they are freed by warming or heating, or by photo-excitation with suitable light, or by applying a voltage which thereby drifts the ions or electrons showing photo-conductivity. Once trapped, the electrons are bound to the lattice field by Coulomb forces, and cannot undergo radiative transitions.

It is thus clear that the mechanism of luminescence is different from that of absorption due to lattice defects originating from colour centres. This leaves doubt whether the bands are characteristic of some impurities, or belong to the parent lattice itself. In order to get an idea of the extent of changes introduced in emission due to impurities, the spectra of rocksalt (impure sodium chloride containing KCl, Mg, Fe, Mn salts etc.) and of a mechanical mixture of KBr containing 5% TiCl were studied, the results are shown in Table II.

TABLE II
Emission spectra of Impurity Phosphors

Phosphor	Band peaks in \AA U.	Remarks
Rocksalt	6350 [†] , 5890, 5650 [†] , 3900	*Denotes that the position of the band is uncertain
KBr+Ti (5%) Mixture	6600 [†] , 6320, 6020, 5760, 5400 [†] , 4035	

Comparing Tables I and II it is at once apparent that the impurity phosphors have roughly the same emission maxima as those of the purer samples. We thus note:



(a)



(b)



(c)



(d)



(e)



(f)



(g)

X-ray luminescence spectra of alkali halides.

(a) NaF, (b) NaCl, (c) NaBr; (d) KBr, (e) KI
(f) KBr + TiCl (mechanical mixture), (g) KBr - Ti (solid solution)

(a) An impurity phosphor prepared by mechanical mixtures has no extra part to play in X-ray luminescence due to minute quantities of added ions. Such a phosphor shows the same bands both in location and intensity profile as those of a pure phosphor (Fig. 2). This shows that the bands presented in Table I are due to the emission of the lattice itself.

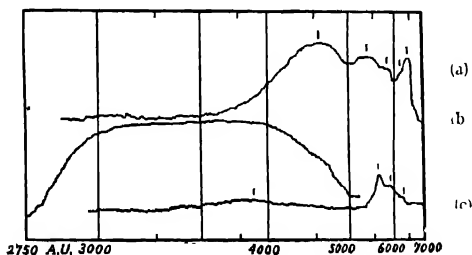


FIG. 2

Records of luminescence spectra of impure alkali halides (reduced) (a) KBr+Tl (5% TlCl by weight as a mechanical mixture) (b) KBr-Tl (solid solution by fusion): (c) Rocksalt.

(b) Though a sample of rocksalt shows roughly the same spectral characteristics as that of pure sodium chloride (Merck, Kahlbaum, or B.D.H. varieties) under X-rays, the very same sample, when suitably excited by copper, iron, or mercury arcs (filtered to cut off the visible portion) invariably emits the pink or yellow colour characteristic of manganese in traces, and green or blue colours due to other impurities; these 'characteristic' impurity emissions are completely absent on X-ray irradiation. The colour centres produced, however, are the same as those for pure sodium chloride, as seen visually.

(c) It is very significant that KBr, mixed with a heavy dose of thallium as TlCl, gives no indication of the very remarkable characteristic thallium emission in the near ultraviolet. It unmistakably shows that our method of excitation does not behave in the same way as ordinary photoexcitation as stated before. If this is once understood, it is easy to see that X-ray luminescence has got nothing to do with mechanical mixtures, unless the impurity in the mixture itself is not strongly luminescent. It should be remarked here that pure TlCl has been found to have a very weak bluish green glow; the spectrum could not be recorded, and the sample changed colour to pink on irradiation. The situation completely changes when thallium is introduced within the lattice by fusion. In that case the thallium emission is always present as shown in figure 2.

Thus we have shown that minute quantities of impurity ions, not rigidly adhered to the original lattice, cannot have any measurable disturbing effects on the X-ray induced emission processes of the lattice itself. The lattice

emission has lately been postulated in case of pure ionic solids ; the lattice emissions of alkaline earth oxides and sulphides have been observed by Kroger (1940), Kudryavtzeva (1946a, 1946b) and Byler (1947), all at low temperatures; in alkali halides, the works of Kudryavtzeva (1934) and Katz (1947) have established lattice emission. As to the carriers of luminescence, the mechanism of 'excitons' developed by Peierls and Frenkel is particularly suitable. This exciton mechanism postulates that an electron raised from a filled band to a non-conducting energy state is still electrostatically bound to the positive 'hole' left behind before being raised to the conduction band; as a result, a number of hydrogen-like discrete energy levels below the conduction band will occur.

ACKNOWLEDGMENT

The author's thanks are due to Prof S. N. Bose, Khaira Professor of Physics, Calcutta University, for facilities of work, and to Mr. H. N. Bose, Khaira Laboratory of Physics, for suggesting the problem and encouragement during the progress of the work.

KHAIRA LABORATORY OF PHYSICS
CALCUTTA UNIVERSITY

REFERENCES

- Bose, H. N. (1947), *P R S*, dissertation (unpublished).
 Bose, H. N. and Sharma, J. 1950, *Proc Nat Inst. Sci Ind*, **26**, 47.
 Byler, W. H. (1947), *J Opt Soc. Amer*, **37**, 911.
 Hirschlaff, R. (1938), 'Fluorescence and Phosphorescence' (Matheson).
 Ivey, H. F. (1947), *Phys. Rev.*, **72**, 341.
 Kalabuchov, N. (1945), *J Phys. USSR*, **9**, 41.
 Katz, M. L. (1947), *Dokl Akad Nauk SSSR*, **68**, 1935.
 Kroger, F. A. (1940), *Physica*, **7**, 1.
 Kudryavtzeva, V. M. (1934), *Z. Physik*, **90**, 489.
 Kudryavtzeva, V. M. 1946a, 1946b), *C. R. Ac. Sc. URSS*, **82**, 495, 581.
 Mollwo E. (1931), *Goett Nachrichten*, **2**, 97.
 Molnar, J. P. (1941), *Phys Rev.*, **59**, 944(A).
 Molnar, J. P. (1944), Ph.D. thesis as quoted by Sertz (1946).
 Motl, N. F. Guiney, R. W. (1940), 'Electronic processes in Ionic Crystals' (Oxford).
 Perrine, J. C. (1923), *Phys. Rev*, **22**, 48.
 Seitz, F. (1946), *Rev. Mod Phys*, **18**, 384.

A NOTE ON THE CRITICAL AREA OF SURFACE FILMS AND EVAPORATION THROUGH THEM

By D. S. SUBRAHMANYAM

(Received for publication, October 18, 1949)

ABSTRACT. Considering the rise of water in two capillary tubes introduced into a basin of water in an isolated system, the surface of water in one of the tubes being contaminated, it is shown theoretically that the surface tension cannot fall in value until the contamination prevents direct communication between the water and vapour phases. A new explanation is thus offered for the existence of critical area of surface films. The theory also throws light on evaporation through surface films and it is pointed out that while Rayleigh's theory explains the phenomena connected with condensed films the new theory will be helpful in explaining the existence of critical area of liquid expanded films.

INTRODUCTION

It was known from the experiments of Pockles and Rayleigh that when a small quantity of a contaminating substance is added to the surface of water and the area gradually decreased the value of surface tension does not perceptibly alter until a critical area is reached. From the value of the thickness of the film corresponding to the critical area, Lord Rayleigh (1899) suggested that the thinnest oil films possibly consisted of only a single layer of molecules which could be regarded as floating objects and which could not thus affect the value of surface tension when the area of the surface exceeded the area they occupied on it. According to this view the diminution in surface tension is to be considered as the surface pressure of the film which is brought into play as the film is compressed. "If the surface were covered by floating corks instead of molecules, it is obvious that no resistance to compression would arise and therefore no surface pressure would be observed until the corks were packed in contact with one another in a layer one molecule thick" (Adam, 1931). Lowering of surface tension is not to be considered as change in surface energy per unit area as such, produced by the contaminating molecules, but only as an elastic force brought into play when the two dimensional film is compressed. Rayleigh's explanation has been the subject of much later work by Langmuir, Adams, Rideal and others, whose experiments have gone to confirm Rayleigh's theory in the main.

An alternative explanation is offered here for the critical area of surface films on a dynamical basis which throws light also on the evaporation that takes place through a surface covered with a film.

THEORY

Lord Kelvin (1881) has shown that the equilibrium vapour pressure over a concave liquid surface must be less, and over a convex surface greater than over a plane surface, the value depending upon the curvature, so that for a liquid surface with a particular curvature the equilibrium vapour pressure has a definite value.

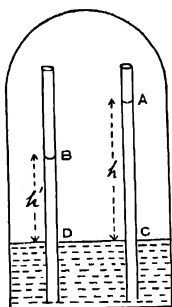


FIG. 1

Imagine two capillary tubes AC and BD , having the same radius r dipping into water in a basin enclosed in an air-tight chamber and let the system be isolated thermally from outside and exhausted of air. Let the meniscus A in AC be uncontaminated and the meniscus B in the other tube, contain some contaminating substance, the quantity however, being such that a part of the surface (however small) is not covered by the substance, so that a continuous interchange of water molecules is possible between the water below and the vapour above. When the system attains a steady state, let h be the height of the water column in AC and h' in BD . Let T and T' be the surface tensions at A and B respectively and let T' be less than T , if possible. Since the effect of contamination on surface tension only is being studied, let it be assumed that the contact angle at B is the same as that at A . It follows then that h' is less than h . Let P be the vapour pressure at the plane surface of water outside, P_1 the vapour pressure at A and P_2 that at a point outside the tube at the same level as B . P_1 is the equilibrium value of the vapour pressure at A , depending upon the curvature of the meniscus there, and it is less than P_2 since the level of B is lower than that of A . If P_e be the equilibrium vapour pressure over the meniscus at B , it may differ from that at A due to two causes: (i) curvature, and (ii) presence of contamination. But since the contact angle at B is the same as that at A and the radius at the bore of the tube is also the same, the curvature cannot be different. The contamination on the surface, if it has any effect at all, should stand in the way of a free exchange of molecules of water in the liquid and vapour states and

should therefore tend to diminish the vapour pressure at *B*. Thus the equilibrium vapour pressure P_e at *B* cannot be greater than that at *A* and it therefore follows that the vapour pressure P_s at the same level as *B* is greater than P_e . Hence condensation must take place at *B* with consequent circulation from *B* to the water surface outside through the water, evaporation there, and condensation again at *B*, a continuous process which is dynamically impossible. Consequently, so long as there is a continuous interchange of water molecules between the liquid and vapour phases at *B*, h' cannot be less than h , nor T' less than T . When the amount of contamination at *B* is, however, such that it completely covers the surface and prevents direct communication between the liquid and vapour phases of water, the above reasoning no longer applies and it will be possible for T' to be less than T .

This reasoning would require that continuous and direct communication between the water in the liquid and vapour phases should be cut off before a fall in surface tension can take place. This, however, may not result in a complete cessation of evaporation. Some of the water molecules possessing large values of kinetic energy may break open the film and escape out and through the openings so made other water molecules will rush out until the opening is again closed by the spreading force of the surrounding film. Thus there are two opposing tendencies: (i) When there is an opening created in the surface film by a fast molecule, the value of surface tension will rise and the level in the capillary tube will tend to go up. (ii) But when the gap is closed the value of surface tension will fall and the level will tend to go down. The actual level obtaining in the capillary tube (and consequently the value of surface tension) will be one of equilibrium between these two opposing tendencies, the process being repeated many times in a second.

EXPERIMENTAL OBSERVATIONS

This explains the gradual fall in the value of surface tension when a film is compressed beyond the critical area. When the film is compressed the cohesive forces between the molecules of the film become stronger, and it will become more difficult for the fast water molecules to break open the film and also the film closes up more quickly. Consequently, the tendency to opposing the lowering of surface tension will become less and less as the film is compressed. Finally the lowest value in surface tension will be reached when evaporation from the surface becomes a minimum. This view is confirmed in a striking manner by the experiments of Seiba and Biesco (1940) on evaporation through surface films. They find that with the normal alcohol of 22 carbons, evaporation is 20% of the rate over water at 20 dynes, and at 48 dynes it is almost nil. With other alcohols and acids, the rate is considerably retarded at 40 dynes.

This view also explains another interesting observation made on evaporation through films. The amount of evaporation through a film depends upon

(i) the readiness with which openings can be created in the film by the fast water molecules and (ii) the rate at which the openings created in the film will be closed by the surrounding molecules of the film. If these molecules are less mobile and do not close up quickly there will be more evaporation through the openings and through the film than if they are more mobile. The mobility of the molecules of a solid substance like stearic acid is very much less than the molecules of a liquid like oleic acid. If, therefore, the second one of the above two effects preponderates, it follows that evaporation through a stearic acid film can be greater than through a film of oleic acid. This was the observation made in the experiments of Rideal (1925) and Langmuir (1927). Defining R , the resistance to evaporation, as the difference between the reciprocals of the loss of weight per sq. cm. of film and water per second, they obtained the following values :

Surface film.	$R/\text{evaporation in vacuo}$		Rate of increase of resistances	
	(a) at 25° C	(b) 35° C	(a)	(b)
None	2.96	1270	1	1
Stearic acid	303.0	165.0	102	97
Lauric acid	573.0	392.0	193	172
Oleic acid	853.0	617.0	288	362

It was considered to be curious that a liquid film should offer more resistance to evaporation through it than a film of solid, but the above reasoning offers an explanation for it.

CONCLUSION

Considering all the phenomena connected with films, it can be taken that the theory presented in this paper supplements Rayleigh's theory. Rayleigh's theory is quite satisfactory in the case of condensed films but is not as satisfactory in explaining the behaviour of liquid expanded film (Adam, 1941). Langmuir tries to explain the behaviour of these films from the similarity between the pressure area curves of a liquid expanded film and the spreading force of a large thin layer of hydro-carbon oil resting on a water surface with a monomolecular gaseous film present at the interface between the oil and the water. The spreading force F_0 of an oil A on water B is

$$F_0 = \gamma_B - \gamma_A - \gamma_{AB}$$

where γ_A , γ_B and γ_{AB} are the surface tensions of the oil-air, water-air and oil-water interfaces respectively. An explanation is thus given in terms of

surface tensions and not compression pressures, and the equation that he obtains is

$$(F - F_0)(A - A_0) = k \cdot T$$

where F is the spreading force of the film, A is the area per molecule, A_0 a constant, k is the gas constant per molecule and T the temperature. This equation gives a rectangular hyperbola for the $F-A$ curve which closely represents the behaviour of the film when compressed beyond the critical area; but it does not explain the existence of the critical area which is also shown by these films. The theory presented in this paper solves this difficulty, being based not on the idea of compression but on surface tension and evaporation through films. While Rayleigh's theory cannot be satisfactorily applied to expanded films, it may be that the theory presented in this paper cannot be applied to some cases of solid condensed films, especially to films of cholesterol and proteins and Rayleigh's compression theory alone applies to them. For, in these cases it is found that there is no appreciable resistance to evaporation even at the pressure of 35 dynes (Sebba and Bresco, 1940). The films are so rigid that the openings created in the film by the bombardment of the fast water molecules do not close for a long time and the film resists the compression exerting appreciable pressure at the same time. This is analogous to a sheet of metal having holes which do not close when the sheet is compressed laterally. It may therefore be concluded that the surface pressure registered by a film may be due to resistances offered by a film when it is laterally compressed or due to a lowering in the surface tension of a film covered surface. Both cases show critical areas; the critical area in the former case is explained by Rayleigh's theory and that in the latter, by the theory presented in this paper.

C. R. R. COLLIER
MILLORE

REFERENCES

- Adam, 1941, *Physics and Chemistry of Surfaces*, 3rd Edition, p. 21.
Adam, 1941, *Physics and Chemistry of Surfaces*, 3rd Ed., p. 65.
Langmuir, 1927, *J. Physical Chemistry*, **31**, 1719.
Rideal, 1925, *J. Physical Chemistry*, **29**, 1585.
Sebba and Bresco, 1940, *Journal of Chemical Society*, **106**, 128.
Rayleigh, 1899, *Phil. Mag.*, **118**, 331.

The following special publications of the Indian Association for the Cultivation of Science, 210, Bowbazar Street, Calcutta, are available at the prices shown against each of them :—

Subject	Author	Price Rs. A. P.
Methods in Scientific Research	Sir E. J. Russell	0 6 0
The Origin of the Planets	Sir James H. Jeans	0 6 0
Separation of Isotopes	Prof. F. W. Aston	0 6 0
Garnets and their Role in Nature	Sir Lewis L. Fermor	2 8 0
(1) The Royal Botanic Gardens, Kew.	Sir Arthur Hill	1 8 0
(2) Studies in the Germination of Seeds.		
Interatomic Forces	Prof. J. E. Lennard-Jones	1 8 0
The Educational Aims and Practices of the California Institute of Technology.	R. A. Millikan	0 6 0
Active Nitrogen A New Theory.	Prof. S. K. Mitra	2 8 0
Theory of Valency and the Struc- ture of Chemical Compounds.	Prof. P. Ray	3 0 0
Petroleum Resources of India ...	D. N. Wadia	2 8 0
The Role of the Electrical [Double ... layer in the Electro Chemistry of Colloids.	J. N. Mukherjee	1 12 0

A discount of 25% is allowed to Booksellers and Agents.

RATES OF ADVERTISEMENTS

Third page of cover	Rs. 32, full page
do. do.	„ 20, half page
do. do.	„ 12, quarter page
Other pages	„ 25, full page
do.	„ 16, half page
do.	„ 10.

15% Commissions are allowed to *bonafide* publicity agents securing orders for advertisements.

CONTENTS

	PAGE
32. B. E. C. and Crystalline structure of Silicate Minerals related to Soils and Clays—By S. K. Mukherjee and A. K. Ganguli	233
33. Some New Relations in the Interval Factors and the General Case of 1^r Electron Configuration—By V. Ramakrishna Rao	257
34. Effect of Time-Lag in the Measurement of Delayed Coincidences with G. M. Counters—By B. D. Nag, S. Sen and S. Chatterjee	261
35. On the X-Ray Luminescence Spectra of Alkali Halides—By Apares Chatterjee	265
36. A Note on the Critical Area of Surface Films and Evaporation through them —By D. S. Subrahmanyam	271

PRINTED BY SIBENDRANATH KANJILAL, SUPERINTENDENT (OFFG.), CALCUTTA UNIVERSITY
 PRESS, 48, HAZRA ROAD, BALLYGUNGE, CALCUTTA AND PUBLISHED BY THE
 REGISTRAR, INDIAN ASSOCIATION FOR THE CULTIVATION OF SCIENCE,
 210, Bowbazar Street, Calcutta.

Vol. 24

INDIAN JOURNAL OF PHYSICS

No. 7

(*Published in collaboration with the Indian Physical Society*)

AND

Vol. 33

PROCEEDINGS

No. 7

OF THE

INDIAN ASSOCIATION FOR THE CULTIVATION OF SCIENCE

JULY, 1950

PUBLISHED BY THE
INDIAN ASSOCIATION FOR THE CULTIVATION OF SCIENCE
210, Bowbazar Street, Calcutta

BOARD OF EDITORS

K. BANERJEE	S. K. MITRA
D. M. BOSE	P. RAY
S. N. BOSE	M. N. SAHA
D. S. KOTHARI	S. C. SIKKAR.

Secretary

EDITORIAL COLLABORATORS

DR. R. K. ASUNDI, M.A., PH.D.
PROF. H. J. BHABHA, PH.D., F.R.S.
DR. P. K. KICHLU, D.Sc.
PROF. K. S. KRISHNAN, D.Sc., F.R.S.
PROF. G. P. DUBEY, M.Sc.
DR. K. RANGADHAMA RAO, M.A., D.Sc.
DR. N. D. SARWATTEY, D.Sc.
DR. N. N. DASGUPTA, M.Sc., PH.D.
PROF. N. R. SEN, D.Sc., F.N.I.
PROF. P. C. MAHANTI, D.Sc., F.N.I.
PROF. S. R. PALIT, D.Sc.,
DR. H. RAKSHIT, D.Sc.,
PROF. K. R. DIXIT, PH.D.
DR. VIKRAM A. SARABHAI, M.A., PH.D.

ASSISTANT EDITOR

MR. A. N. BANERJEE, M.Sc.

NOTICE

TO INTENDING AUTHORS

Manuscripts for publication should be sent to Mr. A. N. Banerjee, Assistant Editor, 210, Bowbazar Street, Calcutta.

The manuscript of each paper should contain in the beginning a short abstract of the paper.

All references to published papers should be given in the text by quoting the surname of the authors followed by the year of publication within braces, e.g., Sen (1942). The actual references should be given in a list at the end of the paper according to the following specimen :

Sen, B. K., 1942, *Ind. J. Phys.*, 16, 339.

The references should be arranged alphabetically in the list.

All diagrams should be drawn on thick white paper in Indian ink, and letters and numbers in the diagrams should be written in pencil.

Annual Subscription—

Inland Rs. 20
Foreign £ 2

SOME RANDOM FADING RECORDS WITH SHORT-WAVE SIGNALS

By P. M. DAS AND S. R. KHASTGIR

(Received for publication, March 29, 1950)

ABSTRACT Some random fading patterns recorded at Dacca with 4840 kc/s signals from Calcutta are shown and analysed. Rayleigh's formula for random fading from the various diffracting centres in the ionosphere was not found to agree with the observed signal variations. It is likely that the discrepancy is due to the two sets of waves reaching the receiver after single reflection from the E- and F-layers or after single and double reflections from the same F-layer

INTRODUCTION

In an investigation on the intensity variation of short-wave signals from Calcutta received at Dacca (distance 240 km) during the evening hours of December, 1948 and January, 1949, the quick random type of variations were at times observed. In the present paper some of these random fading observations are given with a brief reference to the receiving and recording arrangements. The results of these observations are also examined on the supposition that the variation is caused by the interference of waves scattered from a large number of diffracting centres distributed at random in the ionosphere.

The idea of random scattering from the various diffracting centres in the ionosphere had been substantiated, for medium waves and moderate transmission distances, by Ratcliffe and Pawsey (1933), Pawsey (1933) and Khastgir and Ray (1940) who showed that the time-variation of the amplitude of down-coming waves was consistent with the random scattering formula of Lord Rayleigh. For longer distances, however, there was departure from the formula, as was shown by Sen Gupta and Dutt (1941).

The recent view of Ratcliffe (1948) who has taken into account the continual random motion of the diffracting centres in the ionosphere and the consequent Doppler change of frequency of the waves, is not, however, considered in the paper.

THE RECEIVER AND THE RECORDING SYSTEM

A T. R. F. receiver which had one stage H/F amplification followed by a grid-leak detector (and an A/F power amplifier to work a loudspeaker for facilitating tuning) was used with a tuned frame aerial. A mirror galvanometer in the anode circuit of the detector valve, which was balanced for no-

signal anode current indicated current fluctuations due to intensity variations of the signal. The details of the recording apparatus are described elsewhere. Essentially, it consisted of a rotating drum with a lateral movement. The light from a point-source falling on the galvanometer mirror was made to converge after reflection to a sharp focus by suitable condensing lenses on a bromide paper round the drum, which was enclosed in a light-tight box. As the drum was rotated slowly with the help of a reduction gear and an electric motor, the galvanometer spot on the bromide paper recorded the fluctuations of the signals.

RANDOM FADING RECORDS

With Calcutta signals of 4840 kc/s received at Dacca during the evening and early night hours, most of the records revealed periodic patterns.* A number of records showed also quick random fluctuations. In these records, showing quick random fading, there was indication of slow rhythmic variations. A typical record showing quick random fading with a slow periodicity is shown in Fig. 1.

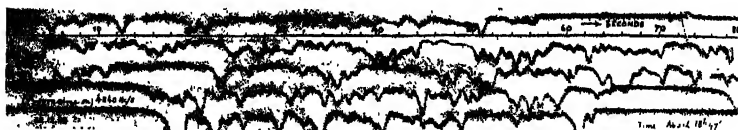


FIG. 1

Quick random fading with a periodicity

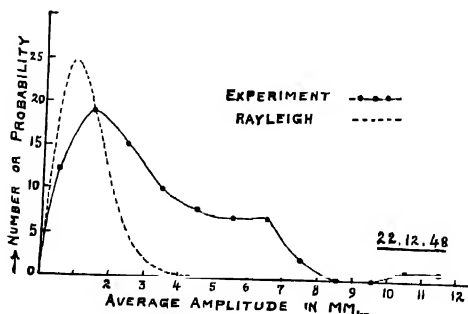


FIG. 2

Amplitude distribution in random fading with 4810 kc/s signal

* The observations of periodic fading are being published elsewhere.

It is interesting to observe that the record reveals extremely high frequencies (4 to 12 mega c/s) in the form of saw-tooth discontinuities. These may be identified with the 'flutter'-phenomena reported by Subba Rao and Somayajulu (1949), the cause of which is yet unknown.

As the transverse displacement in the records was found to vary linearly with the field intensity, the variation of signal intensity was easily obtained from the recorded fading pattern. The actual distribution of amplitudes, lying within a range of 1 mm between zero and 13 mms, is obtained from the fading record given in Fig. 1 and is shown in Fig. 2. Similar distribution curves for two more random fading records are given in Fig. 3

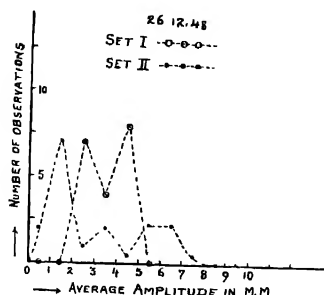


FIG. 3

COMPARISON WITH RAYLEIGH'S CALCULATIONS BASED ON RANDOM SCATTERING

Lord Rayleigh deduced an expression for the probability of occurrence of any resultant amplitude on the assumption of a large number of components of random phases. The probability is given by

$$P'' = \frac{2r}{R^2} e^{-r^2/R^2}$$

where R^2 is the sum of the squares of the component amplitudes and $P''dr$ the probability of a resultant amplitude between r and $r+dr$. Differentiating P'' with respect to r and putting it equal to 0, the maximum value of P'' is found to correspond to $R^2 = 2r_m^2$ where r_m is the most probable amplitude, so that

$$P'' = \frac{1}{r_m^2} e^{-r^2/r_m^2}$$

Substituting the experimental value of r_m for which the number of observations having amplitudes within r and $r+dr$ is maximum, the theoretical values of P'' can be calculated for various values of r . These values are then multiplied by a suitable constant so as to agree with the observed peak value. The theoretical Rayleigh distribution corresponding to the fading record, shown in Fig. 1, is illustrated along with the actual distribution in Fig. 2.

CONCLUSION

It is significant that with 4840 kc/s signal and over a distance of 240 km there is no agreement between the observed distribution and that obtained from Rayleigh's formula for random scattering. In the curve showing the actual distribution of amplitudes in Fig. 2, there is an indication of a smaller peak. The curves in Fig. 3 also reveal two distant peaks. The double peaks appear to suggest dual sets of downcoming waves reflected from the ionosphere. That there were at times two sets of downcoming waves was often indicated by the appearance of a slow type of periodic fading, which could be considered as due to the interference of the waves reflected from the moving ionospheric layer or layers.

Further work on the subject of random fading of radio signals is in progress.

PHYSICS DEPARTMENT,
HINDU UNIVERSITY, BANARAS.

REFERENCES

- Khastgir, S. R. and Ray, A. K., 1940, *Ind. Jour. Phys.*, **14**, 283.
 Pawsey, J. L., 1933, *Proc. Camb. Phil. Soc.*, **31**, 125.
 Ratcliffe, J. A., 1948, *Nature*, **162**, 9, July 3.
 Ratcliffe, J. A. and Pawsey, J. L., 1933, *Proc. Camb. Phil. Soc.*, **23**, 301.
 Sengupta, M. M. and Dutt, S. K., 1941, *Ind. Jour. Phys.*, **15**, 447.
 Subba Rao, N. S. and Somavajulu, Y. V., 1949, *Nature*, **163**, 442.

LINEAR ANALYSIS OF ELECTRONIC SWITCHING*

By RAIS AHMED

(Received for publication, May 2, 1950)

ABSTRACT. A linear analysis of the multivibrator circuit has been made and it is shown that the time of switch over between two relaxation states can be calculated with a fair degree of accuracy. Variation of the time of rise with various circuit parameters has been studied and results have been compared with observational data. By means of this analysis a criterion for the design of fast switching circuits has been indicated.

The current-voltage relationship in a vacuum tube is non-linear and, therefore, any exact analysis of circuits using such tubes would have to depend on the solution of non linear differential equations. In fact, considering the actual grid voltage-plate current characteristic of a tube one may have to resort to graphical methods since analytical expressions for such characteristics are only approximations. It is because of these facts that considerable difficulties have been experienced in the analysis, in particular, of relaxation circuits, which have otherwise proved to be so useful in a very large number of modern timing, switching and controlling devices.

In the case of multivibrators, which form a basis of so many above-mentioned circuits, a number of papers have appeared, *e.g.* Kiebert and Inglis (1945), on the calculation of the relaxation periods. The switching period, which lies between two successive relaxations, has not been fully investigated (Williams, Aldrich, Woodford, 1950; Ahmed, 1948), and many authors, considering lower frequencies of operation, have simply assumed this period to be zero. When multivibrators or similar other circuits are being used these days in ever faster networks, it becomes imperative to investigate the switching period, even with a small margin of error. The designing engineer or physicist must have some quantitative information about the switching time.

The circuit of a symmetrical multivibrator, originally given by Abraham and Bloch (1927), is shown in Fig. 1 and its operation has been explained by several authors. The voltage waveforms at the two grids are shown in Fig. 2; it is the period *ab* which is referred to as the switching time, since it is during this time that one tube is being switched on while the other is being switched off. During *ab* both the tubes are conducting and since the output of one is connected to the other, it is during *ab* that the grid voltage of one, due to cumulative amplification, is rapidly rising while

* A part of this work was done by the author as contract research for Princeton University, N. J., U. S. A.

that of the other is rapidly falling. Basically, therefore, the problem of determining the switch-over time amounts to a solution of the differential equations for the grid voltage in the equivalent amplifying circuit of Fig. 3 with appropriate boundary conditions.

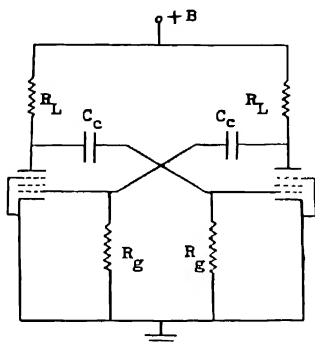


FIG. 1

A symmetrical multivibrator

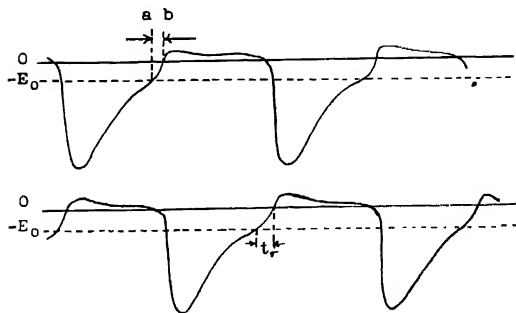


FIG. 2

The grid voltage wave forms of a symmetrical multivibrator

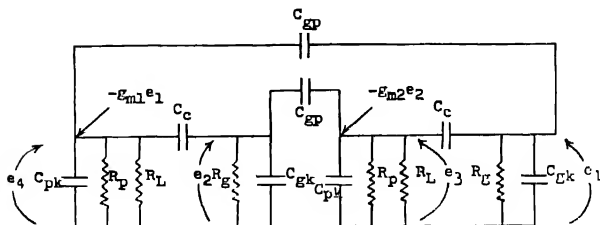


FIG. 3

A-C equivalent circuit of the multivibrator

To facilitate the application of the linear method of circuit analysis some simplifying assumptions have to be made regarding the a-c operation of the multivibrator.

1. It may be assumed that the relaxation time of the circuit is large compared to the switching time. This would permit the omission of the coupling condensers from the equivalent circuit of Fig. 3 and is a natural assumption for low frequency multivibrators. When high frequency multivibrators will be considered these coupling condensers will have to be restored.

2. It may be assumed that there is negligible inductance in the components at the frequencies under consideration.

3. It may be assumed that the tubes used have negligible grid to plate capacitance C_{gp} . This assumption would be valid only for pentode tubes, and at lower frequencies.

4. It may also be assumed that during the interval ab the value of the mutual conductance of the two tubes remains constant and is equal to the normal value g_m . In fact, this is the weakest assumption of all, since the full value of the mutual conductance of the tube that starts to be switched on at the instant a (Fig. 2) is not established till somewhat later than a . However, for the sake of linearising the analysis this assumption has to be made, and it comes close to being true, again, in the case of pentode tubes.

With the above-mentioned assumptions the simple equivalent circuit of Fig. 4 is obtained, and its differential equations are given below (p.285) where

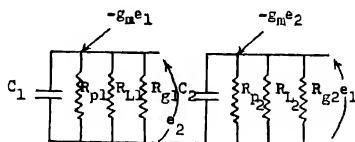


FIG. 4

A simplified a-c equivalent circuit of the symmetrical multivibrator

the total shunting capacitances and conductances are indicated by the letters C and G , and p denotes the time derivative d/dt .

$$(G_1 + pC_1)e_1 + g_{m2}e_2 = 0 \quad (1)$$

$$g_{m1}e_1 + (G_2 + pC_2)e_2 = 0 \quad (2)$$

The determinant of these equations is written in an expanded form below, and it has been equated to zero so that the exponentials arising in the circuit may be determined.

$$p^2 C_1 C_2 + p(C_1 G_2 + C_2 G_1) + (G_1 G_2 + g_{m1} g_{m2}) = 0 \quad (3)$$

If C_1/G_1 , the shunt time constant, is denoted by t_{1s} , and C_2/G_2 by t_{2s} , the mid-frequency amplification g_{m1}/G_1 is denoted by A_1 , and g_{m2}/G_2 by A_2 and $A_1 A_2 = A^2$, then the roots of (3) are

$$p_{1,2} = -\frac{1}{2}(t_{1s} + t_{2s}) \pm \left[\frac{1}{4} \left(\frac{1}{t_{1s}} - \frac{1}{t_{2s}} \right)^2 + \frac{A^2}{t_{1s} t_{2s}} \right]^{\frac{1}{2}} \quad (4)$$

In a symmetrical circuit the roots will be.

$$p_1 = \frac{(g_m - G)}{C}; \quad p_2 = -\frac{(g_m + G)}{C} \quad (5)$$

It is obviously the presence of the positive root p_1 which causes instability and makes the grid voltages e_1 and e_2 rise or fall rapidly to the level where the tube that was previously conducting, now goes off and the other one comes on. It is further seen that the condition of disappearance of the positive root is that A , the mid-frequency amplification should be less than unity. This result could, of course, be anticipated from a simple feedback consideration, but in this case it only confirms the validity of the calculation. It is also clearly indicated that the requirement for a rapid switch-over, or large positive root, is that the quotient g_m/C should be large.

In order to derive an explicit equation for the time of rise for e_1 or e_2 during the switching interval, one of the voltages may be written as follows:

$$e_1 = A_1 e^{p_1 t} + A_2 e^{p_2 t} \quad \dots (6)$$

Before proceeding with the application of the boundary conditions, however, if e_1 is considered to be the expression for the grid voltage of the tube that is being switched on, it is useful to consider the fact that the voltage e_1 starts rising rapidly from a value $-E_0$ (this is not the same as the cut-off voltage $-E_{c0}$ in the case of static plate voltage) that is, the grid voltage at which plate current just starts to flow. The switch-over time may, therefore, be defined as the time required by e_1 , given in equation (6), to rise from a value zero by an amount $|E_0|$. Alternatively, the expression for e_1 may be modified and put in the form

$$e_1 = A_1 e^{p_1 t} + A_2 e^{p_2 t} - E_0 \quad \dots (7)$$

so that the time of switch-over may be defined as the time required by e_1 , given by equation (7), to rise from a value $-E_0$ to zero volts.

It is obvious that these two expressions will yield the same value of the time of switch-over, but it may be added that equation (7) proves to be more convenient for mathematical handling and will therefore be used in all further calculations.

Equation (7) has, then, to be solved with two boundary conditions. The first is that at time $t=0$, $e_1 = -E_0$ and therefore $A_1 + A_2 = 0$. The second boundary condition is that at $t=0$, the slope of e_1 given from equation (7) should be the same as the slope of the grid voltage in the preceding

relaxation period at t just less than zero. This slope can be proved to be continuous by an elaborate mathematical analysis but the following physical explanation also shows the same. The grid whose voltage e_1 is being considered is the grid of the tube that was off at $t < 0$ and which is coupled through the condenser C_c to the plate of the tube that was conducting current at $t < 0$ and continues to conduct till after $t = 0$. With reference to Fig. 4 g_m is the mutual conductance that is assumed to jump from zero to a constant (normal) value. This jump will cause a discontinuity in the derivative of the current flowing into the plate of this tube, but due to the shunting capacitance the voltage at the plate will be continuous. This voltage is transferred by the coupling condenser to the grid of the second tube, and thence to the plate of the second tube. The quantity $g_{m2}e_2$ is continuous because both its constituents are continuous, and since this current determines the slope de_1/dt , it is concluded that de_1/dt must also be continuous.

The relaxing condenser voltage is given by the well-known equation :

$$e_c = (\text{most negative voltage}) e^{-t'/\text{series time constant } T} \quad \dots (8)$$

where t' is measured from the instant the condenser reaches its most

negative voltage, $T = C_c \left(R_g + \frac{R_p R_c}{R_p + R_c} \right)$ and $t = 0$ of equation (7)

corresponds to that value of t' which makes $e_c = -E_0$. Thus,

$$\left(\frac{de_c}{dt} \right)_{e_c = -E_0} = \left(\frac{de_1}{dt} \right)_{e_1 = -E_0} = \frac{|E_0|}{T} = A_1 p_1 + A_2 p_2$$

and finally,

$$e_1 = \frac{|E_0|}{T(p_1 - p_2)} [e^{p_1 t} - e^{p_2 t}] - E_0 \quad \dots (9)$$

THE TRANSIENT SWITCH-OVER TIME

It can now be seen that the switch-over time or the time of rise t_r , being the time required for e_1 to become zero, can be easily calculated. However, the explicit equation for e_2 can also be derived, and if the time t_{r2} , required by e_2 to go from zero to $-E_0$ is shorter than t_{r1} , then of course the amplifying circuit will be opened at the instant t_{r2} and in such a case t_{r2} will be the effective switch-over time of the whole circuit. It may be noticed that as far as the design work is concerned, the exponentials for e_1 and e_2 being the same, the value of either t_{r1} or t_{r2} can be taken as the basis of the calculation.

In order to have an explicit equation for the time of rise, the exponential term with a negative coefficient may be omitted, because this term rapidly decreases to zero and only affects the form of the grid voltage e_1 in the beginning.

Thus,

$$t_r = \frac{\ln[T(\phi_1 - \phi_2)]}{\phi_1} \quad \dots (10)$$

$$= \frac{\ln \left[\left(R_\theta + \frac{R_p R_L}{R_p + R_L} \right) \frac{2g_m C_c}{C} \right]}{\frac{1}{C} \left(g_m - \frac{R_p R_L + R_\theta R_L + R_\theta R_p}{R_p R_\theta R_L} \right)} \quad \dots (11)$$

It is interesting to note that the quantity $-E_0$ does not appear in this expression for t_r due to the special boundary conditions.

The calculated variations of the time of rise, when the various elements in the circuit are varied, have been plotted in Figs. 5, 6 and 7 and a set of

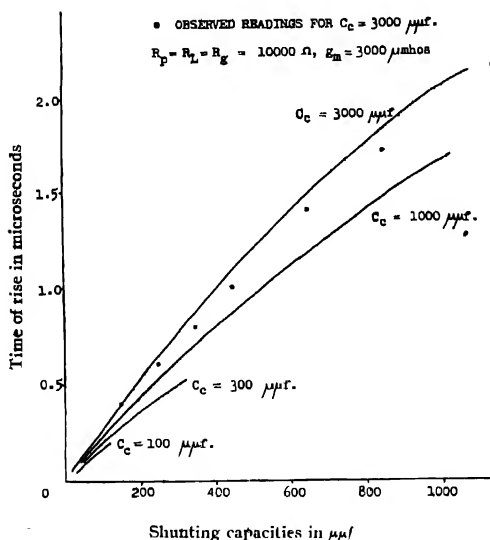


FIG. 5

Calculated curves for the variation of the time rise with shunting capacities $-g_m$ constant

observations to check these results has been given in Table I. Further observational results are found in reference (Ahmed, 1948). In connection with plotting the data in Fig. 5, it may be remarked that the observed time of rise for zero external shunt capacitance was taken as the basis for estimating the effective shunting capacitance. This is found to be $150 \mu\mu f$ (including the effect of $C_{\theta p}$) and so $150 \mu\mu f$ has been added to the externally connected condenser in each observation:

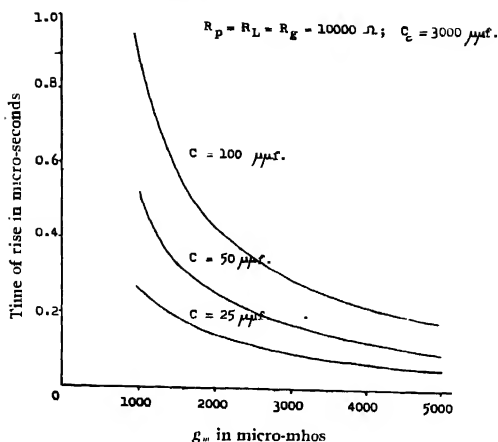


FIG 6

Calculated curves for the variation of the time of rise with mutual conductance C , constant

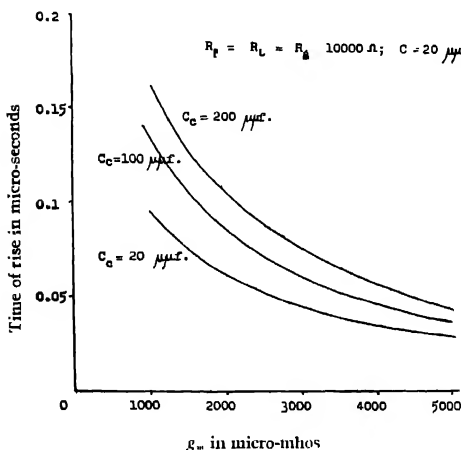


FIG. 7

Calculated curves for the variation of the time of rise with mutual conductance C constant

The divergence between the observed and calculated results is noticeable as the shunting capacitance becomes large as compared to the coupling capacitance. This is natural since the equation for the time of rise was developed on the assumption that the coupling condenser was very much larger than the total shunting capacitance.

TABLE I

Circuit components as in Fig. 5; $C_c = 3000 \mu\text{f}$.

External shunting capacitance	Effective shunting capacitance	Switching time
0 μf	150 μf	0.4 μsec
100 "	250 "	0.6 "
200 "	350 "	0.8 "
300 "	450 "	1.0 "
500 "	650 "	1.4 "
700 "	805 "	1.7 "
1000 "	1150 "	2.2 "

The effect of grid to plate capacitance C_{gp}

Under the same set of assumptions as above, the exponentials which determine the time of rise are given by :

$$p_1 = \frac{1}{C + 4C_{gp}}(g_m - G); \quad p_2 = \frac{-1}{C}(g_m + G) \quad (12)$$

These show clearly that the positive root p_1 has been considerably decreased, and that the time of rise will therefore increase when an appreciable amount of grid to plate capacitance is present. When it is desired to reduce the switch-over time in a circuit, it is necessary to minimise the capacitance C_{gp} . A set of observations is given in Table II to illustrate the effect of C_{gp} and a comparison with the previous set will indicate that C_{gp} is several times more effective per micro-farad in changing the time of rise than the shunting capacitance. From these observations, however, it is not possible to separate the C_{gp} from the rest of the shunting capacitance.

TABLE II

Circuit of Fig. 1 with $R_L = R_g = 10 \text{ k}\Omega$; $C_c = 3000 \mu\text{f}$; 6J5 tubes at 100 volts.

Externally connected C_{gp}	Time of rise
0 μf	0.4 μsec
20 "	0.7 "
30 "	0.9 "
50 "	1.2 "
100 "	1.6 "
200 "	3.0 "

The effect of positive return for the grid

The ends of the grid resistances R_g which have so far been connected directly to the cathodes may also be connected to a source of positive potential E_+ . This will be a purely d-c condition and will, therefore, not change the differential equations (1) and (2). The discharge of the coupling condenser will, however, now take place under different steady-state conditions and so will affect the time of rise. It may be expected even quantitatively that by making the condenser discharge sharper than before the switch-over time will be shortened. In this case the time of rise may easily be shown to be approximately

$$t_r = \frac{\ln \left[T(p_1 - p_2) \frac{|E_0|}{E_+ + |E_0|} \right]}{p_1} \quad (13)$$

A set of values for the time of rise has been calculated and plotted in Fig. 8 and the observations given in Table III, were taken to check the general form of the result.

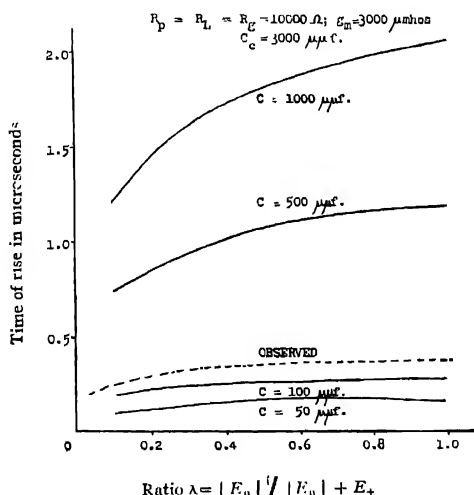


FIG. 8
Calculated variations of the time of rise with
positive grid return voltage

In conclusion it must be stated that by means of a simple linear analysis of the multivibrator circuit in the state when both tubes conduct, it is possible to obtain a fairly accurate idea of the quantitative value for the time of switch-over. The variations of the time of rise with different circuit components can also be predicted. The difference between the observed and

calculated results is explicable on the basis of assumptions made. The equations developed lead to reliable design criteria and, in fact, the author carried out such designs and constructed multivibrators with frequencies of several megacycles per second.

TABLE III

Circuit of Fig. 1 with all resistances = 10 k Ω ; $C_c = 3000 \mu\text{f.}$; 6J5 tubes with 160 volts on the plates.

Positive return voltage	Peak plate voltage	Cut-off voltage	Time of rise
0 v.	145 v.	-14.0 v.	0.37 μ sec.
25 "	112 "	-12.1 "	0.32 "
15 "	96 "	-11.3 "	0.28 "
65 "	78 "	-10.0 "	0.26 "
85 "	60 "	-8.0 "	0.24 "
105 "	41 "	-6.0 "	0.22 "

ACKNOWLEDGMENTS

The author wishes to acknowledge gratefully the advice and guidance of Prof. N. W. Mather and Prof. W. H. Surber of Princeton University, N. J., U.S.A., where a part of this work was done as contract research. Thanks are also due to Prof. P. S. Gill for his permission and encouragement to continue the work.

DEPARTMENT OF PHYSICS
ALIGARH UNIVERSITY

REFERENCES

- Abraham H., and Bloch R., 1927. *Annales de Physique*, **12**, 114.
 Ahmed R. 1948, Master's Thesis, Princeton University, U.S.A.
 Bode H. W., 1947, "Network Analysis and Feedback Amplifier Design," D. Van Nostrand Company, Inc., New York.
 Kiebert M. V., and Ingilis A. F., 1945. *Proc. I.R.E.*, **33**, 534.
 Williams R. M., Aldrich D. F. and Woodford J. B., 1950, *Proc. I.R.E.*, **38**, 65.

AN EXPLANATION OF THE INFLUENCE OF THE FREQUENCY OF THE EXCITING POTENTIAL ON JOSHI EFFECT

By G. V. BAKORE

(Received for publication, March 27, 1950)

ABSTRACT An increase in the supply frequency increases the positive space-charge density which enhances the intensity of ionisation by collision in the discharge space and consequently reduces the "threshold" potential V_m . This high initial positive space charge in dark reduces in effect, the negative space-charge formed under light, which according to Joshi's theory should diminish the light-effect as observed.

An increase in the supply frequency diminishes V_m and hence increases $(V - V_m)$, V being the applied potential. The proportion of the high frequency components of the discharge current decreases with increase in V as also $(V - V_m)$. Hence an increase in the supply frequency decreases the high frequency components which, according to Joshi, leads to a diminution of the Joshi-effect.

Other theories of Joshi-effect are also discussed in this connection.

The light effect Δi , a reversible and (sensibly) instantaneous current change, usually though not invariably, a diminution on irradiation from extreme red to X-rays (Joshi 1944b, 1945b), of chlorine and a number of other gases and vapours have been observed with semi-and full ozoniser discharges.

Joshi (1939) has shown that the measurements of the minimum "threshold" potential V_m , at which the current i increases rapidly with the applied voltage V , are markedly sensitive to changes in frequency. Joshi (1945d) observed that *ceteris paribus* % Δi decreases as the input frequency of the A.C. supply is increased. Mohanti (1949) has observed in oxygen that whereas V_m for 50 cycles is about 2.7 kV, it is as small as 0.7 kV under otherwise identical conditions with 500 cycles. Deshmukh (1949), in iodine vapours, observed that V_m changes from 2.1 kV to 0.27 kV as the frequency of the A.C. supply is varied from 50 cycles to 500 cycles. Mohanti, in oxygen, observed that increase of current i with the applied voltage V is far more rapid at 500 cycles than at 50 cycles. Further, he observed that under constant conditions of the current in the dark (i_D), Δi and % Δi for 50 cycles is larger than for 500 cycles. Thus % Δi decreases from 42% to 21% (current in the dark $i_D = 3$) with increase in frequency from 50 to 500 cycles. Similar results have been obtained by Deshmukh (1949) in iodine vapours when the system was excited in the range of 50 to 500 cycles. Joshi and Lad (1945 e) with chlorine observed that no light-effect is observed when the system is excited with high frequencies in the range of 5—12 mega-

cycles. Mohanti, with oxygen, observed no light effect when the system is excited in the range of 3—11 megacycles. Observations of Tiwari and Prasad (1945), Dasgupta and Laheri (1949), and Das Gupta (1945-46) with chlorine are similar

From the data given above it appears that V_m diminishes as the frequency of the exciting potential is increased. Its influence on the light effect expressed as $\frac{100 \times \Delta i}{i_D} = \% \Delta i$ is also in the same direction and no light effect is observed at very high frequencies (3-12 megacycles).

The processes which occur in an ozoniser discharge are complicated by a number of factors, namely, the dielectric nature of the electrodes and the field distortion due (i) to the deposition of ions on the dielectric surface and (ii) due to the space-charges of positive and negative ions, which owing to differences in mobilities of electrons and ions and diffusion, will accumulate in complicated ways (Loeb, 1939)

At and above the "threshold" potential V_m , the gas breaks down as a dielectric and discharge space consists of electrons, positive and negative ions. At the peak value of the exciting of A.C. potential, the electrons will be ionising by collision and thus positive and negative ions will be created in the gap. As the field declines these will be gradually swept out. In this sweeping the electrons will be first removed and then negative ions with their low mobility will follow. Finally if the gap is short and the fields are high even the slow positive ions will disappear. For longer gaps when the ions cannot cross during the quarter cycle, it is clear that a residue of positive charge will remain in the gap. These will gradually build up a space charge which is enhanced by diffusion of ions, which is more pronounced at low pressures. Hence the reverse cycle will never recall all the ions and the electrons of a given sign that have moved out into the gap. With lower frequency and more uniform fields the condition for gas breaks down should not materially differ from the static break down.

As the frequency of the exciting potential is increased, so that the period of the cycle is small in comparison with the time of crossing of the ions across the gap during the interval of high voltage, the matter changes radically. When the voltage is high, the ions will be generated, but before they reach the respective electrodes, the voltage falls to zero and they will again be driven across the gap to their places as the potential begins to reach high values in the reverse direction. The number of ions reaching the respective electrodes become less and less as the frequency of the exciting potential is increased. Terman (1947), in case of diodes, finds a decrease in the number of electrons reaching the anode with increase in the frequency of the applied A.C. voltage. The positive ions remaining in the gap form an enhancing space charge field for ionisation by electrons from the temporary cathode. In this way the ionisation by collision is facilitated. When the frequency goes up still further the space charge at the

temporary cathode will be increasingly greater and greater causing a progressive lowering of V_m with increase in frequency, as observed. Reukama (1928) found that for 2.5 cm. gap in air, there was a progressive lowering of V_m with increasing frequency from 20,000 to 60,000 cycles. At greater values the lowering approached a limiting value which remained constant upto 425,000 cycles. The absence of further change in V_m with increasing rate of accumulation of ions in the gap is attributed to a loss process which drives positive ions out of the gap.

According to Joshi's theory (1946, 1947a, b), (a), under electrical discharge an activated layer is formed on the electrodes and it is in dynamical equilibrium with the gas phase. (b) As a primary step photo-electric emission occurs from the active layer and (c) the photo-electrons thus emitted are converted into slow moving negative ions due to the electron affinity of the excited medium, and these reduce the current as in the space charge effect.

The magnitude of the light-effect thus depends upon the negative space-charge formed under the action of light. It is therefore to be anticipated that any factor which reduces the negative space-charge should decrease the light-effect. Increase in the supply frequency of the exciting potential causes an increase in the positive space-charge. The increased positive space-charge decreases in effect, the negative space-charge formed under light, thus decreasing the light-effect as observed. Since positive space-charge increases with increase in supply frequency, it follows that the light-effect should decrease with increase in the supply frequency. This deduction, as well as the lowering of V_m with the frequency of the exciting potential, are in agreement with the results obtained by various workers in this field.

It has been shown by Joshi (1940) that the discharge current depends on $(V-V_m)$, where V is the exciting potential. Warburg (1924), Joshi (1945d), Prasad and Jain (1947) and Deb and Ghosh (1948) have shown that the proportion of the high frequency components of the discharge current decreases with increase in the exciting potential V , as also $(V-V_m)$. Deb and Ghosh gave a mathematical expression for the variation of the proportion of the high frequency components in the discharge current with the exciting potential V , as also $(V-V_m)$.

Joshi (1944a, 1945a) has shown that the suppression of these high frequency components under light is mainly responsible for the light-effect. If V_m decreases with the frequency of the exciting potential, $V-V_m$ increases with increase in the frequency of the exciting potential. The proportion of the high frequency components of the discharge current decreases with increase in V , as also $(V-V_m)$. Hence an increase in the frequency of the exciting potential decreases the high frequency components which, according to Joshi, leads to a diminution of the light-effect.

Persad (1945) has advanced an explanation of the light-effect from the stand point of Kramer's quantum mechanical theory of light dispersion.

According to him, on irradiation the gas is excited to the higher vibrational and electronic states. For these, due to the operation of negative terms in Kramer's dispersion formula, the refractive index should be less than that of the normal gas. From the Maxwell's well known relation $n^2 = \epsilon$ (where ϵ is the dielectric constant), it follows that ϵ should decrease with decrease in n . Since ϵ is a measure of the electrostatic capacity of the system he concludes that the Joshi-effect represents a diminution of the displacement as distinct from the conduction or ohmic current. The results of Prasad and Tiwari (1945), Das Gupta (1946), Mohanti (1949) and Deshmukh (1949) do not support Prasad's view. From the observation that the wattage dissipated in the ozoniser decreases on irradiation corresponding to Δi , Joshi (1945c) concludes that the effect results chiefly from a reduction of the ohmic or conduction part of the current. Further, he observes "that the corresponding displacement current may be affected is suggested by a frequent observation of a sensible movement and distortion on irradiation of the steadied wave form on the oscillograph, due, perhaps to a frequency or / and phase shift; by the observed influence on $\% \Delta i$ of capacitative changes in the system, suggesting a change under light of the dielectric constant of the ionised gas as possibly a partial, though at best a minor explanation of this phenomenon of ageing, adsorption and nature of the material".

Deb and Ghosh (1946-47-1948) take the mechanism of the origin of the high frequency components as given by Klemenc,* Hintonberger and Hoffer (1937). According to them, the high frequency components of the discharge current originate from the neutralisation of the surface charges when the applied voltage passes through its zero value. As the surface charges are on the insulating (glass) surface, the neutralisation does not take place in the single spark but in a number of sparks between small isolated elements of the surface charges. Deb and Ghosh advance a view that the action of light is to restrict the formation of the surface charges thus suppressing the high frequency components of the discharge current. The suppression of the high frequency components under light is mainly responsible for the light-effect.

According to these authors "as the frequency of the applied voltage is increased the pulsation time becomes equal to and finally less than the time required for the full deposition of the charges. Increase of frequency therefore causes a decrease in the density of the surface charges. Hence the H.F. components of the discharge current as also the light-effect decrease as the frequency is increased".

The mechanism, although accounts for the decrease in the light-effect with increase in frequency of the exciting potential, fails to show why V_m should decrease with increase in the supply frequency. Both these factors are well accounted for on the suggestions put forward in the present paper.

ACKNOWLEDGMENTS

The author wishes to express his grateful thanks to Prof. S. S. Joshi, University Professor of Chemistry, Hindu University, Banaras, to Prof. M. F. Soonawala, Head of the Department of Physics and Dr. W. V. Bhagwat, Professor of Chemistry, Holkar College, Indore, for their kind interest and valuable guidance.

PHYSICAL LABORATORIES
MAHARAJA'S COLLEGE, JAIPUR

REFERENCES

- Das Gupta, 1946, *Science and Culture*, **11**, 318
- Das-Gupta and Laheri, 1949, Proceedings Indian Sci. Cong 1949, Part III, Phys Sec. Abst. No. 30.
- Deshmukh, 1949, *Proc. Indian Acad. Sci.*, 1949, **29**, 245, 251, 252
- Deb and Ghosh, 1946-47, *Sci. and Cult.*, **12**, 17-19.
- " " 1948, *Jour. Indian Chem. Soc.*, **25**, 445, 451, 462
- Joshi and Narsimhan, 1940, *Curr. Sci.* **9**, 536
- Joshi, 1939, *ibid.*, **8**, 548
- " , 1944a, *Nature*, **154**, 147
- " , 1944b, *Curr. Sci.*, **13**, 278
- " , 1945a, *ibid.*, **14**, 67
- " , 1945b, " **14**, 317
- " , 1945c *Proc. Indian Acad. Sci.*, **A 22**, 225
- " , 1945d, *ibid.*, **A 22**, 389
- " and Lad, 1945 e, *ibid.*, **22**, 293, 295, 296
- Joshi, 1946, *Proc. Indian Sci. Cong. 1946*, Part III. Phys. Sec. Abst. No. 26.
- " , 1947a, *ibid.*, Part III Phys. Sec. Abst. No. 25
- " , 1947b, *Curr. Sci.*, **16**, 19-21
- Klemenc and others, 1937, *Z. Electrochem.*, **43**, 708
- Loeb, 1939, Fundamental Processes of Electrical discharge in gases, 1939, pp. 550-552
- Mohanti, 1949, *Jour. Ind. Chem. Soc.*, **26**, 507-510
- Prasad and Tewari, 1945, *Curr. Sci.*, **14**, 229, 247
- Prasad and Jain, 1947, *Proc. Indian Acad. Sci.*, **25a**, 675.
- R. Persad, 1945, *Nature*, **155**, 362.
- Reukama, 1928, *Trans. Am. Inst. Elect. Eng.*, **47**, 38.
- Terman, 1947, *Radio Engineering* pp. 194.

MULTIPLY SEPARATIONS IN THE f^1 -ELECTRON CONFIGURATION

By K. SURYANARAYANA RAO

(Received for publication, April 26, 1950)

ABSTRACT The separation factors are calculated for the multiplet terms of the f^1 -electron configuration, using Goudsmit's method. A table of the results is given. All the terms are predicted to be normal with the exception of 3D .

In a paper on the "Multiplet Separations" in terms due to equivalent electron configurations, Goudsmit (1928), applying the X-ray doublet law to the optical spectra, has given a general method for calculating the separation factors for equivalent electron configurations by which he calculated the separations for p^n and d^n configurations. Recently, Ramakrishna Rao (1949), extending the method to f -electron configurations, has calculated the separations for f^1 , f^2 , and f^3 electron configurations, which are useful in the analysis of the spectra of rare-earths. It is proposed here to extend the same method to the f^1 -electron configuration, but it may be noted that the mathematical difficulties will increase if we begin to deal with the more complex f -electron configurations. The theory of the method may be briefly outlined as follows :

The doublet separation in optical spectra, which is due to a single electron is given by the formula

$$\Delta\nu = \frac{Rch\alpha^2 Z^4 e f f}{n^3 l(l+1)} \quad \dots (1)$$

which is conveniently written as

$$\Delta\nu = a(l + \frac{1}{2})$$

The multiplet separations arise out of the interaction between the spin and orbital angular momenta of the electron which is well-known to be equal to

$$\Gamma = \sum_i a_i l_i s_i \cos(\overline{l_i s_i})$$

where all the quantities have the usual significance (Pauling and Goudsmit, 1930). This may be written as

$$\Gamma = ALS \cos(LS) = \frac{1}{2} A [J(J+1) - L(L+1) - S(S+1)] \quad \dots (2)$$

with

$$A = \sum_i a_i \frac{S_i}{S} \cos(\overline{S_i S}) \frac{l_i}{l} \cos(\overline{l_i l})$$

in the case of R-S coupling. It is seen from the above formula that the levels in a multiplet are separated by the difference in the values of J . So Γ gives the displacement of the actual multiplets over hypothetical level which is actually the centre of gravity of the multiplet. These Γ -factors obey the same 'Sum' and 'Permanence' rules as do the ' g '-factors. In a weak-field an atom is spatially quantized so that the vector J has the component ' M ' along the field. If the field is increased to such an extent that the ' ls ' coupling is broken, the vectors ' l ' and ' s ' precess independently around the field and

$$\cos(\overline{sl}) = \cos(sH) \cos(lH) = \frac{m_s m_l}{sl}$$

$$\Gamma = A ls \cos(ls) = A m_l m_s \quad (3)$$

Thus the weak-field Γ -values are given by equation (2) and strong-field values are given by formula (3) and using the Γ -permanence rule established by Goudsmit, which states that the sum of Γ -values corresponding to a given value of M is the same for a strong field as for weak one, the separations for any configuration can be calculated.

CALCULATIONS

It has been already shown (Rao, 195c) in a previous paper that in the case of f^4 -electron configuration, the number of valid wave-functions is 400, and Table I is only a typical portion of a very extensive table showing how to obtain the Γ -values in a strong field. In the table,

TABLE I

m_{l_1}	m_{l_2}	m_{l_3}	m_{l_4}	m_{s_1}	m_{s_2}	m_{s_3}	m_{s_4}	M_s	M_L	M	$\frac{\Gamma_1}{a}$	$\frac{\Gamma_2}{a}$	$\frac{\Gamma_3}{a}$	$\frac{\Gamma_4}{a}$	$\frac{\Gamma}{a}$
$\frac{1}{2}$	3	$\frac{1}{2}$	2	$\frac{1}{2}$	1	$\frac{1}{2}$	0	2	6	8	$1\frac{1}{2}$	1	$\frac{1}{2}$	0	3
"	"	"	"	"	"	"	-1	"	5	7	"	"	"	$-\frac{1}{2}$	$2\frac{1}{2}$
"	"	"	"	"	"	"	-2	"	4	6	"	"	"	-1	2
"	"	"	"	"	"	"	-3	"	3	5	"	"	"	$-1\frac{1}{2}$	$1\frac{1}{2}$
$\frac{1}{2}$	3	$\frac{1}{2}$	2	$\frac{1}{2}$	1	$-\frac{1}{2}$	-3	1	3	4	$1\frac{1}{2}$	1	$\frac{1}{2}$	$+1\frac{1}{2}$	$4\frac{1}{2}$
"	"	"	"	"	"	"	-2	"	4	5	"	"	"	1	4
"	"	"	"	"	"	"	-1	"	5	6	"	"	"	$\frac{1}{2}$	$3\frac{1}{2}$
"	"	"	"	"	"	"	0	"	6	7	"	"	"	0	3
"	"	"	"	"	"	"	1	"	7	8	"	"	"	$-\frac{1}{2}$	$2\frac{1}{2}$
"	"	"	"	"	"	"	2	"	8	9	"	"	"	-1	2
"	"	"	"	"	"	"	3	"	9	10	"	"	"	$-1\frac{1}{2}$	$1\frac{1}{2}$

$$M_S = \sum m_s$$

$$M_L = \sum m_l \text{ and } M = M_S + M_L;$$

$$\frac{\Gamma_1}{a} = m_{l_1}, m_{s_1}; \quad \frac{\Gamma_2}{a} = m_{l_2}, m_{s_2}; \quad \frac{\Gamma_3}{a} = m_{l_3}, m_{s_3}; \quad \frac{\Gamma_4}{a} = m_{l_4}, m_{s_4}$$

$$\frac{\Gamma}{a} = \sum \frac{\Gamma_i}{a} = \frac{\Gamma_1}{a} + \frac{\Gamma_2}{a} + \frac{\Gamma_3}{a} + \frac{\Gamma_4}{a}$$

which gives the strong field Γ -value for a particular M -value. Thus all the Γ -factors corresponding to the strong field are obtained and presented in Table II. The weak-field Γ -factors are calculated from formula (2) and are presented in Table III which is given only from $M=10$ to $M=0$, as the other part from $M=-1$ to $M=-10$ is symmetrically disposed to the above part, about the value $M=0$. In this table the letters I, G, M' etc., are actually $A_I, A_G, A_{M'}$, etc., but are abbreviated thus for convenience. Also a prime is used for some of these letters in triplets to distinguish the same kind of terms in triplets and quintets. The numbers in parentheses before some of the states in this table give the number of times those terms occur. Now by equating, according to the Γ -permanence rule, the sum of Γ -values corresponding to a particular value of M in the weak-field to the sum of Γ -factors of the same M -value in the strong field (starting from the highest value of M), it can be seen that only $^3M_{10}$ can be uniquely calculated by putting $^3M' = \frac{1}{2}a$ or $M' = \frac{1}{6}a$ and that for other columns there are more unknowns than the available equations. This mathematical difficulty can be circumvented by treating the quintets separately. For example, the 1I_6 level

is given by the weak-field wave-function $(3^+2^+1^+0^+)$, giving $\frac{\Gamma}{a} = \frac{3}{2} + 1 + \frac{1}{2} + 0 = 3$; so $^12I = 3a$ or $I = \frac{1}{3}a$. Similarly 1G_6 is given by two wave-functions because of its degeneracy in 1I , namely, $(3^+2^+1^+-2^+)$ and $(3^+2^+0^+-1^+)$, giving $\frac{\Gamma}{a} = \frac{3}{2} + 1 + \frac{1}{2} - 1 = 2$ in one case and $\frac{\Gamma}{a} = \frac{3}{2} + 1 + 0 - \frac{1}{2} = 2$ in the other. Thus

the strong-field Γ -values for 1G_6 are the same, which means that the degeneracy does not present any difficulty. Nor is it necessary to know which of the two functions actually belongs to 1G_6 , because the required Γ -values are the same in both the cases. Similarly all the other quintet separations come out to be equal to $\frac{1}{4}a$, except 3S for which the Γ -value is zero, $\frac{1}{4}a$ as can be verified from the five wave-functions each giving zero. Substituting these values of quintets it can be seen that we are left with one unknown in each column. It must be borne in mind here that the triplet levels also cannot be treated separately in the same way because of their intrinsic degeneracy not only amongst themselves but also in the quintets. The results are given in Table IV from which it can be seen that there is only one inverted term, namely, 3D in the f^4 -electron configuration.

TABLE II

M M_S	10	9	8	7	6	5	4	3	2	1	0	-1	-2	-3	-4	-5	-6	-7	-8	-9	-10
2																					
1	$1\frac{1}{2}$	3	3	$2\frac{1}{2}$	$1\frac{1}{2}$	$2\frac{1}{2}$	1	2	0	-2	-4	$-1\frac{1}{2}$	-4	$-2\frac{1}{2}$	-3	-7	-5	-3	$-1\frac{1}{2}$		
0	0	0	0	0	0	0	0	0	0	0	0	0	0	0	0	0	0	0	0	0	0
-1			$-1\frac{1}{2}$	-3	-5	-7	-8 $\frac{1}{2}$	-10	-10	-7	-4	0	1	7	10	10	8 $\frac{1}{2}$	7	5	3	$1\frac{1}{2}$
-2																					
ΣF	$1\frac{1}{2}$	3	$6\frac{1}{2}$	6 $\frac{1}{2}$	7 $\frac{1}{2}$	7 $\frac{1}{2}$	2 $\frac{1}{2}$	-3 $\frac{1}{2}$	-10	-13 $\frac{1}{2}$	-16	-13 $\frac{1}{2}$	-10	-3 $\frac{1}{2}$	2 $\frac{1}{2}$	7 $\frac{1}{2}$	7 $\frac{1}{2}$	6 $\frac{1}{2}$	6 $\frac{1}{2}$	3	$1\frac{1}{2}$

TABLE III : Weak-field Table

$\frac{M}{MS}$	10	9	8	7	6	5	4	3	2	1	0
6I_8			12I	12I	12I	12I	12I	12I	12I	12I	12I
7				4I	4I	4I	4I	4I	4I	4I	4I
6					-31I	-3I	-3I	-3I	-3I	-3I	-3I
5						-9I	-9I	-9I	-9I	-9I	-9I
4							-14I	-14I	-14I	-14I	-14I
5G_8					8G	8G	8G	8G	8G	8G	8G
5						2G	2G	2G	2G	2G	2G
4							-3G	-3G	-3G	-3G	-3G
3								-7G	-7G	-7G	-7G
2									-10G	-10G	-10G
6F_8						6F	6F	6F	6F	6F	6F
4							F	F	F	F	F
3								-3F	-3F	-3F	-3F
2									-6F	-6F	-6F
1										-8F	-8F
5D_4							4D	4D	4D	4D	4D
3								0	0	0	0
2									-3D	-3D	-3D
1										-5D	-5D
0											-6D
5S_2									0	0	0
$^3M_{10}$	9M'	9M'	9M'	9M'	9M'	9M'	9M'	9M'	9M'	9M'	9M'
0		-M'	-M'	-M'	-M'	-M'	-M'	-M'	-M'	-M'	-M'
8			-10M'	-10M'	-10M'	-10M'	-10M'	-10M'	-10M'	-10M'	-10M'
3L_2		8L	8L	8L	8L	8L	8L	8L	8L	8L	8L
8			-L	-L	-L	-L	-L	-L	-L	-L	-L
7				-9L	-9L	-9L	-9L	-9L	-9L	-9L	-9L
3K_8			14K	14K	14K	14K	14K	14K	14K	14K	14K
(2)7				-2K	-2K	2K	-2K	2K	-2K	-2K	-2K
6					-16K	-16K	-16K	-16K	-17K	-16K	-16K

TABLE III : Weak-field Table (contd.)

M	M	10	9	8	7	6	5	4	3	2	1	0
5I_7					$12I'$	$12I'$	$12I'$	$12I'$	$12I'$	$12I'$	$12I'$	$12I'$
(2)6						$-4I'$	$-2I'$	$-2I'$	$-2I'$	$-2I'$	$-2I'$	$-2I'$
5							$-14J'$	$-14J'$	$-14J'$	$-14J'$	$-14J'$	$-14J'$
3H_6					$20H$	$20H$	$20H$	$20H$	$20H$	$20H$	$20H$	$20H$
(4)5						$-4H$	$-4H$	$-4H$	$-4H$	$-4H$	$-4H$	$-4H$
4							$-24II$	$-24H'$	$-24H'$	$-24H'$	$-24H'$	$-24H'$
3G_5							$12G$	$12G'$	$12G'$	$12G'$	$12G'$	$12G'$
(3)4								$-3G'$	$-3G'$	$-3G'$	$-3G'$	$-3G'$
3								$-15G'$	$-15G'$	$-15G'$	$-15G'$	$-15G'$
3F_4								$12F'$	$12F'$	$12F'$	$12F'$	$12F'$
(4)3								$-4F'$	$-4F'$	$-4F'$	$-4F'$	$-4F'$
2									$-16F'$	$-16F'$	$-16F'$	$-16F'$
3D_3									$4D'$	$4D'$	$4D'$	$4D'$
(2)2									$-2D$	$-2D'$	$-2D'$	$-2D'$
1										$-6D'$	$-6D'$	$-6D'$
3P_2										$3P$	$3P$	$3P$
(3)1										$-3P$	$-3P$	$-3P$
0											$-6P$	$-6P$
ΣI		$9M'$	$8M' + 8L$	$-2M' + 7L + 14K + 12I$	$-2M' - 2L + 12K + 12J' + 16I$	$-2M' - 2L - 4K - 4I' + 10H + 13J' + 8G$	$-2M' - 2L - 4K - 4I' + 16H + 12G' + 4I + 10G + 6P$	$-2M' - 2L - 4K - 4I' - 8H + 9G' + 12F' - 10I' + 7G + 7F + 4D$	$-2M' - 2L - 4K - 4I' - 8H - 6G' + 8F' + 4D' - 10I' + 4F + 4D$	$-2M' - 2L - 4K - 4I' - 8H - 6G' - 8F' + 2D' + 3P - 10I' - 10G - 2F + D$	$-2M' - 2L - 4K - 4I' - 8H - 6G' - 8F' - 4D' - 10I' - 10G - 10F - 4D$	$-2M' - 2L - 4K - 4I' - 8H - 6G' - 8F' - 4D' - 6P - 10I' - 10G - 10F - 10D$
M		10	9	8	7	6	5	4	3	2	1	0

TABLE IV

Multiplet	Separation factor A	Multiplet	Separation factor A
3I	$\frac{1}{2}a$	3K	$19/112 a$
3G	$\frac{1}{2}a$	3J	$17/168 a$
3F	$\frac{1}{2}a$	3H	$2/15 a$
3D	$\frac{1}{2}a$	3G	$11/60 a$
3S	0	3F	$7/48 a$
3M	$\frac{1}{8}a$	3D	$-1/24 a$
3I_1	$\frac{5}{24}a$	3P	$1/6 a$

ACKNOWLEDGMENT

The author is deeply indebted to Prof. K. R. Rao for his valuable guidance and also to Dr. V. Ramakrishna Rao for his helpful suggestions.

DEPARTMENT OF PHYSICS, ANDHRA UNIVERSITY
WALFAR

REFERENCES

- Goudsmit, 1928, *Phy. Rev.*, **31**, 946.
 Pauling and Goudsmit, 1930, 'Structure of Line Spectra' 1st Ed., p. 158.
 Rao Ramakrishna 1948, *Ind. Jour. Phys.*, **22**, 423.
 „ „ 1950, *Ind. Jour. Phys.*, (In Press).
 Rao Suryanarayana, 1950, *Ind. Jour. Phys.* **24**, 51.

AN EXPERIMENTAL STUDY OF THE ILLUMINATING SYSTEM OF THE ELECTRON MICROSCOPE

By M. L. DE

Plates IXA and IXB

(Received for publication, June 12, 1950)

ABSTRACT. The paper gives an account of the experimental study of the illuminating system of the electron microscope to determine the most efficient operating condition. The variation of the size of the electron cross-over with different grid filament distances has been observed. An attempt has been made to correlate these observations with the final image quality

INTRODUCTION

It is well-known that the illuminating system of an electron microscope influences to a great extent the quality of the final image. It is, in fact, one of the several factors which determine the ultimate limit of resolution obtainable with any particular instrument and it has, for this reason, been the subject of study, both theoretical and experimental, by several investigators (Ardenne, 1943; Becker *et al.*, 1942; Borries, 1942, 1944; Hillier and Baker, 1945; Hillier and Illis, 1949; Nissen, 1944). The present paper gives an account of the experimental study on the properties of the illuminating system of the new horizontal electron microscope (Dasgupta and others, 1948) installed at the Institute of Nuclear Physics, Calcutta

Figure 1, is a diagrammatic representation of the illuminating system. It consists of a three electrode gun constituted by the hairpin shaped

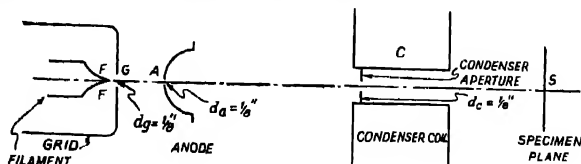


FIG. 1

Schematic diagram of the electron gun

tungsten filament *F*, a cathode shield *G* and the hemispherical anode *A*. The anode is placed at a fixed distance from the cathode-shield, while the filament to shield distance can be varied, within limits, to any desired extent. The cathode shield, for zero-bias operation, is maintained at the filament potential, while for biased operation it is given a negative voltage to serve as the control grid. The condenser lens *C* serves to concentrate the

electron beam emerging through the anode aperture, on to the specimen plane placed at S.

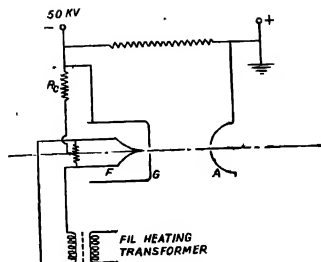


FIG 2

Electrical connection diagram of the gun

The electrical circuit of the gun is shown in Fig. 2. The filament is maintained at a high negative potential of 50 kV, while the anode is at the ground potential. The resistance R_c of 0.5 megohms provides automatic bias to the grid.

Conditions for Efficient Illumination.

The essential requirements which the illuminating system of an electron microscope must satisfy for efficient operation can be stated as follows:

(1) The angle of illumination, *i. e.* the angle which the extreme rays of the illuminating beam make with the beam axis, must have an independent means of control.

(2) The focused illumination on the specimen plane must have a small and preferably a circular size.

(3) The beam must have sufficient intensity to permit taking of micrographs at reasonably short time.

ANGLE OF ILLUMINATION

The mode of illumination of a specimen is shown schematically in Fig. 3. By reason of the electrostatic lens system consisting of the filament-grid-anode assembly, a cross-over of diameter d_k is formed in the space between the grid and the anode. The image of this cross-over can be made to fall on the specimen plane or on planes in front or beyond it, by the proper choice of the current through the condenser lens. With any particular condenser lens, current the image c' of diameter d'_k is formed as shown in the Fig. 3. Then the angular aperture of illumination or half of the angle subtended at the specimen point P by the cross-over image can be expressed as (Borries and Ruska, 1939),

$$\alpha_c = \frac{r_k}{(u_c + v'_c) - u_c v'_c / f_c} \quad \dots (1)$$

The significance of the different quantities in this expression is shown in Fig. 3, and $1/f_c$ is the power of the condenser lens, dependent on its current strength, and $r_k = d_k/2$.

For the new microscope, $u_c = 230$ mm, $v'_c = 370$ mm. so that substituting these values in the above expression, it can be written

$$\alpha_c = \frac{1.18 \times 10^{-5} \times 1_k}{7.04 \times 10^{-3} - 1/f_c} \quad \dots (2)$$

It is evident from Fig. 3 that the aperture d_c of the condenser lens sets a limit to the maximum value of α_c which is given by,

$$\alpha_{c_{max}} = \frac{d_c}{2v'_c} \quad \dots (2)$$

For $d_c = \frac{1}{8}"$, $\alpha_{c_{max}} = 4.3 \times 10^{-3}$ radian

and for $d_c = \frac{1}{16}"$, $\alpha_{c_{max}} = 2.15 \times 10^{-3}$ radian

The variation of α_c , the angle of illumination with the condenser lens power has been calculated for various values of 1_k and the results are shown in Fig. 4.

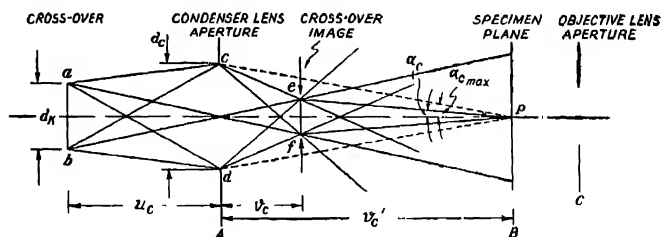


FIG. 3

Ray diagram illustrating the mode of illumination of the specimen

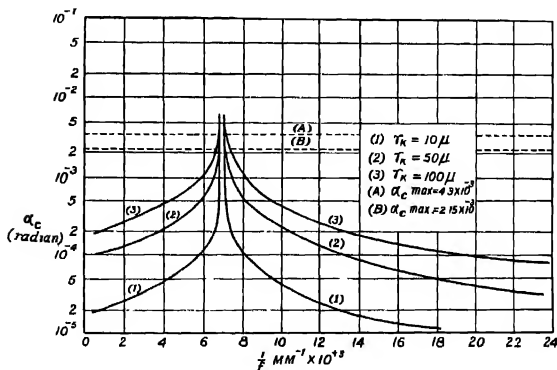


FIG. 4

Variation of α_c , The angle of illumination with the power of the condenser

SIZE OF FOCUSED ILLUMINATION ON SPECIMEN PLANE

From considerations of expression (2) and Fig. 4, two conclusions can be arrived at, viz., for the same condenser lens power, α_c decreases as r_k is reduced and secondly, the rate of variation of α_c with the lens power is more rapid with reduction of r_k . Low value of r_k , i.e. a small size of the cross-over image is, therefore, an essential condition for efficient operation of the illuminating system. The small cross-over size has the additional advantage that, on being focused on the specimen, it illuminates at a time only a small area which is under observation at the particular instant. Heating of the specimen under this condition is, therefore, minimum, so that rise in temperature and the consequent chance of destruction of specimen is least. A small cross-over further ensures better contrast in the final image. In the present experiment the size and shape of the focused spot on the specimen plane was determined for different values of filament to grid spacing.

The projector pole piece as well as the intermediate screen were removed, and a blank 200 mesh wire screen was positioned in the specimen plane. With the filament to grid distance adjusted to a known value, the condenser power was set for parallel illumination of the wire mesh. The objective lens current was next adjusted to get on the final screen an image of the mesh and a photographic record was made of it, reproduced in Plate IXA, Fig. a. From the actual dimension of the mesh and that of its magnified image, an estimate was made of the objective magnification, which was found to be 20X.

The wire mesh was next removed. The objective lens power was kept unchanged from the previous value and the condenser lens current was adjusted to get the smallest focused illuminated spot on the final screen, the focused illuminated spot on the final screen was evidently a magnified form of the focused cross-over image on the specimen plane. A photographic record was made of this focused spot of illumination.

The procedure was repeated for three other values of grid-filament distance. The photographs of these illuminated spots are reproduced in Plate IXA, Figs. b-f. The photographs of Figs. (b) and (c) were taken at a lower objective magnification compared to the rest. The size of these images when divided by the objective magnification, gave the true size of the cross-over images as formed on the specimen plane.

Different grid filament distances, saturation currents and diameters of the corresponding illuminated spots, as deduced from measurements of micrographs shown in Plate IXA, are given in Table I.

Figs. (b) to (f) point to a number of interesting facts. Firstly, the formation of double image of the cross over for close grid-filament distance is apparent from Fig. (b). This picture was taken at the same setting as in Fig. (c) but with a lower beam current of 55 μ a. These two spots of Fig. (b) are found to merge into one single entity in Fig. (c) with the increase of beam current from 55 μ a to 125 μ a.

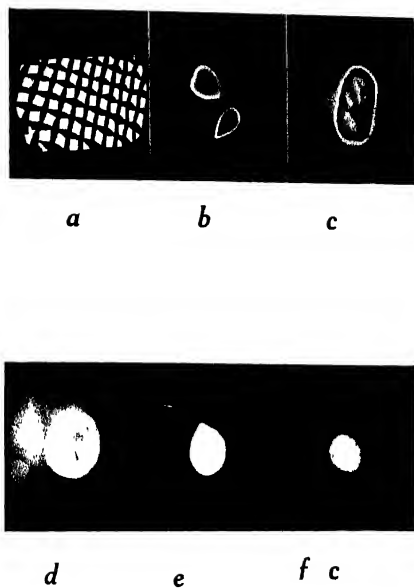
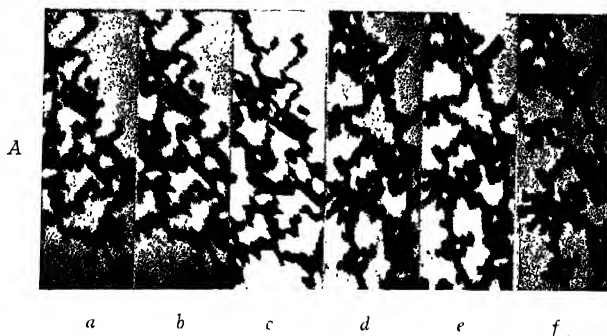
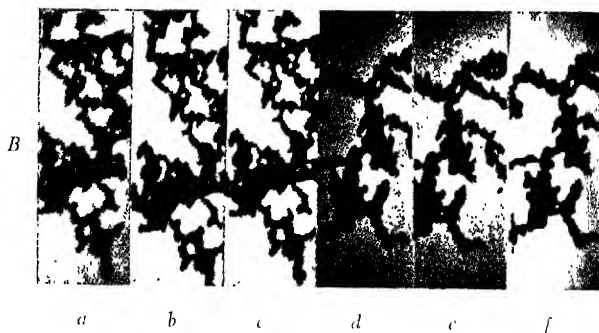


Fig. 5

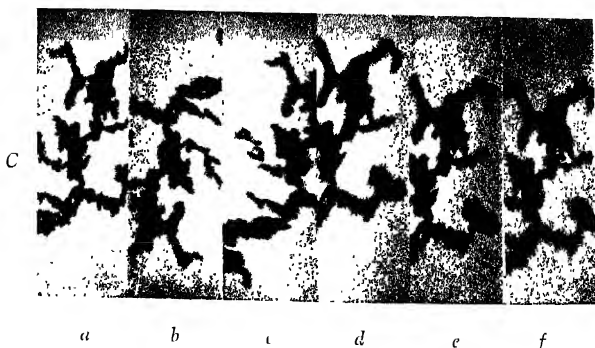
(a)—Magnified image of a wire mesh used as a support for specimen
(b)—(f) Images of illuminated spots for different grid-filament distances



Through-focus series of electron micrographs of benzene smoke for grid-filament setting corresponding to Fig (c), Plate IX



Through-focus series of electron micrographs of benzene smoke for grid-filament setting corresponding to Fig (d), Plate IX



Through-focus series of electron micrographs of benzene smoke for different grid-filament settings.

TABLE I

Variation of the size of the illuminated spot and of saturation current with different grid—filament distance

Figure (Plate IXA).	Filament to grid distance.	Size of spots from micrographs	Objective magnification.	True size of spot on specimen plane.	Saturation value of beam current	Remarks
(c)	1.6 mm.	14 mm. \times 8mm	12.5X	$1120\mu \times 650\mu^*$	125 μ A	Spot non-uniform and non-homogeneous, High beam current.
(d)	2.1 mm.	12mm dia	20.0X	607 μ	40 μ A	Spot nearly circular but non-homogeneous, medium beam current
(e)	3.2 mm	8 mm. dia.	20.0X	400 μ	20 μ A	Spot uniform and homogeneous, low beam current
(f)	4.0 mm	7 mm dia	20.0X	350 μ	5 μ A	Spot uniform and homogeneous, very low beam current

* These sizes are given in microns, 1 micron = 10^{-3} mm.

It is further seen that as the filament to grid distance is increased, a decrease in size, uniformity in shape and improvement in quality are progressively noticed in the spot images. Particularly noticeable is the absence in Figs. (e) and (f) of the internal inhomogeneity of spots which are apparent in Figs. (b), (c) and (d).

IMAGE QUALITY FOR DIFFERENT GRID FILAMENT DISTANCES

The performance of the gun having thus been studied, the dependence of the final image quality on the above mentioned factors was next considered.

With the projector pole piece re-inserted, a specimen was introduced into the microscope, the sample chosen being carbon, obtained by burning benzene and collecting the smoke on a blank wire mesh. For the different values of the grid filament spacings of the previous observation, the specimen was imaged on the final screen with a high condenser current. To obtain the position of exact focus, a through-focus series of pictures were taken for each observation. The pictures are reproduced in Plate IX B, Figs. A, B and C. All micrographs were made at fixed electronic magnification of 10,000X. With the condenser and projector currents fixed, the objective current was varied in steps. Thus in Fig. (A), the objective current was varied from 85.5 to 88ma. in steps of 0.5 ma. Figures of (B) were obtained with objective currents varying from 89 to 92 ma and in Fig. (C) current was varied from 94 to 98 ma. The three series A, B and C correspond respectively to the grid-filament

settings of Figs. (c), (d) and (e), of Plate IXA. In view of very low intensity of illumination corresponding to the setting of Fig. (f), no photograph was taken for this case.

By comparing the Figs. (A), (B) and (C) of Plate IXB it is evident that although the three series were taken with widely different beam currents of 125, 40 and 10 μ a, but with the same exposure time, the change in intensity of illumination is not appreciable. From the point of view of specimen heating, therefore optimum grid filament distance is 3.2 mm. On careful examination the particles in Fig. (C) are found to be more discrete than those in Fig. (A).

CONCLUSION

An operating condition of the electron gun ensuring efficient operation has thus been found to correspond to the grid-filament setting of Fig. (e) (Plate IXA) the distance of the grid to filament being 3.2 mm. and the saturation value of the beam current of the order of 10 μ a

Under this condition the spot of illumination is found to be symmetrical, homogeneous and of small cross-section. The low beam current further permits taking of micrographs without any chance of specimen destruction and drifting.

ACKNOWLEDGMENTS

The author is obliged and thankful to Prof. M. N. Saha, for providing laboratory facilities to carry out the present study. The author is also indebted to Dr. N. N. Dasgupta, for his valuable help and guidance and sincere thanks are due to him. Thanks are also due to the author's colleagues Messrs. D. L. Bhattacharyya and A. K. Chaudhuri for their assistance, and to the Ministry of Education, Government of India for financial aid.

BIO-PHYSICS SECTION,
INSTITUTE OF NUCLEAR PHYSICS,
UNIVERSITY OF CALCUTTA.

REFERENCES

- Ardenne, M. V., 1943, *Z. Phys.*, **121**, 1.
 Baker, R. F., Ramberg, E. G. and Hillier, J., 1942, *J. Appl. Phys.*, **12**, 450.
 Borries, B. V., 1942, *Z. Phys.*, **119**, 498
 Borries, B. V., 1942, *Phys. Z.*, **53**, 190
 Borries, B. V., 1944, *Z. Phys.*, **122**, 539
 Borries, B. V. and Ruska, E., 1939, *Zell f. tech. Phys.*, **20**, 225.
 Dasgupta, N. N., De, M. L., Bhattacharyya, D. L. and Chaudhuri, A. K., 1948, *Ind. J. Phys.*, **22**, 497.
 Hillier, J. and Baker, R. F., 1945, *J. Appl. Phys.*, **16**, 469
 Hillier, J. and Ellis, S. G., 1949, *J. Appl. Phys.*, **20**, 700.
 Nissen, H. F., 1944, *Z. Phys.*, **122**, 523.

CRYSTAL STRUCTURE OF PHENANTHRENE

B. S. BASAK

(Received for publication, June 26, 1950)

ABSTRACT: The crystal structure of phenanthrene has been determined by the help of Fourier synthesis method. Integrated intensities of a large number of axial and prism planes were determined from oscillation, rotation and moving film photographs and absolute values of structure factors were determined by comparison with aluminum. On the basis of these F -values and existing chemical physical and magnetic data, a structure is found out by trial-and-error method. Electron density projection map on the (010) face shows the picture of the molecule quite clearly. The length of one of the molecules makes an angle of 75° with the a -axis and 6° with the (010) plane and the plane of the molecule is inclined at 60° to the (010) plane. The orientation of the second molecule is governed by the twofold screw axis. A three dimensional Fourier summation to give out the detailed structure analysis is in progress.

The crystalline structure of phenanthrene was studied by the X-ray diffraction method previously by Mark and Hengstenberg (1929), who found the following dimensions for the unit cell

$$\begin{array}{ll} a = 8.60 \text{ \AA} & b = 6.11 \text{ \AA} \\ c = 19.24 \text{ \AA} & \beta = 81^\circ 45' \end{array}$$

with 4 molecules in the unit cell. From a study of systematic absent planes they assigned the space-group $C_{2h}^2 - P_{21}/c$ in the monoclinic system to this crystal. We have taken up a complete structure determination of this crystal on account of its importance in the domain of organic chemistry. From over-exposed rotation photographs and goniometric measurements, it was found out that the actual c 's axial length of the unit cell was really half the value found out by Mark and Hengstenberg with the following values for axial lengths and angles

$$\begin{array}{ll} a = 8.57 \text{ \AA} & b = 6.11 \text{ \AA} \\ c = 9.47 \text{ \AA} & \beta = 82^\circ 30' \end{array}$$

No. of molecules in the unit cell = 2.

From an examination of intensities of the (010) planes and from steric and symmetry considerations, the crystal was classified as belonging to the space group $C_{2h}^2 - P_{21}$ in the monoclinic crystal class (Basak, 1948).

Oscillation and moving film pictures about the three crystallographic axes were next recorded. The estimated intensities of the different planes

by comparison with a logarithmic sector wedge were converted to absolute intensities and thence to absolute values of structure factors by matching some of the reflections with standard aluminium powder lines.

In carrying out a two dimensional Fourier summation, the phases of the structure factor terms were determined by the conventional method of trial-and-error. The already existing chemical, magnetic and other data were utilised for narrowing out the field over which trials were to be given. From the magnetic measurements of Krishnan and Banerjee (1936), the molecular orientation in the phenanthrene crystal, assuming a planar configuration of the molecule, comes out to be as follows: The length of the molecule lies in the (010) plane at 78.5° with the a -axis. On the basis of their corrected values for magnetic data, we have made fresh calculations and the inclination of the molecular plane to the (010) crystallographic plane comes

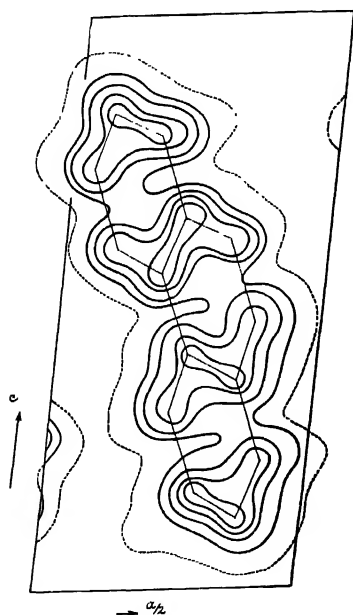


FIG. 1

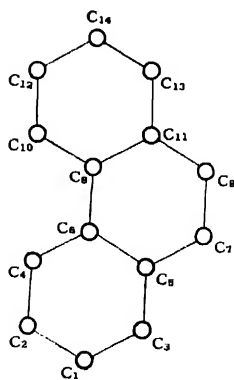


FIG. 2

out to be nearly 60° . By far the strongest reflection happens to be from the (201) crystallographic plane; the measured absolute value of structure factor being about 61% of that had all the atoms been on the (201) plane. The (211) plane too is strong enough, suggesting that the inclination of the molecular plane to the (010) plane is near about 60° . Moreover the crystal has got a very prominent cleavage along the (201) plane. Taking all these

TABLE I
(Part I)

Index of the spot	F Calculated	F Observed	Index of the spot	F Calculated	F Observed
001	-36	35	201	+57	68
002	-19	24	202	-2	6
003	-11	15	203	0	abs
004	-16	30	204	-3	3
005	+13	19	205	-1	5
006	-1	1	206	-2	1
007	+3	abs	207	+3	abs
008	0	abs	208	-6	3
009	-7	1	209	+2	2
00(10)	0	abs	201	-17	18
100	+1	1	202	-9	11
200	-25	30	203	-15	20
300	+13	14	204	+25	33
400	-5	4	205	-4	abs.
500	+7	7	206	-2	1
600	-4	4	207	-2	2
700	-5	7	208	+4	7
800	0	abs	209	-2	2
900	-1	abs	301	+7	5
101	-8	abs	302	-1	1
102	-19	20	303	-3	abs
103	+2	4	304	-11	6
104	-2	4	305	-3	2
105	+7	5	306	-3	abs
106	+5	5	307	+2	1
107	+4	abs	308	+15	11
101	+5	12	309	-6	4
102	0	2	301	-5	5
103	0	abs	302	0	4
104	+14	7	303	+5	2
105	-3	abs.	304	-8	3
106	-6	5	305	+1	3

TABLE I (contd.)

Index of the spot	<i>F</i> Calculated	<i>F</i> Observed	Index of the spot	<i>F</i> Calculated	<i>F</i> Observed
307	+4	abs.	306	+2	abs.
307	+4	abs.	509	+1	abs.
308	-6	abs.	601	+1	abs.
309	+1	abs.	602	+3	3
401	+1	4	603	-3	3
402	-5	5	604	+1	abs.
403	+6	6	605	-3	-3
404	0	6	601	-1	abs.
405	0	abs.	602	-1	abs.
406	+2	abs.	603	+4	4
407	0	2	604	+3	3
408	+5	3	605	+2	abs.
401	-6	5	701	+11	9
402	-5	4	702	-2	abs.
403	+11	7	703	-3	abs.
404	+1	abs.	704	-1	abs.
505	-5	abs.	705	+7	7
406	+2	abs.	706	-4	3
407	+6	4	701	-2	abs.
408	-4	2	702	-2	abs.
501	0	1	703	-4	3
502	-3	abs.	704	+5	7
503	+2	abs.	705	-1	abs.
504	+12	12	706	0	abs.
505	-11	9			
509	+10	12			
501	-3	2			
502	-3	1			
503	-2	abs.			
504	+3	abs.			
505	-3	abs.			

TABLE I (Part II)

Since in these projections, there are no centres of symmetry, only the numerical values of F are given

Index of the plane	F Calculated	F Observed	Index of the plane	F Calculated	F Calculated
020	10	18	110	11	10
040	3	3	210	30	38
060	5	9	310	1	6
011	7	4	410	10	20
012	3	abs.	510	12	11
013	6	abs.	610	5	6
014	11	14	710	2	abs.
015	10	15	120	5	1
016	2	abs.	220	8	5
017	8	7	320	12	11
021	11	15	420	5	4
022	11	21	520	8	7
023	13	19	620	2	abs.
024	4	6	130	4	4
025	3	abs.	230	7	7
030	2	abs.	330	1	abs.
027	11	14	430	5	9
031	10	5			
032	6	abs.			
033	9	9			
034	1	abs.			

TABLE II

Co-ordinates of the atoms

Description of the atom	x/a	y/b	
C_1	0.3850	0.3100	0.1700
C_2	0.2920	0.1249	0.1538
C_3	0.1148	0.4700	0.2105
C_4	0.2289	0.1608	0.2980
C_5	0.3517	0.4469	0.3547
C_6	0.2587	0.2618	0.3985
C_7	0.3815	0.6079	0.4552
C_8	0.1956	0.2377	0.5427
C_9	0.3184	0.5838	0.5994
C_{10}	0.1026	0.0526	0.5865
C_{11}	0.2254	0.3987	0.6432
C_{12}	0.0395	0.0285	0.7307
C_{13}	0.1623	0.3746	0.7874
C_{14}	0.0693	0.1895	0.8312

points into consideration, the molecule is assumed to be oriented with its length in the (010) plane at $78\frac{1}{2}^\circ$ to the a -axis and its molecular plane at 60° to the b -plane. Trials were given by varying the orientations and matching the calculated values of structure factors with the observed ones. The lengths of the aromatic c - c bond were assumed to be 1.41 Å in conformity

with the determinations of similar compounds by Banerjee (1930), Robertson (1933) and others.

After a large number of trials, agreement between observed and calculated F -values was reached at the following orientation. The length of the molecule which itself is planar makes an angle of 6° with the b -plane and 75° with the a -axis while molecular plane is inclined at 60° to the $(c10)$ plane. The orientation of the second molecule in the crystal is governed by the two-fold screw axis of symmetry.

A two-dimensional Fourier summation was next carried out around b -axis using the method of summation described by Lipson and Beevers (1934). From the resultant electron density map the appearance of the molecule can be seen with reasonable clearness.

The x - and z -co-ordinates only are obtained from this projection, while the y -co-ordinates were determined by trial from the F -values of the (okl) and (hko) planes. The agreement between observed and calculated values of structure factors can be seen from Table I.

Projections along the other two axes are in progress and a refinement of the parameters by a three dimensional Fourier summation will be carried out.

ACKNOWLEDGMENT

It is a great pleasure to acknowledge my indebtedness to Prof K. Banerjee for suggesting the problem and for his kind help during the progress of the work.

INDIAN ASSOCIATION FOR THE CULTIVATION OF SCIENCE
210, BOWBAZAR STREET, CALCUTTA

REFERENCES

- Banerjee, K., 1930 *Ind Jour Phys.*, **4**, 557
 Basak, B. S., 1948, *Acta Crystallogr.*, **1**, 224.
 Beevers, C. A. Lipson, H., 1931, *Phil Mag.* **17**, 855
 Krishnan, K. S., Banerjee, S., 1936, *Phil Trans Roy Soc*, 235-343.
 Mark, H. and Mengstenberg, J., 1929, *Z. Kristallogr* **70**, 287
 Robertson, J. M., 1933, *Roy Soc Proc.* **141**, 594

SOME NUCLEAR LEVELS

By M. F. SOONAWALA

(Received for publication, October 10, 1949)

ABSTRACT. The energy levels of Mg^{24} and Be^9 nuclei are derived on the basis of the nuclear structure previously discussed

A view has been put forward that the rare gas nuclei behave as particles with a degree of unsaturation which induces them to combine readily with each other. The nucleus is assumed to consist of the nuclei of the rare gases and protons and neutrons as the principal constituents (Soonawala, 1929, 1942; cf. Mayci, 1948). Further, it has been shown (Soonawala, 1947) that for such a nucleus with two constituents, a simple extension of the elementary Bohr theory of circular orbits enables us to calculate the radii and energies of the quantized orbits depending upon the potential of interaction between the particles. One relation so derived is

$$r^2 = \frac{h^2 s^2 (m_1 + m_2)^2}{8\pi^2 m_1 m_2 M E} \quad (1)$$

where E is the energy of the orbit and r is the distance between the particles revolving about their common centre of gravity and whose mass-numbers are m_1 and m_2 . M is the mass of the proton, s is one of the group numbers given as the reciprocal of any factor common to m_1 and m_2 , or such a fraction plus any integer. If we assume the inter-constituent potential to be of the Yukawa form, $V \cdot e^{-\lambda r}/r$ then,

$$\frac{V \cdot e^{-\lambda r}}{r} = \frac{h^2 s^2 (m_1 + m_2)^2}{8\pi^2 m_1 m_2 M r^2} \quad (2)$$

For given values of V and λ , we can get the distance r for the quantized orbit corresponding to the number s , and Eqn. (1) then gives the energy of the orbit.

The β - and γ -ray spectra of some nuclei are known and schemes of energy levels satisfying these energy differences can be sought. The procedure adopted here is as follows. The distance between the constituents is calculated for the normal state from the known moment of inertia of the nucleus which is taken from the same source as before. This distance is assumed to be equal to r/λ in (2). The highest value of E is taken from the energy data, when known, as the energy of the highest level. A suitable value of s is chosen, and for this purpose trial is made for different values of s starting from the lowest. Eqn. (1) is used to get the inter-constituent distance r from the values of s and E . Eqn. (2) then incidentally gives the value of V , the potential depth. Eqn. (2) is employed to find r for the next smaller value of

s and the same value of V and λ as before. From this, (1) gives the corresponding value of E as the energy of the level. This is carried out for all lower values of s , giving the energies of all these lower levels. The test of the correctness will be provided by comparison with the γ - and β -ray spectra.

The two nuclei discussed here on these lines are Mg^{24} and Be^8 . The spectrum of Mg^{24} is taken as given by Kruger and Ogle (1945). The γ -ray spectrum of Be^8 consists of the two principal transitions of energies 17.6 Mev and 14.8 Mev. Besides these, Hornyak and Lauritsen (1948) have given an energy scheme for Be^8 based on various other experimental data Mg^{24} . The mass-numbers of the constituent particles are 20 and 4. The possible values of s are, therefore, $\frac{1}{2}, \frac{3}{2}, 1, 1\frac{1}{2}, 1\frac{3}{2}, 2, 2\frac{1}{2}$, etc. Working from $s=\frac{1}{2}$ upwards, we find the first evidence of a satisfactory agreement with experimental data for $s=1\frac{1}{2}$. The moment of inertia of Mg^{24} is 5.20×10^{-48} gm cm². This gives $r=1.25 \times 10^{-13}$ cm, which is taken as the value of r/λ . With $s=1.5$ and $E=5.27$ Mev $=8.43 \times 10^{-6}$ erg, $r=3.88 \times 10^{-12}$ cm (2) takes the form

$$\ln r - \lambda r = \ln \frac{h^2 s^2 (m_1 + m_2)^3}{8\pi^2 m_1 m_2 M V} \quad \dots (3)$$

$$(3), \quad \log r - \lambda r / 2.3 = \log \frac{h^2 s^2 (m_1 + m_2)^3}{8\pi^2 m_1 m_2 M V} = y \quad \dots (4)$$

$$(4), \quad \log r - r/a = y, \quad \dots (5)$$

where $a=2.3/\lambda$

Here \ln and \log denote logarithms to the base e and 10 respectively. This gives $V=7.32 \times 10^{-16}$. E and r are then calculated from (1) and (5) for the lower values of s ; i.e., $s=1.25, 1.0, 0.5$, and 0.25 . These are shown in Table I. As shown in Table II, these energy levels are able to explain satisfactorily five of the eight gamma-ray energies. A sixth one, 3.24 Mev, may be said to be explained but not satisfactorily. The energies 2.76 Mev and 2.89 Mev remain unexplained.

A slight alteration of V is seen to produce marked changes in the goodness of fit with the observations. Thus, if $V=7.0 \times 10^{-16}$, the energy levels are as shown in Table I. Here we find that the misfit for 3.24 Mev remains of the same order as before, but the other energies fit in better. Similarly, $V=6.46 \times 10^{-16}$ gives the levels as shown in Table I with less signs of agreement with experimental data.

It is characteristic of the calculations presented here that the lower levels are crowded close together while the upper ones tend to open out more and more. In this connection we may note that the β -ray spectrum of Mg^{24} consists of the three lines 1.84, 1.63 and 1.07 Mev. These may belong to transitions from an outer Na^{24} level to a group such as that formed by the three lowest levels of Mg^{24} as derived above. Alternatively, the transition may be due to an unresolved group at the top.

TABLE I

 Mg^{24} . $1/\lambda = 1.25 \times 10^{-12} \text{ cm.}, a = 2.875 \times 10^{-12} \text{ cm.}$

	$s = 1.5$		1.25	1.00	0.5	0.25	
	r/a						
$V = 7.0 \times 10^{-16}$		1.32	1.55	1.81	2.56	3.28	
	r	3.80	4.46	5.21	7.36	9.45	$\times 10^{-12} \text{ cm}$
	E	5.50	2.80	1.30	0.16	0.25	Mev
$V = 7.32 \times 10^{-16}$	r/a	1.35	1.575	1.84	2.59	3.29	
	r	3.88	4.53	5.29	7.45	9.46	$\times 10^{-12} \text{ cm}$
	E	5.27	2.68	1.25	0.16	0.2	Mev
$V = 6.46 \times 10^{-16}$	r/a	1.27	1.5	2.0	2.77	3.5	
	r	3.65	4.32	5.75	7.97	10.1	$\times 10^{-12} \text{ cm}$
	E	5.94	2.96	1.0	0.14	0.22	Mev

TABLE II

The gamma ray lines and their possible origins.

	$V = 7.32$	7.00	6.46×10^{-16}
gamma energies (Mev)			
1.38 (42)	$2.68 - 1.25 = 1.43$	$2.80 - 1.30 = 1.50$
2.56 (26)	$2.68 - 0.16 = 2.52$
1.26 (25)	$1.25 - 0 = 1.25$	$1.30 - 0.03 = 1.27$
2.68 (16)	$2.68 - 0 = 2.68$	$2.80 - 0.16 = 2.64$
2.76 (15)	$2.80 - 0.03 = 2.77$
2.89 (9)		$2.80 - 0 = 2.8$	$2.96 - 0.14 = 2.82$
3.24 (1)	$5.27 - 1.25 = 4$	$5.5 - 1.3 = 4.2$	$5.94 - 2.96 = 2.98$

Figures in brackets indicate relative intensities.

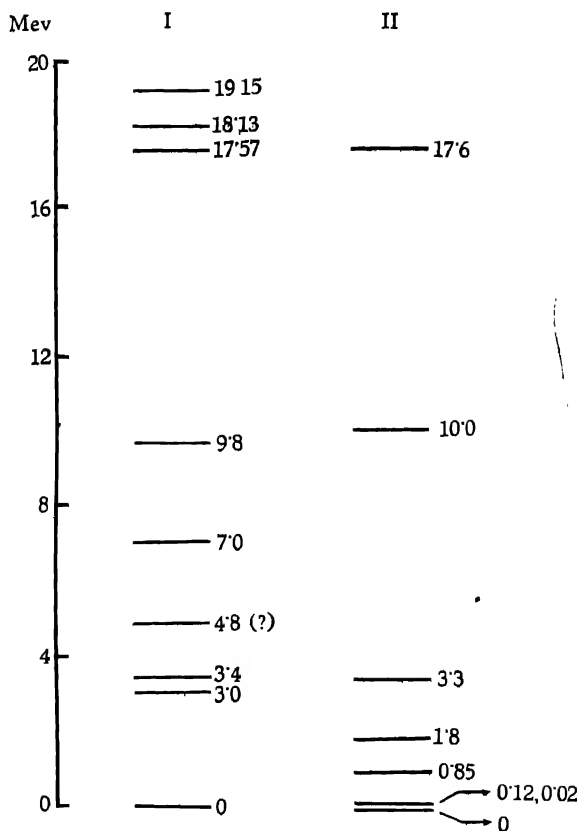


FIG. 1

I shows the levels given by Hornyak and Lauritsen and II shows those calculated by the author.

TABLE III

 Be^8 . $a = 1.38 \times 10^{-12} \text{ cm.}, V = 3.80 \times 10^{-}$

s	2.25	2.0	1.50	1.25	1.00	0.5	0.25
r	1.37	1.60	2.11	2.42	2.77	3.78	$4.75 \times 10^{-12} \text{ cm}$
E	17.6	10.0	3.3	1.8	0.85	0.12	0.02 Mev

Be^8 : Here the constituents are two alpha particles, and hence $m_1 = m_2 = 4$. The values of s are $\frac{1}{2}$, 1, $1\frac{1}{2}$, etc. The lowest value of s giving an indication of satisfactory fit is $s = 2.25$. With $E = 17.6$ Mev as the maximum, $s = 2.25$ gives $r = 1.37 \times 10^{-12}$ cm and $V = 7.63 \times 10^{-17}$. The moment of inertia of Be^8 is 1.2×10^{-48} gm. cm. This gives 3.0×10^{-18} cm as the radius of the orbit; or, $r/\lambda = 6.0 \times 10^{-13}$ cm. The values of r and I for $s = 2, 1.5, 1.25, 1.0, 0.5$, and 0.25 are also given in Table II. The principal lines are 17.6 Mev and 14.8 Mev which are represented here as 17.6 Mev and 14.3 Mev. Bennett and others, (1947) list the transition 14.5 Mev as doubtful and 4.9 Mev as certain; while, Walker and MacDaniel (1948) in their later work confirm the existence of the 14.8 Mev line, but apparently find no trace of the 4.9 Mev transition. Resonance is found for the reaction $\text{Li}^7(p, \gamma) \text{Be}^8$ at 440 kev, but no other below 1.8 Mev. The level schemes of Hornyak and Lauritsen are shown in Fig. 1 compared with those derived in this paper.

Considering the simplicity of our assumptions, it is satisfactory to note that the salient features of the gamma and beta ray spectra are explicable to the extent shown above. A better fit may be possible with a more judicious choice of the constants V and I and of the potential function. A further refinement may be expected to resolve some of the levels into finer structures. Thus, the line 17.6 Mev of the Be spectrum may resolve itself into a group such as shown by the transitions 19.15, 18.13 and 17.57 Mev in the scheme of Hornyak and Lauritsen. This has also been suggested above for the explanation of the beta ray spectrum of Mg^{21} .

DEPARTMENT OF PHYSICS,
MAHARAJA'S COLLEGE,
JAIPUR, (RAJPUTANA).

REFERENCES

- Bennett, Bonner, Richards and Watt, 1947, *Phys. Rev.*, **71**, 11
 Hornyak, W. F., and Lauritsen, T., 1948, *Rev. Mod. Phys.*, **20**, 191.
 Mayer, M. G., 1948, *Phys. Rev.*, **74**, 235.
 Kruger and Ogle, 1915, *Phys. Rev.*, **67**, 273.
 Soonawala, M. F., 1929, *Ind. Jour. Phys.*, **3**, 489.
 " " 1942, " " 16, 291
 " " 1947, " " 21, 137.
 Walker, R. L., and MacDaniel, B. D., 1948, *Phys. Rev.*, **74**, 315

The following special publications of the Indian Association for the Cultivation of Science, 210, Bowbazar Street, Calcutta, are available at the prices shown against each of them :—

Subject	Author	Price Rs. A. P.
Scientific Research	Sir E. J. Russell	0 6 0
The Origin of the Planets	Sir James H. Jeans	0 6 0
Separation of Isotopes	Prof. F. W. Aston	0 6 0
Garnets and their Role in Nature	Sir Lewis L. Fermor	2 8 0
(1) The Royal Botanic Gardens, Kew.	Sir Arthur Hill	1 8 0
(2) Studies in the Germination of Seeds.		
Atomic Forces	Prof. J. E. Lennard-Jones	1 8 0
Aims and Practices of the California Institute of Biology.	R. A. Millikan	0 6 0
Active Nitrogen A New Theory.	Prof. S. K. Mitra	2 8 0
Theory of Valency and the Struc- ture of Chemical Compounds.	Prof. P. Ray	3 0 0
Petroleum Resources of India	... D. N. Wadia	1 8 0
The Role of the Electrical Double layer in the Electro Chemistry of Colloids.	... J. N. Mukherjee	1 12 0

A discount of 25% is allowed to Booksellers and Agents.

RATES OF ADVERTISEMENTS

Third page of cover	Rs. 32, full page
do.	do.	„ 20, half page
do.	do.	„ 12, quarter page
Other pages	„ 25, full page
do.	„ 16, half page
do.	10, quarter page

15% Commissions are allowed to *bonafide* publicity agents securing orders for advertisements.

CONTENTS

	PAGE
37. Some Random Fading Records with Short-wave Signals—By P. M. Das and S. R. Khastgir	277
38. Linear Analysis of Electronic Switching—By Rais Ahmed	281
39. An Explanation of the Influence of the Frequency of the Exciting Potential on Joshi-Effect—By G. V. Bakore	291
40. Multiplet Separations in the f^4 Electron Configuration—By K. Suryanarayana Rao	296
41. An Experimental Study of the Illuminating System of the Electron Microscope—By M. L. De... ..	303
42. Crystal Structure of Phenanthrene—By B. S. Basak	309
43. Some Nuclear Levels—By M. F. Soonawala	315

Vol. 24

INDIAN JOURNAL OF PHYSICS

No. 8

(Published in collaboration with the Indian Physical Society)

AND

Vol. 33

PROCEEDINGS

No. 8

OF THE

INDIAN ASSOCIATION FOR THE CULTIVATION OF SCIENCE

AUGUST, 1950

PUBLISHED BY THE
INDIAN ASSOCIATION FOR THE CULTIVATION OF SCIENCE
210, Bowbazar Street, Calcutta

BOARD OF EDITORS

K. BANERJEE	S. K. MITRA
D. M. BOSE	P. RAY
S. N. BOSE	M. N. SAHA
D. S. KOTHARI	S. C. SIKKAR.

Secretary

EDITORIAL COLLABORATORS

DR. R. K. ASUNDI, M.A., PH.D.
PROF. H. J. BHABHA, PH.D., F.R.S.
DR. P. K. KICHLU, D.Sc.
PROF. K. S. KRISHNAN, D.Sc., F.R.S.
PROF. G. P. DUBEY, M.Sc.
DR. K. RANGADHAMA RAO, M.A., D.Sc.
DR. N. D. SARWATHEY, D.Sc.
DR. N. N. DASGUPTA, M.Sc., PH.D.
PROF. N. R. SEN, D.Sc., F.N.I.
PROF. P. C. MAHANTI, D.Sc., F.N.I.
PROF. S. R. PALIT, D.Sc.,
DR. H. RAKSHIT, D.Sc.,
PROF. K. R. DIXIT, PH.D.
DR. VIKRAM A. SARABHAI, M.A., PH.D.

ASSISTANT EDITOR

MR. A. N. BANERJEE, M.Sc.

NOTICE TO INTENDING AUTHORS

Manuscripts for publication should be sent to Mr. A. N. Banerjee, Assistant Editor, 210, Bowbazar Street, Calcutta.

The manuscript of each paper should contain in the beginning a short abstract of the paper.

All references to published papers should be given in the text by quoting the surname of the authors followed by the year of publication within braces, e.g., Sen (1942). The actual references should be given in a list at the end of the paper according to the following specimen :

Sen, B. K., 1942, *Ind. J. Phys.*, 16, 329.

The references should be arranged alphabetically in the list.

All diagrams should be drawn on thick white paper in Indian ink, and letters and numbers in the diagrams should be written in pencil.

Annual Subscription—

Inland Rs. 30

Foreign £ 2

A SPECTROSCOPIC STUDY OF A CONDENSED SPARK BETWEEN COPPER ELECTRODES IN ILLUMINATING GAS, AIR AND CARBON DIOXIDE AT VARIOUS PRESSURES, PART II

By JAGDEO SINGH

Plates XA, B and C

(Received for publication, June 2, 1950)

ABSTRACT. A detailed study of the nature of the spectra at various portions of a condensed spark in illuminating gas, air and carbon dioxide at various pressures is described, and some of the important observations and results obtained are reported in the present paper.

INTRODUCTION

In a previous communication (Singh and Ramulu, 1945) are reported results obtained during a spectroscopic study of an uncondensed spark discharge maintained between copper electrodes by a large induction coil in illuminating gas, air and carbon dioxide at various pressures ranging from 2 cms of mercury to the atmospheric pressure. A number of observations have been recorded there concerning the characteristic development of line, band and continuous spectra at different pressures and in different parts of spark. Such studies have now been extended to the spectra obtained with a condensed spark discharge in each of the three above-mentioned gases and at similar pressures. In this paper results obtained are collected

EXPERIMENTAL ARRANGEMENT AND PROCEDURE

The general experimental arrangement is similar to that previously described, with some necessary and small modifications. In the present case the discharge tube was not blown to the form of a bulb as previously. The length of the discharge tube was 34 cms., and its internal diameter was 4 cms. The electrodes, one of which was a disc of 1 cm diameter and the other a pointed rod, were of copper and were fused on to the opposite sides of the discharge tube with a distance of 1.3 cms between the free ends. The discharge tube had a quartz window attached to it and an inlet and an outlet, so that the tube could be washed by the gas under experiment a number of times and finally filled with it at the required pressure. The illuminating gas used was the one supplied by the University for laboratory purposes and is reported to be of the same constituents as the one used in the previous work. Carbon dioxide was obtained from a commercial steel cylinder. The purity is not known, but obviously it contains some small quantity of nitrogen. The air used was drawn directly from the atmosphere through drying tubes containing CaCl_2 and P_2O_5 .

The discharges were excited by a transformer delivering 6,000 volts approximately, the primary being fed by 110 volts, 50 cycles/sec-single phase. The condenser (capacity = .0018 μ f., was joined as usual in parallel to the spark gap in the discharge tube. Generally no auxiliary spark gap was used although in a few cases an additional spark gap of variable length was employed.

Spectra were photographed on a medium Hilger quartz spectrograph. Using a Hartman diaphragm of three slots, spectra of the discharges near the disc end, the centre and the pointed end of the horizontal spark have each been photographed successively for a given pressure. These have been denoted by F, C and B respectively in the spectrograms given. Eastman Kodak B-20 and Ilford Selochrome (orthochromatic) plates have been used. All spectra, except a few which have been so indicated, have been taken with the same exposure time *i. e.* 10 minutes.

In Plate X, Fig 1 is representative of spectra obtained with illuminating gas at pressures of 20, 10, 5, 3 and 1 cms of mercury. Fig. 2 is that for air at pressures of 40, 30, 20, 10 and 3 cms. Fig. 3 represents those taken with air at a pressure of 10 cms when auxiliary spark gaps of 1, 2 and 3 mm were used in series with the main spark gap in the discharge tube. Figs. 4 and 5 are for carbon dioxide at pressures of 20, 10, 5 and 1 cms and 32, 18, 10 and 4 cms respectively. Fig. 6 represents spectra obtained for carbon dioxide at a pressure of 10 cms at the point end of the spark with an auxiliary gap of 2 mm and also without it.

RESULTS AND DISCUSSIONS

Before the spectroscopic study of the plates is described, some observations regarding the spark discharge, and attendant fluctuations of pressure, which have been observed, might be mentioned. It was observed that with the condenser and transformer employed, the spark discharge could be obtained up to a pressure of 60 cms in the case of air, while in the case of carbon dioxide and the illuminating gas, the maximum pressures for the spark discharge to take place were only 35 cms and 25 cms. Variations in pressures during the course of the discharge have been observed at different pressures in all the three gases. In the case of the illuminating gas and air the pressure inside the discharge tube goes on increasing up to a certain value after the discharge is started and then becomes constant, whereas in the case of carbon dioxide the pressure first increases to a certain maximum value and then begins to fluctuate almost periodically, the period being greater at higher pressures and smaller at lower pressures. The sudden increase of pressure in the carbon dioxide is also accompanied by a sudden glow, almost filling the whole of the discharge tube up to the window. The maximum increase of the pressure after the discharge is started is found to be at an optimum pressure, below and above which the pressure increase is comparatively less. Table I (*a*, *b* and *c*) gives a comparative idea of the increase of pressure in the three gases at various pressures.



Fig 1

Illuminating gas

Diffuse Group

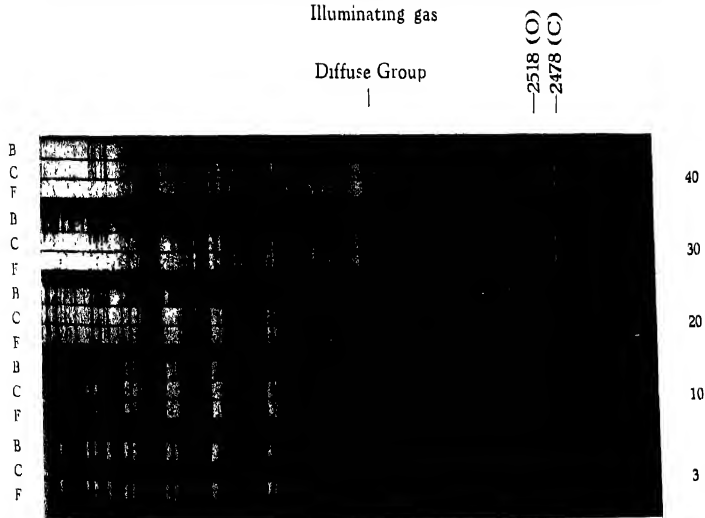


Fig 2

Air

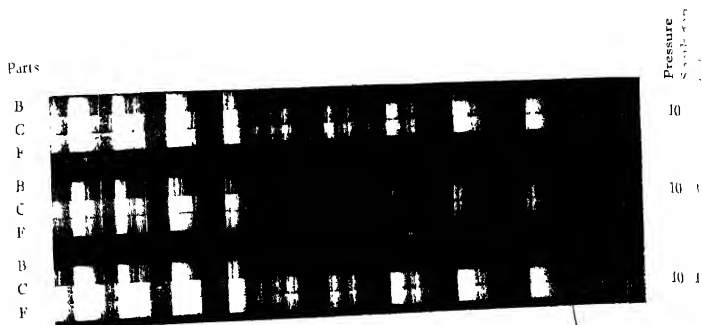


Fig. 3

Air

— 3274 (Cu)
— 3247 (Cu)

— 2518 (O)
— 2478 (C)



Fig. 4

CO₂

This aspect of the pressure fluctuation has been discussed in detail by Sita Ram Swami (1948). According to his observations the range of pressure changes in carbon dioxide can be divided into two classes: (1) The region in which there is a periodic variation of pressure, *i.e.*, pressures from 40 cms to 10 cms. (2) The region in which the variation of pressures is gradual and nonperiodic, covering all pressures below 10 cms. In this region the pressure increase is much less than in the above region and the final pressure reaches a steady value.

According to him these two regions are distinctly marked spectroscopically also. The region (1) is characterised by the emission of atomic lines recorded in the photographic plates, while the region (2) is characterised by the emission of molecular bands only. Thus the pressure variations and the spectral changes are intimately connected.

In the previous work with the large induction coil, the discharge was decidedly unidirectional and either the disc electrode or the bar electrode could be made the cathode, which could be distinguished as such by the nature of the discharge at lower pressures. In the present case, where the discharge is maintained by a transformer, one would expect the discharge to be alternating in type, actually, however, it was found that there was a good deal of rectification and the point electrode was observed to act as the cathode. This occurred at all the pressures investigated into and in all the three gases.

It may be mentioned that rectification in discharge tubes is a well known phenomenon although the quantitative study of it has been but little. Chipionkar has reported certain investigations of this phenomenon but his data are for relatively lower pressures (of the order of 1.8 to 10^{-4} cms of mercury) than those used here. Data for higher pressures seem to be desirable. It is interesting to note that rectification is minimum in the case of the discharge tubes, when the electrodes are identical in shape, size and material.

Study of the Plates XABC has been done on lines similar to those reported before. Observations are restricted to atomic lines, continuous spectra and systems of bands obtained. Atomic lines mostly belonging to the material of the electrodes are prominent at all pressures, beginning from the highest employed up to a pressure of 5 cms in the case of illuminating gas (see Fig. 1), 20 cms in the case of air (see Fig. 2) and 4 cms in the case of carbon dioxide (see Figs. 4 and 5) respectively. Some of the general features of the lines are summarised in Table II.

Emission of continuous spectrum is prominent in the case of illuminating gas and carbon dioxide. It is not so prominent in air at similar pressures in which case the continuous spectrum makes its appearance only at a pressure of 40 cms and extends upto 2400\AA . In the case of illuminating gas and carbon dioxide, the continuous spectrum is stronger in intensity than in the case of air and extends from the red end upto 2400\AA approximately even at comparatively lower pressures. This emission was observed in the illuminating gas at a pressure of 20 cms but

not below. Higher pressures could not be employed. In the case of carbon dioxide, the continuous spectrum was present at the pressures of 20 and 30 cms but not at lower pressures. The continuous spectra in the cases of illuminating gas and carbon dioxide are stronger at the centre of the spark than at either end, whereas in the case of air it is equally strong at F and C. In Table III are summarised some features of the continuous spectrum.

It is difficult to explain the origin of the continuous emission. More detailed investigations on the intensity distribution in the continuous band might throw some light on this point. This, however, has not been attempted.

In the case of air, there is a small region of diffuse spectrum extending through a region of 50\AA with its maximum at 2900\AA . This is stronger at a pressure of 40 cms. and gets weaker at lower pressures and completely disappears at the pressure of 20 cms. This diffuse spectrum is not present in the case of illuminating gas and carbon dioxide.

The observations concerning the developments of bands at the different pressures and in various portions of the spark are summarised in Table IV. They are either very weak or completely absent at higher pressures and increase in intensity as the pressure decreases and are best developed at a pressure of 10 cms in the case of air and between 10 and 5 cms in the other two gases. For the development of the bands, the most striking feature is that in the case of illuminating gas very approximately all the three parts behave similarly, in the case of air F and C behave similarly and in the case of carbon dioxide all the three parts behave differently. In general the 'C' part is weaker below a pressure of 3 cms and stronger after a pressure of 20 cms.

TABLE I(a)

Change of pressure in cms. in the case of Illuminating gas

Time	Initial pressures		
	14 cms.	20 cms.	22 cms.
to sec.	1	2.2	2.2
30 "	1.4	3.6	2.8
1 min	1.8	4.8	3.2
1.5 "	2	5.6	3.6
2 "	2.2	6.0	3.8
3 "	2.4	6.2	3.8
4 "	2.6	6.4	4.0
5 "	2.6	6.6	4.2
6 "	2.6	6.8	4.4
7 "	2.6	6.8	4.4
8 "	2.6	6.8	4.4
9 "	2.6	7.0	4.4
10 "	2.6	7.2	4.4

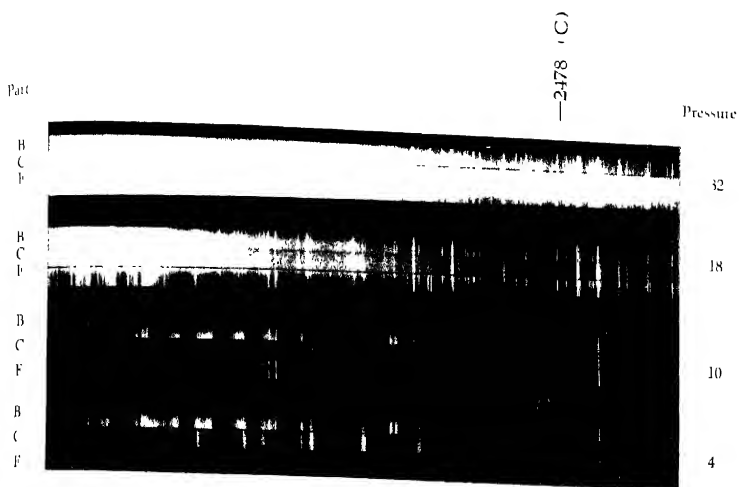


Fig. 5
 CO_2

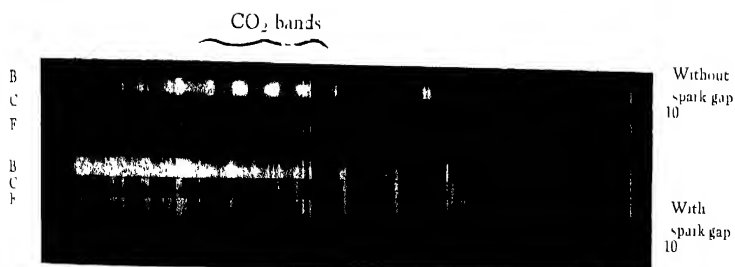


Fig. 6
 CO_2

TABLE I(b)

Air

Time	Initial pressures		
	20 cms.	30 cms.	38 cms.
10 sec	0	0.8	1
30 "	0	1.0	1
1 min.	0	1.0	1
2 "	0	1	1
3 "	0.2	1	1
4 "	0.2	1	1
5 "	0.2	1	1

TABLE I(c)
(Carbon dioxide)

Time	Initial pressures		
	17 cms.	22 cms.	27 cms.
10 sec.	1.2	1.6	1.6
30 "	1.4	2.0	2.4
1 min.	1.6	2.6	3.6
1 " 30 "	1.8	3.0	3.2
2 "	2.0	3.2	3.6
2 " 30 "	2.2	3.6	3.8
3 "	2.4	3.2	4.0
3 " 30 "	2.4	3.4	4.2
4 "	2.4	3.6	4.2
4 " 30 "	2.4	3.0	4.2
5 "	2.4	3.2	4.2
5 " 10 "	—	6.6	—
5 " 30 "	2.4	—	4.2
6 "	2.4	3.4	4.2
6 " 30 "	2.6	3.8	4.2
7 "	2.6	6.6	4.2
7 " 30 "	2.6	3.0	4.2
8 "	2.6	3.6	4.2
8 " 30 "	—	6.6	4.2
8 " 40 "	5.8	—	—

TABLE I(c) (contd.)

Time	Initial pressures		
	17 cms.	22 cms.	27 cms.
9 "	2.4	3.6	4.2
9 " 30 "	2.4	3.6	18.0
10 "	2.6	4.6	3.0
10 " 30 "	2.6	7.6	3.8
11 min	3.8	3.4	4.0
11 " 30 sec.	2.6	3.8	4.2
11 " 50 "	—	7.6	—
12 "	2.6	3.6	4.2
12 " 20 "	3.6	—	—
12 " 30 "	3.6	3.6	16.0
13 "	2.6	3.8	3.0
13 " 30 "	2.6	1.0	3.8
13 " 35 "	3.6	—	—
13 " 50 "	—	13.6	—
14 "	2.6	3.6	4.0
14 " 30 "	3.6	3.8	4.4
15 "	2.1	4.0	1.4
15 " 10 "	3.6	—	—
15 " 30 "	2.6	4.0	4.4
16 "	2.6	13.6	4.4
16 " 30 "	2.6	3.6	4.1
16 " 35 "	3.4	—	—
17 "	2.6	3.6	4.4
17 " 30 "	2.6	13.6	4.4
18 "	2.6	3.6	4.4
18 " 30 "	2.6	4.0	4.4
18 " 35 "	—	13.6	—
18 " 50 "	—	—	16.0
18 " 55 "	3.6	—	—

TABLE I(c) (contd.)

Time	Initial pressures		
	17 cms	22 cms	27 cms
19 min.	2.6	3.8	3.0
19 " 30 sec.	2.6	1.2	3.6
20 "	2.0	13.6	1.0
20 " 30 "	2.6	3.6	4.7
20 " 50 "	3.6	—	—
21 "	2.6	4.0	4.2
21 " 30 "	2.6	4.7	4.2
22 "	2.6	6.6	4.4

In all the three cases there was found to be no increase of pressure at the initial pressures of 5 cms and below.

TABLE II

(Lines)

Illuminating gas	Air	Carbon dioxide
Lines are present from 20 cms up to a pressure of 5 cms. Copper lines are stronger at the ends and weaker at the centre.	They are present from 40 cms up to 30 cms. Copper lines are equally strong at F and C and weaker at B, except the lines at 3274Å and 3274Å which are stronger at the ends and weaker at the centre.	They are present from 30 cms up to 4 cms. Copper lines are stronger at the ends and weaker at the centre.
Lines other than copper (O and C) are stronger at the centre and weaker at the ends (Fig. 1).	Lines other than copper are strong at F, weak at C and weaker at B (Fig. 2).	Lines other than copper are stronger at the centre and weaker at the ends (Figs. 4 and 5).
Copper lines at 3274Å and 3274Å are shaded to the violet at the spark ends F and B but not at the centre. This occurs only at the pressure of 20 cms but not below.	These copper lines are not shaded at all at any pressure and in any part.	These copper lines are shaded to the violet at F and B but not at C at the pressures of 20 and 30 cms. only.

TABLE III

(Continued)

Illuminating gas.	Air	Carbon dioxide
The continuous spectrum is present at the pressures of 10 and 20 cms. At 20 cms it is present in all the three parts of the spark, but is stronger at the centre and extends up to 2400 Å. At 10 cms, it is faintly present in F and C and is stronger at C and extends up to 2700 Å (Fig. 1).	The continuous spectrum is fairly strong at a pressure of 10 cms. and is equally strong at F and C. In this case also it extends up to 2400 Å (Fig. 2).	The continuous spectrum is present at the pressures of 20 and 30 cms. At 30 cms it is present in all the three parts but is stronger at the centre, whereas at 20 cms it is present only at the centre and it extends at both the pressures up to 2400 Å. (Figs. 4 and 5).

TABLE IV
(Bands)

System of bands	Illuminating gas (investigated at pressures 20—1 cms.)		Air (investigated at pressures 40—3 cms.)		Carbon dioxide (investigated at pressures 3.2—3 cms.)	
	At different pressures	At various portions of the spark	At different pressures	At various portions of the spark	At different pressures	At various portions of the spark
First negative nitrogen bands	Absent at all pressures.	Absent in all portions of spark.	They start developing at a pressure of 10 cms. and increase in intensity with a decrease of pressure and are best developed at 3 cms. pressure.	At a pressure of 3 cms. they are stronger in B, slightly weaker in F and weakest in C	Absent at all the pressures.	Absent in all the portions of the spark.
Second positive nitrogen bands.	They start developing at a pressure of 10 cms and are best developed at a pressure of 3 cms	At pressures of 3 cms and below they are quite strong in F and B and weaker in C	They start developing at a pressure of 30 cms. and increase in intensity with decrease of pressure and are best developed at a pressure of 3 cms.	At 3 cms they are stronger in F and B and weaker in C, at a pressure of 10 cms they are strong in C slightly weaker in F and still weaker in B, at the pressures of 20 and 30 cms. they are equally strong in F and C and weak in B	They begin to appear at a pressure of 10 cms and are best developed at a pressure of 5 cms. At lower pressures they become weaker.	At a pressure of 5 cms they are strong in C than in F and B and at a pressure of 1 cm they are weaker in C and stronger in F and B.
Cyanogen violet system.	They are present at all the pressures but become weaker below a pressure of 5 cms	They are equally strong in all the three parts at the pressures of 20, 10 and 3 cms and slightly weaker in F at a pressure of 5 cms. At a pressure of 1 cm, they are slightly weaker in C than in F and B.	Absent at all pressures	Absent in all the portions of the spark	Present at pressures of 20 and 30 cms	They are slightly weaker in F and equally strong in C and B at both the pressures

NO ₂ bands	Absent at all pressures.	Absent in all portions of spark.	They begin to develop at a pressure of 30 cms. and are best developed at a pressure of 10 cms. below which they become weaker.	From 30 to 10 cms. they are equally strong at F and C and weak in B. At a pressure of 3 cms they are stronger in F and weaker in B than in C	Absent at all pressures	Absent in all the portions of the spark.
CO ₂ and CO ₂ bands	Absent at all pressures.	Absent in all portions of spark.	Absent at all pressures	Absent in all the portions of the spark.	They begin to develop at a pressure of 20 cms. and are best developed at a pressure of 5 cms below which they become very weak	They are present only in the B part at pressures from 10 to 4 cms. and at a pressure of 1 cm, they are faintly present both in F and B.
CO Angstrom bands.	They begin to develop at a pressure of 10 cms. and go on increasing in intensity up to a pressure of 1 cm.	They are best developed at a pressure of 1 cm in B part	Absent at all pressures	Absent in all the portions of the spark	They begin to develop at a pressure of 10 cms and are best developed at a pressure of 5 cms and get weaker at lower pressures	At a pressure of 10 cms. they are stronger in F and at B than in C and at 6 cms they are equally strong in B and C and weaker in F and at a pressure of 1 cm they are equally strong in F and B and weaker in C
CO third positive bands.	They begin to develop at a pressure of 5 cms. and are best developed at a pressure of 1 cm.	At a pressure of 3 and 1 cm they are stronger in F and B and weaker in C	Absent at all the pressures.	Absent in all the portions of the spark	They begin to develop at a pressure of 1 cms and are best developed at a pressure of 5 cms	At pressures of 10 and 5 cms. they are stronger in the centre and weaker at the ends, but at 1 cm pressures they become stronger at the ends and weaker at the centre.

By using a spark gap in series with the main spark of the discharge tube, the bands are weakened and the lines strengthened. The lines are best developed with the spark gap of 2 mm in the case of air which is the optimum spark gap for the best development of the lines. The bands are best developed without the spark gap or with the spark gap of minimum distance (1 mm. in this case).

The following are some of the more important observations and results obtained :

(a) After the discharge is excited there is an increase of pressure which is maximum in the illuminating gas, and minimum in air at similar pressures. After attaining the maximum pressure, it remains almost constant in illuminating gas and in air, but it fluctuates periodically in carbon dioxide and each sudden fluctuation is accompanied by a sudden glow filling the whole of the tube.

(b) There is rectification in the discharge tube in all the three gases and at all the pressures investigated.

(c) The lines are stronger at higher pressures and weaker at lower pressures. Most of the lines are due to the material of the electrodes and are confined mostly to the ends of the spark. Lines other than those due to the electrodes are stronger at the centre and weaker at the ends.

(d) Copper lines (3247\AA and 3271\AA) show peculiar shading near the end portions of the spark in the illuminating gas and carbon dioxide at higher pressures.

(e) Continuous spectrum is present only at higher pressures and is stronger in the 'C' part for the illuminating gas and carbon dioxide and equally strong in F and C parts in the case of air

(f) Bands, in general, are best developed at pressures between 10 and 5 cms.

(g) For the development of bands very approximately all the three parts behave similarly in the case of the illuminating gas, F and C behave similarly in the case of air, and all behave dissimilarly in the case of carbon dioxide.

ACKNOWLEDGMENTS

Thanks are due to Dr. R. K. Asuudi, University Professor of Spectroscopy, for his inspiring guidance and valuable suggestions. Thanks are also due to Dr. N. L. Singh for valuable suggestions.

DEPARTMENT OF SPECTROSCOPY,
BANARAS HINDU UNIVERSITY.

REFERENCES

- Chiplonkar, V. T., 1939, *Proc Ind Acad. Sci.*, **10**, 381.
 " " 1941, *ibid*, **13**, 323
 Singh, J. and Sree Ramulu, 1945, *Ind. J. Phys.*, **19**, 235
 Sita Ram Swami, 1948, M.Sc. Thesis, (B.H.U.).

ON THE X-RAY LUMINESCENCE SPECTRA OF THALLIUM-ACTIVATED ALKALI HALIDE CRYSTALS*

By APARESH CHATTERJEE

(Received for publication, June 29, 1950)

Plate XI

ABSTRACT. The X ray luminescence spectra of thallium-activated alkali halides have been investigated at ordinary and low temperatures. The band systems are of two types, the visible part is due to the lattice emission, while the short wavelength part exhibits characteristic thallium emission. The lattice bands gain in intensity due to the presence of thallium. The intensity of the characteristic band is linearly related to the concentration of thallium. It has been shown that Seitz's explanation of the characteristic thallium band emission is inadequate, and an alternative energy level scheme has been proposed.

INTRODUCTION

Since initiated by Pohl and his associates, the thallium-activated alkali halide crystal phosphors occupy an unique place in phosphor research. These substances gave a clue to an attempt of understanding correctly the luminescence processes in crystals in general. The absorption spectra were studied by Hilsch and Pohl (1928, followed by many papers), and Pório (1929). An early explanation of absorption was given by Seitz (1938, 1939), who attributed the absorption peaks at 195, 205, 247.5 $m\mu$ for KCl-Tl to the electronic transitions $^1S_0 \rightarrow ^3P_1$, $^1S_0 \rightarrow ^1P_1$, and $^1S_0 \rightarrow ^1P_1$ of the thallium ions modified by the Madelung field in a lattice. Fialkovskaya (1948a) has reported another temperature-insensitive weak absorption band (at 273 $m\mu$ for KCl-Tl, and at 300 $m\mu$ for KBr-Tl) at high thallium concentrations detectable only in thick single crystals. Koch (1929) has shown that thallium is monatomically dispersed in the lattice.

The emission spectra of these phosphors have been studied by von Meyeren (1930), Büniger (1930), Flechsig (1930), Fromherz (1931), Büniger and Flechsig (1931), Pringsheim (1942), Fialkovskaya (1948b), Hutten and Pringsheim (1948), Shahmova (1948), Bose and Sharma (1950). A report of the earlier work may be found in articles by Hilsch (1937) and Rees (1942); the older literature deals exclusively with emission of the phosphors by using ultraviolet excitation.

Thallium may be introduced in the lattice of the alkali halides by fusion, or by electrolytic dispersion, or by evaporation from a concentrated solution

* Communicated by Prof. S. N. Bose.

(Pringsheim, 1942) or by prolonged grinding of the thallous salts (Hutten and Pringsheim, 1948); the negative ion of the thallous salt is of little consequence in forming such mixed crystals. Perturbations in the original lattice due to the excess of positive ions from ideal stoichiometric proportions are produced in such impurity crystals.

PRESENT WORK

The luminescence spectra of alkali halides activated by thallium have been recently investigated by Bose and Sharma (1950) under cathode rays. The samples were prepared by melting the mixture of weighed quantities of $TlCl$ and the alkali halide at about $900^{\circ}C$. The present investigations were carried out by using the same phosphors under X-ray excitation to confirm and supplement their measurements.

The amount of thallium present in the phosphors is given as the percentage weight of $TlCl$ dissolved in 100 gms of alkali halides, and not as molar ratios. For recording the spectra at liquid oxygen temperatures, a special sample holder was constructed, as shown in Fig. 1. Other experimental arrangements have already been described (Chatterjee, 1950, henceforth referred to as Paper I).

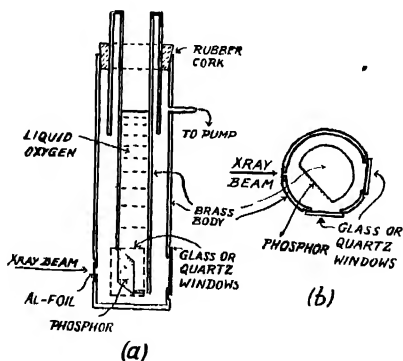


FIG. 1

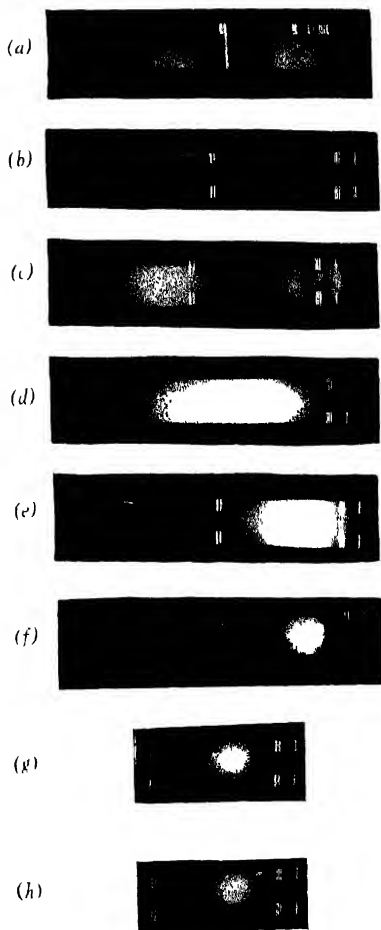
Low temperature phosphor holder

(a) Longitudinal section, (b) Transverse section near the bottom.

The spectra are shown in Plate XI the microphotometer traces in Fig. 2, and the measurements in Table I. Since the measurements are inaccurate by ± 20 AU at $300 m\mu$, and no systematic shifts in the room temperature ($25^{\circ}C$) and low temperature ($-180^{\circ}C$) spectra were found, only the low temperature data are given.

NATURE OF THE EMISSION BANDS

Comparing the present data with those of other workers, it may look surprising that in almost all cases the longer wavelength bands are completely



X-ray luminescence spectra of thallium-activated alkali halides.

(a) NaCl-Tl(1%), (b) NaBr-Tl(2.5%), (c) KCl-Tl(2.5%)
 (d) KBr-Tl(2.5%), (e) KI-Tl(2.5%), long exposure; (f) KI-Tl(2.5%)
 short exposure, (g) KI-Tl(5%), (h) KI-Tl(0.1%)

X-ray Luminescence Spectra of Thallium-activated Alkali halides 333

absent, and visible luminescence has been entirely overlooked. For the convenience of comparison, the older work is summarized in Table II.

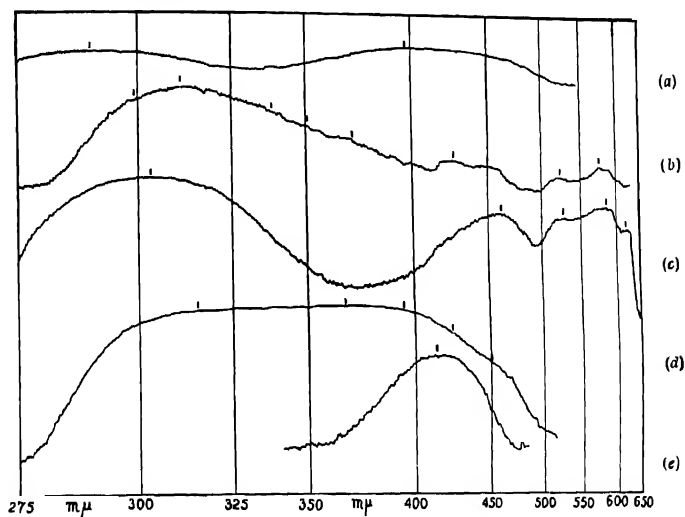


FIG. 2

Microphotometer traces of luminescence spectra (reduced) (a) NaCl-Tl (1.0%); (b) NaBr-Tl (2.5%); (c) KCl-Tl (2.5%); (d) KBr-Tl (2.5%); (e) KI-Tl (0.5%).

TABLE I

X-Ray Luminescence Spectra of Thallium Activated Alkali Halides

Phosphor	Approximate ranges in $m\mu$	peak positions in $m\mu$
NaCl-Tl (1.0%)	496-350 305-270	396.5 289.0 (Tl)
NaBr-Tl (2.5%)	600-505 470-440 400-280 continuous	575, 530 450 445, 366.5, 350.5, 337(?) 299.0 (Tl)
KCl-Tl (2.5%)	650-500 500-405 340-280	617, 583.5, 523.5 460.5 303.0 (Tl)
KBr-Tl (2.5%)	500-275 continuous with peaks difficult to locate.	450, 422 394, 366 315 (Tl)
KI-Tl (0.5%)	660-510 continuous, very faint 470-360	537, 520 419.5 (Tl)

TABLE II

Emission of Tl-activated phosphors using ultraviolet light

Phosphor	von Meyeren (1930) 150°C, 20°C-180°C Peaks in $m\mu$			Bunger and Flechsing (1931)	Pringsheim (1942) Extensions	Hutten and Pringsheim (1948) Peaks
NaCl-Tl	290,	288,	286	288		
NaBr-Tl	315, 298,	308, 295,	305 295			
KCl-Tl	304,	298,	296	270 300	600-560 500-430 405-360 330-280	610, 540 457 385 300
KBr-Tl	320, 297,	350, 319,	360 311	350 318	670-420 430-340 360-310	325
KI-Tl	401,	415,	417	—	—	—
RbCl-Tl	317,	315,	314	—	—	—

When the present work is compared with those of the workers of Pohl's school, it is found that the shortest wavelength bands of our measurement coincide with theirs: these near ultraviolet emission bands are attributed to the thallium present in the lattice as impurity, and hence are characteristic of thallium. But the X-ray luminescence spectra show also a number of bands extending far into the visible region, sometimes covering the whole range. The origin of these longer wavelength bands must necessarily be due to some other causes *not* associated with thallium, and there are only two possibilities: they may well be due to the presence of other impurities, or due to the emission of the parent lattice itself.

In Paper I, we have shown that the X-ray luminescence spectra of pure alkali halides show lattice emission, and if we compare the spectra of pure phosphors with these thallium-activated ones, we can verify that the longer wavelength band patterns and peaks are very closely similar in shape and position in the two cases. We thus arrive at the very important conclusion that the longer wavelength bands owe their origin to the radiative transitions taking place in the original lattice, and are *not* due to any impurities. These phosphors strikingly demonstrate the characteristic emission and the lattice emission side by side.

Pringsheim (1942) and Hutten and Pringsheim (1948) have observed such a phenomenon; in fact, they were first to demonstrate clearly that the

phosphors under consideration show a visible luminescence. However, we are now in a position to account for both ultraviolet and visible luminescence of these phosphors.

From Plate XI, it can be verified that to a first approximation, the bands of the parent lattice are not much affected in position (*cf.* Paper I), except that occasional overlapping, omissions, and enhancements of the weaker bands occur in a few cases.

The characteristic thallium band changes to longer wavelength side with increasing lattice constant of the parent matrix.

The intensity of the thallium band depends on the crystal. It is more for crystals of greater lattice constant, resulting in lesser exposure in recording the spectra. This fact indicates that the emission of the phosphor is also dependent on the ease with which the thallium ions (having large ionic radii) enter the lattice.

Generally, the characteristic thallium emission is more intense than the lattice emission. This is especially true for low thallium content, and is the most important reason why earlier workers did not get visible luminescence by using molar thallium concentrations of the order of 0.1 to 0.5%. On short exposures, only the thallium band is obtained, in a few cases (*e.g.*, KI-Tl, See Plate XI, Figs. e and f), while on long exposures, the lattice bands appear at their appropriate positions, but the thallium band is much widened at the same time.

Though the lattice emission bands do not change in position, they distinctly gain in intensity due to the presence of thallium. This may be exemplified by citing the case of KCl-Tl. A measurably good luminescence spectrum of pure KCl could not be obtained even on an exposure of 20 hours, but KCl-Tl (2.5%) showed the lattice emission bands in 4 hours very distinctly. The lattice bands of pure KBr (*cf.* Paper I) terminate at 455 $m\mu$, but the bands are just measurable from that region in case of KBr-Tl; the weaker lattice bands are enhanced due to the presence of thallium. Another additional proof, though indirect but significant, may be given from Pringsheim's data. It is well known that pure alkali halides *never* fluoresce under ultraviolet excitation, but Pringsheim has prepared thallium-activated phosphors which show visible luminescence quite well under ultraviolet arc. Hence thallium behaves truly as an 'activator' of the lattice emission.

It appears that thallium emits a single band. Though older workers have reported two bands in a few cases, it can be easily verified that one of these bands, particularly the longer ones (at 470 $m\mu$ for KCl-Tl, Bunger and Flechsig, and at 305 $m\mu$ for NaBr-Tl, von Meyeren) is due to the parent lattice (Bose and Sharma, 1950).

The spectra at low temperatures did not show any special features. The lattice bands were not much affected in position and intensity, but the thallium bands were sharpened. No systematic shifts were found.

INTENSITY VARIATION OF THE CHARACTERISTIC BAND WITH CONCENTRATION

Hutten and Pringsheim state that at low thallium concentrations, KCl-Tl fluoresce violet, while with increasing concentrations, the overall fluorescence efficiency increases and extends far into regions of longer wavelengths. To study the intensity variation of the thallium band, KI-Tl phosphors were prepared from melt with 0.1% and 5.0% TlCl (0.07 and 3.35 mol per cent Tl). A linear law was tacitly assumed, and proportional exposures were given, The 0.1% phosphor was exposed for 200 minutes, and the 5% sample for 4.5 minutes. Densitometric measurements were made with the microphotometer, as shown in Fig. 3.

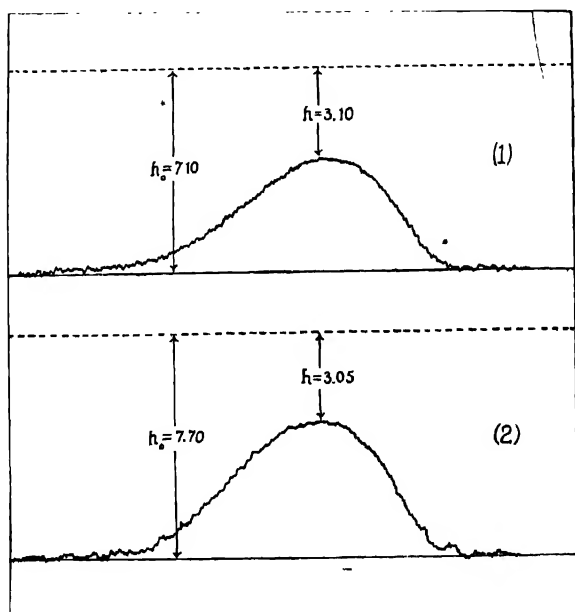


FIG. 3

"Intensity curves of KI-Tl phosphors (reduced to half size).

(1) 5% phosphor, 4.5 minutes; (2) 0.1% phosphor 200 minutes.

The values of h and h_0 are in cms. (see text)."

The concentration n and the photographic density of blackening d are related to the intensity of emission I by the relation

$$n.t = I = I_0 e^{-n.d}, \quad \text{or} \quad n.t/I'_0 = e^{-d}, \quad (I'_0 = I_0 e^{-n}), \quad (1)$$

X-ray Luminescence Spectra of Thallium-activated Alkali halides 337

where t is the time of exposure. If h be the microphotometer height, then

$$h = h_0 e^{-d}, \quad \dots (2)$$

defined by $h = h_0$ (base lines of Fig. 3) when $d=0$, and $h=0$ (top dotted lines) for $d=\infty$. Equating (1) and (2), we get

$$(nt)/I'_0 = h/h_0, \quad \dots (3)$$

If there be two concentrations n_1 and n_2 exposed for t_1 and t_2 under identical conditions, then $(I'_0)_1 = (I'_0)_2$, and

$$\frac{n_1 t_1}{n_2 t_2} = \left(\frac{h}{h_0}\right)_1 / \left(\frac{h}{h_0}\right)_2 \quad \dots (4)$$

Putting numerical values, the left hand side gives 1.125 and the right hand side from Fig. 3 gives 1.102. Thus the agreement is within 2%. Considering the various uncertainties, the most important one being the difficulty of obtaining a desired steady X-ray current from a Hadding tube at a predetermined voltage in both cases, the agreement is much better than expected. We can conclude that the intensity of characteristic thallium emission is linearly related to its concentration in the parent lattice.

CARRIERS OF LUMINESCENCE

Some controversy has recently arisen as to the carriers of luminescence in thallium-activated alkali halides. Seitz (1933) is of opinion that Tl^+ ions enter the lattice in place of vacant positive ion sites, and the levels of ionized thallium are so modified in the lattice field as to give the $^1P_{1,2} \rightarrow ^1S_0$ emission transitions in the near ultraviolet. But Pringsheim (1942), from the similarity of the absorption spectra in solution and in the solid state, and Hutten and Pringsheim (1948), from the X-ray diffraction photographs, are in favour of complex formation of the type (TlX_n) —(cf. Kröger, 1948, p 53). Whatever be the correct explanation, Pringsheim has rightly pointed out

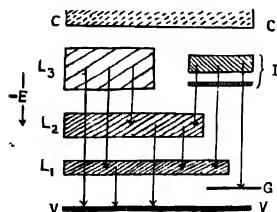


FIG. 4

A new energy level scheme for thallium activated alkali halides. V=valence band (normally filled, combined p levels of halogens, as modified in a lattice field); C=conduction band, normally empty; L_1, L_2, \dots , ionic exciton levels, G=ground state of thallium (ion or complex); I=excited state of thallium.

that Seitz's energy level scheme cannot explain the visible luminescence of the phosphors. Bose and Sharma have also discussed this point. Any energy level scheme which explains the visible part of luminescence must take into consideration the transfer of energy from thallium levels to the valence levels of the ions building up the lattice.

Such a scheme has been presented in Fig. 4. The ionic exciton levels I_1, I_2, \dots , lie between the valence and the conduction bands, and are responsible for lattice emission. The impurity levels are so situated in a perturbed crystal that a transition from one of them directly to its ground state gives rise to the characteristic emission of thallium, and to the ionic states go to enhance the lattice emission bands, *e.g.*, in case of KCl-Tl. Except in case of NaBr-Tl, the impurity levels do not lie at the same height as those of lattice levels, hence the characteristic emission is on the shorter wavelength side, while in case of NaBr-Tl, they distinctly overlap. The transfer transitions from thallium exciton (?) levels (be it due to complex formation, or to substitution at vacant anion sites) are distinctly responsible for exhibiting very wide, extended, and unresolved emission regions in case of NaBr-Tl and KBr-Tl.

ACKNOWLEDGMENTS

The author is thankful to Prof. S. N. Bose, Khaira Professor of Physics, Calcutta University, for the interest he has taken in this work and for laboratory facilities; and to Mr. H. N. Bose, under whose guidance the present work was undertaken, for encouragement and many helpful discussion.

KHAIRA LABORATORY OF PHYSICS,
CALCUTTA UNIVERSITY.

REFERENCES

- Bose, H N, and Sharma, J., 1950, *Proc Nat Inst. Sci Ind*, **26**, 47
 Bunger, W, 1930, *Z Physik*, **66**, 311
 Bunger, W, and Flechsig, W., 1931, *Z Physik*, **69**, 637
 Chatterjee, A., 1950, *Ind. J Phys*, **24**, 265
 I'dor, M., 1929, *Z. Physik*, **66**, 235, 534.
 Fialkovskaya, O V, 1948a, *Dokl Akad Nauk SSSR*, **60**, 40 (*Phys. Abs.*, 4675, 1949)
 Fialkovskaya, O.V, 1948b, *Ibid*, **60**, 475 (*Phys. Abs.* 1397, 1949)
 Flechsig, W, 1931, *Z. Physik*, **67**, 428
 Fromherz, H., 1931, *Ibid.*, **68**, 233
 Hilsch, R, 1937, *Proc Phys Soc*, extra part, **49**, 40.
 Hilsch, R, and Pohl, R W, 1948, *Z. Physik*, **48**, 384
 Hutten, E H., and Pringsheim, P, 1948, *J Chem. Phys*, **16**, 241.
 Koch, W, 1929, *Z. Physik*, **67**, 638
 Kröger, F. A., 1948, *Luminescence of Solids*, Elsevier, p. 53.
 Pringsheim, P, 1942, *Rev Mod. Phys.*, **14**, 132.
 Rees, A. L. G, 1942, *Annual. Rep. Prog. Chemistry*, p. 87.
 Seitz, F, 1938, *J. Chem. Phys.*, **6**, 150.
 Shalimova, K. V, 1948, *J. Exp. Theor. Phys.*, **18**, 1045 (*Phys. Abs.* 1394, 1949).
 von Meyeren, W, 1930, *Z. Physik*, **61**, 321.

THE RELATIVISTIC THEORY OF SCATTERING IN COULOMB FIELD BY ATOMS

By K. C. KAR, S. SENGUPTA AND P. P. CHATTERJI

(Received for publication, April 4, 1950)

ABSTRACT Relativistic theory of nuclear scattering of electrons has been considered from the wavestatistical point of view. It has been shown that to a first order relativistic approximation the ordinary hydrodynamical wave equation is slightly modified. On deriving the wellknown χ -equations with the help of the modified equation we get a new term in the interaction energy which together with the other wellknown interaction terms gives the correct scattering formula.

INTRODUCTION

Relativistic theory of electron scattering has first been given by Mott (1929), using Dirac's linear equation for the electron. In addition to the wellknown $\cos^2 \frac{\theta}{2}$ term he has obtained two correction terms, the second of which is proportional to $(Ze^2)^3$. Later on Sexl (1933) has considered the problem afresh starting with the quadratic form of Dirac's equation (*vide* Dirac, 1947) and has obtained a formula for the scattering intensity differing from Mott's formula only in the last correction term. The controversy over the second correction term has been finally settled by Urban (1942), who, on checking up the calculations of Mott, finds that Mott's method, after proper approximation, also gives exactly the same formula as that obtained by Sexl (*loc. cit.*). It may also be mentioned that Sauter (1933) and recently Sengupta and Chatterji (1950) have obtained the above Mott-Sexl formula without the second correction term by application of Born's method of approximation to the linear equation of Dirac.

Recently Kar (1945, 1947) has considered the problem of high velocity scattering from the wave-statistical point of view and has derived Mott's formula using some new ideas regarding spin-spin interaction. In the present paper we shall show that the introduction of these ideas is not at all necessary and the correct Mott-Sexl formula can be deduced wave-statistically in a perfectly straightforward manner.

It is wellknown that in wavestatistics we take for the phase waves the general hydrodynamical wave equation in the form

$$\frac{\partial^2 D}{\partial t^2} = v^2 \Delta D \quad (1)$$

and from it we obtain the wellknown differential equations for the χ_1 - and χ_2 - waves. We shall presently show that equation (1) is only a first approximation of the actual equation satisfied by the density function in a compressible medium. If we carry the approximation a stage further, we get an equation slightly different from (1). On deriving χ_1 - and χ_2 - equations from it we get a new term in the interaction energy which together with the other wellknown interaction energies gives the correct scattering formulæ.

WAVE EQUATION

The wellknown Bernoulli's equation and the equation of continuity for a fluid in motion can be written in the form

$$\frac{\partial \phi}{\partial t} + \frac{1}{2} w^2 + \frac{\delta P}{\rho_0} = \text{const.} \quad \dots (2.1)$$

$$\frac{\partial \rho}{\partial t} + \text{div}(\rho w) = 0 \quad \dots (2.2)$$

where ϕ is the velocity potential and w the velocity of the fluid.

From (2.2) we get

$$\frac{\partial \rho}{\partial t} + \rho \text{div } w + (w \text{ grad } \rho) = 0$$

or,
$$\frac{\partial^2 \rho}{\partial t^2} + \rho \Delta \phi + (w \text{ grad } \rho) + \text{div}(\rho w) = 0$$

Substituting for ϕ and ρ from (2) we get

$$\frac{\partial^2 \rho}{\partial t^2} - \rho \Delta \frac{\delta P}{\rho_0} - \frac{\rho}{2} \Delta w^2 + (w \text{ grad } \rho) - \text{div}(w \text{ div } \rho w) = 0$$

or,
$$\frac{\partial^2 \rho}{\partial t^2} - v^2 \Delta \rho + (w \text{ grad } \rho) - \frac{\rho}{2} \Delta w^2 - \text{div}(w \text{ div } \rho w) = 0 \quad \dots (3)$$

because,
$$\frac{\delta P}{\rho_0} = \frac{\delta P}{\delta \rho} \frac{\delta \rho}{\rho_0} = v^2 \cdot \frac{\rho - \rho_0}{\rho_0} \quad \dots (3.1)$$

Neglecting the last two terms in (3) we get

$$\frac{\partial^2 \rho}{\partial t^2} - v^2 \Delta \rho + (w \text{ grad}) (\rho - \rho_0) = 0 \quad \dots (4)$$

It is evident from the above derivation that the change of ρ in the last term of (4) is due to motion of the fluid. It is therefore negligible, except for very large velocity, i.e., when w is comparable with c , the velocity of light. Hence for this ρ we can write (in the relativistic region)

$$\rho = \frac{\rho_0}{(1 - \beta^2)^{\frac{1}{2}}}; \quad \beta = \frac{w}{c} \quad (4.1)$$

or approximately,

$$\rho \left(1 - \frac{\beta^2}{2} \right) = \rho_0 \quad \text{i.e.,} \quad \rho - \rho_0 = \frac{1}{2} \beta^2 \rho_0 \quad (4.2)$$

Substituting this value of $\rho - \rho_0$ in the last term of (4) we get

$$\frac{\partial^2 \rho}{\partial t^2} - v^2 \Delta \rho + \frac{1}{2} \beta^2 (\nabla \cdot \text{grad } \rho) = 0 \quad (5)$$

It is evident that for small velocities, the last term can be neglected and then (5) becomes identical with the equation (1)

If we now take the general hydrodynamical wave equation in the form (5), the equation for the phase waves becomes

$$\frac{\partial^2 D}{\partial t^2} - v^2 \Delta D + \frac{\beta^2}{2} (\nabla \cdot \text{grad } D) = 0 \quad (6)$$

Eliminating time we get for the χ -waves

$$\Delta \chi + \frac{4\pi^2 v^2}{c^2} \chi - \frac{\beta^2}{2v^2} (\nabla \cdot \text{grad } \chi) = 0 \quad (7)$$

Now for χ_1 -waves $v \equiv v_1 \equiv w$ and the relativistic frequency v_1 is given by [Kar and Sengupta (1949)]

$$v_1 = \frac{1}{h} \cdot \frac{(E - E_{s-0} + E_0 - V)^2 - E_0^2}{E - E_{s-0} + E_0 - V} \quad (7.1)$$

where E is the total energy, E_{s-0} the well known spin-orbit interaction energy being given by Thomas (1927)

$$E_{s-0} = - \frac{Ze^2}{2m_0^2 c^2 r} \quad (\text{LS}) \quad (7.2)$$

and V is the electrostatic potential energy. Substituting in (7) and remembering that $w = - \frac{1}{m_0} \text{grad } V = - \frac{V'}{m_0} \frac{\mathbf{r}}{r}$, we get,

$$\Delta \chi_1 + \frac{8\pi^2 m_0}{h^2} \left\{ E - V - E_{s-0} + \frac{1}{2E_0} (E - V)^2 \right\} \chi_1 + \frac{V'}{2E_0} \frac{\partial \chi_1}{\partial r} = 0 \quad (8)$$

For χ_2 -waves, we have,

$$\beta = \frac{v_2}{c} \quad (9)$$

where v_2 is the velocity of the χ_2 -waves projected in the q -space being given by [Kar and Sengupta (l.c.)],

$$v_2 = \frac{E}{\{(E - E_{s-0} + E_0 - V)^2 - E_0^2\}^{1/2}} \quad (9.1)$$

Remembering that $v_2 = \frac{E}{h}$, we get for the χ_2 -waves the same equation as (8).

Thus equation (8) may be written in the general form

$$\Delta\chi + \frac{8\pi^2 m_0}{h^2} \left\{ E - V - E_{s=0} + \frac{V'h^2}{16\pi^2 m_0^2 c^2} \frac{\partial}{\partial r} + \frac{(E-V)^2}{2E_0} \right\} \chi = 0 \quad (10)$$

On comparing (10) with the equation deduced in the earlier paper [Kar and Sengupta (1949)] we notice that in addition to the well known relativistic and spin-orbit corrections to energy, we have here a new correction term whose value is given by

$$V_s = \frac{h^2}{16\pi^2 m_0^2 c^2} \cdot \frac{\partial c^2}{r^2} \cdot \frac{\partial}{\partial r} \quad \dots (10.1)$$

It may here be noted that this particular interaction term has also been obtained by Condon and Shortley (1935) by forming, to a first approximation, the relativistic quadratic wave equation from Dirac's linear equation for the electron. They have showed the importance of the term in spectroscopy. We shall presently show that this term has also great importance in scattering and that its contribution to the scattering formula corresponds to Mott-Sexl's first correction.

CALCULATION OF THE SCATTERING INTENSITY

By separating the interaction energies involving V and V^2 we can write (10) in the form

$$\Delta\chi + \frac{8\pi^2 m_0}{h^2} \left\{ E \left(1 + \frac{E}{2E_0} \right) - V \left(1 + \frac{E}{E_0} \right) - E_{s=0} + V_r + \frac{V^2}{2E_0} \right\} \chi = 0 \quad (11)$$

Remembering that E in the above does not contain E_0 , we get from (11), the rest energy of the electron,

$$\Delta\chi + \frac{4\pi^2}{h^2} \left\{ p^2 - 2m_0 V - 2m_0 E_{s=0} + 2m_0 V_r + \frac{V^2}{2} \right\} \chi = 0 \quad \dots (11.1)$$

where $p = \frac{m_0 v}{(1-\beta^2)^{\frac{1}{2}}}$, the relativistic momentum of the electron.

We now consider the scattering of a beam of fast electrons incident on a nucleus by usual Born's approximation method. Outside the potential field the wave function for the incident beam is

$$\chi_0 = e^{2\pi i p \cdot (\mathbf{n}_0 r) / h} \quad \dots (12)$$

where \mathbf{n}_0 is the unit vector along the direction of incidence. χ_0 in (12) is averaged for unit volume. Hence it represents an intensity of v electrons crossing unit area per unit time. Near the nucleus, the wave equation is given by (11.1). This equation can be written in the form

$$\Delta\chi + \frac{4\pi^2 p^2}{h^2} \chi = F\chi \quad \dots (13)$$

$$\text{where} \quad F = \frac{4\pi^2}{h^2} \left\{ 2mV - 2m_0V' - \frac{V'^2}{c^2} + 2m_0E_{r=0} \right\} \quad \dots (13.1)$$

Now we try to find a solution of (13) of the form

$$\chi = \chi_0 + \lambda_1 \chi_1 \quad (13.2)$$

where χ_0 represents the incident wave and $\lambda_1 \chi_1$ the scattered wave.

From (13) and (13.2) we get at once the well known solution

$$\lambda_1 \chi_1 = -\frac{1}{4\pi} \int \frac{e^{2\pi i h^{-1} \mathbf{p} \cdot |\mathbf{r} - \mathbf{r}'|}}{|\mathbf{r} - \mathbf{r}'|} F(\mathbf{r}') \lambda_1 d\mathbf{r}' \quad \dots (14)$$

which has the asymptotic form (for large r)

$$\lambda_1 \chi_1 = -\frac{1}{4\pi} \cdot \frac{e^{2\pi i \mathbf{p} \cdot \mathbf{r}/h}}{r} \int e^{-2\pi i \mathbf{p}(\mathbf{n}\mathbf{r})/h} F \chi_0 d\tau \quad (14.1)$$

where \mathbf{n} is the unit vector along the direction of scattering. In the following we shall replace χ in the integral by χ_0 , the incident wave function, as is usual in the Born's first approximation.

Now the integral in (14.1) consists of four different integrals corresponding to the four different interaction terms in F . The first of the integrals

is, remembering that $V = -\frac{Ze^2}{r}$,

$$I_1 = -\frac{8\pi^2 m Ze^2}{h^2} \int e^{2\pi i \mathbf{p}(\mathbf{n}_0 - \mathbf{n}, \mathbf{r})/h} \frac{1}{r} d\mathbf{r} \quad (15)$$

Now taking polar angle $\theta_1 = 0$ along the direction of the vector $\mathbf{n}_0 - \mathbf{n}$ the integration (15) can be easily performed. If we take into account the correction for critical approach (Kar, 1945), then evidently the lower limit of the \mathbf{r} -integration should be taken r_0 instead of zero, where r_0 is the distance of critical approach. Then we get

$$\begin{aligned} I_1 &= -\frac{8\pi^2 m Ze^2}{h^2} \cdot \frac{h^2}{\pi p^2 |\mathbf{n}_0 - \mathbf{n}|^2} \cdot \cos k r_0 \\ &= -\frac{2\pi Ze^2}{m_0 v^2 \sin^2 \frac{\theta}{2}} \theta^{(1-\beta^2)^{\frac{1}{2}}} \cos k r_0 \quad \dots (15.1) \end{aligned}$$

θ being the angle of scattering and $k = \frac{4\pi m v \sin \frac{\theta}{2}}{h}$. The value of r_0 as has been derived wave-statistically by Kar (1945) is

$$r_0 = 1.35 \cdot \frac{Ze^2}{m_0 v^2} (1 - \beta^2) (\operatorname{cosec} \frac{\theta}{2} - 1) \quad \dots (15.2)$$

It is evident from above that $k r_0$ is generally small for high velocity of incidence and $\cos k r_0$ is only slightly different from one.

The second integration can be written in the form [vide (10.1) and (13.1)],

$$I_2 = -\frac{Ze^2}{2m_0c^2} \int e^{-2\pi i \mathbf{p} \cdot (\mathbf{n}\mathbf{r})/h} \cdot \frac{\partial}{\partial \mathbf{r}} e^{2\pi i \mathbf{p} \cdot (\mathbf{n}_0\mathbf{r})/h} d\mathbf{r} \sin \theta_1 d\theta_1 d\phi_1 \dots \quad (16)$$

If we remember that θ_1 is taken zero along $\mathbf{n}_0 - \mathbf{n}$, then it can be easily shown that

$$(\mathbf{n}_0\mathbf{r}) = r \left(\sin \frac{\theta}{2} \cos \theta_1 + \cos \frac{\theta}{2} \sin \theta_1 \cos \phi_1 \right) \dots \quad (16.1)$$

Substituting this in (16) and performing the differentiation, we get

$$I_2 = -\frac{\pi i p}{h} \cdot \frac{Ze^2}{m_0c^2} \left\{ \sin \frac{\theta}{2} \int e^{i k r \cos \theta_1} d\mathbf{r} \cos \theta_1 \sin \theta_1 d\theta_1 d\phi_1 \right. \\ \left. + \cos \frac{\theta}{2} \int e^{i k r \cos \theta_1} d\mathbf{r} \sin^2 \theta_1 d\theta_1 \cos \phi_1 d\phi_1 \right\} \dots \quad (16.2)$$

The second term evidently vanishes through ϕ_1 -integration. The first integration can be easily performed and we get,

$$I_2 = \frac{\pi Ze^2}{m_0c^2} \left(1 - \frac{(k\tau_0)^2}{6} \right) \dots \quad (16.3)$$

The third integration can be performed in the same way as the first one and we get,

$$I_3 = -\frac{2\pi^2(\pi - 2k\tau_0)(Ze^2)^2}{hc^2m_0v \sin \frac{\theta}{2}} (1 - \beta^2)^{\frac{1}{2}} \dots \quad (17)$$

In the fourth integral there is a factor $(\mathbf{LS}) = L_x S_x + L_y S_y + L_z S_z$. If we write out the well-known operators for L_x , L_y etc., then with the help of (16.1) the integration can be easily performed and it may be seen that,

$$I_4 = 0 \dots \quad (18)$$

Thus we get from (14.1), neglecting terms of the order of $\frac{v^4}{c^4}$,

$$\lambda_1 \chi_1 = \frac{e^{2\pi i \mathbf{p} \cdot \mathbf{r}/h}}{r} \cdot \frac{Ze^2}{2m_0v^2} \cdot (1 - \beta^2)^{\frac{1}{2}} \left\{ \operatorname{cosec}^2 \frac{\theta}{2} \cos k\tau_0 - \frac{v^2}{c^2} \left(1 - \frac{(k\tau_0)^2}{6} \right) \right. \\ \left. + \frac{\pi(\pi - 2k\tau_0)Ze^2v}{hc^2} \operatorname{cosec} \frac{\theta}{2} \right\} \dots \quad (19)$$

If the relative scattered intensity be given by $I(\theta)d\Omega$, then to a first approximation

$$I(\theta) = \left(\frac{Ze^2}{2m_0v^2} \right)^2 (1 - \beta^2)^{\frac{1}{2}} \left\{ \operatorname{cosec}^4 \frac{\theta}{2} \cos^2 k\tau_0 - \frac{v^2}{c^2} \cos k\tau_0 \operatorname{cosec}^2 \frac{\theta}{2} \right. \\ \left. + \frac{2\pi \cos k\tau_0 (\pi - 2k\tau_0) Ze^2v}{hc^2} \operatorname{cosec} \frac{\theta}{2} \right\} \dots \quad (19.1)$$

Neglecting the correction for the critical approach, we get

$$I(\theta) = \left(\frac{Ze^2}{2m_0v^2} \right)^2 (1 - \beta^2) \left(\operatorname{cosec}^4 \frac{\theta}{2} - \frac{v^2}{c^2} \operatorname{cosec}^2 \frac{\theta}{2} + \frac{2\pi^2 Zc^2 v}{hc^2} \operatorname{cosec}^2 \frac{\theta}{2} \right) \quad (20)$$

which is identical with the formula obtained by Mott-Sexl.

In conclusion, it may be mentioned that in deriving the above formula of scattering we have found (Eqn. 18) that the spin-orbit interaction term in F has no contribution to the scattering intensity. Since the other two interaction terms in F have a relativistic origin, it may be easily seen that both the corrections in Mott-Sexl formula (20) are really relativistic.

ACKNOWLEDGMENT

One of the junior authors expresses his indebtedness to the Government of West Bengal for awarding him a scholarship.

PHYSICAL LABORATORY,
PRESIDENCY COLLEGE, CALCUTTA.

REFERENCES

- Condon and Shortley, 1935, *Theory of Atomic Spectra*, p. 130.
Dirac, P. A. M., 1947, *Principles of Quantum Mechanics*, p. 264.
Kar, K. C., 1945, *Ind. Jour. Phys.*, **19**, 146.
" 1947, *ibid.*, **21**, 69.
Kar, K. C., and Sengupta, S., 1949, *ibid.*, **23**, 19.
Mott, N. F., 1929, *Proc. Roy. Soc. A*, **124**, 425.
Sauter, 1933, *Ann. d. Phys.*, **18**, 61.
" 1933, *Zeit. f. Phys.*, **86**, 818.
Sengupta, S. and Chatterji, P. P., 1950, *Curr. Sci.*, (in press).
Sexl, 1933, *Zeit. f. Phys.*, **81**, 178.
Urban, 1942, *ibid.*, **119**, 67.
Thomas, L. H., 1927, *Phil. Mag.*, **3**, 1.

SCINTILLATION TYPE ALPHA COUNTER AND ITS APPLICATION IN U AND TH ESTIMATION OF MINERALS

By SANTIMAY CHATTERJEE AND SOBHANA DHAR

(Received for publication, July 8, 1950)

ABSTRACT. A scintillation type alpha counter using commercial 931-A photomultiplier tubes is described. The screen of Cossor oscillograph-type J, has been used as the phosphor. The luminescence spectrum of the phosphor and the microphotometer analysis are given. The application of such arrangement for uranium and thorium estimation has been described. The apparatus has been used for low counting rate and has been standardised with an electrolytically deposited standard uranium oxide source to give 100% efficiency of counting and 50% maximum geometry. The background counting rate of the system is 1.4 counts per hour due to radio-active contamination in the phosphor and highly ionising cosmic radiations. Integral bias curves for polonium and standard uranium source have been given. Associated electronic circuits have been discussed. The amplifier has an input time constant of 5 micro-seconds. The discriminator pulse width is 100 micro-seconds and can be decreased to one micro-second for high rates of counting to which the apparatus is adaptable. The same arrangement can be used to detect uranium fission by neutrons.

INTRODUCTION

The detection of alpha-particles from very weak sources is of great importance in the study of radio-activity of rocks, minerals, dust and other substances and to detect traces of uranium or thorium present in such substances. Since uranium and thorium in equilibrium with their decay products emit 9.87×10^4 and 2.02×10^4 alphas respectively per gramme per second, it is possible to detect microgrammes of uranium and thorium or less, contained in minerals. The sensitivity is limited by the background rate of counting of the apparatus. It is desirable to construct an apparatus which will be reliable and can be run for long periods of time. It is also desirable that the background rate of counting should be as low as possible and the apparatus should not be affected by the surrounding conditions. A counting arrangement, using a FP54 electrometer tube in conjunction with an ionisation chamber, first used by Evans (1935) and later used in this laboratory by Nag, Das and Das Gupta (1944), did not fully satisfy the requirements. For single alpha counting it had two main disadvantages, *viz.*, (1) the background was rather high, and (2) the arrangement could not be run for long periods of time. Recent work on the use of scintillation counter in detecting radio-active disintegrations has brought to notice the

possibility of using such counters for detection of α -particles, with a fairly low background. During the last few years, many papers have been published on the scintillation α -counters by several authors—Allen, Sherr, Broser, and Kallmann, Boaler and Weidhlg, etc. and specifically about low rate α -counter by Cassen, Reed, Curtis and Baurmash (1949).

In the present work, we have used a commercial photomultiplier tube with a three-stage degenerative feed-back amplifier and have been able to reduce the background, due to all extraneous effects, aside from contaminations and highly ionising radiations, effectively to zero, at the same time maintaining the efficiency of alpha counting at 100% after correction for geometry. The electronic devices have been made reliable, non-microphonic and free from stray pick-ups. The arrangement is not sensitive to β - or γ -radiations and records alphas incident with rates ranging from 1000 counts per second to a few counts per hour. The background, as measured over 20 hours, is 1.4 counts per hour.

DETAILS OF EXPERIMENTAL ARRANGEMENTS

The schematic diagram of the experiment is shown in Fig. 1. The arrangement of the photo-multiplier tube, the phosphor and the sample

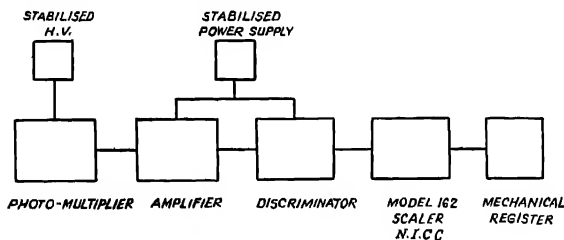


FIG. 1

Block Diagram

holder are shown in Fig. 2. The phosphor deposited on a thin glass plate was fixed just before the photo-cathode of the photo-multiplier by a thin adhesive film of 'durofix'. The standard sample was deposited on a thin platinum foil, having an area of 2.06 cm. \times 5.6 cm. and was mounted on a sample-holder which was fixed in such a manner that the whole of the source remained just in front of the phosphor without actually touching it. The photo-multiplier tube and the sample-holder were enclosed in a light-tight box painted black inside, so that no light could get inside. Mineral samples were ground in an agate mortar and were sieved through a 200-mesh sieve. For dust samples, weighed amounts were pasted on pieces of Scotch tape which were fixed on the sample-holders. Care was taken that the area of the source thus prepared is in no case greater than the area of the phosphor. The sample-

holders were fixed in such a way that the geometry of the source and the phosphor did not change while the sample-holder was replaced. The light-tight box was of convenient size, so that the whole place could be decontaminated without any difficulty.

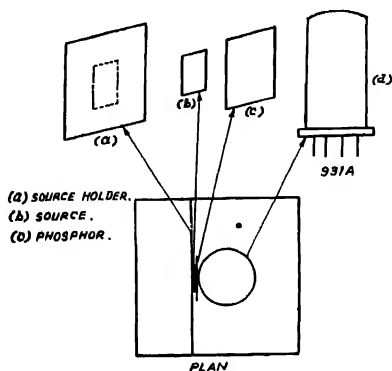


FIG. 2



FIG. 3

X-ray Luminescence Spectrum of Phosphor J

Of the many organic and inorganic phosphors tested, the photo-current pulse due to α -particles was found to be maximum for the sulphide phosphors, specially for Ag-activated zinc sulphide, which had also been noted by Kallmann (1949). It was found by us that the fluorescent screen of the Cossor oscilloscope (Type J), which has a blue emission, gave, with E. C. A. 931-A photo-multiplier tube, even larger photo currents for α particles. Throughout the present work a thin rectangular glass piece 3.2 cm. \times 1.6 cm of the same area as the photo-cathode had been used on which the Type J phosphor was deposited (mentioned hereafter as phosphor J). The luminescence spectrum of the phosphor J under X-ray excitation and standardised by copper arc, is shown in Fig. 3, and the microphotometer record is shown in Fig. 4. It will be found that the maximum light emission is at 4400 Å and ranges from 3950 Å to 5050 Å which suits very well the 931-A tube which has a maximum efficiency at 4200 Å. The luminescence spectrum

suggests that the phosphor is made of zinc sulphide activated with silver. The light-yield being adequate, no reflector has been used.

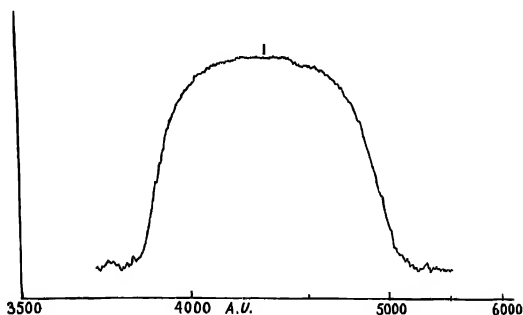


FIG. 4

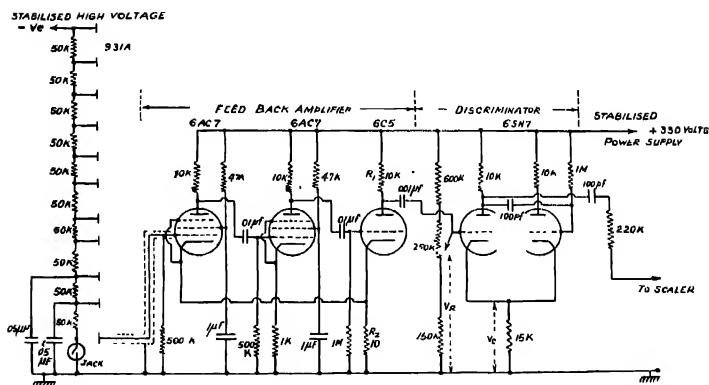


FIG. 5

Circuit Diagram

The circuit diagram is given in Fig. 5. The negative high voltage from a stabilised high voltage source was fed to a voltage dividing network to supply the dynode voltages of the photo-multiplier tube. The current drainage from the high voltage source was kept variable from 1 milliamp. to 2 milliamps., and the voltage per dynode stage could be varied from 50 to 100 volts. It was found necessary to connect two 0.05 microfarad capacitors to the last two dynode stages to bypass all pick-up disturbances and to reduce effectively the current surges through the resistors to a minimum, giving more stable operation and higher pulse heights at the anode. The

anode of the photomultiplier tube is followed by an usual three stage degenerative feedback amplifier shown in the circuit diagram which has an amplification of 1000 over a bandwidth of 10 Mc/s. Two 6AC' tubes were used in the amplifier stages to ensure the wide bandwidth. The amplification can be shown to be equal to R_1/R_2 and thus could be varied by varying the ratio of the resistances to any desired value. The input of 6AC' was taken through a shielded cable to avoid pick-ups at this stage. The discriminator is a cathode coupled multi-vibrator triggered by the positive pulses from the output of the amplifier. The power supply of the amplifier and the discriminator were highly stabilised so that the multi-vibrator remained stable throughout the operation. The potentiometer in the grid arm of the first tube of the multi-vibrator sets the limit to the height of the incoming pulses that will trigger the multivibrator and thus pulses of smaller heights will not be recorded. The discriminator is then followed by a standard laboratory scaler, and a mechanical register. The scaling circuit used by us was triggered by negative pulses and had to be fed from the plate of the first tube of the multi-vibrator discriminator which is normally non-conducting and is triggered only by pulses of pre-determined heights coming through the amplifier. Pulses of smaller heights coming at the grid which do not trigger the multi-vibrator may affect it in another way. These pulses may make the first tube slightly conducting without actually triggering it. This leads to a slight decrease in the plate voltage of the first tube and, as a matter of fact, will produce small pulses at the plate of the first tube. Unless care is taken, the unwanted pulses will get into the scaling circuit which is sensitive upto 0.25 volts. This was avoided by connecting the discriminator to the scaling circuit with a 220K resistor in series with the 100 p.f. capacitor which suppresses all such small pulses and allowed only triggered pulses to pass through. The same effect can be obtained by taking the positive output from the plate of the second tube which is operated only when the multivibrator is triggered. This has to be inverted by means of another tube before feeding it to the scaling circuit. In dealing with multi-vibrator type discriminators, we have always found it necessary to check all pulse-shapes visually by using an oscilloscope. The triggering action of the multivibrators is very interesting and is being investigated by Mr. S. Sen, in this laboratory.

The necessity of introduction of the discriminator will be understood by the explanation of the counting mechanism. A high energy particle, when incident on the phosphor, produces a spark of light whose intensity is proportional to the energy of the incident particle. The spark of light thus produced liberates electrons from the photo-cathode and the electrons after being amplified a hundred thousand times at the nine secondary emitting surfaces, are collected by the collector plate. At the input of the amplifier, these amplified electron bursts produce voltage pulses of a few millivolts magnitude. For particles of same energy the voltage pulses coming out of

the photo-multiplier tubes may be expected to have same sizes, but in practice it was not so. The reason is that the high energy particles can strike any part of the phosphor and the paths travelled by particles may be different. The sparks of light thus produced may have slightly different intensities. As a result the electrons collected at the anode will have somewhat different energies from one another, and as such will have a distribution over pulse heights. These pulses of different heights after amplification come to the input of the discriminator. The scaler and the mechanical register will record pulses greater than a certain voltage, determined by the grid bias of the discriminator multivibrator ($V_c - V_H$). For different settings of the grid bias, an integral curve of counting rate versus discriminator bias will be obtained. The discriminator bias can be converted into the corresponding minimum pulse-height from the relation $x = (V_c - V_H - k)$, where x is the required pulse height, V_c is the cathode bias, V_H is the voltage in the grid arm, and k is the difference between the cathode bias and the voltage in the grid arm of the multi-vibrator at the point when the multi-vibrator just starts to oscillate. Let $N = \phi(x)$ represent the integral bias curve, then the pulse-height distribution curve will be given by $N' = -d\phi(x)/dx$. Integral bias curves and the corresponding pulse-height distribution curves are shown in Figs. (6), (7), (9) and (10).

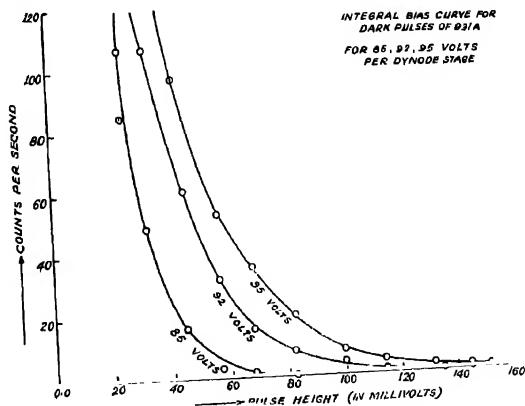


FIG. 6

The chassis containing the photo-multiplier tube was kept on four soft and thick blocks of rubber to make it shock-proof. This was found necessary to eliminate all microphonics completely. The amplifier was designed to handle both high and low counting rates. It may be mentioned that for recording high counting rates, the amplifier must necessarily have a wide band-

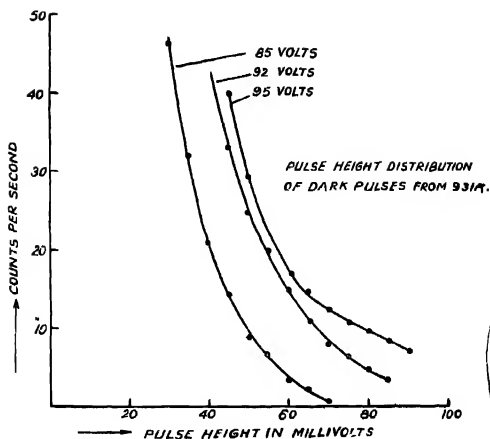


FIG 7

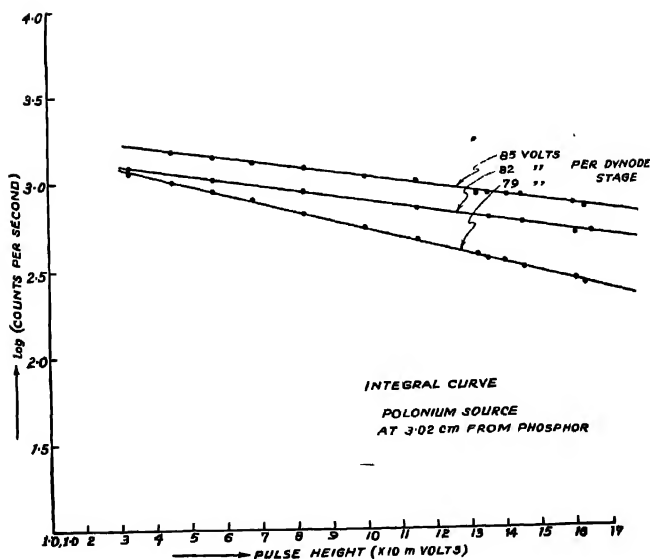


FIG. 8

width, while for recording low counting rates, it is desirable, though not necessary, that the amplifier should have a narrow bandwidth. The amplifier used had an input time constant of 5 micro-seconds, and a bandwidth of 10 Mc/s. In recording low counting rates with a wide band amplifier, the

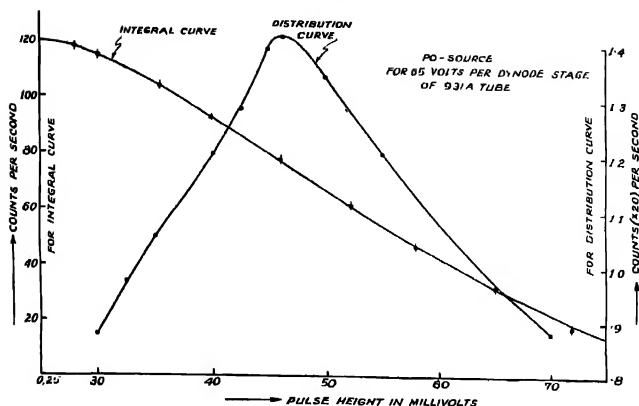


FIG. 9

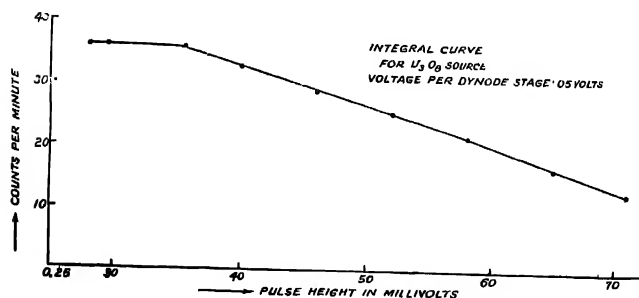


FIG. 10

elimination of stray pulses becomes important and has been successfully dealt with by proper shielding of the different parts of the apparatus. The commercial scaler used had a scale of 128 and a resolving time of 0.25 micro-second so that it could record more than 10,000 counts per second without appreciable counting loss. The mechanical register which can record 10 counts per second without being choked, sets the limit of the counting rate per second of the whole arrangement. The discriminator circuit has been kept at a resolving time less than 10^{-4} second, and can be reduced to 1 micro-second, if desired.

RESULTS

It has been found that all 931-A tubes are not equally sensitive, and the tube amplification varies over a wide range. Six 931-A tubes were selected for the experiment after inspection of their characteristics. The integral bias

curve for the dark pulses as also the pulse height distribution for different voltages are shown in Fig. 6 and Fig. 7. In the present case, the whole arrangement had to be made insensitive to β - and γ -radiations. For achieving this end, the amplification of the photo-multiplier tube was reduced to a minimum by reducing the voltage per stage of the dynodes to as low as 66 volts. This at the same time reduces the dark pulses by a considerable amount. Phosphor J is very insensitive towards β - or γ -radiations at this voltage. This was tested by using a 0.5 millicurie RaE β -source and also by using a 10 millicurie Radon tube γ -source. But the arrangement remains very sensitive to the α -particles incident on the phosphor J. For identical conditions, phosphor J was replaced by anthracene of same area as phosphor J but it did not record any alpha without the use of a reflector. Even when a reflector was used, it was not as efficient as type J. The same trial with thallium activated potassium iodide showed that it was much inferior to phosphor J. It has been mentioned earlier that α -particles produce much greater ionisation in the phosphor and the voltage pulses due to them are accordingly quite high. The integral bias curve for the α -particles from a polonium source, having a comparatively high specific activity and placed at a distance of 3.0 cm. from the phosphor is shown in Fig. 8.

This arrangement has, in fact, a bad geometry, for α -particles may strike the phosphor at any angle with any energy, as a result of which a probability distribution for the pulse heights has been obtained. A polonium source of comparatively less specific activity was placed just in front of the phosphor J so that all γ -particles coming out within that 50% geometry struck the phosphor. In this case, pulses recorded will have a continuous height distribution, starting from a minimum. This minimum pulse height will depend on the range, i.e., the energy of the incident alpha, upon the thickness of the source and also on the geometry of the arrangement. The integral bias curve and the pulse height distribution are shown in Fig. 9. The minimum pulse height has been found to be less than the expected value due to thickness of the source used. The method of preparation of the polonium source was described by A. K. Saha (1946). The same experiment was repeated with a very weak uranium oxide standard source.

The sample for the purpose of standardisation of the apparatus was prepared by electrochemical deposition of the uranyl ions on a platinum foil and then converting it to the stable oxide U_3O_8 . The method has been described by Biswas and Patro (1949). The current density for the best deposition was found to be near about 0.164 amps. per sq. cm. The uranium oxide thus deposited on the platinum foil (0.6 cm \times 2.06 cm.) had a total weight 0.12 mgm. The standard source was mounted in a manner shown in Fig. 2. The integral bias curve is shown in Fig. 6 for pulse heights up to 100 millivolts. It will be seen that for pulse heights up to 38 millivolts the total counting rate is constant. The experiment is repeated

with the discriminator set to admit pulses greater than 36 volts and the counting rate is taken for a long run. The average for over 10 hours gives a counting rate of 36 counts per minute. The background counting rate for an average over 20 hours is 1.4 counts per hour. The largest dark pulse that could be detected with 66 volts per dynode stage had been 18 millivolts. With the phosphor removed and with the same setting of the discriminator bias, no dark pulse could be detected for a constant run of ten hours. The background recorded with the phosphor mounted had been due to the contaminations present in the box and in the phosphor itself. It can be calculated that 0.12 mgm of uranium oxide gives 73.2 alphas per minute for 100% geometry. The accuracy of weighing is ± 0.00001 gm. corresponding to ± 3.2 counts per minute. Thus within the accuracy of weighing of the standard source the efficiency of α -counting is 100% with 50% geometry.

A number of natural minerals and dust samples were tested for alpha activity; the most interesting of them being a dust sample from a contaminated room, 4.88 mgm. of which emitted 4.6 alphas per hour averaged over a counting period of 8 hours.

URANIUM AND THORIUM CONTENT DETERMINATION

The theory of the emission of alpha particles from a solid of finite thickness has been worked out by Finney and Evans (1935). The same authors have also worked out the methods for the determination of the thorium and the uranium contents of minerals. We have used the same method with recalculated values of constants for the present arrangement. The number of particles n_a emitted by a thick source per sq. cm. per second through an absorber of thickness a has been given as

$$n_a = (N\mu/4) (R - \rho - a)^2 / (R - \rho) \quad \dots (1)$$

where, N = the number of α -particles emitted per cm.² of the source with a mean range of R air cm.
 μ = absorption coefficient of the source.
 ρ = minimum residual range above the absorber which can be recorded by the instrument.

N can be expressed as

$$N = 6.0234 \times 10^{23} \times Q\lambda d/W \quad (2)$$

where Q = the fractional concentration of the radio-active material per gm.,
 λ = decay constant,
 d = density of the material,
 W = atomic weight.

In a natural source, uranium, actinium and thorium are present in various concentrations in equilibrium with their decay products. Hence the number of alpha particles produced per cm.² per second is essentially the same for each member of the radio-active series, and are given by

$$N_U = 1.2343 \times 10^4 \text{ U. d.}$$

$$N_{Th} = 0.3373 \times 10^4 \text{ Th. d.}$$

$$N_{Ac} = 0.0493 \times 10^4 \text{ U. d.,}$$

where U and Th are the uranium and thorium concentrations in gm. per gm. of the source respectively. Thus the counting rate for a thick mineral source containing only uranium will be

$$\left(\frac{1.2343 \times 10^4 \text{ U} \mu d}{4} \right) \sum \frac{(R - \rho - a)^2}{(R - \rho)}$$

where the summation extends for all values of the ranges R , which are members of the uranium series. The presence of the actinium and the thorium series is to be taken into account as well. The counting rate for an absorber of equivalent thickness a air cm. can be written as

$$n_a = v_a U + w_a \text{ Th} \quad \dots (3)$$

Let

$$H = \Sigma(R - \rho - a)^2 / (R - \rho)$$

then,

$$v_a = (3.086 H_U + 0.123 H_{Ac}) \mu d \cdot 10^3 \quad \dots (4)$$

$$w_a = (0.843 H_{Th}) \mu d \cdot 10^3 \quad \dots (5)$$

Branching is taken into account in the expression

$$H = \Sigma \Delta j (R - \rho - a)^2 / (R - \rho)$$

where Δj is a numerical parameter equal to the ratio of the alpha particles emitted from any nucleus to the number emitted by its parent.

For $\rho = 0.03 \text{ cm.},$

$$H = \Sigma R \Delta j + a^2 \Sigma \Delta j / (R - 0.03) - (2a + 0.03) \Sigma \Delta j.$$

$$= P_j + a^2 Q_j - (2a + 0.03) j \quad \dots (6)$$

The values of R , Δj , j , P_j , Q_j for the three series are given in Table I. The values of a -ranges have been taken from Gamow's book. The values of Δj , j have been taken from Finney and Evans and the values of P_j , Q_j have been calculated for $\rho = 0.03 \text{ cm}$. In all these evaluations, summation is taken over those alphas which have $R \geq (a + \rho)$. The value of ρ for the present arrangement has been found experimentally by using a polonium source which emits mono-energetic alpha particles of mean 3.83 air cm. The absorber thickness required to cut off the alpha particles completely was 3.80 air cm, giving $\rho = 0.03 \text{ air-cm.}$

TABLE I

 $\rho = 0.03 \text{ cm.}$

Uranium Series	Mean range R in air-cm	ΔI	I	P_1	Q_1
Radium C'	6.87	0.9908	1	6.87	0.1461
Radium A	4.64	1	2	11.51	0.3630
Radium C (av.)	4.06	0.0002	2	11.51	0.3630
Radon	4.04	1	3	15.55	0.6124
Radium F	3.83	1	4	19.38	0.8755
Radium	3.29	1	5	22.67	1.1821
Uranium II	3.24	1	6	25.91	1.4937
Ionium	3.15	1	7	29.06	1.8142
Uranium I	2.69	1	8	31.75	2.1901
<i>Thorium Series</i>					
Thorium C'	8.53	0.65	0.65	5.54	0.0765
Thorium A	5.62	1	1.65	11.16	0.2554
Thoron	4.99	1	2.65	16.15	0.4570
Thorium C	4.71	0.35	3	17.80	0.5318
Thorium X	4.26	1	4	22.06	0.7682
Radiothorium	3.96	1	5	26.02	1.0227
Thorium	2.84	1	6	28.86	1.3786
<i>Actinium Series</i>					
Actinium C'	6.53	0.003	0	0	0
Actinium A	6.44	1	1	6.44	0.1360
Actinon (av.)	5.68	1	2	12.12	0.3330
Actinium C (av.)	5.42	0.997	3	17.52	0.5181
Radioactinium	4.66	1	4	22.18	0.7340
Actinium X	4.31	1	5	26.49	0.9676
Protoactinium	3.63	1	6	30.12	1.2454
Actinouranium	3.24	1	7	33.36	1.5569

The counting rates n_1 and n_2 with two different absorber thicknesses for identical conditions of the source and the recording system, will be given by

$$n_1 = v_1 U + w_1 \text{Th}$$

$$n_2 = v_2 U + w_2 \text{Th}$$

which will lead to

$$\frac{\text{Th}}{\text{U}} = \left(\frac{v_1}{w_1} \right) \left(\frac{n_2 - v_2}{n_1 - v_1} \right) / \left(\frac{w_2}{w_1} - \frac{n_2}{n_1} \right) \quad (7)$$

n_1 and n_2 can be found experimentally, $v_1/10^3\mu d$, $w_1/10^3\mu d$, $v_2/10^3\mu d$ and $w_2/10^3\mu d$ can be found with the help of Table I and eqns. (4), (5), and (6), and thus Th/U ratio can be determined. The experimental results of a few samples are given in Table II.

TABLE II

$\rho = 0.03 \text{ cm}$

Sample	a_1	n_1	v_1	w_1	a_2	n_2	v_2	w_2	Th/U
Thorianite	0.7 cm.	85.33	68.33 ⁰⁵	17.5636	4.09	6.124	3.8885	1.8038	1.87
Monazite	0.4 cm	11.22	87.3965	20.1940	3.79	0.102	5.2204	2.3728	4.54
G. S. I. (Lab 1226 No. 5)	0.6 cm	0.17	72.6507	18.1177	3.99	0.011	4.3309	1.9510	0.55

TABLE III

Sample	No. of α 's emitted per gm. per sec.	Th/U	U in gm. per gm. of mineral	Th in gm./gm. of mineral
Thorianite	18.86×10^3	1.87	13.42×10^{-3}	25.59×10^{-3}
Monazite	571.60	1.51	2.94×10^{-3}	13.34×10^{-3}
G. S. I. (Lab 1226 No. 5)	17.24	0.55	4.15×10^{-4}	2.29×10^{-4}

If the total counting rate is N_α per gm per second for 4π solid angle then,

$$N_\alpha = x[10.2688 + p \times 2.0238] \times 10^4$$

where x is the amount of uranium present in 1 gm. of the sample and p is the Th/U ratio. A few results are given in Table III. In finding the Th/U ratio, the most suitable thickness has been found to be 4 to 5 air cm. The geometry of the source and the phosphor has to be checked critically. The accuracy of the experiment will mostly depend upon the accuracy of finding the distance between the source and the phosphor. The discriminator bias is set at such a position that all the alphas incident on the phosphor are recorded. An accuracy of 5% can easily be obtained.

DETECTION OF FISSION

With the same arrangement we have been able to detect fission. About 6 mgm of uranium oxide was placed in front of the phosphor. The dis-

criminator bias was set to admit pulses greater than 83.5 volts so as to cut off all alpha particles coming from the uranium source. The background had been one count per 4 hours and that probably due to the piling up of the alpha particles. A 40 millicurie radium-beryllium neutron source was placed at a distance of 6 cm. from the uranium source. Paraffin blocks of 3 cm. total thickness were placed between the neutron source and the uranium source for slowing down the neutrons. An average of 2 fission counts per hour was obtained.

DISCUSSION

The elimination of dark pulses and the methods of obtaining a reproducible geometry have made it possible to use scintillation counters as alpha-detectors. The problem of thin windows, which is so often faced with G.M. counters, does not arise here. Early in 1947, Allen in his improved electron multiplier reported to have obtained 100% efficiency for a moderately high counting rate of alpha particles at nearly zero discriminator bias. He observed 1800 counts per minute from a calibrated polonium source which emitted 1600 alphas per minute and the result was within the accuracy of the calibration of the source. The background counting rate has not been mentioned. Cassen (*et al* 1949) have described a low rate alpha counter with 931-A and IP28 tubes. With 80 volts per dynode stage, the background counting rate obtained was 2 to 3 per hour and the efficiencies of alpha counting were 64.8% and 68.0% with 50% geometry. They have not given the integral bias curve in their paper. With a suitable choice of phosphor we have increased the light yield so that the tube amplification could be reduced by reducing the voltage per dynode stage. This has completely reduced the dark pulses without affecting the alpha counting efficiency of the system. From the integral bias curve, the region of operation, where all the alphas are detected, is obtained and observations are taken in this region to maintain the 100% efficiency. The nature of integral bias curve shown in Fig. 9 has also been observed by Kallmann (1949) and by Boaler and Weidling (1949). They have not reported about the efficiency of their arrangement. The small size of the phosphor, which is the primary detecting medium, restricts the use of such arrangements to narrow beam measurements. Such arrangements will be very useful for quick determination of weak alpha activity and can be conveniently used for analysis of uranium and thorium contents of minerals. The thorium content in the thorianite reported here is much less than what has been found by other workers. This is probably due to the fact that only a small amount of the rock sample was available to us and proper sampling could not be made.

ACKNOWLEDGMENTS

We express our gratitude to Professor M. N. Saha, F.R.S., Director of the Institute of Nuclear Physics, for his kind interest in the work, and to

Dr. B. D. Nag for suggesting the problem and for his constant guidance. Our thanks are due to Mr. B. M. Banerjee, Mr. S. K. Sen, and Mr. A. Chatterjee for their valuable suggestions. We are also indebted to Dr. W. D. West, Director of Geological Survey of India for helping us with a few mineral samples.

INSTITUTE OF NUCLEAR PHYSICS,
CALCUTTA UNIVERSITY.

REFERENCES

- Allen, J. S., 1947, *R. S. I.*, **18**, 739
 Biswas, S. and Patro, A. P., 1949, *Ind Jour Phys.*, **23**, 97
 Boaler and T. Weidling, 1949, *Arkiv f. Fysik*, **Band I**, 335.
 Broser, I. and Kallmann, H., 1947, *Nature*, **2** (a), 430.
 Broser, I. and Kallmann, H., 1949, *Nature*, **163**, 21
 Curran, S. C. and Baker, W. R., 1948, *R. S. I.*, **19**, 116.
 Cassen, D., Reed, C. W., Curtis, L. and Baumash, L., 1949, *Nucleonics*, **5**, No 4, 55.
 Finney, G. D. and Evans, R. D., 1935, *Phys. Rev.*, **48**, 503.
 Kallmann, H., 1949, *Phys. Rev.*, **75**, 623
 Michaelis, L. G., 1949, *Helv. Phys. Acta*, **23**, Supplement 3, 155.
 Nag, B. D., Das, S. and Dasgupta, A., 1944, *Proc Nat Inst. Sci.*, **10**, 167
 Saha, A. K., 1946, *Proc Nat Inst Sci*, **12**, 159
 Sherr, R., 1947, *R. S. I.*, **18**, 767.

A STUDY OF THE SWITCHING ACTION IN A MULTIVIBRATOR CIRCUIT. PART I

By B. M. BANERJEE

(Plates XIII, B and C)

ABSTRACT. An experimental arrangement for taking oscillograms of the rapid changes in the electrode voltages when current transfers from one tube to another in a plate-coupled multivibrator is described. Oscillograms with different values of the circuit parameters are shown. The results of this investigation are summarized.

INTRODUCTION

The multivibrator circuit has come into extensive use in the electronics of television, radar and experimental nuclear physics. Its wide application no doubt promoted extensive studies on its mode of operation. As a result much of it is now well-known. The author had the opportunity of exploring this circuit in a variety of ways, chiefly in experimental nuclear physics (Banerjee, 1945). He has also made some new observations on this circuit. It is felt that the literature published up till now* (Donald, 1947, etc) fails to give proper importance to and clarify adequately the phenomenon occurring at the time when switching takes place, *i.e.*, when current from one valve transfers to the other. It is therefore intended to deal with this particular part of multivibrator action in a series of publications.

SWITCHING ACTION IN A MULTIVIBRATOR

For clarity and convenience, the mode of operation of the multivibrator circuit will be discussed briefly. The multivibrator may be described as a two-stage resistance-capacity coupled amplifier in which the output is fed back to the input. The plate-coupled circuit is shown in (Fig. 1). When such a circuit is connected to the high tension supply, current

* The literature (Kiebert and Inglis, 1915) and text books (M. I. T. Staff, 1916) (Pink, 1947) published until very recently do not deal with the switching phenomenon in any detail—nor do they give the facts in a summarized form as has been done in this paper. Williams *et al* (1950) present the results of a theoretical analysis on the switching action of a multivibrator circuit. They discuss the effects of circuit parameters on speed of switching in connection with the discussion on triggering delay in triggered switching, the determination of which is the chief aim of their paper. In the chapter on "Generation of fast waveforms" ("Waveforms", by David Sayre McGraw Hill & Co., 1949) the methods of obtaining "fast switching" has been discussed. Sayre also attempts for a theoretical analysis of the switching action. The theoretical analysis by the author which will come out in the second part of this paper is more complete and is somewhat different.

alternately switches from the tube T_1 to T_2 and switches back from T_2 to T_1 , at regular intervals. We shall study what happens at the time of switching. The plate-coupled multivibrator will be discussed first.

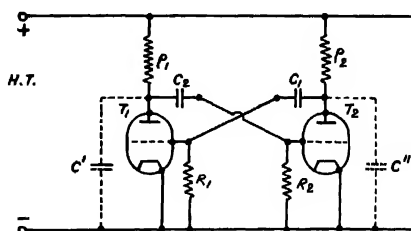


FIG. 1

Starting with the condition in which T_1 current is flowing and T_2 current shut off, let us examine the phenomenon when current transfers from T_1 to T_2 . In T_2 grid voltage advances slowly towards zero from the high negative value it attained previously when current in T_2 was shut off. This is due to the negative charge in the condenser C_2 leaking off through R_2 . As the grid voltage crosses the cut off limit, current flows again through T_2 . The feedback chain is completed and the regenerative switching process starts. Current rapidly increases in T_2 and diminishes in T_1 . Within a short time—one or two microseconds, current in T_2 rises to the maximum limit and that in T_1 cut off completely. Thereafter the anode voltage of T_2 and the grid voltage of T_1 go on falling; the anode voltage of T_1 goes on rising, while the grid voltage of T_2 diminishes slightly. Within another short period of a few microseconds (or a few tens of microseconds), the anode voltage of T_2 and the grid voltage of T_1 drop to their lowest values and the anode voltage of T_1 approaches the maximum value, the H.T. line voltage. The whole phenomenon may therefore be considered to consist of two distinctly separate parts, *viz.*, the switching of currents in the tubes in the first one or two microseconds and the completion of the consequent voltage changes in the following few microseconds or few tens of microseconds. This latter part appears to be fairly well known now-a-days. Before World War II, it was believed that the whole phenomenon takes place immediately.

The changes of current and voltage that take place at the time of switching on absorb finite time, few microseconds, because some stray capacities, indicated by C' and C'' (Fig. 1) are to be charged and discharged through finite resistances. The first part of the switching process in which the current is flowing in both the tubes T_1 and T_2 , is a regenerative process and is an exponential one with positive index. We shall discuss this part in a later publication. An experimental set up for oscillographic study on a

free-running multivibrator will be described in this publication. The second part of the switching phenomenon has been ~~and~~ studied in the first phase of these experimental investigations. The results of these investigations will be summarized and explained. As mentioned before, these appear to be well known. A new experimental arrangement is described in the present paper.

EXPERIMENTAL ARRANGEMENT

The experimental set-up consists of the following parts :

- (1) The multivibrator ~~to be tested~~ ^{to be tested}.
- (2) An isolating cathode follower tube for applying the test multivibrator electrode voltage to one plate (Y_1) of the double-beam cathode ray tube.
- (3) A synchronized high-speed sweep which may be adjusted to start just before the switching takes place.
- (4) A time marker arrangement feeding a shocked sine wave to the other plate (Y_2) of the double beam cathode ray tube.
- (5) An intensifying arrangement to switch on the cathode ray beam at the forward stroke of the high speed sweep.

The circuit diagram is given in Fig. 2.

The test multivibrator consists of two 6SJ7 tubes connected as a free running plate-coupled multivibrator. The 6SJ7 tubes may be connected as a triode or a pentode. The isolating cathodes follower consists of two sections of the double triode 6SN7 in parallel. The grids may be connected to any electrode of the test multivibrator. The cathode feeds the oscilloscope plate Y_1 and deflects the corresponding beam of the double beam tube. The oscilloscope plate receives a voltage signal at low impedance which is the same as the signal on the grids of the cathode follower. The multivibrator electrode under investigation is loaded only with the relatively small input capacity of the cathode follower compared to the cathode ray tube. The remote end of the cathode resistance goes to the +45 volts of the dry battery when plate voltages are measured and to -60/120 volts when grid voltages are to be measured. The plates of the cathode follower may be connected to the +300 volt or +500 volt supply.

The synchronized high speed sweep produces a saw tooth sweep voltage which may be adjusted to start just before the switching takes place. It consists of the 6SN7 synchronizing amplifier, the 50 pF, 5 k differentiating circuit, the 6SJ7 biased amplifier, the 6SN7 sweep multivibrator locked to the test multivibrator frequency, the 6SH7 sweep generator and the 6H6 diode clamp tube. Its mode of operation is given below.

The grids of the tube T_1 of the test multivibrator and that of the synchronizing amplifier are connected together. When the test multivibrator is

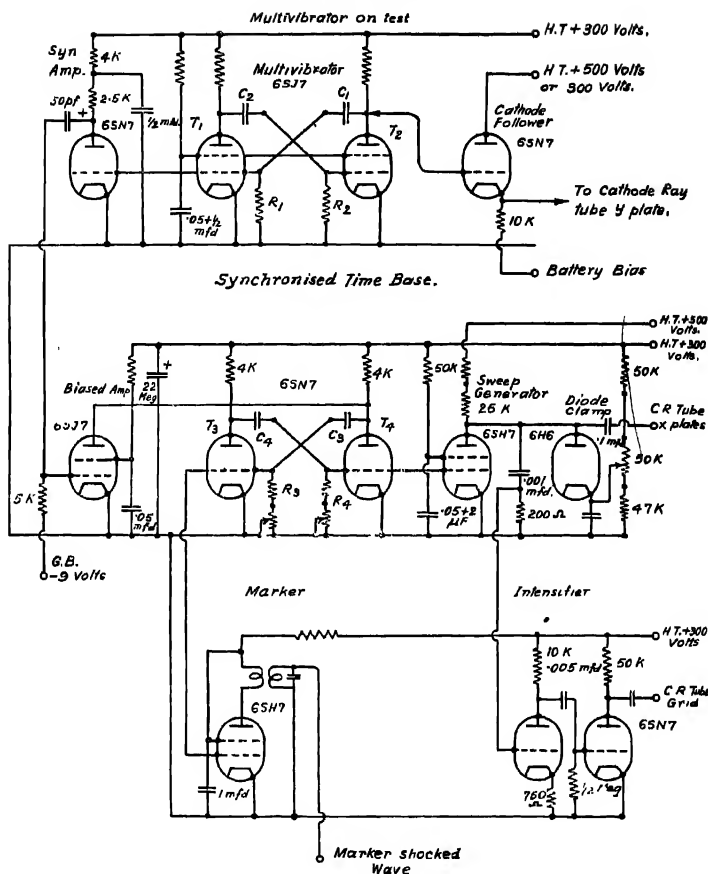


FIG. 2

switched on, T_1 is cut off and synchronizing amplifier tube is also cut off. The positive rectangular pulse at its anode is differentiated by the 50 pf., 5 k circuit to form a positive spike at the grid of the 6SJ7 biased amplifier. The positive spike passes through this 6SJ7 tube biased to cut off and triggers the sweep multivibrator—bringing about current transfer from T_3 to T_4 . This marks the synchronized zero time of the whole period and the system.

The switching of the sweep multivibrator drives the voltage of the grid of T_4 to a little positive above zero and together with it the grid of the sweep generator 6SH7, as they are connected together. The .001 Mfd. sweep capacitor therefore discharges through the 6SH7 sweep tube.

The sweep multivibrator switches back after some time, as T_3 grid voltage comes near zero from the high negative value it attained at zero time—the time of the triggered switching. This time τ_3 depends upon C_3R_4 . When the sweep multivibrator switches back and current is transferred from T_4 to T_3 , T_1 grid becomes highly negative and its anode current is cut off. The 6SH7 sweep tube is simultaneously cut off. The 001 Mfd. sweep condenser therefore charges through the 50 kilohm resistance at the plate of the 6SH7 tube. This is applied to the oscilloscope Plates X through the 0.1 Mfd. capacity and produces the forward sweep. As the sweep condenser voltage exceeds the voltage set by the cathode potentiometer of the diode clamp tube, it conducts and prevents further rise of condenser voltage during the sweep. The exponential sweep is thus brought to a halt and is confined to the nearly linear region.

As the test multivibrator switches back, current is transferred from T_2 to T_1 , after a time τ_1 which is determined by C_1R_1 .

If τ_3 is made just smaller than τ_1 by adjusting of R_3 and C_3 , the forward stroke of the sweep starts just before this switching (from T_2 to T_1) in the test multivibrator. The voltages at this switching time are therefore delineated on the greatly expanded sweep of the oscilloscope and their variations in times of the order of microseconds become observable.

The test multivibrator switches again, from T_1 to T_2 , after another time τ_2 , determined by C_2R_2 . This marks the completion of one period and the sweep multivibrator is again triggered. The sweep multivibrator must not switch, of itself, earlier. If the sweep multivibrator were allowed to run free, it would have taken a time τ_1 dependent upon C_1R_4 , for the return switching. Thus the total period of the test multivibrator is $(\tau_1 + \tau_2)$ and the total period of the sweep multivibrator when allowed to run free is $(\tau_3 + \tau_4)$. For proper synchronization $(\tau_3 + \tau_4)$ must be greater than $(\tau_1 + \tau_2)$. If this condition is not satisfied, the sweep multivibrator will complete its period and switch on by itself before the test multivibrator has switched on and thus cannot be synchronized with the test multivibrator. Thus the following two conditions are to be satisfied for proper adjustment,

τ_3 just smaller than τ_1 , and

$(\tau_3 + \tau_4)$ greater than $(\tau_1 + \tau_2)$.

These are accomplished by adjusting the continuously variable resistances R_3 and R_4 and by changing C_3 and C_4 until suitable values are obtained. These adjustments are most easily made with the double-beam oscilloscope. After removing the synchronizing link between them, the test multivibrator signal and the sweep voltage are both applied to the two oscilloscope plates. These are alternately locked with the internal time base of the oscilloscope

and their frequencies estimated. Keeping the variable parts of R_3 and R_4 at about half values, the frequency of the sweep multivibrator is made smaller than the test multivibrator by adjustment of R_3 , R_4 , C_3 and C_4 . Then the synchronizing link is restored and the continuously variables in R_3 and R_4 adjusted until the forward stroke of the sweep is seen to come at the switching time. The internal time base of the oscilloscope is then disconnected and the circuit time-base is applied. Adjustment of R_3 brings the switching phenomenon at the desired position in the expanded sweep. (Fig. *a* and *b* in Plate XIII A).

The time marker is provided by shocked oscillations in an L C circuit. At the forward sweep of the time-base, *i.e.*, when current in the sweep multivibrator transfers from T_4 to T_3 , T_3 grid is powerfully driven positive. As the grid of the 6SH7 (shocked oscillation tube) is connected to T_3 , it is also driven positive. The sudden burst of current in the primary of the oscillator coil excites a powerful damped oscillation at the natural frequency of the LC circuit. This is applied to the second beam of the oscilloscope tube and used as a time marker.

The intensifier consists of a two stage resistance coupled amplifier which derives its input from the 200-ohm resistance in series with the sweep condenser. The charging current of the sweep condenser produces a small positive voltage across this resistance with respect to ground. The amplified voltage of a magnitude of about 100 volts positive, is applied through a high voltage coupling condenser, to the cathode ray tube grid. It therefore switches on the normally shut off beams at the forward stroke of the time base. This unblanking voltage remains positive only so long as the sweep condenser charges, *i.e.*, only when the cathode ray spot moves in the forward direction. As soon as the spot movement stops, due to conduction in the clamping diode, the positive voltage goes off and the cathode ray beams are blanked out. There is no opportunity for steady spots remaining illuminated to produce halo and reduce visibility in this circuit.

RESULTS OF EXPERIMENTS

Oscillograms of rise of plate-voltage in tube T_2 , fall of grid voltage in T_2 and fall of plate voltage in T_1 , with plate load resistances of 600,000 ohms, 100,000 ohms and 20,000 ohms, both when the 6SJ7 tubes were connected as triodes as well as pentodes will be found in Plates XIIA, B and C. ~~By~~ ^{When} connecting as a pentode, the common screen dropping resistor was made equal to twice the corresponding plate resistance. The condensers C_1 and C_2 were both 15 pf. tubular ceramic condensors and the grid leaks R_1 and R_2 were one megohm carbon resistors of small size. The 15 pf. 1 Meg. combination gave a relatively small repetition time and was necessary to minimize "jitter" of the oscilloscope patterns. A few oscillograms with 50 pf.

ceramic condensers for C_1 and C_2 will also be found in oscillograms *a*, *b*, *q*. Besides, oscillogram (*a*) in Plate XIIA shows the grid voltage of T_2 together with that of the synchronized sweep on the internal time base of the Cossor model 339A oscilloscope and the same grid voltage with the expanded synchronized sweep. Further oscillograms (*n*) and (*s*) prove the simultaneous beginning of the rise of grid voltage in tube T_1 and fall of grid voltage in tube T_2 , and the rise of plate voltage in tube T_2 compared with the fall of plate voltage in tube T_1 .

The oscillograms were taken on a Cossor model 339A oscillograph using a 09D double-beam tube. This tube retains admirably good focus with large assymetric deflection voltages and with the large change of grid voltage needed for full intensification of the forward sweep.

The time marker circuit provides a damped sine wave of 1.1 Mc/s, generated by shock excitation of a high 'Q' tuned circuit. The repetition frequency of the test multivibrator altered with changes of plate load resistance. They were measured by comparing with the sine waves from a beat oscillator.

The results may be summarized broadly as follows:

(1) The rise of plate voltage with time is exponential and has a time constant approximately given by $C_1\rho$.* It may be represented by the equation

$$(H. T. \text{ Voltage} - \text{Plate voltage}) =$$

$$(H. T. \text{ Voltage} - \text{Plate voltage at start of switching}) \exp -t/C\rho.$$

This voltage changes very slowly compared to all other electrode voltages. This is directly affected by changes in the coupling capacity C_1 and by changes in the load resistance ρ .

(2) The fall of plate voltage with time is roughly exponential† and has a time constant dependent mainly upon the stray capacitances C' (sum of tube output and input capacitances plus the wiring capacity) and the plate resistance of the tube. This change of voltage is the most rapid of all the voltage changes. It is affected by changes of the plate load resistor by a small amount—an increase in the plate load resistor diminishing the rapidity of the change. Changes in the coupling capacity produce a still smaller change in the rapidity of fall—an increase of capacity increases the rapidity.

(3) The fall of grid voltage is a complicated function of time, a combination of two exponentials, roughly. It is dependent mainly on the same factors as those which control the plate voltage fall, being derived from it.

* For accurate estimation, C_1 must include the stray capacities across the plate of T_2 .

† The divergence from an exponential curve is very great, yet it is so called because the simple theory indicates an exponential.

It is affected greatly by C_2R_2 ; an increase of C_2R_2 produces an increased rapidity. It is slower than the fall of plate voltage but may be faster or slower compared to the rise of plate voltage.

(4) When the magnitude of the plate load resistors are equal to or slightly greater than the tube plate resistance, and the coupling capacities are comparable to or as small as the stray capacities, the rise and fall of plate voltage are almost equally rapid, (compare oscillograms of 20k load resistance), while the fall of grid voltage is slower than either.

(5) The rise of plate voltage is affected little by a change from triode to pentode connection. The fall of plate voltage and grid voltage are affected appreciably, the chief difference being a slight change in the character of these waveforms. However, the slopes are not appreciably greater with multivibrators using pentodes, so that when rapid switching is desired, multivibrators using triodes may be as good as multivibrators using pentodes.

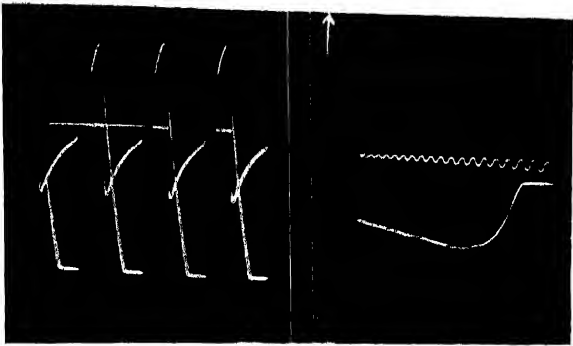
CONCLUSION

The switching action—the phenomenon that takes place in a multivibrator when current transfers from one tube to another, has been studied in this paper. The switching phenomenon is divided into two parts. In the first part, currents in the two tubes change—increasing to the maximum limit in one tube and decreasing to zero in the other. The voltage changes during this current transfer are usually small—of the order of five to fifteen volts. This completes itself within the first one or two microseconds. After this current transfer, the electrode voltages go on changing and reach their final values within another few or few tens of microseconds. This change is considerable, being a good fraction of the H. T. supply voltage. Oscillograms of this switching action has been taken with the help of a circuit that starts a high-speed sweep just before the switching. The second part of the switching phenomenon is shown clearly in these oscillograms. The first part occupies relatively small portions of these oscillograms and hence no comments are made as to its nature. The results of these investigations with regard to the second part are summarized above.

The switching action in a multivibrator is important because waveforms generated when switching very often form the basis of the timing signals utilised in radar, television and experimental nuclear physics. A critical knowledge of this switching phenomenon is helpful in obtaining increased accuracy of timing, which is very important in the proper functioning of these systems.

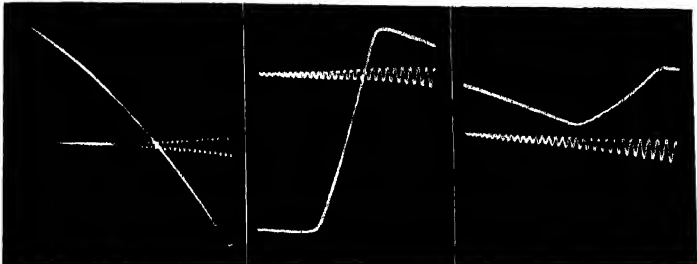
OSCILLOGRAMS

Oscillograms were taken on a four-inch Cossor double-beam oscilloscope (Model 339 A).



a

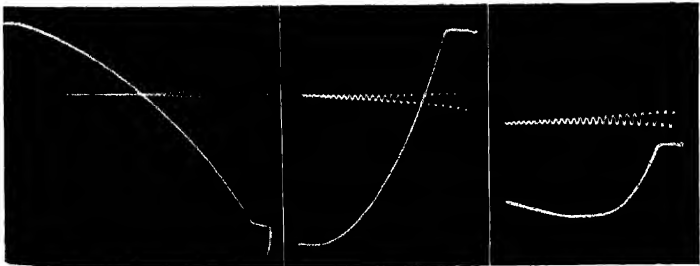
b



c

d

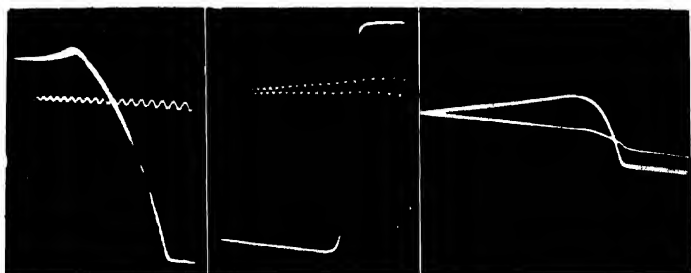
e



f

g

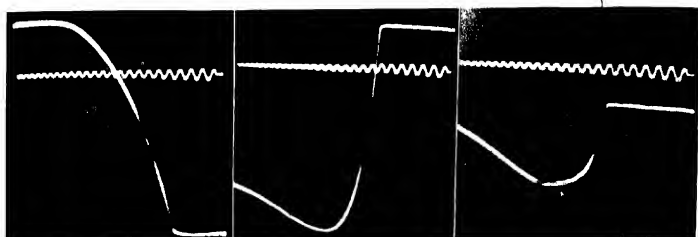
h



l

m

n

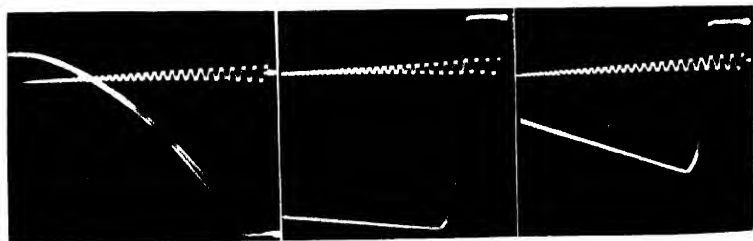


l

i

j

k



o

p

q

The cathode ray spot moves from right to left at the forward stroke of the high-speed sweep. The damped oscillation of the tune marker is from a high Q LC circuit that resonates at 1 Mc/s.

The switching phenomenon was studied on a symmetrical circuit in which $\rho_1 = \rho_2$, $C_1 = C_2$, $R_1 = R_2$; the stray capacitances C' and C'' are also nearly equal; (see Fig. 1). As a result it is immaterial as to which of the tubes is utilised to get the oscillograms. Thus the plate voltage rise in T_1 will be the same as that in T_2 ; the plate voltage fall in T_2 will be the same as that of T_1 ; the grid voltage fall in T_1 will be the same as that in T_2 ; the grid voltage rise in T_2 will be the same as that of T_1 . While the latter of the tubes referred to above were usually exploited in the experiments, it was verified that this conclusion generally holds true ~~for all~~.

As the rise in grid voltage is usually too small to be of much experimental value, most of these oscillograms have been omitted.

Oscillogram (a) in Plate XIIA top left, shows the synchronized high-speed sweep (long up-and-down strokes) and the grid voltage of T_2 (the smaller pattern in the middle of the oscillogram). It will be seen that the forward stroke of the sweep—the long line from top to bottom—is synchronized with the fall of grid voltage of T_2 .

Oscillogram (b) in Plate XIIA top right, shows the fall of grid voltage in T_2 expanded on the high-speed sweep. The cathode ray spot moves from right to left at the forward stroke of this time base.

Oscillograms (c), (d), (e) show respectively the plate voltage rise, plate voltage fall, and grid voltage fall, where T_1 and T_2 are two 6SJ7 tubes connected as triodes with plate load resistances $\rho_1 = \rho_2 = 600,000$ ohms, coupling capacities $C_1 = C_2 = 15$ pf and grid leak resistances $R_1 = R_2 = 1$ Meg. The repetition frequency was 6500 c.p.s.

Oscillograms (f), (g) and (h) similarly show the plate voltage rise, plate voltage fall and grid voltage fall respectively with the same circuit constants as above but with the 6SJ7 tubes connected as pentodes. Repetition frequency = 6500 c.p.s.

Oscillograms (i), (j) and (k) in Plate XIIB show respectively the plate voltage rise, plate voltage fall and grid voltage fall where T_1 and T_2 are pentode connected and $\rho_1 = \rho_2 = 100,000$ ohms. Other circuit constants are same as before. Repetition frequency = 8900 c.p.s.

Oscillograms (l), (m) and (n) in Plate XIIB similarly show the plate voltage rise, plate voltage fall and grid voltage rise and fall, with T_1 and T_2 —6SJ7 tubes of as triode connected. Other circuit constants are same as those for oscillograms (i), (j), (k). Repetition frequency = 9500 c.p.s.

Oscillograms (o), (p), (q) in Plate XIIB show the plate voltage rise, plate voltage fall and grid voltage fall respectively, with connected tubes as 6SJ7

triode and with coupling capacities of 50 pf for C_1 and C_2 . Other circuit constants and same as those for oscillograms (i), (j), (k). Repetition frequency = 4650 c.p.s.

Oscillograms (r), (s), (t) in Plate XIIC show respectively the plate voltage rise, plate voltage rise and fall superimposed, and grid voltage fall with triode connected 6SJ7 tubes and with $\rho_1 = \rho_2 = 20,000$ ohms. $R_1 = R_2 = 1$ Meg. and $C_1 = C_2 = 15$ pf, same as in other oscillograms. Repetition frequency = 14,400 c.p.s.

Oscillograms (u), (v), (w) in Plate XIIC are respectively the plate voltage rise, plate voltage fall and grid voltage fall with pentode connection of 6SJ7 tubes and other circuit constants remaining same as in (r), (s), (t). Repetition frequency = 8500 c.p.s.

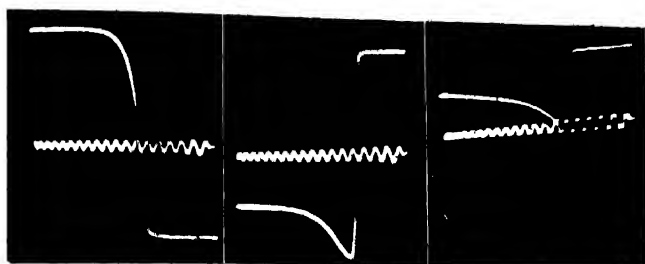
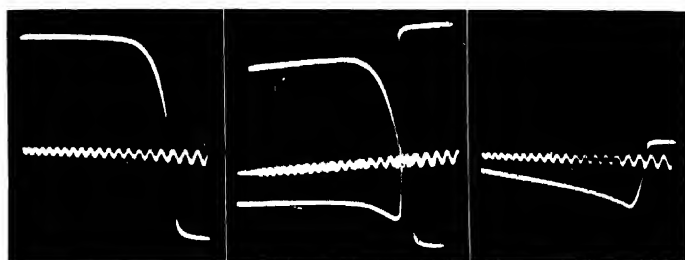
ACKNOWLEDGMENT

The author is indebted to Professor M. N. Saha, F.R.S., for his kind interest and encouragement during the progress of the work.

INSTITUTE OF NUCLEAR PHYSICS,
CALCUTTA UNIVERSITY.

REFERENCES

- Banerjee, B. M., 1945, *Ind. Jour Phys.*, **18**, 75.
 Banerjee, B. M., Saha A. K. and Ghosh, A., 1946. *Proc. Nat. Inst. Sciences Ind.*, **12**, 173
 Sayre, 1949, *Waveforms*, Chapter V, pp. 159-204. McGraw Hill.
 Donard G. Fink, 1947, *Radar Engineering*.
 Kiebert and Inglis, 1945, *Proc. I. R. E.*, **33**, 534.
 M I T., Staff, 1946, *Principles of Radar*, Second Edition
 Williams, Aldrich and Woodford (1950), *Proc. I. R. E.*, **38**, 65.

*u**v**w**r**s**t*

REVIEWS

A general kinetic theory of liquids—By M. Born and H. S. Green. Macmillan & Co. Ltd., Publishers, London, 1950. Price 10s. 6d.

This little volume contains six articles reprinted from Proc. Roy. Soc. A. of 1946-47. Of these, the first, third, fourth and fifth articles are written jointly by M. Born and H. S. Green, the remaining by the junior writer alone, being communicated by Prof. Born.

In the first three papers the writers claim to have given a general kinetic theory of liquid. Here the well known problems of classical statistical mechanics are discussed by taking a law of distribution not in the usual Maxwellian form in which the potential energy is neglected but in a more general form with the potential energy $\phi(r)$. It is apparent that unless $\phi(r)$ is defined for the liquid state the theory should be applicable to any state within the limits of classical statistics. The quantum extensions of the above theory has been made in their fourth paper. In this connection it may be mentioned that Fermi statistics with magnetic potential energy has already been used by Pauli (Zeit. f. Phys. Vol. 41, p. 97, 1927) for calculating the paramagnetic susceptibility. Thus, the idea of taking potential energy in the distribution function is not new.

In the fifth paper is discussed the corresponding thermodynamics.

The sixth and the last paper is rather interesting. Here the finer variation of density has been considered using Schrödinger wave equation, the potential $\phi(r)$ being taken for liquid after Lennard-Jones and the total density is taken to be the product of the Maxwellian and Schrödinger densities (*vide* Eq. 2.51). This idea is well known in wave statistics where the total density is taken as the product of Fermi and Schrödinger densities.

Lastly, the mode of presentation appears to be as unattractive as in the well known book 'Kristallgitter' written by the senior writer of the papers.

K. C. K.

History of Physics—By Max von Laue. Pp. 150 viii. Academic Press Inc., Publishers, New York, 1950. Price \$ 2.30

In writing this short history of physics, the author has covered the following topics: (1) Measurement of time, (2) Mechanics (3) Gravitation and action at a distance, (4) Optics, (5) Electricity and Magnetism, (6) The reference system of Physics, (7) The basis of the theory of heat (8) The law of conservation of energy, (9) Thermodynamics, (10) Atomistics, (11) Nuclear Physics, (12) Physics of crystals, (13) Heat radiation and (14) Quantum Physics. The most difficult task in writing such a history is to date the discoveries accurately and in several cases some confusion may

arise in finding out the actual discoverer. The author has made it clear in the introduction how he has got rid of this difficulty. According to him a discovery should be dated only from that time at which it was so clearly and definitely stated that it had a distinct effect on further progress.

The topics mentioned above are so varied that a specialist in any one of these branches of Physics would take a very long time to collect all the facts incorporated in the book from existing literature. The situation is, however, different to the distinguished author, because not only he has himself made very valuable contributions to our knowledge in many of the topics mentioned above but he has also kept in close touch with the advancement in the other topics, as can be clearly seen from the elegant manner in which he has described from historical point of view the developments in those branches of Physics

The author has dealt with only the early history in the case of most of the topics and in doing so he has started with the earliest work on the topic on record and has stopped at some stage of development which is for different topics. For instance, the chapter on Nuclear Physics starts with the discovery of radio-activity in 1896 and ends with the measurement of the wavelength of γ -rays emitted by fission fragments of plutonium in 1949, but the chapter on Optics starts with the idea of formation of images published in the thirteenth century and ends with Loretz's theory of the Zeeman effect. Of course Planck's quantum theory is responsible for recent development in Optics. These developments come under Quantum Physics, but this chapter again is not written in such detail as would allow the discovery of the Raman effect to be at least mentioned, although the Compton effect has been included.

To almost every physicist the book will be found to be useful in forming clear notion about the sequence of events in the early development in some of the topics in which he himself may not have specialised.

The book is nicely got up, but as the historical discussions are short there are no diagrams. The price seems to be moderate.

S. C. S

The following special publications of the Indian Association for the Cultivation of Science, 210, Bowbazar Street, Calcutta, are available at the prices shown against each of them :—

Subject	Author	Price Rs. A. P.
Methods in Scientific Research	... Sir E. J. Russell	0 6 0
The Origin of the Planets	... Sir James H. Jeans	0 6 0
Separation of Isotopes	... Prof. F. W. Aston	0 6 0
Garnets and their Role in Nature	... Sir Lewis L. Fermor	2 8 0
(1) The Royal Botanic Gardens, Kew.	... Sir Arthur Hill	2 8 0
(2) Studies in the Germination of Seeds.	... "	
Interatomic Forces	... Prof. J. E. Lennard-Jones	2 8 0
The Educational Aims and Practices of the California Institute of Technology.	... R. A. Millikan	0 6 0
Active Nitrogen A New Theory.	... Prof. S. K. Mitra	2 8 0
Theory of Valency and the Struc- ture of Chemical Compounds.	... Prof. P. Ray	3 0 0
Petroleum Resources of India	... D. N. Wadia	2 8 0
The Role of the Electrical Double layer in the Electro Chemistry of Colloids.	... J. N. Mukherjee	2 12 0

A discount of 25% is allowed to Booksellers and Agents.

RATES OF ADVERTISEMENTS

Third page of cover	Rs. 32, full page
do. do.	" 20, half page
do. do.	" 12, quarter page
Other pages	" 25, full page
do.	" 16, half page
do.	" 10, quarter page

15% Commissions are allowed to bona fide publicity agents securing orders for advertisements.

CONTENTS

PAGE

44.	A Spectroscopic Study of a Condensed Spark between Copper Electrodes in Illuminating Gas, Air and Carbondioxide at various Pressures—By Jagdeo Singh	321
45.	On the X-ray Luminescence Spectra of Thallium-activated Alkali Halide Crystals—By Aparesh Chatterji	331
46.	The Relativistic Theory of Scattering in Coulomb Field by Atom—By K. C. Kar, S. Sengupta and P. P. Chatterji	339
47.	Scintillation type Alpha Counter and its Application in U and Th Estimation of Mineral—By Santimoy Chatterjee and Sobhana Dhar	346
48.	A Study of the Switching Action in a Multivibrator Circuit—By B. M. Banerjee	361
	Reviews	371

PRINTED BY SIBENDRANATH KANJILAL, SUPERINTENDENT (OFFG.), CALCUTTA UNIVERSITY PRESS, 48, HAZRA ROAD, BALLYGUNGE, CALCUTTA AND PUBLISHED BY THE BROMFIELD, INDIAN ASSOCIATION FOR THE CULTIVATION OF SCIENCE, 210, Bowbazar Street, Calcutta.

VOL. 24

INDIAN JOURNAL OF PHYSICS

No. 9

(Published in collaboration with the Indian Physical Society)

AND

VOL. 33

PROCEEDINGS

No. 9

OF THE

**INDIAN ASSOCIATION FOR THE
CULTIVATION OF SCIENCE**

SEPTEMBER, 1950

PUBLISHED BY THE

INDIAN ASSOCIATION FOR THE CULTIVATION OF SCIENCE

210, Bowbazar Street, Calcutta

BOARD OF EDITORS

K. BANERJEE	S. K. MITRA
D. M. BOSE	P. RAY
S. N. BOSE	M. N. SAHA
D. S. KOTHARI	S. C. SIKKAR.

Secretary

EDITORIAL COLLABORATORS

DR. R. K. ASUNDI, M.A., PH.D.
PROF. H. J. BHABHA, PH.D., F.R.S.
DR. P. K. KICHLU, D.Sc.
PROF. K. S. KRISHNAN, D.Sc., F.R.S.
PROF. G. P. DUBEY, M.Sc.
DR. K. RANGADHAMA RAO, M.A., D.Sc.
DR. N. D. SARWATHEY, D.Sc.
DR. N. N. DASGUPTA, M.Sc., PH.D.
PROF. N. R. SEN, D.Sc., F.N.I.
PROF. P. C. MAHANTI, D.Sc., F.N.I.
PROF. S. R. PALIT, D.Sc.,
DR. H. RAJSHI, D.Sc.,
PROF. K. R. DIXIT, PH.D.
DR. VIKRAM A. SARABHAI, M.A., PH.D.

ASSISTANT EDITOR

MR. A. N. BANERJEE, M.Sc.

NOTICE

TO INTENDING AUTHORS

Manuscripts for publication should be sent to Mr. A. N. Banerjee, Assistant Editor, 20, Bowbazar Street, Calcutta.

The manuscript of each paper should contain in the beginning a short abstract of the paper.

All references to published papers should be given in the text by quoting the surname of the authors followed by the year of publication within braces, e.g., Sen (1942). The actual references should be given in a list at the end of the paper according to the following specimen :

Sen, B. K., 1942, *Ind. J. Phys.*, 16, 329.

The references should be arranged alphabetically in the list.

All diagrams should be drawn on thick white paper in Indian ink, and letters and numbers in the diagrams should be written in pencil.

Annual Subscription—

Inland Rs. 20

Foreign £ 2

A SPECTROSCOPIC STUDY OF AN UNCONDENSED SPARK BETWEEN COPPER ELECTRODES IN THREE DIFFERENT GASES AT VARIOUS PRESSURES.

PART III

By JAGDEO SINGH

(Received for publication, June 2, 1950)

Plates XIII A and B

ABSTRACT. A study is made of the uncondensed spark spectra in illuminating gas, air and carbon dioxide by using a transformer as a source of excitation. Some observations concerning the development of lines, bands and continua in the spectra of the uncondensed spark are reported in the present paper.

INTRODUCTION

In Parts I and II of this series (Singh and Ramulu, 1945, 1950) are discussed some aspects of the uncondensed spectra of three different gases, the illuminating gas, air and carbon dioxide and some observations have been made concerning the developments of lines, bands and continua. In the studies of the uncondensed spark spectra mentioned above, an induction coil was used as a source of excitation. Before taking the condensed spectra (Part II), observations regarding the uncondensed spectra were also repeated under similar conditions. It is the purpose of the present paper to report some observations concerning the developments of lines, bands and continua, in the spectra of the uncondensed spark obtained by using a transformer as a source of excitation.

EXPERIMENTAL ARRANGEMENT AND PROCEDURE

The experimental arrangements are exactly the same as discussed in Part II of the series, dealing with the condensed spark. The spectra have been photographed on a medium Hilger quartz spectrograph and the plates used were Eastman Kodak B-20 in the case of air and Ilford selochrome (orthochromatic) plates in the case of the illuminating gas and carbon dioxide.

Fig. 1 (Plate XIII A) represents those taken with the illuminating gas at the pressures of 10, 5, 3, 1 and 0.5 cm* under similar conditions as the Fig. 1 of the condensed spark. Fig. 2 is a representative of those taken with air at the pressures of 38, 20, 10 and 3 cms, under similar conditions as

* Cms of mercury

TABLE I

System of bands	Illuminating gas (investigated at pressures: 10-0.5 cms)		Air (investigated at pressures 30-3 cms)		Carbon dioxide (investigated at pressures 12-0.5 cms.	
	At different pressures.	At various portions of the spark	At different pressures	At various portions of the spark	At different pressures.	At various portions of the spark.
First negative nitrogen bands.	Absent at all the pressures	Absent in all the parts	They make their appearance at a pressure of 20 cms and increase with decrease of pressure and are strongest at a pressure of 3 cms.	At all pressures they are stronger in <i>F</i> , less strong in <i>B</i> and least in <i>C</i> .	Absent at all pressures	Absent in all parts
Nitrogen second positive bands.	These bands are present at all pressures. From 10 cms upto 3 cms they are equally strong; at lower pressures they become slightly weaker.	Between 10 and 3 cms they are equally strong in all the three parts, below a pressure of 3 cms they are weaker in <i>C</i> part	They are present at all pressures and are best developed between 10 and 3 cms.	At 38 cms they are stronger in <i>B</i> than in any other part, at 20 cms they are equally strong in <i>F</i> , <i>C</i> and <i>B</i> and at a pressure of 3 cms they are equally strong in <i>F</i> and <i>B</i> and weaker in <i>C</i>	They make their appearance at a pressure of 6 cms and are best developed at a pressure of 1 cm and below	They are slightly stronger in <i>F</i> than in <i>C</i>
Cyanogen violet bands.	They are present at all pressures and are equally strong upto a pressure of 3 cms below which they weaken	Between 10 and 3 cms they are equally strong in <i>F</i> , <i>C</i> and <i>B</i> and at lower pressures they weaken	Absent at all pressures.	Absent in all the parts.	Absent at all pressures	Absent in all the parts

NO γ bands	Absent at all pressures.	Absent in all the parts	They are present at all pressure and are best developed at a pressure of 10 cms	At 38 cms they are equally strong in <i>F</i> and <i>C</i> , at 20 cms they are stronger in <i>C</i> than in other parts; at 10 cms they are equally strong in <i>F</i> and <i>C</i> and weak in <i>B</i> , at 3 cms they are stronger in <i>F</i> than in <i>B</i> and <i>C</i> .	Absent at all pressures	Absent in all the parts.
CO Angstrom bands	They are present at all pressures. They increase in intensity as the pressure is decreased and are strongest at 0.5 cm.	They are equally strong in <i>F</i> and <i>B</i> and weaker in <i>C</i> at all pressures.	Absent at all pressures	Absent in all the parts.	They are present at all pressures	At 12 and 10 cms they are stronger in <i>B</i> and very weak in <i>F</i> and <i>C</i> ; at the pressures of 6 cms and below they are equally strong in <i>F</i> and <i>B</i> and absent in <i>C</i> .
Co third positive band at 2840 Å.	Present at all pressures	Up to a pressure of 3 cms it is equally strong in <i>F</i> , <i>C</i> and <i>B</i> and below this pressure it is equally strong in <i>F</i> and <i>B</i> and weaker in <i>C</i> .	Absent at all pressures.	Absent in all the parts	It makes its appearance at a pressure of 6 cms. and is present at all pressures below	At a pressure of 6 cms it is stronger in <i>F</i> , slightly weaker in <i>B</i> and completely absent in <i>C</i>

Fig. 2 (Plate XIII A) of the condensed spark. Fig. 3 (Plate XIII B) is a representative of those taken with carbon dioxide at the pressures of 12, 10, 3, and 1 cm along with the Figs. 4 and 5 of the condensed spark.

RESULTS AND DISCUSSION

Before coming to the spectroscopic studies, some general features of the spark are described. In this case the maximum pressures upto which the spark could pass are only 15, 40 and 18 cms in the cases of the illuminating gas, air and carbon dioxide respectively, as against 25, 60 and 35 cms of the condensed spark. The maximum rise of pressure in illuminating gas at a pressure of 10 cms is 1.6 cms in the case of air there is no rise upto a pressure of 40 cms and in carbon dioxide the maximum rise at a pressure of 20 cms is 0.2 cm and at a pressure of 20 cms it is 1 cm. There is, however, no fluctuation of pressure as was observed in the condensed spark in carbon dioxide.

Even in this case of the uncondensed spark there is found to be rectification in the discharge tube in all the three gases used.

The line and the continuous spectra are practically absent in this case. The resonance lines of copper (3247 and 3274 Å) are completely absent in illuminating gas and carbon dioxide, but present in the air spectra at all the pressures and are stronger at the ends and weaker in the middle. The carbon lines (2483 and 2298 Å) have appeared in the illuminating gas spectra at the pressure of 3 cms and in the carbon dioxide spectra at the pressures of 6, 3 and 1 cm in the *F* part only. They are absent at all other pressures. It may be pointed out that it was not so in the condensed spark spectra. The carbon lines, as present in the condensed spark, were present only at higher pressures and were stronger at the centre and weaker at the ends of the spark.

The bands are best developed both in the condensed and the uncondensed at a pressure of 10 cms in the case of air and from 10 to 5 cms in the case of illuminating gas and carbon dioxide. The general development of the bands is summarized in Table I. As regards the developments of the bands, both in the condensed and the uncondensed, the air spectra are exactly alike, the illuminating gas spectra are a bit less alike and the carbon dioxide spectra are least alike. In the case of the illuminating gas all the three parts (*F*, *C* and *B*) behave alike, in the case of air, *F* and *C* and in the case of carbon dioxide *F* and *B*, more or less behave alike. The *C* part is weaker below 1 cm in both the sparks and in all the three gases, and is weaker in uncondensed carbon dioxide spectra at all pressures.

The developments of CO_2 and CO_2^+ bands in the carbon dioxide spectra are rather peculiar. At 12 and 10 cms they are very much stronger in the *B* part as compared to the *F* and *C* parts; whereas at a pressure of 6 cms they are equally strong in *F* and *B* and weaker in *C* and at a pressure of 3 cms they are strong in the *F* part as compared to *B* and *C* though they are present

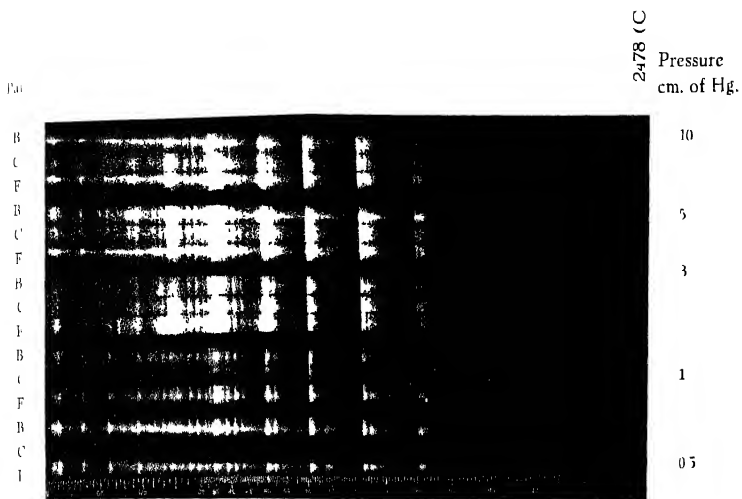
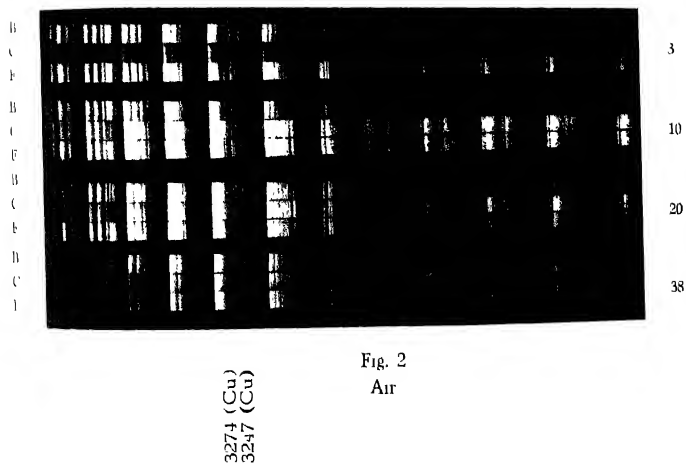


Fig 1
Illuminating gas



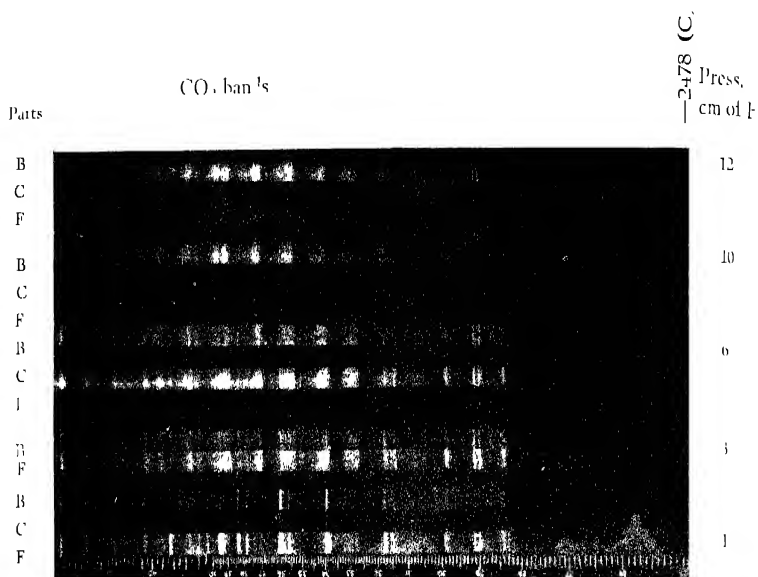


Fig. 3
CO₂

both in *F* and *B* parts. It may be pointed out that this was not so in the condensed spark spectra, where they were best developed in the *B* part only at the pressures of 10 and 5 cms.

The cyanogen violet bands were developed in the carbon dioxide spectra only at the higher pressures (20 and 30 cms) in the case of the condensed spark. They are, however, always absent in the uncondensed spark spectra in carbon dioxide. They are always absent also in the air spectra both in the condensed and the uncondensed. As pointed out in the previous publication, it is quite likely that for the development of the cyanogen violet bands a great concentration of carbon seems necessary.

The complete absence of $\text{N}\gamma$ bands in the illuminating gas (containing 48% of nitrogen and 12% of oxygen) is rather surprising. As pointed out previously, it is quite likely that for the developments of these bands a very low concentration of nitrogen and oxygen in the presence of the other substances is required.

The following are some of the more important points.

(a) The copper lines are all absent in the spectra of illuminating gas and carbon dioxide at all the pressures, but the resonance lines of copper are present in the spectra of air at all the pressures and are stronger at the ends and weaker at the centre. There is no shading of the line in this case.

(b) In the uncondensed spark spectra of the illuminating gas and carbon dioxide some carbon lines have appeared at the pressures of 3 cms and 6, 3 and 1 cm respectively in the *F* part only. They are absent at higher and lower pressures than mentioned above.

(c) Continuous spectrum is absent in all the gases and at all the pressures investigated.

(d) The developments of some of the band systems, like CN , $\text{N}\gamma$ and CO_2 have been discussed.

ACKNOWLEDGMENTS

Thanks are due to Dr. R. K. Asundi, University Professor of Spectroscopy for his inspiring guidance and valuable suggestions. Thanks are also due to Dr. N. L. Singh for valuable suggestions.

DEPARTMENT OF SPECTROSCOPY,
BENARES HINDU UNIVERSITY

REFERENCES

- Singh, J and Sree Ramulu, 1915, *Ind. J. Phys.*, **10**, 235
" " " " *Ind. J. Phys.* (communicated)

ON THE RAMAN SPECTRA OF THREE MONO-SUBSTITUTED *n*-BUTANE COMPOUNDS IN THE SOLID STATE*

By S. B. SANYAL

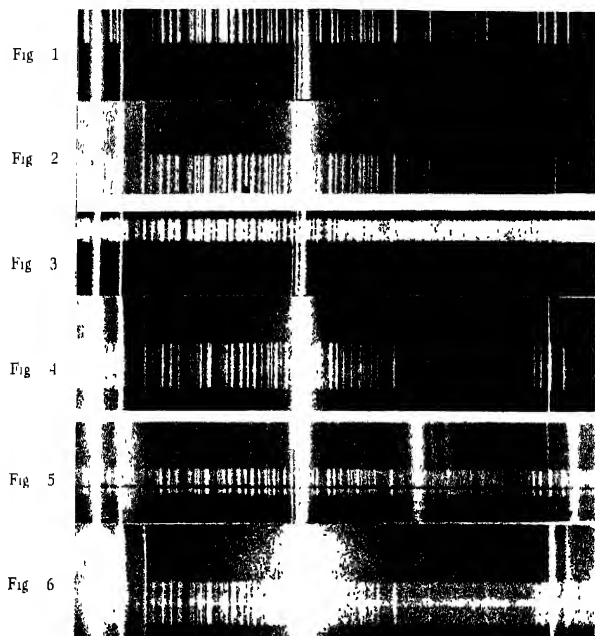
(Received for publication July 15 1950)

Plate XIV

ABSTRACT. The Raman spectra of *n*-butyl bromide, *n*-butyl amine and *n*-butyl alcohol have been studied in the solid state at about -150°C and compared with those of the corresponding liquids at about 30°C. It is observed that most of the lines due to the oscillations of the C-C-C chain disappear with the solidification in all these cases. Also, two intense lines at 558 cm⁻¹ and 642 cm⁻¹ due to C-Br valence oscillations are observed in the case of butyl bromide in the liquid state, but the line 558 cm⁻¹ disappears when the liquid is solidified. It has been pointed out that the results cannot be explained by assuming that two forms of isomeric single molecules are present in the liquid state and that one of the forms disappears in the solid state, as has been done by previous authors. It has further been pointed out that if association of molecules in the liquid state is postulated, the results can be explained satisfactorily.

INTRODUCTION

The Raman spectra of many disubstituted ethane compounds have been studied by previous workers and it has been observed that some of these compounds, which are in the liquid state at ordinary temperatures, yield a smaller number of Raman lines when solidified at low temperature. According to the general explanation offered by the various previous workers the disappearance of some of the lines in the solid state is due to the disappearance of one of the two forms of molecules which are supposed to exist in the liquid state. It was pointed out by Sirkar and Bishui (1945) that there are certain difficulties about explaining, on this hypothesis, all the changes observed in the case of ethylene dibromide. Such disappearance of some of the lines is also observed in the case of substituted propane compounds (Mizushima *et al.*, 1940) and the results obtained in these cases have also been explained on the same hypothesis. An alternative hypothesis has, however, been put forward by Bishui (1948a) to explain these phenomena. The Raman spectra of *n*-butyl bromide and some other derivatives of *n*-butane have been studied in the liquid and solid states by Nakamura (1939) and it has been concluded from the results that two molecular forms exist in the liquid state of these compounds and in the solid state one of the forms disappears. Since it



Raman Spectra

- Fig. 1. *n*-Butyl bromide at 30°C
Fig. 2. " " " -150°C
Fig. 3. *n*-Butylamine at 30°C
Fig. 4. " " " -150°C
Fig. 5. *n*-Butylalcohol " 30°C
Fig. 6. " " " -150°C

was found that such a hypothesis could not explain satisfactorily all the facts observed in the case of substituted ethane and propane compounds it was thought worthwhile to re-investigate the Raman spectra of some mono-substituted *n* butane derivatives in order to find out whether in these cases also an alternative hypothesis is necessary to explain the observed facts. For this purpose the Raman spectra of *n*-butyl bromide, *n*-butyl amine and *n*-butyl alcohol in the liquid and solid states have been studied in the present investigation. The polarisation of the Raman lines of *n*-butyl bromide and *n*-butyl amine in the liquid state has also been studied in order to understand the significance of the changes which are observed to take place with the change of state of these substances.

EXPERIMENTAL

The liquids used were obtained from the old stock of the laboratory and were of chemically pure variety. They were further distilled in vacuum before use. The technique used was the same as that adopted in the previous investigation (Sanyal, 1950). In order to find out the state of polarisation of the Raman lines, the horizontal and vertical components in the transversely scattered spectrum were photographed on the same plate with the help of a Wollaston prism. The light from the Hg arc was focused on the horizontal tube containing the liquid with the help of a condenser in this case and as there was some convergence of the incident rays, the horizontal component of the totally depolarised Raman lines was practically of the same intensity as that of the vertical component.

RESULTS

The spectrograms are reproduced in Plate XIV. The frequency-shifts of the Raman lines are given in Tables I, II and III. The data for the liquid state observed by some previous workers in the case of these substances are also included in the tables for comparison. As usual the letter D put against the frequency-shifts indicates that the value of the depolarisation factor is $6/7$. Similarly the letter P indicates that $\rho < 6/7$. The Raman spectra of *n*-butyl bromide and other mono-substituted butane compounds were studied previously by Nakamura (1939) in the liquid and solid states, but as the literature is not available to the present author it has not been possible to incorporate these data in the tables.

DISCUSSIONS

n-Butyl bromide.

The results given in Table I for *n*-butyl bromide show that some of the lines observed in the case of the liquid state disappear when the liquids are solidified. Such a phenomenon is reported to have been observed also by Nakamura (1939) and they have explained it on the hypothesis that two

TABLE I

n-Butyl bromide. C₄H₉Br

Liquid at 30°C		Solid at -150°C
Wood and Collins (1932) $\Delta\nu$ in cm ⁻¹	Present author $\Delta\nu$ in cm ⁻¹	Present author $\Delta\nu$ in cm ⁻¹
218 (3)		50 (2), e, k.
235 (3)	235 (2b), \pm e, k, P	
276 (5)	272 (4), \pm e, k, P	
345 (1)		
387 (2)		
411 (2)		
457 (5)	460 (1), e, k, P	
550 (20)	558 (10), \pm e, k, P	V
540 (10)	642 (6), e, k, P	610 (4), e, k
736 (5)	738 (2), e, k, P	616 (1), e, k
796 (6)	797 (2), e, k, P	V
833 (0)		
865 (5)	863 (2), e, k, P	V
893 (11)	850 (1b), e, k, P	902 (2), e, k
509 (2)		
967 (1)		
1011 (2)	1010 (6b), e, k, P	1015 (2), e, k
1048 (8)	1049 (4), e, k, P	V
1097 (8)	1094 (2), e, k, P	1100 (1), e, k
1214 (5)		
1260 (4)		
1294 (5)	1296 (2), e, k, P	1290 (0), e, k
1441 (10)	1440 (5b), e, k, P	1430 (1), e, k
2660 (0)		1450 (1), e, k
2733 (1)		
2833 (2)	2815 (1), e, k, P	2815 (2), e, k
2868 (10)	2866 (5), e, k, P	2865 (5), e, k
2902 (5)	2905 (2b), e, k, P	2911 (48), e, k
2934 (10)	2937 (5), e, k, P	2937 (18), e, k
2963 (10)	2960 (5), e, k, P	2960 (5), e, k
3008 (3)	3008 (1b), e, k, P	3000 (18), e, k.

Raman Spectra of Three Mono-substituted *n*-Butane Compounds 381

TABLE II

n-Butyl amine, $C_4H_9NH_2$

Liquid at 30°C		Solid at -150°C
Bayley (1933) $\Delta\nu$ in cm^{-1}	Present author $\Delta\nu$ in cm^{-1}	Present author $\Delta\nu$ in cm^{-1}
330 (o)		
338 (1)	350 (1b), e, k, P	?
399 (4)	396 (6), e, k, P	396 (2), e, k
440 (1)		
472 (o)		
495 (o)		
794 (1)	794 (1b), e, k, P	
813 (1)		
842 (1)		
872 (1)	872 (o), e, k; P	871 (1), e, k
896 (2)	894 (1), e, k; P	
935 (1)		
962 (1)	968 (1), e, k, P	
1030 (2)	1034 (2), e, k, P	
1050 (3)		1049 (2), e, k
1083 (3)	1074 (1), e, k; P	
1123 (1)	1121 (o), e, k; P	1119 (2), e, k
1184 (o)		
1301 (4)	1298 (3), e, k; D	1300 (3), e, k
1442 (7)	1440 (5b), e, k; D	1424 (3), e, k
1459 (4)		1455 (3), e, k
1476 (o)		
2727 (o)	2733 (1b), e, k; P	2868 (3b), e, k
2873 (10)	2868 (8b), e, k; P	
2906 (7)	2908 (6), e, k; P	2887 (8s), e, k
2930 (7)	2937 (6), e, k, P	2930 (2), e, k
2960 (2)	2960 (4), e, k; P	2958 (2), e, k
3317 (1)	3386 (4b), e, k; P	3319 (2s), e, k
3383 (o)	3378 (2b), e, k; P	

TABLE III

n-Butyl alcohol. C_4H_9OH

Liquid at 30°C		Solid at -150°C
Wood and Collins (1932) $\Delta\nu$ in cm^{-1}	Present author $\Delta\nu$ in cm^{-1}	Present author $\Delta\nu$ in cm^{-1}
350 (3)	356 (1), e, k	356 (1), e, k
394 (6)	391 (3), e, k	391 (2), e, k
448 (3)	447 (1b), e, k	
483 (2)	498 (1b), e, k	
514 (2)		
805 (4)	811 (4), e, k	811 (p), e, k
825 (8)	820 (5), e, k	820 (a), e, k
845 (3)	842 (o), e, k	
877 (4)	879 (1), e, k	
901 (4)	902 (1), e, k	908 (1), e, k
944 (4)	941 (1), k(e)	
963 (4)	960 (1), k(e)	
1025 (4)	1018 (1), e, k	
1051 (4)		
1067 (4)	1060 (4b), e, k	
1104 (6)	1110 (4), k	1110 (o), k
1135 (1)		
1296 (1)	1298 (8), e, k	1298 (o), e, k
1447 (10)	1440 (8b), e, k	1440 (1), e, k
1476 (4)	1476 (2), e, k	
2660 (1)		
2733 (1)	2720 (2), e, k	2882 (4), e, k
2865 (10)	2882 (15), e, k	2896 (3), e, k
2903 (10)	2911 (10), e, k	2911 (4), e, k
2932 (10)	2937 (8), e, k	2937 (2), e, k
2963 (15)	2963 (10), e, k	2963 (2), e, k

forms of molecules exist in the liquid state and one of the forms disappears in the solid state. We shall examine this hypothesis carefully to find out how far they can explain the observed facts. For this purpose it will not

Raman Spectra of Three Monosubstituted *n*-Butane Compounds 381(b)

be irrelevant to discuss here the results obtained in the case of lower alkyl halides. If we examine the data for the Raman spectra of ethylene dibromide, *n*-propyl bromide and also for analogous chlorides in the liquid and solid states, we find that the lines having frequency-shifts below 1060 cm^{-1} , which disappear in the solid state, are too many to be accounted for by assuming that they all belong to the rotational isomer other than that present in the solid state. For instance, in the case of ethylene dibromide, according to Mizushima *et al* (1938), the number of lines having frequency-shifts below 1056 cm^{-1} , which disappear in the solid state is twelve, whereas, according to Sirkar and Bishui (1945), this number is at least nine. If these lines were due to the vibrations of the group Br-C-C-Br of *cis* or *gauche* form the total number would be only six. Hence the observed number is too large to be produced by such a form. According to Bishui (1948a), in the case of propyl bromide there are altogether four lines having frequency-shifts between 1024 and 848 cm^{-1} in the liquid state, but only one line with a frequency-shift 1020 cm^{-1} is observed in the solid state. All these lines are probably due to oscillations of the C-C-C chain. If the molecules would have two forms, the lines due to C-C oscillations would have identical frequencies in both the cases and even if they were of slightly different frequencies, the number of such lines in one case would be the same as that in the other. Hence if the disappearance of the lines were due to disappearance of the one of the forms in the solid state, we would expect half the number of the lines observed in the liquid state to be present in the solid state. Actually, however, only one line is observed in this region in both the cases of propyl chloride (Mizushima, *et al*, 1940) and propyl bromide in the solid state. These results have been shown diagrammatically in figure 7, in which the data for butyl bromide and butyl amine are also included. Hence it is quite evident that the other three lines are due to the C-C oscillations modified by some extraneous causes. We shall try to find out these causes by comparing these results with those obtained in the case of substituted *n*-butane compounds.

It is seen from Table I that there are six lines having frequency-shifts between 1049 and 738 cm^{-1} in the case of *n*-butyl bromide in the liquid state and in the case of solid state there are only two lines having frequency-shifts 902 and 1015 cm^{-1} respectively. It is also observed that the line 558 cm^{-1} , which is the strongest in the spectrum due to the liquid disappears in the solid state and the line 642 cm^{-1} splits up into two lines at 640 and 646 cm^{-1} respectively in the solid state. Simultaneously, some changes occur also in the lines due to the C-H oscillations. The line 2937 cm^{-1} , which is the strongest of the lines, due to C-H valence oscillations in the liquid, becomes weaker in the spectrum due to the solid. Also, the line 2906 cm^{-1} shifts to 2911 cm^{-1} , becomes a little sharper and increases in intensity in the solid state. It is thus seen that the changes observed in the lines 558 and 642 cm^{-1} due to C-Br oscillations with the change of state

is indirectly connected with the changes in the C-H oscillations. According to the argument put forward in the previous paragraph in the case of

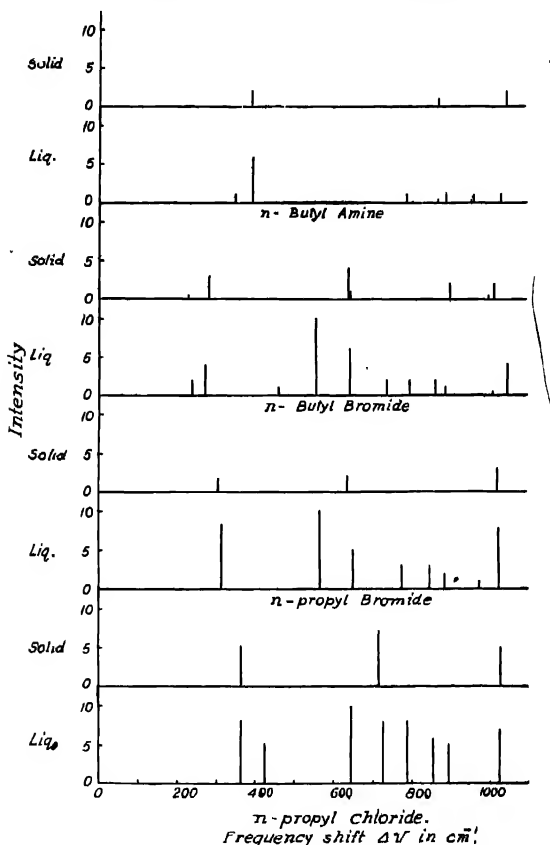


FIG. 7

n-propyl bromide, in the present case also the disappearance of the lines 738, 796 and 864 cm^{-1} produced probably by C-C oscillations cannot be due to the disappearance of one of two isomeric forms which might be postulated to exist in the liquid state. It is quite evident that it is not the geometrical configuration which creates such numerous lines due to C-C oscillations in the liquid state, but it is probably the change in the strength of the C-C bond in some of the molecules due to proximity of the Br atom of a neighbouring molecule that such different frequencies of the C-C oscillations are produced. The hypothesis put forward by Bishui (1948a) can explain the

facts observed in the present investigation quite satisfactorily. If it would be assumed that the frequency of C-Br oscillation has two values owing to the presence of two types of C-Br bond having two different strengths and that one of them disappears in the solid state, the observed facts could be explained. The normal C-Br bond evidently gives rise to the line 558 cm^{-1} , as can be seen from the Raman spectra of ethyl bromide (Bishui, 1948b) in both liquid and solid states. Owing to the random arrangement of molecules in the liquid state the C-Br bond may be strengthened by the influence of intermolecular field in the case of some of the molecules and this would give rise to the line 642 cm^{-1} . In the solid state there would be regular arrangement of the molecules in the lattice and there being only one halogen atom at the end of the molecule probably all such C-Br bonds are influenced by the neighbouring molecules and only C-Br oscillations of the associated molecule in the solid state are produced. The crystalline field is asymmetric and this may be the reason of splitting up of the line into two. The lines at 738 , 796 , 854 and 1049 cm^{-1} may be due to vibrations of the C-C group affected by the influence of the Br atom of the neighbouring molecules. When the random orientation ceases in the solid state such an influence is restricted only to one or two of the carbon atoms in the molecule and therefore these lines disappear. The fact that the lines due to some of the C-H oscillations undergo changes in the intensity in the solid state shows that the association mentioned above takes place through the H and Br atoms and such association alters indirectly the strength of the C-C bond in the molecule and directly the strength of the C-H and C-Br bonds.

It can further be seen from Table I that a new line at 50 cm^{-1} appears in the Raman spectrum of butyl bromide when the substance is solidified. It will be seen from the other two tables that no such new lines in the low-frequency region appear in the case of butyl amine and butyl alcohol. Thus the presence of halogen atom in the molecules seems to be responsible for the origin of this line. It can further be concluded that the line is not due to rotational oscillation of the molecules pivoted in the lattice as postulated by Kastler and Rousset (1941), because in that case the other two substances would also have yielded such new lines in the solid state.

n-Butyl amine.

In the case of *n*-butyl amine it is seen from Table II that the lines 1034 and 1074 cm^{-1} observed in the liquid state merge into one to form a sharp line at 1049 cm^{-1} . This last line is most probably due to C-NH₂ valence oscillation, as there is a line at 1037 cm^{-1} in the case of methyl amine. Hence it has to be inferred from these results that in the liquid state the frequency of this oscillation has two different values owing to the influence of a virtual bond on some of the molecules and absence of such an influence in the case of other molecules. As the random orientation changes to an ordered one in the crystal the

influence of the intermolecular field becomes the same for both the types of molecules but it is smaller than that in the liquid state so that the frequency of the C-NH_2 oscillation is intermediate between those observed in the liquid state. Remarkable changes take place also in the lines due to N-H and C-H oscillations with the change of state. The line 2868 cm^{-1} , which is the most intense line in the spectrogram due to the liquid, becomes much weaker and the line 2908 cm^{-1} , due to the liquid shifts to 2887 cm^{-1} , and becomes more intense when the liquid is solidified. On the other hand, the line 2937 cm^{-1} shifts to 2930 cm^{-1} and becomes much weaker with the solidification of the substance. All these lines are due to vibration of the CH_2 group and it is unlikely that any rotation of the C-NH_2 group about a C-C bond would change the intensity and frequency of the lines due to oscillations of the CH_2 group so enormously. The facts clearly show that the H atoms take part in forming virtual bonds and consequently, the frequencies of the C-H oscillations are altered so much.

Both the lines 3316 and 3378 cm^{-1} observed in the liquid state are due to N-H oscillations in the liquid state. Since both these lines are polarised they are not due to the symmetric and antisymmetric modes respectively of the NH_2 group. They are probably due to the N-H oscillations in the associated and single molecules respectively. In the solid state probably the former type persists and the latter disappears and so the line 3376 cm^{-1} also disappears. There is another fact which deserves mention in this connection. The intensity of the line 872 cm^{-1} is small in the liquid state, but it increases very much in the solid state. On the other hand, the neighbouring lines 794 , 894 and 968 cm^{-1} , which are stronger than the line 872 cm^{-1} in the liquid state, are absent in the spectrogram due to the solid. These lines are probably due to oscillations of the C-C-C-C chain. As in the case of *n*-butyl bromide, in this case also, only less than half the number of lines is observed in this region in the case of the solid. This fact cannot be explained on the hypothesis that it is due to the disappearance of one of two isomeric forms, and therefore, it has to be concluded again that the influence of intermolecular field due to random distribution of the molecules in the liquid state changes the strength of some of the C-C bonds.

n-Butyl alcohol.

The data given in Table III for *n*-butyl alcohol in the liquid and solid states show that in this case also the lines having frequency shifts lying between 1060 cm^{-1} and 811 cm^{-1} undergo remarkable changes in intensity and position with the solidification of the substance. The number of such lines in this region is nine in this particular case, while it is only six in the case of butyl amine. In the latter case probably both the lines 1034 cm^{-1} and 1074 cm^{-1} are due to C-NH_2 oscillations. Therefore, only the remaining four lines are produced by the vibration of the C-C-C-C chain. In the

case of butyl alcohol on the other hand, probably the line 1060 cm^{-1} is due to the C-OH oscillation and the remaining eight lines with frequency-shifts ranging from 811 cm^{-1} to 1018 cm^{-1} are due to the oscillations of the C-C-C-C chain. In the solid state the intensity of the line 1060 cm^{-1} becomes extremely small, whereas the feeble line 902 cm^{-1} shifts to 908 cm^{-1} and becomes more intense than either of the strong lines 820 cm^{-1} and 1060 cm^{-1} . The weakening of the line 1060 cm^{-1} in the solid can hardly be explained on the assumption that one of the two isomeric molecular forms present in the liquid state disappears in the solid state, because if such a disappearance would actually take place there would be another strong line in this region due to the C-OH oscillation in the case of the solid state. Since no such line is present, it has to be inferred that in the solid state great changes occur in the strength of the C-OH bond. On examining the relative intensities of the lines due to C-H valence oscillations in both liquid and solid states it is found that the relative intensities and frequency-shifts remain almost unaltered with the change of state, excepting the fact that the most intense broad line 2882 cm^{-1} splits up into two sharper lines at 2882 cm^{-1} and 2896 cm^{-1} . This fact shows that the strength of the C-H bond is not affected very much with the change of state. On the other hand the intensity of the lines 1298 and 1440 cm^{-1} diminishes considerably in the solid state. As these lines are due to deformation oscillation of a CH_2 or a pair of CH_2 groups the diminution in intensity may be due to the attachment of an H atom to a neighbouring molecule. These results are quite different from those observed in the case of butyl amine, because in that case the relative intensities and the positions of the lines due to C-H valence oscillations undergo considerable changes with the change of state. Hence these changes are due to different causes in the two cases and they may be due to association of the molecules in which the hydrogen atoms of the CH_2 group take part in the case of butyl amine and the OH group takes part in such an association the case of butyl alcohol. It appears therefore that in all these cases the random distribution of the molecules around each molecule affects the strength of the C-C bond giving rise to different C-C valence frequencies and the regular arrangement in the solid state produces a smaller number of such lines.

CONCLUSIONS

The results obtained in the present investigation thus show that in the case of mono-substituted normal butane compounds the changes observed to take place in the Raman spectra with the change of state of the substances cannot be explained by assuming that two types of single molecules exist in the liquid state and one of them disappears in the solid state. There are other facts which support such a conclusion. If in the liquid only two types of rotational isomers of the molecules were present they would be single molecules. On the other hand, the values of Kerr constant of substances

having polar molecules in solutions and in the liquid and vapour states show (Stuart and Volkmann, 1933) that in the liquid state the molecules are highly associated in many such cases and especially in acetone and ethyl alcohol. Hence it is expected that as the molecules of all the three compounds studied in the present investigation are polar, they are also highly associated in the liquid state. Hence any postulate in which the existence of only single molecules is assumed in the case of liquids having polar molecules cannot be accepted as a correct one.

ACKNOWLEDGMENT

The author is indebted to Prof. S. C. Sirkar for his kind interest in the present work and to the Authorities of the Indian Association for the Cultivation of Science for kind permission to carry out the investigation in the Optics Department of the Association.

INDIAN ASSOCIATION FOR THE CULTIVATION OF SCIENCE,
210, BOWBAZAR STREET, CALCUTTA

REFERENCES

- Baylev, P. L., 1933, *Phys. Rev.*, **44**, 510.
 Bishui, B. M., 1948 a, *Ind. J. Phys.*, **22**, 333.
 Bishui, B. M., 1948 b, *Ind. J. Phys.*, **22**, 447.
 Kastler, A. and Rousset, A., 1941, *Comptes Rendus*, **212**, 640.
 " " *Jour de Physique*, **2**, 49.
 Mizushima, S. I. and Morino, Y., 1938, *Proc. Ind. Acad. Sc.*, **8A**, 315.
 Mizushima S. I. and Morino, Y. and Nakamura, S., 1940, *Sc. Papers of Inst. Phys. & Chem. Research Tokyo.*, **37**, 205.
 Nakamura, S., 1939, *J. Chem. Soc. Japan*, **60**, 1010.
 Sanyal, S. B., 1950, *Ind. J. Phys.*, **24**, 151.
 Sirkar, S. C. and Bishui, B. M., 1945, *Ind. J. Phys.*, **19**, 24.
 Stuart, H. A. and Volkmann, H., 1933, *Z. f. Phys.*, **83**, 444.
 Wood R. W. and Collins, G., 1932, *Phys. Rev.*, **42**, 386.

TIDES IN THE IONOSPHERE

By A P MITRA

(Received for publication, July 25, 1950)

ABSTRACT. The paper presents in a connected form results of recent investigations, both theoretical and experimental, on tidal effects in the ionosphere. An account of the electromagnetic theory of tides, as developed by Martyn, is given. Results of estimation of ionospheric tides by comparative study of ionospheric data at Calcutta, Delhi and Chungking are also presented.

INTRODUCTION

It has been known for a long time that tidal motions, similar to those in the oceans, exist in the upper atmospheric regions. The presence of these motions leads one naturally to expect that the ionospheric layers, situated as they are in the high regions of the atmosphere, would participate in these tidal motions and that ionospheric records, if analysed, would reveal the effects of such motions. This is, in fact, what has been found. Analysis of the daily records of h' , h_{\max} and f^oF_2 have shown that their values oscillate with the solar and lunar tides. The motions of the ions and electrons as produced by the tidal motions of the air is, however, by no means simple, on account of the influence of the terrestrial magnetic field. Hence the observed tidal variations of ionospheric quantities are not always easy to interpret in terms of tidal air motions.

In recent years a complete theory of tidal oscillations in the ionosphere—the electrodynamical theory—has been developed by Martyn (1947a,b; 1948; 1949). According to this theory, though the tidal motion is predominantly a horizontal motion, the ions and electrons are constrained to move along the terrestrial magnetic lines of force. This motion has, in general, a vertical component except at the magnetic equator. But even at such low latitudes vertical ion—(and electron) drift can occur if a horizontal electric field exists; such a field must occur if the "dynamo theory" of magnetic variations is valid. It has been shown by Martyn that these characteristic motions of ions and electrons, besides explaining the observed tidal variations, also explain many of the known anomalies of the behaviour of F_2 -layer, and the small but significant departures of the behaviour of regions E and F₁ from that of the ideal Chapman region. Another fact that has emerged from these considerations is that the usual methods of measuring α from observations of the diurnal variation of ionization need reconsideration.

In the present paper we shall present in a connected form the results of analysis of ionospheric data for determining tidal effects, and also the electro-dynamical theory of the same as developed by Martyn.

The principal ionospheric parameters recorded are h' , h_{\max} and f^o , for regions F, F₁ and F₂. Hourly or bi-hourly measurements of each of these data for long periods are necessary for deducing the tidal variations. The solar tidal variations are usually much larger than the lunar ones but are more difficult to isolate. This is because the solar diurnal ionospheric variations must have a strong non-tidal 12-hourly harmonic due to the ionizing effect of solar rays of 24-hour fundamental periodicity. Lunar ionospheric tidal effects, though of much smaller amplitude, are free from these complications and are easier to deduce.

LUNAR TIDAL EFFECTS

(i) *Introduction.*—The methods used for the determination of the lunar barometric tide and the lunar magnetic variations may also be used for deriving the lunar tidal variations of ionospheric characteristics. The solar diurnal variation is first removed from the data. They are then rearranged in lunar time reckoned from the lower transit. The data for each calendar month are arranged in lunar time on one sheet and added up. Selected groups of months are then subjected to harmonic analysis.

As an instance of the analysis of ionospheric data for deducing tidal variations, we may refer here to the work of Appleton and Weekes (1939)—the earliest work of its kind—on the lunar semi-diurnal variation of $h' E$ at

TABLE I

Lunar ionospheric tides—Region II
(semi-diurnal)

Station	$h' E$ variations		$f^o E$ variations		Remarks
	Amplitude (km)	Phase of the maximum (lunar hours after transit)	Amplitude (per centum)	Phase of the maximum (lunar hours after transit)	
Slough (51°N, 0.6°W)	0.03	11.25			Average of 1 year's accurate data (Appleton and Weekes)
Canberra (35.3°S, 149°E)	J 0.19	J 6.3	J 0.09	J 6.6	Average of 4 years' routine data (Martyn)
	E 0.16	E 5.3	E 0.21	E 3.8	
	D 0.26	D 4.2	D 0.20	D 3.2	
	Mean: 0.15	Mean: 5.2	Mean: 0.13	Mean: 4.8	
Brisbane (27.5°S, 153.0°E)	0.5	4.5			Average of 4 years' routine data (Martyn)

J—Northern solstice months, E—Equinox months and D—Southern solstice months.

Slough, England. They worked with the data of eleven different periods (in the years 1937-38), each period covering 12-14 days. The height measurements were carried out on 1.8 Mc/s. As this frequency was below three-quarters of the critical frequency, the true height was practically the same as the equivalent height. The hourly means for the whole period of observations were plotted and a smooth curve was drawn through them. The departures of the individual readings from this curve were then tabulated and subjected to harmonic analysis, which yielded the components of the lunar variations. The normal accuracy of measurement, which was made every quarter of an hour, was 0.5 km. Though the amplitude of the variation was comparable with the error of each measurement, a strongly marked and statistically reliable semi-diurnal variation was revealed. This could be expressed in the form $0.93 \sin (2l' + 112^\circ)$ km., where l' is the lunar hour angle. The maximum is therefore attained about $\frac{1}{4}$ hour before the lunar transit. Fig. 1. shows the semi-diurnal variation of the height of the E-layer

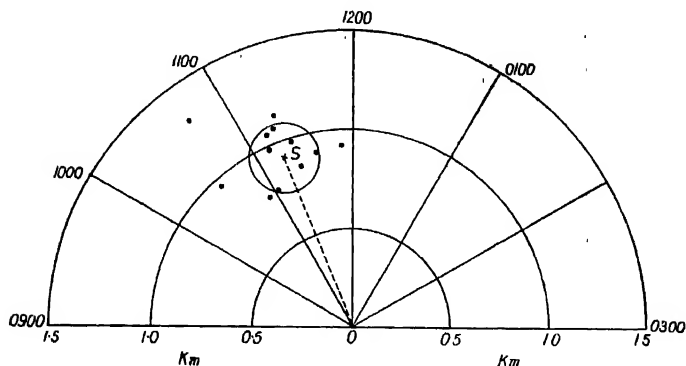


FIG. 1

Harmonic dial illustrating lunar semi-diurnal oscillation of Region E

on the harmonic dial. It will be noticed that the points are closely grouped, so that the probable error circle does not enclose the centre of the dial; this shows that the result obtained is statistically significant. Further, they lie not far from the point S, which was derived from an independent series of midday values.

(ii) *E-layer*.—Table I shows the amplitudes and phases of lunar semi-diurnal variations of region E characteristics observed in three different places. It will be seen from the table that at the same place of observation,

the hours at which $h'E$ and $f^{\circ}E$ attain their maximum values are about the same.*

The mean phase appears to have a strong latitude effect. It will be seen that while the maximum occurs at Canberra ($35^{\circ}S$) nearly 5 hours *after* lunar transit, it occurs nearly one hour *before* lunar transit at Slough ($51^{\circ}N$). This result will be discussed in sec. d(iv).

TABLE II
Lunar ionospheric tides—Region F_1
(Semi-diurnal)

Station	$h'F_1$ variation		$f^{\circ}F_1$ variation		Remarks
	Amplitude (km.)	Phase of the maximum (Lunar hours after transit)	Amplitude (per centum)	Phase of the maximum (Lunar hours after transit)	
CANBERRA ($35.3^{\circ}S, 149^{\circ}E$)	J 0.85 E 0.64 D 1.13 Mean, 0.83	J 5.3 E 7.0 D 6.1 Mean: 6.1	J 0.14 E 0.16 D 0.24 Mean 0.16	J 11.0 E 7.3 D 6.8 Mean; 7.5	Average of 10 years' data (Martyn)
HUANCAYO ($12^{\circ}S, 75^{\circ}30'W$)	0.22	7.2			Ten years' data (Martyn)
WASHINGTON ($39.0^{\circ}N, 77^{\circ}5'W$)	0.7	6.4			7 months' data (Martyn)
WATHEROO ($30^{\circ}5'S, 115.9^{\circ}E$)	1.3	5.0			21 months' data (Martyn)

J—Northern solstice months, E—Equinox months and D—Southern solstice months.

(iii) F_1 layer.—Lunar tidal variations of the heights and ionization densities of the F_1 layer have also been determined. The amplitudes are of the same order of magnitude as those of the E layer. The maximum of these variations occur 6 hours after lunar transit, approximately as for Region E.

Table II shows the amplitudes and phases of the semi-diurnal lunar tidal variations of $h'F_1$ and $f^{\circ}F_1$ as observed at Canberra, Watheroo and Washington.

* It should be noted, however, that according to Martyn (private communication to Professor S. K. Mitra) the small lunar variation in $f^{\circ}E$ cannot yet be considered as reliably determined.

TABLE III

Lunar ionospheric tides—Region F₂
(semi-diurnal)

Station	$h'F_2$ variation		$h_{max}F_2$ variation		f^oF_2 variation		Remarks
	Amplitude (km.)	Phase of maximum (lunar hrs.)	Amplitude (km.)	Phase of maximum (lunar hrs.)	Amplitude per centum	Phase of maximum (lunar hrs.)	
CANDERRA (35.3°S, 149°E)	1.6	5.6	1.7	5.7		9.5	Average of 4 years' data (Martyn).
HUANCAYO (12°S, 75.3°W)	2.3	9.2	5.2	8.4	1.7	4.3	Average of 3 years' data (Martyn).
WASHINGTON (35.0°N, 77.5°W)	3.1	6.0			1.4	9.8	Average of 4 years' data (Birkard).
BURGHFAD (57.5°N, 5.5°W)					1.3	7.6	Average of 4 years' data (Martyn).
WATHEROO (30°S, 116°E)	2.0	6.9	2.3	4.5	1.3	10.4	Average of 6 years' data (Martyn).
*CALCUTTA (22.6°N, 88.4°E)			2.0	4.0	0.5	6.0	Average of 3 years' data (Baral).
OTTAWA (45.5°N, 75.8°W)	0.6	3.2				11.4	Average of 2 years' data (Martyn).

* Unpublished.

It will be noticed from the table that the phase of $h'F_2$, according to observations of Martyn, does not show any regular variation with latitude.

(iv) F_2 -layer.—For this region the lunar tidal variations are much more well-marked than those for regions E and F₁. Analysis of only 3-4 years of ionospheric data is sufficient to reveal the semi-diurnal lunar tidal harmonic. The oscillations of h_{max} and f^o are approximately in phase quadrature. (This may be compared with the case of region E or F₁ where these oscillations are nearly in phase.)

A close analysis of the tidal effects in region F_2 also reveals another type of tidal variation which can be described as the *luni-solar* variation. It has been found (Martyn, 1947b) that the harmonic coefficients of the lunar variations sometimes depend markedly on solar time.

Table III shows the lunar tidal variations of the characteristics of region F_2 , as deduced from the recorded data at a number of stations.

SOLAR TIDAL EFFECTS

(i) *Regions E and F_1 .*—Solar tidal variations for the E and F_1 regions have not yet been properly derived. As mentioned earlier, they are difficult to isolate, being superposed on the much larger semi-diurnal harmonic of the solar ionization effect. Further, the amplitudes of the variations are small, being of the same order as the lunar tidal variations. Nevertheless, close examination of the E and F_1 records reveals certain features in their semi-diurnal variations which, according to Martyn, are ascribable to tidal effects.

The ionization variations of the E and F_1 regions are known to be regular, as required by Chapman's formula. N_{\max} varies nearly as $(\cos \lambda)^{\frac{1}{2}}$ and h_{\max} as $\log \sec X$, where X is the zenith angle of the sun. (It may be noted that actual available data are normally scaled values for h' , the minimum equivalent height, rather than h_{\max} . But for the purpose of assessing the diurnal variation of h_{\max} one may take monthly scaled values of h' .) It thus follows, that the Chapman variations of E and F_1 are symmetrical about midday. Examination of records show, however, that in practice there are significant departures from this ideal Chapman variation—which cannot be due to observational errors but which, according to Martyn, can be well explained as due to tidal effects.

Martyn has examined the h' records of Washington (14 years) and Huancayo (11 years). It is found that there are significant deviations of h' from Chapman variation for region F_1 , amounting to ± 4 kms. Further, at Huancayo, the deviations from the Chapman curve are in an upward direction in the morning for all seasons. Corresponding to this, in the Washington curves there is a deviation in the downward direction. These features are common to both E and F_1 variations. The origin of these variations, according to the electrodynamical theory of Martyn will be discussed in sec. d(iv).

(ii) *Region F_2 .*—A simple evidence of the solar tidal motion in region F_2 is obtained from a study of the times at which h' (or h_{\max}) for this region reaches maximum value in course of its diurnal variation. Martyn has drawn the diurnal variation of both $h'F_2$ and $h_{\max}F_2$ for Mount Stromlo (Canberra) averaged over 4 years (1941-44). Similar curves have also been

drawn for Calcutta, Delhi and Chungking. In Fig. 2 are given curves delineating the diurnal variation of $h_{\max} F_2$ for Calcutta and Delhi, and $h'F_2$ for Chungking averaged over 3 years (1946-48). Two maxima are clearly seen, one at about midday and the other at about midnight. The midday maximum *might* be explained as a heating effect, but, it would be difficult to

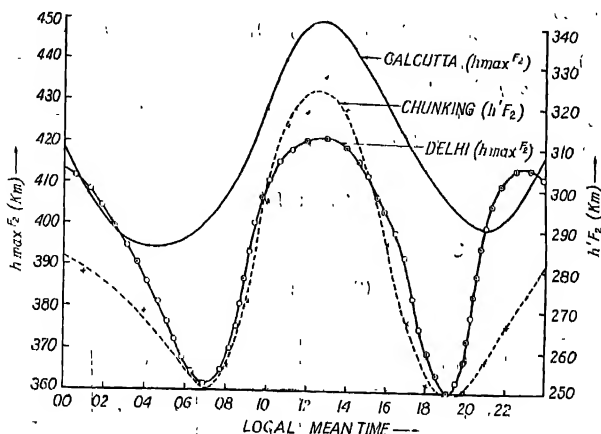


FIG. 2

Average diurnal height variation for region F_2 for Calcutta, Delhi and Chungking, 1946-48 inclusive ($h_{\max} F_2$ for Calcutta and Delhi, $h' F_2$ for Chungking)

attribute the midnight maximum to such a cause. On the assumption of a tidal motion of 12 hourly periodicity both the midday and midnight maxima are explained.

Monthly mean hourly values of $h'F_2$ for a period of 100 months (April, 1937—August, 1945) for Mount Stromlo have also been closely examined (Table IV). An average periodicity of almost exactly 12 hours in the occurrence of maxima over 100 months is found. Similar observations made at Calcutta over 36 months showed similar periodicity. An interesting point may be noted in the Fig. 3. Each maximum shows a seasonal swing, the maximum occurring about one hour before midday (and midnight) in summer and one hour after midday (and midnight) in winter. The fact that in this swing of the maxima from summer to winter a constant time-difference of 12 hours is preserved, supports the hypothesis that the variations observed are due to tidal effects.

Solar tidal effects in the variation of N^m , for Region F_2 have also been observed (Table IV). This effect, however, is generally masked by the large variation due to the ionizing action of the ultraviolet solar radiation. To

observe the effect of this tidal motion it is therefore advisable to compare the diurnal variation of N_{max} at two or more latitudes for which the ionizing term (which is proportional to $\cos^2\lambda$) varies little but for which the tidal term varies markedly. This has been done by Martyn, the three stations chosen for the purpose being Cape York (11°S), Brisbane (28°S) and Canberra A.C.T. (35°S) (all situated near longitude 140°E). Similar analysis has been made with records of Calcutta (22.5°N), Chungking (29.4°N) and Delhi (28.6°N). In Fig. 4 curve I depicts differences between corresponding mean hourly values of $f^\circ F_2$ at Calcutta and Chungking. Curve II depicts the same quantity for Calcutta and Delhi. The curves clearly show that there is a semi-diurnal variation in $\delta/f^\circ F_2$ for pairs of stations.

TABLE IV
Solar ionospheric tides—Region F,
(Semi-diurnal)

Station	$h_{max} f_2$ variation		$f^\circ F_2$ variation		Remark
	Amplitude (km)	Time of maximum after midnight (solar hours)	Amplitude (Mc/s)	Time of maximum after midnight (solar hours)	
MOUNT STROMLO (35.3°S , 149°E)	J 13.9 E 15.4 D 17.4 Mean: 15.9	J 12.5 E 11.6 D 11.5 Mean: 11.9			Average of 4 years' data (Martyn)
HUANCAYO (12°S , 75.3°W)	50		1.5		Average of 3 years' data (Martyn)
CALCUTTA (22.5°N , 88.5°E)	17.6	12.5	J 0.65 E 1.10 D 1.43 Mean: 1.06	J 10.5 E 11.5 D 14.5 Mean: 11.8	Average of 3 years' data (A.P. Mitra)
DELHI (28.5°N , 77.1°E)	13.36	13.0	J 0.45 D 0.75 Mean: 0.60		Average of 3 years' data (A.P. Mitra)
CHUNKING (29.4°N , 106.8°E)	23.47	13.0	J 0.77 D 0.74 Mean: 0.60		Average of 3 years' data (A.P. Mitra)

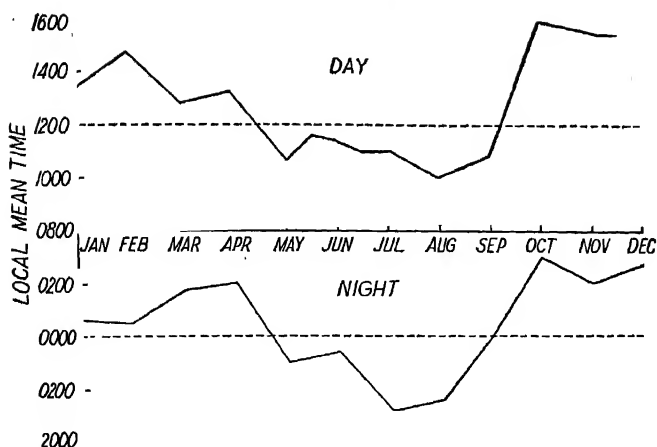


FIG. 3

Seasonal variation of the average time of occurrence of maximum $h_{\max} F_2$ at Calcutta, 1946-48 inclusive.

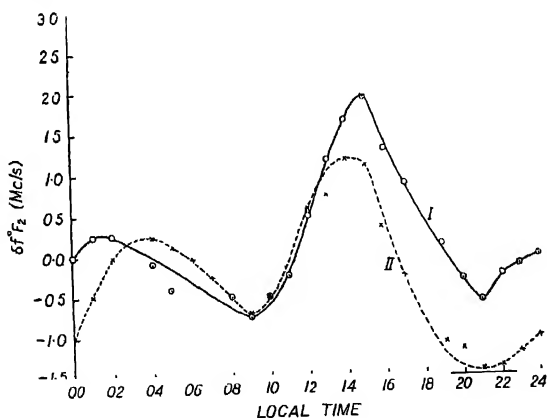


FIG. 4

Difference between average diurnal variation of $f^o F_2$ at Calcutta, Delhi and Chunking, Curve I, Calcutta-Chunking, — Curve II, Calcutta-Delhi.

ELECTRODYNAMICAL THEORY AND ITS APPLICATIONS

(i) *Introduction—Vertical ionic drift velocity.*—We now proceed to discuss after the electrodynamical theory of Martyn the tidal effects in the ionospheric regions. The main facts of the theory are as follows:

would have existed in the absence of these collisions. Now, the force F_0 itself is given by $F_0 = mvc_0$, where c_0 is the horizontal air velocity. Then the ionic velocities along the x , y , z -axes are given by

$$\dot{x}' = \frac{F_{\perp}}{mv} \cdot \frac{v^2}{v^2 + \omega^2} = c_{\perp} \frac{v^2}{v^2 + \omega^2},$$

$$\dot{y}' = -\frac{F_{\perp}}{eH} \frac{\omega^2}{v^2 + \omega^2} = -c_{\perp} \frac{v\omega}{v^2 + \omega^2},$$

$$z' = c_{\parallel},$$

where c_{\parallel} and c_{\perp} are components of c along z and x respectively, and $\omega = He/m$.

It is seen that the ionic velocities along x and z are independent of the ionic sign. Both have vertical components. When $v \ll \omega$, as in the F_2 region, the x velocity is negligible, and the vertical ionic velocity (v_1) is very nearly equal to $C_{\parallel} \sin I$, where I is the magnetic dip. v_1 is thus very nearly equal to the vertical component of the air velocity along the magnetic field.

The ionic velocity along OY depends on the ionic sign. Ions of opposite sign will move in opposite directions giving rise to an electric current and thus possibly to a polarization of the medium. The component of any resulting polarisation field perpendicular to the magnetic field (E_{\perp}) will produce ionic drift. In particular, vertical ionic drift will be produced by the component E_{\perp}' of E_{\perp} lying in the horizontal plane containing H . The magnitude of this vertical ionic drift (v_2) is, as shown by Martyn,

$$v_2 = \frac{E_{\perp}'}{H} \cdot \frac{\omega^2}{v^2 + \omega^2} \cos I$$

Further, the sense of this drift is opposite to that of the previous one.

At any latitude the total vertical ionic drift (v) is thus the sum of the two drift velocities: $v = v_1 + v_2$, v_1 being due to the vertical component of the air motion along the magnetic field and v_2 due to polarization caused by motion of the ions across the magnetic field.

Now v_1 and v_2 , as is easily seen, vary strongly with latitude. In middle latitudes the air velocity along the magnetic field has a large vertical component and v_1 has a maximum. In low latitudes, on the other hand, the magnetic field is nearly horizontal. The value of v_1 is, therefore, small. On the other hand, v_2 has its maximum at the magnetic equator, where $\cos I$ is greatest. Both v_1 and v_2 tend to zero at the poles, the former because a horizontal wind has no component along the (vertical) magnetic field, and the latter because $I = 90^\circ$.

Thus at all places, save the poles, there are vertical ionic drifts, though for causes distinctly different in high and low latitudes. And, since v_1 and v_2 are opposite in sign, the vertical drift in high latitudes will be in opposite direction to that in low latitudes. The reversal of phase occurs in an intermediate latitude where v_1 and v_2 are numerically equal. This latitude is found to be about 35° .

Another, and formally identical way of looking at the above results is to concentrate attention on the two electric fields—"the dynamo field," and the polarisation field already described. We may combine these two fields and find the vertical drift due to the combination. This is exactly equivalent to combining v_1 and v_2 , and is a very useful concept in practice. For example, from the world-wide current circuits associated with the magnetic variations the distribution of electric fields in the responsible ionospheric region is known at any time. Hence the vertical drift distribution is also known. The change of phase of the vertical drift already mentioned to occur at about latitude 35° is identical with the change of phase of the east-west current which occurs at the current foci in this latitude.

Now, the drift velocity, in general, may be expected to change with height. Due to the resulting velocity gradient the ionic concentration at a given point will change with time. Taking this "hydrodynamical continuity equation" factor into account, the equation for $\partial N/\partial t$ now becomes

$$\frac{\partial N}{\partial t} = I(z, t) - \alpha N^2 + \frac{\partial}{\partial z}(Nv) \quad \dots (1)$$

where I —rate of ion production per cm^3 ,

α —effective co-efficient of recombination

z —the reduced height (h/H_0 where h is measured from the datum level; H_0 scale height)

v —the vertical ionic velocity measured positively downwards.

Let us consider the relative importance of this new term $\frac{\partial}{\partial z}(Nv)$. For the E_1 and F_1 regions the effect of the new term is expected to be small. This is because both I and α are much larger in these regions than in region F_2 . Further, in the regions occupied by E_1 and F_1 , the vertical gradient of v may be small. In region F_2 , however, v may be expected to fall rapidly with height due to damping of a type similar to that which operates in Arago's disc (inductive drag). Hence in this region the third term might be expected to preponderate over the first two. We may expect $v = v_0 e^{-\gamma z}$, where γ is a positive constant of the order unity and the height is measured in scale height. Now, as N may also be supposed to vary exponentially with height the magnitude of the third term will be that of Nv if v is measured in units of H_0 . The ratio of the order of magnitude of the new term and the recombination term is thus $v/\alpha N$. Substituting typical values of α and N , it is found that the new term becomes important if v is of the order $10^{-4}H_0$, or 400 cm/sec. It is to be noted that the wind velocity associated with the solar tide at ionospheric levels is likely, on theoretical grounds, to be several hundred times that near ground level (which is 30 cm/sec.).

(ii) *Characteristics of the drift velocity.*—Martyn has made further detailed study of the drift velocity regarding its variation of phase and amplitude with the latitude, the hour of the day and the season of the year.

The characteristics of the vertical ionic drift velocity as obtained by him may be summarised thus:

(1) The magnitude of the drift velocity is of the same order as that of the horizontal tidal motion, being in the average about 300 cm/sec. in region F_2 .

(2) The drift velocity is periodic in time with several harmonics. The most important of these is the semi-diurnal. In region F_2 this has important seasonal variation.

(3) The drift velocity v may vary with height both in amplitude and in phase. Also, in region F_2 the drift velocity decreases with height, as already explained, and may be expressed as

$$v = v_0 e^{-\gamma z} \sin(\omega t + \sigma_z).$$

(4) The drift motion in latitudes above and below 35° are in opposite phases for the E region.

(5) The amplitude of the drift velocity v varies with latitude for both semi diurnal harmonics (seasonal and non-seasonal). The latitudinal distribution may be assumed as shown in Fig. 6.

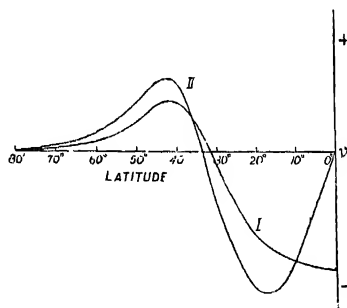


FIG. 6

Latitude distribution of vertical drift velocity (arbitrary units)
Curve I, semi-diurnal, curve II, seasonal.

(6) In the Taylor-Pckeris theory, as exemplified by Weekes and Wilkes (1947), the phase of the tidal air motion may vary greatly at different heights. According to Martyn, the phase of vertical drift in the F₂ region is as shown in Table V.

TABLE V

High latitude		Low latitude	
↑ ₃	↓ ₉	↓ ₃	↑ ₉

The arrow followed by the number is used to indicate the hour at which the drift has its maximum upwards \uparrow and maximum downward \downarrow velocity.

(7) In region F_2 there is a strong seasonal harmonic. Thus account must be taken of two semi-diurnal drifts, one of which is constant in amplitude at a given place throughout the year, while the other changes phase completely from summer to winter. According to Martyn, the first of these harmonics has the phase shown in Table VI

TABLE VI			
High latitude		Low latitude	
\uparrow_{12}	\downarrow_6	\uparrow_6	\downarrow_{12}

The second, or seasonal harmonic, has the phases given in Table VII.

TABLE VII				
	Summer		Winter	
High latitude	↑ ₃	↓ ₉	↑ ₉	↓ ₃
Low latitude	↑ ₉	↓ ₃	↑ ₃	↓ ₉

At a given location the phase and amplitude of the resultant of these two semi-diurnal harmonics are obtained by combining the latter in the proportions appropriate to the latitude, as given by (5) above

(iii) *Effects of a vertical drift on a Chapman region.*—Let us now consider an initial Chapman distribution of ionization. Let the ionizing radiation be absent (night time condition) and let the effective recombination coefficient α be small (F_2 region condition). We consider how the electron density distribution will change with height and with time, if there is a vertical drift of the ions caused by the tidal action.

The initial Chapman distribution is given by

$$N_0 = n_0 \exp \frac{1}{2} (1 - z - \sec \chi e^{-z}) \quad (2)$$

Since only the effect of the vertical drift is present, the equation for N is simply the hydrodynamical "continuity equation"

$$\frac{\partial N}{\partial t} = \frac{\partial}{\partial z} (Nv) \quad (3)$$

Putting $v = v_0 e^{-z}$ (vide *supra*) and using (2) and (3) and integrating we obtain

$$N = n_0 \eta^{-(2\gamma+1)/\gamma} e^{\frac{1}{2}(1-z)} \exp \left(-\frac{1}{2} \sec \chi \eta^{-1/\gamma} e^{-z} \right)$$

where

$$\eta = (1 + \gamma v_0 t e^{-\gamma z})$$

A maximum in N occurs at the height z_m given by

$$\sec X e^{-z_m \eta_m} - \frac{\gamma + 1}{\gamma} - \frac{2\gamma + 1}{\eta_m} + 2\gamma = 0$$

The effect of the vertical drift velocity on the Chapman region may now be deduced from the above relation. They may be summarised qualitatively as follows:

(1) The region moves in the direction of the ionic drift—upwards when the drift is upwards and downwards when the drift is downwards

There is exception to this rule only when the amplitudes or the phases of the drift velocity change very rapidly with height.

(The above rule, of course, applies only when α and I_0 are negligible, otherwise, the velocity of movement of the region may lead the drift velocity by 2 or 3 hours.)

An interesting case arises when in a Chapman region the gradient of the drift velocity is steep in the top portion of the region but is small in the bottom portion. In such case, the top part of Chapman region is subject to the exceptional case of rule (1). If there is appreciable drift, the top portion of the region moves upwards strongly no matter in what direction the drift flows—downwards or upwards. The bottom portion also moves, upwards for upwards drift velocity and downwards for downwards drift velocity, but this motion is small compared to the upward motion of the top part. As a result of this drift motion the original single Chapman region is bifurcated into two ionized regions. However, if the drift velocity is small then the separation takes place only if the drift velocity is downwards. This is because for small drift motion the top region (γ large) moves oppositely to the drift, while the lower region (γ small) moves with the drift. Thus under the influence of upward drift both regions merge together.

(2) N_0 (i.e. the maximum ion density of the undisturbed Chapman region) decreases when the drift velocity is downward and increases when it is upwards. The variation in N_{\max} (i.e. the maximum ion density which results from the action of the drift) is proportional to the height gradient of v .

(iv) *Interpretation of the ionospheric tidal effects.—Regions E and F₁.*—For these two regions Eqn. (1) must be solved with all the three terms in the right hand. The solution is necessarily complicated, but has been made by Kirkpatrick (1948), taking the following numerical values of the parameters:

$$\sigma = 4^\circ, \alpha = 10^{-8} \text{ cm}^2/\text{sec}, H = 11 \text{ km}, \omega = 30^\circ/\text{hr}, \\ v_0 = 22.5 \text{ Km/hr}, N_m = 1.5 \times 10^5/\text{cm}^3.$$

These are sufficiently representative of conditions in region E at the equator during the equinoctial periods.

According to Kirkpatrick's calculations, the departure from Chapman value for region E is ± 2 percent for N_{\max} , and 2.5 km. for $\delta h'$. This may be compared with ± 4 km., the observed deviation in h' for region F₁, as mentioned earlier. The value is somewhat higher than the calculated value of ± 2 km, but it is to be remembered that in region F₁ the recombination rate is lower than in region E.

The reversal in the sense of the deviation from the Chapman curve as one passes from Watheroo to Washington is explained by the fact that the current focus passes along a latitude between Washington and equator. Indeed, this latter fact may be adduced as a strong argument in favour of the interpretation of the observed $h'F_1$ anomalies as due to vertical drift associated with the "dynamo" electric forces produced by the solar tide. It also follows from this interpretation that the currents in region F₁ are very nearly in phase with currents caused by the solar diurnal magnetic variation.

The electrodynamical theory also explains the observed difference in phase in the lunar tidal variations of $h'E$ between high and low latitudes. As will be noticed from Table I at Slough (high latitude) the maximum value of $h'E$ is reached $\frac{3}{2}$ hour before the lunar transit and at Canberra and Brisbane (low latitude) this is reached 5.1 and 4.5 lunar hours respectively after lunar transit. This is due simply to the change in phase of the vertical drift velocity (as explained in Sec. d (i)) as one passes from low latitude to high latitude.

Region F.—As explained earlier, for region F₂ the first and second terms in the right of Eqn. (1) are relatively unimportant. This is also corroborated by observations during solar eclipses. During eclipse, N_{\max} in region F₂, unlike that in region E and F₁, is practically unaffected, though I has decreased considerably. This shows that both the rate of ion production term and the recombination term have small values. The F₂ region may thus be assumed, to a first approximation, to behave as a Chapman region which is being acted upon mainly by vertical ionic drift. This case has been discussed in Sec. d (iii), where it has been shown that the variation caused by the drift in such a region bears little or no resemblance to the Chapman variation. In fact, the observed diurnal and seasonal variations of N_{\max} and h_{\max} are profoundly influenced by the effects of the periodic variations of the drift velocity.

Let us consider the case of F₂ ionization for a typical high latitude station. Here, in summer the daytime value of N_{\max} is low but the

corresponding value of h_{\max} is high. There is also marked afternoon increase in ionization. In winter the daytime value of N_{\max} is large and h_{\max} increases from morning to noon. These effects are explained by the electrodynamical theory as follows: From Tables VI and VII it is seen that in summer, in the morning hours the drift velocity is downwards, the seasonal harmonic being somewhat larger than the other (Fig. 6). For such condition the overall N_{\max} is reduced considerably below the Chapman value and h_{\max} rises. (The relevant important cause of reduced N_{\max} is the flow of electrons downward to regions of comparatively high recombination coefficient, where a large number of electrons are lost). In the afternoon, the drift is upwards. This preserves the ionization and leads to increased concentration in the early evening as observed. In winter the phase of the tidal drift, as seen from Table VII, is upwards from 6 hours. N_{\max} approximates to, or may even rise above, the Chapman value, but h_{\max} rises little.

For a low latitude station in summer the average N_{\max} is slightly higher than the winter value. Also h_{\max} rises steadily in the morning both in summer and in winter. At some stations there is a night maximum in N_{\max} in summer. From Table VI we notice that in summer v is directed upwards in the morning hours. The general level of N_{\max} is maintained near the Chapman value, with some increase in height. From 12 to 18 hours the drift is downwards and N_{\max} and h_{\max} fall. From 18 to 24 hours there may occur a further concentration leading to abnormally high N_{\max} . After midnight the ionization may decrease markedly till dawn.

In winter, at low latitudes, the drift is downwards in the morning, and low average values of ionization might be expected, as for the corresponding case in high latitudes. This does not happen. It is recalled that in winter there is a phase reversal somewhere between the F_1 and F_2 layers (compare Tables V and VII). At the level of reversal, the amplitude of v must be small. Thus during the morning hours before noon, the tidal drift, though downwards, has a small and decreasing amplitude. This is not so effective in removing the undersurface (and maximum) of the region as the corresponding drift in high latitudes in summer, which sweeps downwards through both regions unchecked.

Martyn's tidal theory also explains the bifurcation of the F-layer into two separate layers F_1 and F_2 at daytime. The main facts of bifurcation are as follows: In summer the bifurcation is prominent in all latitudes. In winter it is much less marked, being practically non-existent in high latitudes, and only little in low latitudes. As already explained, a single Chapman region may, under certain condition, be bifurcated into two regions as a result of the drift velocity. This condition, namely, a steep velocity gradient in the upper part of the Chapman region (or a steep gradient of recombination coefficient, which has the same effect) obtains in the single F layer in the morning. The observed bifurcation may then be understood

as follows: In summer, at low latitudes, the F_2 region must move up and separate itself from F_1 ; at high latitudes bifurcation occurs for the reason mentioned in (iii *supra*). In winter, at low latitudes, the small downward drift soon after sunrise may cause a small bifurcation. At high latitudes, however, the small upward drift in winter tends to merge the regions together (iii *supra*). At these latitudes, instead of bifurcation, the whole F layer is slowly lifted from the sink without any separation between the two regions.

From the brief account of the electrodynamical theory given above it is clear that the theory is a definite step forward in our understanding of tidal phenomena and anomalous variations in the ionosphere. The theory, however, is still in the formative stage. Much more work, both observational and theoretical, has to be done, to fill the many gaps that still exist.

ACKNOWLEDGMENTS

It is a pleasure to record my thanks to Dr. D.F. Martyn, F.R.S., for his taking trouble in going through the manuscript and making valuable suggestions for improving it. Thanks are also due to the Council of Scientific and Industrial Research, Government of India, for financial assistance.

The author is indebted to Professor S.K. Mitra, D.Sc., F.N.I., for giving him permission to work in his laboratory and for his helpful interest in the work.

INSTITUTE OF RADIO PHYSICS AND ELECTRONICS,
UNIVERSITY COLLEGE OF SCIENCE,
CALCUTTA

REFERENCES

- Appleton, E.V and Weekes, K., 1939, *Proc. Roy. Soc. A.*, **171**, 171
 Burkard, O., 1948, *Terr. Magn. Atmos. Elec.*, **53**, 273
 Kirkpatrick, C. B., 1948, *Aust. J. Sci. Res. A.*, **1**, 423.
 Martyn, D. F., 1947 a, *Proc. Roy. Soc. A.*, **189**, 241
 Martyn, D. F., 1947 b, *Proc. Roy. Soc. A.*, **190**, 273.
 Martyn, D. F., 1948, *Proc. Roy. Soc. A.*, **194**, 429, and 445
 Martyn, D. F., 1949, *Nature*, **163**, 34.
 Weeks, K and Wilkes, M. V., 1947, *Proc. Roy. Soc. A.*, **192**, 80

ON THE STRUCTURE OF SODA CELLULOSE FROM RAW JUTE FIBRE*

By N. N. SAHA AND MRS. USHA SAHA

(Received for Publication, July 28, 1950)

Plate XV

ABSTRACT. Raw jute fibres were treated with NaOH solutions of different strengths and each of the products thus obtained was washed separately with absolute alcohol and water. These products were analysed by taking X-ray diffraction photographs as well as by chemical method. It has been found in the present investigation that the soda cellulose from jute fibre has the same structure for all the concentrations of the reacting NaOH solution up to about 45%. The structure of this soda cellulose is different from that of soda cellulose I and soda cellulose II obtained from ramie by Hess and Trogus. Thus in the case of raw jute fibre only one type of soda cellulose is formed.

It is further shown that in the hydrated cellulose obtained from raw jute fibre there is hardly any trace of native cellulose.

INTRODUCTION

The absorption of alkalis by cellulose fibre is one of the most important reactions of cellulose and has been the subject of investigation by various workers for a long time, but the mechanism of this reaction is still a disputed matter. In most of these investigations cotton and ramie fibres, containing about 98% of cellulose and small percentage of lignin, were used as the source of cellulose.

The presence of lignin, as shown by Sirkar and Saha, (1947) and Saha (1947 and 1948) in their investigations with raw jute fibre, has great influence on the final product obtained by mercerisation, acetylation, nitration, etc. It is, however, expected that the nature of reaction between caustic soda solution and jute fibres containing about 12 % of lignin and its influence on mercerisation may be different from that observed in case of cotton and ramie.

The nature of this reaction was investigated by Gladstone (1853) in the case of cotton by determining the amount of caustic soda in the product obtained by treating cotton with NaOH solution of different strengths and washing the product with absolute alcohol. Similar investigations in the case of raw jute fibre had not been carried out by previous workers. Further, the X-ray examination of the products obtained after controlled washing with absolute alcohol of soda cellulose prepared from jute fibre may reveal the structure of the product obtained with NaOH solution of different strengths

Communicated by Prof. S. C. Sirkar

and the results may throw some light on the actual mechanism of the formation of soda cellulose and of mercerisation. With these objects in view the present investigation was undertaken.

EXPERIMENTAL

(a) Chemical treatment

Raw jute fibres, cut to small lengths, were boiled in water to make the fibres free from adhering impurities. These fibres, after being dried, were made into small bunches and weighed. The bunches were then treated with equal volumes of NaOH solutions of different concentrations for about ten minutes. Some of these bunches after treatment were thoroughly washed with water and the rest with absolute alcohol until the wash-liquid gave no test for alkali. To determine the end of the washing operation Wesselow's mixed indicator was used. All the samples were then dried and weighed.

The amount of alkali taken up by the fibres was determined in the case of samples washed with absolute alcohol. These samples were dipped in measured quantities of water over and over again until the total alkali taken up by cellulose was brought into solution. The end of this operation was also determined as before. The amount of NaOH in the resulting solution was then determined by titration, using Wesselow's indicator which was found to be more sensitive than phenolphthalein used by earlier workers.

(b) X-ray analysis of the products

X-ray diffraction patterns of the product obtained by treating raw jute fibre with 5%, 10%, 20%, 30% and 45% NaOH solutions in a closed vessel, washing the treated fibres in absolute alcohol and drying them in air were then photographed. Similar photographs due to products washed with water were also taken in the same camera making all the strands parallel and holding them taut during the exposure. The photographs were taken with a camera having a very fine slit, using unfiltered $\text{CuK}\alpha$ radiation from a rotating-target 3 KW X-ray tube*.

RESULTS AND DISCUSSION

The data for the amount of NaOH absorbed per 100 gm. of cellulose and moles of NaOH absorbed per base mole of cellulose ($\text{C}_6\text{H}_{10}\text{O}_5$) for different concentrations of NaOH solution are given in columns 1 and 2 respectively in Table I. The results are represented graphically in Fig. 1. The X-ray diffraction photographs of the samples washed with water as well as with absolute alcohol were analysed and the spacings of the (101) and (002) planes obtained in these cases are given in columns IV and V of Table I. Some of the photographs are reproduced in Plate XV.

* The tube was constructed and set up by Mr. S. K. Chowdhury under the guidance of Prof. S. C. Birkar.



Fig. 2

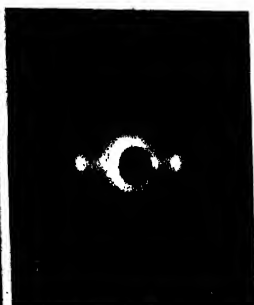


Fig. 3

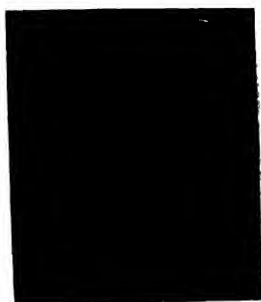


Fig. 4

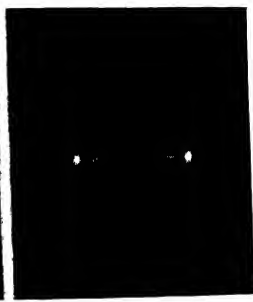


Fig. 5

Fig. 2. Soda cellulose, 30% NaOH solution.

Fig. 3. " " 45% " "

Fig. 4. Hydrated cellulose from raw jute.

Fig. 5. Raw jute.

TABLE I

Strength of NaOH in normality	gms. of NaOH per 100 gms. of cellulose	Moles of NaOH per base mole of cellulose ($C_6H_{10}O_5$)	Product washed with water d_{101}	Product washed with alcohol d_{002}
1.11	2.792	112	Same as in native	Same as in native
2.29	4.95	200	"	"
3.53	5.867	237	Partial conversion	Partial conversion
4.82	6.015	245	7.96 Å	8.2 Å
8.02	6.48	.262	7.96 Å	8.2 Å
12.8	6.7	.260	7.96 Å	8.2 Å

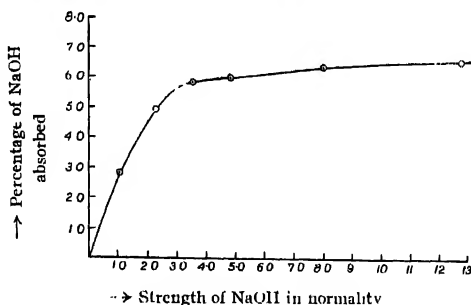


FIG. 1

It can be seen from Table I and the curve given in Fig. 1 that the absorption of caustic soda by cellulose in jute fibre increases steadily up to the strength of about 15% (3.53N) and over the range from 15% to about 20% (5N) the absorption remains nearly constant. Beyond this range it increases very slowly as the concentration of NaOH solution is increased. The break in the absorption curve at a concentration of about 15% indicates the formation of a compound. Calculation shows that in case of jute fibre a compound of molecular ratio $(C_6H_{10}O_5)_1 NaOH$ is formed, whereas in case of cotton it was shown by Champetier (1933) that compounds like $(C_6H_{10}O_5)_2 NaOH$, and $(C_6H_{10}O_5)_3 NaOH$, are formed, depending on the strength of the reacting alkali solution used. The reason for the formation of a compound containing lower proportions of NaOH in the case of jute fibre seems to be the presence of lignin which apparently impedes the penetration of NaOH solution into the micelles.

It is well known that the process of mercerisation with NaOH solution takes place in two steps in the case of cotton and ramie fibres. First, soda cellulose is formed. The structure of this product known as soda cellulose I obtained with NaOH solutions of strength below 21% is different from that of the product (soda cellulose II) obtained with more concentrated solutions as shown by Hess and Trogus (1930). Secondly, on washing these soda celluloses with water, mercerised cellulose having a definite structures different from that of soda cellulose is obtained. It can be seen from Table I that the soda cellulose obtained from raw jute fibre has the same structure for all concentrations of the reacting NaOH solution up to 45%. The structure of soda cellulose obtained from raw jute fibre is, however, found to be different from that of either soda cellulose I or soda cellulose II obtained by Hess and Trogus (1930) from cotton. The spacings observed in the two cases are given in Table II. The spacings given in last column of Table II are those obtained by calculating them from the pattern due to soda cellulose I reproduced by Hess and Trogus.

TABLE II

Equatorial reflection.	hkl	Spacing in Å Soda cellulose from raw jute (Present author)	Spacings in Å. Soda cellulose I (Hess and Trogus)
A_1	101	8.2	12.66
A_2	101	4.64	4.6
A_3	001	4.40	4.3

It thus appears from Tables I and II that in the case of raw jute fibre the presence of lignin prevents the NaOH solution from penetrating completely inside the micelles and forming compounds of type $(C_6H_{10}O)_2 NaOH$ and consequently, the micelles are distended and distorted less than in the case of soda cellulose from cotton. The spacing of (101) plane in the latter case is about one and half times that in the former case. The whole process of mercerisation of these fibres is thus the distortion of the micelles caused by penetration of NaOH inside the micelle and retention partially of the distorted structure even after washing away of the absorbed NaOH with water, and this mercerised jute has been called hydrated cellulose from jute.

It was previously pointed out by Sirkar and Saha (1947) that ageing for three months does not alter the structure of hydrated cellulose obtained by treating raw jute fibre with 30% of NaOH solution, washing the product in water and drying it in air. Mukherjee and Woods (1950) have, however, recently reported that although conversion of jute fibre into soda-cellulose is cent per cent, the hydrated cellulose obtained by washing the soda cellulose in water and drying it in free air is not quite stable, as part of it is reconverted into native cellulose. As this is contradictory to the fact reported by Sirkar and Saha (1947) that the structure of hydrated cellulose obtained from jute

fibre is a stable one, the question has been reinvestigated. The intensity of the reflections from (101) and $(10\bar{1})$ planes of native cellulose has been taken as the measure of the proportion of the native cellulose present in the hydrated cellulose for this purpose, because these spacings in native cellulose are quite different from those in hydrated cellulose.

In figure 4 of Plate XV the pattern due to hydrated cellulose from jute fibre obtained with 30% NaOH solution is reproduced, and figure 5 shows the pattern due to raw jute fibre taken with the same camera. It can be seen from a comparison of these two figures that the intensity in the position of the (101) and $(10\bar{1})$ reflections from native cellulose in the pattern due to hydrated cellulose shown in figure 4 is negligible. Hence it has to be concluded that if there is any reconversion of hydrated cellulose from jute fibre to native cellulose the proportion of such reconversion is negligible in comparison with the stable portion.

ACKNOWLEDGMENTS

The work was carried out under a scheme formulated by Prof. M. N. Saha, F.R.S., and financed by the Indian Central Jute Committee. The authors are indebted to Prof. M. N. Saha, F.R.S., for his kind interest in the work, to Prof. S. C. Sirkar, D.Sc., F.N.I., for helpful suggestions during the progress of the work and to the Indian Central Jute Committee for the financial help.

UNIVERSITY COLLEGE OF SCIENCE,
92, UPPER CIRCULAR ROAD,
CALCUTTA

REFERENCES

- Champetier, G., 1933, *Ann. Chem.*, **20**, 5
 Gladstone, J., 1853, *Trans. Chem. Soc.*, **5**, 17
 Hees and Trognus, 1930, *Z. f. Physik. Chem. B.*, **11**, 381
 Mukherjee, R. R. and Woods, H. J., 1950, *Nature*, **165**, 818.
 Saha, N. N., 1947, *Proc. Nat. Inst. Sc. India*, **13**, 339
 " " 1948, *Ind. J. Phys.*, **22**, 245.
 Sirkar, S. C. and Saha, N. N., 1947, *Proc. Nat. Inst. Sc. India*, **13**, 1

A SPEED LIMIT FOR ROCKETS ?

By WILLIAM SQUIRE

(Received for publication, July 31, 1950)

ABSTRACT. Some fallacies in the arguments put forward in the paper "Plausible Speed Limit for Metallic Projectiles" by Dixit, are pointed out

In a recent paper, Dixit (1949) attempts to prove that a powered metallic projectile travelling in space cannot attain the velocity of escape from the earth's gravitational field because:

1. Radiation is insufficient to dissipate the heat generated by the power plant.
2. Velocities greater than that of sound in the metal will adversely affect the structure of the metal.

The first argument, although plausible, is incorrect because it does not consider that the original system consists of the projectile plus several times its mass of fuel. Most of the heat is carried off by the exhaust gas. This is clearly seen if a rocket motor with regenerative cooling (Zucrow, 1948), i.e., one where the fuel is heated to the boiling point by being used as a coolant, is considered. Except for the combustion chamber, no part of the projectile is exposed to the temperatures above the boiling point of the fuel. If the projectile is initially at a higher temperature above the boiling point of the fuel and the combustion chamber discarded at the end of combustion it is possible for the projectile to lose heat. Therefore the "efficiency" criterion

$$\frac{\text{Kinetic energy imparted to projectile}}{\text{Kinetic energy + heat imparted to projectile}}$$

could exceed unity, showing that it is not a suitable criterion.

The second argument seems to contradict the special theory of relativity. If, as is claimed, "At velocities greater than the sound velocity in a solid we can expect the characteristic frequencies, the Debye characteristic temperature and the melting point to be altered," could not an observer in the rocket travelling in space at a uniform velocity determine his "absolute" velocity by measuring these properties?

CORNELL AERONAUTICAL LABORATORY, INC N Y.

REFERENCES

- Dixit, K R, 1949, *Ind. Jour. of Phys.*, 23, 469-76.
Zucrow, M J, 1948, *Principles of Jet Propulsion*, Chapter 12, John Wiley, New York.

A TIME BASE CIRCUIT FOR A HIGH PRECISION IONOSPHERIC SOUNDING APPARATUS

By B. M. BANERJEE AND R. ROY

(Received for publication, Aug. 5, 1950)

Plates XVI A and B.

ABSTRACT. The paper describes a high precision timebase circuit designed specifically for an ionospheric sounding apparatus. This time-base circuit produces a ten-line raster time-base on the face of the oscilloscope tube. Each line of the raster takes 33.3 micro-seconds which corresponds to 50 kms of ionospheric height. This gives a reading accuracy of about $1/4$ km. The time base also provides for 15 kc/s positive and negative marker pips which mark off 5 km intervals. It also provides for an intensifying pulse on the grid of the cathode ray tube over the 33.3 microseconds interval corresponding to any one of the ten lines selected out by an ingenious line-selector arrangement.

INTRODUCTION

The usual method of investigating the ionosphere consists of sending a series of short pulses from a pulse transmitter, receiving the "reflected" echoes from the ionospheric layers in a receiver, and displaying them on an oscilloscope. The time base of the oscilloscope produces a sweep of the cathode ray beam from left to right. The transmitted pulse and the ionosphere-echo produce momentary vertical displacements of the oscilloscope spot as the output of the receiver is connected to the vertical deflecting plates of the oscilloscope. The sweep length between the transmitted pulse and the ionosphere echo represents the delay between the transmitted and the reflected pulse which again represents the height of the ionised layers. This delay or equivalent height may be calculated from the sweep length between the pulses and the sweep velocity of the time base. The sweep circuit is highly important in as much as the accuracy of these height measurements depends wholly on it. This paper describes a time base which gives an accuracy much higher than hitherto obtainable.

REQUIREMENTS OF A HIGH PRECISION IONOSPHERIC SOUNDING TIME BASE

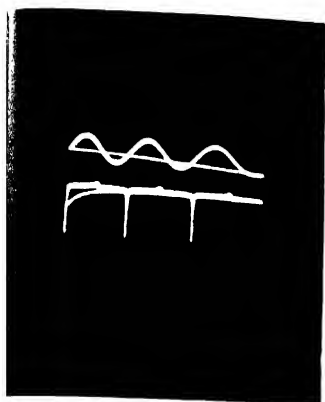
The ionised regions from which reflections are obtained extend up to a height of 400 kilometers and the sounding apparatus should be designed such that it is capable of measuring a maximum height of 500 kilometers. A height of 500 kms corresponds to a total time delay of 3.33 milliseconds. A

single-line time base cannot usually measure times with an accuracy better than half per cent of 3.33 milliseconds, *i. e.*, 16 microseconds. This time corresponds to a height of 2.5 kms.

Increased accuracy may be obtained by a raster time base—one that gives a succession of lines up and down over the tube face. The cathode ray beam in such a time base will move from left to right at a high speed, and after it goes to the extreme right hand position, jumps back to the left within a short time and again moves from left to right. At the same time, as it moves from left to right, it also moves upwards at a slower rate so that when it jumps back after the completion of the first line, the spot does not come over the first position, but is shifted slightly upwards. The second line is therefore separated from the first, and the third line from the second and so on. If there are n lines in the raster, we get the length of the sweep virtually increased n times, which means that the resolution is increased n times.

The object of this paper is to describe a time base, designed specifically to suit the requirements of ionospheric sounding. It produces a raster of ten lines, each of 333 microseconds duration. Each line therefore corresponds to a height of 50 kilometers. Thus a total height of 500 kilometers is scanned. After scanning 500 kilometers, the light spot moves out and remains steady outside the pattern until the repetition period is over. The repetition frequency chosen for the present is 150 c.p.s., so the repetition time is 6.66 milliseconds. The second reflection from the F_2 layer will come at a time delay between 3.3 and 6.6 milliseconds and will therefore appear at the steady position of the spot. It may be inspected at that position, if necessary. The third and fourth reflection will come with a delay between 6.6 and 9.9 milliseconds and may cause confusion, superposing itself on the next raster. But it is presumed that its amplitude will by that time become sufficiently small to make it indistinguishable. If necessary, the repetition frequency may be reduced to 100 c.p.s. or 50 c. p. s. when the confusion with the higher order reflections will be avoided altogether. The high repetition frequency is chosen chiefly to compensate for the loss of brilliance of the oscillograph trace due to the fast sweeps.

The ten line raster, on a double beam tube occupies practically the whole space on the face of the tube. The spacing between the lines is therefore quite small. As a result, if the pulse echoes are big enough, they may cut through the lines making it difficult to recognize as to which line they actually belong. To obviate this difficulty, a device has been provided by which any one of the desired lines may be selected and intensified. In this condition of operation, other lines are blanked out and the desired line is intensified by a positive pulse on the grid of the oscilloscope tube over the 333 microseconds interval covered by that line.



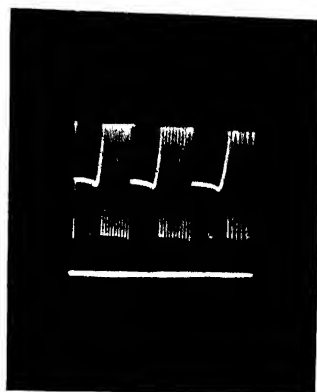
(a)



(b)



(c)



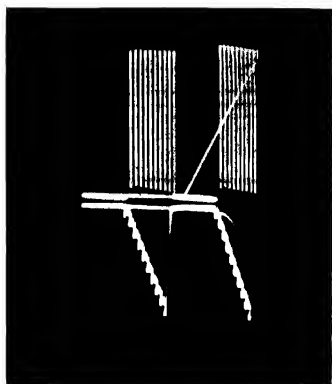
(d)

(a) Top—150 c p s. sine wave. Bottom—Positive spikes generated from it

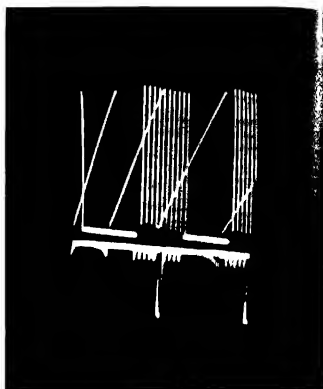
(b) Top—Output of the cathode-coupled multivibrator Bottom—Sweep waveform from the boot-strap vertical time base

(c) Saw tooth waveform obtained with the aid of vertical deflection coils

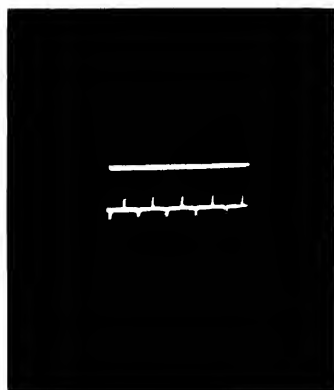
(d) Shock-excited 3000 c p s. sinusoidal oscillations.



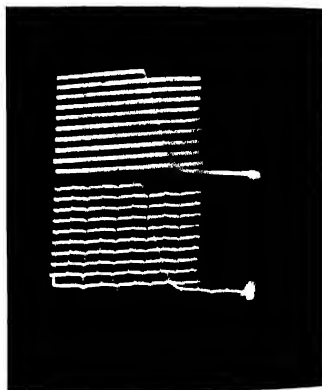
(e)



(f)



(g)



(h)

(e) Time base sweeps. Top—Horizontal Bottom—Vertical

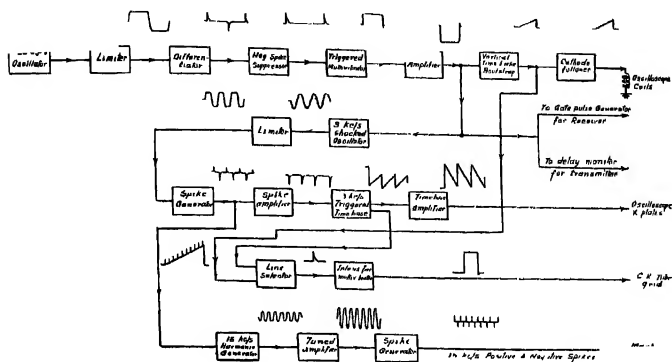
(f) Action of line selector and intensifier. Top—Sawtooth wave-form of the horizontal time base
Bottom—Line selector selects and intensifier gives the positive pulse at the fifth line of the horizontal time base

(g) Single line selected and intensified. Markers on one beam of the C.R. tube.

(h) 10 line raster time base with markers on one beam of the C.R. tube

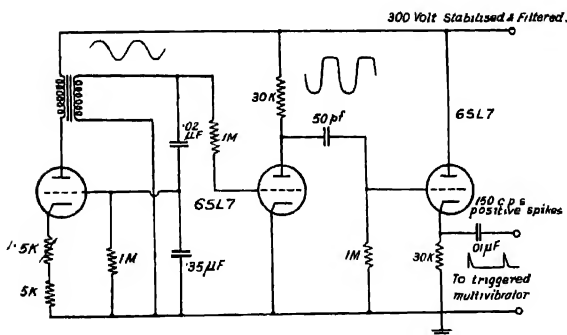
DETAILS OF THE CIRCUIT

The scheme for the time base may be understood from the block diagram given in Fig. 1. It starts with a sine wave oscillator (Fig. 2)



Block diagram of timer

FIG. 1



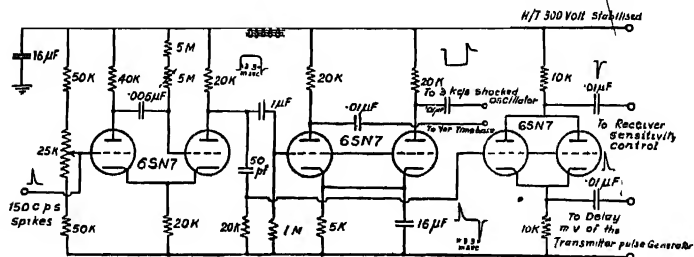
Repetition frequency generator 150 c.p.s. sine-wave oscillator, limiting amplifier, spike generator, negative-spike-suppressor.

FIG. 2

which generates a very pure sine wave at 150 c. p. s. It applies a 200 volt, 150 c. p. s. A. C. to the high μ triode (6SL7) limiter grid through one-megohm series resistance. The limiter clips off this sine wave and produces an almost rectangular wave at its anode, about 200 volts peak amplitude. This is applied to the 50 pf., 1 megohm differentiating or spike generator circuit. The spikes are applied

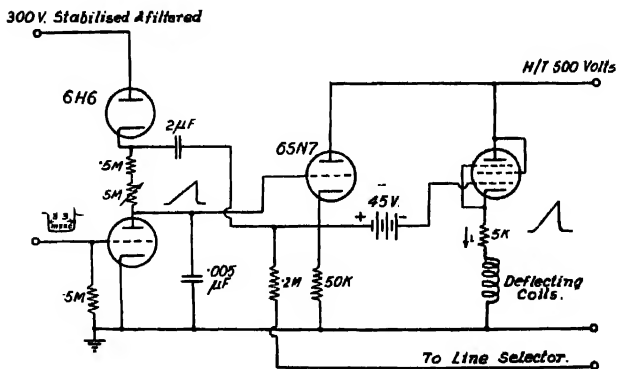
to a high μ triode (6SL7) cathode follower. This allows only the positive spikes to pass through. The negative spikes cannot produce a voltage change greater than four or five volts

The positive spikes of about 50 microseconds duration and 40-50 volts amplitude are applied to the trigger grid of a one-kick cathode-coupled multivibrator (Fig. 3) which generates a 100 volt positive rectangular output pulse of 3.3 milliseconds duration. A 6SN7 amplifier inverts this wave into a negative rectangular pulse of 180, 200 volts peak amplitude and 3.3 milliseconds duration. This cuts off the current in the 6SN7 time base generator (Fig. 4). The current coming from the 300 volt stabilised supply, through the one megohm charging resistance charges the .005 mfd. time base condenser. The condenser voltage goes on increasing linearly with time. The cathode voltage of cathode follower 6SN7 also goes on increasing with time. This voltage is reappplied to the other end of the one megohm charging resistance through the 2 mfd coupling condenser. The 6H6 diode



Triggered multivibrator and amplifier.

FIG. 3



150 c. p. s. boot-strap vertical deflection time base

FIG. 4

presents a very high impedance at its cathode voltage increases above the H. T. supply voltage, due to the application of the cathode follower output

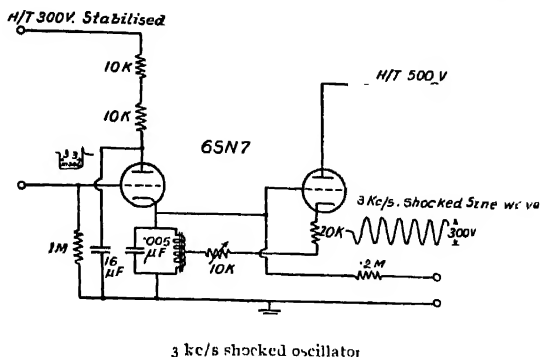
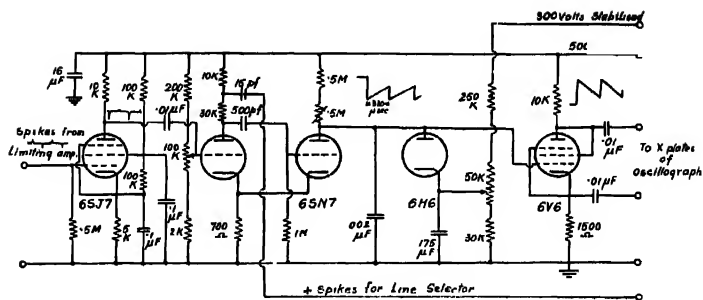


FIG. 5

to its cathode during the charging stroke. As a result of this connection, in spite of the increase in voltage of the time base condenser, the voltage across the one-megohm charging resistance remains practically undiminished, and so also the charging current. Thus we get an almost linear rise of voltage with time. The cathode follower 6V6 tube delivers the current necessary for the vertical deflection coil. The vertical sweep of 3.3 milliseconds is therefore established.

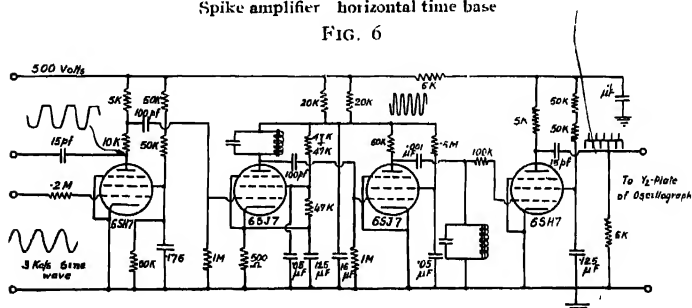
The 180-volt, 3.3 milliseconds negative rectangular pulse from the amplifier also excites the 3000 c.p.s. shocked oscillator (Fig. 5). The abrupt stopping of current in the 6SN7 excites an oscillation of 150 volts peak amplitude in the cathode LC circuit. This 3000 c.p.s. oscillation is the frequency or time standard of the whole time base. The small natural damping ($Q=70$) of this circuit is compensated exactly by the right hand section of the 6SN7 giving positive feed back controlled by the 10 kilo-ohm potentiometer. The natural damping of this shocked oscillation is exactly compensated by adjustment of this potentiometer, while viewing the shocked oscillation on the oscilloscope. Ten complete periods of 3000 c.p.s. oscillation take place in 3.33 milliseconds.

The 150-volt peak 3000 c.p.s. oscillation is again applied through a 0.2 megohm series resistance to the 6SN7 limiter grid (Fig. 7). At its anode we get a 3000 c.p.s. rectangular wave of about 150 volts amplitude. The spike generator circuit applies positive and negative spikes of 40-50 volts to the grid of the 6SJ7 spike amplifier (Fig. 6), normally biased to cut off. The positive spikes get through this amplifier as negative pulses of 50-80 volts amplitude and 7 microseconds duration. This gets on to the grid of the 3000 c.p.s. horizontal time base.



Spike amplifier horizontal time base

FIG. 6

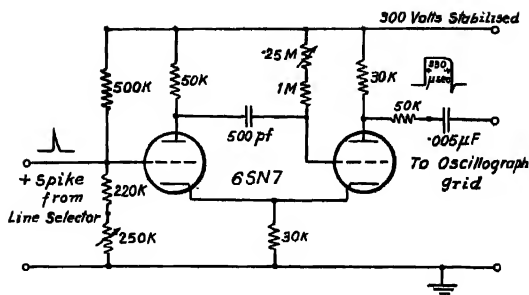


3000 cps limiting amplifier 15 kc/s harmonic generator, limiter
and 15 kc/s marker generator

FIG. 7

The first negative pulse discharges the 0.02 mfd. time base condenser from the voltage set by the clamping diode to a small value. When the discharge is complete, the condenser charges through the one-megohm charging resistance—from the 500 volts positive line. The condenser voltage rises exponentially until the second negative pulse again discharges it. The ten pulses produce the ten discharges and following the discharge ten charging strokes. The exponential rise is amplified by the 6V6 amplifier. The natural curvature of the 6V6 characteristic compensates for the exponential curvature so that we get practically a linear sweep. After the tenth pulse and tenth discharge the condenser voltage rises and is clamped by conduction in the 6H6 diode, to its cathode voltage set to between 50-100 volts.

The positive and negative spikes from the 3000 c. p. s. spike generator excite the 15 kc/s harmonic generator tuned by a 15 kc/s LC circuit whose Q value is 30 (Fig 7). This is further amplified by the 15 kc/s tuned amplifier feeding about 60 volts to the 15 kc/s limiter through a 100, 0.00 ohm series resistance. The 15 kc/s rectangular wave at the anode of the



Intensifier multivibrator

FIG. 9

of this positive unblanking rectangular pulse may be adjusted to 333 microseconds by the $1/4$ megohm variable grid resistance.

CONCLUDING REMARKS

The merits and drawbacks of the time base described in this paper may be judged best if this time base is compared with typical and representative timing circuits that have been developed for radar ranging in the last war. This arrangement allows for a precision which outmatches all radars excepting those meant for precision long-range gunfire control. The possible reading error in this arrangement is of the order of one in two thousand at maximum range. This compares favourably with the best of gunfire control radars—such as the SCR-584. The weak spot of the circuit described in this paper is the determination of the timing by an *LC* circuit in comparison with the highly stable crystal control timing of the SCR-584. The crystal control timing of the SCR-584 gives better accuracy in absolute measurements. As regards comparison of ranges, this circuit is as good as the SCR-584 circuit. When measurements are made in terms of potentiometer settings of delay multivibrators, the accuracy obtained cannot be superior to that obtained in the circuit described in this paper.

It is not convenient or even practical to copy the SCR-584 scheme in developing a time base for a high precision ionosphere sounding apparatus. Besides requiring two type J oscilloscopes, it will need a greater number of frequency dividing multivibrators to obtain the very low repetition frequencies needed for the ionosphere apparatus. The arrangement we have made satisfies the requirements of ionosphere sounding more easily than a copy of any of the timing system developed for radar work.

This paper is the first publication of the research activities in a scheme for developing improved ionospheric sounding apparatus entitled "A New Technique of Investigating the Ionosphere".

ACKNOWLEDGMENTS

The authors are grateful to the Council of Scientific and Industrial Research for financing the aforesaid scheme. The authors are also grateful to Professor S. K. Mitra, D.Sc., M.B.E., the then Chairman of the Radio Research Committee, for his kind support and continued interest. Finally the authors are indebted to Professor M. N. Saha, D.Sc., F.R.S., but for whose personal interest and encouragement the scheme would never have been undertaken. They are also indebted to Mr. B. K. Banerjee, for suggesting the proposed "New Technique" of Ionosphere Sounding.

INSTITUTE OF NUCLEAR PHYSICS
CALCUTTA UNIVERSITY

REFERENCE

D. G. Fink, (1947), "Radar Engineering", McGraw Hill Book Co. New York, N. Y.

REVIEW

Principles of a New Energy Mechanics.—By J. Mandelker. Publisher : Philosophical Library, New York. pp. viii + 73, price dollar 3.75

The new mechanics starts essentially from the same basic relation as that of the special theory of relativity. The postulate involved is that the quadratic expression $x^2 + y^2 + z^2 - c^2 t^2$ retains the same value in any other system that may be moving with a constant velocity v relative to the initial one. x , y , z and t are the co-ordinate variables of the four dimensional space-time continuum. In the special theory of relativity, c , the velocity of light, is an absolute constant and t is as much related to a frame of reference as x , y and z . Dr. Mandelker, on the other hand, retains the same t in different frames (moving relatively to each other) but he changes c in such a way that the invariance of the above expression is preserved. His approach is a step back to the Newtonian idea of time as an unvarying and inexorable entity ; but the product ct maintains the four-dimensional vector character. The kinetic energy formula of Dr. Mandelker which he styles as " the hub of the new mechanics " takes the form

$$E_k = m_0 c^2 [1 - \sqrt{1 - v^2/c^2}]$$

According to this, the maximum kinetic energy which a particle can possess is $m_0 c^2$. In cosmic ray showers, high energy electrons throw off a part of their kinetic energy in the production of photons (Bremsstrahlung) which in their turn create pairs. The kinetic energy transferred in each process is always greater than $2m_0 c^2$. One wonders how such transfers of high energy would fit in within the frame work of the new mechanics. The new mechanics gives the same variation of mass with velocity as the theory of relativity and it explains that the velocity of any particle can never exceed the velocity of light.

The experimentally determined value of the velocity of light c would correspond to that frame of reference which is fixed to the earth whose variation of velocity could be detected, in principle at least, from the measurements of the value of c on the earth.

We feel that the point of view of Dr. Mandelker is fascinating in the novelty of ideas and may set a new path of development in the theory of relativity if the fuller implications of his new mechanics and their fit to different physical phenomena are explained in details.

D. B.

PROCEEDINGS
OF THE
INDIAN ASSOCIATION FOR THE
CULTIVATION OF SCIENCE

THE EARTH'S MAGNETISM AND ITS CHANGES*

By

PROF. S. CHAPMAN

INTRODUCTION

May I first of all express my appreciation of the honour done me by your Society in inviting me to deliver the Ripon Lectures for 1949. It is a great pleasure to me to visit India as a scientific guest of your government, to take part in the Indian Science Congress and other gatherings of Indian scientists, and to meet my fellow scientists in your Universities and research institutions, many of them already old friends by personal meetings abroad, or familiar by name through their distinguished contributions to knowledge.

Among the subjects on which I have some competence to address you, it seems to me that the one I have chosen is especially appropriate for consideration by a general and scientific audience in India, and not least in this great city and port of Calcutta. The history of the growth of our knowledge of the earth's magnetism has many links with the history and scientific endeavours of India; and the fact of the directive influence of this magnetism on the compass has been and is one of great importance in oceanic navigation, which has so profoundly influenced India's history in recent centuries, and on which the growth and prosperity of Calcutta so largely depend. Moreover, in recent years the work of the eminent physicists of this city has greatly enhanced our knowledge of solar and upper atmospheric phenomena that are closely associated with the changes in the earth's magnetism.

EARLY HISTORY OF MAGNETIC SCIENCE

The attractive property of the lodestone or natural magnet was known to the ancient Greeks; they were aware that the lodestone not only itself attracted iron, but could also impart its own attractive power to iron, by stroking it, so that it too became magnetic. For well over a millenium this was the only magnetic knowledge of which we have reliable evidence. But in the twelfth century of the Christian era accounts were given, by Guy de Provence in France, and by Alexander Neckam in England, of the use of the magnetic *compass* by mariners; this showed that, perhaps many decades before, the *directive* property of the magnet had been discovered—that a magnetized rod or needle, if free to turn, will set itself along a particular direction, lying (in most places) approximately north and south—and that this property had been seized upon and practically applied for the benefit of seamen, to indicate to

* Text of Ripon Professorship Lecture delivered in the Indian Association for the Cultivation of Science, Calcutta, on 14. 1. 49 and 15. 1. 49.

them the direction upon the trackless ocean, under clouded skies, when the guidance of the heavenly bodies was denied to them. For a long time it was believed that the compass needle itself was controlled by the poles of the heavens, about which the celestial sphere appears daily to revolve.

The thirteenth century supplied another great landmark in magnetic history—a famous letter by a French soldier-scientist, Petrus Peregrinus (Peter the Pilgrim), who in 1267 wrote, for the instruction of a neighbour, an account of his magnetic experiments. In some of these he used lodestones cut to the spherical form. He showed that every magnet has two poles, of which one seeks the north, and the other the south; and that whereas *unlike* poles attract, *like* poles repel each other—the first clear statement of magnetic repulsion, a property as potent as magnetic attraction, though, so far as our records indicate, it had escaped the notice of the Greek natural philosophers.

For many centuries it was thought that the magnetic compass pointed truly to the geographical north (or south), but experience and the growth of skill in measurement gradually led to the recognition that this is not so—in general, the compass deviates or *declines* from the geographical meridian. The angle between the northward meridian and the line from the south-seeking to the north-seeking pole of the needle is called the magnetic *declination* (or, by mariners, the magnetic *variation*). Our earliest records of this discovery are not written records; they are marks made upon portable sundials used (in the fifteenth century and later) as time-keepers for travellers; these sundials, made notably at Nuremberg in Germany, were provided with a small magnetic compass to enable the dial to be set in the meridian plane; and when it became known to the dial-makers that the compass needle did not itself lie along the meridian, they indicated by a mark the direction along which the needle should lie, when the gnomon was correctly oriented—thus giving the magnetic declination at Nuremberg at the time. Gradually also it was found that the magnetic declination is not everywhere the same, so that the mariner or land traveller, in order to infer the true north from the compass direction, must know the magnetic declination of the locality in which he is. Map-makers began to mark the compass declination upon their charts, supplying another unwritten early record of knowledge of the magnetic direction.

Enlightened mariners realised the need to measure the magnetic declination along the main sea routes and at the chief ports, by making astronomical observations (when the state of the sky permitted) to determine the true north, and comparing it with their compasses. Prominent among such pioneers was the Portuguese navigator Joao de Castro, Viceroy of the Portuguese settlements in India; on a voyage from Portugal to India in 1538-1541, round the Cape of Good Hope and up the east coast of Africa onwards to India, he made a series of 43 measures of declination, constituting what may be regarded as the first major contribution to the magnetic survey of the globe. His results were recorded in the log of his voyage, which remained enshrined in the Portuguese naval archives for centuries. Modern researchers have delved

into these archives and into those of the English, Spanish and Dutch Admiralties, to unearth their many treasures of early magnetic data, till then unpublished and unremembered. These data proved, from intercomparison of measures made by different mariners at about the same time and place, to be accurate to about one degree: the early observers had the advantage, which was lost with the advent of steel ships, that their wooden vessels did not disturb the natural magnetic field of the earth and the direction of the compass.

THE GROWTH OF MAGNETIC KNOWLEDGE IN
RECENT CENTURIES

The next great step in magnetic science was the discovery in 1576 of the magnetic dip, by Robert Normad of London, a maker of ships' instruments. He found that a needle, perfectly balanced horizontally on its pivot before magnetization, did not remain horizontal when magnetized. On giving the needle freedom to turn in the vertical plane through the magnetic north (the compass direction), by resting it on a horizontal axle at right angles to this plane, he found that the north end of the needle pointed downward at an angle (called the magnetic *dip*) of 71° to the horizontal. From this observation he drew the conclusion that the control of the direction of the compass is exerted by a "point respective" within the earth, and not by the pole of the heaven.

In 1600 A.D. William Gilbert of Colchester, physician to Queen Elizabeth, published his book *de Magnets*, one of the first great modern experiment treatises on physical science. It contained a wealth of new discoveries concerning electrostatics and magnetism, and an extensive critical survey of all available earlier literature on magnetism. But its outstanding feature is summed up in the pregnant sentence "*Magnus magnes ipse est globus terrestris*"—the terrestrial globe is itself a great magnet. Gilbert based this conclusion on experiments with tiny pivoted magnetic needles placed at various points on a spherical lode-stone—a model magnetic earth. He showed that they dipped increasingly towards the sphere, when moved from the 'magnetic equator' (the circle midway between the two poles of the sphere), where they rested horizontally (parallel to the magnetic axis joining the two poles), to the poles where they stood upright on the sphere. He showed also that the controlling influence on the needles came from the whole body of the sphere, and not merely from any one point in it. His inferences were based on Norman's discovery, and extended and corrected Norman's own conclusion.

Not long afterwards, in 1635, William Gellibrand, Gresham Professor of Astronomy in London, announced that the compass direction is not constant at London, whereas it had always hitherto been supposed to remain the same at any one place. The compass direction, and later the dip and intensity of the earth's magnetic force, were thus found to undergo a slow

'secular' variation, now observed at London for nearly four centuries, and over a shorter time elsewhere. As Fig. 1 shows, the compass direction at

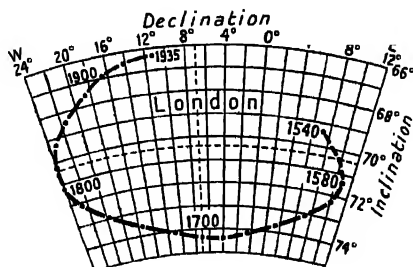


FIG. 1

The direction of the magnetic force at London since A. D. 1582 }

London moved westwards from 11° East in 1580 to 24° West in 1800, since when it has been moving steadily eastward; the dip increased to a maximum of over 74° in 1680, and has since decreased to what has been in recent years the nearly constant value 67° . The diagram suggests that the magnetic direction may return after the lapse of about five centuries to its value in 1576, but only time can confirm this conjecture. The secular course of the magnetic direction elsewhere does not accord with the supposition of a cycle of five centuries or so in the variation of the magnetic direction, nor is there any warrant for the hypothesis that the magnetic axis of the earth has any regular rotation round the geographical axis. The secular variation of the earth's magnetic field is not predictable from our present knowledge, and to keep up-to-date in our information as to the distribution of direction and intensity of the magnetic field over the earth, it is necessary to maintain magnetic observatories, and to make magnetic surveys of the globe every fifteen or twenty years.

In the seventeenth century observations of the magnetic declination gradually increased in number, and covered an ever greater area, as also, more slowly, did those of the magnetic dip. The first ocean voyage for the specific scientific purpose of measuring the declination was made by Edmond Halley in the north and south Atlantic shortly before 1700, in which year he published his results in the form of the first magnetic chart. This showed the *isogonic lines* along each of which the declination has the same value (indicated beside the line); from these lines, by interpolation, the magnetic declination at any point can be found. Halley's chart was an instant success, and two or three years later he published a more extensive chart showing also the isogonic lines over the Indian and (in part) Pacific oceans, using observations collected from eastern voyages; part of this map, including India, is shown in Fig. 2. For comparison a recent world isogonic chart is shown in Fig. 3.

Though such charts are in the form most serviceable to mariners and others for the purpose of reading off the declination at any place, they give no direct visual representation of the distribution of compass direction over the earth. This is best seen from the *magnetic meridian lines*, as shown in Fig. 4, which at each point have the direction of the compass there. The

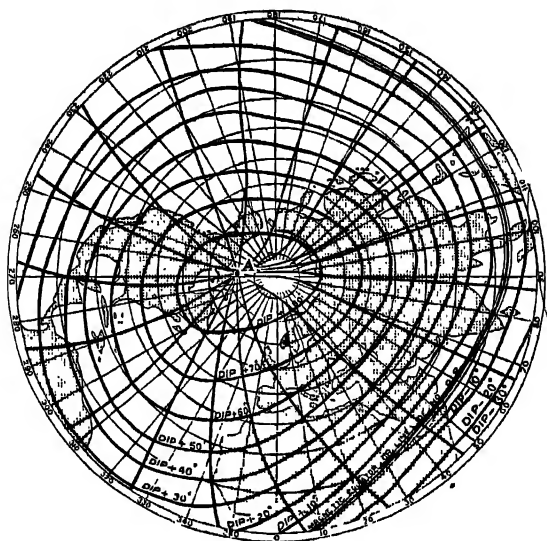


FIG. 4

Lines of horizontal magnetic force, and lines of equal inclination, for the Northern hemisphere, epoch 1830 (After Airy [G 9])

meridians diverge from the south pole of magnetic dip, where the north-seeking end of a freely poised magnet points vertically upward, and converge to the north magnetic dip pole, where the dip (downward) is 90° . The diagram shows also the *isoclinic* lines, or lines of equal dip. The line of no dip is called the magnetic equator. The two dip poles are not antipodal; the line joining them misses the earth's centre by several hundred miles; owing to slight regional irregularities of the earth's field in the polar regions, they differ somewhat from the magnetic *axis poles*; these are the ends of the axis parallel to the direction of uniform magnetization agreeing most closely with the earth's actual field. This magnetic axis is inclined at 11° to the geographical axis.

In the eighteenth century Coulomb proved that the attractions and repulsions between magnetic poles vary as the inverse square of the distance between them, and later Poisson developed the theory of the field of

magnetised bodies in general. For a uniformly magnetised sphere this theory gave the simple formula $\tan I = 2 \cot \theta$ for the dip I at a place at angular distance θ from the magnetic pole; it also indicated that the magnetic intensity increases twofold in going from the magnetic equator to the magnetic poles on such a sphere.

THE BEGINNING OF MAGNETIC OBSERVATORIES

Gauss, in 1832, first showed how to measure the magnetic intensity F at any point on the earth, and after that time it became possible to draw also isodynamic lines, or lines of equal F , the twofold increase of F from magnetic equator to magnetic pole, indicated by Poisson's theory for a uniformly magnetised sphere, was approximately verified for our terrestrial globe. Gauss also applied a mathematical (spherical harmonic) analysis to the available data for the earth's field, and so was able to establish rigorously the conclusion reached by Gilbert over 200 years before, that the surface magnetic field of the earth originates from within; later analyses have gradually reduced the estimated fraction that may possibly be of external origin, to less than one per cent; they also indicate that, contrary to what was thought for a time, there is no reliable evidence for the presence of any part of the field attributable to electric currents crossing the earth's surface, apart from the very minute currents associated with atmospheric electricity.

Gauss was also a pioneer in the establishment and equipment of magnetic observatories, of which those at Göttingen and Greenwich were among the earliest. Some years later magnetic observatories were established at Bombay and Trivandrum in India, and at Batavia in Java—observatories which have earned a most honourable place in magnetic history for their important observations, and for the reductions and interpretations of their data. The great two-volume discussion by Moos of 40 years' Bombay magnetic data is one of the classics of terrestrial magnetism.

There are now about 100 magnetic observatories distributed over the globe, the northern hemisphere having the preponderant share of them. They continuously record the variations of the magnetic elements—usually the declination, and the horizontal and vertical components of the intensity. Besides providing our most accurate information as to the secular magnetic variation, they are indispensable for the reduction of magnetic survey measurements to a common standard and epoch.

The magnetic observatories provide a mass of data rather embarrassing in its volume and detail. In the course of a century many workers have gradually devised suitable means of study of these data. The experience thus gained enables the much younger science of ionospherics—the study of the ionised regions of the upper atmosphere of the earth by means of radio techniques—to progress more rapidly in the geophysical interpretation of its data (of even greater richness and volume), than would otherwise have

been possible. At many observatories the main types of magnetic change have been elucidated; besides the secular variation there are several distinct types of transient variation. Chief among those is the daily variation periodic in a solar day; and there is also a smaller daily variation, generally of about one-fifteenth the intensity, periodic in a lunar day. These regular variations change with the season and wax and wane in amplitude, approximately in parallel with the 11-year cycle of spots on the sun; they also undergo moderate changes from day to day. One exceptionally important early investigation of the lunar daily magnetic variation was that made by Broun from the declination records at Trivandrum. In addition to these regular periodic changes, there are frequent *irregular* disturbances of the earth's magnetic field, when specially intense these are called *magnetic storms*. As in the case of the regular daily variations, these have been studied in great detail at a number of magnetic observatories, for example at Bombay.

After investigating the regular magnetic variations, and the nature of magnetic disturbances, as they affect the records of several individual magnetic observatories, the next step is to synthesize the results to obtain a world view of these phenomena. The study of the geographical distribution of these variations may be termed the *morphology* of the solar and lunar daily magnetic variations and magnetic disturbance. It is a complex subject because it deals with the changing distribution, over a sphere, of a "vector field", that is of a magnetic *force* that has both intensity and direction. Despite the difficult nature of the task, much progress has been made in obtaining comprehensive graphical representations which summarize and synthesize an immense mass of detailed data.

THE MAIN GEOMAGNETIC FIELD

The first approximation to the earth's magnetic field is the field of a uniformly magnetized sphere, concentric with the earth, and of equal or smaller radius, uniformly magnetized along a direction inclined at 11° to the geographical axis; the earth's diameter along this direction is called the *geomagnetic axis*, and its ends, which are at $78^\circ.5$ N, 69° W, and $78^\circ.5$ S, 111° E, are called the *geomagnetic axis poles*. The strength of this, the main part of the earth's magnetic field, is 0.31 at the *geomagnetic equator* (the circle midway between the axis poles), and 0.62 at the axis poles (measured in the magnetic unit called the gauss, and denoted by G).

The actual field of the earth differs, however, from this simple regular field, so that the *dip poles*, where the field is vertical, do not coincide with the axis poles; their positions in 1945 were at 71° N, 96° W and 73° S, 156° E, not antipodal. Likewise, the *magnetic equator*, where the dip I is zero, differs from the geomagnetic equator, and is not a great circle. The horizontal intensity is not constant along the magnetic equator, being notably greater (0.41) at 100° W than at about 30° E, where it is about 0.281. The

magnetic equator nearly touches the southern tip of India, and the dip increases from approximately zero there to about 30° in the north of India; a rough average value of the total intensity over India is 0.4 gauss.

These departures of the earth's field from that of a uniformly (obliquely) magnetized sphere imply the existence of considerable "regional anomalies," as can be seen, for the *horizontal* component of the field, in Fig. 5. These include a field which, over most of Asia, converges towards a centre at about 40°N , 110°E ; another large regional anomaly extends over the south Atlantic ocean, and there are yet others in the South Indian and southeast Pacific oceans.

Besides these great and widespread departures from a simple spherical-magnet field, there are very numerous anomalies of a more local nature; the greatest of these is near Kusk in Russia. It is over 150 miles long, but, where most intense, quite narrow—little over a mile wide, the vertical intensity is everywhere above normal, and ranges up to 1.9 gauss. It is due to a magnetic ore containing up to 40 per cent of iron, extending nearly up to the earth's surface. Another great local anomaly is at Kiruna in northern Sweden, due to magnetic ore which is of great commercial value; there the vertical intensity rises to 3.6 gauss.

Many of these local anomalies are mysterious in that the magnetization of the rocks which produce the anomaly is opposite to that which the earth's present magnetic field would tend to induce. It is known that many substances, such as lava and pottery, become magnetized by the earth's field

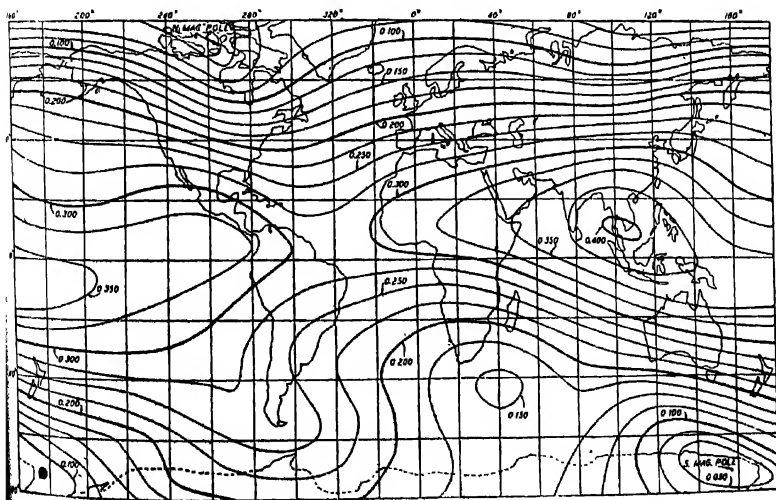


FIG. 5

Lines of equal horizontal intensity, 1922

during the process of cooling, and some of these substances seem able to retain thereafter, over long periods, the magnetism thus acquired, despite subsequent changes in the field. In South Africa and elsewhere there are systems of volcanic dykes of early geological age (*e.g.*, paleozoic) which radiate from a centre of volcanic activity, and may extend outwards 100 miles or more; they consist of thin sheets of igneous rock, often no more than 100 yards wide, that has welled upwards through cracks made in existing strata; and their vertical magnetization has the "wrong" sense. One explanation of this is that 200 million years ago, when they were formed, the earth's magnetization was in a sense opposite to the present sense; but this hypothesis cannot easily be accepted, though no alternative one has as yet been established.

Observation of local magnetic anomalies affords one of the cheapest and simplest ways of searching for hidden deposits that are commercially valuable—such as oil, gold, iron and so on; but naturally there are some kinds of deposit that cannot be detected in this way.

The earth's magnetic field is now known with fair accuracy and in much detail over most of the earth's *surface*. This knowledge can be used to infer very approximately the distribution of the field *above* the surface outside the earth, at any height; the distribution of the main "smoothed" field over any external concentric sphere is approximately the same as over the surface, except that the intensity is reduced proportionately to the *inverse cube* of the distance from the earth's centre; the anomalous part of the field decreases upwards much more rapidly, so that its relative importance becomes steadily less; thus the further we go outwards from the earth's surface, the more nearly does the field agree with that of a uniformly magnetized sphere. The main fact of the inverse-cube law of decrease has been confirmed up to heights of the order 100 miles by radio and rocket measurements of the magnetic field in the ionosphere, in the outer layer of the earth's atmosphere.

THE ORIGIN OF THE EARTH'S MAGNETISM

The distribution of the magnetic field within the earth is much less certainly known. The question is closely bound up with the long-standing mystery of the *origin* or *cause* of the earth's magnetism. Very many answers to this question have been proposed, but the matter remains in doubt. It has generally been considered that the approximate alignment of the earth's magnetic axis with the geographical axis is not merely a coincidence, and that the earth is a magnet because of its *rotation*. Numerous ways in which the rotation could produce the magnetism have been suggested, but most of them have proved on examination to be quite inadequate to explain the existing *strength* of the field.

New interest was added to the question in 1913 when the great American astronomer Hale, who had discovered strong magnetic fields in sunspots,

announced the detection of a general magnetic field of the sun. He gave the polar intensity as 50 gauss, and stated that the direction of the field bore the same relation to the rotation of the sun as obtains between the magnetism and the rotation of the earth.

Much more recently, H. W. Babcock has discovered strong magnetic fields in certain stars

Consideration of the relation between the fields and the rotation and angular momentum of the earth and sun, and later of Babcock's first-measured magnetic star, led Blackett to propose that all three cases were manifestation of a hitherto unrecognized fundamental property of rotating matter, perceptible only in bodies of great size and mass, he found that the ratio of the magnetic moment to the angular momentum could be expressed in simple terms involving the constant of gravitation and the speed of light; the ratio was somewhat uncertain, however, both for the sun and magnetic star.

Bullard pointed out that if Blackett's hypothesis were true, so that matter ordinarily considered non-magnetic did in fact contribute to the earth's field, the variation of this field with depth, in the (approximately non-magnetic) outer crust of the earth, should be different from the inverse-cube relation hitherto assumed to exist there. This remark led Blackett to organize a series of researches on the depth-variation of the geomagnetic field, by taking measurements in deep mines at points where natural local magnetic disturbances, and disturbance due to iron or steel mine-structures, were absent or small. The consequences of Blackett's hypothesis did not differ from those of the classical theory in the case of the vertical magnetic force (near the earth's surface), but they did differ as regards the horizontal force; they indicated a downward *decrease* (for some distance) instead of the hitherto assumed increase

At first the mines magnetic measurements gave some support to Blackett's hypothesis, but continued research on these lines has not confirmed the earlier results.

Moreover, the astronomical support for the hypothesis has also practically disappeared. For many years after Hale's announcement of the general solar magnetic field, a cloud of doubt and uncertainty hung over the matter; after the second world war a young German astronomer, Thiessen, reported new measurements of the sun's field, agreeing substantially with those of Hale; but a year or two later he made new measures which disclosed no such field, and most recently (since these lectures were given in Calcutta) he finds that the field, if present at all has a polar intensity of the order of one gauss, and has the sense opposite to that originally announced by Hale and later confirmed by himself.

The only inference to be drawn from these various announcements is that the observers are seeking to measure something too small for their

methods to determine with any certainty, or else that their measures are valid and that the sun is a magnetically variable star.

The latter possibility is made more credible by a further discovery, by Babcock, of a strongly magnetic star which changes the polarity of its magnetization every nine days. It appears most unlikely that this can be associated with a concurrent change in the sense of rotation, and the observation therefore strikingly contradicts Blackett's hypothesis.

Bullard has lately developed a promising theory, entirely on classical lines, to account for some of the outstanding features of the secular variation of the earth's magnetic field, by inductive effect of large-scale eddies in the supposed convective motions within the earth's liquid core; in the presence of the main geomagnetic field this motion will induce electromotive forces that will impel electric currents in that part of the core; the magnetic field of these currents, as the convective motions and electric currents vary, will be observed at the earth's surface as a secular magnetic variation.

Still more recently Bullard has extended his analysis with the aim of explaining the general magnetic field itself, as maintained by currents induced by dynamo action, in conjunction with the field, by large scale convection in the core. These researches seem to have much promise, an interesting consequence associated with them is the possibility that deep inside the earth the lines of magnetic force do not lie in meridian planes through the magnetic axis (as they do outside the earth). his theory suggests that the deep-lying magnetic field has a considerable component that is normal to these meridian planes.

THE REGULAR MAGNETIC VARIATIONS

The secular magnetic variation, though extremely rapid compared with most long-term changes proceeding from the depths of the earth, is slow according to our every-day judgments about rates of change. The earth's magnetic field undergoes also much more rapid variations, partly regular, partly irregular. These are of several different kinds, and though they have been much studied for at least a century and a half, there is almost certainly much more to discover about them.

The principal regular magnetic variations have a daily period, or rather two daily periods, one relating to the sun and the other jointly to the sun and moon. The *solar* daily magnetic variation is often, for brevity, referred to by the symbol S , to which the suffix q is often added to indicate that the solar daily variation considered is that which is seen in its purest form on magnetically *quiet* days. The *lunar* (or more correctly *luni-solar*) daily magnetic variation is similarly denoted by the symbol L .

These variations S_q and L are not absolutely regular—they certainly change somewhat from day to day, besides undergoing a fairly regular (and substantial) *seasonal* change. They have mostly been studied in the form of

averages from many days in the same calendar month or season, sometimes combined from several years' data.

Each magnetic element is affected by these daily changes, in distinctive ways which depend on the latitude of the station concerned, and to a less extent (in general) on the longitude—because to a first approximation, in middle and low latitudes, the same variations occur all round any circle of latitude, at corresponding *local times*—indicating that the variations are determined by the situation of the station on the earth as seen from the sun (or moon).

Mathematical analysis of these *transient* variations, both regular and irregular, as distributed over the earth, shows that their main cause is *above* the earth's surface—unlike the main field and its secular variation, whose origin is internal. There is, however, a part of each transient variation which is of internal origin, and the reason for this is simple. The main part of the varying magnetic field associated with each type of transient variation, produced above the surface, and observed at the surface, penetrates also below the surface, and its changes induce electric currents there, wherever the earth and its oceans have sufficient electrical conductivity. The external and internal parts of the field can be separately determined from the observations, and from the relation between them we can get information, obtainable in no other way, about the electrical conducting properties of the earth, deep down, far beyond the levels at which, in mines, these properties could be measured *in situ*. The salty oceans conduct electricity very well, and moist land conducts fairly well; dry earth and rocks are bad electrical conductors, but it is inferred from the transient magnetic variations that below 200 miles' depth the earth's electrical conductivity is considerably greater, and increases downwards.

There is reasonable certainty that the daily magnetic variations S_q and I , are due to systems of electric currents flowing in the ionosphere—the layers of the earth's atmosphere, extending upwards from about 50 miles height, which assist world-wide radio communication by deflecting radio waves, so that they travel round the earth's curved surface, instead of losing themselves in outer space. The exact levels of these ionospheric S_q and I , systems of electric current are not yet certainly known, but seem likely to be between 50 and 100 miles height.

Both these current systems are strongest over the sunlit hemisphere, as is natural because there the ionization of the ionosphere is likewise strongest. This ionization is due to absorption of solar radiation, and decays throughout the night, during which this radiation is cut off.

At the equinoxes the main features of these current systems are two circulations of currents (for S_q and also for I) in the northern and southern parts of the sunlit hemisphere; about 60,000 amperes flow in each of these circulations in the case of S_q , and about 5,000 amperes in the case of I . In northern summer the circulation in the northern hemisphere is increased, and

it also extends somewhat across the equator, invading the domain of the reduced southern circulation; in the southern summer these relations are reversed. The systems of current are stronger in sunspot maximum years than at the minimum of the eleven-year sunspot cycle. These changes are parallel to those of the distribution of ionization and electric conductivity in the ionosphere.

These electric current systems are produced by *dynamo action* of the atmosphere moving in the presence of the earth's main magnetic field, in the same way as electric current is generated by the motion of the armature in an electric dynamo.

Such motions are produced by the sun, partly by its thermal and partly by tidal action on the atmosphere. The moon's action is effectively only tidal. These daily motions of the atmosphere due to the sun and moon have long been studied at ground level, and in many ways they must have the same general character in the ionosphere, where, however, they are much advanced in amplitude and speed; this is clearly shown by radio observations of the ionized layers, which, for instance, have revealed that the E layer undergoes a lunar tidal rise and fall, twice in each lunar day, with a range exceeding one *mile*.

The study of the daily magnetic variations has told us much, and has still much more to tell, about the variations of that part of the solar radiation that is intercepted high in the atmosphere, and can only be observed directly from very high flying rockets and also about the motions and structure of the upper atmosphere.

GEOMAGNETIC DISTURBANCE

Often the continuous records of the changes of the magnetic elements, while showing the presence of the regular solar daily variation, also show superimposed *irregular* magnetic changes. These are called magnetic disturbance or activity, or, when specially intense, *magnetic storms*.

Magnetic storms are world-wide phenomena, and have many remarkable properties and associations, particularly with the sun. These are shown most clearly in the case of *great* magnetic storms, which always begin suddenly, and simultaneously all over the earth, to within less than a minute.

Many, probably all, great magnetic storms are preceded by local eruptions of brilliant light on the sun, to which are given the name *solar flares*; usually they occur in the vicinity of sunspots.

The observation of a bright solar flare is generally accompanied by a *radio fade-out*—a failure of communication on many radio transmissions, usually beginning suddenly at the commencement of the flare, and persisting throughout the life of the flare—generally from 20 minutes to an hour or so. In the same interval, the S_{ϕ} daily magnetic variation is temporarily enhanced over *sunlit* hemisphere of the earth. These two phenomena are both attributed to the formation of extra ionization at an ionospheric level lower than

usual, namely at about 50 miles' height—it is caused by the absorption of extra ultraviolet radiation from the flare, of a more penetrating kind than that which produces the ordinary ionised layers. These 'immediate' effects of a solar flare occur in some degree wherever on the sun's disc the flare is situated—even where it is quite near the edge of the disc. They are not exactly contemporaneous with the flares because the visible and ultraviolet radiations by which the flare is seen, and by which it affects the ionosphere, travel with the speed of light, which takes about ten minutes for its passage from the sun to the earth.

If the flare is near the edge of the sun's disc, it may produce no further effect upon the earth. But often, when it is both intense and not too far from the centre of the sun's disc, a great magnetic storm commences about a day later. The interval may range from 16 to 36 hours or so, and is generally interpreted as indicating the time taken for solar gas, ejected during the flare, to reach the earth. The corresponding speed is of the order of 10000 mile a second. Solar observers have observed the ejection of solar gas from the sun at the edge of the disc, with a speed sufficient to carry the gas right away from the sun's gravitational attraction, and travel onwards into space, sometimes with a speed comparable with that inferred for the gas supposed to produce the magnetic storm. But such ejection from the 'edge' of the disc does not produce a storm—for this to happen, the ejection has to include the direction towards the earth, though the angle of scatter from the flare may be a wide one.

The weaker magnetic storms cannot in general be associated with solar flares, but they show a property—not shared by the greater storms—that links them rather definitely with the sun. This is a tendency to recur after the lapse of a polar rotation: often there are multiple—sometimes intermittent—recurrences extending over several solar rotations. This is interpreted as indicating the continued or intermittent emission of solar gas, in a stream with a more limited angle than that associated with flares, over one or more solar rotations; as the sun rotates the direction of the stream changes, like that of water from a hose when the nozzle is rotated, as in a garden sprinkler: the magnetic storm occurs if the stream 'hits' the earth. The recurrence of the storm is not a certainty, because there may be some interruptions or slight changes of direction of the emission, so that the earth is not 'hit' at every rotation.

Magnetic storms are not perceptible by our senses—they are made known to us chiefly by the magnetic records; but they affect human life, because they produce, or are accompanied by, disturbances of telegraphic and radio communication, and they have even been known to affect electric power lines. They are also accompanied by unusually intense and widespread displays of the *aurora polaris* or *polar lights* (known in the northern hemisphere as *aurora borealis* or *northern lights*, and in the southern hemisphere as *aurora australis* or *southern lights*). These lights commonly occur only around the

magnetic polar regions, but during magnetic storms they extend more widely, and have even been seen in India, (*e.g.* from Bombay) in one very great magnetic storm, in 1872. They show many connections with the earth's magnetism, and it is reasonably certain that their distribution is governed (in essentially the same way as is that of the cosmic rays) by the deflecting action of the earth's magnetic field upon the electrical particles in the solar gas, which must be thought of as more or less completely ionised. But there are still many features of the aurora that as yet we cannot adequately explain.

The same is true of magnetic storms; but it is likely that a magnetic storm is produced partly in the solar gas in the region around the earth, *beyond* our atmosphere: and partly by strong systems of electric currents flowing *in* our atmosphere, along the auroral zones and across the polar caps encircled by them. The current in the zones may be as great as two million amperes.

A great magnetic storm may last for a period of from half a day to two or three days, but after the irregular disturbance has died down there remains an effect of the storm that decays only gradually, over a period that may be reckoned in days or even weeks. It seems not unlikely that this after-effect is due to a ring of gas round the earth, somewhat resembling Saturn's rings, at a distance of a few earth-radii from the earth's centre; this ring carries an electric current that diminishes the horizontal component of the earth's surface magnetic field, and that slowly decays. During the decay there may be loss of gas from the ring to the polar regions, maintaining auroral displays at a low level of intensity after the solar stream of gas has ceased to pour on towards the earth.

There is much need for further research and discovery in this field, but the brief account I have given will, I hope, indicate some of the interesting possibilities and the future opportunities for students of the subject. May India continue to add, by its magnetic and solar observatories, to our knowledge of the important facts of these problems and to their interpretation.

The following special publications of the Indian Association for the Cultivation of Sciences, 210, Bowbazar Street, Calcutta, are available at the prices shown against each of them :—

Subject	Author	Price Rs. A. P.
Methods in Scientific Research	... Sir E. J. Russell	0 6 0
The Origin of the Planets	... Sir James H. Jeans	0 6 0
Separation of Isotopes	... Prof. F. W. Aston	0 6 0
Garnets and their Role in Nature	... Sir Lewis L. Fermor	2 8 0
(1) The Royal Botanic Gardens, Kew.	... Sir Arthur Hill	1 8 0
(2) Studies in the Germination of Seeds.	
Interatomic Forces	... Prof. J. E. Lennard-Jones	1 8 0
The Educational Aims and Practices of the California Institute of Technology.	... R. A. Millikan	0 6 0
Active Nitrogen A New Theory.	... Prof. S. K. Mitra	2 8 0
Theory of Valency and the Struc- ture of Chemical Compounds.	... Prof. P. Ray	3 0 0
Petroleum Resources of India	... D. N. Wadia	2 8 0
The Role of the Electrical 'Double layer in the Electro Chemistry of Colloids.	... J. N. Mukherjee	1 12 0

A discount of 25% is allowed to Booksellers and Agents.

RATES OF ADVERTISEMENTS

Third page of cover	Rs. 32, full page
do.	do.	„ 20, half page
do.	do.	„ 12, quarter page
Other pages	„ 25, full page
do.	„ 16, half page
do.	„ 10, quarter page

15% Commissions are allowed to bona fide publicity agents securing orders for advertisements.

CONTENTS

	PAGE
49. A Spectroscopic Study of an Uncondensed Spark between Copper Electrodes in three different Gases at various Pressures. Part III—By Jagdeo Singh	373
50. On the Raman Spectra of three Mono-substituted n -Butane Compounds in the Solid State—By S. B. Sanyal	378
51. Tides in the Ionosphere—By A. P. Mitra	387
52. On the Structure of Soda Cellulose from Raw Jute Fibre—By N. N. Saha and Mrs. Usha Saha	405
53. A Speed Limit for Rockets?—By William Squire	410
54. A Time Base Circuit for a High Precision Ionospheric Sounding Apparatus—By B. M. Banerjee and R. Roy	411
Review	420
The Earth's Magnetism and its Changes—By S. Chapman	...

Vol. 24

INDIAN JOURNAL OF PHYSICS

No. 10

(Published in collaboration with the Indian Physical Society)

AND

Vol. 33

PROCEEDINGS

No. 10

OF THE

**INDIAN ASSOCIATION FOR THE
CULTIVATION OF SCIENCE**

OCTOBER, 1950

**PUBLISHED BY THE
INDIAN ASSOCIATION FOR THE CULTIVATION OF SCIENCE
210, Bowbazar Street, Calcutta**

NOTICE

BOARD OF EDITORS

K. BANERJEE	S. K. MITRA
D. M. BOSE	P. RAY
S. N. BOSE	M. N. SAHA
D. S. KOTHARI	S. C. SIKKAR.

Secretary

EDITORIAL COLLABORATORS

DR. R. K. ASUNDI, M.A., PH.D.
PROF. H. J. BHABHA, PH.D., F.R.S.
DR. P. K. KICHLU, D.Sc.
PROF. K. S. KRISHNAN, D.Sc., F.R.S.
PROF. G. P. DUBEY, M.Sc.
DR. K. RANGADHAMA RAO, M.A., D.Sc.
DR. N. D. SARWATTEY, D.Sc.
DR. N. N. DASGUPTA, M.Sc., PH.D.
PROF. N. R. SEN, D.Sc., F.N.I.
PROF. P. C. MAHANTI, D.Sc., F.N.I.
PROF. S. R. PALIT, D.Sc.,
DR. H. RAKSHIT, D.Sc.,
PROF. K. R. DIXIT, PH.D.
DR. VIKRAM A. SARABHAI, M.A., PH.D.

ASSISTANT EDITOR

MR. A. N. BANERJEE, M.Sc.

Manuscripts for publication should be sent to Mr. A. N. Banerjee, Assistant Editor, 210, Bowbazar Street, Calcutta.

The manuscript of each paper should contain in the beginning a short abstract of the paper.

All references to published papers should be given in the text by quoting the surname of the authors followed by the year of publication within braces, *e.g.*, Sen (1942). The actual references should be given in a list at the end of the paper according to the following specimen :

Sen, B. K., 1942, *Ind. J. Phys.*, 18, 329.

The references should be arranged alphabetically in the list.

All diagrams should be drawn on thick white paper in Indian ink, and letters and numbers in the diagrams should be written in pencil.

Annual Subscription—

Inland Rs. 20
Foreign £ 2

ABSORPTION SPECTRUM OF ANISOLE

By K. SREERAMAMURTY.

(Received for publication, August, 14, 1950)

Plates XVIIIA and B

ABSTRACT. The ultra-violet absorption spectrum of anisole vapour has been photographed in the region $\lambda 2840-2350$. Most of the observed band heads have been interpreted in term of the ground state, the excited state and difference frequencies. Difference frequencies of 26, 56 and 25 cm^{-1} have been newly proposed. The data were compared with the results of earlier investigations on Raman effect and ultra-violet absorption.

INTRODUCTION

The present paper is part of a general investigation of the electronic band spectra of polyatomic molecules with special reference to the ultra-violet absorption bands of organic molecules such as those of the different substituted compounds of benzene. Brief preliminary reports of the results of this investigation are already published elsewhere.* The absorption spectrum of anisole vapour and its interpretation in terms of the electronic states and vibrational frequencies of the molecule are discussed in this paper.

The spectrum of benzene in the near ultra-violet region at 2600\AA has been attributed to the transition $A_{1g}-B_{2u}$. This transition between two electronic vibrationless levels is normally forbidden in the symmetry class D_{6h} to which the benzene molecule belongs. It can, however, be allowed by the superposition of ϵ_g^+ vibration on any one of the electronic levels. Sponer, Nordheim, Sklar and Teller (1939) have shown the analysis of the near ultra-violet absorption spectrum of benzene to correspond to a structure arising from such an allowed transition. Later work of Garforth and Ingold (1948) and Asundi and Padhye (1949) have confirmed this scheme. Sklar (1939) has further shown that, by substitution, the electronic structure of the benzene nucleus can be modified. The modification occurs by an inductive effect depending on the electro-negativity of the substituent and a resonance effect due to an unshared pair of electrons on the substitute. The symmetry characteristics of the benzene molecule are reduced from D_{6h} to C_{2v} by such a substitution and makes the forbidden transition into an allowed one.

A number of molecules involving this mono-substitution of benzene, such as monochlorobenzene, (Sponer and Wollman 1941), monofluorobenzene, (Wollman 1946, benzonitrile,) (Hirt and Howe 1948), Phenol, (Matsen-Ginsburg and Robertson 1945,) aniline (Ginsburg and Matsen 1945,) etc.,

* Sreeramamurty, Curr. Sc. 1948, Vol. 19, p. 48

have already been investigated by several workers, following the treatment of Spomer and Wollman (1941). The electronic transition is interpreted as A_1-B_1 with the electronic moment lying in the plane of the ring and perpendicular to the axis of substitution. This transition is an allowed one and in all spectra it is found to give rise to a strong band in the ultra-violet region. Anisole, having the constitution $C_6H_5.OCH_3$, is one of the above type of molecules arising from the substitution of the OCH_3 group in place of one of the H atoms of benzene. The author has attempted to study and analyse the spectrum to examine how far it is in conformity with the other spectra referred to and to establish the ground and excited state frequencies of anisole.

Previous work on the absorption spectrum of anisole consists of two investigations: (a) Kato and Somcno (1938) and (b) by Matsen and Ginsburg (1946). Kato and Somcno attributed the absorption to the ring π electrons and reported three difference frequencies, 800, 953 and 403 cm^{-1} (cf. Spomer and Teller., *Rev. Mod. Phys.*, 13,76,1941). Ginsburg and Matsen proposed the five upper state frequencies: 527, 759, 934, 954 and 1270 cm^{-1} (cf. Hirt and Howe., *J Chem. Phys.*, 16,485, 1948). The Raman spectrum was studied by Ganesan and Venkateswaran (1929), Kohlrausch and Pongratz (1934) and others.

EXPERIMENTAL

The spectrum is photographed on the medium quartz and large quartz spectrographs. Several pictures have been taken with different lengths of the absorbing column ranging from 2.5 cms to 50 cms. and at different temperatures from -15°C to 80°C . The temperature of the reservoir of the liquid is varied from -15°C to about 60°C .

Anisole supplied by B. D. H. and purified by vacuum distillation is used. For higher temperatures, an all-quartz cell is employed and at lower temperatures and longer columns pyrex glass tubes with quartz windows attached to the ends by means of shellac are used. The liquid is contained in a small glass bulb attached to the absorbing column by a side joint. The conventional hydrogen lamp, working on 2000V and taking a current of 300 ma, served as the source of continuous radiation. Pictures for preliminary examination are also taken with an iodine continuum as the source. The Littrow as well as the medium quartz spectra are measured on several plates.

Ilford Special Rapid plates are used to photograph the spectrum. Exposure times varied from half-an-hour for medium quartz to about 4 hours on the large quartz Littrow.

For longer exposures the absorption tube is evacuated and refilled a number of times during an exposure to avoid the accumulation of decomposition products, if any.

Plate XVIIA illustrates the development of the spectrum under different experimental conditions

About 250 bands are measured in the region $\lambda 2860$ to $\lambda 2380$. The data are contained in Table I. Wavelength, wavenumber in vacuum, intensity (visual estimate), difference in cm^{-1} from the (0, 0) band and the assignment are given in the respective columns.

ANALYSIS AND DISCUSSION

The 0,0 band represented by the prominent head on the short wavelength end of the first strong group is located at $\nu 36389$. The bands occurring on the long wavelend of this 0,0 band have the different Raman frequencies or combinations. The portion of the spectrum to the violet represents the major part of it. The first strong bands to the blue of the 0,0 band are assigned to the totally symmetric frequencies; these represent the fundamental frequencies of the excited state. A difference table has been set up giving the difference in cm^{-1} of the transitions from the 0,0 head. Among these differences, combinations have been formed using the probable frequencies. Of these probable frequencies, those occurring frequently are found to correspond to the separations of the strong bands from the 0,0 band. These are taken as the upper state frequencies. The rest of spectrum is analysed on the basis of these frequencies.

Microphotogram of the spectrum showing the general features is indicated in Plate XVIIIB. It is clear from the picture that the 0,0 band is not the most intense in the spectrum. The totally symmetric C-C vibrations 936 and 951 cm^{-1} are the strongest and of these the 951 transition is more intense. Also a few combination frequencies are stronger than the 0,0. This may be due to the 0,0 transition being normally forbidden but allowed in the substituted benzenes by the excitation of the vibration of proper symmetry.

The 0,0 band seems to show a shift towards the red end as the temperature and pressure are increased. The frequency varies from $\nu 36389$ at 2.5 cms to about $\nu 36401$ at largest pressures. Accompanying this band on the violet side, are a set of satellite bands, approximately equally spaced, presenting the appearance of a structure. At higher temperatures of the absorbing column and the container as also with longer absorbing columns, the 0,0 band showed a broadening on either side and one or more of the satellites merged into this as the temperature and pressure are increased. This might be the cause for the appearance of the shift in the 0,0 band. Hence the wavelength and wavenumber of the 0,0 band as well as of those involving the totally symmetric frequencies are taken from measurement on plates at low temperatures where the heads are sharp enough to give accurate values.

Corresponding to the Raman frequencies 210, 264, 440, 523, 610, 781, 816, 991, 1021 or 1033 and 1297 cm^{-1} , the transitions $0-1 \times v$, resulting in bands at 210, 264, 440, 523, 610, 786, 818, 987, 1029 and 1301 cm^{-1} are identified to the red side of the 0,0 band. The band of weak intensity 818 cm^{-1} to the red of the 0,0 band might probably correspond to the Raman frequency 816 cm^{-1} analogous to 824 cm^{-1} in phenol. If, as in phenol, this represents an antisymmetric frequency it may be that such a frequency appears in the case of molecules with OX substitution.

The ϵ_g^+ vibration 606 cm^{-1} in benzene is supposed to split up in substituted benzenes into one of about 600 cm^{-1} and another of a somewhat smaller value of symmetry β_1 . 610 and 523 cm^{-1} may correspond to the two vibrations.

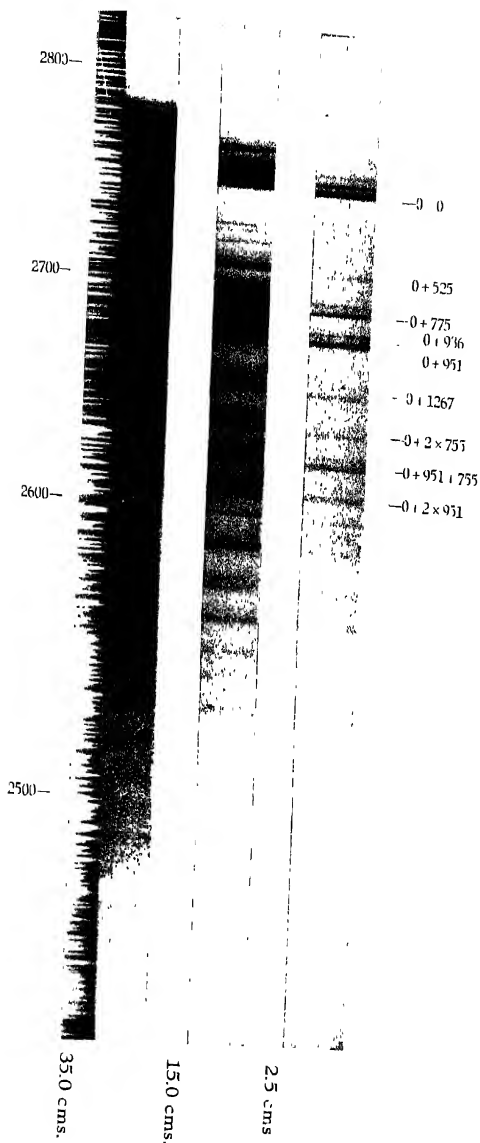
The frequencies of 1170 and 1242 cm^{-1} which appear in Raman data with a fairly large intensity of 5 (in the scale 0 to 10) (*cf.* Magat, Numerical data on Raman effect) are significantly absent though the 1297 frequency which appears in Raman effect with the same frequency occurs with medium intensity. Similarly, the frequencies 1453 and 1587 cm^{-1} are absent. The Raman line at 3065 cm^{-1} is reported to be of intensity 9. This frequency could not be observed even on plates taken at high pressures.

There are some intense bands close and to the red of the 0,0 band 26, 56 and 125 cm^{-1} distant which cannot be identified with any of the Raman frequencies. These may be the difference frequencies representing the $1-1$ transitions. 26 and 56 cm^{-1} give bands of large intensity and involve low frequencies in the ground state. The 26 cm^{-1} frequency might be from the Raman frequency 210 cm^{-1} . In such a case, we should expect a band about 185 cm^{-1} to the violet of the 0,0 band. Actually, there is a band of medium intensity with frequency difference of 183 cm^{-1} . Similarly, if 56 cm^{-1} is from 264 cm^{-1} in the ground state, then 203 cm^{-1} of medium intensity may correspond to the upper state frequency.

The upper state vibrational frequency of 525 cm^{-1} would be ω'_0 (Sponer's notation) or 6b (Wilson's notation) mode of vibration characteristic of the benzene ring. 936 and 951 cm^{-1} represent the ω'_1 or 1 or the 'breathing' frequency and ω'_2 or 18a modes of vibration respectively. 362 may have to be associated with 440 and 497 with 529 cm^{-1} .

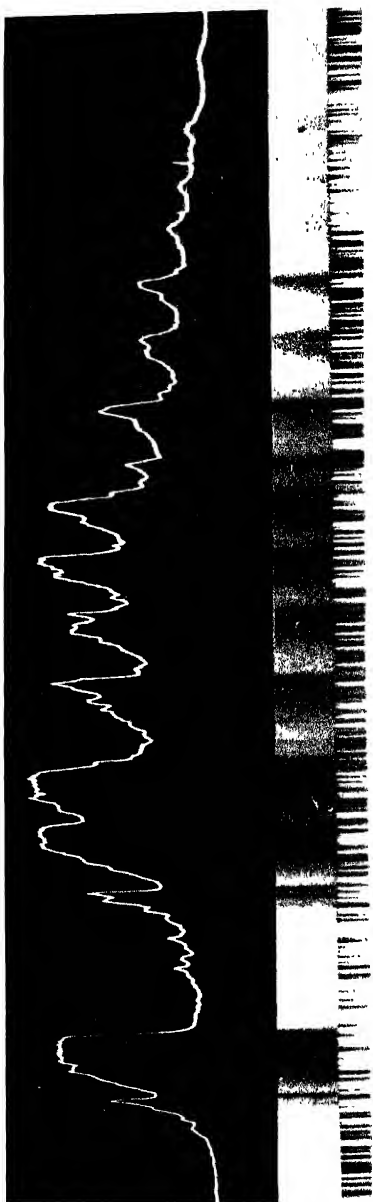
Kato and Somene have reported frequency differences of 800, 953 and 403 cm^{-1} . 953 may be 951 of the present work. 800 and 403 cm^{-1} are not observed.

The upper state and the ground state frequencies are listed in Table II along with the Raman frequencies with which they are probably associated. Frequencies above 1300 cm^{-1} are not given. The excited state frequencies as reported by Matsen and Ginsburg (*cf.* Hirt and Howe, J. 1948) are indicated in Column 4.



Development of the spectrum of anisole at laboratory temperature

$0+2 \times 951$ --
 $0+951+755$ --
 $0+2 \times 755$ --
 $0+1267$ --
 $0+951$
 $0+755$ --
 $0+525$ --
 $0-0$



Microphotograph of the spectrum of anisole

Absorption Spectrum of Anisole

425

TABLE I

Wavelength	Wavenumber	Int.	Diff. from 0, 0	Assignment
2858.16	34977	w	1412	
49.11	35088	m	1301	0-1301
40.24	198	m	1191	
33.81	278	m	1111	0-987-125
29.24	334	w	1055	0-1055
27.19	360	w	1029	0-1029
25.06	387	m	1002	
23.89	402	m	987	0-987
22.04	425	vw	964	
18.95	464	w	925	0-818-2x56
17.79	478	vw	911	
16.68	492	vvw	897	
12.59	541	m	845	0-786-56
10.97	564	m	825	
10.39	571	w	818	0-818
08.37	597	mst	792	
07.94	603	m	786	0-786
06.27	624	mst	765	
03.34	661	w	728	0-610-2x56
01.26	687	vw	702	
2798.81	719	m	670	0-610-56
96.82	744	w	645	
94.10	779	m	610	0-610
91.68	810	m	589	
89.60	837	st	552	
87.30	866	m	523	0-523
86.18	881	w	518	
84.53	902	w	487	
82.78	925	w	464	0-440-26
82.03	934	m	455	
80.86	949	m	440	0-440
79.16	972	w	417	

TABLE I (contd.)

wavelength	Wavenumber	Int.	Diff. from o, o	Assignment
2778.23	35984	vw	405	
74.50	36032	m	357	
73.63	043	m	346	
72.66	056	w	333	
72.09	063	mw	326	
70.69	071	m	318	
69.88	092	m	297	o - 264 - 26; o - 786 + 497
68.51	110	w	279	
67.36	125	m	264	o - 264
66.53	136	m	253	
66.23	140	w	249	
64.98	156	mst	233	
63.21	179	w	210	o - 211
61.59	200	vw	189	
60.77	211	vw	178	o - 125 - 2 × 26
59.81	224	w	165	o - 3 × 56
58.75	238	mst	151	o - 125 - 26
56.78	264	mst	125	o - 125
55.78	277	m	112	o - 2 × 56
54.19	298	m	91	
53.22	310	mst	79	
51.52	333	st	56	o - 56
49.22	363	st	26	o - 26
48.50	373	vst	16	
47.31	389	vst	0	o - 0
46.75	396	mst	7	
46.20	403	m	14	
45.73	409	w	20	
45.45	413	w	24	
44.78	422	m	33	
43.65	437	mw	48	
42.83	448	w	59	o - 440 + 525 - 26; o - 440 + 497

TABLE I (contd.)

Wavelength	Wavenumber	Int.	Diff. from 0, 0	Assignment
2742.41	36456	w	67	
40.87	474	w	85	0-440+525
38.58	504	w	115	
37.00	526	w	137	
35.70	542	w	153	
35.30	548	vw	159	
34.52	559	m	170	0+170
33.48	572	mw	183	
32.06	592	m	203	
30.69	610	m	221	
29.93	620	m	231	
28.02	646	mst	257	0-264+525
27.33	655	w	266	
25.99	673	w	284	0-440+755-26
25.10	685	mw	296	
24.58	692	w	303	
23.64	705	w	316	0-440+755
22.78	716	mw	327	
21.61	732	vw	343	0+2X170
20.18	751	mst	362	0-362
19.98	768	w	379	
18.44	774	m	385	
17.31	790	mw	401	0+525-125
15.46	815	vw	426	
14.64	826	m	437	
12.60	854	mst	465	0+525-56
10.25	886	mst	497	0-497; 0+525-26
07.14	901	vw	512	0+3X170
08.18	914	st	525	0+525
05.98	944	w	555	
04.30	967	vw	578	

TABLE 1 (contd.)

Wavelength	Wavenumber	Int.	Diff. from o, o	Assignment
2702.28	36995	vw	606	
2711.61	37004	vvw	615	
2720.26	023	w	634	0+755-125
2698.08	052	w	663	0+525+170-26
2676.21	078	st	689	0+525+170
2654.43	089	st	700	0+755-56
2632.99	109	w	720	0+2 × 362
2611.24	119	mw	730	0+755-26
2589.87	138	mst	749	
2568.41	144	vst	755	0+755
2546.13	162	m	773	
2524.65	169	vw	780	
2502.53	198	mw	809	
2480.84	207	m	818	
2458.45	226	mf	837	
2436.66	266	m	877	
2414.32	270	st	881	0+936-56
2392.21	285	m	896	0+951-56
2370.66	307	st	918	
2348.39	325	vst	936	0+986
2326.30	340	vst	951	0+951
2304.90	360	m	971	
2282.46	366	w	977	
2260.53	379	st	990	
2238.51	393	w	1004	
2216.44	408	m	1019	0+1267-2 × 125
2194.93	443	m	1054	0+2 × 525
2172.25	453	vw	1064	0+525+170+362
2150.12	511	w	1122	0+755+362; 0+951+170
2127.79	529	mw	1140	0+1267-125
2105.19	538	vvw	1149	

TABLE I (contd.)

Wavelength	Wavenumber	Int.	Diff. from α, α	Assignment
2662.26	37551	mw ?	1162	$0 + 939 + 231$
61.41	563	m	1174	
60.80	571	m	1182	$0 + 951 + 238$
60.33	578	mw	1189	$0 + 1267 - 3 \times 26$
60.05	582	mw	1193	
59.18	594	mw	1205	$0 + 951 + 2 \times 125$
58.79	600	m	1211	$0 + 1267 - 56$
57.96	612	m	1223	
56.87	627	m	1238	$0 + 1267 - 26$
55.84	642	m	1253	
54.87	656	mst	1267	$0 + 1267$
53.77	672	m	1283	$0 + 1536 - 2 \times 125$
52.65	687	vw	1298	$0 + 936 + 362$
50.54	717	mw	1328	
46.45	775	vw	1386	
44.61	802	mw	1413	$0 + 1536 - 125$
43.42	819	m	1430	
42.16	837	w	1448	$0 + 951 + 497$
41.52	846	m	1457	$0 + 936 + 525$
40.24	864	m	1475	$0 + 951 + 525, 0 + 1536 - 56$
37.75	900	mst	1511	$0 + 2 \times 755, 0 + 1536 - 26$
36.98	911	m	1522	
35.97	925	m	1536	$0 + 1536$
34.29	950	w	1561	
33.26	964	w	1575	$0 + 3 \times 525$
28.84	38028	mD	1639	$0 + 936 + 755 - 56$
25.19	081	st	1692	$0 + 936 + 755$
24.07	097	st	1708	$0 + 951 + 755$
23.70	103	m	1714	
22.60	119	mw	1720	
21.67	132	mst	1743	

TABLE I (contd.)

Wavelength	Wavenumber	Int.	Diff. from 0, 0	Assignment
2621.28	38138	mw	1749	
20.49	149	mw	1760	
19.18	169	w	1780	
18.60	177	w	1788	
16.63	206	w	1817	
15.72	219	m	1830	
12.65	263	m	1874	$0+2 \times 936$
11.57	280	mst	1891	$0+951 \times 936$
11.23	284	mst	1895	
10.73	292	mstBd	1903	$0+$
08.78	321	m	1932	
06.43	355	w	1966	
06.00	362	w	1973	$0+1536+497-56$
02.43	414	m	2025	
01.73	424	mw	2035	$0+1536+497$
2598.83	467	mw	2078	$0+2 \times 951+170$
96.78	498	m	2109	
94.38	533	m	2144	
92.30	564	mw	2175	$0+951+755+525-56$
90.51	591	w	2202	$0+525+755+951-26$
88.53	621	mst	2232	$0+951+755+525$
86.74	647	w	2258	$0+1267+2 \times 497$
86.33	654	mw	2265	$0+3 \times 755; 0+2 \times 951+362$
84.52	680	mw	2291	
83.83	691	w	2302	
82.47	711	mw	2322	$0+1267+2 \times 525$
80.25	744	vw	2355	
78.62	768	vvw	2379	
76.03	808	m	2419	$0+2 \times 951+525$
73.28	849	mw	2460	$0+951+2 \times 755$
72.86	855	mst	2467	$0+1536+936$

TABLE I (contd.)

Wavelength	Wavenumber	Int.	Diff. from 0, 0	Assignment
2571.00	38884	vvw	2495	$0 + 1536 + 951$
68.89	916	w	2527	$0 + 2 \times 1267$
66.68	949	w	2560	
64.90	976	w	2587	
63.94	991	w	2602	
60.60	39042	st	2653	$0 + 2 \times 951 + 755$
58.46	974	w	2685	
56.74	101	w	2712	
54.59	134	vw	2745	
52.49	166	vw	2777	$0 + 1267 + 2 \times 755$
48.26	231	m	2842	$0 + 2 \times 951 + 936$
46.55	257	w	2868	
46.41	275	vw	2886	
43.93	298	vvw	2909	
41.33	338	w	2949	
39.46	366	mw	2977	
38.73	378	w	2989	
37.13	403	vvw	3014	
35.32	431	mw	3042	$0 + 1536 + 2 \times 755$
33.04	466	w	3077	$0 + 2 \times 1536$
31.40	492	w	3103	
28.44	538	vw	3149	$0 + 1267 + 951 + 936$
27.02	560	mw	3142	
24.62	597	mw	3208	
20.54	662	m	3273	
19.15	684	vvw	3295	
12.30	792	w	3403	$0 + 1536 + 2 \times 936$
06.97	877	w	3488	
01.49	964	w	3575	
00.09	987	w	3598	
2498.01	40020	vw	3631	

TABLE I (contd.)

Wavelength	Wavenumber	Int.	Diff. from o, o	Assignment
2494.80	40071	w	3682	
89.49	157	w	3768	
88.68	170	w ?	3781	
83.96	246	vw	3857	
81.71	282	w	3893	
77.61	349	w	3960	
69.04	489	va	4100	
62.36	599	vw	4210	
12.65	41436	vw	5047	
2388.22	859	vw	5470	

TABLE II

Ground state		Excited state		
Raman ultra-violet		Author	Matsen & Ginsburg	Kato & Soneno
Kohlrausch & Pongratz	Author			
210 (4)		170 m		
264 (4)				
440 (5)	440 m	362 mst		403
529 (2)	523 m	497 st		
610 (4)	610 m	525 mst	527	
781 (10)	786 m	755 vst	759	
816 (1)	818 w			800
901 (2)	987 m	936 st	934	
1021 (4)				
1033 (3)	1029 w	951 vst	954	953
1066 (0)	1055 w			
1150 (2)				
1170 (5)				
1242 (5)				
1297 (5)	1301 m	1267 mst	1270	

ACKNOWLEDGMENT

The author wishes to express his indebtedness to Prof. K. R. Rao for his kind guidance.

PHYSICS DEPARTMENT,
ANDHRA UNIVERSITY, WALTAIR.

REFERENCES

- Asundi and Padhye, 1949, *Ind. J. Phys.*, **23**, 199
 Ganesan and Venkateswaran, 1929, *Ind. J. Phys.*, **5**, 195
 Garforth and Ingold, 1948, *J. C. S.*, p 417
 Ginsburg and Matsen, 1945, *J. Chem. Phys.* **13**, 309
 Hirt and Howe, 1948, *J. Chem. Phys.* **16**, 480
 Kato and Someno, 1938 *Sci. Pap. Inst. Phys. Chem. Res, Tokyo*, **34**, 912
 Kohlrausch and Pougatz, 1934, *Monatsh*, **65**, 6
 Matsen, Ginsburg, and Robertson, 1945, *J. Chem. Phys.* **13**, 309
 Matsen and Ginsburg, 1946, Paper presented before the symposium on Color and Electronic spectra of complex molecules, Chicago, Illinois, December 130
 Sklar, 1939, *J. Chem. Phys.* **7**, 984
 Sponer, Nordheim, Sklar and Teller, 1939, *J. Chem. Phys.* **7**, 207.
 Sponar and Teller, 1941, *Rev. Mod. Phys.* **13**, 74.
 Sponar and Wollman, 1941, *J. Chem. Phys.* **9**, 816.
 Wollman ,, 1946, *ibid* **14**, 123.

ABSORPTION SPECTRA OF THALLIUM HALIDES

By P. TIRUVENGANNA RAO

(Received for publication, May 2, 1950)

Plates XVIII, B

ABSTRACT The absorption spectra of TlI, TlCl and TlBr have been investigated in the region $\lambda 6500-\lambda 2200$. An examination of the new absorption photographs obtained for TlI in the present work, has led to an important modification in the analysis of the main system $^1\Pi-^1\Sigma^+$, reported earlier in emission. The origin had to be located at $\nu 26339.6$ instead of at $\nu 25780.0$ and the vibrational quantum numbers ν' and ν'' had to be increased by 11 and 13 units respectively. The revised vibrational constants are

$$\begin{array}{lll} \omega_e' = 93.4 & \omega_e'' = 123.5 \\ \nu_e = 26361.7 & x_e' \omega_e' = 0.10 & x_e'' \omega_e'' = 0.09 \end{array}$$

No systems of TlI attributable to the transitions $^3O^+-^1\Sigma^+$ and $^1\Pi-^1\Sigma^+$ have been obtained in absorption.

The two systems of TlCl lying between $\lambda 4200-\lambda 3800$ and one for TlBr in the region around $\lambda 3950$ reported in emission have not occurred in absorption.

INTRODUCTION

In the previous investigation on the emission spectrum of thallium iodide, the author (T. Rao and K. Rao., 1949) referred to the possible existence of bands due to the electronic transition $^1\Pi-^1\Sigma^+$. If at all they are excited, they are expected to occur in the ultraviolet. Under conditions of emission in a transformer or oscillator discharge, they were not obtained. As they might appear probably in absorption, experiments have been carried out to investigate this point. Incidentally the investigation is extended to cover the entire region in the case of thallium iodide and of the remaining halides of thallium as well. This work has led to a very important modification in the analysis of the main system of TlI itself, namely in the location of the origin of the system, which could not be very definitely identified from emission spectrum. The $^1\Pi-^1\Sigma^+$ transition itself could not be obtained even in absorption. In the present paper these results are described and a comparison is also made of the absorption spectra of all the thallium halides.

The existing results on the absorption spectra of thallium halides can be briefly summarised in the following table.

TABLE I

Molecule	Authors	Description	Region	Transition
TlF	Butkow & Boizova, Howell & Coulson.	A continuum	$\lambda 2200$	$^1\Pi - ^1\Sigma^+$
		A band system	around $\lambda 2200$	
		"	$\lambda \lambda 2800-2600$	
TlCl	Butkow, II & C	"	$\lambda \lambda 3300-3800$	$^3\Pi - ^1\Sigma^+$
		"	$\lambda \lambda 3400-3200$	
		A continuum	$\lambda \lambda 2545-2475$	
TlBr	Butkow, II & C	"	$\lambda 3106$	$^3\Pi - ^1\Sigma^+$
		"	$\lambda 2890$	
		"	$\lambda 2890$	
TlI	Butkow	A band system	$\lambda \lambda 3600-3400$	$^3\Pi - ^1\Sigma^+$
		A continuum	$\lambda 3330$	
TII	Butkow	Diffuse bands	$\lambda \lambda 4200-3800$	

(H & C—Howell and Coulson).

The foregoing table indicates clearly that while the study of the absorption spectra of the fluoride, chloride and bromide of thallium is sufficiently extensive, very little is known of the absorption of thallium iodide. For this molecule, the brief region $\lambda 4200 - \lambda 3800$ where 13 diffuse bands were recorded by Butkow is obviously a portion of that in which the extensive system in emission is described by the author in the earlier paper. In the present experiments, the entire region from $\lambda 6500 - 2200$ is investigated for all the molecules.

EXPERIMENTAL

The usual experimental arrangement is employed for the study of the absorption spectra.

Source:—The source of continuous spectrum from $\lambda 6500 - \lambda 2900$ is a special ultraviolet ribbon lamp constructed by the General Electric Company. The lamp has a special thin sucked-in window having a lens action and transmits down to $\lambda 2900$.

From $\lambda 2900$ down to $\lambda 2100$, the source of continuous spectrum is the one described by Ramasastry (1948) consisting of an H. F. oscillator discharge through iodine vapour. This source has been found by us as very useful and simple in all experiments in absorption in the ultraviolet.

Absorption tube:—The absorption tube was of pyrex tubing 40 cm. long and 1 cm. in diameter open at both ends to avoid windows on which the substance might deposit itself. A circular diaphragm of the same diameter as the tube is held in position, at each end of the tube, to act as a

shield for extraneous light. These diaphragms are found very necessary to get good pictures. The substance is spread near the centre of the tube.

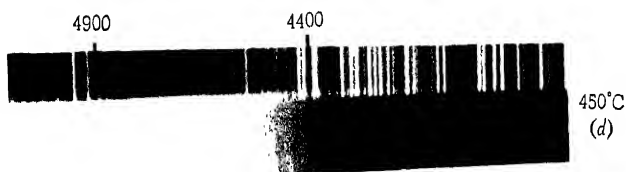
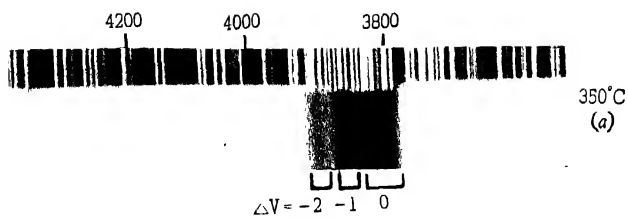
Furnace :—This is an electric furnace of hinged design, having units of helical coils of nichrome wire. It is of a very convenient design permitting inspection of the tube frequently. It is operated on 220 volts and 5 amperes. Any temperature up to 600°C can be easily obtained by regulating the current. The measurement of temperature is done by a standardised thermocouple supplied by the Cooley Electric Manufacturing Corp. (U.S.A.). The actual temperature range in which the absorption was studied in these molecules, extended from 350°C to 600°C . This range was found suitable for the complete development of the absorption spectra.

Instruments :—Hilger medium quartz and a Fuess glass instrument were mainly used. For thallium iodide, the Fuess spectrograph was more suitable. Exposures were of 5 to 10 minutes' duration, on Ilford Special Rapid Panchromatic plates.

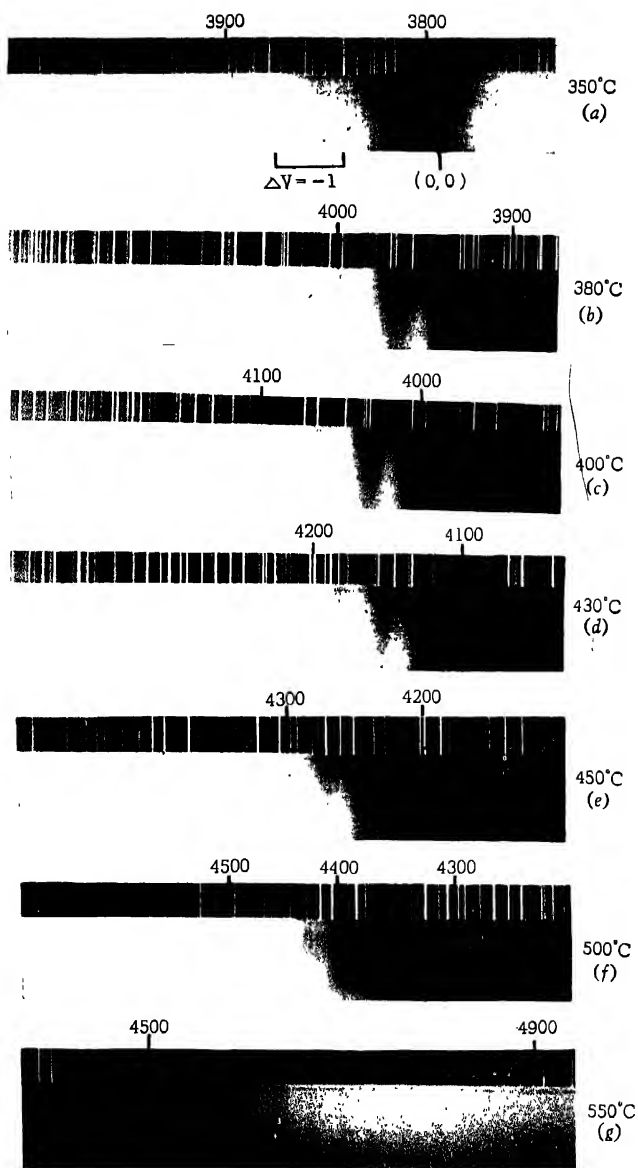
RESULTS

TI I :—Plate XVIIIA and strips (a) to (d) show the absorption spectra of thallium iodide at various temperatures taken on the medium quartz spectrograph. At 350°C four discrete groups of bands at about $\lambda 3800$ and upwards, appear, the one in the extreme violet end being the strongest. The intensity of these groups decreases as we go towards longer wave-lengths. Some of these groups show banded structure which is partially resolved. This at once indicated the need for taking the picture on a higher dispersion instrument. At 380°C absorption extends to longer wave-lengths to about $\lambda 4100$ while between $\lambda 3950$ – $\lambda 3960$ there is complete absorption in the place of discrete bands. At 400°C absorption extends up to $\lambda 4500$. As the temperature increases, the shorter wave edge of absorption extends down to $\lambda 3700$.

Plate XVIII B strips (a) to (g) show the complete absorption spectrum of thallium iodide at various temperatures taken on the Fuess glass instrument of higher dispersion. At 350°C , the groups recorded previously on medium quartz instrument around $\lambda 3800$ appear well resolved into discrete bands. This is just the region of the spectrum which is obscured partly by the intense TI 3775 line, in emission. This picture proved to be of utmost importance in the location of the origin of the system. At higher temperatures as well, photographs with this instrument show well resolved discrete structure in places where just diffuse bands are found under the smaller dispersion of the quartz instrument. The extension of the spectrum towards longer wave-length side with increasing temperature may be clearly seen in the absorption photographs shown in Plate XVIII B strips (a) to (g). It is seen that at the highest temperature 550°C , the bands become exceedingly diffuse and extend up to $\lambda 4700$, which may be assumed to be the longer wave length



Til absorption spectra at various temperatures
(medium quartz spectrograms)



TII absorption spectra at various temperatures
(Fuess spectrograms)

Absorption Spectra of Thallium Halides

limit of the band system. At about the same temperature, the absorption bands of iodine are also recorded above $\lambda 5000$, probably because of the presence of free iodine formed as a product of thermal dissociation. These absorption photographs of thallium iodide, obtained so clearly for the first time in the present work, proved very useful in arriving at a definite analysis of the main system.

The second system of TlI observed in emission and analysed as $^3O^+ - ^1\Sigma^+$ is not obtained in absorption.

ANALYSIS OF TlI BANDS

In arriving at the analysis of the main system of this molecule from a study of the emission photographs, reference was made to one main difficulty in obtaining the starting point. The origin of the system had to be located at the violet end of the observed bands mainly from a consideration of analogy with the other thallium halides. The absorption photographs have clearly confirmed this view, for, both in emission and in absorption the violet limit is about $\lambda 3800$. The red end limit is at about $\lambda 4700$ in absorption while it extends further to the red in emission. With increasing temperature, a gradual extension of the spectrum is observed in absorption towards the region of longer wave-lengths. Further the intensity of absorption is maximum in the most refrangible part of the spectrum.

The difficulty in exactly locating the origin from the emission photographs only, as was previously stated, is partly because this end is obscured by the intense Tl 3775 line. In this respect, the absorption spectrum has proved more useful. A close examination of these spectra has indicated that the origin of the system lies further to the violet than that located previously. The existence of well-defined and more prominent bands in the region $\lambda 3795 - \lambda 3813$ necessitated this change. A re-assignment of the vibrational quantum numbers based on the shift in the origin of the system had to be made, adopting the very strong bands between $\lambda 3795.49$ to $\lambda 3838.59$ as the $\Delta v = 0$ sequence. Table II gives the new assignments derived from the absorption pictures. Only the most refrangible portion of the bands below $\lambda 3896.56$ are shown in this table. The wave-length and wavenumber data of the remaining bands are those given already in the previous paper. But the vibrational numbering should be changed consistently with the new numbering shown in Table II. It implies that for all the bands with wavenumbers below $\nu = 25780.0$ cm. (which is assigned as the 0, 0 band previously), the values of the vibrational quantum numbers v' , v'' should be increased by 11 and 13 respectively.

In the light of this new v' , v'' numbering, the constants of the system are re-calculated. There is obviously an alteration chiefly in the value of v_0 , the remaining constants being almost identical on account of the very

TABLE II

TII Bands ($\lambda 3790$ - $\lambda 3900$)

Wave-length	Int	Wavenumber (Abs.)	Wavenumber (emission) data	Classification	
				Abs. (ν' , ν'') Revised	emis. (ν' , ν'')
3795.49	10	26339.6	..	0.0	..
59.53	10	26311.6	...	1.1	...
3804.22	10	26279.2	..	2.2	..
08.59	10	26249.1	..	3.3	...
13.18	10	26217.4	26218.9	4.4	5.0
17.56	9	26187.3	26187.6	5.5	6.1
21.76	8	26158.6	26159.4	6.6	7.2
26.06	6	26129.5	26132.3	7.7	4.0
30.52	6	26098.7	26102.6	8.8	5.1
34.42	6	26072.2	26071.0	9.9	6.2
38.59	6	26043.9	26043.8	10.10	3.0
43.13	6	26013.1	26014.7	7.8	4.1
47.52	6	25983.4	25984.2	8.9	5.2
52.42	6	25950.4	25953.9	9.10	2.0
56.87	6	25920.5	25921.9	10.11	3.1
3861.32	6	25890.6	25890.0	11.12	4.2
65.78	5	25860.7	25863.8	12.13	1.0
69.76	5	25834.1	25836.3	13.14	2.1
74.15	5	25804.8	25807.5	14.15	3.2
78.41	4	25776.5	25780.0	11.13	0.0
82.69	5	25748.1	25750.8	12.14	1.1
87.29	4	25717.6		13.15	
96.56	4	25656.4	25654.8	11.14	0.1

TABLE III

Molecule	Approximate interval separations
TlF	1682
Tl ⁺ I	1106*
TlBr	872*
Tl I	740

small magnitude of the anharmonic constants. These new values are given below (for comparison, the old values are also quoted in the foot note).*

$$\nu_e = 26361.7 \quad \omega'_e = 93.4 \quad \omega''_e = 123.5 \quad x'_e \omega'_e = 0.10 \quad x''_e \omega''_e = 0.09$$

The interval separations between the origins of the two systems $^3I - ^1\Sigma^+$ and $^3O^+ - ^1\Sigma^+$, is also altered on account of the change in the value of ν_e .

Table III gives the new value for Tl I along with those of the corresponding ones for the other thallium halides.

$$* \quad \nu_e = 25794.7 \quad \omega'_e = 91.2 \quad \omega''_e = 121.2 \quad x'_e \omega'_e = 0.10 \quad x''_e \omega''_e = 0.09$$

* Values determined approximately from continua occurring on the shorter wave side of the main system.

ABSORPTION SPECTRA OF OTHER
HALIDES OF THALLIUM

TlF: The absorption spectrum for this molecule is not taken as it has been thoroughly investigated previously by Howell

TlCl:—For this molecule the author recorded two new systems of bands in emission, the analyses of which have already been reported in a previous paper (T. Rao, 1949). It has been shown that these two systems occurring in the region $\lambda 4200$ – $\lambda 3800$ have a common lower state which is the same as the upper state of the ultraviolet system around $\lambda 3200$ analysed by Howell and Coulson. The author suggested that it is improbable to expect these systems in absorption as the ground state is not involved in the emission of the systems. This study of the absorption spectrum of TlCl was undertaken primarily to see whether these systems can be actually observed in absorption. No such systems are observed in the neighbourhood of $\lambda 3800$ and $\lambda 4200$. For the sake of completeness, the absorption spectra of the system occurring around $\lambda 3200$ were taken at various temperatures.

Both Butkow and Howell and Coulson observed a continuum at 3100 at about 200°C , while at about 450°C , Howell and Coulson recorded another continuum at $\lambda 2890$. In the present work, the continuum around $\lambda 3106$ consists actually of two discrete continua, one with maximum at $\lambda 3110$ and the other $\lambda 3160$. Further, both Butkow and Howell and Coulson recorded the spectrum up to $\lambda 3400$ while in the present work, the spectrum extends up to $\lambda 3500$. As these additional bands have already been obtained in emission and analysed by Howell and Coulson, no quantitative data are given here. The ultraviolet absorption of TlCl around $\lambda 2520$ has also been recorded.

TlBr:—For this molecule, Howell and Coulson (1938) reported a brief system around $\lambda 3950$ as occurring only in emission, the lower state of which is found to be the upper state of the main system in the region $\lambda 3400$ – $\lambda 4500$. A revised analysis of this system is already given in a previous paper by the author. That the brief system occurs only in emission has also been confirmed by the author's experiments on absorption.

A discussion of the electronic transitions and the interpretation of the different band systems has already been given in the previous paper. The absorption experiments detailed above confirm that the lower state of the main systems in all these molecules is the ground state.

ACKNOWLEDGMENT

The author is indebted to Prof. K. R. Rao for his interest and guidance.

DEPARTMENT OF PHYSICS
ANDHRA UNIVERSITY
WALTAIR.

REFERENCES

- Butkow, 1929, *Zelts., f. Physik.*, **66**, 232.
Butkow and Boizova, 1934, *Phys. Zett. O. Sowjet*, **6**, **6**, 765.
Howell, 1937, *Proc Roy. Soc.*, **160**, 242
Howell and Coulson, 1938, *Proc. Roy. Soc.*, **166**, 238.
Howell and Coulson, 1941, *Proc Phys. Soc*, **53**, 706.
Ramasastry, 1947, *Ind. Jour. Phy.*, **21**, 271.
Tiruvenganna Rao and K. R. Rao, 1949, *Ind. Jour. Phy.*, **23**, 115.
Tiruvenganna Rao, 1949, *Ind. Jour. Phy.*, **23**, 393.

ON THE ORIGIN OF FLUORESCENCE IN DIAMOND *

By B. M. BISHUI

(Received for publication, August 30, 1950)

Plates XIXA—G

ABSTRACT. The fluorescence and absorption in the visible region exhibited by six specimens of diamond including one of type II have been investigated at different temperatures and the birefringence shown by these crystals at 30°C and 275°C has been photographed. The intensity of fluorescence excited by different monochromatic radiations in the region of 4046 Å has also been studied qualitatively. The results show that the integrated intensity of the band at 4156 Å increases at lower temperatures and diminishing gradually with the rise of temperature of the crystal, it vanishes abruptly at a temperature which is different for the different crystals; but at 275°C the band is absent in all the cases. The rate of increase of intensity at lower temperatures diminishes gradually with the lowering of temperature.

The absorption band at 4156 Å and its companions also disappear at 275°C but the birefringence shown by the crystals is not altered very much at this temperature. It is further observed that the intensity of fluorescence increases when the incident monochromatic radiation has the same wavelength as that of the absorption band at 4045 Å but it diminishes when the wavelength lies between 4045 Å and 4156 Å and does not coincide with that of any of the absorption bands.

It has been concluded from these results that the fluorescence behaves in the same way as impurity fluorescence and that the impurity is of chemical nature. It is pointed out that the fluorescence is not due to lattice defect produced by strain in the tetrahedral lattice, because there is no exact correlation between microscopic strain and fluorescence in diamonds of Type I.

INTRODUCTION

Fluorescence of diamond was first observed by Robert Boyle in 1663 and the subject has attracted the attention of many investigators since then. Special attention of the physicist was drawn to this phenomenon by Robertson, Fox, and Martin in 1934, who observed that there are actually two distinct classes of diamonds, one (Type II) being transparent to 2200 Å. and the other (Type I) having a continuous absorption in the ultra-violet region starting from about 3000 Å. and extending towards the shorter wavelengths. Recently, however, this subject has engaged the attention of a large number of physicists after a new theory was put forward by Sir C. V. Raman (1944) regarding the structure of diamonds. It is well known that according to the results of X-ray analysis the diamond lattice consists of two identical interpenetrating face-centred cubic lattices, one being displaced from the other along the body-diagonal. It is also known

* Communicated by Prof. S. C. Sirkar.

from study of the Raman spectra that the carbon atoms are joined to each other through covalent tetrahedral bonds and the lattice is not an ordinary molecular lattice, but the whole single crystal is a giant molecule. Further, the crystal is diamagnetic, and shows no pyroelectric properties.

It is a fact, however, that as far as the symmetry of the external facets of the crystal is concerned sometimes it is of holohedral class and sometimes only of the tetrahedral class. This latter fact, that the external symmetry of the crystal is sometimes of tetrahedral class, led Sir C. V. Raman (1944) to postulate the theory that if the electronic configuration of the carbon atoms possesses a tetrahedral symmetry, in two different types of diamond there may not be a centre of symmetry at that point midway between two representative atoms. In fact, four different cases can arise out of this consideration giving four different kinds of structures in the diamond crystal. The four types have been called by him Td I, Td II, Oh I, and Oh II. Td I and Td II are exactly identical in all respects. There is, however, no centre of symmetry at the mid point between two representative carbon atoms joined by each of the C-C bonds in these two cases. In Oh I and Oh II, on the other hand, there is such a centre of symmetry. If we examine the hypothesis carefully we can see that both in Td I and in Td II the resultant angular momenta of the two electrons in each C-C bond are in the same direction, while both in Oh I and Oh II they are in the opposite directions. It is known that different types of molecules are formed by the same two atoms owing to two different orientations of the spin moments of nuclei. For instance, ortho- and para-hydrogen molecules are formed by two different orientations of the nuclear spin moments. In the same way Td I and Oh I structures are assumed to be formed in the case of diamond lattice by two different orientations of the resultant angular momenta of the bonding electrons. In that case it is difficult to understand the differentiation between Oh I and Oh II, because when two bonding electrons have got their spin moments directed in opposite directions it is very difficult to say which of them belongs to which atom and the spin moments can be represented by two arrows pointed in opposite directions only in one way. The two geometrical figures drawn to show that two different orientations are possible are in reality exactly identical. They represent the same relative dispositions of the spin moments, and as stated earlier in a bond in which two electrons take part it is not possible to say whether the spin is directed away from or towards the other atom. Similarly, when two moments are directed in the same way it is immaterial which way the resultant is formed and the two lattices Td I and Td II have exactly same physical properties. There may be, of course, slight irregularity at the surface in the crystal along which two such lattices may join each other in such a way that the resultant spin moment in one is directed in a sense opposite to that in the other. It is also well known that the directions of the C-C bonds in diamond lattice are definitely along the arrows in the figure which represents Oh I as revealed

by X-ray studies, and they cannot be along the arrows given in the other three types, Td I, Td II and Oh II. It is, therefore, difficult to understand how the structures may be different although the arrangement of the carbon atoms as well as the dispositions of the electronic bonds are exactly identical in all the four types mentioned above. It is also a fact that in both types of crystals showing respectively tetrahedral and octahedral external symmetry, the internal arrangement of carbon atoms is exactly identical, and the lack of centre of symmetry midway between two representative carbon atoms has never been detected by the results of X-ray investigation.

It has been assumed in the new theory that diamond has usually the lower symmetry and interpenetration of different types of the structures mentioned above produces different types of diamonds. It has also been assumed that inter-twinning of tetrahedral and octahedral structures may exhibit a set of planes parallel to each other in which alternate layers have got different physical properties. From study of luminescence exhibited by a large number of crystals, it has been concluded that interpenetration of Td I and Td II structures gives rise to blue luminescence without any birefringence and this diamond is opaque to ultraviolet light. The interpenetration of octahedral and tetrahedral structures similarly gives rise to yellow luminescence and the crystal shows structural birefringence and is partially opaque to ultraviolet light. The lamellar intertwinning of two structures Oh I and Oh II is assumed to produce a diamond which is both non-luminescent and transparent to ultraviolet light. This crystal has been identified as those which show streaky birefringence.

Some evidences in support of the theory mentioned above have also been adduced later. These evidences have been found in the results of investigations on infra-red and Raman spectra, X-ray reflections, and luminescence. As regards the infra-red absorption spectrum of diamond, it has been pointed out that according to Placzek's (1934) theory, in the case of an octahedral symmetry the three-fold degenerate vibration should be active in the Raman effect, but inactive in the infra-red spectra. Actually in the case of certain types of diamond the 1332 cm^{-1} line appears both in the Raman spectra as well as in infra-red absorption spectrum showing a tetrahedral symmetry of the crystal, while in other types the line appears only in the Raman effect and is absent in the infra-red spectrum. The results reported by Robertson and Fox (1930) have been cited in this connection. On careful examination of the results, one can easily find that the correspondence between the infra-red band at 8μ and the line 1332 cm^{-1} is not enough to show that they are produced by the same vibration. because 1332 cm^{-1} corresponds only to about 7.5μ and not to 8μ . Further the line 1332 cm^{-1} is extremely sharp while the band at 8μ is broad. Hence it is hardly likely that the band at 8μ is produced by the same vibration as the line 1332 cm^{-1} . Although Krishnan and Ramanathan (1946) tried to show that the 1332 cm^{-1} vibration is active in the infra-red by mentioning that this frequency occurs half way

down the absorption minimum at this place in the infra-red absorption spectrum, Sutherland (1946) criticised their statement and pointed out that the frequency of absorption minimum can never be considered to be an absorption frequency. As regards Piaczek's theory regarding the selection rules for the appearance of a line in the infra-red and the Raman spectra, it is the symmetry of the distribution of electric charges in the vibrating molecule which is usually taken into consideration. It is well known that if a centre of symmetry is maintained during a mode of vibration, the corresponding line is allowed only in the Raman effect and forbidden in the infra-red. The relative orientations of the angular momenta of the electrons around the oscillating atoms can hardly affect either the distribution of electric charges or the magnitude of electric moment generated during oscillation. Hence it is difficult to understand how in the case of the two structures Td I and Oh I there can be any difference as far as the selection rules mentioned above are concerned, because the distribution of electric charges is exactly the same in both Td I and Oh I structures.

As regards evidence from X-ray reflection from diamond, the intensities of Laue spots obtained from different types of diamond have been compared by Krishnan (Raman, 1943) and it has been shown that the Laue spots due to weakly blue luminescent diamond are weaker than those due to strongly blue luminescent diamond. This fact has, again, been explained on the assumption that the former diamond possesses a perfect structure of tetrahedral type and, therefore, extinction is very great, while in the latter type there is a mixture of Td I and Td II structures which produces strains giving rise to small variations in the spacings and consequent increase in the intensity of X-ray reflections. Hariharan (1944) also measured the intensity of Bragg reflection from (111) plane of a large number of diamond crystals of different types and found a correlation between the intensity of X-ray reflection with that of fluorescence exhibited by these crystals. It has to be pointed out, however, that the presence of laminae each containing several planes of the same spacing is necessary for producing any appreciable intensity in X-ray reflection. Such mosaic structure can hardly be produced by the interpenetration of Td I and Td II structures and in fact, it has been pointed out in the original theory that no stress is produced by such interpenetration. These crystals, on the other hand, show birefringence of widely varying magnitudes. Hence the strain present in the crystals is much too large to be accounted for on the assumption, that it is produced by interpenetration of Td I and Td II structures, and it is probably produced by some other causes during crystallisation of the molten carbon. These facts, therefore, do not seem to furnish any strong evidence in support of the new theory.

The main evidence adduced in support of this new theory of diamond structure consists in the results of investigations on the luminescence of different types of diamond carried out by different workers. The work was

systematically started first by P. G. N. Nayar (1941a, 1941b). He studied the fluorescence spectra of about a dozen diamond crystals of different types at different temperatures ranging from 200°C down to the temperature of liquid oxygen. He observed a sharp fluorescence band at 4156Å accompanied by a set of diffuse bands at 4278, 4387, 4514 and 4613Å with a continuous spectrum superposed on these and extending up to 6300Å. These characteristic spectra were observed in all the crystals studied by him, but the intensities were different in different crystals and the ratio in the two extreme cases was of the order of 10,000 to 1. He also used monochromatic exciting radiation and found that the whole fluorescent spectrum was excited by radiation of any wavelength less than 4156Å. The intensity of the bands, however, increased when the exciting line was of wavelength 4156Å and the bands vanished when the exciting wavelength was slightly larger than 4156Å. It was concluded from the results observed by him that the fluorescence was not due to any impurities, but was probably connected with the structural perfection of diamonds. As regards the temperature dependence of the fluorescence spectra, he observed that as the temperature rises the bands become broader unsymmetrically and shift towards longer wavelength and at temperature above 200°C, the fluorescence disappears completely.

These investigations were further extended in the case of a very large collection of diamonds by (Miss) Anna Mani (1944), who studied both the absorption and fluorescence spectra of 32 diamonds of different types. Some of the diamonds studied by her were of Type II. She confirmed the observations of Nayar that the intensity of fluorescence varies enormously from crystal to crystal, although the fluorescence spectrum has almost the same structure in the case of all the different types of diamonds. Type II diamond was found to produce extremely feeble fluorescence spectra. She also studied the absorption spectra of all these diamonds at different temperatures and found that in the case of all the different types of diamond at about -180°C, the whole absorption spectrum starting from 4152Å was a mirror image of the fluorescence spectrum. She further deduced some frequencies from those of the observed fluorescence and absorption bands and these were assumed to be those of oscillations of the diamond lattice. Recently, Chandrasekharan (1948) studied the integrated intensity of the fluorescence band 4156Å of diamond at different temperatures and came to the conclusion that only the width of the band changes with the change of temperature and that its integrated intensity remains almost constant at different temperatures.

From a careful scrutiny of all the spectra reproduced by Nayar, Anna Mani, and Chandrasekharan it was found that the interpretation given by the authors to the results obtained by them was not quite satisfactory in all the cases, and hence a re-investigation of this problem was thought worthwhile. A collection of diamonds of different varieties was, therefore, made from the local market and in this matter the firm of Messrs Benud Behari Dutt & Sons co-operated whole-heartedly. They allowed the crystals to be

examined in the laboratory of the Indian Association for the Cultivation of Science and changed for better ones if not found suitable. In this manner it was possible to collect about a dozen crystals belonging to different types varying from highly fluorescent rose diamond to the ultraviolet transparent type. Two crystals of the latter type were obtained, one having a light pinkish colour while the other was a thin small crystal absolutely colourless. The absorption and fluorescent spectra of some of these crystals have been studied at different temperatures. First of all, the integrated intensity of the fluorescence band at 4156\AA has been determined at different temperatures for six of these diamonds, the intensity being compared with that of Raman line excited by 4358\AA line of mercury. Next, the absorption bands at different temperatures of these diamonds have been studied in the visible region. The birefringence exhibited by these crystals at room temperature and at 275°C has also been studied. Finally, in the case of one of these diamonds the variation in the intensity of the fluorescence band at 4156\AA with the change of wavelength of the monochromatic exciting line has been investigated. These results have been compared with those reported earlier and discussed in the light of the theory mentioned earlier and attempts have been made to offer an alternative explanation.

EXPERIMENTAL

In a series of experimental investigations special stress was laid on measurement of relative intensities of fluorescence spectra at different temperatures in the case of different crystals of diamond. Previous workers compared these intensities, taking either the intensity of 4046\AA line of mercury as a standard or by keeping the time of exposure constant in all the cases and estimating the blackenings produced by fluorescence spectra in the different cases. It was, however, considered essentially necessary to find out a true standard which could be used to compare the relative intensities of fluorescence in the case of different crystals. The intensity of the Raman line excited by 4358\AA line of Hg was found to be such a suitable standard. Fortunately, in the case of these specimens of diamond studied in the present investigation this Raman line was quite strong and was not masked by the fluorescence spectra in any case, although in the case of two of the crystals there was a weak fluorescence band superposed on this Raman line. This, however, did not present a very serious difficulty in estimating the intensity of the fluorescence band at 4156\AA relative to that of the Raman line and this method was probably much more reliable than that adopted by previous workers. The complete mercury arc spectrum beyond 4156\AA towards the ultraviolet region was used to excite fluorescence and a Fuess glass spectrograph was used to photograph the fluorescence spectra. In all the cases the direction of observation was along the normal to the (111) face and the mercury arc was placed in front of the crystal slightly on one side so that the fluorescence from the region of the crystal immediately behind

its front surface could be observed. Thus the 4156\AA band was not weakened very much, although there is an absorption band exactly at this position. For studying these spectra at low temperatures, the technique used by the author for the investigations of Raman spectra at low temperatures was employed. The crystal was suspended inside a transparent Dewar vessel and liquid oxygen was introduced in this vessel through a double walled glass tube entering through the cork at the mouth of this vessel and the surface of the liquid oxygen always remained just below the crystal. The crystals were mounted one by one in a copper frame part of which was kept immersed in the liquid oxygen so that in each case the crystal was in contact with copper at the temperature of liquid oxygen and was not actually immersed in the liquid oxygen itself. The temperature was measured with a pentane thermometer. A sketch of this arrangement is given in Figure 1. The dimensions of the diamonds used are as follows:

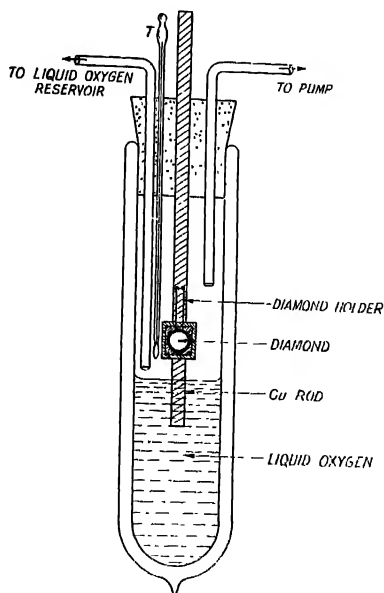


FIG. 1

D I (rose diamond) — $9\text{ mm.} \times 7\text{ mm.} \times 1.5\text{ mm.}$, D II — $8\text{ mm.} \times 5\text{ mm.} \times 1.2\text{ mm.}$, D III — $5\text{ mm.} \times 5\text{ mm.} \times 1\text{ mm.}$, D IV (triangular plate) — base, 11 mm. , height, 8 mm. , thickness, 1.5 mm. , D V — $10\text{ mm.} \times 8\text{ mm.} \times 2\text{ mm.}$ and D VI — $14\text{ mm.} \times 12\text{ mm.} \times 2\text{ mm.}$

For studying the luminescence at higher temperatures, the crystal was suspended inside a cylindrical electric heater provided with a glass window,

In order to measure the integrated intensity of the 4156 \AA band relative to that of the Raman line excited by 4358 \AA line, microphotometric records of the band and the Raman line were taken with a Kipp and Zonen type self-recording microphotometer and the intensities were estimated after taking into account the intensity of the background with the help of blackening-log intensity curves. These latter curves were drawn with the help of intensity marks taken with a standard tungsten ribbon lamp and using different known widths of the slit of the spectrograph. The integrated intensity of the band was determined by calculating the intensities at five points in the band and finding the area of the peak obtained by plotting intensity against width.

For studying the absorption spectra in the visible region, an ordinary 100-watt straight-coil filament lamp was used as the source of light and for studying these spectra at low temperatures, the technique used for studying the fluorescence spectra at low temperatures was employed. In the case of particular crystal D VI monochromatic exciting bands of different wavelengths in the neighbourhood of 4156 \AA , towards the shorter wavelength side were used to find out whether the intensity of the fluorescence band at 4156 \AA depended on the wavelength of the exciting line. A 100-Watt straight coil filament lamp was used as source of light and a Fuess glass spectrograph with a slit in the plane of the photographic plate was used as the monochromator.

The birefringence patterns of the six crystals mentioned above were photographed keeping the crystals first at room temperature and then at about 275°C . Only those portions of the crystals which had opposite parallel faces were used for this purpose, the other portions being covered with suitable black screens. Each of the specimens was mounted in a cylindrical electric heater with its mouths open. The birefringence pattern of one of the crystals was photographed first without passing any current through the heater. A suitable current was then passed through the heater to obtain a temperature of 275°C near the crystal and again the birefringence pattern was photographed. This was repeated for all the six crystals. A pair of large Nicol's prisms made by Messrs. Adam Hilger Ltd. was used in the crossed position and a parallel beam of light was obtained from a point source with the help of a good lens. An ordinary camera was used to photograph the patterns.

RESULTS

(a) *Fluorescence spectra at different temperatures*

The fluorescence spectra observed at different temperatures with the six crystals of diamond are reproduced in Plates XIX—C. In exciting these spectra unfiltered mercury arc light was used, and therefore, these spectra also contain the Raman lines excited by the Hg lines 4046 \AA and 4358 \AA . It can be seen from these spectrograms in Figures 2-7, Plates XIX A, B, C, that the nature of the fluorescence spectrum is different for different crystals, as observed by previous workers also. The band at 4156 \AA is present in all the spectrograms,

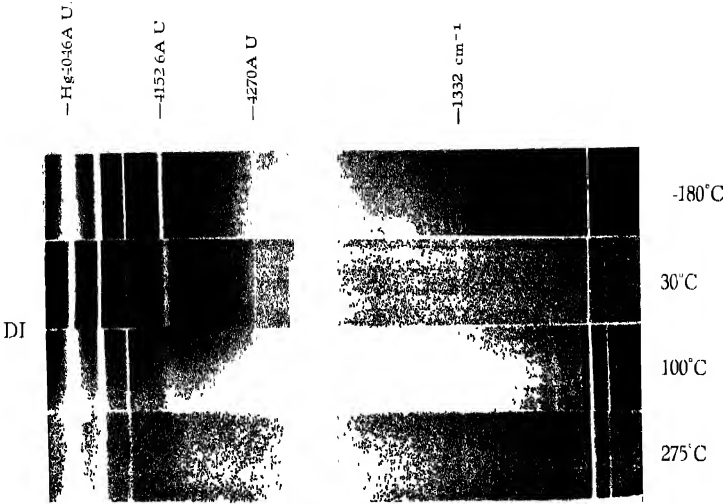


Fig. 2

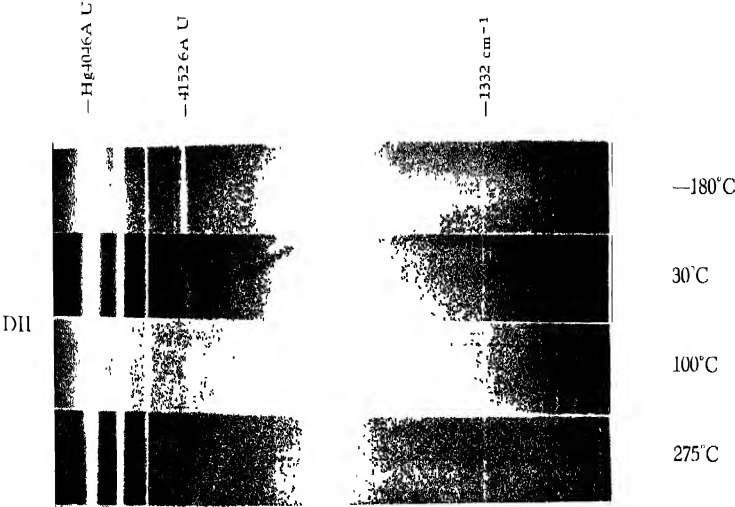


Fig. 3

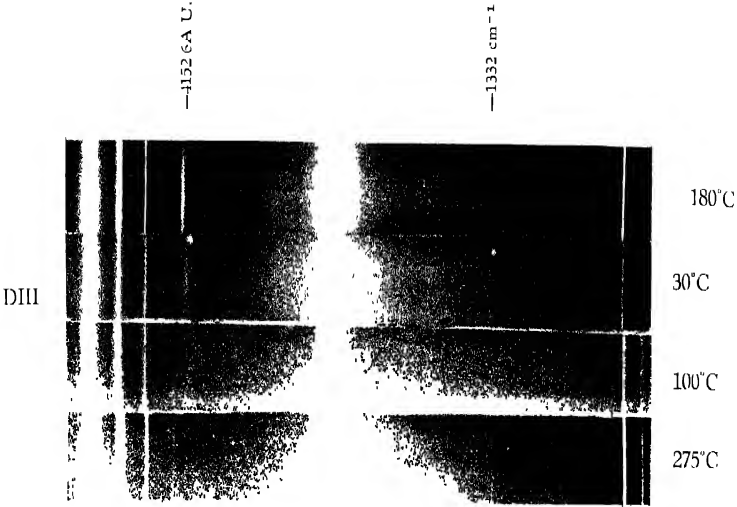


Fig. 4

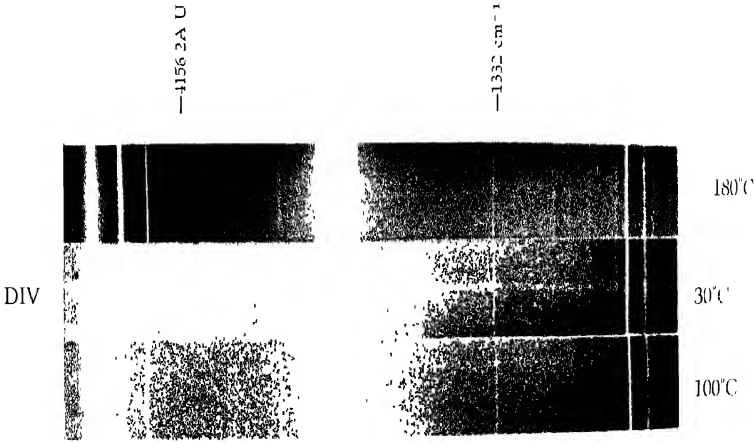


Fig. 5

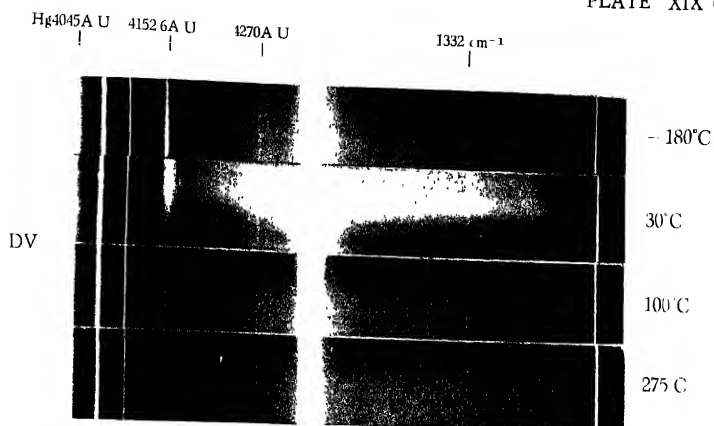


Fig. 6

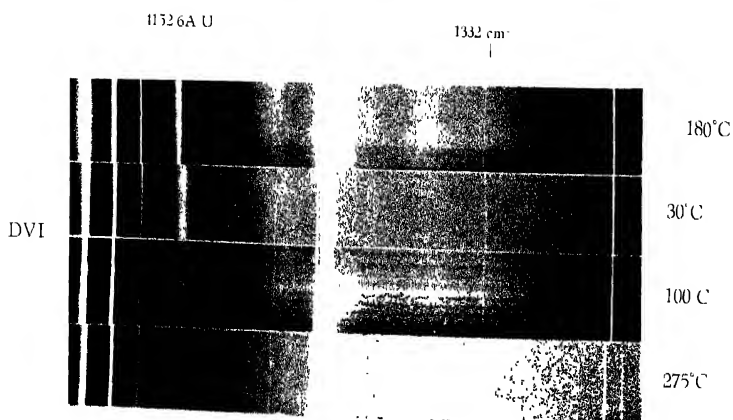


Fig. 7

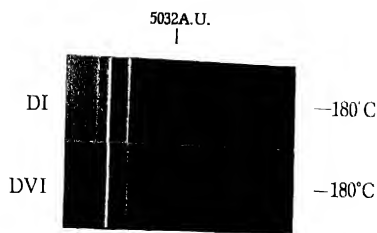


Fig. 8

but with different intensities. Even in the case of D IV, which is a diamond transparent to light of wavelength larger than 2250\AA there is a feeble band at 4156\AA at room temperature. Excepting D IV, all the remaining five crystals D I, D II, D III, D V and D VI are opaque to ultraviolet light in the region of about 3000\AA and they exhibit a few fluorescence bands on the longer wavelength side of the band at 4156\AA . The crystals D II and D VI are slightly pinkish in colour and the latter shows at -180°C an extra band at 5032\AA as shown in Figure 8, Plate XIXC. In the case of D V also, this band is just visible at -180°C . The broad bands accompanying the band at 4166\AA have their centres at 4278\AA , 4378\AA , 4552\AA and 4648\AA respectively in the case of all the five crystals mentioned above, D V shows a peculiar phenomenon, *e.g.*, that one half of the crystal produces the fluorescence bands with great intensity, while the other half produces much feebler fluorescence, although the intensity of the Raman line 1332 cm^{-1} is the same in case of both the halves.

The change of temperature of the crystals brings about changes in position, intensity and width of the bands. In all the cases the 4156\AA band observed at room temperature is found to shift exactly to 4152.6\AA when the crystal is cooled down to -180°C . This can be seen from the Figures 2-7. The other bands on longer wavelength side shift by different amounts towards shorter wavelengths. The band at 4278\AA shifts to 4270\AA at -180°C and this shift seems to be larger than that of the band 4156\AA . The shift of the band at 4648\AA is also the same as that of the 4278\AA band as can be seen clearly from Figure 7.

All the bands become narrower at -180°C and become gradually broader at temperatures higher than room temperature. In the case of D V, there is continuous fluorescence in the region between 4156\AA and 5200\AA besides the bands mentioned above.

Quantitative data regarding the changes in the integrated intensity of the band at 4156\AA with the change of temperature of the crystals are given in Table I, in which the data for the three temperatures 100°C , 30°C and -180°C are given. In each case the ratios of the integrated intensities of the Raman line 1332 cm^{-1} excited by 4358\AA at the two temperatures -180°C and 30°C and also at the two temperatures 30°C and 100°C are given. Similar data have been included also for the band at 4156\AA . Hence the absolute ratio of intensities of this band at the three temperatures can be calculated. The calculated relative integrated intensities of the band at -180°C , 30°C and 100°C , assuming in each case the intensity at -180°C to be 222 are given in Table II. The curves obtained by plotting logarithms of these intensities against inverse of temperature are reproduced in Figure 9. As no point has been obtained between -180°C and 30°C , it has been assumed in drawing these curves that they are continuous between 30°C and -180°C . It will be seen from Figure 9 that the intensity increases at lower temperatures and diminishes

at higher temperatures in all the cases. The rate of increase, however, falls off at lower temperatures and in the case of D V and DVI, this rate is very

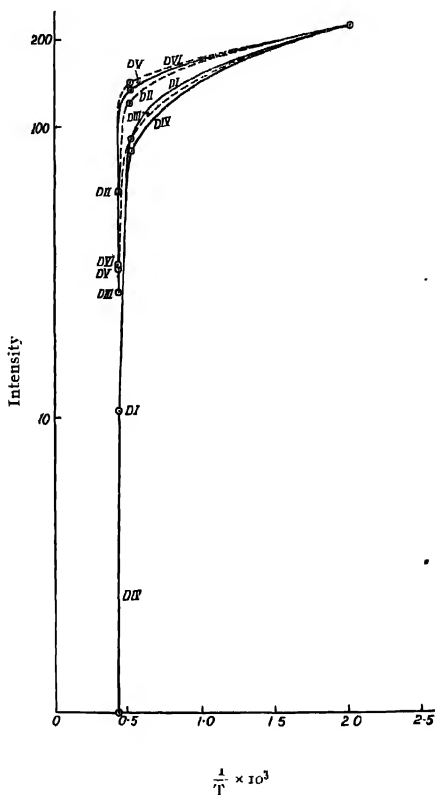
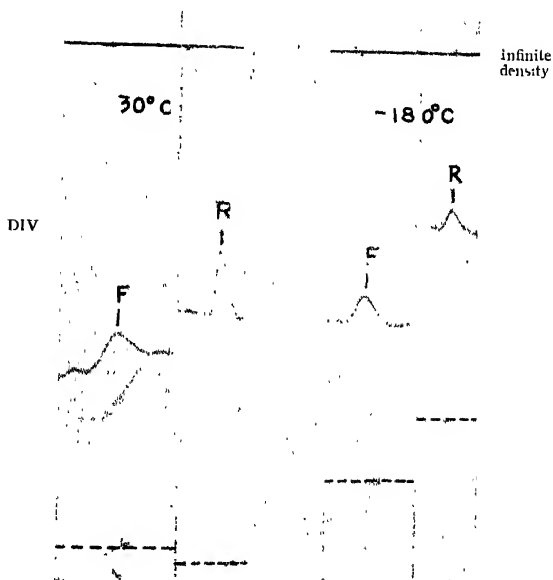
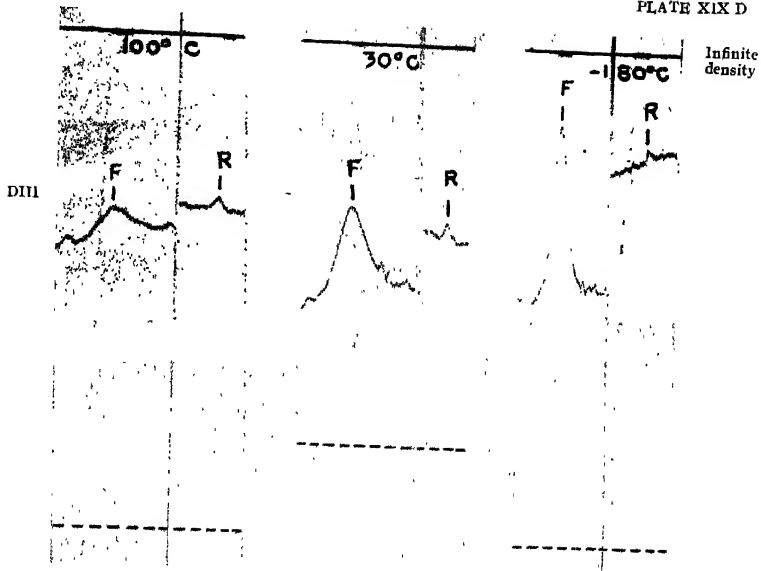


FIG. 9

small at -180°C . These results will be discussed later. Some microphotometric records are reproduced in Plate XIX D.

Plates XIX A, B, C show that except in the case of D VI, all the fluorescence bands disappear completely at 275°C . In the case of D VI, the band at 4156 \AA persists with a small intensity at 275°C . It can also be seen that the bands become only slightly broader before they just disappear, leaving no trace of any continuous background. These results are thus contradictory to those reported by Chandrasekharan (1948) according to whom the integrated intensity remains constant at all temperatures and only the width of the bands changes with temperature.



F—Fluorescence band at 4156\AA R—Raman line

FIG. 10

TABLE I

Diamond No.	Temp.	I 4156 Å (arbitrary unit)	I 1332 cm ⁻¹ (arbitrary unit)	I-180		I 30°	
				I 30°		I 100°	
				4156 Å band	1332 line	4156 Å band	1332 line
D I	100°C	23	3.5			5.4	0.63
	30°C	125	2.2	2.22	0.91		
	-180°C	277	2.0				
D II	100°C	9	2.0			3.67	1.85
	30°C	33	3.7				
	-180°C	30	1.8	91	0.49		
D III	100°C	23	2.1			3.48	1.05
	30°C	80	2.2				
	-180°C	134	1.5	1.68	0.68		
D IV	100°C	0	4				
	30°C	9	4				
	-180°C	13	5	1.44	0.55		
D V	100°C	44	4.0			12.73	3.5
	30°C	560	14.0				
	-180°C	234	3.6	0.41	0.25		
D VI	100°C	80	6.4			3.75	87
	30°C	300	5.6				
	-180°C	500	6.0	1.66	1.07		

The advantage of taking the intensity of the Raman line as a standard for comparing the intensities of the 4156 Å band at different temperatures can be seen at once from a glance at Figures 2 and 3, Plate XIX A and Figure 7, Plate XIX C. For instance, the Rayleigh line 4108 Å is much less intense in the spectrogram for 30°C than in the spectrogram for -180°C, but the Raman line 1332 cm⁻¹ is more intense in the former than in the latter spectrogram. Hence if any of the undisplaced Hg lines would be taken as a standard for comparing the intensities of the band at 4156 Å, results

TABLE II

Diamond No.	Relative Intensities of 4156 Å band.		
	-180°C	30°C	100°C
D I	222	91	16.6
D II	222	120	60.5
D III	222	90	27
D IV	222	84	0
D V	222	135	32.4
D VI	222	143.7	33.4

quite different from those given in Table I would be obtained and such results would be thoroughly unreliable. The method adopted in the present paper has another advantage, *e.g.*, the efficiency of fluorescence of the different crystals can also be estimated roughly. This is possible because, the same blackening-log intensity curve has been used to determine the intensity of the Raman line 1332 cm^{-1} in all the cases and also a single similar curve has been used to determine the intensity of the band at 4156 Å in all the cases. Hence the ratio of the intensity of the fluorescence band 4156 Å to that of the Raman line 1332 cm^{-1} calculated for any of the crystals at any temperature can be compared with such a ratio obtained in the case of any other crystal at the same temperature. Such results are given in Table III. These calculated ratios are, however, not the actual ones but their relative values give the relative fluorescence efficiencies of the crystals in the band 4156 Å . Hence the values given in the last column of Table III represent these fluorescence efficiencies multiplied by a constant K .

TABLE III

Diamond No.	Temperature	$K \times I_f / I_R$
D I	30°C	57
D II	"	9
D III	"	36
D IV	"	1
D V	"	40
D VI	"	54

As regards the influence of temperature on the intensities of the bands 4278 Å, 4378 Å, 4552 Å and 4648 Å, it can be seen that except in the case of D III and the D IV, in all other cases, the intensities of these bands relative to that of the Raman line increases when the crystals are cooled down from 30°C to -180°C. In the case of D IV, these bands are absent at both the temperatures and in the case of D III, the intensities of the bands do not seem to increase appreciably with the lowering of temperature of the crystal.

The spectrograms also do not reveal the presence of the sharp lines in the fluorescence spectra, although such lines were observed by (Miss) Anna Mani (1944) in the case of a few crystals of diamond studied by her. Thus these lines do not seem to be produced by the diamond lattice itself and may be due to impurities.

(b) Birefringence at different temperatures.

It can be seen from the birefringence patterns reproduced in Plate XIXE that birefringence does neither diminish nor disappear at a temperature at which the fluorescence disappears almost completely. As regards the nature of birefringence shown by different types of diamonds, it is clearly seen that D III, which is a diamond showing blue luminescence, exhibits a regular birefringence pattern. In the case of D IV, which is a diamond transparent to ultra violet region up to 2250 Å, the birefringence pattern does not show any streaky character as can be seen from Plate XIXE. The restored light extends uniformly over the major portion of the crystal excepting a small region. These results do not agree with fact observed by Raman and Randall (1944) that all the crystals of Type II show streaky birefringence. Again it can be seen from Plate XIXE that percentage of the area showing birefringence in the case of D III is less than that in the case D V and it is of the same order as that in D II. Further the percentage is almost the same in the case of the two crystals D II and D VI. The relative fluorescence efficiencies of the two crystals D II and D VI at the band 4156 Å are, however, widely different from each other. The significance of these results will be discussed later.

(c) Monochromatic excitation of fluorescence.

The spectrograms obtained by using incident light consisting of bands about 30 Å broad in the region of the 4046 Å are reproduced in Figures 12(a), 12(b) and 12(c), Plate XIXE. The wave-lengths of the centres of the bands are 3990, 4046 and 4110 Å respectively. It can be seen from Figures 12(a) and 12(b) that in both the cases the fluorescence band at 4156 Å as well as its broader companions in the visible region are present, although with small intensity. These fluorescence bands are thus excited by the bands of wavelengths 3990 and 4046 Å respectively. In Figure 12(c) the

exciting band is at 4110 \AA but the fluorescence bands are almost absent, excepting the band at 4156 \AA which seems to have been excited very feebly. It thus appears that the intensity of fluorescence diminishes when the wave-length of the exciting band is increased from 4046 \AA to 4110 \AA , although the latter wavelength is shorter than 4156 \AA . This fact was observed by Nayar (1941a) also, but he did not discuss its significance. It will be seen in the next section that there is a broad absorption band with its centre at about 4045 \AA in the absorption spectrum of diamond. The facts mentioned above indicate that when any portion of the exciting band has wavelength coinciding with that of any portion of the broad band at 4045 \AA , the intensity of the fluorescence bands excited by the band is increased. In fact the efficiency of a monochromatic line at 4046 \AA in exciting the fluorescence band at 4156 \AA is very large as can be seen from Figure 12(d) in which light from a mercury arc filtered through highly concentrated solution of sodium nitrite was used as the incident light. Although all the lines of wavelength shorter than 4046 \AA have been cut off and the intensity of the line 4046 \AA has been diminished considerably by the filter, yet the fluorescence band at 4156 \AA is distinctly visible in the spectrogram. Evidently, the line 4046 \AA is responsible for exciting this band, because the lines 4077 and 4108 \AA are much weaker.

Again, from a comparison of Figures 12(a) and 12(b), it can be seen that when the mean wavelength of the exciting band changes from 4046 \AA to 3990 \AA , the intensity of the fluorescence band diminishes considerably, this diminution being less in the case of the fluorescence band 4156 \AA than in the case of the other bands on the longer wavelength side. Thus the intensity of the latter bands with respect to that of the band 4156 \AA seems to depend on the wavelength of the exciting band in the region between 3990 \AA to 4110 \AA .

(d) *Absorption Spectra in the Visible Region.*

The absorption spectra of all the six diamonds mentioned earlier were investigated in the visible region both at about 30°C and at -180°C respectively and in the case of D II at 275°C also. Some of the spectrograms are reproduced in Fig. 13, Plate XIX G. No absorption band in the visible region was observed in the case of D IV inspite of repeated trials, although the fluorescence band at 4156 \AA is present with small intensity in luminescence spectrum of this diamond. Evidently, the absorption at 4152.6 \AA is too small to be recorded even at -180°C in this case. Both the diamonds D II and D VI show an intense absorption band at 4156 \AA at room temperature accompanied by a few other bands on the shorter wavelength side. The band at 4156 \AA shifts to 4152.6 \AA and becomes a little sharper, when the crystals are cooled down to -180°C . These observations are in agreement with those of Nayar (1941b). In the case of the other three diamonds D I,

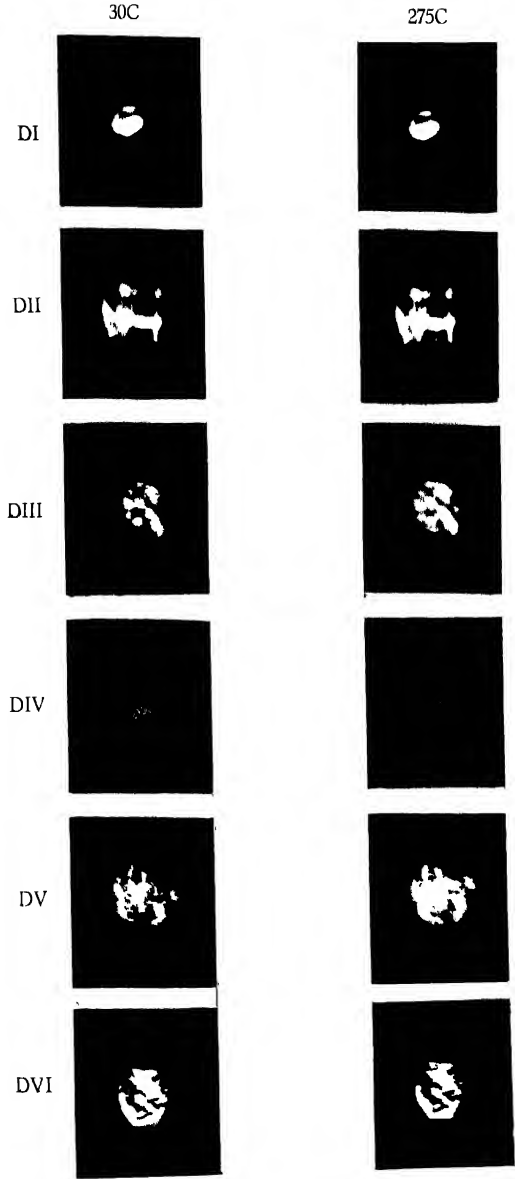


Fig. 11

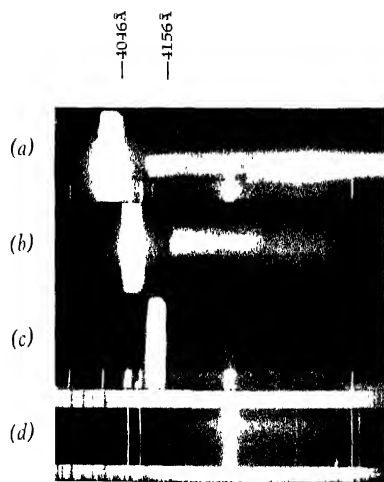


Fig 12

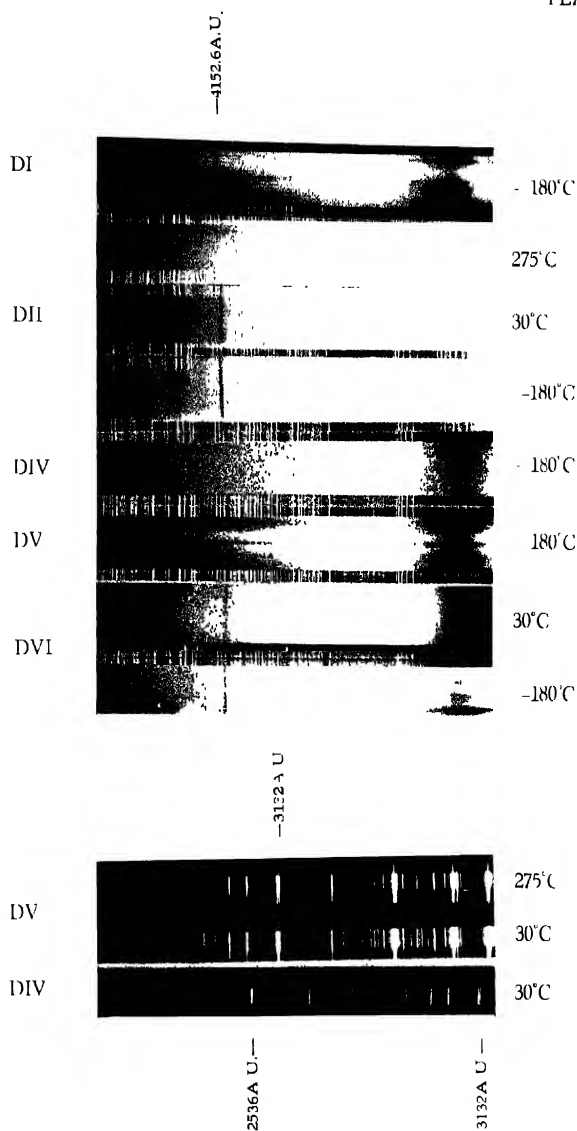


Fig. 13

Absorption spectra

D III and D V at room temperature, the absorption band at 4156 \AA is found to be very feeble, but at a temperature of about -180°C the band shifts to 4152.6 \AA and becomes sharper and more intense as can be seen from the spectrograms reproduced in Plate XIX G. The band with its centre at about 4045 \AA observed in the case of both the diamonds D II and D VI at 30°C shifts to 4041 \AA at -180°C . This band is found to be more diffuse in the case of D I, D III and D V. When D II is heated to 275°C the absorption band at 4156 \AA disappears. In the case of D I, D III and D V also, the intensity of this band at 30°C is very small and the band disappears at about 100°C . Thus even in the case of those diamonds which show an intense absorption band at 4156 \AA at the room temperature, this band disappears at about 275°C . These results are in agreement with those observed by Nayar (1941b).

The influence of temperature on the intensity of continuous absorption beyond 3000 \AA towards shorter wave-lengths has also been studied in the case of D II. The mercury lines transmitted in this region by the diamond at 30°C and 275°C are shown in Fig. 13. It can be seen that the temperature has very little influence on the position of the long wavelength edge of continuous absorption in this region. The transparency of D IV to Hg lines of wavelength shorter than 2536 \AA is clearly indicated in the last spectrogram in Fig. 13. It is evident that the crystal belongs to Type II and the other five diamonds of Type I remains different from D IV even at 275°C .

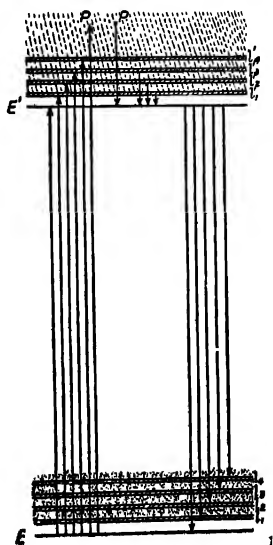


FIG. 14

It can be seen from the spectrogram for D II that there is very little absorption in the region between the band 4152.6 \AA and band at 4045 \AA , and in the region beyond 4045 \AA towards the shorter wavelength there is continuous absorption with some broad maxima separated from each other. These observed facts are in agreement with the scheme of energy levels shown in Fig. 14 and deduced from the properties of the observed fluorescence and absorption bands. The fact that the intensity of fluorescence diminishes abruptly if the wavelength of the exciting band increases from 4046 \AA to about 4110 \AA is also explained satisfactorily. This happens because the absorption of light of wavelength at and in the neighbourhood of 4110 \AA is very small and consequently intensity of fluorescence produced by transitions from the level E' to the sub-levels of E is very small. The absorption spectra also show that light of any wavelength shorter than about 4045 \AA is absorbed in different degrees depending on the wavelength contrary to the hypothesis put forward by Nayar (1941b) that only light of energy corresponding to that of the band at 4156 \AA enhanced by the energies of vibrations of the lattice is absorbed. In fact, the energy diagram shown in Fig. 14 conforms to the theory put forward by Seitz (1938) according to which the electronic energy levels in semi-conductors consist of the Bloch-Wilson bands together with narrow continuous bands lying in the forbidden region between the former bands.

It is further observed that at the lower temperature the absorption band at 4152.6 \AA is much sharper than the fluorescence band of the same wavelength. Hence if a thick crystal be used, the fluorescence band may appear as a doublet because its core will be absorbed owing to self-reversal and the edges will be transmitted freely. This band has actually been observed to consist of a doublet with its centre of gravity at 4152 \AA in the case of a large number of diamonds of fairly large size by (Miss) Anna Mani (1944). She has interpreted the results on the assumption that the band itself is originally a doublet. Actually, however, the appearance of the doublet is due to self reversal of the band. As thin crystals were used in the present investigation and they were irradiated from the front, the fluorescence band at 4152.6 \AA was always found to be a single band and not a doublet as can be seen from Plates XIX A, B, and C.

DISCUSSIONS ON THE ORIGIN OF FLUORESCENCE IN DIAMOND

The variations in intensities of the fluorescence band at 4156 \AA at different temperatures observed in the case of the six specimens of diamond indicated in Fig. 9 show that in all these cases the intensity increases as the temperature, of the crystal is lowered and when the temperature is raised above room temperature the intensity gradually diminishes upto about 160°C , but the rate of diminution becomes higher at still higher temperatures, till the band disappears at about 275°C . Since the birefringence

exhibited by the crystals persists at 275°C, this disappearance is a purely temperature quenching. Such an effect is observed in the case of almost all phosphors activated by chemical impurities and is caused by the presence of a large activation energy for radiationless transition. The results reported by Williams and Eyring (1947) in the case of Zn_2SiO_4 phosphor activated by manganese are similar to those observed in the present investigation. It is further observed that the absorption band at 4156 Å together with its companions of shorter wavelength disappears at about 275°C, although the continuous absorption starting from about 3000 Å persists at this higher temperature. Hence the presence of the former narrow absorption bands are necessary for the excitation of the fluorescence bands. These facts suggest that the narrow absorption bands are due to some impurities and the evidences discussed below show that these impurities are of chemical nature and they are not due to lattice defect produced by strain in the pure diamond lattice.

According to the theory put forward by Sir C. V. Raman (1944) slight inhomogeneity in the lattice in diamond of Type I produces these new absorption bands while in Type II large amount of strains cannot produce such an effect. This difference in the behaviour of the two types of diamond is attributed to the difference in the relative orientations of the resultant angular momenta of the two bonding electrons in the C-C bond. Those portions of the crystal of Type I which show birefringence should, therefore, exhibit very strong fluorescence and the intensity of fluorescence would be determined by the relative volumes of the inhomogeneous and isotropic parts in the crystal. Such exact correspondence between the intensity of fluorescence and the birefringence is not observed in all the cases. For instance, in the case of D II and D VI (Plate XIX E) the difference in the volume showing birefringence is not very large, but the intensity of fluorescence in the latter case is six times that in the former case as shown in Table III. Again, D V shows birefringence throughout its volume, while only a part of the whole volume of D VI is birefringent. The fluorescence, however, is more intense in the latter case than in the former. In fact, in the arrangement for photographing the fluorescence spectrum an image of the illuminated diamond was focussed on the slit of the spectrograph, in each case, but no discontinuity in intensity along the length of the bands corresponding to the discontinuity in birefringence was observed in any case. The discontinuity observed in the case of D V also does not correspond to the birefringence pattern exhibited by this crystal, as shown in Plate XIX E. Further, it is a fact that in certain diamonds of Type I, some portions which show strong fluorescence do not show strong birefringence and on the other hand, some portions showing strong birefringence do not exhibit fluorescence at all. Such instances can also be found in the results reported by previous authors. The birefringence and luminescence patterns of D 200 studied by

Sir C. V. Raman (1944) in Plate V of his paper, indicate that some portions not showing strong birefringence fluoresce strongly, and *vice versa*. Rendall (1944) studied the ultraviolet transparency of the same diamond and it can be seen from the photograph reproduced in Plate XXVI of the paper that the portion of the crystal not showing any luminescence in Plate V mentioned above is not quite transparent to ultraviolet light, and, therefore, this portion of the crystal is not of Type II. Hence strain has failed to produce luminescence in this portion of the crystal of Type I. Thus the presence of chemical impurities is to be postulated to explain the observed fluorescence. Such impurities may be so minutely dispersed in certain volumes of the crystal that there may not be any macroscopic strain, but local lattice defects will give rise to fluorescence. Similarly, in other portions of the crystal, larger amount of the impurity may produce visible striations and strong birefringence. This would account for the correspondence of birefringence and fluorescence in certain portions of the crystal.

The difference in the positions of the edge of the continuous ultraviolet absorption by the two types of diamond strongly indicates the presence of chemical impurity in diamond of Type I. The absorption starts at about 3000 \AA in this type, while in Type II it starts at 2250 \AA . If the absorption in the former case would be the characteristic of the C-C bond, the strength of the bond would be slightly different from that in Type II. The frequency of the Raman line at 1332 cm^{-1} is, however, exactly the same in the two cases. Hence the strength of the C-C bond in the two cases is exactly the same and the difference in the absorption spectra is due to the presence of chemical impurity in diamonds of Type I and its absence in diamonds of Type II. The fluorescence band at 5032 \AA is due to a different chemical impurity as this band is not present in all crystals of Type I. This band cannot be due to Oh I structure, because no amount of strain can produce any fluorescence in this crystal as can be inferred from the fact that diamond of Type II showing streaky birefringence does not exhibit fluorescence. Further, if the interpenetration of octahedral and tetrahedral structures would produce this fluorescence in diamond of Type I, there would be correspondence between fluorescent laminae and those showing alternately transparency and opacity to ultraviolet light of wavelength 2300 \AA . No such general correspondence has ever been established. The observations made by Blackwell and Sutherland (1949) show that even some diamonds of Type II exhibit yellow luminescence. Evidently, this is not due to interpenetration of Type I and Type II structures, because in that case these diamonds would show absorption in the region of 3000 \AA . This fact indicates clearly that some type of impurity producing absorption in the region of 3000 \AA is absent in this type of yellow luminescent diamond and another type of chemical impurity produces the yellow luminescence without changing the ultraviolet absorption.

There is another property of the absorption and fluorescence bands which shows that strain has nothing to do with the fluorescence exhibited by diamonds of Type I. The position of the absorption and fluorescence band in the region of 4156 \AA is determined by the temperature alone and at a particular temperature, it is the same for different crystals showing different degrees of birefringence. Evidently, the position of energy level of the chemical impurity depends on interatomic distances which are determined by the temperature of the crystal.

The photo-conductivity of diamond of Type I is generally much less than that shown by diamond of Type II, as shown by Robertson, Fox and Martin (1934). This cannot be due to presence of laminae in Type I and their absence in Type II, because the latter show streaky birefringence. The difference may be due to presence of chemical impurity in Type I, which entraps the ejected electrons moving through the lattice. Further, the radiations in the region 2300 \AA , which are most effective in producing photo conductivity, are absorbed by a thin layer on the surface in crystals of Type I.

Robertson, Fox and Martin (1934) have pointed out that all diamonds of Type I having origin in widely different parts of the world show the same absorption band at 4156 \AA . This is not a genuine difficulty, because diamond must have crystallised from a melt contained in a particular environment and it is not unlikely that a common impurity has entered into the lattice in varying amounts in all the crystals. In exceptional cases, when this impurity was absent, diamond of Type II was formed. The streaky birefringence exhibited by diamond of this type may be due to the fact that just before crystallisation of the melt, the formation of C-C bonds was started and there was sudden contraction of the volume which produced standing ultrasonic waves in the solidifying mass. These waves were frozen in when the crystallisation was complete. In the case of the pure melt, the strata of compression and rarefaction were parallel and such a diamond shows streaky birefringence. In case any impurity was present, the waves were distorted, the distortion depending on the nature and quantity of the impurity.

ACKNOWLEDGMENT

The author is indebted to Prof. S. C. Sirkar for his kind interest and helpful suggestions during the progress of the work and to Prof. M. N. Saha, F.R.S., for his kind permission to use the microphotometer in his laboratory at the University College of Science, Calcutta.

INDIAN ASSOCIATION FOR THE CULTIVATION OF SCIENCE,
210, BOWBAZAR STREET, CALCUTTA.

REFERENCES

- Anna Mani (Miss), 1944, *Proc. Ind. Acad. Sc.* **19A**, 231.
- Blackwell, D. E. and Sutherland, G. B. B. M., *Jour. de Chimie Physique*, **46**, 9.
- Chandrasekharan, V., 1948, *Proc. Ind. Acad. Sc.*, **27A**, 316.
- Hariharan, P. S., 1944, *Proc. Ind. Acad. Sc.*, **19A**, 261.
- Krishnan, R. S. and Ramanathan, K. G., 1946, *Nature*, **157**, 45, 582.
- Nayar, P. G. N., 1941a, *Proc. Ind. Acad. Sc.*, **13A**, 483
- „ „ 1941b, *Ibid*, **14A**, 1.
- Placzek, G., 1934, *Handbuch der Radiologie*, **6**, 2nd. Auf. Teil II, p. 231.
- Raman, Sir C. V., 1943, *Current Science*, **12**, 33.
- Raman, Sir C. V., 1944, *Proc. Ind. Acad. Sc.*, **19A**, 189.
- Raman, Sir C. V. and Rendall, G. R., 1944, *Proc. Ind. Acad. Sc.*, **9A**, 265
- Robertson, R. and Fox J. J., 1930, *Nature*, **26**, 279.
- Robertson, R., Fox J. J. and Martin, A. E., 1934, *Phil. Trans. Roy. Soc. A*, **232**, 482.
- Sutherland, G. B. B. M., 1946, *Nature*, **57**, 45, 582.
- Williams F. E. and Eyring, H., 1947, *J. Chem. Phys.*, **15**, 289.

ULTRASONIC VELOCITIES IN ORGANIC SOLUTIONS. I

By K. C. LAL

(Received for publication, June 20, 1950)

ABSTRACT. Measurements on supersonic velocities and compressibilities of solutions of different concentrations of benzoic acid in toluene and xylene at various temperatures are reported.

It has been found that velocity increases with dilution and the adiabatic compressibility increases with concentration. The ultrasonic velocity in solutions decreases with the increase in temperature.

INTRODUCTION

Parthasarathy (1936, 1937) in a series of papers reported determination of acoustic velocity in a variety of pure organic compounds and discussed the relation between the sound velocity and chemical constitution. Ram Pershad (1941) pointed out that the determination of velocities and compressibilities of the mixtures is expected to throw appreciable light on the state of cohesion as a function of molecular fields of liquids and also the structure of molecules as derived from the resulting intermolecular action. Wilson and Richards (1932) and Parthasarathy (1936) have reported some observations on supersonic velocities and compressibilities of mixtures. Ram Pershad (1941, 1942) has reported results on the determinations of velocity and adiabatic compressibilities in liquid mixtures and has also discussed their relationship with the constitution of the mixtures. With these considerations it was thought worthwhile to determine the ultrasonic velocity in solutions with a solid solute and to find out whether the laws which hold for liquid mixtures also hold for solid mixtures or not. In this paper results are reported for the solutions of benzoic acid in xylene and toluene. In the subsequent papers of this series, the results in other solvents will be reported and attempts will be made to correlate them with the chemical constitution of the constituents of the solutions.

EXPERIMENTAL

The method of the diffraction of light by sound waves originated by Debye and Sears (1932) in America and by Lucas and Biquard (1932) in France was employed in the present investigation.

The high frequency generator is based on the principle of energy feedback from the plate to the grid circuit. It is a simple standard high frequency valve oscillator employing a Hartley circuit modified to suit the conditions of the investigations.

The optical arrangement followed was similar to the one used in getting grating spectra. A monochromatic source of light was focused on the slit of a collimator and the parallel beam of light passing through a cell with plane parallel windows was focused by an objective on a photographic plate. As a source, a mercury arc with filters was used—4358Å and 5461Å of the mercury arc were used.

Since the thickness of the camera lens was considerable, the distance of lens to plate was measured from the centre of the lens to the photographic plate.

Determination of frequency:—The experimental arrangement once set up was not disturbed till all the solutions had been investigated. The solutions were changed by simply removing the cell and changing solutions. The constants of the apparatus therefore remained the same.

The calibration of the high frequency generator was carried out by a precision wavemeter supplied by Gambrell Bros., Ltd., London.

In order that the effect of damping of the oscillations by the superincumbent liquid might be negligible, the quartz crystal was suspended within less than half a centimetre below the surface of the liquid.

Temperature Control:—Ireyer Hubbard and Andrews, (1929) find that the temperature coefficient of sound velocity in liquids is fairly high; hence, attempt was made to record the observations with a little change of temperature as possible. The experimental vessel was surrounded with a double-spaced copper jacket which was surrounded by a wooden vessel. The upper and the lower portions were covered with wooden slabs. The upper slab contained three holes for inserting the crystal, the stirrer and the thermometer. The space between wooden jacket and the copper chamber was packed with asbestos to avoid loss of heat and also to fix the position of the vessel.

At low temperatures the copper vessel was filled with ice and the change in temperature was recorded by means of a sensitive thermometer of least count 0.1°C . This arrangement was found to give a fairly steady temperature during the course of the observations; the maximum variation in temperature being not more than 0.5°C .

RESULTS

Ultrasonic velocity was found out in the following solutions of different concentrations and at different temperatures:—

1. Benzoic acid in xylene.
2. Benzoic acid in toluene.

Kahlbaum's or Merck's purest xylene and toluene were employed. They were redistilled before actual use. Kahlbaum's purest benzoic acid was recrystallized and used as a solute.

Densities of the solutions were determined separately with a specific gravity bottle at the same temperature.

The velocities were calculated from the simple formula

$$\sin \theta = p \frac{\lambda}{\Delta}$$

where θ is the angle of diffraction which is measured by

$$\sin \theta = \frac{d}{\lambda}$$

where d is the distance between two diffraction fringes and λ is the distance between the centre of the camera lens and the plate.

λ is wavelength of light used.

Δ is wavelength of sound to be determined and p is the number of orders.

Both the 4358 Å and 5461 Å of the mercury lines were used as incident beams to check up against each other and the results obtained agree very well with each other.

The adiabatic compressibility was calculated from the relation

$$\sqrt{\beta \rho}$$

where v is the velocity of sound, ρ the density and β the adiabatic compressibility. The results are given in the following tables.

TABLE I
Benzoic Acid in Toluene
(a) Variation of Velocity with Concentration

No.	Concentration	Temperature °C	Density gms/c c.	Frequency Mcs /sec.	Wavelength mm.	Velocity metres/sec.	Compressibility $\times 10^6$
1	M/5	31.8	0.8678	4.25	0.2810	1198	81.36
2	M/10	31.8	0.8660	4.25	0.2823	1200	81.2
3	M/20	31.8	0.8643	4.25	0.2833	1204	80.8
4	Pure Toluene	30.9	0.8639	4.25	0.2847	1210	80.1
1	M/5	20		4.25	0.2856	1214	
2	M/20	20		4.25	0.2889	1228	
3	Pure Toluene	20		4.25	0.2930	1246	
1	M/5	10		4.25	.289	1232	
2	M/10	10		4.25	
3	M/20	10		4.25	.293	1245	
4	Pure Toluene	10		4.25	.300	1276	
1	M/5	3		4.25	.302	1282	
2	M/20	2.8		4.25	.306	1301	
3	Pure Toluene	3		4.25	.308	1308	

(b) Variation of Velocity with Temperature

No.	Concentration	Temperature °C	Velocity metres/sec.
1	M/5	31.8	1198
		20	1214
		10	1232
		3	1282
2	M/20	31.8	1204
		20	1228
		10	1245
		2.8	1301
3	Pure Toluene	30.8	1210
		20	1246
		10	1276
		3	1308

TABLE II

Benzoic acid in xylene

1) Variation of Velocity with Concentration

No.	Concentration	Density	Temperature °C	Frequency Mc/s	Wavelength mm.	Velocity metre/sec.	Compressibility $\times 10^6$
1	M/5	0.8648	18.5	4.13	.2993	1236	76.7
2	M/10	0.8640	18.5	4.13	.2999	1239	76.3
3	M/20	0.8589	18.5	4.13	.3000	1241	76.6
4	Pure Xylene	0.8572	18.5	4.13	.3020	1249	75.7
1	M/5		10	4.13	.305	1262	
2	M/10		10	4.13	.307	1266	
3	M/20		10	4.13	.308	1270	
4	Pure Xylene		10	4.13	.309	1276	
1	M/5		2.3	4.13	.3116	1289	
2	M/10		2.3	4.13	.3130	1294	
3	M/20		2.3	4.13	.3143	1297	
4	Pure Xylene		2.3	4.13	.3160	1304	

(b) Variation of Velocity with Temperature

No.	Concentration	Temperature °C	Velocity meters/sec.
1	M/5	18.5	1236
		10	1262
		2.3	1289
2	M/10	18.5	1239
		10	1266
		2.3	1294
3	M/20	18	1241
		10	1270
		2.3	1297
4	Pure Xylene	18	1249
		10	1276
		2.3	1304

I N F E R E N C E S

1. The velocity in a pure solvent is always greater than that in the solution.
2. The presence of a solid constituent in a solution, however small it may be, always lowers the velocity.
3. The velocity in a solution increases with dilution.
4. The adiabatic compressibility of a solution increases with concentration.
5. The velocity decreases with the rise in temperature.

A C K N O W L E D G M E N T S

In conclusion the author wishes to express his grateful thanks to Dr. D. B. Deodhar for suggesting the problem and guidance during the progress of this investigation, and his deep indebtedness to Dr. P. N. Sharma for encouragement and helpful discussions.

PHYSICS DEPARTMENT
LUCKNOW UNIVERSITY

R E F E R E N C E S

- Debye and Sears, 1932 *Proc. Nat. Acad. Sc.*, **18**, 409.
 Prevot, Hubbard and Andrews. 1929, *Jour. Amer. Chem. Soc.* **51**, 759.
 Lucas and Biqard, 1932, *C. R.*, **194**, 2132, and **195**, 121.
 Lucas and Biqard, 1932, *Jour. de Phys et la Rad.*, **3**, 464.
 Parthasarathy, 1936a, *Proc. Ind. Acad. Sc.*, **2A**, 497.
 Parthasarathy, 1936b, *Proc. Ind. Acad. Sc.*, **3A**, 285, 482, 519.
 Parthasarathy, 1936c, *Proc. Ind. Acad. Sc.*, **3A**, 297.
 Parthasarathy, 1937, *Proc. Ind. Acad. Sc.*, **4A**, 59, 213.
 Ram Pershad, 1941, *Ind. Jour. Phys.*, **18**, 323.
 Ram Pershad, 1942, *Ind. Jour. Phys.*, **18**, 1, 307.
 Wilson and Richards, 1932, *Jour. Phys. Chem.*, **36**, 1268.

AN AUTOMATIC PRESSURE STABILISING DEVICE FOR A DIAPHRAGM TYPE WILSON CLOUD CHAMBER*

By RANJIT KUMAR DAS

(Received for publication, Sept. 6, 1950)

ABSTRACT. An automatic electro-mechanical air pressure stabilising device is described. The development has been necessary for the use of a specially designed metallic diaphragm of a shallow cloud chamber. A stabilisation factor of $\pm 0.02\%$ has been reached.

INTRODUCTION

Economy of space between the pole pieces is a very important factor in Wilson chamber work, in a magnetic field. This is all the more keenly felt where the pictures are to be photographed by reflection from a plane mirror set at 45° to the plane of the chamber. All the lateral pin-control type chambers, (e.g., the one used by Blackett in his early work) use three conical leak-tight plugs carrying wedge-shaped end-pieces for controlling the expansion ratio. These wedge-pieces have a considerable thickness parallel to the axis of the chamber and they effectively draw upon the space between the pole-pieces. An economy in this direction was made by using a circular brass sheet with annular corrugations as the diaphragm, the movement of which produced the requisite expansion of the cloud chamber.

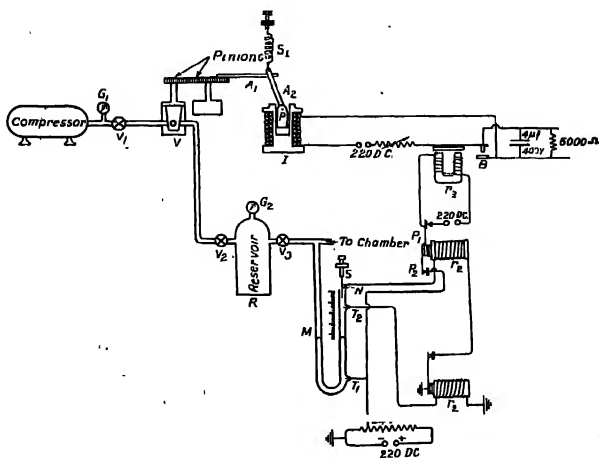
It was found that for a definite gas pressure in the glass compartment (in our case, 6 cm. of Hg) the compressing pressure in the back compartment could be varied within a rather small critical range (in our case, 2 cm. of Hg., with optimum at 96 cm. differential pressure). In other words, working of such a chamber depends critically upon the supply of air at a stabilised compressing pressure within a narrow range.

THE MECHANISM OF THE DEVICE

Fig. 1 gives a schematic diagram of the device used to secure the requisite pressure stabilisation. T_1 and T_2 are stiff tungsten wires sealed in the right limb of the U-tube mercury manometer M . T_1 is in permanent contact with mercury. T_2 is sealed at the lower limit (in our case 95.6 cm. of Hg.) of the working differential pressure range. S is a brass screw carrying a fine needle N at the end and can be worked down in the manometer as shown in the diagram. The upper limit of the working pressure is determined by the

* Communicated by Prof. M. N. Saha,

position of the tip of the needle T_2N is the differential range of pressure (of course; the optimum lies in between the two limits for which the apparatus is adjusted) within which the pressure remains automatically stabilised.



Schematic diagram of the automatic pressure stabiliser

FIG. 1

Normally, the cup-cone valve system V allows a regulated supply of air from the compressor at a pressure of a couple or two pounds per sq. inch. above the final stabilised pressure into the reservoir R . The mercury in the manometer rises and touches T_2 , thus completing the energising coil of the 24-volt relay r_1 . Simultaneously the prongs of this relay closes the earth end of the second relay r_2 in the sequence. Mercury continues to rise and touches the needle tip N . Immediately r_2 is energised, closing the two pairs of prongs P_1 and P_2 . Now P_1 closes the magnetising coil of a 220-volt colliery-bell relay, the armature of which carries a $\frac{1}{4}$ inch diameter and $\frac{1}{2}$ inch long brass stud. The rod makes contact with the brass disc B and closes the magnetising coil of the iron-cored solenoid I . The axial field of the solenoid attracts the rod towards the bottom of the core cavity. This translatory motion of the rod R_1 is converted into the rotatory motion of the coupled pinions by means of the lightly pivoted cross arms A_1 and A_2 . The rotation of the pinions displaces the air passage through the truncated cone completely from the pair of diametrical openings through the cup. The air supply from the compressor is thus automatically and very effectively cut off.

Now, through unavoidable minor leakages and use in the cloud chamber, the pressure in the stabiliser tank falls so that the needle loses its contact

with mercury. In spite of this, the relay r_2 remains energised through the auxiliary prong P_2 and thus the relay r_3 and the solenoid circuit in the automatic sequence remain closed. As mercury falls just below T_2 , the prongs of the relay r_1 open, breaking the magnetising circuit of the relay r_2 . Simultaneously, the relay r_3 in the solenoid circuit gets opened in succession and the tension of the spring S_1 restores the valve to its previous position and the cycle of operation repeats.

When the solenoid circuit breaks, a sufficiently large back E. M. F. develops at the contacts, producing heavy sparking there. This is the reason why the contacts are made of a brass rod and a disc rather than the lightly built prongs of relay r_2 which could otherwise be used directly.

DISCUSSION

The volume of the reservoir was nearly 5500 times greater than the chamber volume. The actual requirements of the compressed air for expansion of the chamber was small, so that when the chamber works, stabilisation for more than half an hour was easily secured. This arrangement gives a stabilisation factor of $\pm .02\%$. By taking wide manometer limbs to reduce the convexity of the mercury meniscus due to surface tension and increasing the proportionate volume of the stabiliser tank, the stabilisation factor can be easily pushed down to $\pm .005\%$.

ACKNOWLEDGMENTS

The author wishes to record his sincere thanks to Prof. M. N. Saha, D.Sc., F.R.S., for his kind interest in the work and also to Dr. P. C. Bhattacharyya for his constructive criticism and to Sri G. N. Sarkar, M.Sc., for substantial help.

INSTITUTE OF NUCLEAR PHYSICS,
UNIVERSITY OF CALCUTTA

ANNOUNCEMENT

INTERNATIONAL UNION OF CRYSTALLOGRAPHY

The Second General Assembly and International Congress of the Union will be held in Stockholm from 27 June to 3 July 1951. Delegates to the General Assembly will be nominated by the National Committees. Crystallographers through out the world are, however, cordially invited to attend the International Congress. The Union is unfortunately not in a position to provide funds to assist delegates in meeting travelling expenses. All those attending will be required to pay a membership fee of 50 Swedish crowns.

The subjects selected for consideration are :

- | | |
|---|-------------------------------------|
| (1) Instruments and Measurements | (7) Proteins and Related Structures |
| (2) New Developments in Structure Determination | (8) Random and Deformed Structures |
| (3) Mineral Structures | (9) Thermal Transformations |
| (4) Metal Structures | (10) Crystal Growth |
| (5) Inorganic Structures | (11) Neutron Diffraction |
| (6) Organic Structures | (12) Miscellaneous |

No report of the Congress shall be published. Full abstract of the contributions will, however, be distributed in advance.

Arrangements have been made for a visit to Uppsala University. It is proposed to hold two symposia on (i) Advanced Technique in Structure Determination and (ii) Electron Diffraction in Liquids and Gases. These symposia are intended primarily for specialists in these fields, but in so far as accomodation is available, all crystallographers will be welcome.

Contributions may be presented in any language, preferably in English, French or German.

Crystallographers intending to attend are requested to complete Form B and return it to the General Secretary not later than 15 February, 1951. Offers of papers are cordially invited and should be submitted, preferably in Form C to the Secretary, Programme Committee, not later than 15 February, 1951. Forms are obtainable (in India) from Secretary to the Govt. of India, Dept. of Scientific Research, North Block, Central Secretariat, New Delhi. Crystallographers, whose contributions are accepted, will be notified shortly and will be requested to submit an abstract of their papers not later than 31 March, 1951.

All correspondence concerning contributions to the Congress or Symposia should be submitted to the Secretary, Programme Committee (F. E. Wickman, Stockholm 50, Sweden), and other correspondence to the General Secretary of the Union (R. C. Evans Crystallographic Laboratory, Cavendish Laboratory, Cambridge, England).

The following special publications of the Indian Association for the Cultivation of Science, 210, Bowbazar Street, Calcutta, are available at the prices shown against each of them :—

Subject	Author	Price Rs. A. P.
Methods in Scientific Research	... Sir E. J. Russell	0 6 0
The Origin of the Planets	... Sir James H. Jeans	0 6 0
Separation of Isotopes	... Prof. F. W. Aston	0 6 0
Garnets and their Role in Nature	... Sir Lewis L. Fermor	2 8 0
(1) The Royal Botanic Gardens, Kew.	... Sir Arthur Hill	1 8 0
(2) Studies in the Germination of Seeds.	
Interatomic Forces	... Prof. J. E. Lennard-Jones	2 8 0
The Educational Aims and Practices of the California Institute of Technology.	... R. A. Millikan	0 6 0
Active Nitrogen A New Theory.	... Prof. S. K. Mitra	2 8 0
Theory of Valency and the Struc- ture of Chemical Compounds.	... Prof. P. Ray	3 0 0
Petroleum Resources of India	... D. N. Wadia	2 8 0
The Role of the Electrical [Double layer in the Electro Chemistry of Colloids.	... J. N. Mukherjee	1 12 0

A discount of 25% is allowed to Booksellers and Agents.

RATES OF ADVERTISEMENTS

Third page of cover	Rs. 32, full page
do. do.	„ 20, half page
do. do.	„ 12, quarter page
Other pages	„ 25, full page
do.	„ 16, half page
do.	„ 10, quarter page

15% Commissions are allowed to bona fide publicity agents securing orders for advertisements.

CONTENTS

	PAGE
55. Absorption Spectrum of Anisole—By K. Sreeramamurthy	421
56. Absorption Spectrum of Thallium Halides—By P. Tiruvenganna Rao	434
57. On the Origin of Fluorescence in Diamond—By B. M. Bishui	441
58. Ultrasonic Velocities in Organic Solutions. I.—By K. C. Lal	461
59. An Automatic Pressure Stabilizing Device for a Diaphragm-type Wilson Cloud Chamber—By Ranjit Kumar Das	466

Vol. 24

INDIAN JOURNAL OF PHYSICS

No. 11

(Published in collaboration with the Indian Physical Society)

AND

Vol. 33

PROCEEDINGS

No. 11

OF THE

**INDIAN ASSOCIATION FOR THE
CULTIVATION OF SCIENCE**

NOVEMBER, 1950

PUBLISHED BY THE
INDIAN ASSOCIATION FOR THE CULTIVATION OF SCIENCE
210, Bowbazar Street, Calcutta

BOARD OF EDITORS

K. BANERJEE	S. K. MITRA
D. M. BOSE	P. RAY
S. N. BOSE	M. N. SAHA
D. S. KOTIHARI	S. C. SIKKAR.

Secretary

EDITORIAL COLLABORATORS

DR. R. K. ASUNDI, M.A., PH.D.
PROF. H. J. BHABHA, PH.D., F.R.S.
DR. P. K. KICHLU, D.Sc.
PROF. K. S. KRISHNAN, D.Sc., F.R.S.
PROF. G. P. DUBEY, M.Sc.
DR. K. RANGADHAMA RAO, M.A., D.Sc.
DR. N. D. SARWATTEY, D.Sc.
DR. N. N. DASGUPTA, M.Sc., PH.D.
PROF. N. R. SEN, D.Sc., F.N.I.
PROF. P. C. MAHANTI, D.Sc., F.N.I.
PROF. S. K. PALIT, D.Sc.,
DR. H. RAKSHIT, D.Sc.,
PROF. K. R. DIXIT, PH.D.
DR. VIKRAM A. SARABHAI, M.A., PH.D.

ASSISTANT EDITOR

MR. A. N. BANERJEE, M.Sc.

NOTICE

TO INTENDING AUTHORS

Manuscripts for publication should be sent to Mr. A. N. Banerjee, Assistant Editor, 210, Bowbazar Street, Calcutta.

The manuscript of each paper should contain in the beginning a short abstract of the paper.

All references to published papers should be given in the text by quoting the surname of the authors followed by the year of publication within braces, e.g., Sen (1942). The actual references should be given in a list at the end of the paper according to the following specimen :

Sen, B. K., 1942, *Ind. J. Phys.*, 16, 329.

The references should be arranged alphabetically in the list.

All diagrams should be drawn on thick white paper in Indian ink, and letters and numbers in the diagrams should be written in pencil.

Annual Subscription—

Inland Rs. 20
Foreign £ 2

THE ELECTRICAL CONSTANTS OF SOIL AT ULTRA-HIGH FREQUENCIES

By P. N. SUNDARAM

(Received for publication, July 12, 1950)

ABSTRACT. A detailed study of the variation of the dielectric constant and conductivity of soil with frequency, sand content and moisture content has been made within the wavelengths between 4 and 7 metres. A modified Lecher-wire system, completely immersed in the soil for the required length, was used for recording observations. Experiments were conducted with two 'brown fine clay' samples of soil within the University area of Banaras.

INTRODUCTION

The knowledge of electrical constants of soil has been found to be of great importance for radio as well as electrical engineers. In electrical engineering, for example, it is necessary to have proper earth connections at specific points, in the supply and distribution systems, resistances of which are entirely dependent upon the conductivity of the soil. Several electrical devices, employed in tapping oil and mineral resources, have become indispensable to geophysicists for the geodetic survey of any place.

But in the propagation of radio signals, these soil properties influence even the design of the transmitter, irrespective of the use of an earthed antenna. A knowledge of the electrical constants of soil around the transmitter is essential for computing the primary 'service area' of any broadcasting station. The efficiency of reception is very much influenced by the conductivity of soil in the neighbourhood of the receiving station. Moreover, the knowledge of soil constants has been made indispensable by the increasing use of shorter-waves during the last two decades.

For special short-distance communications, like blindlanding beams for aviation and police conversations by wireless, ultra short waves (*i.e.*, wavelengths below 10 metres) are extensively used. Being almost immune from fading they insure complete privacy of conversation.

In view of this recent trend towards the use of very short waves, variations with frequency, moisture content and sand content of the electrical constants of soil at ultra-high frequencies were investigated.

EXPERIMENTAL ARRANGEMENTS

The experimental arrangement was essentially the same as adopted by Banerjee and Joshi (1938) with a modification in the method of observation as described below.

Two hard drawn copper wires stretched horizontally formed the Lecher wires. A series of condensers were placed at the input end in series with the

parallel wires as shown in the figure 1. The two ends of the central condenser were connected to the two ends of a vacuum thermojunction and the other two terminals of the junction to a galvanometer G.

A wooden box, of a length variable between 50 cm. and 250 cm. was made to keep the soil. Two slits were cut on opposite smaller sides of the box nearly to the bottom. The parallel wires were passing through these slits.

An ordinary retroaction type of valve generator, O (Fig. 1) formed the

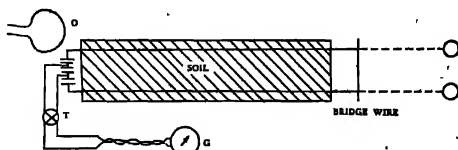


FIG. 1
(The Lecher-wire system)

source of oscillations. The same oscillator could give different frequencies of oscillations by merely changing the inductance in the circuit. By loosely coupling the inductance of the oscillator to the input end of the parallel wires, oscillations were set up in the parallel wire system. To minimise the chance of boundary reflection of the waves at the surface of separation of the two media in the soil and the air, the box was shifted to such a position that its end, nearer to the input end, coincided with a potential node.

METHOD OF OBSERVATIONS

As the box was gradually filled with soil, it was found that the shift of the nodes was towards the box. The wires were covered with soil and compressed, and the number of nodes shifted in the soil was noted. The final node next to the end of the box was located and the distance l of the node from the box was measured. Then, if λ_a and λ_s be the wavelengths in air and soil respectively,

$$\lambda_a/\lambda_s = N\lambda_a - Z/L,$$

where N is the total number of nodes between the input end of the box kept at the node, to the node next to the other end of the box outside it, and L is the length of the soil box. This is the wave-shift method as employed by Smith-Rose and McPetrie (1934).

The resonance curves were then drawn by plotting the distance along parallel wires, against deflections of the galvanometer, as a short-circuiting metal bridge (Fig. 1) was gradually moved along the parallel wires. The attenuation constant α was found by the 'half-width' method from these resonance curves using the relation,

$$\alpha = 2\pi d/n\lambda_s^2$$

where d is the half-width, that is the distance between the points on the

resonance graph, where the deflections of the galvanometer are half that of the maximum deflection at the node, proportionately calculated for a half-wavelength in soil, n the number of the node from input end. Observations taken in a similar way clearly indicated that the calculated value of the attenuation constant α varies markedly with the length of the wires immersed in the medium. This anomalous variation of the calculated attenuation constant has been discussed by the author (Sundaram, 1950).

Since reliable results could not be obtained, by this method, to determine λ_s/λ , and α , the resonance curve for the first potential node in soil was drawn, and from it the node itself was located and d_s , the half-width in soil was read. Thus λ , the wavelength in soil was directly measured in soil and α was calculated from $\alpha = 2\pi d_s/\lambda$. With this modified method, the variation of the electrical constant of soil with frequency, moisture content and sand content was studied in detail. Six different frequencies, that is, 43.17 Mc/sec., 52.08 Mc/sec., 60.48 Mc/sec., 69.12 Mc/sec. and 74.07 Mc/sec., all in the ultra high range, were employed; their corresponding wavelengths being 6.95 m., 6.28 m., 5.76 m., 4.96 m., 4.34 m., and 4.05 m. respectively.

VARIATION OF THE SOIL CONSTANTS WITH FREQUENCY AND SAND CONTENT

Mixtures of very dry sand and equally dry soil were prepared and the variation of the electrical constants of soil with increase in frequency and also of the influence of contained sand was studied. In Tables I and II are given the results of the experiments conducted.

TABLE I

Variation of dielectric constant (in e. s. u.) with frequency and sand content.

Frequency Mc/sec.	Pure soil	Sand content					Pure sand
		10%	20%	30%	40%	50%	
43.17	3.17	3.11	2.99	2.94	2.85	2.88	2.45
47.77	3.21	3.21	3.06	3.04	3.04	3.02	2.57
52.08	3.04	3.12	3.03	2.95	2.95	2.95	2.53
60.48	2.86	2.92	2.82	2.81	2.87	2.81	2.53
69.12	2.79	2.79	2.70	2.66	2.77	2.70	2.53
74.07	2.72	2.80	2.76	2.73	2.80	2.76	2.42

TABLE II

Variation of conductivity (in 10^8 e. s. u.) with frequency and sand content.

Frequency Mc/sec.	Pure soil	Sand content					Pure sand
		10%	20%	30%	40%	50%	
43.17	17.91	18.18	16.85	15.94	14.60	14.36	0.834
47.77	20.17	18.86	16.43	14.13	14.53	14.21	0.746
52.08	19.88	19.45	16.67	17.00	14.93	14.02	0.812
60.48	18.77	20.73	15.21	16.64	17.16	13.77	0.819
74.07	26.17	23.54	25.77	21.07	18.87	16.73	1.270

Fig. 2 represents one of the typical curves for the variation of the dielectric constant with frequency for dry soil alone and Fig. 3 that of the

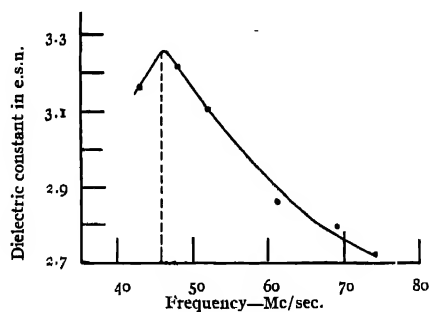


FIG. 2
(Dry soil)

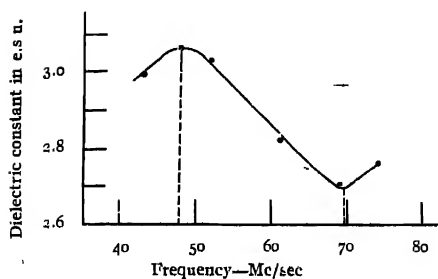


FIG. 3
(10% sand)

mixture of soil with 10% sand, drawn from the observations in first three columns of Table I. The important characteristics of these curves are the humps or the crests at about 47 Mc/sec. and the troughs between 65 and 70 Mc/sec. The crest or the maximum is observed in all the curves including those for pure soil and pure sand, the observation for which are shown in the second and eighth columns of Table I. We, therefore, conclude that this maximum is a common property of soil and sand both. The presence of this crest in the value of dielectric constant, suggests some resonance effects in the medium at the frequency of about 47Mc/sec. On the other hand, the trough is a characteristic of the mixtures only. It is absent both in the case of pure soil or pure sand alone. It is more pronounced in the case of the sample containing 20% sand, being less marked in other cases. A similar trough in the value of dielectric constant is obtained in case of pure soil with high percentage of moisture as shown later.

Fig. 4 is a typical curve for conductivity. Its variation with frequency

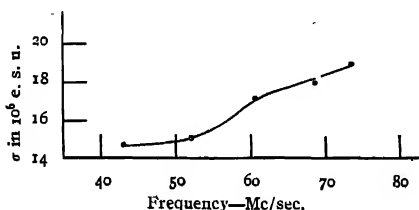


FIG. 4
(40% sand)

is not so regular as that of dielectric constant. The conductivity of sand itself varies very little with frequency and in this fact we find that it influences the conductivity value of the mixture markedly. The mean variation of conductivity with frequency decreases with increase of sand content in our sample of soil.

THE INFLUENCE OF MOISTURE AND FREQUENCY OF THE SOIL CONSTANTS

Here also the same six different frequencies were employed to study the variation of the soil constants with frequency and moisture content. The soil samples were not artificially moistened as this imparts a non-uniform and irregular distribution of moisture to the samples. The electrical constants were measured at different percentages by weight of the moisture content, during the natural course of the evaporation of soil samples, initially

containing a large percentage of moisture. Several samples were experimented upon but only the typical results of one sample are recorded here. In Tables III and IV are given the results of these experiments.

TABLE III

Variation of dielectric-constant with frequency and moisture

Frequency Mc/sec.	Moisture content				
	5.3%	7.2%	9.1%	11.5%	15.5%
43.17	4.49	5.03	5.37	5.37	4.63
47.77	4.63	5.03	5.41	5.70	5.10
52.08	4.80	4.73	5.53	5.40	4.69
60.48	4.27	4.44	5.04	4.95	4.38
69.12	3.89	4.11	4.66	4.52	3.72
74.07	3.94	3.94	4.55	4.36	4.23

TABLE IV

Variation of conductivity (in 10^6 e. s. u.) with frequency and moisture

Frequency Mc/sec.	Moisture content				
	5.3%	7.2%	9.1%	11.5%	15.5%
43.17	34.86	42.00	42.00	36.67	34.94
47.77	36.59	44.21	38.79	46.62	41.65
52.08	39.87	45.52	44.67	44.20	39.01
60.48	41.02	43.02	47.55	46.30	43.55
69.12	44.50	44.05	49.71	49.15	36.96
74.07	46.49	46.49	52.25	46.31	53.13

Fig. 5 is a typical curve representing the variation of dielectric constant with frequency for the same sample of the soil with different percentages of moisture in it. There is the usual crest at 47 Mc/sec., which we saw was due to the soil itself. It is present in all cases and in general we find that the dielectric constant decreases with frequency. At higher moisture contents, however, the trough is obtained at about 69 Mc/sec., as shown in Fig. 6. It

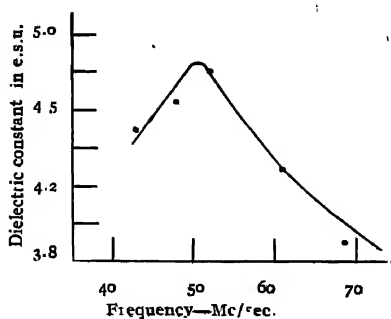


FIG. 5.
(5.3% moisture)

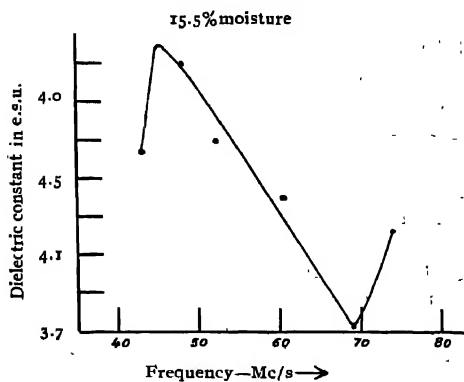


FIG. 6.
(15.5% moisture)

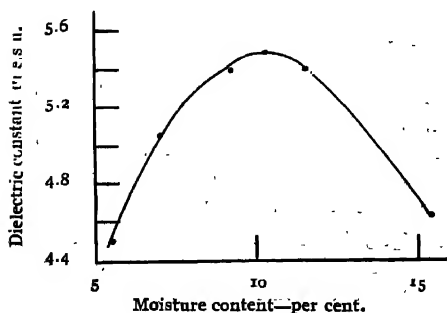


FIG. 7.
(Frequency, 43.17 Mc/s)

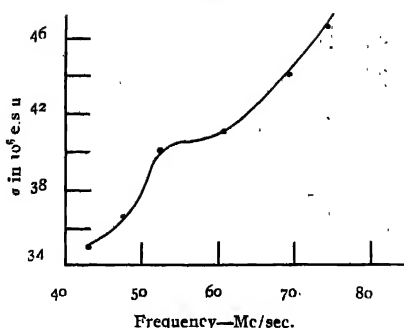


FIG. 8.
(5.3% moisture)

will be observed that the curve in Fig. 6 is similar to the ones for the mixture of sand and soil as mentioned earlier. It may therefore be said that the effect of the sand on the soil is very similar to that of a large amount of water in the sample as far as the variation of dielectric constant is concerned.

The curve in Fig. 7 represents the typical variation of the dielectric constant with moisture content. The results of the previous investigators in this field indicated that the dielectric constant increased with increasing moisture contents, tending towards the constant value. But it is clear from these curves that the dielectric constant has a definite maximum between 10% and 12%. This shows that the effect of moisture on dielectric constant is maximum in this range. There is also a gradual shift of this maximum towards higher moisture contents as the frequency is increased between 40 Mc/sec. and 56 Mc/sec. Between 52 Mc/sec. and 75 Mc/sec., however, this shift is in the opposite direction, *i.e.*, towards smaller percentages of water content. The fact that this crest is observed at all frequencies prevents us from attributing it to any resonance effects which can occur only at particular frequencies.

Fig. 8 represents a curve showing the variation of the electrical conductivity of the soil with frequency, which shows that the electrical conductivity of a sample of soil, containing very little moisture, increases with frequency within the range investigated. It may be mentioned that such curves show maxima and minima with increase of moisture content, which are also shown in the conductivity measurements below.

The curve in Fig. 9 illustrates the influence of moisture on the soil conductivity. The interesting feature of such curves is the maximum between 8% and 10% of moisture. Perhaps if higher frequencies are experimented with more maxima may be observed as in the case of dielectric constant mentioned above.

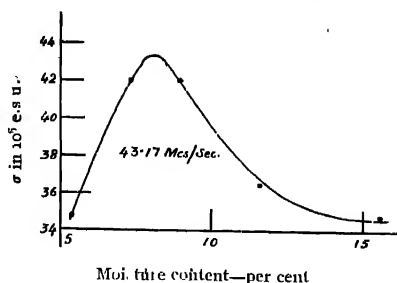


FIG. 9

(Frequency, 43.17 Mc/s)

SUMMARY AND CONCLUSIONS

The dielectric constant of the first sample is 3.17 at 43.17 Mc/sec, increasing at first to 3.21 at 47.77 Mc/sec., gradually decreasing to 2.72 at 74 Mc/sec. With increase of sand content the dielectric constant decreased. Its value for pure sand is 2.15 at 43.17 Mc/sec. increasing to 2.57 at 47.77 Mc/sec. and then gradually decreasing to 2.42 at 74 Mc/sec. The second sample has a dielectric constant of 4.49 at 43.17 Mc/sec. at first increasing to 4.63 at 47.77 Mc/sec and then gradually decreasing to 3.94 at 74 Mc/sec. At all frequencies the dielectric constant increases with increase of moisture content up to 10% or 12%. But when the percentage of moisture is still greater it is found that the dielectric constant decreases. It appears as though water has its maximum effect at about 10% or 12%. It was similar in the case of conductivity also.

The value of the electrical conductivity of the first sample is 17.91×10^6 e. s. u. at a frequency of 43.17 Mc/sec. The variation with frequency is not very regular. Its mean variation with frequency decreases with increase of sand content. The conductivity of the second sample is 34.8×10^6 e. s. u. at 43.17 Mc/sec. The electrical conductivity of dry soil, increases with frequency. As in the case of dielectric constant the effect of moisture seems to be maximum between 8% and 10%.

Lastly, the important feature of the results of these observations is that they indicate that a mixture of dry soil and dry sand shows a similar behaviour in 'resonance effects' as the moist soil, within the range of frequencies employed.

ACKNOWLEDGMENTS

These experiments were performed in the Banaras Hindu University and the author has great pleasure to record his grateful thanks to Dr. S. S. Bauerjee, D.Sc., for his suggestions during the course of the work,

NATIONAL PHYSICAL LABORATORY OF INDIA,
NEW DELHI.

REFERENCES

- Banerjee, S. S. and Joshi R. D (1938) *Phil. Mag.*, **25**, 1025
Smith Rose, R. L. and McPetrie, J. S (1934) *Proc. Phys. Soc.*, **46**, 649
Sundaram, P. N (1950) *Science and Culture*, **15**, 441

ON THE DISINTEGRATION OF SCANDIUM (46) AND THE METHOD OF DELAYED COINCIDENCE FOR THE STUDY OF SHORT-LIVED METASTABLE STATES IN ISOMERIC NUCLEI

BY B. D. NAG, S. SEN, AND S. CHATTERJEE

(Received for publication, Sept 9, 1950)

ABSTRACT. A metastable state having a half-life of 12.15 ± 0.2 micro-seconds has been found in titanium (46) decaying from 85 days scandium (46). The method of delayed coincidence used for the purpose has been discussed with reference to the effect of time-lag in G-M counters. The distribution function for the time-lag is found to differ from the Gaussian error function. A mathematical expression relating the decay constant of the metastable state to the delay in one of the channels has been derived assuming a Gaussian distribution of the initial pulses as a first approximation.

The disintegration scheme of scandium (46) has been examined. The two beta-rays were separated by putting aluminium absorbers and the values of their energy maxima were obtained as 0.34 mev and 1.52 mev from the Feather plots. This confirms the results obtained by Walke, Peacock and Wilkinson.

INTRODUCTION

The disintegration of scandium (46) to titanium (46) by β^- -emission has been investigated by several workers. Walke (1940) reported two groups of beta-rays having maximum energies 0.26 mev and 1.5 mev and a γ -ray of energy 1.25 mev. Meitner (1945) could not find the high energy beta-ray group and attributed Walke's results to scattering. Later work on scandium (46) by Miller and Deutsch (1947), Jurney (1948) and others revealed that there is only one group of beta rays of maximum energy 0.36 ± 0.01 mev and two groups of gamma-rays of energies 0.89 ± 0.02 mev and 1.12 ± 0.02 mev. Further β - γ and γ - γ coincidences show that each β -ray of the 0.36 mev group is followed by the cascade emission of the two gamma-rays. Peacock and Wilkinson (1948) reported the presence of the beta-ray group having end-point energy of 1.49 mev in addition to the beta-rays with end-point energy 0.36 mev, thus confirming the earlier results obtained by Walke. They also found that 2 percent of the beta-rays belong to high energy group.

Feister and Curtiss (1947) have verified that only the low energy beta-rays are present. Mandeville and Scherb (1948) also could not find any hard beta-rays having end-point energy in the vicinity of 1.5 mev. In a communication, Goldhaber and Muelhaue (1949) mention a metastable state of half-life of 20 seconds in scandium (46). Nag, Sen, and Chatterjee (1949)

reported a metastable state in titanium (46) having a half-life of 13.2 micro-seconds.

Method of delayed coincidence.—The method by which the half-lives of short-lived metastable states of the isomeric nuclei are determined is generally known as "delayed coincidence" method. The method of delayed coincidence has engaged attention of many workers for the last few years and led to the discovery of a number of nuclear isomers with short decay periods. The first workers in this line were Rossi and Nereson (1942) who found the decay period of meson by this method. DeBenedetti and McGowan (1946) first introduced the method of delayed coincidence to the study of short-lived metastable state of isomeric nuclei.

In the method of delayed coincidence there are two counters, each followed by a channel leading to a coincidence stage. A time delay is being introduced in one of the channels, so that two simultaneous events in the counters will not come out of the channels simultaneously but will be shifted in time. But when the two events in the counters are delayed by the same time as introduced in the channel, then only the events will emerge simultaneously and they will be in coincidence. Thus the natural delay in the events can be known in terms of the delay introduced in the circuit.

DeBenedetti and McGowan found isomeric states in Ta^{181} (22 μ -secs.) Tc^{187} (0.65 μ -sec.), Tm^{169} (1 μ -sec) and Tm^{171} (2.5 μ -secs), using multi-vibrators for introducing the delay. Their researches were carried out at delays between 10^{-4} to 10^{-6} sec. Independently of their work, Hürzel, Stoll and Wülfel (1948) have used the same method for the study of isomers in Pr^{141} (70 μ -sec), Tc^{127} (1200 μ -sec). The same method has been followed by Bunyan, Laundby, Ward and Walker (1948-49) and their searches for short period activities has been extended to the region between 3×10^{-7} and 10^{-4} secs. Van Name (Jr.) (1948) has used the coaxial lines to introduce a delay instead of the variable width multivibrator. Recently, DeBenedetti, McGowan and Francis (Jr.) (1949) have replaced Geiger-Müller counter by anthracene scintillation counters and have increased the limit of the delay to 10^{-7} sec.

ANALYSIS OF TIME LAG IN COUNTERS

The radiation from a radio-active source passing through the Geiger-Müller counter produces a primary ionisation. The electrons from the region of primary ionisation travel to the region near the anode, where an electron avalanche occurs, which thereafter travel along the length of the central wire. This process takes a short time of the order of microseconds depending on the geometry of the counter and the nature of the gas in the counter, thus introducing an intrinsic time lag between the ionising event and the registering of its effect in the recording circuit. The time lag in

counters was noted by Montgomery and Montgomery (1940) and its effect on coincidence measurements was taken into consideration by Rossi and Nereson (1942). The relation between the initial radiation passing through the counter and the corresponding grid voltage rise of the first tube is statistical in nature, so that the time lag between the cause and the effect follows statistical distribution law. Van Name (1938) explained his observed results assuming the time lag in counters to follow a triangular distribution law. This, however, seems to be too simplified a treatment. Bradt and Scherrer (1943) found an agreement of the observed results by assuming Gaussian law for the distribution function of the time lag in counters. They used a coincidence arrangement with a variable resolving time. Bunyan, Laundry and Walker (1949) have assumed the same law and have given a mathematical expression for the probability of delayed coincidence. The authors (Nag, Sen and Chatterjee, 1950) have earlier reported a general expression for the same. In the following section we have given a complete analysis of the effect of time lag in counters in the measurement of delayed coincidences, assuming the Gaussian law. We have shown that the Gaussian law is only an approximation and has got to be corrected to get the real picture.

Let us consider the case of two exactly identical counters each followed by two channels *A* and *B* leading to a coincidence stage (Fig. 1). In

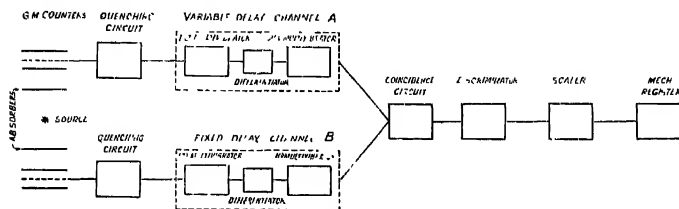


FIG. 1

channel *A* there is an arrangement by which a time delay can be introduced to the event passing through that channel. We assume Gaussian distribution of the time lag between the primary ionising event and the occurrence of the corresponding pulses at the input of the coincidence stage and consider that radiations from a radio-active source are emitted in immediate succession and pass through both the counters. Let t_A and t_B be the average inherent time lags for the two channels and let a deliberate delay t_d be introduced on the pulses in the channel *A*. Let the Gaussian distribution have a standard deviation $t_0/\sqrt{2}$, where t_0 represents the standard deviation of the difference between the time lags of the two counters. Let the pulse-widths of the channels *A* and *B* be τ_A and τ_B , which, for simplicity, will be taken to be equal to τ . This will give a resolving time of the order of 2τ .

If now an event occurs at the counter leading to channel *B* at $t=0$ the

probability that the corresponding pulse will be recorded at the input of the coincidence stage between time t and $t + dt$ will be,

$$\frac{1}{t_0 \sqrt{\pi}} \exp. \left\{ - \left(\frac{t - \bar{t}_0}{t_0} \right)^2 \right\} dt$$

Similarly for an event occurring in the counter leading to channel A in which the pulses are delayed by time t_d , the probability of recording the pulse at the coincidence stage between time t' and $t' + dt'$ is :

$$\frac{1}{t_0 \sqrt{\pi}} \exp. \left\{ - \left(\frac{t' - \bar{t}_0 - t_d}{t_0} \right)^2 \right\} dt'$$

After a pulse has reached the coincidence stage through channel B a coincidence will be recorded only if the pulse through the channel A reaches the coincidence stage between time $t - \tau$ and $t + \tau$. Thus the probability of such delayed coincidences can be written as,

$$\psi(t_d) = \int_{-\infty}^{\infty} \left(\frac{1}{t_0 \sqrt{\pi}} \right)^2 \exp. \left\{ - \left(\frac{t - \bar{t}_0}{t_0} \right)^2 \right\} dt \int_{t-\tau}^{t+\tau} \exp. \left\{ - \left(\frac{t' - \bar{t}_0 - t_d}{t_0} \right)^2 \right\} dt' \quad (1)$$

This is a double integral of surface elements dt and dt' . By transformation of the expression in terms of ξ and η , where $\xi = t + t'$ and $\eta = t - t'$ and $dt \cdot dt'$ being given by the Jacobian

$$\begin{vmatrix} d\xi/dt, & d\eta/dt \\ d\xi/dt', & d\eta/dt' \end{vmatrix} d\xi d\eta$$

the value of the integral will come out as

$$\begin{aligned} \psi(t_d) &= \frac{1}{2t_0^2 \pi} \int_{-\infty}^{\infty} \exp. \left(- \frac{1}{2t_0^2} \xi^2 \right) d\xi \int_{\tau}^{-\tau} \exp. \left\{ - \frac{1}{2t_0^2} (\eta + \Delta + t_d)^2 \right\} d\eta \\ &= \frac{1}{2} \left[\phi \left(\frac{t_d + \Delta + \tau}{t_0 \sqrt{2}} \right) - \phi \left(\frac{t_d + \Delta - \tau}{t_0 \sqrt{2}} \right) \right] \quad \dots (2) \end{aligned}$$

where $\Delta = \bar{t}_A - \bar{t}_B$ and $\phi(x) = (2/\sqrt{\pi}) \int_0^x e^{-z^2} dz$.

It will be no loss of generality to take $\Delta = 0$; which is true when counters are identical, since this will only lead to a displacement of the curves along the t_d -axis by an amount Δ .

This expression has been obtained by Bunyan *et al* and we shall discuss certain objections which can be raised against some steps used in the deduction of the equation (2).

In equation (1) the limits of integration for t have been taken to be $-\infty$ and $+\infty$, whereas the limits should actually be t_d and $+\infty$, for there can be no coincidence before the pulse through the delayed channel has reached the coincidence stage, that is, before the fixed delay time t_d has elapsed. This has introduced an error $\epsilon(t_d)$ in the value of $\psi(t_d)$ so that we have

$$\psi(t_d, t_0) - \psi_1(t_d, t_0) = \epsilon(t_d, t_0)$$

where $\psi_1(t_d, t_0)$ denotes the corrected value of $\psi(t_d, t_0)$.

In Fig. 2, curves A and B stand respectively for the assumed Gaussian distributions in channels A and B and the points P and Q correspond

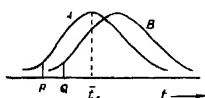


FIG. 2

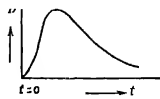


FIG. 3

respectively to $t = 0$ and $t = t_d$. Hence the contribution to the integral in equation (1) which arises from the product of corresponding ordinates of the curves A and B to the left of Q is actually the value of $\epsilon(t_d, t_0)$. As t_d changes from 0 to ∞ the ordinates coming from B remain the same but those of the ordinates coming from A which make dominant contributions to the value of $\epsilon(t_d, t_0)$, increase monotonically in the beginning, become largest when $t_d = t_0$, then gradually fall towards zero.

Hence $\epsilon(t_d, t_0) < \epsilon(0, t_0)$ (3), for sufficiently large t_d .

Let us for the present assume that $\psi_1(t_d, t_0)$ versus t_d curve for some value of t_0' agrees exactly with the experimentally determined (coincidence, delay) curve. Suppose we now fit a theoretical $\psi(t_d) - t_d$ curve to the above curve by finding a t_0 such that

$$\psi(0, t_0) = \psi_1(0, t_0')$$

Thus $\epsilon(0, t_0') = 0$ but ψ and ψ_1 involve different parameters t_0 and t_0' . If t_0 and t_0' are nearly equal and the validity of the treatment resulting in relation (3) is assumed in this case also, it follows that the experimental curve runs below the theoretical curve for small values of t_d and above it for large values of t_d , that is, for large t_d the experimental coincidence numbers will appear to tend to zero less rapidly than given by the theoretical curve. This is exactly the result obtained by us and also by Bunyan and others (1949).

The above discussion naturally loses much of its value, in fact $\epsilon(t_d, t_0)$ becomes always negligible, if the Gaussian distribution is very sharp, that is, t_0 is very small in comparison with t_0 . But as there is no information on this point, we have no a-priori grounds to ignore the conclusions reached above.

It must also be noticed that the distribution curves *A* and *B* (Fig. 2) should in no case extend to the left of *P* and *Q* respectively. This implies that instead of being symmetric Gaussian, the actual distribution is asymmetric, possibly of the type shown in Fig. 3. But this will not alter the above conclusions to any significant extent, unless the nature of asymmetry is considerably different from that shown in Fig. 2. The actual distribution in counter can in principle be investigated and an analytical expression for the distribution function is being investigated.

Next we consider the case in which a radio-active source, instead of emitting instantaneous radiations, gives out radiations which are naturally delayed. This implies that the nucleus formed by the decay of the parent nucleus has a metastable state with a decay constant λ . The presence of a finite half-life of the intermediate nucleus introduces in this case another probability factor $f(t)$ for the coincidence of the two emitted radiations. Let the probability that a nucleus will disintegrate between time t and $t+dt$ be $f(t)$. Then for a total number of nuclei N , the number that will disintegrate

in time t is $\int_0^t f(t) dt$. From fundamental considerations we know this to be

$$N_0 \left(1 - e^{-\lambda t} \right) \text{ and thus } f(t) = \lambda e^{-\lambda t}$$

Let us assume that the radiation which is first emitted enters the channel *A* and that the following radiation enters the channel *B* so that the probability of delayed coincidence for all disintegrations taking place between time $t'' = 0$ and $t'' = \infty$ becomes,

$$\begin{aligned} \Psi_1(\lambda, t_d) &= \int_0^\infty \lambda e^{-\lambda t''} \psi(t_d - t'') dt'' \\ &= \frac{1}{2} \left[\phi \left(\frac{t_d + \tau}{t_0 \sqrt{2}} \right) - \phi \left(\frac{t_d - \tau}{t_0 \sqrt{2}} \right) \right] \\ &+ \frac{1}{2} \left[\left\{ 1 + \phi \left(\frac{t_d - \tau}{t_0 \sqrt{2}} - \frac{\lambda t_0}{\sqrt{2}} \right) \right\} \exp. (\lambda \tau) - \left\{ 1 + \phi \left(\frac{t_d + \tau}{t_0 \sqrt{2}} - \frac{\lambda t_0}{\sqrt{2}} \right) \right\} \exp. (-\lambda \tau) \right] \times \\ &\quad \exp. (-\lambda t_d + \frac{1}{2} \lambda^2 t_0^2) \quad \dots (4) \end{aligned}$$

It is, however, equally probable, according to the symmetric geometry of the source and counters, that the first radiation may enter channel *B* and the following one to channel *A*. In that case, the probability of delayed coincidence is

$$\begin{aligned} \Psi_2(\lambda, t_d) &= \int_0^\infty \lambda e^{-\lambda t''} \psi(t_d + t'') dt'' \\ &= \Psi_1(\lambda, -t_d) \quad \dots (5) \end{aligned}$$

Therefore the total probability of delayed coincidence is

$$\Psi(\lambda, t_d) = \frac{1}{2}\Psi_1(\lambda, t_d) + \frac{1}{2}\Psi_1(\lambda, -t_d) \quad (6)$$

Equation (6) can be written in the form

$$K\Psi(\lambda, t_d) = \int_0^\infty e^{-\lambda t''} \dot{\psi}(t_d - t'') dt'' + \int_0^\infty e^{-\lambda t''} \dot{\psi}(t_d + t'') dt''$$

where K is a constant given by $2/\lambda$.

It can be shown that

$$\begin{aligned} K\dot{\Psi}(\lambda, t_d) &= \int_0^\infty e^{-\lambda t''} \left\{ \dot{\psi}(t_d - t'') + \dot{\psi}(t_d + t'') \right\} dt'' \\ &= 0, \text{ for } t_d = 0. \end{aligned}$$

and

$$\begin{aligned} K\ddot{\Psi}(\lambda, t_d) &= \int_0^\infty e^{-\lambda t''} \left\{ \ddot{\psi}(t_d - t'') + \ddot{\psi}(t_d + t'') \right\} dt'' \\ &= \lambda \int_0^\infty e^{-\lambda t''} \left\{ -\dot{\psi}(t_d - t'') + \dot{\psi}(t_d + t'') \right\} dt'' \\ &= 2\lambda \int_0^\infty e^{-\lambda t''} \dot{\psi}(t'') dt'', \text{ at } t_d = 0. \end{aligned}$$

But since $\frac{d\dot{\psi}(t'')}{dt''}$ is negative, $\frac{d^2\Psi(\lambda, t_d)}{dt_d^2}$ is also negative. Because $\frac{d\Psi(\lambda, t_d)}{dt_d}$ is

zero and $\frac{d^2}{dt_d^2}\Psi(\lambda, t_d)$ is negative at $t_d = 0$ and for all values of the parameters

λ, t_0, τ , it proves conclusively that $\Psi(\lambda, t_d)$ is maximum at $t_d = 0$ in all cases. This is entirely expected from a priori considerations and later it will be shown that this expression gives a more accurate fit to the experimental curves. In the case where the geometry of the counters is not quite symmetrical but each of the counters can receive both radiations in different proportions, the analytical expression is similar with some modification and can be written as

$$\Psi(\lambda, t_d) = \alpha\Psi_1(\lambda, t_d) + \beta\Psi_1(\lambda, -t_d) \quad (7)$$

where α, β are the fractions of the total radiation entering the counters.

It can also be seen that at $t_d = 0$, eqn. (6) becomes $\Psi(\lambda, 0) = \Psi_1(\lambda, 0)$. For all values of t_d , $\Psi(\lambda, t_d) \leq \Psi(\lambda, 0)$, since $\Psi(\lambda, t_d)$ is maximum at $t_d = 0$.

From this it can be shown that, $\frac{\Psi_1(\lambda, 0)}{\Psi_1(\lambda, t_d)} \gg \frac{1}{2} + \frac{1}{2} \frac{\Psi_1(\lambda, -t_d)}{\Psi_1(\lambda, t_d)}$. Now because

$$\frac{\Psi_1(\lambda, -t_d)}{\Psi_1(\lambda, t_d)} \text{ is a non-negative quantity, the expression, } \frac{\Psi_1(\lambda, 0)}{\Psi_1(\lambda, t_d)} > \frac{1}{2}. \quad \dots \quad (8)$$

This is a good check for all experimental curves.

EXPERIMENTAL ARRANGEMENT AND DETAILS

The schematic diagram is shown in Fig. (1), and the circuit diagram in Fig. (4). The two G. M. counters are placed symmetrically with respect

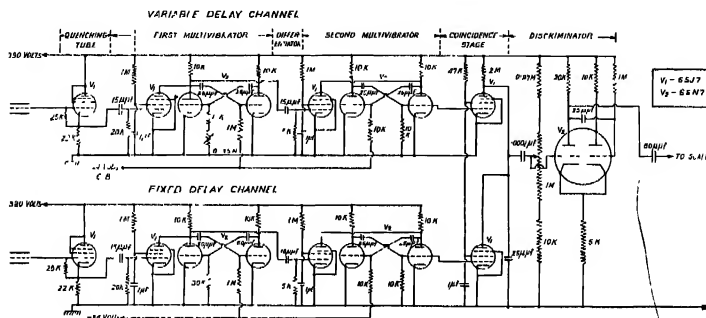


FIG. 4

to the source and a sufficient thickness of matter is placed between them to cut down all β -rays below energies 1.5 mev. The counters are exactly similar having a gamma detection efficiency of about 0.2% and are 3" long and 1" in diameter. The diameter of the central wire is 5 mil. The counters have a starting potential of 850 volts with a plateau of about 200 volts. The lengths of the counters are specially made short to shorten the width of the pulse distribution of the counter and obtain sharp pulses of about 0.25 microsecond rise time.

The pulses from the counters are taken through cathode follower quenching circuits and led to the input of the delay channel. A delay channel consists of an one-shot multivibrator with variable width followed by a differentiator circuit and then a second multivibrator which sharpens and equalises the pulses. For each counter there is one such delay circuit. The delay introduced in one channel is fixed and that in the other is variable. The former is called the "fixed delay channel" and the latter the "variable delay channel". The negative pulse from the quenching circuit triggers the first multivibrator. The consequent square top pulse is differentiated into two pulses, positive and negative, separated by the pulse-width of this multivibrator. The second multivibrator is triggered by negative pulse only and thus the pulse from the second multivibrator will emerge as shifted in time. The differentiator circuit consists of a small resistance and a small condenser.

The simultaneous events in the two counters after going through two channels separately will suffer a shift with respect to each other. This re-

lative shift between the two pulses can be varied by varying the pulse-width of the first multivibrator of the "variable delay channel". Thus if the events causing ionisation in the counter have an intrinsic time-delay between themselves, that can be counter-balanced in the delay unit to record a coincidence, the delay between the events being given by the time delay introduced in the circuit.

In the present arrangement the equalising and pulse-sharpening multivibrators have a pulse-width of 0.5μ second. The first multivibrator of the "fixed channel" has a pulse-width of one microsecond, while that of the variable channel has a pulse-width variable continuously from 1 microsecond to 20 microseconds. The electronic resolving time of the circuit is 0.5 microsecond as measured from the random coincidence counts.

The output pulses from the delay unit are led to the input of the coincidence stage followed by a discriminator circuit. It can be seen from the circuit diagram (Fig. 4) that the grids of 6SJ7, forming the coincidence stage, have been connected directly to the grids of the pulse-equalising multivibrators, to minimise any further broadening of the pulses. The discriminator circuit which cuts off the partials is essentially an one-shot multivibrator set to be triggered only by positive pulses greater than a pre-determined amplitude. The pulses from the discriminator are led to the standard laboratory scalar of 128 to be finally recorded in the mechanical register.

It has been observed that the output pulses of the multivibrator are somewhat modified by the shape and size of the input pulses bringing in uncertainties in triggering the multivibrators and changing the resolving time of the circuit. Care has always been taken to minimise this. Highly stabilised power supplies have been used. At all stages, the pulses are made as sharp as possible and their amplitudes more or less equal.

The delay time introduced in the circuit is directly measured in micro-seconds by comparing with the damped oscillation generated by the time marker circuit specially made for the purpose. As the pulses are very sharp (of the order of a micro-second) it is essential to have a special time base and intensifying arrangement. The diagram for sweep generator with intensifying arrangement and the time marker circuits is shown in Fig. 5.

In the circuit V_1 (6SN7) is a multivibrator triggered by positive pulses fed from a pulse generator. The rectangular negative output of the multivibrator cuts off the current in the sweep generator valve V_2 (6SJ7). The anode voltage of the 6SJ7 therefore rises exponentially—the condenser 0.001 mfd. being charged through the 30 kilo ohms anode resistance. This is applied to the X-plates of the oscillograph and produces the horizontal sweep. The diode 6U6 limits the rise up to a voltage set by the 100 kilo ohms potentiometer. Above this voltage, the diode conducts and prevents further rise of voltage. The movement of the cathode-ray beam is therefore brought to a halt at this point. As the rectangular pulse of the multivibrator ter-

the oscilloscope cathode-ray tube. The "brilliance control" on the oscilloscope is adjusted to normally cut off the beam entirely. The beam is switched on by the amplified positive voltage at the forward stroke only. Thus the phenomenon only on the short rapid forward stroke is presented, at other times the tube remains dark.

Simultaneous with the generation of the rapid forward sweep, the positive pulse from the other tube of the multivibrator "shock excite" a "medium wave" tuned circuit generating damped oscillations at a frequency of 1 Mc/s. These may be applied when desired, to one beam of the double beam oscilloscope and used as time marker

Sharp pulses from a pulse generator (Banerjee, 1945) are introduced simultaneously through the delay channels and the output of the delay channels are connected to the two vertical plates and the time base voltage is applied to the horizontal plate of the double beam oscilloscope (Cossor). The time separation of the two pulses on the oscilloscope screen is then measured in comparison with the damped oscillation on the same as shown in Fig. 6.

EXPERIMENTAL RESULTS

The experimental results have been shown in Fig. 7, where coincidences per minute are plotted against time-delay in microsecond for cobalt (60) and titanium (46). Cobalt (60) (Mukherjee and Das, 1948) is known to emit

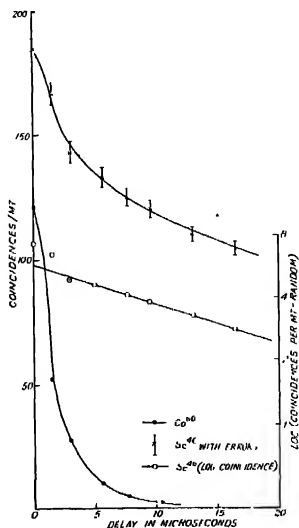


FIG. 7

two gamma rays in immediate succession without any delay and is thus a convenient source for calibrating the counters and the electronic circuits. The curve obtained for cobalt (60) is due to the normal pulse distribution of the counters. The logarithm of the coincidence counts per minute (random counts being subtracted) against time delay in microseconds is plotted for titanium (46) in the same figure and from this, the half life of the isomeric state is found to be 13.2 ± 0.8 micro-second, without the correction for the pulse-width distribution of the counter.

In Fig. 8 are given the theoretically computed curves from equations (2), (4), (5) and (6). For cobalt (60), $\frac{\psi(t_d)}{\psi(0)}$ is plotted against time delay t_d . It will be seen that the experimental curve approaches more slowly than the theoretical curve. This is, as explained earlier, probably due to the non-

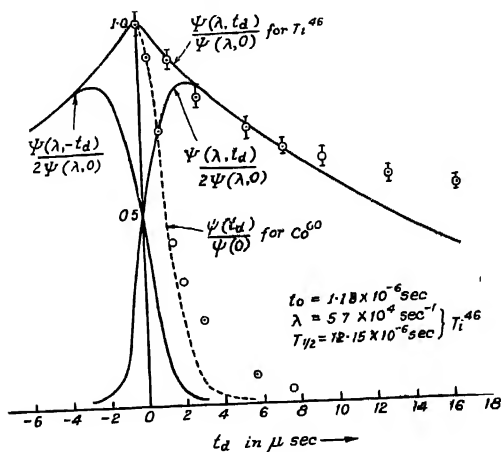


FIG. 8

Gaussian nature of the distribution function of the time lag in counters. It is found that for a family of curves, with different values of t_0 , the best fit with the experimental curve is obtained with a value of $t_0 = 1.13 \times 10^{-6}$ secs.

For scandium (46), $\frac{\psi(\lambda, t_d)}{\psi(\lambda, 0)}$ is plotted against t_d and for $t_0 = 1.13 \times 10^{-6}$ secs, the best fit with the experimental value is obtained for $\lambda = 5.7 \times 10^4 \text{ sec}^{-1}$. This gives a half life of 12.15 ± 0.2 microseconds. The error is calculated from the difference of the two extreme values of λ for which the curves just touch the experimental points.

The two functions in the expression (6) are plotted separately for titanium (46) excited state and the resulting curve $\frac{\Psi(\lambda, t_d)}{\Psi(\lambda, 0)}$, it will be found (in Fig. 8), lies on the experimental points. As we previously expected $\frac{\Psi(\lambda, t_d)}{\Psi(\lambda, 0)}$ is maximum at $t_d = 0$.

Bunyan, Laundby and Walker (1940) have also calculated the probability for the delayed coincidence and their expression is similar to $\Psi_1(\lambda, t_d)$ of our case. In their case, the expression $\frac{d}{dt_d} \Psi(\lambda, t_d)$ is not zero at $t_d = 0$ and so $\Psi(\lambda, t_d)$ is maximum at some positive value of t_d and not at $t_d = 0$. This is justified because Bunyan *et al* in observing α - β and β - γ coincidences have used proportional counters to detect α which does not detect β and proportional counter sensitive only to β and not to γ . So the probability that the first radiation may enter channel B and that the following radiation may enter channel A, does not arise. But for all general cases including γ - γ coincidences the complete expression for probability will be given by equation (6).

It has been mentioned earlier that equation (8) is a good check for all the experimental curves. Using this check for the published curves of delayed coincidences against delay time, it is found to agree in all cases, except in one (Fig. 3 of Bunyan *et al*, 1949). Probably some errors were made in the time co-ordinate.

The maximum energies of the betaparticles in course of the disintegration were determined by the absorption measurements of beta-rays, using aluminium absorbers for which a thin source was mounted on aluminium

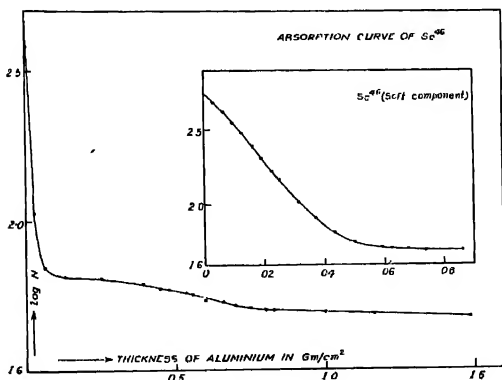


FIG. 9

foil. The semi-log plot of the number of counts per minute against thickness of absorbers of aluminium in gm/cm^2 is shown in Fig. 9. The strength of the source was 100 micro-curies initially. The absorption curve shows the existence of the two groups of beta-rays and confirm the results obtained by Walke (1940) and Peacock and Wilkinson (1948). The energy maxima of the two groups as determined by Feather plots are 0.34 mev. and 1.52 mev. These values are corrected for the window thickness for the counter and the errors are due to scattered electrons, thickness of the source and in counting. The total number of counts taken for each point is 10,000. The errors introduced in counting and self-absorption are estimated as ± 0.006 mev for low energy beta-ray group and ± 0.015 mev for the high energy beta-ray group. Absorption curve for RaE in equilibrium with RaD and its decay products has been used for the Feather plot. The proportion of the two groups of beta-rays have been calculated assuming the efficiencies of our counters to be same for the high and the low energy beta-rays and calculating the areas under each of the absorption curves extrapolated to zero absorption. The number of disintegration in the low energy beta-ray group is found to be 97.7% of the total number of beta-rays, corrections if any, due to scattered electrons from gamma-rays are not taken into account.

Coincidence experiments between β - γ and γ - γ were performed with various absorbers between the source and the two counters. β - γ coincidence experiments were performed with an aluminium absorber in front of the β -counter to cut off β -rays below 0.36 mev. and absorbers in front of the γ -ray counter were changed to obtain the decrease in coincidence counts and hence to decide whether the 1.12 mev. γ -ray or 0.89 mev. γ -ray was being observed in the coincidence experiments. The half-value thickness indicated a γ -ray of energy less than 1 mev. The number of coincidences between the high energy β -ray (1.5 mev.) and the following γ -ray (0.89 mev.) was 1.6 times that between two γ -rays. Corrections for the γ -counts in the β -ray counter were not made as the observations were thought definitely conclusive that the 0.89 mev. γ ray was in coincidence with 1.52 mev. β -rays. Further confirmation was obtained in the delayed coincidences, measurements in which delayed coincidences following the same-decay period were observed were observed between the 1.52 mev. β -ray and the 0.89 mev. γ -ray, as was observed between the two γ -rays. Observations on β - β coincidences gave counting rates no greater than the accidental rate, after correcting for the γ -counts in the β -ray counters. Taking the efficiencies of the β -ray counters into account and the numbers of γ -rays counted by these counters, the proportion of the high energy β -ray is estimated as 2.2%, which is in accordance with absorption experiments.

We repeated Peacock and Wilkinson's observations and confirmed that the ratio of the intensities of the two β -rays was observed to remain the same over the period of observation which was about one half-life (85 days). Our conclusion is that the high energy electrons of

maximum energy 1.52 mev. is due to a beta-disintegration of the same state of scandium (46) that emits the low energy beta-rays of maximum energy 0.34 mev. This agrees with the observations of Peacock and Wilkinson (1948) regarding the energy level scheme.

DISCUSSION

Sc^{46} decays to Ti^{46} by a complex process which is illustrated in Fig. 10. The composite half-life is 85 days and the end-energies of the two

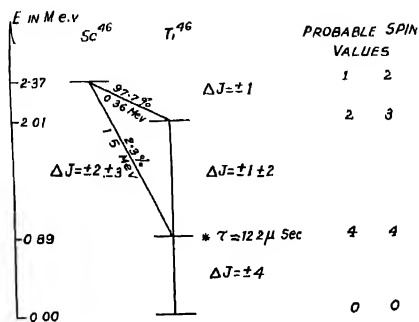


FIG. 10

β -disintegrations are 0.36 and 1.50 mev. respectively. If the disintegration constant be determined by λ_1 and λ_2 , the probabilities of disintegrations of the low and high energy rays respectively, then we obtain,

$$\lambda_1 : \lambda_2 = \text{ratio of activities} = 42.5$$

and

$$\lambda = \lambda_1 + \lambda_2.$$

From these we obtain $t_1 = 7.5 \times 10^6$ secs for 0.36 mev. β -disintegration and $t_2 = 3.2 \times 10^8$ secs. for 1.50 mev. β -disintegration. This is explicable in terms of selection principles.

The values of ' ft ' for the two transitions are computed from the equation given by Konopinski (1943).

For β -disintegration with end energy 0.36 mev., we obtain $f = 0.25$, $t = 7.5 \times 10^6$ secs and therefore ' $ft' \approx 1.9 \times 10^6$ '. The transition is of 1B type. Using G-'I' selection rules we should have $\Delta J = 0, \pm 1$ (no $0 \rightarrow 0$).

Similarly for β -disintegration with end energy 1.50 mev., $f = 43.5$, $t = 3.2 \times 10^8$ secs and ' $ft' = 1.4 \times 10^{10}$ '. The transition is 2B (or higher B) type and $\Delta J = \pm 2, \pm 3$ (no $0 \rightarrow 2$).

Using Weizsäcker formula given by $\tau = 10^{-14} \left(\frac{\hbar c}{ER} \right)^{2(\Delta J - 1)}$ the spin difference (ΔJ) between the ground state and the observed metastable state ($\tau = 12.15 \times 10^{-6}$ secs.) of Ti^{46} has been calculated to be ≈ 4 .

If the spin of the ground state of Ti^{46} is assumed to be zero, the decay scheme of Sc^{46} in light of the informations obtained at present may be indicated as in Fig. 10.

The conversion coefficient of 0.89 mev. gamma-ray as calculated from the expression given by Dancoff and Morrison, (1939) is found to be 1.04×10^{-2} . No detectable conversion electrons above the scattering background were obtained by us experimentally.

The isotopic weight of Sc^{46} is 45.96909 determined from the Q of the d-p reaction of scandium (45) given by Davidson (1939). The isotopic weight of Ti^{46} is known to be 45.9661. Thus we find that $\text{Sc}^{46} - \text{Ti}^{46} = 2.4$ mev. This agrees with the total energy release in β and γ transitions, as obtained from the energy level scheme, within the experimental errors of mass determination.

In the nuclear chart ${}_{21}\text{Sc}^{46}$ lies between ${}_{20}\text{Ca}^{46}$ and ${}_{22}\text{Ti}^{46}$. The isotopes Ca^{46} and Ti^{46} are stable, their abundance being given as 0.0033 % and 7.95 % respectively. Thus Sc^{46} may either transform to Ca^{46} by K-capture or positron emission or it may decay to Ti^{46} by electron emission.

M. N. Saha and A. K. Saha (1946) have given, on the basis of Bethe-Weizsäcker mass formula, expressions for the energy release in β^- and β^+ disintegration and in K-capture. The formulae are for a nucleus, ${}_Z\text{M}^A$ (e. g. ${}_{21}\text{Sc}^{46}$.)

$$E^- = A^-(Z, A) - \chi(Z, A)$$

$$E^+ = A^+(Z, A) - \chi(Z, A)$$

$$E^h \approx E^+ + 2m$$

Here χ is the spin dependent term, A^- and A^+ are given by the formulae,

$$A^- = 0.766 + \frac{4\beta(I-1)}{A} - \frac{0.58(A-I+1)}{A^{1/3}}$$

$$A^+ = -1.788 - \frac{4\beta(I+1)}{A} + \frac{0.58(A-I-1)}{A^{1/3}}$$

where I = isotopic number = $N - Z$ (here $I = 4$) and β is a constant whose value in this region is found to be between 19.5 mev. and 22.5 mev.

Applying for Sc^{46} and taking $\beta=19.5$ mev., we easily get $A^-=-1.11$ mev : since the observed value of $E^-=2.37$ mev., $\chi(22, 46)=-3.48$ mev.

The value of $A^+ = -3.63$ mev., hence $E^+ = -0.15$ mev., i.e., there would be no positron emission.

But $E^k = 1.02 + 0.45 = 0.87$ mev., hence K -capture is possible. We then have $f^k \approx 0.17$.

There is no evidence in previous observations about the transformation of Sc^{46} to Ca^{46} by positron emission. Walke, Williams, and Evans (1939) obtained photographs of the tracks of photo-electron in the cloud chamber, and deduced that Sc^{46} decays to Ca^{46} by K -capture. Meitner (1945) also deduced that Sc^{46} decays by K -capture to Ca^{46} . The ratio of K -capture to β^- -emission is given as 3 : 2. But the results are stated to be preliminary. We have not been able either to prove or disprove the existence of K -capture on account of the small amount of Sc^{46} at our disposal.

The source used was scandium oxide irradiated by neutrons and prepared for us by the atomic energy establishment at Harwell, U. K.

ACKNOWLEDGMENTS

Our thanks are due to Prof. M. N. Saha, F. R. S. for his kind interest in the work. We are indebted to Mr. B. M. Banerjee for his help in the electronic circuits. We also wish to thank Messrs. U. C. Guha, S. Datta-Mazumdar and A. P. Patro for helpful discussion in the theoretical part of the work.

INSTITUTE OF NUCLEAR PHYSICS
CALCUTTA UNIVERSITY

REFERENCES

- Banerjee, B. M., 1945, *Ind. J. Phys.*, **19**, 75.
 Bradt, H. and Scherrer, P., 1943, *Helv. Phys. Acta*, **16**, 251 & 259.
 Bunyan, D. E., Laundby, A., Ward, A. H. and Walker, D., 1948, *Proc. Phys. Soc.*, **61**, 300.
 Bunyan, D. E., Laundby, A. and Walker, D., 1949, *Proc. Phys. Soc.*, **62**, 253.
 Dancoff, S. M. and Morrison, P., 1939, *Phys. Rev.*, **55**, 122.
 Davidson, W. L. (Jr.), 1939, *Phys. Rev.*, **55**, 1062.
 De Benedetti, S. and McGowan, F. K., 1946, *Phys. Rev.*, **70**, 569 (14).
 De Benedetti, S. and McGowan, F. K., 1948, *Phys. Rev.*, **74**, 738.
 Feister, I. and Curtiss, L. P., 1947, *J. Research Nat. Bur. Stand.*, **58**, 411.

- Goldhaber, M. and Muelhause, C. O., 1948, *Phys. Rev.*, **74**, 1877.
- Hirzel, O., Stoll, P. and Waller H., 1947, *Helv. Phys. Acta*, **20**, 241.
- Jurney, E. T., 1948, *Phys. Rev.*, **74**, 1049.
- Konopinski, E. J., 1943, *Rev. Mod. Phys.*, **15**, 209.
- Mandeville, C. F. and Scherb, M. V., 1948, *Phys. Rev.*, **73**, 141.
- McGowan, F. K., De Benedetti, S., and Francis, J. B. (Jr) 1949, *Phys. Rev.*, **75**, 1761 (L).
- Meitner, L., 1945, *Arkiv. F. Mat. Astro. Och. Fys.* **A**, **32**, No. 6.
- Miller, A. and Deutsch, M., 1947, *Proc., Am. Phys. Soc.*, **22**, 7.
- Montgomery, C. G. and Montgomery, D. D., 1940, *Phys. Rev.*, **57**, 1045.
- Mukherjee, A., and Das, S., 1948, *Ind. J. Phys.*, **22**, 311.
- Nag, B. D., Sen, S., and Chatterjee, S., 1949, *Nature*, **164**, No. 4180, 1001 (L).
- Nag, B. D., Sen, S., and Chatterjee, S., 1950, *Ind. Jour. Phys.*, **24**, 261.
- Peacock, C. and Wilkinson, R. G., 1948, *Phys. Rev.*, **74**, 297 & 1240 (A).
- Rossi, B. and Nereson, S., 1942, *Phys. Rev.*, **62**, 417.
- Saha, M. N. and Saha, A. K., 1946, *Proc. Nat. Inst. Sci. India*, **2**, 193.
- Van Name, F. W. (Jr), 1949, *Phys. Rev.*, **75**, 100.
- Walke, H., Williams E. J. and Evans, G. R., 1930, *Proc. Roy. Soc.*, **A171**, 360.
- Walke, H., 1940, *Phys. Rev.*, **57**, 163.

A TRIGGERING DEVICE FOR ARC DISCHARGE LAMPS USED IN CLOUD CHAMBER PHOTOGRAPHY*

By RANJIT KUMAR DAS

(Received for publication, Sept. 6, 1950)

ABSTRACT A new triggering circuit is described. The circuit has been designed for the specific purpose of cloud chamber photography. In addition to its normal function as a trigger, it effectively controls the requisite time delay between the passage of a cosmic ray particle and its subsequent illumination for photography.

INTRODUCTION

Every cloud chamber worker is fully alive to the vital importance of a powerful light source for momentary illumination of the sensitive volume of the chamber. Until recent years, the illumination was provided almost exclusively by the simultaneous supercharging of several low voltage (usually 110 volts) electric glow lamps at a higher voltage; carbon arcs and various high voltage transformer-operated devices, such as, the mercury pool arc discharge lamps, were also used. These latter tubes, though satisfactory sources of illumination, are rather troublesome in that they require pre-heating of mercury to produce sufficient mercury vapour before an arc discharge can be initiated. The introduction of modern Kr-Xe filled lamps has ushered in a new era in the technique of cloud chamber photography. These tubes provide an intense momentary illumination rich in photographically useful wavelengths. They require a sharp high voltage pulse on an external electrode for the initiation of the arc discharge. The few triggering devices found in the literature utilise some variants of the basic triggering circuit developed by Edgerton (1931, 1937,) and Germeshausen (1935). This circuit and its variants employ the rather costly and bulky high power thyratrons FG 17, FG 67 etc. in association with one or more ionization transformers. Apart from the high cost, the local non-availability of the requisite high power thyratrons has led us to develop the triggering circuit described in this paper. This circuit, besides having its primary function as a trigger, serves another very useful purpose in conjunction with the cosmic-ray pulse recorder circuit which will be described in the sequel.

THEORY OF THE TRIGGER CIRCUIT

It is well known that whenever an inductive circuit, of inductance L , say, is associated with a current variation di/dt in it, an E. M. F. $e = -L di/dt$

* Communicated by Prof. M. N. Saha.

is developed at one of its terminals. The greater this time rate of current variation the larger is the magnitude of the E. M. F. developed. In the present circuit this time rate of decay current has been highly augmented by the extremely sharp stoppage of the current through an inductance L in series with the plate of an 807 tube. The abrupt current stoppage has been made possible by the use of a very steeply descending wave-front of a nearly rectangular pulse generated by a properly adjusted multivibrator unit.

THE CIRCUIT OPERATION

The portion of the circuit within the dotted rectangle in Fig. 1 is the trigger circuit proper. Tubes T_1 and T_2 constitute the multivibrator unit. When a negative pulse of proper magnitude arrives at the input of the tube T_1 , the multivibrator, by its cumulative feed-back effect, generates an approximately rectangular pulse at the output with steeply ascending and descending sides. The length of the pulse is chiefly determined by the feed-back condenser C_4 and the voltage swing is nearly the full potential applied to it.

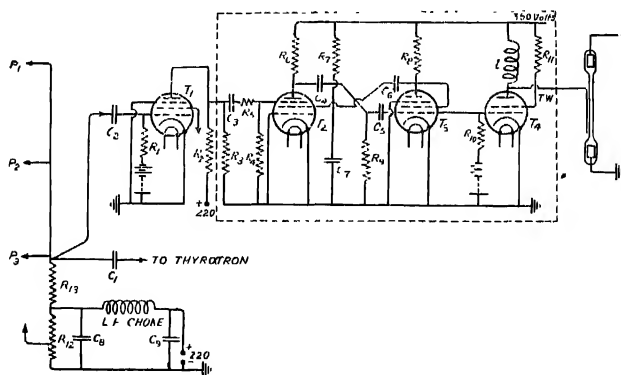


FIG. 1

Schematic diagram of the trigger circuit.

$C_1 = C_2 = 0.01$, $C_3 = 0.0002$, $C_4 = C_5 = 1$, $C_6 = 0.01$, $C_7 = 0.005$, $C_8 = C_9 = 10$
 $R_1 = R_3 = R_4 = R_9 = R_{10} = 10^6$, $R_2 = 25 \cdot 10^6$, $R_5 = 10 \cdot 10^3$, $R_6 = 1 \cdot 10^4$, $R_7 = 10^5$, $R_8 = 5 \cdot 10^4$
 $R_{11} = 20 \cdot 10^3$, $R_{12} = 5 \cdot 10^3$, $R_{13} = 10^6$.

P_1 , P_2 , P_3 → plates of coincidence pulse amplifiers.

$T_1 = 6SJ7$, $T_2 = 6V6$, $T_3 = 6V6$, $T_4 = 807$

(All resistances are in ohms and capacitances in microfarads).

This rectangular output pulse generated by the multivibrator actuates a similar current pulse in the plate circuit of the biased tube 807. Due to the extreme steepness of the voltage pulse, the current through the inductance L in the plate circuit of the 807 tube is abruptly cut off and the consequent

high time rate of decay of the plate current generates a momentary voltage pulse $L di/dt$, the magnitude of which exceeds a few thousand volts, depending on the inductance of the coil and the screen grid voltage of the 807 tube. This pulse is sufficiently large to trigger the flash tubes.

DISCUSSION

In earlier works we used a 6L6 tube in series with the trigger coil. The circuit worked satisfactorily for the first few months. Subsequently, however, troubles developed in the form of sparking between the plate and cathode and, as a result, the required triggering at the flash tube did not occur. With the 807 tube this difficulty was completely overcome and the triggering was cent per cent successful. With new flash tubes the triggering coil might conveniently be an air cored I. F choke. But as the tube aged more and more hard triggering was necessary and an iron-cored I. F choke served the purpose quite satisfactorily. It was found convenient to use an iron-cored choke right from the beginning. The length of the wire connecting the copper trigger proper to the coil was found to have a definite bearing on the performance of the circuit. For wire lengths exceeding an optimum value, practically no triggering was obtained. Further, unlike in other triggering practices, the output triggering voltage pulse could not be led along two channels to operate two flash tubes simultaneously. With apparently equal lengths of connecting wire it was found that sometimes one and sometimes the other tube flashed. The number of times both the tubes flashed simultaneously was practically negligible. This preferential behaviour of the triggering pulse could not be explained on any known ground. One possibility suggested that there is some inherent difference in the construction of two apparently identical flash tubes (Type IT 126 Int. G. E. C.).

One peculiarity of the above circuit is that contrary to usual practice, the negative input pulse is fed to the suppressor grid rather than to the normal control grid of the tube T_2 . This is necessitated by the fact that with the normal control grid the multivibrator becomes extremely sensitive, so much so, that the slightest voltage variation at the input (in this case a little over 1.5 volts) trips the circuit. This is highly undesirable for the specific purpose at hand. The flash tube is expected to illuminate the sensitive volume of the chamber only when there is real synchronization with a recordable event. Any spurious flash means wastage of photographic films and the risk of superposed exposures. By shifting the input channel to the suppressor, the multivibrator has been made insensitive to any input pulse less than -32 volts. In this way the number of spurious flashes due to electrical pick-ups has been reduced almost to nil.

To synchronize a flash with a recordable event in the cloud chamber, the tripping in the trigger circuit is done by the coincidence pulse from the common plate resistor R_{13} of the parallel connected amplifier valves. This

pulse is positive in sign and requires a reversal of sign before it can operate the trigger unit. This sign-reversal is done by feeding the coincidence pulse to the input of a normally biased tube T_1 . A pulse of current flows through the plate circuit of the amplifier and a negative voltage pulse of more than 150 volts is obtained.

A great advantage of the circuit is that the requisite delay between the passage of a cosmic ray particle through the chamber and the subsequent flashing of discharge tubes can be efficiently controlled by manipulating the capacitances C_1 and C_2 in the multivibrator unit.

ACKNOWLEDGMENTS

The author wishes to express his thanks to Prof. M. N. Saha, D. Sc., F.R.S., for his kind interest. He is much indebted to Sri B. M. Banerjee, M. Sc., for his unstinted help in designing the circuit, and to Dr. P. C. Bhattacharyee for valuable discussion.

INSTITUTE OF NUCLEAR PHYSICS
CALCUTTA UNIVERSITY.

REFERENCES

- Edgerton, H. E., 1931, *Elec Eng.*, **50**, 327
 Edgerton, H. E., 1937, *J Appl. Phys*, **1**, 8.
 Edgerton, H. E. and Geimeshausen, K. J., 1935, *Rev. Sci. Instr.*, **3**, 535.

PHOTOGRAPHIC EMULSION STUDIES OF THE LATITUDE EFFECT

By K. R. DIXIT

(Received for publication, September, 16, 1950)

ABSTRACT. Nuclear emulsions exposed and studied under identical conditions except for a change of 39° in the magnetic latitude show a significant difference of about 43 per cent. in the number of single tracks ($>100\mu$). The experiments appear to suggest that the causes which produce the stars and the singles ($>100\mu$) at an altitude of 2200 m are independent of one another.

Nuclear emulsion 50μ Ilford C 2 plates were exposed simultaneously for about 15 days, near Ootacamund and near Simla. The plates exposed simultaneously at the two places, were from the same batch manufactured at the same time. After the exposures were over, the plates from the two places were brought to Bombay by rail and processed together within a week. During the exposure the plates were wrapped in a black paper, and kept in a light-tight cardboard box, which in its turn was kept in a thin tin box hermetically sealed. The plates were kept horizontal during the time of exposure to the cosmic radiations. For processing the plates the standard Powell technique was used. After processing, the plates were scanned with a binocular microscope at a magnification of 320. This magnification enabled us to note all the details and at the same time maintain a reasonable scanning speed. More details were observed with a higher dry magnification and also with oil immersion. Photomicrographs of interesting events were also taken. To maintain uniformity and remove all personal differences in scanning, the materials exposed simultaneously at Ootacamund and Simla were scanned by the same scanner.

Scanning of a reasonable amount of emulsion from each of three batches has been completed. From each group of plates exposed at one place, an area of about 70 sq cms and a volume of about 0.35 ml has been scanned. In all the total area scanned so far is about 500 sq cms and a volume of about 2.5 mls. Tables II to VII show the results of the scanning. Tables II and III, IV and V, VI and VII, refer to pairs of simultaneous exposures at the two places. Each pair of tables represents the results of scanning by the same observer and represents comparable data. In choosing events mentioned in the tables, as due to cosmic rays, the usual precautions were taken and stars were excluded when stars up to five-fold did not have at least one ray longer than 60μ . The singles included in the tables are all longer than 100μ . This kind of selection may exclude from counting some events which may be due to cosmic rays (like the 20μ short singles of Taylor, Bhabha and collaborators (1950): we also observed a large number of such short singles in plates exposed both at Ootacamund and Simla but we have

not studied them systematically so far) but is not likely to include any event produced by the radioactive contamination. As our object in the present series of experiments was mainly to study the latitude effect by the use of photographic plates—as this technique has not yet been used as widely as the counter technique in the investigation of the latitude effect—the above discrimination in favour of the true cosmic ray events, in selection, was considered most desirable.

The information about the dispositions of the two places where the plates were simultaneously exposed is given in Table I.

TABLE I

	Ootacamund	Simla
Geographic Latitude ...	11°24'N	31°06'N
Geographic Longitude ..	76°44'E	77°10'E
Magnetic latitude (Dip)	6°	45°
Magnetic longitude (Declination)	1°	1°25'
Altitude	7300 ft.	7280 ft.

It will thus be seen that the differences between the two sets of observations could be attributed to the change in the magnetic latitude.

TABLE II

Batch A. Exposed at Ootacamund.

Area scanned 70.5 sq. cms.

Volume scanned 0.35 ml.

Event	Total number observed	Number in ml. per day
3 fold	58	11
4 fold	36	7
5 fold	33	6.3
6 fold	2	~ 0.4
7 fold	1	~ 0.2
9 fold	2	~ 0.4
10 fold	1	~ 0.2
Stars with more } than 5 rays }	6	~ 1.2
Singles > 100 μ	749	143
Singles > 1000 μ	5	~ 1

Details of the extra long singles

1-1000 μ

1-4000 μ

1-1100 μ

1-6500 μ

1-2700 μ

TABLE III

Batch A. Exposed at Simla.

Area scanned 71.25 sq. cms.

Volume scanned 0.36 ml.

Event	Total number observed	Number in ml. per day
3 fold	61	10.7
4 fold	47	8.2
5 fold	39	6.8
6 fold	4	~ 0.8
7 fold	2	~ 0.1
8 fold	1	~ 0.2
9 fold	1	~ 0.2
Stars with more } than 5 rays }	8	~ 1.6
Singles > 100 μ	1188	
Singles > 1000 μ	10	

Details of the extra long singles.

1-1000 μ 1-1500 μ 2-1100 μ 2-1800 μ 1-1200 μ
 1-1900 μ 1-1300 μ 1-4400 μ

TABLE IV

Batch B. Exposed at Ootacamund.

Area scanned 71.25 sq. cms.

Volume scanned 0.36 ml.

Event	Total number observed	Number in ml. per day
3 fold	53	10
4 fold	32	6
5 fold	19	3.8
6 fold	2	~ 0.4
8 fold	1	~ 0.2
Stars with more } than 5 rays. }	3	~ 0.6
Singles > 100 μ	702	132
Singles > 1000 μ	4	~ 0.8

Details of the extra long singles.

1-1200 μ 1-2700 μ 1-1700 μ 1-3000 μ

TABLE V

Batch B. Exposed at Simla.

Area scanned 70.5 sq. cms.

Volume scanned 0.35 ml.

Event	Total number observed	Number in ml. per day
3 fold	50	9
4 fold	33	6
5 fold	23	4.5
8 fold	1	~ 0.2
Stars with more } than 5 rays. }	1	~ 0.2
Singles > 100 μ	1083	104
Singles > 1000 μ	9	~ 1.7

Details of the extra long singles

1-1000 μ 1-2400 μ 4-1100 μ 1-3900 μ 2-1200 μ

TABLE VI

Batch C. Exposed at Ootacamund.

Area scanned 71.25 sq. cms.

Volume scanned 0.36 ml.

Event	Total number observed	Number in ml. per day
3 fold	41	7.6
4 fold	30	5.6
5 fold	10	~ 2
7 fold	2	~ 0.1
8 fold	1	~ 0.2
12 fold	1	~ 0.2
16 fold	1	~ 0.2
Stars with more } than 5 rays. }	5	~ 1
Singles > 100 μ	753	141
Singles > 1000 μ	8	~ 1.6

Details of the extra long singles.

1-1300 μ 1-2000 μ 3-1700 μ 1-2300 μ 1-1900 μ 1-3300 μ

It will be seen that the two places where simultaneous exposures were given are comparable in every respect, except for a change of dip of about 39° . Further as the plates in one simultaneous exposure belonged to the same batch, were processed at the same time and were scanned by the same scanner, no significant differences could be expected to occur on this account.

N.B. :—The longest two end in emulsion and have been identified as protons and their energies are about 30 Mev. and 40 Mev. respectively

TABLE VII

Batch C. Exposed at Simla

Area scanned 69.75 sq. cms Volume scanned 0.35 ml.

Event	Total number observed	Number in ml. per day
3 fold	29	5.2
4 fold	28	5
5 fold	22	4
6 fold	2	~ 0.4
10 fold	1	~ 0.2
Stars with more } than 5 rays }	3	~ 0.6
Singles $> 100 \mu$	1093	195
Singles $> 1000 \mu$	14	2.5

Details of the extra long singles

2-1000 μ	1-2100 μ	1-1100 μ	1-2300 μ
2-1600 μ	2-2400 μ	1-1700 μ	1-2700 μ

A comparison of Tables II to VII will show a very significant difference in the number of singles ($> 100 \mu$) between the two places. The ratio of such singles comes out as about 1.43 ± 0.01 . This difference can be considered as real, significant and not statistical, specially as we are dealing with a very large number of singles and also as the number of these events does not show a great fluctuation from one group of plates to another group of plates.

Beets, Morand and Winand (1949) find with G5 and C3+B plates a difference of 2.4 in the number of stars (> 2 branches) at an altitude of 4500 m. between geomagnetic latitudes 44°N and 1°S . This factor is deduced by them from observations made at 4500 m altitude in the geomagnetic latitude of 1°S and at an altitude of 3470 m at geomagnetic latitude 44°N . By using the same mode of calculation, we can find out what this ratio should have been if their observations were made at an altitude of about 2200 m., and we find that the result comes out at about 1.5. No great significance, however, need be attached to the similarity between the

value of Beets *et al* and our value. Their results at the two places of observation are not as strictly comparable as ours. Further the ratio determined by them was for stars (> 2 branches), whereas, the ratio determined by us is for singles ($> 100 \mu$). The ratio of the number of stars and the number of singles is, however, nearly constant (Thomson, 1949) under the same conditions.

According to Thomson (1949), some single tracks must be due to primary protons, but these are too few to account for more than 1 per cent. (These are probably the extra long singles mentioned in Tables II to VII). Tracks from stars outside the emulsion amount to about 10 per cent. and the neutrons which presumably accompany the stars might be expected to produce about 1 per cent. by knocking on the protons in the emulsion. The remaining 88 per cent., according to him, must have some independent cause. Our results appear to indicate that this independent causative radiation is influenced by the magnetic field of the Earth.

According to Forster (1950) the number of heavy particle tracks (singles) found in the emulsion shows an exponential decrease with altitude similar to that of stars. From this observation he suggests that the majority of single tracks found in the photographic emulsion originate in nuclear disintegrations (stars) produced in the neighbourhood of photographic plates. If we apply this suggestion of Forster to the majority of singles ($> 100 \mu$) observed by us they will have to be regarded as part of the stars produced in the neighbourhood of the photographic plates; and we shall have to assume that such stars are produced by some radiation which is sensitive to the magnetic field of the Earth. Such an interpretation is difficult to reconcile with the view that the majority of star-producing particles at altitudes below 4000 m are energetic neutrons (page, 1950), or that only 17 per cent. of all stars are caused by ionising primary particles (page, 1950). Our experiments thus appear to support the view of Thomson that the majority of singles ($> 100 \mu$) is produced by some independent cause, and that this independent causative radiation is affected by the magnetic field of the Earth.

THE INSTITUTE OF SCIENCE
MAYO ROAD, BOMBAY 1.

REFERENCES

- Beets, C., Morand M. and Winand L., 1949, *C. R. Acad. Sci. Paris*, **229**, 1227.
 Forster, H. H., 1950, *Phys. Rev.*, **78**, 247.
 Page, Nora, 1950, *Proc. Phys. Soc.*, **63A**, 250.
 Taylor, H. J., Bhabha, H. J., Daniel, R. R., Heeramaueck, J. R., Swami, M. S. and Shrikantia, G. S., 1950, *Proc. Ind. Acad. Sci.*, **31A**, 130.
 Thomson, G. P., 1949, *Phil. Mag.*, **40**, 589.

ON THE ABSORPTION OF U.H.F. RADIO WAVES BY OPALESCENT BINARY LIQUID MIXTURES*

By (MISS) ANJALI CHOUDHURY

(Received for publication, October 7, 1950)

ABSTRACT The absorption of ultra high frequency radio waves in two opalescent mixtures, *e.g.*, (1) nitrobenzene (50%)+hexane (50%) at 14°C and (2) aniline (46%)+cyclohexane (54%) at 34.5°C have been investigated in the frequency range 300–510 megacycles per sec. It has been observed that in each case a new absorption peak appears on the low-frequency side of the original peak observed in the case of one of the pure constituents having polar molecules. There is also another peak in the position of the original peak, but its height is much smaller than that in the pure liquid. It is concluded from these results that in the case of each of the two mixtures the polar molecules form two types of groups, in one of which the nature of packing of the molecules is identical with that in the pure liquid and in the other type the molecules are more closely packed.

The non-polar molecules of the solvent do not seem to be able to penetrate into these groups of polar molecules. It is pointed out that this method gives definite information regarding the change in the intermolecular field which takes place with the mixing up of polar molecules with non-polar molecules and furnishes definite information regarding the composition of the groups formed in opalescent mixtures.

INTRODUCTION

It was first shown by Krishnan (1935a) that the value of ρ_h observed in the case of the light scattered transversely by opalescent binary liquid mixtures is different from unity, although in the case of clear solutions the value is unity. This discrepancy was explained by Krishnan on the hypothesis that in the clear solution the scattering is due to single molecules whereas, in the opalescent mixture it is due to clusters of molecules. It was also assumed that the size of the cluster changes with the change of temperature of the opalescent mixture and at temperatures far away from the critical temperature, at which the mixture shows opalescence, the groups vanish. These light scattering data only show that there is local fluctuation in density in the mixture owing to the presence of small elementary volumes larger than single molecules and of such composition as produces heterogeneity in the elementary volumes. No information regarding the actual composition of elementary volumes or groups of molecules can, however, be obtained from the light-scattering data excepting the fact that the scattering is due to ellipsoidal particles of size not very small in comparison with the wavelength of light. It has, however, been shown recently by Sirkar and Sen (1949a) and also by Sen (1949) that the anomalous absorption

* Communicated by Prof. S. C. Sirkar

of ultra high frequency radio waves observed by Drude (1897) and other workers is exhibited by many organic liquids and polar molecules if the temperature of the liquids is suitably adjusted and a suitable range of frequency of incident radio waves is chosen. It is well known that applying Debye's theory, we can find out from the frequency of the absorption peak the viscous forces acting on the individual molecules. Since these forces are produced by the surrounding molecules, comparison of the position of the absorption peak observed in the case of the pure liquid with that observed in the case of the opalescent mixture gives us an idea of the change which takes place in the intermolecular forces on mixing the liquid with another liquid to form the binary mixture. This method is thus suitable for studying the nature of intermolecular field acting on the individual polar molecule in the opalescent binary mixture and is expected to furnish definite information regarding the composition of the groups of molecules which are responsible for the opalescence of the mixture. It has, therefore, been decided to study the absorption of U.H.F. radio waves in a large number of opalescent binary liquid mixtures in order to find out the nature of the clusters of molecules formed in the mixture, and in the present paper results obtained in the case of two such mixtures have been discussed.

EXPERIMENTAL

The experimental arrangement used in the present investigation is the same as that described by Sen (1950). The mixture studied are nitrobenzene-hexane, and aniline-cyclohexane. In the former case the mixture contains equal weights of the two liquids and in the latter case it contains 46% by weight of aniline and 54% of cyclohexane. The nitrobenzene-hexane mixture shows opalescence at 14°C while the other mixture is opalescent at 34.5°C . In the second case temperature of opalescence mentioned by Krishnan (1935b) is 30°C , but it was found that at 30°C the liquids quickly separate from each other, the heavier one settling at the bottom, whereas, at 34.5°C no such separation takes place. Constant-temperature baths were used to keep these mixtures at the temperatures of opalescence. During the experiment, first, an empty bottle identical with that used to contain the mixture was placed between the oscillator and the detector and the reading in the detector at resonance was found with this empty bottle placed as the absorber. The bottle was then replaced by the bottle containing the opalescent mixture taken off from the constant-temperature bath. The detector was adjusted again for resonance and the reading was taken very quickly, so that the temperature of the mixture did not alter appreciably during this short period. This process was repeated for different frequencies of incident radio waves and also for the two opalescent mixtures. The absorption exhibited by pure nitrobenzene at 14°C , by pure aniline at 14°C and at 34°C and also by clear solution of nitrobenzene in hexane at 30°C was studied in this way in the frequency-range 300-510 mega cycles per sec.

RESULTS AND DISCUSSION

The values of the attenuation coefficient calculated from the ratio of the reading observed in the galvanometer in the detector circuit with the empty absorption cell as the absorber and that with the absorption cell filled with the mixture or the liquid, as the case may be, as the absorber are given in Tables I and II. In calculating the attenuation co-efficients in the case of the mixtures, a thickness equivalent to the proportion of the liquid in the mixture has been taken. The values have been plotted in figures 1 and 2 to show graphically the changes in the position of absorption peaks.

TABLE I
Nitrobenzene + *n*-hexane mixture

Frequency in Mc/sec.	Pure liq. at 14°C.		Mixture at 14°C		Mixture at 30°C	
	I_0/I	Atten. coeff.	I_0/I	Atten. coeff.	I_0/I	Atten. coeff.
510	6.0	.461	1.82	.309	2.0	.357
505	6.66	.488	1.92	.336	1.875	.323
500	7.75	.527	2.0	.357	1.875	.323
490	6.0	.461	1.90	.330	1.666	.263
480	3.42	.316	1.70	.272	1.594	.240
470	2.64	.249	1.60	.242	1.575	.234
460	2.33	.218	1.53	.219	1.562	.230
450	2.33	.218	1.50	.209	1.534	.220
440	2.10	.191	1.50	.209	1.527	.217
430	2.20	.203	1.67	.262	1.517	.214
420	2.10	.190	1.605	.244	1.531	.219
410	1.76	.145	1.41	.177	1.526	.217
400	1.75	.144	1.36	.159	1.515	.214
390	1.73	.142	1.36	.159	1.458	.194

It can be seen from figure 1 that pure nitrobenzene exhibits a peak at about 497 megacycles per sec. at 14°C, while at 26°.7C this liquid shows a peak at about 505 Mc/sec (Sen, 1950¹). The value of the attenuation coefficient at the peak at the latter position is about 0.3 while this value increases to 0.53 at 14°C. In the case of the opalescent mixture at 14°C again, there is a peak at 497 megacycles per sec., but the height of this peak is much smaller than that observed in the case of the pure liquid at this

TABLE II

Aniline (46%) + cyclohexane mixture

Frequency in mc/sec	Pure liquid at 14°C		Pure liquid at 34°.5 C		Mixture at 34°.5 C	
	I_0/I	Atten. coeff	I_0/I	Atten. coeff.	I_0/I	Atten. coeff.
510	1.55	.112	1.45	.096	1.19	.096
505	1.58	.118	1.44	.093	1.12	.092
500	1.78	.148	1.42	.090	1.11	.096
490	1.50	.104	1.36	.080	1.09	.048
480	1.36	.079	1.29	.065	1.06	.035
470	1.30	.067	1.25	.057	1.07	.037
460	1.29	.065	1.25	.057	1.08	.044
450	1.27	.061	1.23	.053	1.13	.068
440	1.28	.063	1.23	.053	1.10	.054
430	1.27	.061	1.22	.052	1.09	.046
420	1.27	.062	1.22	.052	1.08	.044
410	1.25	.057	1.21	.050	1.07	.037
400	1.24	.055	1.21	.048	1.07	.036
390	1.23	.052	1.20	.046	1.07	.037

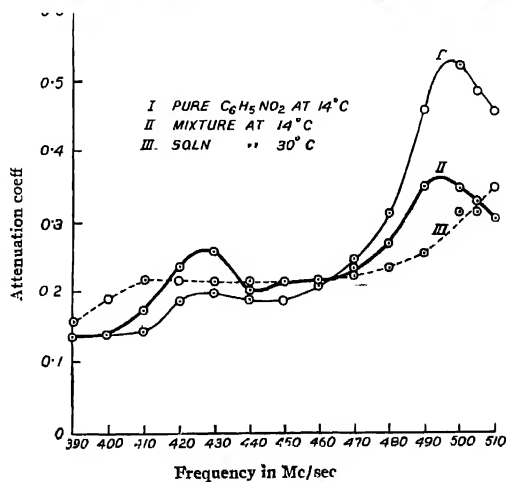


FIG. 1

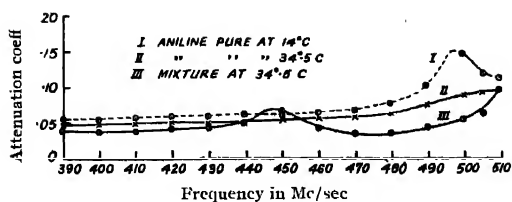


FIG. 2

temperature. Another new peak, however, appears in this case at about 427 megacycles per sec. In fact, pure nitrobenzene at 14°C also shows a very low hump at this position and this hump develops into a higher peak in the case of the opalescent mixture.

In the case of aniline at 34°.5 C there is hardly any absorption maximum in the range 300-510 megacycles per sec, but the absorption begins to increase monotonously at 480 megacycles per sec. and it seems that there may be a peak at a frequency much higher than 510 megacycles per sec. When the liquid is cooled down to 14°C an absorption peak at 498 megacycles per sec. is observed. In the case of the opalescent mixture at 34°.5 C, however a new peak at 447 megacycles per sec. is observed and the absorption begins to increase monotonously at 490 megacycles per sec. with the increase in the frequency of the radio waves.

The results mentioned above indicate that in both the opalescent mixtures, of the total number of polar molecules certain percentage has the same time of relaxation as that in the pure liquid at the same temperature, but a considerable proportion of the molecules has a time of relaxation larger than that of the molecules in the pure liquid. Since this time of relaxation is proportional to the product of the viscous force and the cube of the radius of the molecule, the observed increase in the time of relaxation may be due to an increase in either of these two factors. If there would be association of molecules in these groups, the radius of the molecule would at least be doubled and in that case the increase in the time of relaxation would be very large, but the observed increase is too small to be accounted for in this way. Hence the viscous force acting on the molecule in these groups is larger than that acting in the pure liquid. It is to be inferred, therefore, that in the opalescent mixture there are groups of molecules in which the molecules are of the same species and in some of these groups they are packed exactly in the same way as in the pure liquid, whereas, in others they are more closely packed, so that the viscous forces acting on the individual molecule are larger in the latter case than in the former. The molecules in these groups are however, free to oscillate with the incident electromagnetic field.

It can be seen from figure 1 that in the case of clear solution of nitrobenzene and hexane at 30°C, there is practically no absorption-maximum in

the range 390-510 megacycles per sec. The absorption increases a little at 410 megacycles per sec., remains almost constant over the range from 420-480 megacycles per sec and then increases rapidly at higher frequencies, showing that there is a peak at frequencies above 530 megacycles per sec. These results show that when the molecules of hexane intermix with those of nitrobenzene to produce a solution of uniform composition the time of relaxation of the nitrobenzene molecule diminishes appreciably and consequently the absorption peak shifts to higher frequencies. This shift again is not due to breaking up of associated groups of molecules in the solution, because in that case the shift would be much larger than what is actually observed. So the shift is due to diminution in the viscous forces. Thus it is clearly demonstrated that the study of the shift of absorption peak in this U. H. F. region gives us an idea about the change in the intermolecular forces in the mixture.

The arguments put forth above show that in opalescent mixtures, molecules of the constituent liquids do not mix with each other, but those of each liquid form very small elements of volume and such volumes disperse in the whole mixture in such a way that a heterogeneity in the density is created. The opalescence is produced by this heterogeneity.

Incidentally, it has to be pointed out that the absorption curves for the pure liquids at different temperatures obtained in the present investigation confirm the hypothesis put forward by Sirkar and Sen (1949b) that with the lowering of temperature the absorption peak becomes sharper and its height increases.

ACKNOWLEDGMENT

The author is indebted to Prof. S. C. Sirkar for his kind interest and guidance throughout the progress of the work.

OPTICS DEPARTMENT,
INDIAN ASSOCIATION FOR THE
CULTIVATION OF SCIENCE,
CALCUTTA

REFERENCES

- Drude, P., 1896, *Wied. Ann.*, **58**, 1.
 Krishnan, R. S., 1935a, *Proc. Ind. Acad. Sc.* **1**, 1, 211
 „ 1935b, *Proc. Ind. Acad. Sc.* **1**, 1, 915.
 Sen, S. N., 1949, *Ind. J. Phys.*, **23**, 495.
 „ 1950, *Ind. J. Phys.*, **24**, 163.
 Sirkar, S. C. and Sen, S. N., 1949a, *Nature*, **164**, 1048.
 „ 1949b, *Science and Culture*, **15**, 155

FINE STRUCTURE IN THE EAST-WEST COSMIC-RAY INTENSITY AT LAHORE ($\lambda = 22^\circ\text{N}$), INDIA*

By OM PARKASHI

Part I

(Received for publication, August 23, 1950)

ABSTRACT The paper deals with the fine-structure measurements taken at Lahore ($\lambda = 22^\circ\text{N}$) in 1947 and their statistical analysis by the method developed by Warren. A triple coincidence telescope, consisting of three internally quenched G. M. counters, 35 cm long, 2.5 cm in diameter, with a distance of 25 cm between the extreme counters, has been employed. The intensity measurements have been made in both the eastern and western azimuths from $0-42^\circ$ at 6 degree steps.

The results indicate a possibility of the existence of the negative primaries. However, to have a significant decision about this point we need more data. The presence of silicon band (13.2 Bev) in the primary cosmic-rays is definitely shown, its edge extending to about 21° in the east of the zenith. This supports earlier experiments by Millikan and his co-workers in India and the banded nature of the primary cosmic-rays.

A comparison between our results and those of Schremp and Banos, at Mexico, ($\lambda = 29^\circ\text{N}$) shows a striking similarity as regards the west-east excess. Any divergence has been traced to be due to the difference in latitude of the two places. The oxygen band (7.5 Bev) and the nitrogen band (6.5 Bev) which are effective in the western azimuth at Mexico do not show up at Lahore, and this explains all the differences. The work brings out the importance of such measurements and emphasises the need of more extensive observations at such latitudes with coordinated programme.

INTRODUCTION

On the considerations of the banded nature of penumbra (*i. e.* regions of allowed and forbidden energy bands) Schremp (1938) stated that for intermediate latitudes ($10^\circ-40^\circ$), the penumbra will exhibit its most important aspect, giving rise to a highly anomalous behaviour of the directional intensity distribution of cosmic-rays. The theory of this anomalous intensity distribution, termed as 'Fine-structure', involves the geo-magnetic effects on the primary energy spectra at infinity and the absorptive effects on their passage through the atmosphere. Both of these effects account for the prominences and depressions observed in the zenith angle-intensity distribution curves.

The first experimental evidence of the existence of fine-structure came from the work of Cooper (1939, 1940) and Ribner (1939), at Missouri ($\lambda = 49^\circ$) and from the extensive work of Schremp and Banos (1940, 1941) at Mexico

* The data of the present work were collected at Lahore in 1946-47.

Cooper (*loc. cit*) found three approximately symmetrical prominences (i.e., increase of intensity over the normal $\cos^2 z$ (z =zenith angle) distribution) at $z=5-10^\circ$, 20° and 40° and Ribner (*loc. cit*) obtained one pair of symmetrical prominences at 20° both in the eastern and western azimuths together with an indication of peaks in the neighbourhood of 10° and 40° .

Vallarta (1939) has emphasised the importance of such studies, as they can be useful in the analysis of primary cosmic rays, their energy spectra at infinity and their behaviour on the passage through the atmosphere. In addition, this type of study can help in the elucidation of the hypothesis of atom-annihilation energy bands present in the primary cosmic radiation.

Millikan (1949) has shown that the silicon band of energies should appear vertically at 20°N in India. Millikan (1947) has further stated that so far as India is concerned, this hypothetical band may properly be said to predict and explain both qualitatively and quantitatively the latitude (and other directional) effects. The existence of this band was shown from a series of balloon flights made in India [Neher and Pickering (1942); Millikan, Neher and Pickering (1942)] during 1939-40, using Geiger counters in vertical double coincidence. The most significant point, that was observed, was that within the uncertainty of measurements, there was no change in the intensity of radiation coming in near the vertical from $3-17^\circ\text{N}$, while from $17-25^\circ\text{N}$, there was an increase of 21%. This increase was interpreted to be due to primary charged particles in the energy range 15 down to 11.5 B ev, thus indicating the existence of the supposed Si band. It is seen that this band will be effective at the latitude of Lahore (22°N) and should produce some observable effect in the east-west intensity distribution.

Further, as indicated above, Schremp (*loc. cit*) has (see also Bhattacharya, 1942) attributed this fine structure to the effects of penumbra. However, the most extensive work on fine structure at the high latitude of Missouri does not corroborate the above view. Even if the effect of penumbra is not negligible, the azimuthal symmetry of the fine structure, as observed at Missouri and Mexico, cannot be understood in terms of penumbra effects. Instead, it seems that the fine-structure is due to a discrete energy spectrum of primary particles showing up as a result of the 'main cone' or 'Full light' in appropriate directions in the sky. Since the work of Johnson (1938) shows that the primaries are mainly (or entirely?) positively charged and since the most effective energy band at Lahore is 14 B ev band (corresponding to the silicon band), the appearance of main cone should be a step-function '—' the intensity being higher to the west where the primaries of the given energy are allowed than to the east where they are not.

Realising the importance of these points and the information that can be obtained from the directional studies in deciding these, the present study of the fine-structure in the intensity distribution in the E-W azimuths was undertaken at Lahore ($\lambda=22^\circ\text{N}$). The importance of this work is further

shown from the fact that there is not much data of this type for these latitudes, the only work, existing, being of Schremp and Banos (*loc. cit.*) at Mexico (29°N).

APPARATUS AND EXPERIMENTAL PROCEDURE

The cosmic-ray telescope (Parkash and Sarna, 1948) used in the present work consisted of three internally quenched G. M. counters, 35 cm long, 2.5 cm in diameter, mounted in parallel positions on a light wooden frame. The distance between the extreme counters was 25 cm. The telescope subtended an angle of 11.3° in the zenith, though as shown by Cooper (*loc. cit.*) the actual resolution is much better than the dimensions indicate. For the present set-up more than half of the rays are incident through an angle of about 2° on each side of the mean zenith angle. The triple coincidences were recorded by a circuit (Parkash and Sarna, 1948) after its thorough testing for discrimination against doubles and singles. With the plane of the telescope in the magnetic meridian so that the rotation would be in the local east-west plane; the observations were taken at every 6° intervals, ranging from $0-42^{\circ}$ in the eastern and western azimuths. The telescope was alternately kept inclined towards east and west at a particular zenith angle for about half an hour, and the process repeated. The total number of counts in each position was calculated and reduced to a common temperature and pressure of 20°C and 74.5 cm of Hg respectively. The probable errors were calculated as usual.

RESULTS AND DISCUSSION

At sea level, the zenith angle-intensity curve is represented by the square of the cosine of the zenith angle. Thus if I_0 is the vertical intensity, at any zenith angle z , then $I_z = I_0 \cos^2 z$ and the observed anomalies are represented by $\Delta z = I_z - I_0 \cos^2 z$. As Cooper (*loc. cit.*) has remarked, it is

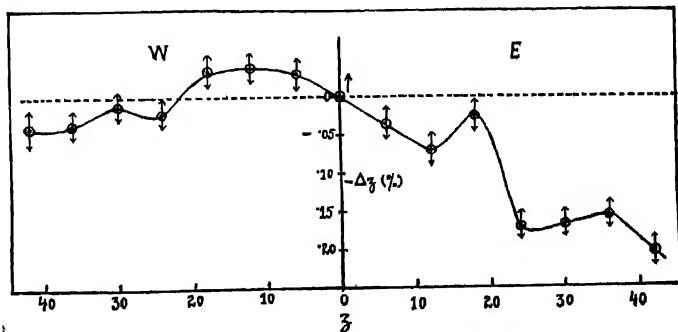


FIG. 1

$\Delta z-z$ curve for the eastern and western azimuths at Lahore, (22°N), India.

more convenient to plot the deviation Δz or per cent Δz for the empirical cos square curve against z than the zenith angle-intensity curve. This flattens out the distribution curve and shows any prominences and depressions as oscillatory about a perfect cos square distribution. Table I gives the results of the present measurements. Fig. 1 is a plot of the percentage deviation Δz against z . The arrows show the extent of probable errors.

TABLE I

Fine-structure data in the eastern and western azimuths at Lahore (22°N), India.

Zenith angle (z), degrees	Time in minutes	Total number of counts at 20°C and 74.5 cm Hg	Counts/min $I_z \pm pe$	$I_0 \cos^2 z \pm pe$	$\Delta z \pm pe$ $\Delta z = I_z - I_0 \cos^2 z$	Per cent $\Delta z \pm pe$ $= \left(\frac{I_z}{I_0 \cos^2 z} - 1 \right) 100$
0° (vertical)	2370	7999	3.337 ± 0.025	3.337 ± 0.025	0.000	0
6	W 340	1157	3.402 ± 0.067	3.304 ± 0.025	$+0.098 \pm 0.072$	$+0.030 \pm 0.022$ (X100)
	E 319	1017	3.188 ± 0.067		-0.116 ± 0.072	-0.035 ± 0.022
12	W 471	1562	3.316 ± 0.056	3.193 ± 0.024	$+0.123 \pm 0.061$	$+0.039 \pm 0.019$
	E 427	1268	2.968 ± 0.056		-0.225 ± 0.061	-0.070 ± 0.019
18	W 472	1476	3.127 ± 0.055	3.018 ± 0.023	$+0.109 \pm 0.060$	$+0.036 \pm 0.020$
	E 420	1237	2.945 ± 0.056		-0.073 ± 0.061	-0.024 ± 0.020
24	W 443	1200	2.729 ± 0.053	2.785 ± 0.021	-0.056 ± 0.057	-0.020 ± 0.020
	E 431	996	2.311 ± 0.049		-0.474 ± 0.053	-0.170 ± 0.019
30	W 651	1610	2.473 ± 0.041	2.502 ± 0.019	-0.029 ± 0.045	-0.011 ± 0.018
	E 593	1235	2.083 ± 0.040		-0.419 ± 0.044	-0.167 ± 0.017
36	W 593	1250	2.108 ± 0.040	2.185 ± 0.016	-0.077 ± 0.013	-0.035 ± 0.020
	E 666	1228	1.841 ± 0.035		-0.341 ± 0.038	-0.156 ± 0.017
42	W 409	725	1.772 ± 0.044	1.844 ± 0.014	-0.072 ± 0.046	-0.039 ± 0.025
	E 402	590	1.468 ± 0.041		-0.376 ± 0.043	-0.204 ± 0.023

Some of the marked peculiarities apparent from Fig. 1 are:

(i) A very marked west-east excess, similar to one observed by Schremp and Banos (*loc. cit.*) in the Mexico curve.

(ii) There is a prominence at 18° in the eastern azimuth together with an indication of another at 36° and a flat prominence at about 12° with an indication of another at 30° in the western azimuth. It may be noticed that the magnitudes of these 'anomalies' is greater in the eastern than in the western azimuth.

(iii) The intensity falls off less rapidly in the west than in the east.

Vertical counts were recorded daily, twice, during the period of observations and the average counting rate obtained after applying temperature and pressure corrections.

iv. There are two depressions at 12° and 24° in the east and an indication of one at 24° in the west.

The 18°E prominence, also present in Mexico curve, is believed by Schremp and Banos (*loc. cit.*) to be due to the presence of negative primaries. In fact, the existence of negative primaries has been shown (Swann, 1933) to be necessary, even otherwise. Vallarta *et al* (1939) have shown the existence of negative primaries from the considerations of data on diurnal variations. Though the sea level effects seem to be mostly due to positive particles, they may not be really due to the excess of positives over the negatives but merely due to the difference in the penetrating power of the two types of primaries, (Evans, 1941); or it may be that there is an excess of negative slow primaries (Alfven, 1938), which might get absorbed in the upper parts of the atmosphere by a process different from that of the positives, (Vallarta and Bouckart, 1935). Janossy (1948) is also of the opinion that the primaries are of two types, probably electrons and protons. The recent rocket experiments of Singer (1950), the balloon experiments of Hulsizer and Rossi (1948) and of Schein, Jesse and Wollan (1941) and the high altitude experiments on E-W asymmetry by Johnson and Barry (1939) have proved the non-existence of electrons as the primary particles. If now we exclude the possibility of electrons as the negative primaries, then negative protons (Arley, 1946) may form the negative primaries. Even on Millikan's atom-annihilation hypothesis, Klein (1950) has shown that, for the annihilation to take place, there must be the presence of anti-matter near ordinary matter in the inter-stellar space; the two atoms of matter and anti-matter annihilating themselves on collision and generating two primary cosmic-rays which may be protons and anti-protons. These anti-protons, on reaching the top of the atmosphere, might interact with matter in a different way from the protons. That this is so, is, in a way, evident from the measurements on the directional dependence of the positive excess in the meson spectrum. Quercia, *et al* (1950) have found a marked difference in the relative abundance of negative and positive mesons in the eastern and western azimuths. There are relatively more negative mesons than the positives in the east and vice versa.. (This may be explained either (i) on the supposition that higher energy positive primaries reaching the eastern azimuths produce mesons in a different way than the lower energies reaching the western azimuth, or, (ii) there are negative primaries (negative protons) which somehow produce more negative mesons. The latter view appears more justified in view of the evidences from other sources).

The relatively rapid and greater decrease of intensity in the east, clearly seen in Fig. 1, may be attributed to the presence of negative primaries (negative protons) which, along with their progeny, are absorbed more quickly while traversing down the atmosphere. The prominence at 18°E in Fig. 1 also supports this view. (The prominence at Lahore is less marked than

at Mexico. This is due to the fact, that, the edge of positive primaries of 13.2 Bev nearly extends to this angle, while at Mexico this extends to farther east. Thus, the contribution of the positive component being nearly zero at 18°E at Lahore, the prominence is not so marked.)

The marked west-east excess, present in both Lahore and Mexico curves, is probably due to the presence of the already mentioned silicon band (13.2 Bev) with its edge extending to the east of zenith to about $18-24^\circ$ at Lahore and farther east at Mexico. That, there is such a band of energies, with its edge at about $18-24^\circ$, is clearly shown by the marked depression at 24° in the eastern azimuth. This might correspond to 36° depression in Mexico curve. The depression at 12°E , if real, probably indicates the presence of another narrow band within the silicon band.

The western azimuth does not show anything real beyond statistical fluctuations, though there is an apparent anomaly near the zenith. The anomalies observed at 12° and 42° in the western azimuth in Mexico curve, but absent from ours, seem most probably due to the presence of positive primaries of the oxygen band (7.5 Bev) and the nitrogen band (6.5 Bev) effective at that latitude (29°N) but absent from Lahore (22°N), India, due to geo-magnetic cut-off.

From the present investigation, therefore, we conclude that :

- i. Negative primaries (probably negative protons) form a part of the primary cosmic-rays.
- ii. Most of the west-east excess is due to the presence of the silicon band, of which, the existence is definitely shown, thus supporting the atom annihilation hypothesis, as modified by Klein, as the major source of cosmic rays.
- iii. In conjunction with Mexico data, the banded nature of the primaries is responsible for fine-structure.

The above discussion clearly brings out the importance of such measurements in deciding these vital issues. These are needed the most at intermediate latitudes where other atom annihilation bands will also show their peculiarities. The existing data are very meagre and a coordinated programme using similar equipment is desired.

Part II

STATISTICAL ANALYSIS OF LAHORE DATA

In order to see the significance of the above conclusions, the data of Part I have been analysed by the method developed by Warren (1946). Whereas, we have visualised the fine-structure as departures from the normal \cos square curve, here we consider it as departures from the $\log I - \log \cos Z$ curve which under normal distribution is a straight line.

Table II gives the summary of the interpretations of Lahore data. Fig. 2 is the logarithmic plot of cosmic-ray intensity measured at Lahore. The

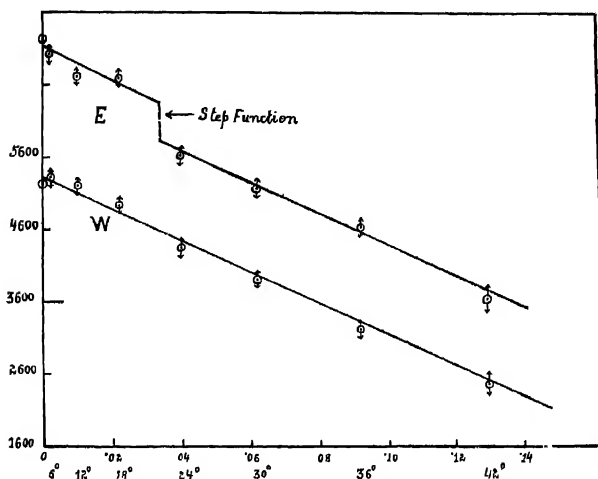


FIG. 2

Logarithmic graph of cosmic-ray intensity measured at Lahore. The ordinates are the logarithms of the relative intensities and abscissae are the negative logarithms of the cosine of z .

ordinates are the logarithms of cosmic-ray intensity and the abscissae are the negative logarithms of the cosine of the zenith angles.

TABLE II

SUMMARY OF INTERPRETATIONS OF LAHORE DATA

Name of fitted line (s)	points fitted	Parameter values				χ^2	N	$P(>\chi^2)$
		a_1	a_2	b_1	b_2			
Single line for all	all, E & W	.1243		2.54		84.1	13	10^{-6}
Single line W	all, in W & 0°	.4430		2.173		5.299	6	.51
Single line E	all in E & 0°	.4046		2.873		19.20	6	.015
Combined, both of above	all, 0° twice					21.50	12	.018
Step function, E combined with single line W.	all in E & 0° all, 0° twice	.4313	-.3718	2.218		6.07 12.27	5 11	.224 .35
Step function, only one step at 21° E. (parallel lines with a break)	all	.4490	-.3689	2.124		15.91	12	.196
Step function, two non parallel lines, with a break at 21° E.	all	.4398	-.3684	2.133	2.120	15.9	11	.15

* (For various constants, refer to Warren (*loc.cit.*)).

As mentioned in Part I, the appearance of the main cone should be a step function 'L' giving higher intensity to the west where the primaries are allowed than to the east where they are not. We, therefore, tried to fit the data with the use of such a step function. It is evident from Fig. 1, that it is easy to fit a straight line inside of six out of eight of the probable errors. Since there remains six degrees of freedom and the probable error is selected so that there is an equal chance of the discrepancy falling inside and outside the limit, we see that we can do better than the expected three outside, even from this crude consideration. The more detailed calculations verify this exactly and the agreement between the observations and a single straight line (on the log-log graph) is exactly as good as would be expected from the observational errors; or we might infer (as we mentioned in Part I) that the data in the west do not show anything that can be reliably distinguished from statistical fluctuations. To be convincing of the break between 18° and 24° in the west, the counting errors should be one third or ten times as many counts recorded per point. (If real, this break will correspond to the edge of negative primaries with slight overlapping near the zenith. It may be mentioned that no other low energy bands (oxygen or nitrogen bands) are allowed at the place of observation).

In the east, however, the situation is quite different. Here the discrepancy is quite real and the calculations show only one chance in three hundred that these data were obtained from a 'true' distribution, that is a single straight line. Here we have an example of this simple type of fine-structure with a single energy band of positive primaries that appears only west of this limit. This can be calculated as a step-function by fitting parallel straight lines to the observations in the east of azimuth. This gives a good probability of agreement (1 in 4.5) and appears to fit in quite readily with the simple interpretations given above. The step at 21° E appears to be due to the edge of the silicon band (13.2 Bev) extending to about $18-24^\circ$ in the east of the zenith and, hence, established its existence.

The marked west-east excess, as stated in Part I, is also due to this band of positive primaries.

To decide the point that the step at $18-24^\circ$ E might be the only statistically significant irregularity, we tried to fit a single straight line to all the points in both the azimuths west of this edge and a parallel line (or non-parallel) to the east of it. The probability of agreement is 1 in 5 (1 in 6.5) showing a very good agreement with the hypothesis that the western excess is due the single edge in the east between $18-24^\circ$ E, corresponding to about .50 millistormers or about 14 Bev. However, to decide about other conclusions apparent from our observations, we need more data.

ACKNOWLEDGMENTS

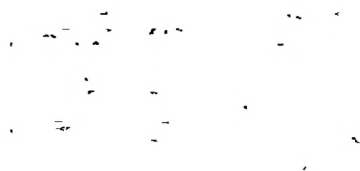
The author wishes to thank Dr. H. R. Sarna, Director of the Punjab University, Physics Laboratories, Government College, Hoshiarpur for his

kind encouragement and to Dr. P. S. Gill (now Head of the Department of Physics, Aligarh University) for some very useful discussions about the subject. He is particularly thankful to Mr. D. T. Warren, of the University of Denver, Colorado (U.S.A.), for helping in the analysis of the present data. Most of the discussion in Part II of this paper is due to his help. Thanks are also due to S. Harbhajan Singh (previously of Government College, Lahore), Head Instrument Maker, for helping in constructing and setting up the apparatus.

PHYSICS DEPARTMENT
PUNJAB UNIVERSITY

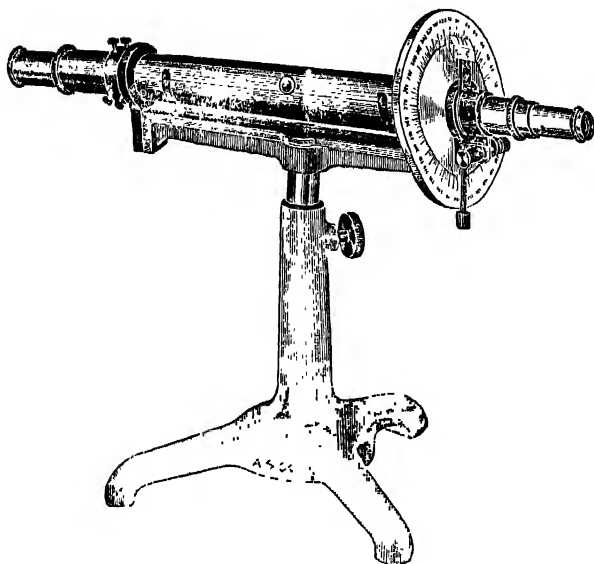
REFERENCES

- Alfven, H., 1938, *Phys. Rev.*, **54**, 97.
 Arley, N., 1946, " " , **69**, 78.
 Bhattacharya, P. C., 1942, *Proc. Nat. Inst. Sci. India*, **8**, 273.
 Cooper, D. M., 1939, *Phys. Rev.*, **55**, 12-2 L.
 " " , 1940, " " , **56**, 288.
 Evans, F., 1941, *Phys. Rev.*, **59**, 1.
 Hulsizer, R. L., and Rossl, B., 1948, *Phys. Rev.*, **73**, 1402.
 Janossy, L., 'Cosmic-rays', Oxford University Press, p. 313.
 Johnson, T. H., and Barry J. G., 1939, *Phys. Rev.*, **56**, 219.
 Johnson, T. H., 1938, *Rev. Mod. Phys.*, **10**, 193.
 Millikan, R. A., 1949, *Rev. Mod. Phys.*, **21**, 1.
 " " , 1947, 'Electrons etc.' Chicago University Press, p. 563.
 Millikan, R. A., Neher, H. V. and Pickering, W. H., 1942, *Phys. Rev.*, **61**, 397.
 Neher, H. V. and Pickering, W. H., 1942, *Phys. Rev.*, **61**, 407.
 Paikash, Om and Sarna, H. R., *Ind. Jour. Phys.*, **22**, 19.
 Quercia, I. F., Rispoli, B and Scutti, S., 1950, *Phys. Rev.*, **78**, 824.
 Ribner, H. S., 1939, *Phys. Rev.*, **55**, 1271L.
 " " , 1939, " " , **56**, 1069.
 Schein, M., Jesse, W. R., and Wollan, E. O., 1941, *Phys. Rev.*, **59**, 615.
 Schremp, E. J., 1938, *Phys. Rev.*, **53**, 915A.
 " " , 1938, " " , **54**, 157.
 Schremp, E. J. and Banos, A., 1940, *Phys. Rev.*, **58**, 662L.
 " " and " " , 1941, " " , **59**, 614L.
 Singer, S. F., 1950, *Phys. Rev.*, **77**, 730.
 Swann, W. F. G., 1933, *Phys. Rev.*, **44**, 124.
 Vallarta, M. S., and L. Bouckart., 1935, *Phys. Rev.*, **47**, 434.
 " " Graff, C. and Kusaka, S., 1939, *Phys. Rev.*, **55**, 1.
 Vallarta, M. S., 1939, *Rev. Mod. Phys.*, **11**, 139.
 Warren, D. T., 1946, *Phys. Rev.*, **69**, 78.



POLARIMETER

IDEAL FOR CHEMISTS—RESEARCH & INDUSTRIAL
LABORATORIES



Fitted with Lippich device which makes the instrument sufficiently accurate and at the same time simple. Can be used with sodium burner or an electric lamp with suitable filter interposed into position between the source of light and the polarimeter.

The circular head attached near the analysing Nicol and a Vernier movable with this enables reading of the optical rotation accurate to 0.1 degree. A 200 mm tube for the container of the solution under study for its optical activity is supplied with the instrument. Mounted upon a suitable base.

For further information please write to us.

THE ANDHRA SCIENTIFIC Co. Ltd.

Head Office & Factory

MASULIPATAM

*Sales Warehouse &
Show Room*

**4, Blacker's Road, Mount Rd.
MADRAS 2.**

Branches:

**BOMBAY
CUTTACK
HYDERABAD
VIZAGAPATAM.**

The following special publications of the Indian Association for the Cultivation of Science, 210, Bowbazar Street, Calcutta, are available at the prices shown against each of them :—

Subject	Author	Price
		Rs. A. P.
Methods in Scientific Research	Sir E. J. Russell	0 6 0
The Origin of the Planets	Sir James H. Jeans	0 6 0
Separation of Isotopes	Prof. F. W. Aston	0 6 0
Garnets and their Role in Nature	Sir Lewis L. Fermor	2 8 0
(1) The Royal Botanic Gardens, Kew.	Sir Arthur Hill	
(2) Studies in the Germination of Seeds.		
Interatomic Forces	Prof. J. E. Lennard-Jones	1 8 0
The Educational Aims and Practices of the California Institute of Technology.	R. A. Millikan	0 6 0
Active Nitrogen A New Theory.	Prof. S. K. Mitra	
Theory of Valency and the Struc- ture of Chemical Compounds.	Prof. P. Ray	3 0 0
Petroleum Resources of India	D. N. Wadia	2 8 0
The Role of the Electrical 'Double layer in the Electro Chemistry of Colloids.	J. N. Mukherjee	1 12 0

A discount of 25% is allowed to Booksellers and Agents.

RATES OF ADVERTISEMENTS

Third page of cover	Rs. 32, full page
do. do.	„ 20, half page
do. do.	„ 12, quarter page
Other pages	„ 25, full page
do.	„ 16, half page
do.	„ 10, quarter page

15% Commissions are allowed to *bonafide* publicity agents securing orders for advertisements.

CONTENTS

	PAGE
60. The Electrical Constants of Soil at Ultra-high Frequencies—By P. N. Sundarām	469
61. On the Disintegration of Scandium (46) and the Method of Delayed Coincidence for the Study of Short-lived Metastable States in Isomeric Nuclei—By B. D. Nag, S. Sen, and S. Chatterjee	479
62. A Triggering Device for Arc-discharge Lamps in Cloud Chamber Photography—By Ranjit Kumar Das	497
63. Photographic Emulsion Studies of the Latitude Effect—By K. R. Dixit	501
64. On the Absorption of U. H. F. Radio Waves by Opalescent Binary Liquid Mixtures—By (Miss) Anjali Choudhury	507
65. Fine Structure in the East-West Cosmic-ray Intensity at Lahore ($\lambda = 42^\circ \text{N}$), India—By Om Parkash	513

VOL. 24

INDIAN JOURNAL OF PHYSICS

No. 12

(Published in collaboration with the Indian Physical Society)

AND

VOL. 33

PROCEEDINGS

No. 12

OF THE

**INDIAN ASSOCIATION FOR THE
CULTIVATION OF SCIENCE**

DECEMBER, 1950

**PUBLISHED BY THE
INDIAN ASSOCIATION FOR THE CULTIVATION OF SCIENCE
210, Bowbazar Street, Calcutta**

BOARD OF EDITORS

K. BANERJEE	S. K. MITRA
D. M. BOSE	P. RAY
S. N. BOSE	M. N. SAHA
D. S. KOTHARI	S. C. SIKKAR

Secretary

EDITORIAL COLLABORATORS

DR. R. K. ASUNDI, M.A., PH.D.
PROF. H. J. BHABHA, PH.D., F.R.S.
DR. P. K. KICHLU, D.Sc.
PROF. K. S. KRISHNAN, D.Sc., F.R.S.
PROF. G. P. DUBEY, M.Sc.
DR. K. RANGADHAMA RAO, M.A., D.Sc.
DR. N. D. SARWATTEY, D.Sc.
DR. N. N. DASGUPTA, M.Sc., PH.D.
PROF. N. R. SEN, D.Sc., F.N.I.
PROF. P. C. MAHANTI, D.Sc., F.N.I.
PROF. S. R. PALIT, D.Sc.,
DR. H. RAKSHIT, D.Sc.,
PROF. K. R. DIXIT, PH.D.
DR. VIKRAM A. SARABHAI, M.A., PH.D.

ASSISTANT EDITOR

MR. A. N. BANERJEE, M.Sc.

NOTICE

TO INTENDING AUTHORS

Manuscripts for publication should be sent to Mr. A. N. Banerjee, Assistant Editor, 2 & 3, Lady Willingdon Road, Jadavpur, Calcutta-32.

The manuscript of each paper should contain in the beginning a short abstract of the paper.

All references to published papers should be given in the text by quoting the surname of the authors followed by the year of publication within braces, e.g., Sen (1942). The actual references should be given in a list at the end of the paper according to the following specimen :

Sen, B. K., 1942, *Ind. J. Phys.*, 16, 329.

The references should be arranged alphabetically in the list.

All diagrams should be drawn on thick white paper in Indian ink, and letters and numbers in the diagrams should be written in pencil.

Annual Subscription—

Inland Rs. 20

Foreign £ 2

ON ALPHA-DISINTEGRATION: PART I SOME USEFUL THEORETICAL TABULATIONS AND GRAPHICAL PLOTS

By RANJIT KUMAR DAS

(Received for publication, October 3, 1950)

ABSTRACT. Starting from the well-known mass defect formula

$$\Delta M = \alpha A - \beta \frac{(N-Z)^2}{A} - \gamma A^{2/3} - \delta \frac{Z^2}{A^{1/2}}$$

an expression has been deduced for the total energy released in an α -disintegration. The calculation has been confined to groups of nuclides with, $Z=44, 45, 46, 47, 48, 49, 50, 51, 52$, and 54 . Useful theoretical data are given in ten tables. β, γ, δ and Q curves are plotted on ten separate graphs and their outstanding characteristics briefly discussed.

INTRODUCTION

It is well-known that when a nuclide $M(A, Z)$ disintegrates into the daughter nuclide $M(A-4, Z-2)$, emitting an α -particle $M(4, 2)$, we can write the reaction scheme as follows

$$M(A, Z) = M(A-4, Z-2) + M(4, 2) + Q \quad \dots (1).$$

where Q is the energy released in the α -disintegration process, including the recoil energy of the daughter nuclide. It is, of course, tacitly assumed that the resulting nuclide is in the ground state, so that there is no subsequent gamma ray emission. Whenever there is emission of a gamma photon following an α -disintegration the gamma energy has to be deducted from the theoretically possible value of Q to get the nearest approach to the experimentally observed value.

If by any means we can accurately measure the nuclear masses involved in the above reaction scheme, we can straightforwardly calculate the energy of disintegration. Unfortunately, the only practical means at our disposal of measuring nuclear masses accurately, namely, mass-spectrographic investigation, has not yet been much successful with heavy nuclei. However, using the Bethe-Weizsacker (1936) mass defect formula, we can theoretically calculate the possible energy release involved in an α -disintegration process.

Glueckauf (1948) has utilised the accurately known mass values of the lightest elements upto a mass number $A=40$, and with somewhat reduced accuracy upto $A=60$, to calculate directly the binding energy of the last alpha particle in the nucleus (which is the alpha disintegration energy with opposite sign). Although these nuclei are not radioactive in nature, the

resulting plots are very interesting in that, the lines of constant α -energy values show qualitatively the same kind of fluctuations as are noticeable in similar experimental curves obtained for high atomic weight nuclei. Pryce (1950) has recently published some theoretical calculations on the energy of α -particles from radioactive bodies and has tabulated the results in the form of energy release from various isotopes (existing or hypothetical) of all the elements from Pt ($Z=78$) to Cm ($Z=96$). Considering the fact that there are at present several collateral alpha decay chains of artificially produced radioactive nuclides (Seaborg and Perlman, 1950; Studier and Hyde, 1947; Meinke, Ghiorso and Seaborg, 1948) we have calculated the theoretical α -energy release from them with a view to extending the study of correlation between theoretical predictions and experimental findings. As the calculations are of an involved nature and hence time consuming; the final data have been supplied in tabular forms and relevant curves plotted for the different I values.

DERIVATION OF THE ENERGY RELEASE FORMULA

The exact nuclear mass of a nuclide $M(A, Z)$ can be expressed as

$$M(A, Z) = NM_n + ZM_p - \alpha A + \beta \frac{(N - Z)^2}{A} + \gamma A^{2/3} + \delta \frac{Z^2}{A^{1/3}}$$

from which, the mass defect ΔM is

$$\begin{aligned} \Delta M &= \alpha A - \beta \frac{(N - Z)^2}{A} - \gamma A^{2/3} - \delta \frac{Z^2}{A^{1/3}} \quad \dots (2) \\ &= \alpha A - \beta \frac{I^2}{A} - \gamma A^{2/3} - \delta \frac{Z^2}{A^{1/3}} \end{aligned}$$

From (1), $Q = M(A, Z) - M(A-4, Z-2) - M(4, 2)$

or, in terms of $\Delta M(A, Z)$,

$\Delta M(A-4, Z-2)$ and $\Delta M(4, 2)$

$$Q = \Delta M(A-4, Z-2) + \Delta M(4, 2) - \Delta M(A, Z).$$

Now, substituting for ΔM 's their respective expressions involving the constants α , β , γ , and δ , we have, after slight rearrangements,

$$\begin{aligned} Q(\text{in Mev}) &= -4\alpha + 28.16 - 4\beta \frac{I^2}{A(A-4)} + 13.08[A^{2/3} - (A-4)^{2/3}] \\ &\quad + .58 \left[\frac{Z^2}{A^{1/3}} - \frac{(Z-2)^2}{(A-4)^{1/3}} \right] \\ &= -27.88 - 75.6 \frac{I^2}{A(A-4)} + 13.08[A^{2/3} - (A-4)^{2/3}] + .58 \left[\frac{Z^2}{A^{1/3}} - \frac{(Z-2)^2}{(A-4)^{1/3}} \right] \end{aligned}$$

In working out the above expression for Q , we have used values of the constants α , β , γ , and δ , calculated with the help of up-to date mass data:

α	(14.01)
β	(18.9)
γ	(13.08)
δ	..	.	(.58)

The binding energy of the α -particle has been taken as 28.16 Mev

Meanings of symbols used:

M = actual mass of the nuclide.

A = Mass number

N = The number of neutrons in the nuclide

Z = The .., .., protons .., .., ..

I = Isotopic number = $(N - Z)$

M_p = Mass of the proton.

M_n = Mass of the neutron.

TABULATION AND GRAPHICAL PLOTS

With the help of the above expression we have calculated, term by term, the total energy release for the nuclear species characterised by $I=44, 45, 46, 47, 48, 49, 50, 51, 52$, and 54 . No series with $I=53$ has yet been found. For convenience of tabulation, nuclides with the same I value have been divided into two groups from amongst the four possible ones, *viz*, even-even, even-odd, odd-odd and odd even—the first word referring to the number of protons in the nuclide and the second, to the number of neutrons.

The tabulated data have been presented in the form of graphical plots (Figs 1—10). On each graph for the same I , have been plotted the net contributions from the β , γ , and δ terms, as well as the theoretical energy Q , against the corresponding nuclide. The scales of ordinates are necessarily different. This procedure has been adopted to present a comparative picture of the variations of the different quantities with the mass number.

Nuclides plotted immediately close to the abscissa denote class (A) of the tables, while those farther below or up denote class (B). The order of the ordinates, for all the plots, is respectively β , γ , δ , and Q , starting from the extreme right.

TABLE I
Nucleides, $I = 44$

(A) Even-Even group

Nucleides	J^2 $A(A-4)$	$[A^2/3 - (A-4)^2/1]$	$\left[\frac{Z^2}{A^{1/3}} - \frac{(Z-2)^2}{(A-4)^{1/3}} \right]$	Net contribution from			Calc. Q (in Mev)
				β -term	γ -term	δ -term	
92U^{228}	0.03790720	0.437080	51.740	2.865790	5.726420	30.00020	4.990
90Th^{224}	0.03028570	0.44030	50.940	2.97000	5.750120	29.54520	4.454
88Ra^{220}	0.04074070	0.44310	50.130	3.08000	5.795740	29.07400	3.919
86Rn^{216}	0.04227810	0.44590	49.310	3.106220	5.832370	28.59980	3.356
84Po^{212}	0.04390420	0.44860	48.500	3.319150	5.866768	28.13000	2.798

(B) Odd-Odd group

91Pa^{226}	0.03858720	0.43900	51.340	2.917190	5.74220	29.77920	4.724
89Ac^{222}	0.04000330	0.44180	50.530	3.024250	5.778740	29.30739	4.182
87Fr^{218}	0.04149770	0.44450	49.730	3.137300	5.814060	28.84340	3.640
85At^{214}	0.04309950	0.44710	49.000	3.256820	5.848100	28.42000	3.131

TABLE II
Nucleides: $I = 45$

(A) Even-Odd group

Nucleides	J^2 $A(A-4)$	$[1/2]^{1/3} - (A-4)^{1/3}/8]$	$\left[\frac{Z^2}{A^{1/3}} - \frac{(Z-2)^2}{(A-4)^{1/3}} \right]$	Net contribution from			Calc. Q (in Mev)
				β -term	γ -term	δ -term	
92U^{229}	0.03930130	0.43720	51.700	2.971193	5.718570	29.98600	4.853
90Th^{225}	0.0407340	0.43970	50.999	3.078730	5.751270	29.52140	4.314
88Ra^{221}	0.04222530	0.44240	50.081	3.192230	5.786580	29.04090	3.755
86Rn^{217}	0.04381120	0.44520	49.280	3.312130	5.82320	28.60210	3.233
84Po^{213}	0.04548610	0.44790	48.450	3.438750	5.858530	28.10100	2.641

(B) Odd-Even group

91Pa^{227}	0.04000310	0.43500	51.300	3.024230	5.742390	29.75400	4.552
89Ac^{223}	0.04146440	0.44110	50.490	3.134710	5.769580	29.28420	4.039
87Fr^{219}	0.04300630	0.44370	49.689	3.251350	5.803590	28.81960	3.492
85At^{215}	0.04463790	0.44660	48.861	3.374620	5.841520	28.33930	2.926
83Bi^{211}	0.0463660	0.44930	48.040	3.505040	5.876400	27.86200	2.353

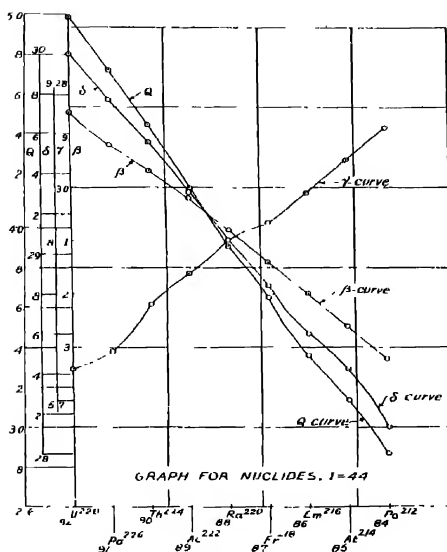


FIG. 1

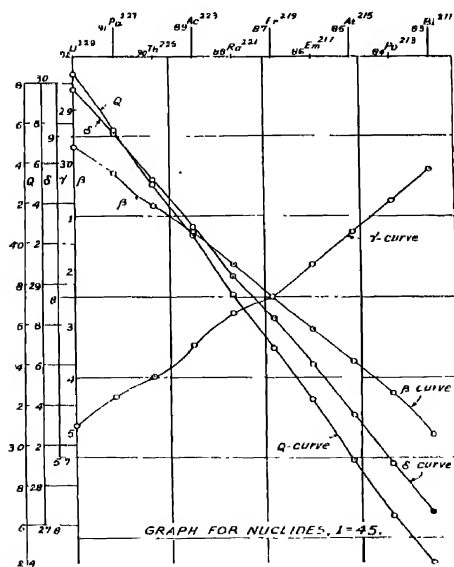


FIG. 2

TABLE III

Nuclides : $I=46$

(A) Even-Even group

Nuclides	$\frac{I^2}{A(A-4)}$	$[A^{2/3} - (A-4)^{2/3}]$	$\left[\frac{Z^2}{A^{1/3}} - \frac{(Z-2)^2}{(A-4)^{1/3}} \right]$	Net contribution from			Calc. Q (in Mev).
				β term	γ -term	δ -term	
$^{92}\text{Tl}^{230}$	0.04070790	0.43660	51.660	3.077520	5.710720	29.96280	4.716
$^{90}\text{Th}^{226}$	0.04121490	0.43910	50.850	3.188420		29.40300	4.168
$^{88}\text{Ra}^{222}$	0.04372260	0.44180	50.110	3.305430	5.778740	29.06371	3.657
$^{86}\text{Rn}^{218}$	0.0453571	0.44440	49.170	3.428990	5.812750	28.51860	
$^{84}\text{Rn}^{214}$	0.047085	0.44720	48.410	3.559620	5.849370	28.07780	2.48

(B) Odd-Odd group

$^{91}\text{Pa}^{228}$	0.04143170	0.43770	51.260	3.12230	5.725110	29.75180	4.134
$^{89}\text{Ac}^{224}$	0.04293830	0.44040	50.440	3.246130	5.760430	29.25520	3.890
$^{87}\text{Fr}^{220}$	0.04452850	0.44300	49.650	3.366360	5.795740	28.79700	3.346
$^{85}\text{At}^{216}$	0.04620890	0.44590	48.820	3.493390	5.831060	28.31560	2.773
$^{83}\text{Bi}^{212}$	0.04798620	0.44860	48.000	3.627740	5.867680	27.84000	2.200

TABLE IV

Nuclides : $I=47$

(A) Even-Odd group

Nuclides	$\frac{I^2}{A(A-4)}$	$[A^{2/3} - (A-4)^{2/3}]$	$\left[\frac{Z^2}{A^{1/3}} - \frac{(Z-2)^2}{(A-4)^{1/3}} \right]$	Net contribution from			Calc. Q (in Mev)
				β -term	γ -term	δ -term	
$^{96}\text{Cm}^{239}$	0.03933054	0.43091	53.199	2.973900	5.636302	30.85542	6.038
$^{94}\text{Pu}^{235}$	0.04069264	0.43335	52.411	3.076363	5.68216	30.39837	5.124
$^{92}\text{U}^{231}$	0.04212673	0.43587	51.606	3.184781	5.70177	29.93148	4.568
$^{90}\text{RaAc}^{227}$	0.04363799	0.43845	50.822	3.295034	5.734917	29.47674	4.033
$^{88}\text{AcX}^{223}$	0.04523210	0.44108	50.006	3.419547	5.769326	28.93619	3.406
$^{86}\text{An}^{219}$	0.04691516	0.44375	49.192	3.446785	5.804140	28.53350	3.011
$^{84}\text{AcA}^{215}$	0.04869354	0.44653	48.371	3.581260	5.84061	28.05517	2.335
$^{82}\text{AcB}^{211}$	0.05057581	0.44936	47.543	3.823532	5.877601	27.57493	1.749

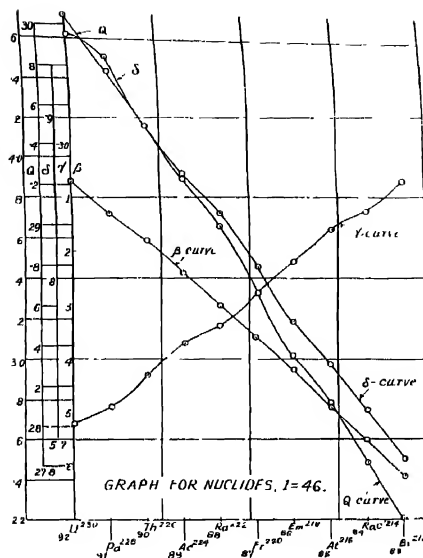


FIG. 3

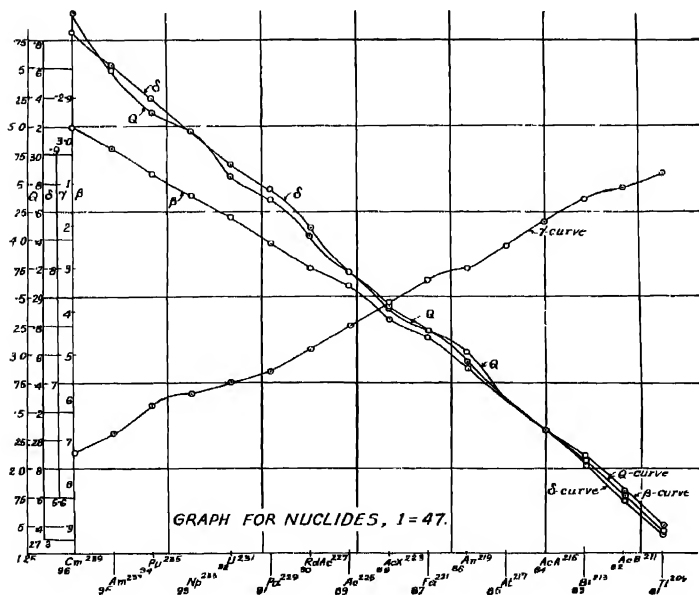


FIG. 4

TABLE IV (contd.)

(B) Odd-Even group

$^{95}\text{Am}^{231}$	0.04000290	0.43095	52.806	3.024220 5.657754 30.627470	5.491
$^{97}\text{Np}^{233}$	0.04140034	0.43458	52.012	3.129862 5.684338 30.166960	4.961
$^{91}\text{Pa}^{229}$	0.04287233	0.43718	51.316	3.241153 5.718314 29.76330	4.360
$^{89}\text{Ac}^{225}$	0.04442431	0.43973	50.310	3.335880 5.751666 29.17085	3.716
$^{87}\text{Fr}^{221}$	0.04610150	0.44243	49.600	3.460497 5.786983 28.76800	3.214
$^{85}\text{At}^{217}$	0.04779214	0.44512	48.782	3.613086 5.822160 28.29357	2.623
$^{83}\text{Bi}^{213}$	0.04962150	0.44791	47.958	3.751386 5.859054 27.81565	2.043
$^{81}\text{Tl}^{209}$	0.05155793	0.45082	47.126	3.897800 5.883640 27.33308	1.439

TABLE V

Nuclides, $I=48$

(A) Even-Even group

Nuclides	$\frac{I^2}{A(A-4)}$	$[4^{2/3} - (A-4)^{2/3}]$	$\left[\frac{Z^2}{1^{1/3}} - \frac{(Z-2)^2}{(A-4)^{1/3}} \right]$	Net contribution from			Calc. Q in Mev.
				β -term	γ -term	δ -term	
$^{96}\text{Cm}^{240}$	0.04067796	0.43029	53.150	3.075253	5.628193	30.82922	5.502
$^{94}\text{Pu}^{246}$	0.04208064	0.43276	52.371	3.181296	5.660492	30.37518	4.974
$^{92}\text{U}^{232}$	0.04355716	0.43425	51.562	3.292922	5.679981	29.92915	4.436
$^{90}\text{Th}^{228}$	0.04583525	0.43877	50.784	3.465133	5.730110	29.45471	3.840
$^{88}\text{Th}^{224}$	0.04675323	0.44039	49.955	3.354544	5.760301	28.97970	3.325
$^{86}\text{Th}^{220}$	0.04848483	0.44310	49.150	3.665420	5.795847	28.50700	2.757
$^{84}\text{Th}^{216}$	0.05031455	0.44583	48.329	3.803771	5.831465	28.03827	2.186
$^{82}\text{Tl}^{212}$	0.05221062	0.44866	47.501	3.950070	5.868472	27.55058	1.584
$^{80}\text{Hg}^{208}$	0.0549563	0.45151	46.670	4.104976	5.905575	27.06859	0.989

(B) Odd-Odd group

$^{95}\text{Am}^{238}$	0.04137037	0.43150	52.760	3.12760	5.64420	30.60600	5.243
$^{93}\text{Np}^{240}$	0.04280036	0.43400	51.972	3.236385	5.676711	30.14375	4.704
$^{91}\text{Pa}^{230}$	0.04432464	0.43650	51.369	3.350950	5.709420	29.69150	3.880
$^{89}\text{Ac}^{226}$	0.0459220	0.43908	50.369	3.471700	5.743164	29.21400	3.605
$^{87}\text{Fr}^{222}$	0.04760722	0.44182	49.559	3.599000	5.779000	28.67810	2.978
$^{85}\text{At}^{218}$	0.0491870	0.44438	48.471	3.735851	5.812490	28.11317	2.312
$^{83}\text{Ra}^{214}$	0.05126833	0.44742	47.916	3.875886	5.849636	27.79128	1.885
$^{81}\text{Ra}^{210}$	0.05325934	0.45009	47.082	4.026407	5.887076	27.30755	1.288

TABLE VI
Nuclides : $I=49$

(A) Even-Odd group

Nuclides	$\frac{J^2}{A(A-1)}$	$[A^{2/3} - (A-1)^{2/3}]$	$\left[\frac{Z^2}{A^{1/3}} - \frac{(Z-1)^2}{(A-1)^{1/3}} \right]$	Net contribution from			Calc. Q (in Mev)
				β -term	γ -term	δ -term	
$^{90}\text{Cm}^{211}$	0.01203057	0.42972	53.119	3.177067	5.610737	30.80902	5.172
$^{91}\text{Pu}^{217}$	0.04347985	0.43211	52.330	3.287076	5.652291	30.35139	1.837
$^{92}\text{U}^{231}$	0.0449978	0.43160	51.534	3.401908	5.681506	29.88972	4.292
$^{90}\text{Th}^{229}$	0.04659874	0.43713	50.731	3.524864	5.718050	29.42400	3.739
$^{88}\text{Ra}^{225}$	0.04828557	0.43973	49.921	3.650380	5.751665	28.95591	3.177

(B) Odd-Even group

$^{95}\text{Am}^{239}$	0.04271003	0.43004	52.727	3.231827	5.636302	30.5132	5.048
$^{93}\text{Np}^{235}$	0.04422953	0.43335	51.916	3.343752	5.668216	30.11302	1.557
$^{91}\text{Pa}^{231}$	0.04779827	0.43580	51.148	3.461591	5.704110	29.66830	4.028
$^{89}\text{Ac}^{227}$	0.04830000	0.43813	50.429	3.585776	5.734606	29.30010	3.578
$^{87}\text{Ac}^{223}$	0.04916353	0.44008	49.401	3.710761	5.769326	28.65257	2.825

TABLE VII
Nuclides : $I=50$

(A) Even-Even group

Nuclides	$\frac{J^2}{A(A-1)}$	$[A^{2/3} - (A-1)^{2/3}]$	$\left[\frac{Z^2}{A^{2/3}} - \frac{(Z-2)^2}{(A-1)^{2/3}} \right]$	Net contribution from			Calc. Q (in Mev)
				β -term	γ -term	δ -term	
$^{96}\text{Cm}^{242}$	0.04340578	0.42012	53.084	3.281770	5.612890	30.78871	5.240
$^{94}\text{Pu}^{238}$	0.04489074	0.43150	52.284	3.393663	5.644020	30.32468	4.695
$^{92}\text{U}^{234}$	0.04539377	0.43400	51.475	3.51170	5.676720	29.79841	4.083
$^{90}\text{Th}^{230}$	0.04809543	0.43650	50.690	3.636010	5.709420	29.40021	3.594
$^{88}\text{Ra}^{226}$	0.04982856	0.43910	49.881	3.767410	5.743426	28.93100	3.027
$^{86}\text{Rn}^{222}$	0.0516452	0.44617	49.160	3.904376	5.765100	28.51280	2.434
$^{84}\text{RaA}^{218}$	0.05235640	0.45101	48.150	4.050340	5.799210	27.92600	1.895
$^{82}\text{RaB}^{214}$	0.05562970	0.45622	47.417	4.205606	5.836556	27.50286	1.254

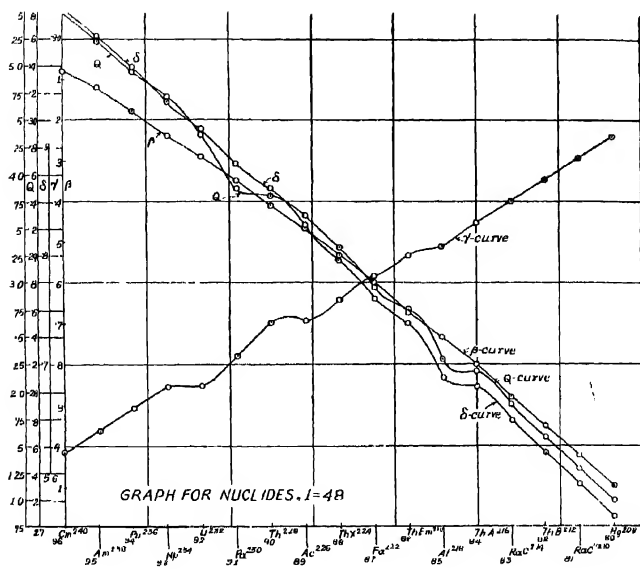


FIG. 5

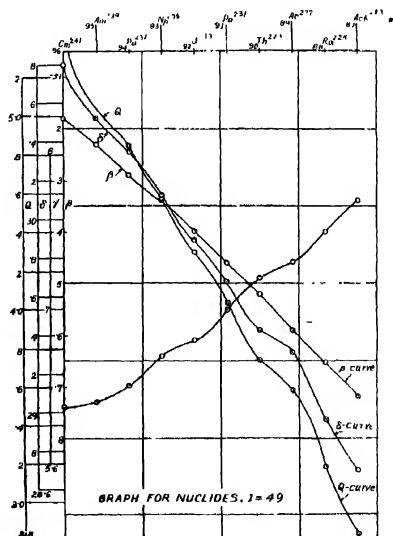


FIG. 6

TABLE VII (contd.)

(B) Odd-Odd group

$^{95}\text{Am}^{240}$	0.04413842	0.43041	52.687	3.336864	5.629762	30.55847	4.971
$^{93}\text{Np}^{236}$	0.04566041	0.43273	51.890	3.451928	5.660500	30.10200	4.431
$^{91}\text{Pa}^{232}$	0.04618672	0.43525	51.153	3.571050	5.693070	29.66874	3.908
$^{89}\text{M}^{228}\text{Th}_2$	0.0489505	0.43777	50.227	3.700558	5.726030	29.13165	3.277
$^{87}\text{Pa}^{224}$	0.05073051	0.44040	49.028	3.835327	5.760439	28.43629	2.481
$^{85}\text{Ac}^{220}$	0.05260942	0.44309	48.072	3.977271	5.795615	27.88059	1.919
$^{83}\text{Bi}^{216}$	0.05459468	0.44583	47.866	4.127357	5.831450	27.71948	1.574
$^{81}\text{Tl}^{212}$	0.05660447	0.44866	47.000	4.286102	5.868469	27.16000	0.962

TABLE VIII

Nuclides. $I = 51$

(A) Even-Odd group

Nuclides	$\frac{I^2}{A(A-1)}$	$[A^{2/3} - (1-1)^{2/3}]$	$\left[\frac{Z^2}{A^{1/3}} - \frac{(Z-1)^2}{(A-1)^{1/3}} \right]$	Net contribution from			Calc. Q (in Mev)
				ρ term	γ -term	δ -term	
$^{96}\text{Cm}^{243}$	0.04178537	0.42852	53.030	3.385766	5.605040	30.75261	5.102
$^{94}\text{Pu}^{239}$	0.04631000	0.43001	52.240	3.501034	5.636302	30.31022	4.565
$^{92}\text{U}^{235}$	0.0479177	0.43315	51.452	3.622281	5.666910	29.84216	4.007
$^{90}\text{U}^{231}$	0.04960237	0.43587	50.651	3.749049	5.701177	29.37758	3.440
$^{88}\text{Ra}^{227}$	0.05138182	0.43845	49.841	3.884467	5.731016	28.90777	2.873

(B) Odd-Even group

$^{95}\text{Am}^{241}$	0.04553820	0.42952	52.645	3.442680	5.618133	30.35110	4.650
$^{93}\text{Np}^{237}$	0.04710165	0.43234	51.851	3.560884	5.655006	30.07510	4.299
$^{91}\text{Pa}^{233}$	0.04874712	0.43460	51.052	3.686980	5.684566	29.54106	3.650
$^{89}\text{Ac}^{229}$	0.0504835	0.43716	50.247	3.816323	5.718050	29.02208	3.144

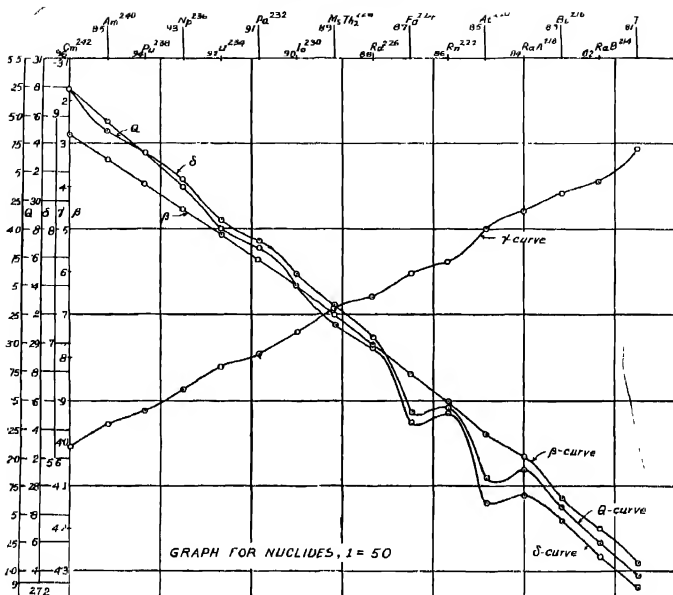


FIG. 7

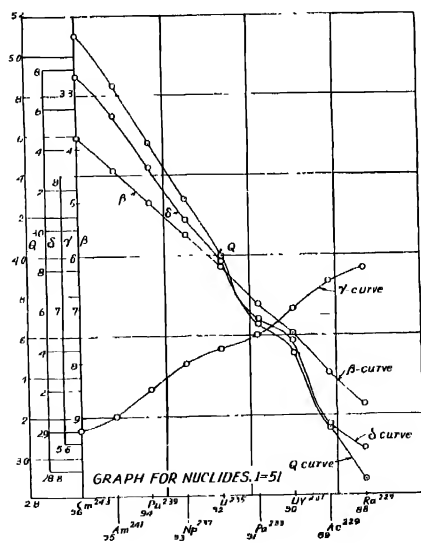


FIG. 8

TABLE IX
Nuclides: $I=52$

(A) Even-Even group

Nuclides	$\frac{I^2}{A(A-4)}$	$[A^{2/3} - (A-4)^{2/3}]$	$\left[\frac{Z^2}{A^{1/3}} - \frac{(Z-2)^2}{(A-4)^{1/3}} \right]$	Net contribution from			Calc. Q (in Mev)
				β -term	γ -term	δ -term	
$^{26}\text{Cm}^{244}$	0.04617486	0.42701	52.909	3.460818	5.50761	30.7394	4.566
$^{94}\text{Pu}^{240}$	0.01774010	0.43031	52.208	3.600152	5.624152	30.28064	4.170
$^{92}\text{U}^{236}$	0.04038631	0.43276	51.413	3.733605	5.66050	29.81932	3.806
$^{90}\text{Th}^{232}$	0.05111916	0.43523	50.609	3.864010	5.69287	29.27897	3.227
$^{88}\text{MsTh}^{228}$	0.05306790	0.43778	49.801	4.011058	5.725135	28.88457	2.718
$^{86}\text{Rn}^{224}$	0.05487010	0.44041	48.983	4.148180	5.76056	28.41014	2.143

(B) Odd-Odd group

$^{27}\text{Am}^{242}$	0.04604768	0.42912	52.605	3.540244	5.61289	30.44742	4.631
$^{93}\text{Np}^{238}$	0.04855274	0.43270	51.811	3.670586	5.650515	30.05037	4.159
$^{91}\text{Pa}^{234}$	0.05324152	0.43279	51.019	3.798760	5.660892	29.58579	3.568
$^{89}\text{Ac}^{220}$	0.052020	0.43651	50.198	3.932701	5.70965	29.11483	3.012
$^{87}\text{Fr}^{226}$	0.05389158	0.43908	49.393	4.074430	5.752584	28.64940	2.448

TABLE X
Nuclides: $I=54$

(A) Even-Even group

Nuclides	$\frac{I^2}{A(A-4)}$	$[A^{2/3} - (A-4)^{2/3}]$	$\left[\frac{Z^2}{A^{1/3}} - \frac{(Z-2)^2}{(A-4)^{1/3}} \right]$	Net contribution from			Calc. Q (in Mev)
				β -term	γ -term	δ -term	
$^{96}\text{Cm}^{246}$	0.04901581	0.42668	52.922	3.703041	5.58359	30.70475	4.705
$^{94}\text{Pu}^{242}$	0.05062840	0.42918	52.129	3.827524	5.601760	30.23482	4.321
$^{92}\text{U}^{238}$	0.05235040	0.43152	51.452	3.958370	5.61160	29.84216	3.635
$^{90}\text{UX}_1^{234}$	0.05418060	0.43400	50.506	4.096054	5.676732	29.20348	2.994
$^{88}\text{Ra}^{230}$	0.0567682	0.43752	50.028	4.241047	5.725750	28.97582	2.650

(B) Odd-Odd group

$^{95}\text{Am}^{241}$	0.04979518	0.42792	52.516	3.764510	5.59720	30.45927	4.412
$^{93}\text{Np}^{240}$	0.05148307	0.42931	51.730	3.892120	5.617653	30.03400	3.760
$^{91}\text{Pa}^{236}$	0.05325832	0.42276	50.933	4.026330	5.65130	29.54114	3.426
$^{89}\text{Ac}^{232}$	0.05512705	0.44389	50.121	4.167605	5.67227	29.07180	2.894



DISCUSSION

It will be seen from the plots that the β -curves have almost a constant slope, the net contribution of the β -terms to the α -energy Q diminishing monotonically with decreasing mass number. The average slope of these curves, considering the straightest portion of each, is about '035 per mass unit.

Most of the γ -curves are characterised by undulations—flat maxima and minima occurring alternately. This feature is very prominent for $I=44$, 45, 46, 48, 49, 50, 51, and 54. Another peculiarity of these curves is that even in the same curve the undulations do not occur with any regularity with respect to mass number. On the other hand, for $I=44$, 45, and 48 there is practically no undulation for a considerable run of the curves towards the ends.

The δ and Q curves show a pronounced tendency to run more or less parallel. This is specially true for curves with increasing I values. Also, with increase of I there is a tendency for the occurrence of undulations. This is very marked for $I=47$, 48, 49, 50 and 51. We can infer from this that the main contribution toward the energy release comes from δ -term. This is also apparent from the tables, in which the leading contributor is the δ -term. Another interesting fact is that when the Q -points belonging to the same class (A) or (B) are joined separately, the resulting mean curve is more or less straight. This theoretical prediction of irregularity in the energy release curves of nuclides with the same I value is in qualitative agreement with experimentally obtained curves (Peilman, Ghiorso and Seaborg, 1950). In any similar theoretical plots the relative trend of the curves will not change by altering the constants β , γ , and δ because, such an alteration will introduce only a change in the scale of the ordinates in the ratio of the altered values of the constants to their respective values used here. The full significance of these theoretical plots in relation to experimental findings will be dealt with subsequently.

ACKNOWLEDGMENTS

It is a pleasure to record gratitude to Prof. M. N. Saha, D.Sc., F.R.S., for initiating the author to the problem and guiding in all phases. Thanks are due to Dr. S. Biswas for collecting some of the data which will be presented in the second part.

REFERENCES

- Bethe, H. A. and Bacher R. F., 1936, *Rev. Mod. Phys.*, **8**, 165
 Gluckauf, E., 1948, *Proc. Roy. Soc. (London)*, **61**, 25
 McInke, W. W., Ghiorso A., Seaborg G. T., 1948, *Phys. Rev.*, **75**, 311
 Price, M. H. L., 1950, *Proc. Phys. Soc. (London)*, **63**, 692
 Perlman, I., Ghiorso, A. and Seaborg G. T., 1950, *Phys. Rev.*, **77**, 39
 Studier, M. H. and Hyde, E. K., 1947, *Phys. Rev.*, **75**, 314
 Seaborg, G. T. and Perlman, I., 1950, *Rev. Mod. Phys.*, **20**, 585
 Weizsacker, C. F. v., 1935, *Zeits. f. Physik*, **96**, 431

ON THE RAMAN SPECTRA OF NAPHTHALENE AT LOW TEMPERATURE*

By A. K. RAY

(Received for publication, October 11, 1950)

Plate XX

ABSTRACT The Raman spectra of a homogeneous crystalline mass of naphthalene have been studied for three different temperatures, *e.g.*, 30°C , -100°C and -180°C , using a spectrograph having a dispersion of 11.8 \AA/mm in the region of 4046 \AA . A new Raman line at 95 cm^{-1} has been observed in the case of the crystal at 30°C besides the other five lines in the low frequency region reported by previous authors. The line 75 cm^{-1} , which is broad at 30°C , becomes sharper at lower temperatures and all the six lines shift away from the Rayleigh line with the lowering of temperature. It is pointed out that if these lines would be due to rotational oscillations of the two molecules in the unit cell they would shift nearer to the Rayleigh line with the lowering of temperature and the actual shift in the opposite direction indicates that there is a coupling between the molecules.

It is further observed that all the other lines of higher frequencies become sharper at low temperatures and there is no indication of any splitting of any of the lines into two components. It is concluded from these results that these latter lines are due to oscillations of single molecule in the crystal, having no phase relation with the oscillation of its neighbours.

INTRODUCTION

The Raman spectra of naphthalene in different states have been investigated by a large number of workers since it was first observed by Gross and Vuks (1935) that in solid state at about 0°C this substance yields four new Raman lines at 45, 73, 100 and 124 cm^{-1} respectively. These lines were attributed to lattice oscillations by the same authors. It was, however, pointed out by Sirkar (1937) that one of these lines of naphthalene is more intense than the most intense line at 1380 cm^{-1} of the naphthalene molecule, but since the unit cell has a centre of symmetry, translational oscillations of molecules are forbidden in the Raman effect and, therefore, this intense line cannot be due to such oscillations of the lattice. Kastler and Rousset (1941) and also Bhagavantam (1941) independently pointed out that these new lines are due to rotational oscillations of the molecule in the lattice about the three axes of the molecule. Nedungadi (1942) investigated the Raman spectra of a single crystal of naphthalene with different orientations of the incident light vector with respect to the axes of the crystal and found out the matrix elements of the tensor components of the deformation ellipsoids corresponding to the new lines in the low frequency region and

*Communicated by Prof. S. C. Sirkar

also those for the lines in the high frequency region due to oscillations of the single molecule. He concluded that the characteristics of the matrices observed by him confirmed the theory put forward by Bhagavantam (1941) that the new lines in the low frequency region were due to rotational oscillations of the molecule about its three axes, there being two such oscillations, one symmetric and another anti-symmetric to the two-fold axis of the rotation of the unit cell, in each of these three cases. From the nature of the matrices of the tensor observed in the case of Raman lines of higher frequencies he concluded that each of these lines is composed of two oscillations of the pair of molecules in the unit cell, one symmetric and another anti-symmetric to the two-fold axis of rotation. It has recently been shown by Sirkar and Ray (1950) that the characteristics of the Raman spectra of solid benzene at different temperatures observed by them do not confirm the theory put forward by Bhagavantam (1941) and in fact the results show that the Raman lines of frequencies higher than those of the new Raman lines in the low frequency region are much sharper in the case of the solid than in the case of the liquid and they are due to incoherent scattering of single benzene molecule in the lattice. Such a conclusion has also been drawn by Frulimig (1949) from the results observed in the case of solid diphenyl ether.

The theory mentioned above can be tested only by studying the temperature-dependence of the positions and the number of new lines in the low frequency region and also the influence of temperature on the width of the other lines of higher frequencies. Since in the case of naphthalene in the solid state it has been concluded by previous workers (Kastler and Roussel, 1941, Nedungadi, 1942) that the results observed confirm the theory mentioned above, the study of the influence of temperature on the properties of the Raman lines of solid naphthalene would be of interest. In the present paper results of such an investigation have been discussed.

EXPERIMENTAL

The experimental technique used is the same as that used in the case of solid benzene by Sirkar and Ray (1950). Naphthalene scales from May & Baker were first sublimed and then distilled repeatedly under reduced pressure in Pyrex containers. Finally a Pyrex tube provided with a long narrow neck was partially filled up with the molten distillate and the tube was sealed. The molten mass was kept in a suitable bath so that it crystallised very slowly to form a very homogenous mass. The Raman spectra of this mass at three different temperatures, *e.g.*, 30°C, -100°C, and -180°C were photographed exactly in the same way as indicated in a previous paper (Sirkar and Ray, 1950). Iron arc spectrum was photographed in each plate in order to find out whether any of the lines shifts with the change of temperature.

RESULTS AND DISCUSSION

Results obtained are given in Table I. In this table frequency-shifts observed by Hilmi Benel (1940) and Nedungadi (1942) for the single crystal at room temperature have also been included. The spectrograms are reproduced in Plate XX.

TABLE I

Hilmi Benel (1940) Single-crystal at room temp $\Delta\nu$ in cm^{-1}	Nedungadi (1942) Single crystal at room temp $\Delta\nu$ in cm^{-1}	Present author		
		Crystal at 30°C $\Delta\nu$ in cm^{-1}	Crystal at about -100° $\Delta\nu$ in cm^{-1}	Crystal at about -180°C $\Delta\nu$ in cm^{-1}
	38	38 (1), c,k	38 (1), c,k	30 (1), c,k
	47	46 (1), e,k	48 (1), e,k	50 (1), e,k
	75	75 (4b), e,k	78 (4), e,k	86 (4), e,k
		95 (2), e,k	97 (1), e,k	106 (2), e,k
	107	102 (2), e,k	109 (2), e,k	120 (3), e,k
	121	122 (1), e,k	125 (1), e,k	141 (2), e,k
393	389 (2)	397 (6), e,k	397 (6), e,k	507 (6), e,k
	403 (1)	465 (6), e,k		107 (6), e,k
508	512 (10)	508 (1), e,k	508 (4), e,k	511 (4), e,k
726	721 (1)	724 (6), e,k		
763	761 (13)	761 (4), e,k	761 (4), e,k	763 (1), e,k
786	784 (1)			
946				
952	948 (1)	950 (1), e,k		
980	972 (1)			
1024	1021 (6)	1024 (3), e,k	1025 (3), e,k	1027 (35), e,k
	1102 (1)			
1147	1143 (3)	1142 (1), e,k	1142 (1), e,k	1144 (18), e,k
1168	1169 (2)			
	1215 (3)			
1244	1242 (2)	1240 (1), e,k		
	1258 (1)	1256 (1), e,k		1258 (1), e,k
	1260 (2)			
	1321 (1)			
1382	1384 (15)	1381 (10), e,k	1383 (10), e,k	1388 (118), e,k
1446	1442 (1)	1444 (1), k		1441 (1), k
1463	1403 (3)	1460 (2), e,k	1461 (2), e,k	1463 (3), e,k
	1519 (6)	1520 (6), k	1520 (6), k	1520 (6), k
	1537 (1)			
1577	1576 (7)	1577 (3), e,k	1578 (3), e,k	1580 (4), e,k
1596				
1630	1624 (1)			
	3000 (1)			
	3026 (1)			
3055	3058 (8)	3055 (48), k	3055 (48), k	3062 (35), k
	3080 (1)			

(a) Lines due to intermolecular oscillation

The positions of the new lines in the low frequency region at different temperatures of the crystals were also studied previously by Shkar (1936). The frequency shifts observed at different temperatures by different authors are given in Table II for comparison.

TABLE II

Gross & Vukc (1935) at 0°C $\Delta \nu$ in cm^{-1}	Nedungadi (1942) at about 28°C $\Delta \nu$ in cm^{-1}	Sirkar (1936)		Present author		
		at 30°C $\Delta \nu$ in cm^{-1}	at about -180°C $\Delta \nu$ in cm^{-1}	at 30°C $\Delta \nu$ in cm^{-1}	at about -100°C $\Delta \nu$ in cm^{-1}	at about -180°C $\Delta \nu$ in cm^{-1}
	38			38 (1)	38 (1)	39 (1)
		42				
45(4s)	47			46 (1)	48 (1)	50 (1)
73(8b)	75	71	80	75 (4b)	78 (4)	84 (4)
				95 (2)	97 (1)	106 (2)
109(3)	107	102	120	102 (2)	109 (2)	120 (3)
124(2)	121	116	142	122 (1)	125 (1)	141 (2)

It can be seen from column 5 of Table II that even at room temperature there are six new Raman lines in the low frequency region. The line at 75 cm^{-1} is broad and Nedungadi (1942) concluded from values of tensor components that this line is actually an unresolved doublet with its components at 72 and 76 cm^{-1} . The feeble but sharp line at 95 cm^{-1} was not observed by any of the previous workers. In the present investigation it has been observed that the line 75 cm^{-1} is broad at room temperature but it becomes sharper and shifts away from the Rayleigh line at lower temperatures. In fact all the lines in this region shift away from the Rayleigh line when the solid mass is cooled down to -180°C . If the line 75 cm^{-1} would be a doublet it would be split up into two components at -180°C , because the distance between the components of the other two pairs increases at low temperature. As on the contrary it becomes sharper at the lower temperatures, it is doubtful whether this line consists of unresolved doublet. The line at 102 cm^{-1} , observed at room temperature, shifts to 120 cm^{-1} and also its intensity increases when the temperature of the crystal is lowered to -180°C .

As pointed out in an earlier paper by Sirkar and Ray (1950), the changes which take place in the position and intensity of these lines with the change of temperature are contradictory to the hypothesis put forward by Kastler and Rousset (1941) and by Bhagavantam. If the rotational oscillations would be executed by free single molecules pivoted in the lattice there would hardly be any splitting up of the lines due to symmetric and antisymmetric oscillations of the two molecules in the unit cell. The fact that three doublets are observed at room temperature and the distance between the components of each doublet increases with the lowering of temperature shows that there is strong coupling between the two molecules executing

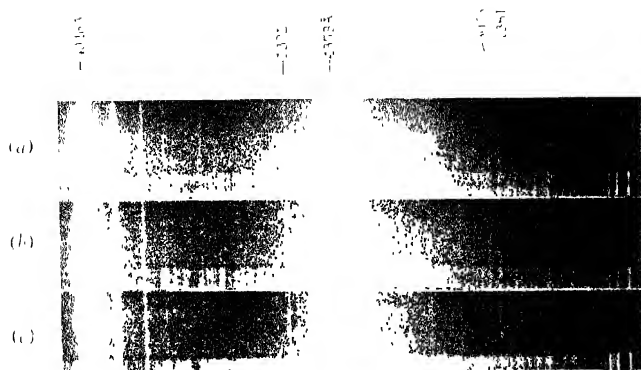


Fig. 1

(a) Solid at air temperature (b) Solid at about -100°C
 (c) Solid at air temperature

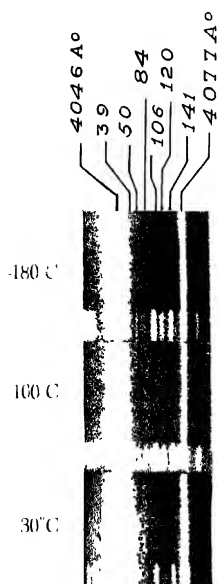


Fig. 2

Raman spectra of naphthalene

the oscillations. This conclusion is further corroborated by the fact that the lines shift away from the Rayleigh line with the lowering of temperature. In the case of rotatory oscillation of uncoupled molecules the frequency-shift of the lines due to such oscillations would diminish with the lowering of temperature, because in the case of polar molecules such a diminution in the frequency of such oscillations has been observed by previous workers (Sen, 1949). On the other hand the observed increase in the frequency shift can be explained satisfactorily on the assumption that there is coupling between the neighbouring molecules and the strength of the coupling increases with the diminution in the distance between neighbouring molecules at lower temperatures. The slight increase in the intensity of the line 120 cm^{-1} with the lowering of temperature to -180°C also cannot be explained on the hypothesis that the line is due to oscillation of a pair of single molecules in the unit cell.

(b) Lines due to intramolecular vibrations

The data given in Table I show that prominent Raman lines of the naphthalene molecule in the solid state are all single lines and Plate XX shows that these lines are very sharp. These lines, therefore, are due to incoherent scattering due to the single molecules, because in the case of the lines in the low frequency region it has been observed that the oscillation of molecules coupled to each other produce doublets in which the components are separated from each other. As pointed out by Sirkar and Ray (1950), the probability of the occurrence of the same mode of oscillation simultaneously in the case of the two molecules in the unit cell of the crystal in this case is very small in view of the fact that there are so many modes of oscillations. The chance for the exact coincidence of the phases of the two molecules in the unit cell executing the same mode of oscillation is still less. Hence from theoretical point of view only incoherent scattering due to single molecule is expected in the case of such organic molecular crystals and the results observed in the present investigation corroborate such a view. The results obtained also in the case of crystals of benzene by Sirkar and Ray (1950) and those obtained by Fröhling (1949) in the case of solid diphenyl ether also led to the conclusion that the Raman lines due to intramolecular oscillations in the crystals are due to incoherent scattering by single molecule. All these results, therefore, show that the theory put forward by Bhagavantam (1941) regarding the structure of Raman lines due to molecular crystal is not correct.

As regards the magnitudes of tensor components of the deformation ellipsoid observed independently by Nedungadi (1942) and Hilmi Benel (1946) it can be seen that the magnitudes observed by the two authors are quite different from each other in certain cases. For instance, in the case of the line 1382 cm^{-1} Nedungadi finds that all the tensor components have finite values while the other author finds $\epsilon_{\alpha\alpha}$, $\epsilon_{\beta\beta}$ and $\epsilon_{\gamma\gamma}$ to be equal to

zero. Further if the lines would be due to superposition of oscillations of the pair of molecules in the unit cell symmetric and antisymmetric to the two-fold axis, all the tensor components would be present in the case of each of the Raman lines. Contrary to such an expectation, both the authors find that some of the tensor components are absent. This fact also shows that the lines are due to oscillations of the single molecule and during oscillations of certain modes the polarisability of the molecule along certain directions does not change at all. This is due to the planar structure of the molecules in the crystal.

Some of the lines are observed to shift slightly towards longer wavelengths with the lowering of temperature of the crystal. Such a change also takes place with the solidification of the molten mass, as can be seen from the data published by Nedungadi (1942) and Hilmi Benel (1940). These changes may indicate some form of coupling between the molecules in the unit cell of the crystal.

ACKNOWLEDGMENT

The author is indebted to Prof. S. C. Sirkar for his kind interest and guidance throughout the progress of the work.

OPTICS DEPARTMENT,
INDIAN ASSOCIATION FOR THE CULTIVATION OF SCIENCE,
210, BOWBAZAR STREET, CALCUTTA

REFERENCES

- Bhagavantam, S., 1931, *Proc. Ind. Acad. Sc.*, **13A**, 543.
 Pruhling, A., 1919, *Jour. de Chimie Physique*, **46**, 35.
 Gross, W. and Vuks, M., 1935, *Nature*, **135**, 100, 431, 998.
 1936, *Jour. Phys. Rad.*, **5**, 1.
 1938, " **6**, 457.
 Hilmi Benel, 1940, *Thesis, Bordeaux*.
 Kastler, A. and Ronset, A., 1941, *Comptes Rendus*, **212**, 645.
 Nedungadi, T. M. K., 1942, *Pro. Ind. Acad. Sc.*, **15A**, 376.
 Sen, S. N., 1949, *Ind. J. Phys.*, **23**, 495.
 Sirkar, S. C., 1936, *Ind. J. Phys.*, **10**, 75.
 " 1937, " **11**, 343.
 Sirkar, S. C. and Ray A. K., 1950, *Ind. J. Phys.*, **24**, 189.

THE WAVE STATISTICAL THEORY OF ALPHA-DISINTEGRATION

BY K. C. KAR AND M. I. CHAUDHURY

(Received for publication, September 18, 1950)

ABSTRACT The present paper is an attempt to study the phenomenon of alpha-decay from a completely new standpoint. All the previous theories are based on the leakage hypothesis, first introduced by Gamow (1928). The recent experiments of Chang (1946) are, however, "in serious disagreement" with the above theories. So the need of reformulation of the above hypothesis has been stressed by Chang and others.

According to the present theory the alpha particles do not leak through the potential barrier by some unknown mechanism, but actually surmount the barrier as required by classical mechanics. And on coming out of the nucleus they are acted upon by a retarding attraction field of Yukawa type, which will obviously reduce the initial high energy to the low observed value. Instead of the usual wave equation, we have taken those from the principles of wave statistics, given by Kar (1940), which give a physical interpretation for the internal mechanism of disintegration.

The chief advantages of the present theory are

- (1) An *explicit* formula for the nuclear radius, *independent of λ* , has been obtained for the first time [*vide* Eq. (36)]. The values of nuclear radii have been calculated from the observed energy values (Table I). The values thus obtained are unique for given z -values, unlike the numerous values given by the previous theories.
- (2) The maximum values of the extra-nuclear Yukawa type field have been calculated from the formula obtained [*vide* Eq. (35.1)]. The order of the magnitudes obtained agree with the values of nuclear binding energies calculated from mass-defects, etc.
- (3) The formula for disintegration constant λ differs in the exponential part from the Gamow-factor, in having the internal energy of the alpha particle instead of its observed value. This will explain the discrepancy between the previous theories and the recent experimental results.
- (4) It explains qualitatively the general decrease in the number of spectral lines as we go up a radioactive series.

INTRODUCTION

The first attempt to give a wave-mechanical treatment of the problem of alpha-decay was made by Gamow (1928), and Condon and Gurney (1928). The difficulty in explaining the difference between the observed low energy of the emitted alpha particles and the high energy of the potential barrier at the surface of the nucleus (indicated by scattering experiments) led them to introduce the well-known hypothesis of leakage. It is also assumed that the energy of the alpha particles inside the nucleus is complex and that the imaginary part is the cause of the leakage (Gamow, 1937).

Since then attempts have been made by Sexl (1929), Kar (1933), Bethe (1937), Preston (1946) and many others* to study the phenomenon of alpha-decay. Each attempt was initiated with the purpose of removing the lack of mathematical rigour at places in Gamow's theory noticed by the different authors. But the fundamental hypothesis of leakage and the complex energy for a real particle were retained throughout by others except by Kar (1933), who gave up the latter hypothesis though retained the former. All these theories have given almost the same formula for disintegration constant λ , as obtained by Gamow.

The experimental agreement of Gamow's formula was found to be more or less satisfactory. However, recently with the collection of more accurate data, Berthelot (1942) has suggested that for better agreement, comparison with the experimental Geiger-Nuttall curve should be made for isotopes only. More recently, objections have also been raised by Chang (1946), who has discovered low energy spectral lines for alpha-rays from Ra, Ra²²⁶, etc. According to him, the existing theory of alpha-disintegration is "in serious disagreement" with his experimental results. For, "the theoretical intensity varies much more rapidly than the observed intensity." Another serious objection, pointed out by Chang and also admitted by Gamow (1949), is that unacceptably large spin changes, as calculated from Gamow's theory, occur in the case of normal-normal and normal-high alpha transformations. He has also pointed out that if the internal energy of the alpha particles be supposed to be higher than the observed value, in contradiction to the fundamental hypothesis of leakage, the discrepancy can be reconciled. Hence while stressing the need of "reformulation" of the current decay theory, Chang (1946) has suggested a modification in a qualitative way. He assumes that penetration occurs through the barrier at a higher energy level than the corresponding observed low energy and that the original difficulty of energy difference can be explained by postulating some sort of semi-static interaction between the outgoing alpha particle and the product nucleus, resulting in the transfer of the balance energy back to the residual nucleus. However, as the exact mechanism of this transfer of energy is not known the position remains more or less as vague as in Gamow's conception of leakage.

SECTION 1

In the proposed theory, we shall suppose that the alpha particle does not leak through the barrier due to some unknown mechanism but actually surmounts the potential hill with energy higher than or just sufficient to overcome it, as required by classical mechanics. We also assume that as the alpha particle just comes out of the nucleus, a retarding attraction field of Yukawa type is at once set up between the outgoing alpha particle and the product nucleus. This extra-nuclear attraction field would obviously reduce

* See references.

the initial high energy of the alpha particle to the observed low value. As, however, this short range attraction force is operative only when the alpha particle has left the nucleus, the minimum energy with which it can come out from inside the nucleus is equal to the peak energy of the Coulomb field, i.e., $2z^*e^2/r_0$, where r_0 =nuclear radius, and z^* =charge number of the product nucleus. If the attraction potential $U(r)$ is effective upto a short distance, reducing to an insignificant value at r_1 (say), no further reduction in the energy of the alpha particle can take place beyond this range. Thus the total energy of the alpha particle at r_1 is equal to the final observed kinetic energy.

Now from what has been stated above, the whole phase space may be divided into three regions, namely.

Region 1. $0 < r < r_0$, i.e., the interior of the nucleus.

In this region the potential energy U' may be taken to be constant. Thus $E' + U' = E_1$, the total kinetic energy inside the nucleus.

Region 2. $r_0 < r < r_1$, i.e., the extent of the short range force.

In this region the Coulomb potential $V = 2z^*e^2/r$. The short range attraction potential actually varies from $U(r_0)$ at r_0 to $U(r_1) = 0$ at r_1 . We shall, however, assume for simplicity the mean constant potential U_0 in the wave equation for this region.

Region 3. $r_1 < r < \infty$, i.e., outside the influence of the short range force.

In this region, the Coulomb potential $V = 2z^*e^2/r$, $U(r) = 0$, kinetic energy $= (E_3 - V)$, where E_3 is the total energy of the alpha particle, and is obviously the observed alpha energy, $\frac{1}{2}Mv^2$.

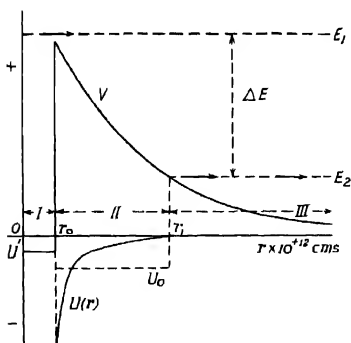


FIG. 1(a)

→ indicates α -particle, V =coulomb potential. I, II, III are the respective regions. ΔE =difference of internal and observed energy of the α -particle $U(r)$ =Extra-nuclear attraction potential of nuclear force type. U_0 . its mean (rectangular, outside) U' =Internal rectangular potential.

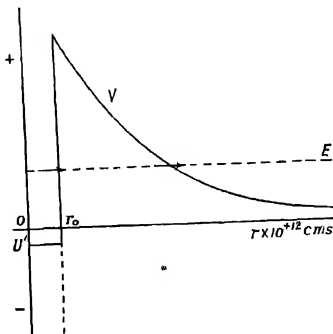


FIG. 1(b)

E =Internal α -energy=observed α -energy
 U' =Attraction potential (internal, rectangular)

The distribution of fields assumed in the proposed theory is shown in Fig. 1(a). For comparison the distribution assumed by the previous workers is given in Fig. 1(b),

Region 1. In this region the wave equation from the principles of wave statistics, is given by

$$\Delta\chi_1 + \frac{8\pi^2 ME_1}{h^2} \left(1 + \frac{b^2 h^2}{16\pi^2 E_1^2} \right) \chi_1 = 0$$

where χ_1 represents the wave function for the alpha particle for q-space. This wave equation differs from that of Schrodinger in having the term $b^2 h^2 / 16\pi^2 E_1^2$, where b is the damping co-efficient. It is to be noted that for mechanism of disintegration, Kai (1940) has suggested from hydrodynamical analogy that when viscosity develops in the highly dense but compressible nuclear phase fluid, alpha particle comes out as a result of damping. Thus damping factor b provides a physical interpretation for disintegration, and b is defined by $b.D_t dt = dD_t$, where D_t is the number density of alpha particles just inside the surface of the nucleus. Now since the emission is assumed to be spherically symmetrical, we have $l=0$, and so the radial component of the wave function χ_1 for region 1 satisfies

$$\frac{d^2 R_1}{d\tau^2} + \frac{2}{\tau} \frac{dR_1}{d\tau} + \frac{8\pi^2 M.E_1}{h^2} \left(1 + \frac{b^2 h^2}{16\pi^2 E_1^2} \right) R_1 = 0 \quad \dots (1)$$

Putting $R_1 = \frac{R'_1}{\tau}$, in Eq. (1) we have

$$\frac{d^2 R'_1}{d\tau^2} + \frac{8\pi^2 ME_1}{h^2} \left(1 + \frac{b^2 h^2}{16\pi^2 E_1^2} \right) R'_1 = 0 \quad \dots (1.1)$$

The solution of Eq. (1.1) gives

$$R_1 = \frac{R'_1}{\tau} = \text{const.} \frac{\sin \alpha_1 \tau}{\tau} \quad \dots (1.2)$$

where

$$\alpha_1^2 = \frac{8\pi^2 ME_1}{h^2} \left(1 + \frac{b^2 h^2}{16\pi^2 E_1^2} \right) \quad \dots (1.3)$$

Regions 2 and 3. Outside the nucleus b is absent. Consequently, on taking corresponding energies, we have the wave equation for the region 2 ($\tau_0 < \tau < \tau_1$) as

$$\Delta\chi_2 + \frac{8\pi^2 M}{h^2} (E_2 + U_0 - V(\tau)) \chi_2 = 0 \quad \dots (1.4)$$

and for the region 3 ($\tau_1 < \tau < \infty$) as

$$\Delta\chi_3 + \frac{8\pi^2 M}{h^2} (E_3 - V(\tau)) \chi_3 = 0 \quad \dots (1.5)$$

These are identical with the usual wave equations except for the term U_0 in region 2. Therefore the modified R -equations for these external regions are

$$\frac{d^2 R_2}{d\tau^2} + \frac{2}{\tau} \frac{dR_2}{d\tau} + \frac{8\pi^2 M}{h^2} (E_2 + U_0 - V(\tau)) R_2 = 0 \quad \dots (2)$$

and
$$\frac{d^2 R_3}{d\tau^2} + \frac{2}{\tau} \frac{dR_3}{d\tau} + \frac{8\pi^2 M}{h^2} (E_3 - V(\tau)) R_3 = 0 \quad \dots (3)$$

On putting $R_2 = \frac{R_2'}{\tau}$, and $R_3 = \frac{R_3'}{\tau}$, respectively in (2) and (3), we have

$$\frac{d^2 R_2'}{d\tau^2} + \frac{8\pi^2 M}{h^2} (E_2 + U_0 - V(\tau)) R_2' = 0 \quad \dots (2.1)$$

and
$$\frac{d^2 R_3'}{d\tau^2} + \frac{8\pi^2 M}{h^2} (E_3 - V(\tau)) R_3' = 0 \quad \dots (3.1)$$

where M = mass of alpha particle, E = total energy of the α -particle, $V(\tau) = 2z^*e^2/\tau$, $z^* = z - 2$. The subscripts 2, and 3 respectively refer to regions 2 and 3.

To solve Eq. (2.1) we put

$$\left. \begin{aligned} \rho &= \alpha_2 \tau \\ \alpha_2 &= 4\pi \sqrt{2M(E_2 + U_0)/h} \end{aligned} \right\} \quad \dots (2.2)$$

where

Therefore Eq. (2.1) becomes

$$\frac{d^2 R_2'}{d\rho^2} + \left(1 - \frac{K_2}{\rho}\right) R_2' = 0 \quad \dots (2.3)$$

where

$$K_2 = \frac{4\pi z^* e^2 \sqrt{M}}{h \sqrt{2(E_2 + U_0)}} \quad \dots (2.4)$$

Again by substituting

$$\left. \begin{aligned} \rho &= 2x \\ K_2 &= K_2'/2 \end{aligned} \right\} \quad \dots (2.5)$$

Eq (2.3) can further be simplified and we have

$$\frac{d^2 R_2'}{dx^2} + \left(1 - \frac{K_2'}{x}\right) R_2' = 0 \quad \dots (2.6)$$

Similarly from Eq. (3.1) we have evidently

$$\frac{d^2 R_3'}{dx'^2} + \left(1 - \frac{K_3'}{x'}\right) R_3' = 0 \quad \dots (3.2)$$

where we have put

$$\left. \begin{aligned} \rho' &= \alpha_3 \tau = 2x' \\ \alpha_3 &= 4\pi \sqrt{2ME_3}/h \\ K_3 &= \frac{4\pi z^* e^2 \sqrt{M}}{h \sqrt{2E_3}} = \frac{K_3'}{2} \end{aligned} \right\} \quad \dots (3.3)$$

Now Eqs. (2.6) and (3.2) are standard differential equations. P. Debye (1909) has given a solution by the method of steepest descent, which has been used by Preston (1946). We shall, however, follow the method given by Schlechinger (1900), and quoted by Sexl (1929). Both the methods, of course, lead to the same solution.

It would be useful to give a brief sketch of the method to be followed. Let us assume a solution of (2.6) in the form

$$R_2' = e^{\int g \cdot dx} \quad \dots (4)$$

where

$$g = g_0 + \lambda g_1 + \dots \quad \dots (4.1)$$

in which λ and g_1 are small. On substituting (4) in (2.6) and neglecting the small quantities $\lambda dg_1/dx$ and $\lambda^2 g_1^2$, we have

$$g_0' + g_0^2 + 2\lambda g_0 g_1 + 1 - \frac{K_2'}{x} = 0 \quad \dots (5)$$

where

$$g_0' = \frac{dg_0}{dx}.$$

The following three cases may now be considered :

Case 1. Let x be very small and K_2' very great. Along with x , r becomes very small. So the solution refers to a region inside the nucleus. Thus the case is apparently invalid for an equation holding for a region where there is Coulomb field.

Case 2. Let x and K_2' be both great. Hence from Eq. (5), equating terms of the same order we get

$$\left. \begin{aligned} g_0 &= \pm \sqrt{\frac{K_2'}{x} - 1} \\ \lambda g_1 &= -\frac{1}{2} \cdot \frac{d}{dx} \cdot \ln g_0 \end{aligned} \right\} \quad \dots (4.3)$$

Using Eq. (4.3) in (4) we have for the solution

$$R_2' = \frac{\text{const.}}{\sqrt{\frac{K_2'}{x} - 1}} \cdot e^{\pm \int \sqrt{\frac{K_2'}{x} - 1} \cdot dx} \quad \dots (6)$$

Here again the solution (6) may be of two different forms according as,

(a) $\frac{K_2'}{x} > 1$, and so putting $\frac{K_2'}{x} = \frac{1}{\cos^2 u}$, the solution becomes

$$R_2' = \text{const.} \cdot \sqrt{\cot u} \cdot e^{\pm K_2(2u - \sin 2u)} \quad \dots (6.1)$$

or, as,

(b) $\frac{K_2'}{x} < 1$, and so putting $\frac{K_2'}{x} = \frac{1}{\cosh^2 u}$, the solution becomes

$$R_2' = \text{const.} \sqrt{\coth u} e^{\pm i \{K_2 (\sinh 2u - 2u) - \pi/4\}} \quad \dots (6.2)$$

Case 3. Let x be very great and K_2' finite, so that $\frac{K_2'}{x} \ll 1$. Hence from Eq. (5), on equating terms of the same order we get

$$\left. \begin{aligned} g_0 &= \pm 1 \\ \text{and } \lambda g_1 &= -\frac{1}{2} \cdot \frac{d}{dx} \cdot \ln g_0 \pm \frac{K_2'}{2ix} \end{aligned} \right\} \quad \dots (4.4)$$

Therefore, using (4.4) in (4), the solution becomes

$$R_2' = \text{const.} e^{\pm i \left(\frac{a_2}{2} r \mp K_2 \ln \frac{a_2}{2} \cdot r - \frac{\pi}{4} \right)} \quad \dots (7)$$

It may easily be shown from (2.2), (2.4) and (2.5) that

$$\frac{K_2'}{x} = \frac{2z^* e^2 / r}{E_2 + U_0} \quad \dots (7.1)$$

Region 2. In this region near r_0 , $\frac{2z^* e^2}{r} > E_2 + U_0$, because even for zero initial kinetic energy of the α -particle, $(E_{kin})_{r_0} = E_2 + U(r_0) - \frac{2z^* e^2}{r_0} = 0$ i.e. $\frac{2z^* e^2}{r_0} = E_2 + U(r_0)$ and $U(r_0) > U_0$ {Fig. 1 (a) and 1 (b)}. Then from r_0 outwards as the Coulomb potential $\frac{2z^* e^2}{r}$ decreases, it must be equal to $E_2 + U_0$ at certain value $r = r'$, i.e., at r' ,

$$\frac{2z^* e^2}{r'} = E_2 + U_0 \quad \dots (7.2)$$

So for the region 2(a) i.e., for $r_0 < r < r'$, from Eq. (7.1), $\frac{K_2'}{x} > 1$, hence for this range we have to take the solution as (vide (6.1))

$$R_2 = \frac{R_2'}{r} = \frac{\text{const.}}{r} \sqrt{\cot u} \cdot e^{\pm i K_2 (2u - \sin 2u)} \quad \dots (8)$$

Again for the region 2(b) i.e., for $r' < r < r_1$, $\frac{2z^* e^2}{r} < E_2 + U_0$ and so from Eq. (7.1) $\frac{K_2'}{x} < 1$. Therefore in this range we have to take the solution as (vide (6.2))

$$R_2 = \frac{R'_1}{r} = \frac{\text{const.}}{r} \cdot \sqrt{\coth u} \cdot e^{\pm i \left\{ K_2 (\sinh 2u - 2u) - \frac{\pi}{4} \right\}} \quad \dots (8.1)$$

If, however, r_1 is sufficiently great, so that $\frac{K'_2}{x} \ll 1$ near r_1 , we should take solution as {vide (7)},

$$R_2 = \frac{\text{const.}}{r} \cdot e^{\pm i \left(\frac{\alpha_2}{2} \cdot r - K_2 \ln \frac{\alpha_2}{2} \cdot r - \frac{\pi}{4} \right)} \quad \dots (8.2)$$

instead of Eq. (8.1). But as we do not know where r_1 actually falls, we should start by taking both the solutions (8.1) and (8.2) for the region 2 (b), finally rejecting the one found to be inappropriate from other considerations.

Region 3. In this region beyond r_1 , $\frac{2z^*e^2}{r}$ is definitely very small, and

so we have, $\frac{K'_3}{r} = \frac{2z^*e^2/r}{E_3} \ll 1$, similar to Eq. (7.1). Therefore we have to take the solution of Eq. (3.2), corresponding to (7) as

$$R_3 = \frac{\text{const.}}{r} \cdot e^{\pm i \left(\frac{\alpha_3}{2} \cdot r - K_3 \ln \frac{\alpha_3}{2} \cdot r - \frac{\pi}{4} \right)} \quad \dots (9)$$

Boundary Conditions :

Of the boundary conditions of continuity at $r=r_0$, and at $r=r_1$, the latter is useful in giving valuable informations regarding the size of the nucleus, and the magnitudes of the attraction potential $U(r)$ at r_0 in the region 2. So we consider it first. The other boundary condition will be considered in Sec. 2.

The R -components of the wave equations (1.4) and (1.5) satisfy the combined boundary conditions at $r=r_1$, namely,

$$\left\{ \frac{d}{dr} \cdot \log R_2 \right\}_{r=r_1} = \left\{ \frac{d}{dr} \cdot \log R_3 \right\}_{r=r_1} \quad \dots (10)$$

As already discussed under Eq. (7.1), R_2 may have two forms near r_1 , according as $\frac{K'_2}{x} < 1$ or $\ll 1$. Taking the real part of the first form, given

in (8.1) (the unknown constant, in general, being considered complex) we have

$$R_2 = \frac{\text{const.}}{r} \cdot \sqrt{\coth u} \cdot \cos \left\{ K_2 (\sinh 2u - 2u) - \frac{\pi}{4} + p_2 \right\} \quad \dots (10.1)$$

where p_2 is the unknown epoch. On taking the above value of R_2 , the left hand side of (10) becomes

$$-\frac{1}{r_1} + \frac{1}{4r_1 \left(1 - \frac{\alpha_2 r_1}{4K_2} \right)} - \frac{\alpha_2}{2} \sqrt{1 - \frac{4K_2}{\alpha_2 r_1}} \times \tan \left\{ K_2 (\sinh 2u_1 - 2u_1) - \frac{\pi}{4} + p_2 \right\} \quad \dots (11)$$

Again taking the real part of the second form of R_2 , given in Eq. (8.2) we have

$$R_2 = \frac{\text{const.}}{r} \cdot \cos\left(\frac{\alpha_2}{2} r - K_2 \ln \frac{\alpha_2}{2} r - \frac{\pi}{4} + p_2'\right)$$

where p_2' is the corresponding epoch. With this value of R_2 , the l. h. s. of (10) becomes

$$-\frac{1}{r_1} \left(\frac{\alpha_2}{2} - \frac{K_2}{r_1} \right) \times \tan\left(\frac{\alpha_2}{2} r_1 - K_2 \ln \frac{\alpha_2}{2} r_1 - \frac{\pi}{4} + p_2'\right) \quad \dots \quad (11.1)$$

For the right hand side of (10) we take the real part of R_1 , given in Eq. (9) and get

$$R_1 = \frac{\text{const.}}{r} \cdot \cos\left(\frac{\alpha_1}{2} r - K_1 \ln \frac{\alpha_1}{2} r - \frac{\pi}{4} + p_3\right)$$

where p_3 is the unknown epoch. On substituting the above value of R_3 , we have for the right hand side of (10)

$$-\frac{1}{r_1} \left(\frac{\alpha_1}{2} - \frac{K_1}{r_1} \right) \times \tan\left(\frac{\alpha_1}{2} r_1 - K_1 \ln \frac{\alpha_1}{2} r_1 - \frac{\pi}{4} + p_3\right) \quad \dots \quad (12)$$

Now for the left hand side of (10) we can take either (11) or (11.1). Equating (12) successively with (11) and (11.1), we have after transformation

$$\begin{aligned} -\frac{1}{2r_1 \left(2 - \frac{r_1}{2} \cdot \frac{\alpha_2}{K_2} \right)} - \frac{\alpha_2}{2} \sqrt{1 - \frac{4}{r_1} \cdot \frac{K_2}{\alpha_2}} \times \tan\left\{K_2 \left(\sinh 2u_1 - 2u_1 \right) - \frac{\pi}{4} + p_2\right\} \\ = -\left(\frac{\alpha_3}{2} - \frac{K_3}{r_1} \right) \times \tan\left(\frac{\alpha_3}{2} r_1 - K_3 \ln \frac{\alpha_3}{2} r_1 - \frac{\pi}{4} + p_3\right) \quad \dots \quad (13) \end{aligned}$$

$$\begin{aligned} \text{and} \quad \left(\frac{\alpha_2}{2} - \frac{K_2}{r_1} \right) \times \tan\left(\frac{\alpha_2}{2} r_1 - K_2 \ln \frac{\alpha_2}{2} r_1 - \frac{\pi}{4} + p_2'\right) \\ = \left(\frac{\alpha_3}{2} - \frac{K_3}{r_1} \right) \times \tan\left(\frac{\alpha_3}{2} r_1 - K_3 \ln \frac{\alpha_3}{2} r_1 - \frac{\pi}{4} + p_3\right) \quad \dots \quad (13.1) \end{aligned}$$

We cannot proceed further with the equations (13) and (13.1) without ascertaining the nature of the resultant field in the region 2. The scattering experiments of Rutherford (1927) with U_1 nucleus suggest that the resultant field in region 2 should in general be repulsive. Thus even if the total energy of the emitted alpha particle is wholly potential at r_0 , its energy at r_1 , should in general be partly potential and partly kinetic. If the particle comes out with the minimum energy, then evidently its kinetic energy ξ at r_0 is zero, and so we have at r_0 ,

$$(E_{kin})_{r_0} = \xi = (E_2)_{\min} + U(r_0)_{\xi=0} - \frac{2ze^2}{r_0} = 0 \quad \dots \quad (15)$$

and at r_1 , since $U(r_1) = 0$,

$$(E_{kin})_{r_1} = (E_2)_{\min} - \frac{2ze^2}{r_1} = \eta_0 \quad \dots \quad (16)$$

where $(E_2)_{\min}$ is the total energy in region 2, corresponding to $\xi=0$. But the alpha particle cannot always come out with the minimum energy, *i.e.* we cannot have always $\xi=0$. On the other hand, ξ may have as many discrete values as there are energy levels in the nucleus higher than the peak of the barrier. When the decaying nucleus emits the alpha particles from different energy levels, the product element will be left in the corresponding excited states. This product nucleus, like all other isomers, is likely to possess different spin values corresponding to its different excited states. Again as the interaction potential is of Yukawa type and spin dependent, $U(r)$ in (15) will change in magnitude with spin. Now, since the spin-difference is associated with the difference of energy states of the nucleus and hence with the initial k. e. ξ of the emitted alpha particle, $U(r)$ is evidently indirectly related to the initial kinetic energy of the alpha particle. Thus Eq. (15) may be taken in the general form

$$E_2 + U(r_0)\xi - \frac{2z^*e^2}{r_0} = \xi \quad \dots (17)$$

On comparing (17) with (15) we have at once

$$E_2 = (E_2)_{\min} + \xi + \beta \quad \dots (18)$$

where

$$\beta = U(r_0)_{\xi=0} - U(r_0)\xi \quad \dots (18.1)$$

We shall, however, show later on that β is positive and consequently

$$U(r_0)_{\xi=0} = U(r_0)_{\max} \quad \dots (18.2)$$

Now since we have defined the second boundary r_1 as the distance at which the attraction potential is sensibly zero, it is reasonable to believe that for the small change β in $U(r_0)$, the change in the value of the potential at such a great distance r_1 is insignificant. Thus only the kinetic portion of the total energy of the alpha particle changes at the second boundary r_1 , with any change in the initial kinetic energy ξ at r_0 . Therefore, similar to (17), we should take Eq. (16) at r_1 in the general form

$$E_2 - \frac{2z^*e^2}{r_1} = \eta \quad \dots (19)$$

where, [*vide* (18)]

$$\eta = \eta_0 + \xi + \beta \quad \dots (19.1)$$

Now if S be the ratio of the straight mean $U(r_0)_{\xi}/2$ to the true mean U_0 for the attraction potential in region 2, we have, corresponding to Eq. (17),

$$E_2 + U_0 - \frac{2z^*e^2}{r} = \xi' \quad \dots (20)$$

where

$$U_0 = \frac{U(r_0)_{\xi}}{2s} \quad \dots (20.1)$$

Comparing Eq. (20) and (17), U_0 is seen to be the actual attraction potential at r , where ξ' is the corresponding kinetic energy. Again, since $U(r)$ is of Yukawa type, the mean value U_0 , given by (20.1) and which has been taken

constant for the wave equation (1.4) or (2), must be less than the straight average $U(r_0)\xi/2$. Hence in Eq. (20.1) we have

$$s > 1 \quad \dots (21)$$

It will be shown later on [*vide* Eq. (32.2)] that $s < 2$. It is obvious that for the lower limit $s=1$, ξ' and $\bar{\tau}$ in (20) are the averages of the corresponding quantities at the two boundaries r_0 and r_1 . It may be easily seen that for the upper limit $s=2$, we have

$$\bar{\tau} = \frac{4r_0r_1}{3r_0 + r_1} \quad \dots (20.2)$$

$$\xi' = (3\eta + \xi)/4 \quad \dots (20.3)$$

Now having thus defined U_0 for the second region we get at once from (2.2) and (2.4)

$$\frac{\alpha_2}{K_2} = \frac{2(E_2 + U_0)}{z^*e^2} \quad \dots (22)$$

Now, substituting in the equation of continuity (13) the values of α_2/K_2 , α_2 , and r_1 from (22), (2.2) and (19) respectively, we have after transformation

$$\begin{aligned} & \frac{E_2 - \eta}{2(U_0 + \eta)} \tan \left\{ K_2 (\sinh 2u_1 - 2u_1) - \frac{\pi}{4} + p_2 \right\} + \frac{8\pi z^* e^2 \sqrt{2M(U_0 + \eta)}}{h(E_2 - \eta)} \\ &= \frac{8\pi z^* e^2 \sqrt{M}}{h \sqrt{2E_2}} \frac{(E_2 + \eta)}{(E_2 - \eta)} \cdot \left\{ \frac{\tan \left(\frac{\alpha_2}{2} r_1 - K_2 \ln \frac{\alpha_2}{2} r_1 - \frac{\pi}{4} + p_3 \right)}{\tan \left\{ K_2 (\sinh 2u_1 - 2u_1) - \frac{\pi}{4} + p_2 \right\}} \right\} \quad \dots (23) \end{aligned}$$

Similarly from (2.2), (2.4) and (19), the alternative equation (13.1) transforms into

$$\frac{2\sqrt{1 + U_0/E_2}}{(1 - \eta/E_2)} - \frac{1}{\sqrt{1 + U_0/E_2}} = \frac{(1 + \eta/E_2)}{(1 - \eta/E_2)} \cdot \frac{\tan \left(\frac{\alpha_2}{2} r_1 - K_2 \ln \frac{\alpha_2}{2} r_1 - \frac{\pi}{4} + p_3 \right)}{\tan \left\{ \frac{\alpha_2}{2} r_1 - K_2 \ln \frac{\alpha_2}{2} r_1 - \frac{\pi}{4} + p_2 \right\}} \quad \dots (23.1)$$

Now from the optical analogy, that the transmitted waves do not suffer any phase change at a boundary, it is reasonable to assume that the matter waves do not undergo any change of phase at the boundary r_1 . Hence the ratio of the tangents of the phase angles at r_1 , on the right hand side of both equations (23) and (23.1) become 1, and so we have

$$\left. \begin{aligned} & \frac{(E_2 - \eta)}{2(U_0 + \eta)} \cdot \frac{1}{\tan \left\{ K_2 (\sinh 2u_1 - 2u_1) - \frac{\pi}{4} + p_2 \right\}} + \frac{8\pi z^* e^2 \sqrt{2M(U_0 + \eta)}}{h(E_2 - \eta)} \\ &= \frac{8\pi z^* e^2 \sqrt{M}}{h \sqrt{2E_2}} \frac{(E_2 + \eta)}{(E_2 - \eta)} \end{aligned} \right\} \quad (23.2)$$

and
$$\frac{2\sqrt{1+U_0/E_2}}{(1-\eta/E_2)} - \frac{1}{\sqrt{1+U_0/E}} = \frac{(1+\eta/E_2)}{(1-\eta/E_2)} \quad \dots (23.3)$$

On solving (23.3) for $\sqrt{1+\frac{U_0}{E_2}}$, it may be easily shown that either

$$U_0=0, \text{ or } = \left\{ \frac{1}{4} \left(1 - \frac{\eta}{E_2} \right) - 1 \right\} \times E_2 \quad \dots (23.4)$$

The second value of U_0 in (23.4) is negative, as $\frac{\eta}{E_2} < 1$. Thus both the possible values of U_0 obtained in (23.4) should be rejected, as going against our fundamental conception of U_0 . We are thus left with the only equation of continuity (23.2)

To find the unknown epoch p_2 in (23.2), we consider the behaviour of the solution R_2 , given in Eq. (8.1) for the region 2(b), i.e. for $r' < r < r_1$. Since r' is not a boundary, R_2 should be valid at r' . At $r=r'$, the real part of the solution R_2 in (8.1) as given in (10.1) is

$$R_2 = \left| \frac{\text{const.}}{r} \cdot \sqrt{\coth u} \cdot \cos \left\{ K_2 (\sinh 2u - 2u) - \frac{\pi}{4} + p_2 \right\} \right|_{r=r'} \quad \dots (23.5)$$

where
$$(\coth u)_{r=r'} = \sqrt{\frac{1}{1-4K_2/\alpha_2 r'}}$$

Again from (2.2), (2.4) and (7.2) we have $\frac{4K_2}{\alpha_2 r'} = 1$ Therefore

$$(\coth u)_{r=r'} = \infty \quad \dots (24)$$

i.e., the solution R_2 in (23.5) is infinite, which is impossible. Therefore in order to make the solution bounded at r' , we must take in (23.5)

$$\cos \left\{ K_2 (\sinh 2u - 2u) - \frac{\pi}{4} + p_2 \right\} \Big|_{r=r'} = 0$$

$$K_2 (\sinh 2u - 2u) - \frac{\pi}{4} + p_2 \Big|_{r=r'} = \frac{\pi}{2} \quad \dots (24.1)$$

From Eq. (24), $|u|_{r=r'} = 0$ and $(\sinh 2u)_{r=r'} = 0$. Hence from (24.1) we at once get

$$p_2 = 3 \cdot \frac{\pi}{4} \quad (25)$$

Using (25) in (23.2) we have finally for the continuity equation

$$\frac{E_2 - \eta}{2(U_0 + \eta)} \cdot \frac{1}{\tan \left\{ K_2 (\sinh 2u_1 - 2u_1) + \frac{\pi}{2} \right\}} + \frac{8\pi z^* e^2 \sqrt{2M(U_0 + \eta)}}{h(E_2 - \eta)} \quad (26)$$

$$= \frac{8\pi z^* e^2 (E_2 + \eta)}{h\nu(E_2 - \eta)}$$

where v is the observed velocity of alpha particle, given by $E_2 = \frac{1}{2} M v^2 = E_3$. The first term in (26) is very small compared to the second and the third, as can be seen by putting the approximate values for all the quantities involved. So neglecting this term, to a first approximation we find

$$\frac{U_0}{E_2} = \frac{1}{4} - \frac{\eta}{2E_2} + \frac{\eta^2}{4E_2^2} \quad \dots \quad (26.1)$$

Now using (26.1), the correction term in (26) becomes

$$2\left(1 - \frac{3\eta}{E_2}\right) / \tan \theta \quad \dots \quad (27)$$

where
$$\theta = \pi \left\{ \frac{z^* \times 0.1393 (\sinh 2u_1 - 2u_1)}{v - 10^{-9} \times \sqrt{\frac{5}{4} - \frac{\eta}{2E_2}}} + 0.5 \right\} \quad \dots \quad (27.1)$$

neglecting the small $\frac{\eta^2}{E_2^2}$ term.

Again to find $2u_1$ and $\sinh 2u_1$ in (27.1) we note that by definition

$$\cosh 2u_1 = \frac{\alpha_2 r_1}{4K_2} = \frac{1 + U_0/E_2}{1 - \eta/E_2} = \frac{5/4 - \frac{\eta}{2E_2}}{1 - \eta/E_2} \quad \dots \quad (27.2)$$

from which $2u_1$ and $\sinh 2u_1$ can be calculated if η/E_2 is known. Substituting (27) in (26) we have

$$\frac{8\pi z^* e^2 \sqrt{2M(U_0 + \eta)}}{h(E_2 - \eta)} = \frac{8\pi z^* e^2 (E_2 + \eta)}{h v (E_2 - \eta)} - \frac{2\left(1 - \frac{3\eta}{E_2}\right)}{\tan \theta} \quad \dots \quad (28)$$

Therefore

$$U_0 + \eta = \frac{1}{8} M v^2 \left(1 + \frac{2\eta}{E_2}\right) - \frac{M v^3 \hbar \left(1 - \frac{3\eta}{E_2}\right)}{8 z^* e^2 \tan \theta} + \text{higher term}$$

or
$$U_0 + \eta/2 = \left\{ \frac{1}{4} - \frac{\hbar v \left(1 - \frac{3\eta}{E_2}\right)}{4 z^* e^2 \tan \theta} \right\} \times E_2 \quad \dots \quad (29)$$

Determination of β

At the outset it need be pointed out that since β is involved only in U_0 , Eq. (29) is unaffected even if we take $\beta = 0$ always. In that case, however, we have to assume with Gamow and others that the size of a nucleus of same z^* fluctuates as it is raised to different energy states by emitting different α -groups. Thus we have to assume as many as 13 radii for the same RaF nucleus. This seems to us less plausible than our conception of constant r_0 , which follows from (29) with discrete β -values. So let us now decide whether β is positive or negative.

Let us first assume that β is negative, and we have then from (20.1) and (18.1)

$$U_0 = \frac{[U(r_0)]_{\xi=0}}{2s} + \frac{\beta}{2s} \quad \dots (30)$$

It is evident from (30) that when $\beta=0$, U_0 is minimum. Hence

$$(U_0)_{\min} = [U(r_0)]_{\xi=0/2s}.$$

$$(U_0)_{\max} = [U(r_0)]_{\xi=0/2s} + \frac{\beta_{\max}}{2s}.$$

and so

$$(U_0)_{\max} - (U_0)_{\min} = \beta_{\max}/2s \quad \dots (30.1)$$

Again when $\beta=0$, $\xi=0$, therefore $(U_0)_{\min}$ corresponds to $(E_2)_{\min}$ and so in that case $\eta=\eta_0$ [vide (19.1).] Also when β is maximum, ξ is also maximum, and $(U_0)_{\max}$ corresponds to $(E_2)_{\max}$, and in that case $\eta=\eta_{\max}$. Therefore neglecting the small correction term $3\eta/E_2$ in (29) we have similar to (30.1).

$$(U_0)_{\max} - (U_0)_{\min} = \frac{1}{4} (E_2)_{\max} - (E_2)_{\min} - \frac{\eta_{\max} - \eta_0}{2} - \frac{\hbar}{4z^* e^2} \left\{ \frac{v_{\max} (E_2)_{\max}}{\tan \theta_0} - \frac{v_{\min} (E_2)_{\min}}{\tan \theta_{\max}} \right\} \quad \dots (31)$$

Again from (19.1) and (18) for negative β

$$\eta_{\max} - \eta_0 = (E_2)_{\max} - (E_2)_{\min} = \xi_{\max} - \beta_{\max} \quad \dots (31.1)$$

Now substituting (31.1) in (31)

$$(U_0)_{\max} - (U_0)_{\min} = -\frac{1}{4} (\xi_{\max} - \beta_{\max}) - \frac{\hbar}{4z^* e^2} \left\{ \frac{v_{\max} (E_2)_{\max}}{\tan \theta_0} - \frac{v_{\min} (E_2)_{\min}}{\tan \theta_{\max}} \right\} \quad \dots (31.2)$$

From (30.1) and (31.2) we have

$$\beta_{\max} = \frac{s}{(s-2)} \xi_{\max} + \frac{\hbar s}{z^* e^2 (s-2)} \left\{ \frac{v_{\max} (E_2)_{\max}}{\tan \theta_0} - \frac{v_{\min} (E_2)_{\min}}{\tan \theta_{\max}} \right\} \quad \dots (32)$$

Since in (30) β is assumed to be negative, β_{\max} in (32) should be positive. So the right hand side of (32) should also be positive, i.e., $s > 2$. Again, if β is negative, $\xi_{\max} - \beta_{\max} = (E_2)_{\max} - (E_2)_{\min}$, (vide 18). So $\xi_{\max} > \beta_{\max}$. Therefore

we have in (32), $\frac{s}{s-2} < 1$ which is impossible if $s > 2$. Thus β cannot be

negative. Hence β is positive which means, as assumed in (18.2), that the attraction potential $U(r)$ becomes higher as the nucleus is raised to higher excited states due to emission of alpha particles at lower energies. Thus it follows that $U(r)$ or U_0 is related indirectly to the kinetic energy of the outgoing alpha particle as already mentioned.

Now since β is positive, we shall have instead of (32)

$$\beta_{\max} = \frac{s}{(2-s)} \xi_{\max} + \frac{\hbar s}{z^* e^2 (2-s)} \left\{ \frac{v_{\max} (E_2)_{\max}}{\tan \theta_0} - \frac{v_{\min} (E_2)_{\min}}{\tan \theta_{\max}} \right\} \quad \dots (32.1)$$

From (32.1) and (21) we have evidently

$$1 < s < 2. \quad \dots (32.2)$$

Since from (18), $\xi_{\max} + \beta_{\max} = (E_2)_{\max} - (E_2)_{\min} = \text{range of } \alpha\text{-energy spectrum}$ we have from (32.1)

$$\beta_{\max} = \frac{s}{2} (E_2)_{\max} - (E_2)_{\min} + \frac{\hbar s}{2z^2 e^2} \left\{ \frac{v_{\max} (E_2)_{\max}}{\tan \theta_0} - \frac{v_{\min} (E_2)_{\min}}{\tan \theta_{\max}} \right\} \dots (32.3)$$

$$\text{and } \xi_{\max} = \frac{(2-s)}{2} (E_2)_{\max} - (E_2)_{\min} - \frac{\hbar s}{2z^2 e^2} \left\{ \frac{v_{\max} (E_2)_{\max}}{\tan \theta_0} - \frac{v_{\min} (E_2)_{\min}}{\tan \theta_{\max}} \right\} \dots (32.4)$$

Now it follows from (32.3) and (32.4) that in the case of the elements which do not show alpha energy spectrum, $\xi = \beta = 0$. These elements possess only one effective energy level higher than the peak of the potential barrier. There are, however, other energy states lower than the peak of the barrier. These levels being of insufficient energy are incapable of emitting alpha particles. With smaller values of z , the potential barrier becomes less high and consequently the number of alpha transformations giving rise to spectrum will increase, and necessarily the range of the alpha energy spectrum becomes wider. It is remarkable that the present theory thus provides a qualitative explanation for the observed fact that as we go up a radioactive series, z increases, the number of spectral lines in general decreases till it becomes one (*vide* Table I). Irregularities, however, must be due to some structural complexities

EVALUATION OF NUCLEAR RADIUS r_0

Since β is positive, writing for $U(r_0)$ from (18.1) and (18.2), we have from (20.1)

$$U_0 = \frac{U(r_0)_{\max}}{2s} - \frac{\beta}{2s} \quad \dots (33)$$

Therefore

$$(U_0)_{\min} = \frac{U(r_0)_{\max}}{2s} - \frac{\beta_{\max}}{2s} \quad \dots (33.1)$$

Since β_{\min} corresponds to ξ_{\max} and hence $(E_2)_{\max}$, we have from (29)

$$(U_0)_{\min} = \left\{ \frac{1}{4} - \frac{\hbar v_{\max} (1 - 3\eta_{\max} / (E_2)_{\max})}{4z^2 e^2 \tan \theta_0} \right\} \times (E_2)_{\max} - \frac{\eta_{\max}}{2} \quad \dots (34)$$

Again from (15) and (18.2), we have

$$r_0 = \frac{2z^2 e^2}{(E_2)_{\min} + [U(r_0)]_{\max}} \quad \dots (35)$$

On substituting for $U(r_0)_{\max}$ from (33.1) and using (34) we get

$$U(r_0)_{\max} = \left\{ \frac{s}{2} - \frac{\hbar v_{\max} (1 - 3\eta_{\max} / (E_2)_{\max})}{z^2 e^2 \tan \theta_0} \right\} \times (E_2)_{\max} - s \left(\eta_{\max} - \frac{\beta_{\max}}{s} \right) \dots (35.1)$$

TABLE I

Name of decaying element	z*	No of α -energy groups	obsd. $(E_2)_{\max}$ Mev,	obsd. $(E_2)_{\min}$ Mev.	$U(r_0)_{\max}$ Mev.	Nuclear radius $r_0 \times 10^{-12}$ cm.	Produced by
U ₁ ²³⁸	90	1	4.270		4.360	3.024	
U ₁₁ ²³⁴	90	1	4.780		3.473	3.139	⁹¹ UX ₂ ²³⁴ β -decay
Io ²³⁰	88	1	4.810		3.409	3.083	⁹² U ₁₁ ²³⁴ α -decay
Ra ²²⁶	86	7	4.793	3.947	2.629	3.765	⁹⁰ Io ²³⁰ α -decay
Rn ²²²	84	1	5.486		3.674	2.640	⁸⁸ Ra ²²⁶ α -decay
Ra A ²¹⁸	82	1	5.998		3.890	2.380	⁸⁶ Rn ²²² β -decay
Ra C ²¹⁴	82	13	10.509	7.683	3.526	2.105	⁸³ RaC ²¹⁴ β -decay
Ra F ²¹⁰	82	13	5.303	3.685	4.327	2.947	⁸³ RaF ²¹⁰ β -decay
Ra C ²¹¹	81	3	5.517	5.333	3.781	2.560	⁸² RaB ²¹⁴ β -decay
Th ²³²	88	1	4.20		3.384	3.341	...
Rd Th ²²⁸	88	2	5.418	5.335	3.784	2.779	⁸⁰ MsTh ₁₁ ²²⁸ β -decay
Th X ²²⁴	86	1	5.680		3.814	2.608	⁹⁰ RdTh ²²⁸ α -decay
Th ²²⁰	84	1	6.280		4.077	2.334	⁸⁸ ThX ²²⁴ α -decay
Th A ²¹⁶	82	1	6.774		4.222	2.146	⁸⁶ Th ²²⁰ α -decay
Th C ²¹²	82	3	10.553	8.776	7.50	1.450	⁸³ ThC ²¹² β -decay
Th C ²¹²	81	6	6.054	5.601	4.151	2.392	⁸² ThB ²¹² β -decay
Ac U ²³⁵	90	1	4.330		3.643	3.249	
Pa ²³¹	89	1	5.00		3.523	3.007	⁹⁰ UY ²³¹ β -decay
Rd Ac ²²⁷	88	11	6.051	5.674	5.513	2.265	⁸⁸ Ac ²²⁷ β -decay
Ac X ²²³	86	3	5.720	5.533	3.896	2.626	⁹⁰ Rd Ac ²²⁷ α -decay
An ²¹⁹	84	3	6.826	6.436	4.449	2.221	⁸⁸ Ac X ²²³ α -decay
Ac A ²¹⁵	82	1	7.365		4.381	2.009	⁸⁶ An ²¹⁹ α -decay
Ac C ²¹¹	82	1	7.434		4.390	1.997	⁸³ Ac C ²¹¹ β -decay
Ac C ²¹¹	81	2	6.619	6.262	4.273	2.213	⁸² Ac B ²¹¹ β -decay

Now from (35) and (35.1) we get after transformation

$$r_0 = \frac{4z^{*2}c^4 \tan \theta_0}{(E_2)_{\max} \{ (s+2)z^{*2}e^2 \tan \theta_0 - s\hbar v_{\max} (1 - 3\eta_{\max} / (E_2)_{\max}) \}} - I, \quad (36)$$

where $\tan \theta_0$ corresponds to v_{\max} and is given in (27.1), and

$$L = 2z^{*2}e^2 \tan \theta_0 (s\eta_{\max} + \xi_{\max})$$

from (32.4) neglecting small term involving \hbar , we have

$$L = 2z^*e^2 \tan \theta_0 \left(s\eta_{\max} + \frac{(2-s)}{2} \text{range} \right) \quad \dots (36.1)$$

For the elements which do not show energy spectrum (36.1) takes the simple form

$$L = 2sz^*e^2\eta_0 \tan \theta_0 \quad \dots (36.2)$$

It should be noted that the formula for r_0 in (36) contains s and η_0 , yet to be found. The value of η_0 will be obtained from the formula to be deduced later on (*vide* 40). Hence we are in a position to calculate r_0 for different nuclei, if we take at present for s its limiting value† $s=2$ (*vide* 32.2). In addition to the size of the nucleus, information regarding the limiting values of the attraction potential $U(r)$ at r_0 , are also known (*vide* 35.1). It is remarkable that the magnitude of the short range potential calculated from our theory ranges over several Mev which agrees with the order of the magnitude obtained from other methods (e.g. nuclear binding energy calculation from mass defects, etc). Table I gives the calculated values of r_0 , $U(r_0)_{\max}$, for the elements of all the three radioactive series with $s=2$.

It is to be noted that Eq. (36) gives an *explicit* formula for the size of a nucleus. Previously, the values of nuclear radii were obtained from an *implicit* $\log \lambda - E$ relation. This method seems to be only approximate because, (1) the $\log \lambda - E$ relation, given by the leakage theory, is open to the objections raised by Chang (1948), Berthelot (1942) and others, (2) this $\log \lambda - E$ relation really contains an unknown averaging (normalizing) factor, and in calculating r_0 , all the previous workers, instead of finding that unknown factor, have taken it to be unity, and (3) these r_0 values are calculated from a relation in which λ and E are variable, so that in the case of energy spectrum r_0 should be different for the different values of the observed energy for the same z^* . Thus, for example, for the element RaC', there should be at least 13 values of nuclear radii for the same element, which appears to be improbable.

On the other hand, our explicit formula for r_0 is *independent* of λ , and comes out in terms of constant quantities, such as z^* , M , e , $(E_2)_{\max}$, etc.

Determination of η

From what has been discussed under Eq. (16) and also from the Eq. (18.1), it is seen that as ξ at r_0 increases, $U(r_0)$ decreases. Similarly at distance r , the attraction potential U_0 may also be taken related in the same way with the corresponding kinetic energy of the alpha particle $\xi' = (\xi + 3\eta)/4$. [*vide* (20.3)]. This suggests a simple relationship between the two and we take tentatively

$$U_0 \times (\xi + 3\eta)^n = F(\xi) \quad \dots (37)$$

where n is an unknown constant and F is a slowly varying function of ξ .

† Numerical calculations suggest that s should be very close to 2.

A constant F leads to absurd result, as can easily be seen by comparing the two extreme cases of (37), namely $\xi = \xi_{\max}$. Now for $\xi = \xi_{\max}$ we have from (37)

$$(U_0)_{\max} \times (\xi + 3\eta)^n_{\max} = F(\xi_{\max}) \quad \dots (37.1)$$

Or, using (33.1) and (19.1)

$$\frac{U(r_0)_{\max}}{2s} - \frac{\beta_{\max}}{2s} = \frac{F(\xi_{\max})}{(4\xi_{\max} + 3\eta_0)^n} \left\{ 1 + \frac{3\beta_{\max}}{4\xi_{\max} + 3\eta_0} \right\}^n \quad \dots (37.2)$$

Since $3\beta_{\max} < (4\xi_{\max} + 3\eta_0)$, we have from (37.2)

$$\frac{U(r_0)_{\max}}{2s} - \frac{\beta_{\max}}{2s} = \frac{F(\xi_{\max})}{(4\xi_{\max} + 3\eta_0)^n} - \frac{6nsF(\xi_{\max})/(4\xi_{\max} + 3\eta_0)^n}{(4\xi_{\max} + 3\eta_0)} \frac{\beta_{\max}}{2s} \quad \dots (38)$$

Again, since $\beta_{\max} \ll U(r_0)_{\max}$, we have from (38), on equating terms of the same order

$$\frac{U(r_0)_{\max}}{2s} = \frac{F(\xi_{\max})}{(4\xi_{\max} + 3\eta_0)^n} \quad \dots (38.1)$$

and

$$\frac{6ns}{(4\xi_{\max} + 3\eta_0)} \frac{F(\xi_{\max})}{(4\xi_{\max} + 3\eta_0)^n} = 1 \quad \dots (38.2)$$

Substituting (38.1) in (38.2) we have

$$3nU(r_0)_{\max} = 4\xi_{\max} + 3\eta_0 \quad \dots (39)$$

Now putting $U(r_0)_{\max}$ from (33.1) and using (34), (32.3) and (32.4), we have after transformation, if $sn = s'$

$$n_0 = -\frac{s'}{2(s' + 1)} \cdot (E_2)_{\max} - \frac{(3s' - 4s + 8)}{6(s' + 1)} \cdot [(E_2)_{\max} - (E_2)_{\min}]$$

$$\frac{2ns \left(\frac{4 + 3n}{4} \frac{\gamma_{\min}(E_2)_{\min} - \gamma_{\max}(E_2)_{\max}}{\tan \theta_{\max} \tan \theta_0} \right)}{3(s' + 1)z^*e^2} \quad \dots (39.1)$$

It may be shown from Eq. (27) that if we assume $\eta \geq \frac{1}{3}E$, we have impossible results. Let us first put $\eta = \frac{1}{3}E$. In that case Eq (27) or the first term on the left hand side of (23) becomes zero, i.e., we shall have $2K_2 = 0$, which is impossible [vide (2.4).] Again if $\eta > \frac{1}{3}E$, the numerator of (27) becomes negative and so the term on the left hand side of (13) becomes positive, which is impossible. Hence we conclude that $\eta < \frac{1}{3}E$. Using this condition we can easily find from (39.1) that for the elements which do not show alpha energy spectrum s' is certainly less than 2. Again since lower limit of $\eta = 0$, for the average value of η , $s' = 1/2$. With this value of s' , in the general case, we have from (39.1) neglecting the higher term

$$\eta_0 = \frac{1}{6} (E_2)_{\max} - \frac{1}{6} \left((E_2)_{\max} - (E_2)_{\min} \right) \quad \dots (40)$$

and hence

$$\eta_{\max} = \frac{1}{6} (E_2)_{\max} + \frac{5}{6} \left((E_2)_{\max} - (E_2)_{\min} \right) \quad \dots (40.1)$$

SECTION 2

Disintegration constant λ

We now consider the condition of continuity at the first boundary $r=r_0$. This condition of continuity gives a formula for the viscosity coefficient b , from which we shall deduce the disintegration constant λ .

Since near r_0 , $K'_2/x > 1$, we have to take the solution (8) for the region just outside r_0 . In order to deduce the proper sign in the exponential, we consider the behaviour of the solution at r' , upto which it is valid. Now at $r=r'$, $\cot u$ in Eq. (8) is from (6.1)

$$(\cot u)_{r=r'} = \sqrt{(4K_2/a_2 r') - 1} = \infty$$

since from (2.2), (2.4) and (7.2) $4K_2/a_2 r' = 1$.

Therefore in order to make the solution bounded at r' , we shall have to take

$$e \pm K_2(2u' - \sin 2u') = 0 \quad \dots (41)$$

Now since $\cot u = \infty$, $u = n\pi$, where $n=0, 1, 2, 3$ etc. But if we put $n=0$, we get $e \pm K_2(2u' - \sin 2u') = 1$, and the function becomes infinite both for positive and negative sign of the exponential. Hence $n=1$ at least. As K_2 is large, for $n=1, 2, 3$ etc., the condition (41) is satisfied only if the negative sign is taken. Thus Eq. (8) becomes

$$R_2 = \frac{\text{const.}}{r} \cdot \sqrt{\cot u} \cdot e^{-K_2(2u - \sin 2u)} \quad \dots (42)$$

Now the boundary conditions at $r=r_0$ give

$$\left| \frac{\delta}{\delta r} \cdot \log \cdot \frac{\sin \alpha_1 r}{r} \right|_{r=r_0} = \left| \frac{\delta}{\delta r} \log \sqrt{\cot u} \cdot e^{-K_2(2u - \sin 2u)} \right|_{r=r_0} \quad \dots (43)$$

The left hand side of (43) is $\alpha_1 \cot \alpha_1 r_0 - \frac{1}{r_0}$,

$$\text{where} \quad \alpha_1^2 = \frac{8\pi^2 M E_1}{h^2} \left(1 + \frac{b^2 h^2}{16\pi^2 E_1^2} \right).$$

$$\text{Since} \quad \frac{b^2 h^2}{16\pi^2 E_1^2} \ll 1,$$

we have

$$\alpha_1 r_0 = \sqrt{\frac{8\pi^2 M E_1}{h^2}} \cdot r_0 + \sqrt{\frac{8\pi^2 M E_1}{h^2}} \cdot \frac{b^2 h^2}{3^2 \pi^2 E_1^2} \cdot r_0 = A + B \text{ (say)} \quad \dots (43.1)$$

So

$$\alpha_1 \cot \alpha_1 r_0 = \alpha_1 \cot (A+B) = \alpha_1 \cot A - \alpha_1 B - \alpha_1 B \cot^2 A + B^2 \alpha_1 \cot A.$$

Now since A is of the order of 40 , and $\cot A$ of the order 4 , by putting $\cot A = \delta/A$ and the values of A and B from (43.1) and on neglecting terms

containing b^4 and b^6 being too small, we have after transformation,

$$\alpha_1 \cot \alpha_1 r_0 - \frac{1}{r_0} = -\frac{1}{r_0} + \frac{1}{r_0} \left\{ \delta - b^2 \left(\frac{\delta(\delta-1)h^2}{32\pi^2 E_1^2} + \frac{M r_0^2}{4E_1} \right) \right\} \quad \dots (43.2)$$

Now the right hand side of (43) is

$$-\frac{1}{r_0} + \frac{1}{4r_0(1-\alpha_2 r_0/4K_2)} + \frac{\alpha_2}{2} \sqrt{\frac{4K_2}{\alpha_2 r_0} - 1} \quad \dots (43.3)$$

Equating (43.2) with (43.3) we have

$$\delta - b^2 \left(\frac{M r_0^2}{4E_1} + \frac{\delta(\delta-1)h^2}{8E_1^2} \right) = \frac{1}{2 \left(2 - \frac{r_0}{2} \cdot \frac{\alpha_2}{K_2} \right)} + \frac{\alpha_2 r_0}{2} \sqrt{\frac{4}{r_0} \cdot \frac{K_2}{\alpha_2} - 1} \quad \dots (44)$$

Now from (22) and (20), and using (20.2) for \bar{r} , we get

$$\frac{\alpha_2}{K_2} = 4(1 + \xi' \bar{r} / 2z^* e^2) / \bar{r} \quad \dots (44.1)$$

$$\text{and} \quad \frac{\alpha_2 r_0}{2} = \frac{K_2}{2r_1} (3r_0 + r_1) \left(1 + \frac{\xi' \bar{r}}{2z^* e^2} \right) \quad \dots (44.2)$$

Therefore the right hand side of (44) becomes after transformation

$$\frac{1}{3 \left\{ \frac{r_1}{r_1 - r_0} - \frac{2\xi' r_0 r_1}{3z^* e^2} \right\}} + K_2 \left\{ 1 - r_0^2 \left(\frac{3}{2r_1} - \frac{1}{2r_0} + \frac{\xi'}{z^* e^2} \right)^2 \right\}^{\frac{1}{2}} \quad \dots (45)$$

On combining (45) and (44), on neglecting 1 compared to 3δ , we get

$$b^2 \left(\frac{M r_0^2}{4E_1} + \frac{\delta(\delta-1)h^2}{8E_1^2} \right) = \delta - K_2 \left\{ 1 - \frac{r_0^2}{r_1^2} \left(\frac{3}{2} + \frac{\xi' r_1}{z^* e^2} - \frac{r_1}{2r_0} \right)^2 \right\}^{\frac{1}{2}}$$

Since again $\xi' \ll z^4 e^2 / r_1$, we have finally for b , on putting $r_0^2 / r_1^2 = n'$, and simplifying

$$b = \frac{v'}{r_0} \sqrt{\frac{2\delta - K_2 \left\{ 2 - \frac{n'}{2} \left(3 - \frac{1}{\sqrt{n'}} \right)^2 \right\}^{\frac{1}{2}}}{\sqrt{1 + \delta^2 h^2 / M^2 v'^2 r_0^2}}} \quad \dots (46)$$

Now we have by definition

$$b = \frac{1}{D_s} \cdot \frac{dD_s}{dt} = \frac{1}{N_s} \cdot \frac{dN_s}{dt} \quad \dots (47)$$

where D_s is the probable number density at the surface and N_s is the probable number of α -particles in a thin shell of width Δr_0 , just inside the surface. Again

$$\frac{dN_s}{dt} = \frac{dN_a}{dt} = \frac{1}{N} \frac{dN}{dt} = \lambda \quad \dots (48)$$

where N_α is the total number of alpha particles inside a given nucleus, and N , the total number of nuclei in the sample. Therefore from (47), (48), and (46) we have

$$\lambda = b \cdot N_\alpha = \frac{v'}{r_0} \cdot \frac{\sqrt{2\delta - K_2 \left\{ 2 - \frac{n'}{2} \left(3 - \frac{1}{\sqrt{n'}} \right)^2 \right\}^{\frac{1}{2}}}}{\sqrt{1 + \delta^2 \hbar^2 / M^2 v'^2 r_0^2}} \cdot \frac{C_1^2 \sin^2 \alpha_1 r_0}{4\pi r_0^2 \Delta r_0}$$

or, from (42)

$$\lambda = C \cdot \frac{\sqrt{2\delta - K_2 \left\{ 2 - \frac{n'}{2} \left(3 - \frac{1}{\sqrt{n'}} \right)^2 \right\}^{\frac{1}{2}}}}{\sqrt{1 + \delta^2 \hbar^2 / M^2 v'^2 r_0^2}} \cdot \frac{v'}{r_0} \cot u_0 \cdot e^{-2K_2(2u_0 - \sin 2u_0)} \quad (49)$$

where

$$C = 4\pi C_2^2 \Delta r_0.$$

and C_1 and C_2 are the averaging factors for the solution inside and just outside r_0 .

In the expression for λ , the exponential part is important. However, it requires to be mentioned that in the exponential of our formula, unlike the previous formulae, we have in K_2 , not the observed energy E_α , but $E_2 + U_0$. A study of Chang's curve will show that if $\log \lambda - E$ curve is plotted against the internal energy, i.e., $E_2 + U(r_0)$, the discrepancy can be resolved.

The quantitative agreement of our formula for λ will be considered later on, only when C in Eq. (49.1) and δ' in (39.1) can be known exactly.

PHYSICAL LABORATORY,
PRESIDENCY COLLEGE, CALCUTTA,

REFERENCES

- Berthelot, 1942, *J. Phys. Radium*, **3**, 52.
 Bethe, H., 1937, *Rev. Mod. Phys.*, **9**, 162.
 Chang, W. Y., 1946, *Phys. Rev.*, **69**, 73.
 „ „ „ *ibid.*, **70**, 632.
 „ 1948, „ **74**, 1195.
 Condon and Gurney, 1928, *Phys. Rev.*, **33**, 127.
 Debye, P., 1909, *Math. Ann.*, **67**, 535.
 Frenkel, 1929, *Zeit. f. Phys.*, **68**, 61.
 Gamow, G., 1928, *Zett. f. Phys.*, **51**, 204.
 „ 1937, *Constitution of Atomic Nuclei and Radioactivity*.
 Gamow, G., and Critchfield, C. L., 1949, *Theory of Atomic Nucleus and Nuclear Energy Sources*.
 Kar, K. C., 1933, *Phil. Mag.*, **16**, 1097.
 „ 1940, *ibid.*, **29**, 169.
 Langer, R. E., 1937, *Phys. Rev.*, **51**, 669.
 Preston, M. A., 1946, *Phys. Rev.*, **69**, 535.
 Rice, O. B., 1930, *Phys. Rev.*, **35**, 1538.
 Rutherford, 1930, *Radiations from Radioactive Substances*, page 241.
 „ 1927, *Phil. Mag. Ser.*, **7**, **4**, 580.
 Saha, A. K., 1914, *Proc. Nat. Inst. Sci. Ind.*, **10**, 373.
 Schlegelinger, 1900, *Differential gleichungen Sammlung*, Bd. 13, 190 (Leipzig).
 Sexl, T., 1929, *Zett. f. Phys.*, **54**, 445.
 „ „ „ *ibid.*, **66**, 62.

THE 43-DAY ISOMER OF CADMIUM (115)*

By P. S. GILL†, C. E. MANDEVILLE AND E. SHAPIRO

ABSTRACT. The 43-day activity of Cd^{115} was induced in pure metallic cadmium irradiated by slow neutrons in the Oak Ridge pile. After chemical purification, the radiations were analyzed with the utilization of conventional absorption and coincidence techniques. It is concluded that the 43-day activity decays with the emission of beta rays of energy 1.41 Mev and at least two gamma rays having respectively energies of 0.10 Mev and 1.10 Mev. These gamma rays are coincident with an inner beta spectrum having an end point at approximately 0.38 Mev. The beta-gamma coincidence data show that only 0.85 per cent. of the total beta radiation is contained in the softer group. Gamma-gamma coincidences indicate cascade emission of gamma rays.

INTRODUCTION

When cadmium is irradiated by slow neutrons, several induced activities are produced. Among these are the 2.5-day Cd^{113} , the 43-day Cd^{115} , and the 330-day Cd^{109} . For the purposes of the present investigation, pure metallic cadmium was irradiated by slow neutrons for a period of several months in the Oak Ridge pile. The source was permitted to decay for a period of one month to allow for the disappearance of the 2.5-day period. The residual activity was then purified as follows:—

Carrier quantities of lead, silver, antimony, and indium ions were added to a 6N- H_2SO_4 solution of irradiated cadmium. Saturation with H_2S precipitated silver, antimony, and residual lead sulfide which were removed by filtration. The acidity of the filtrate was reduced to 0.3N, and indium and cadmium sulfides were precipitated with H_2S . These latter sulfides were filtered off and dissolved in warm dilute nitric acid. The solution was made ammoniacal, precipitating indium hydroxide which was removed by filtration. The filtrate was made slightly acid, then it was saturated with H_2S , precipitating cadmium sulfide which was filtered off and dried for experimental use.

The 43-day activity in cadmium was first reported three years ago, (Seren, Engelkeimer, Sturm, Friedlander, and Turkel, 1947). These early measurements indicated a maximum beta ray energy of 1.5 Mev and that a gamma ray of energy 0.45 Mev accompanied each disintegration. Somewhat different data concerning the energies and intensity of the gamma rays have been obtained by the writers. A preliminary report has already been published, (Gill, Mandeville, and Shapiro, 1950).

* Assisted by the Joint Program of the ONR and the U. S. AEC

† Guest physicist, Bartol Research Foundation, 1950.

‡ The 330-day cadmium decays only by orbital electron capture, and no gamma rays are emitted. Its presence is therefore considered to have no effect upon the measurements described in this paper.

THE MEASUREMENTS

Using a thin window "bubble" counter as a detector, the beta rays of the 43-day activity were absorbed in aluminum as shown in figure 1. The end point, occurring at about 600 mg/cm², corresponds to a maximum energy of 1.41 Mev, (Feather, 1938).

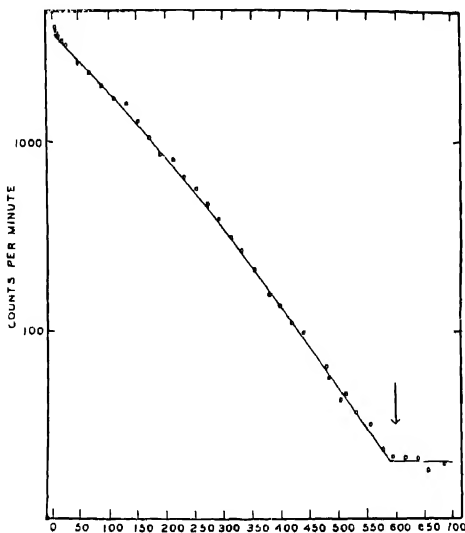


FIG. 1

MG/CM²—AluminiumAbsorption in aluminium of the beta rays from 43-day Cd¹¹⁵

Using the well known technique of coincidence absorption, the gamma ray energy was measured by absorbing in aluminum the Compton secondary electrons produced in a block of aluminum. These data are shown in figure 2. The end point of the coincidence absorption curve corresponds, according to a previously published calibration curve (Mandeville and Scherb, 1948), to a quantum energy of 1.10 Mev. The quantum radiations were also absorbed in lead. The lead absorption curve shows that a gamma ray of energy about 0.10 Mev was present along with a relatively weak gamma ray at 2 Mev.

The gamma ray measurements led to results so markedly different from the earlier data (Seren, Englekemeir, Sturm, Friedlander, and Turkel, 1947) that the cadmium source was allowed to decay further, and additional chemical purification was carried out. It was thought that additional separations should be performed to remove any residual silver and indium

which might still remain in the otherwise pure source. Indium (114), in particular, was considered as a possible impurity, because its half-period and gamma ray spectrum are very similar to the observed characteristics of cadmium (115). The radioactive cadmium sulphide was redissolved in nitric acid, and carrier quantities of silver and indium were added. Silver chloride was precipitated with the addition of dilute HCl and indium was separated from cadmium in the manner described in the introduction of this paper. By this time, the 43-day cadmium activity had decayed for about two months. Absorption experiments were performed as previously indicated, and the results were the same as those obtained after the first chemical purification and after one month of decay.

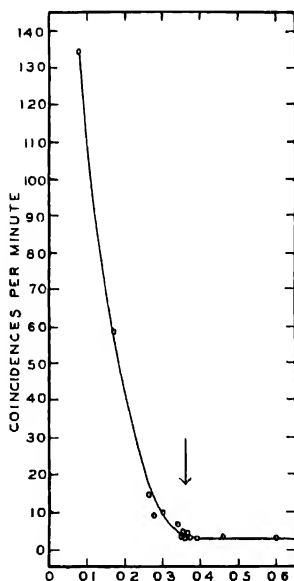


FIG. 2
MG/CM²—Aluminium
Coincidence absorption of the secondary
electrons of the gamma rays
from Cd¹¹⁵.

Using the exceptionally pure cadmium, beta-gamma coincidences were observed as a function of the surface density of aluminium placed before the beta ray counter. These data are shown in figure 3 where the beta-gamma coincidences are observed to decrease from a maximum value of 0.014×10^{-3} coincidence per beta ray at zero absorber thickness to zero at 110 mg/cm^2 . This coincidence rate is a very small one. Calibrating the beta gamma coinci-

dence arrangement with the beta-gamma coincidence rate of Sc^{46} (2 Mev of gamma ray energy coupled with each beta ray) and assuming that each beta ray of the inner group is accompanied on the average by 1.10 Mev of gamma ray energy, it was concluded that the softer group of beta rays at 0.38 Mev must constitute one per cent of the total beta radiation. A gamma-gamma coincidence rate of 0.07×10^{-1} coincidence per gamma ray was observed when a source of the 43-day period was placed between two gamma ray counters in coincidence, showing that cascade emission of gamma rays occurs in the disintegration of Cd^{115} .

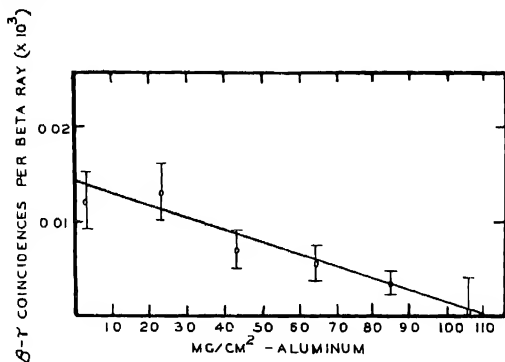


FIG. 3

The beta-gamma coincidence rate of the 43-day Cd^{115} as a function of the surface density of aluminium placed before the beta ray counter

At the conclusion of these measurements, it was learned that Bell, Cassidy, and Hughes of the Oak Ridge National Laboratory, had independently obtained results similar to those of the authors. Using high resolution, obtained with a coincidence spectrometer employing scintillation counters, they observed gamma rays at 1.29, 0.93, 0.72, 0.52, 0.198, and 0.074 Mev. They also concluded that 0.7 per cent. of the beta rays of the 43-day Cd^{115} are coupled with gamma rays. If it is assumed that each beta ray of the inner spectrum is followed on the average by 1.29 Mev of gamma ray energy, the beta-gamma coincidence rate observed by the present authors indicates that 0.85 per cent of the total beta radiation is contained in the softer spectrum. Bell, Cassidy, and Hughes have shown that the faint radiation at 2 Mev is related to an impurity.

A DISINTEGRATION SCHEME FOR THE 43-DAY Cd^{115}

The above reported absorption and coincidence measurements show that the hard beta spectrum of the 43-day Cd^{115} is non-coincident with gamma radiation and must therefore proceed to the ground state of In^{115} , the residual nucleus. The inner spectrum at 0.38 Mev leads to an excited state of In^{115} .

ACKNOWLEDGMENTS

The authors wish to acknowledge with gratitude the kind interest of Dr. W. F. G. Swann, Director of the Bartol Research Foundation, and a grant from the American Philosophical Society which made possible the visit of one of them (P. S. G.) to the United States

MUSLIM UNIVERSITY, ALIGARH
AND
BARTOL RESEARCH FOUNDATION
OF THE FRANKLIN INSTITUTE,
PENNSYLVANIA, U. S. A.

REFERENCES

- Feather, N., 1938, *Proc. Camb. Phil. Soc.*, **34**, 599.
Gill, P. S., Mandeville, C. E., and Shapiro, E., 1950, *Phys. Rev.*, **80**, 248,
Mandeville, C. E., and Scherb, M. V., 1948, *Nucleonics*, **3**, 2.
Seren, L., Ringelkemeir, D., Sturm, W., Friedlander, H. N., and Turkel, S., 1947,
Phys. Rev., **71**, 409.

REVIEW

Physical Aspects of colour—By Dr P. J. Bouma (English Translation By W de Goot) Pp. 312 N. V. Philips. Gocilampenfabrieken, Eindhoven (The Netherlands), 1947. Price Rs. 15/-.

This book deals with the science of measurement of colour. The original manuscript written in Dutch by Dr P. Bouma, an Illuminating Engineer, was published in 1946 and the present translation in English was published in 1947 after the death of Dr. Bouma in January, 1947. Some of the sections have been rewritten in this English translation in order to incorporate results of some recent investigations in this line.

The author has indicated in the preface that he has approached the subject from the points of view of experimental physics and illuminating engineering. The book is divided into fourteen chapters. After explaining in the first chapter parts played by light sources, coloured objects and the eye in making the colour visible, the author deals with the influence of brightness on colour sensation and also with the functions of relative luminosity curves at high and low brightnesses. In Chapter III the convention of expressing any colour by defining its position in a plane colour triangle has been explained with illustrations and the next chapter deals with the convention of colour space in which any colour has a fixed position according to its brightness.

Chapters V and VI deal with the XYZ system adopted by Commission Internationale de l'Éclairage (C. I. E.) and the method of calculation of colour co-ordinate in this system has been explained with the help of suitable examples. In Chapter VII a few special light sources have been described and their functions in colorimetry have been explained. Chapters VIII and IX deal with methods in objective and subjective colorimetry. Chapter X deals with various types of defective colour vision and in the next chapter a brief review of the historical development of colour science has been given. Chapters XII and XIII deal with discrimination of hues and character of colour sensation respectively. In the last chapter some applications of colorimetry, especially those in illuminating engineering and colour reproduction, have been discussed in detail. In the Appendix there are some tables useful for the measurement of colour and also a bibliography of the references has been included at the end.

The book is extremely helpful to illuminating engineers and to those who are interested in reproduction of colour. There are 113 illustrations and the get-up leaves nothing to be desired. The price seems to be quite moderate. The book is available with the Technical & Scientific Literature Department, Messrs. Philips Electrical Co. (India) Ltd., 2 Heysham Road, Calcutta.

S. C. S.

The following special publications of the Indian Association for the Cultivation of Science, 210, Bowbazar Street, Calcutta, are available at the prices shown against each of them :—

Subject	Author	Price Rs. A. P.
Methods in Scientific Research	Sir E. J. Russell	0 6 0
The Origin of the Planets	Sir James H. Jeans	0 6 0
Separation of Isotopes	Prof. F. W. Aston	0 6 0
Garnets and their Role in Nature	Sir Lewis L. Fermor	2 8 0
(1) The Royal Botanic Gardens, Kew.	Sir Arthur Hill	1 8 0
(2) Studies in the Germination of Seeds.		
Interatomic Forces	Prof. J. E. Lennard-Jones	2 8 0
The Educational Aims and Practices of the California Institute of Technology.	R. A. Millikan	0 6 0
Active Nitrogen A New Theory.	Prof. S. K. Mitra	2 8 0
Theory of Valency and the Struc- ture of Chemical Compounds.	Prof. P. Ray	3 0 0
Petroleum Resources of India	D. N. Wadia	2 8 0
The Role of the Electrical [Double layer in the Electro Chemistry of Colloids.	J. N. Mukherjee	1 12 0

A discount of 25% is allowed to Booksellers and Agents.

RATES OF ADVERTISEMENTS

Third page of cover	Rs. 32, full page
do. do.	„ 20, half page
do. do.	„ 12, quarter page
Other pages	„ 25, full page
do.	„ 16, half page
do.	„ 10, quarter page

15% Commissions are allowed to *bonafide* publicity agents securing orders for advertisements.

CONTENTS

	PAGE
66. On Alpha Disintegration. Part I. Some useful Theoretical Tabulations and Graphical Plots—By Ranjit Kumar Das	523
67. On the Raman Spectra of Naphthalene at Low Temperatures—By A. K. Ray	539
68. The Wave Statistical Theory of Alpha Disintegration—By K. C. Kar and M L. Chaudhury	545
69. The 43-day Isomer of Cadmium (115)—By P. S. Gill, C. E. Mandeville and E. Shapiro	566
Review—S. C. S.	571
Physical Aspects of Colour—By Dr. P. J. Bouma.	